uOttawa

Nano-composite Membranes and Zero Thermal Input Membrane Distillation for Seawater Desalination

Mohammadali Baghbanzadeh

Thesis submitted to the
Faculty of Graduate and Postdoctoral Studies
In partial fulfilment of the requirements
For the Doctorate in Philosophy degree in Chemical Engineering

Department of Chemical and Biological Engineering
Faculty of Engineering
University of Ottawa

This thesis is dedicated to my wonderful parents, *Kamal Baghbanzadeh* and *Eghbal Aryan* for their endless love, support, and encouragement and for being a great source of motivation and inspiration.

Résumé

Dans cette thèse, le procédé de dessalement d'eau de mer en ayant recours à la méthode de distillation à base de membranes (DM) a été développé. Concernant l'approche utilisée, une technologie innovatrice présentant l'avantage d'être respectueux de l'environnement et économe en énergie, appelée méthode de distillation pour membranes à demande thermique nulle (DMDTN) a été proposée. Cette approche utilise l'énergie thermique disponible dans l'eau de mer, garantissant un procédé de dessalement autonome, ne nécessitant pas une source d'énergie thermique externe, qui s'avère être l'une des sources majeures de consommation énergétique et de dépense en coût de revient lors du procédé conventionnel DM.

Des études de faisabilité économique ont été entreprises concernant le processus DMDTN. Ces dernières, ont montré que l'eau potable pouvait être produite à un prix de revient de 0.28 $\$/m^3$, correspondant à la moitié du prix de dessalement classique. En ce qui concerne la membrane, une nouvelle membrane a été développée en faisant usage de nanomatériaux incorporés dans le fluorure de polyvinylidène (FPVD). A cet effet, diffèrent nanomatériaux comprenant, le SiO_2 super hydrophobe, l'amine modifiée hydrophile SiO_2, l'oxyde de cuivre CuO et le $CaCO_3$ ont été utilisés. En outre, il a également été démontré que la structure de la membrane et par conséquence ses performances pouvaient être affectées par les propriétés des nanoparticules, la concentration, la présence de matériau de support, le rapport de mélange FPVD, et le temps de pénétration. Dans ce travail, la plus performante des membranes développées (à savoir la membrane à distillation dans le vide (MDV)) permet d'obtenir un accroissement de 2500% du rendement par rapport à celui de la membrane FPVD pure pour les conditions de température d'alimentation et de pression suivantes : 27.5 °C, pour une pression de 1.2 kPa, quand un poids

de 7.0 wt.% de nanoparticules hydrophiles SiO_2 est ajouté à l'intérieur de la membrane contenant le FPVD protégée par des fibres non tissés mixtes de polyester. La membrane en question possède une sélectivité presque parfaite.

Abstract

In this PhD thesis, seawater desalination by Membrane Distillation (MD) has been explored from the perspective of process and membrane. Regarding the process, an innovative, energy efficient, and environmentally friendly Zero Thermal Input Membrane Distillation (ZTIMD) process was proposed. ZTIMD uses thermal energy stored in seawater, which makes the process sustainable by being independent of the external sources of thermal energy, which is one of the major contributors to the cost and energy consumption of conventional MD desalination processes. Economic feasibility study was carried out for the ZTIMD process, and it was demonstrated that drinking water could be produced with a cost of $\$0.28/m^3$, which is approximately half of the cost of conventional desalination processes. Regarding the membrane, novel MD membranes were developed through incorporation of nanomaterials in polyvinylidene fluoride (PVDF). Different nanomaterials including superhydrophobic SiO_2, amine modified hydrophilic SiO_2, CuO, and $CaCO_3$ were used for this purpose. It was shown that membrane structure and consequently its performance could be affected by the nanoparticle properties, concentration, presence of backing material, PVDF blend ratio, and penetration time. In a best membrane developed in this work, almost 2500% increase was observed in the Vacuum Membrane Distillation (VMD) flux over that of the neat PVDF membrane at a feed temperature of 27.5 °C and vacuum pressure of 1.2 kPa, when 7.0 wt.% hydrophilic SiO_2 nanoparticles were added into a PVDF membrane supported with Non-Woven Fabric (NWF) polyester. The membrane possessed near perfect selectivity.

Acknowledgement

I would like to express my heartfelt appreciation to those amazing people helped me accomplish this work.

First and foremost, my deepest gratitude goes to my beloved parents Kamal Baghbanzadeh and Eghbal Aryan for their endless love, support, and encouragement in my life. I would like to express my sincere gratitude to my dearest sisters Sima Baghbanzadeh and Sara Baghbanzadeh for their constant encouragement, motivation, and kindness.

I would like to express my sincere gratitude to both of my supervisors, Dr. Christopher Q. Lan and Dr. Takeshi Matsuura for the support, insight, and smarts they have given throughout my PhD program. Their support, background knowledge, and patience helped me accomplish this thesis.

I would like to extend my heartfelt gratefulness to Dr. Dipak Rana who was always there to answer my questions. His support and encouragement is unforgettable.

Laboratory assistance, experimental guidance, and support from Louis Tremblay, Franco Ziroldo, and Gerard Nina are highly appreciated.

I would like to acknowledge the financial support that I received from the Government of Ontario for the Ontario Trillium Scholarship (OTS).

Last but not the least, special appreciation goes to my friends and lab partners (I cannot list all of them in here, but they are always on my mind), Hoda Azimi, Nadine Hirceaga, Johnson E. Efome, Viyash Murugesan, Yifan Yang, Zuolong Chen, Zhiyu Wang, Licheng Peng, Fan Yang, and Esther Nsaka for their help, support, inspiration, and friendship during the years.

Table of Contents

Résumé iii
Abstract v
Acknowledgement vi
Table of Contents vii
List of Figures xvi
List of Tables xxi
Nomenclature xxiv
Chapter 1:
Introduction 1
1-1- Introduction 2
1-2- Project Objectives 3
1-2-1- Zero Thermal Input Membrane Distillation (ZTIMD) 4
1-2-2- Nanocomposite MD Membranes 4
1-3- Novelty of the Thesis 5
1-4- Structure of the Thesis 6
References 7
Chapter 2:
Membrane distillation 11
Abstract 12
2-1- Introduction 12
2-2- Applications of Membrane Distillation Technology 14
2-3- Different Kinds of Membrane Distillation Configuration 15
2-3-1- Direct Contact Membrane Distillation (DCMD) 15
2-3-2- Air Gap Membrane Distillation (AGMD) 16
2-3-2-1- Memstill and Aquastill 17
2-3-3- Permeate Gap Membrane Distillation (PGMD) 18
2-3-4- Sweep Gas Membrane Distillation (SGMD) 19
2-3-5- Vacuum Membrane Distillation (VMD) 20
2-3-5-1- Vacuum Gap Membrane Distillation (VGMD) 21
2-3-5-2- Memsys 22
2-3-5-3- Difference Between VMD and Pervaporation (PV) 23
2-4- Distillation Membranes 25
2-4-1- MD Modules 25
2-4-1-1- Plate and Frame 25

2-4-1-2- Hollow Fiber 26
2-4-1-3- Tubular 26
2-4-1-4- Spiral Wound 27
2-4-2- Applicable Membranes for MD 27
2-4-2-1- Nanocomposite Membranes 27
2-4-3- Membrane Characteristics in MD 28
2-4-3-1- Liquid Entry Pressure (Wetting Pressure) 28
2-4-3-2- Membrane Thickness 29
2-4-3-3- Porosity and Tortuosity 29
2-4-3-4- Mean Pore Size and Pore Size Distribution 30
2-4-3-5- Thermal Conductivity 30
2-4-3-6- Membrane Fabrication 31
2-5- Transport Phenomena in MD 32
2-5-1- Mass Transfer in MD 32
2-5-2- Heat Transfer in MD 36
2-5-2-1- Thermal Efficiency and Heat Loss 39
2-5-3- Temperature and Concentration Polarization 39
2-5-4- Fouling 41
2-5-5- Operating Parameters 41
2-5-5-1- Feed Temperature 42
2-5-5-2- Permeate Temperature 42
2-5-5-3- Feed Concentration 42
2-5-5-4- Feed Flow Rate 42
2-5-5-5- Air Gap Thickness 42
2-5-5-6- Membrane Properties 42
2-6- Conclusion 43
References 43
Chapter 3:
Zero thermal input membrane distillation, a zero-waste and sustainable solution for fresh water shortage 50
Abstract 52
3-1- Introduction 53
3-2- Methodologies 57
3-2-1- Zero Thermal Input Membrane Distillation (ZTIMD) 57
3-2-2- Process Simulation 61
3-2-3- Results and Discussion 71

3-2-3-1- Effects of Concentrated Brine Discharge Temperature ($T_{f,out}$) on the Water Production Cost ... 72
(a) Major Contributors to the Water Production Cost ... 76
(b) Effects of the Membrane Characteristics on the Water Production Cost ... 85
3-2-3-2- Effects of Minimum Approach Temperature in the External Heat Exchanger, (ΔT_{min}) on the Water Production Cost ... 85
3-2-3-3- Effects of Process Feed Temperature ($T_{f,in}$) on the Water Production Cost ... 90
3-2-4- Feasibility of ZTIMD ... 96
3-3- Conclusion ... 100
3-4- Sample Cost Calculation for the Best Case Scenario ... 102
3-4-1- Capital Cost ... 104
3-4-2- Operation and Maintenance Cost ... 104
3-4-3- Overall Water Cost ... 104
3-4-4- Thickness of Required Insulation Material for Only 1 °C Increase in Coolant Temperature from Bottom of the Sea to the Surface ... 105
References ... 108

Chapter 4:

Effects of inorganic nano-additives on properties and performance of polymeric membranes in water treatment: a review ... 117
Abstract ... 119
4-1- Introduction ... 119
4-2- Nanomaterials as Additives for Enhanced Membrane Performance ... 122
4-2-1- Carbon Nanotube (CNTs) ... 123
4-2-2- Silica (SiO_2) ... 124
4-2-3- Titanium Dioxide (TiO_2) ... 124
4-2-4- Aluminum Oxide (Al_2O_3) ... 125
4-3- Nanomaterials Incorporated Polymeric Membranes in UF/MF ... 126
4-3-1- Improvement of the Performance of UF/MF Membranes by Nano-additives ... 128
4-3-1-1- Permeability ... 128
4-3-1-2- Rejection ... 129
4-3-1-3- Fouling ... 130
4-3-1-4- Mechanical and Thermal Stability ... 130
4-3-2- Effects of the Nano-additives on the UF/MF Membranes Properties ... 131
4-3-2-1- Porosity and Mean Pore Size ... 131
4-3-2-2- Roughness ... 132
4-3-2-3- Hydrophobicity/Hydrophilicity ... 133
4-3-2-4- Morphology ... 133

4-4- Nanomaterials Incorporated Polymeric Membranes in NF 135
4-4-1- Improvement of the Performance of NF Membranes by Nano-additives 136
4-4-1-1- Permeability 136
4-4-1-2- Rejection 138
4-4-1-3- Fouling 138
4-4-2- Effects of the Nano-additives on the NF Membranes Properties 139
4-4-2-1- Porosity and Mean Pore Size 139
4-4-2-2- Roughness 139
4-4-2-3- Hydrophobicity/Hydrophilicity 139
4-4-2-4- Morphology 140
4-5- Nanomaterials Incorporated Polymeric Membranes in RO 141
4-5-1- Improvement of the Performance of RO Membranes by Nano-additives 142
4-5-1-1- Permeability 142
4-5-1-2- Rejection 144
4-5-1-3- Fouling 145
4-5-2- Effects of the Nano-additives on the RO Membranes Properties 146
4-5-2-1- Roughness 146
4-5-2-2- Hydrophobicity/Hydrophilicity 146
4-5-2-3- Morphology 146
4-6- Nanomaterials Incorporated Polymeric Membranes in FO 147
4-6-1- Improvement of the Performance of FO Membranes by Nano-additives 148
4-6-1-1- Permeability 148
4-6-1-2- Rejection 150
4-6-1-3- Fouling 151
4-6-1-4- Mechanical and Thermal Stability 152
4-6-2- Effects of the Nano-additives on the FO Membranes Properties 152
4-6-2-1- Porosity and Mean Pore Size 152
4-6-2-2- Roughness 152
4-6-2-3- Hydrophobicity/Hydrophilicity 153
4-6-2-4- Morphology 153
4-7- Nanomaterials Incorporated Polymeric Membranes in MD/PV 154
4-7-1- Improvement of the Performance of MD/PV Membranes by Nano-additives 156
4-7-1-1- Liquid Entry Pressure (LEP_w) 156
4-7-1-2- Permeability 156
4-7-1-3- Rejection 160

4-7-1-4- Fouling 160
4-7-1-5- Mechanical and Thermal Stability 161
4-7-2- Effects of the Nano-additives on the MD/PV Membranes Properties 161
4-7-2-1- Porosity and Mean Pore Size 161
4-7-2-2- Roughness 162
4-7-2-3- Hydrophobicity/Hydrophilicity 162
4-7-2-4- Morphology 163
4-8- Discussion and Concluding Remarks 165
References 171
Chapter 5:
Effects of hydrophilic CuO nanoparticles on properties and performance of PVDF VMD membranes 187
5-1- Introduction 190
5-2- Experimental Methods 193
5-2-1- Materials 193
5-2-2- Membrane Fabrication 193
5-2-2-1- Preparation of Casting Solution 194
5-2-2-2- Preparation of Casting Suspension Containing Nanomaterials 194
5-2-2-3- Membrane Preparation 194
5-2-3- Membrane Characterization 195
5-2-3-1- Morphology 195
5-2-3-2- Nanomaterials Distribution within the Membrane Layers 195
5-2-3-3- Pore Size 195
5-2-3-4- Porosity 195
5-2-3-5- Thickness 196
5-2-3-6- Wettability 196
5-2-3-7- Roughness 196
5-2-4- Membrane Performance 197
5-2-4-1- Permeability 198
5-2-4-2- Rejection 198
5-2-4-3- Water Liquid Entry Pressure (LEP_w) 198
5-3- Results and Discussion 199
5-4- Conclusion 215
Chapter 6:
Effects of hydrophilic silica nanoparticles and backing material in improving the structure and performance of VMD PVDF membranes 220
6-1- Introduction 223

6-2- Experimental Methods 225
6-2-1- Materials 225
6-2-2- Membrane Fabrication 225
6-2-2-1- Viscosity of the Dope Suspension 226
6-2-3- Membrane Characterization 226
6-2-3-1- Morphology 226
6-2-3-2- Nanomaterials Distribution within the Membrane Layers 226
6-2-3-3- Pore Size 226
6-2-3-4- Porosity 227
6-2-3-5- Thickness 227
6-2-3-6- Wettability 227
6-2-3-7- Roughness 227
6-2-4- Membrane Performance 228
6-2-4-1- Permeability 228
6-2-4-2- Rejection 228
6-2-4-3- Water Liquid Entry Pressure (LEP_w) 228
6-2-4-4- Nanoparticles Leaching 229
6-3- Results and Discussion 229
6-3-1- Effects of Hydrophilic SiO_2 Nanoparticles on the Properties and VMD Performance of Nanocomposite Membrane 229
6-3-2- Effects of backing material on the Properties and VMD Performance of Nanocomposite Membrane 237
6-4- Conclusion 250
Acknowledgments 252
Chapter 7:
Effects of polymer ratio and film-penetration time on the properties and performance of nanocomposite PVDF membranes in membrane distillation 256
Abstract 258
7-1- Introduction 259
7-2- Materials and Methods 261
7-2-1- Materials 261
7-2-2- Membrane Fabrication 261
7-2-3- Membrane Characterization 262
7-2-3-1- Morphology 262
7-2-3-2- Pore Size 262
7-2-3-3- Porosity 263

7-2-3-4- Thickness 263
7-2-3-5- Viscosity of Dope Suspension 263
7-2-3-6- Wettability 264
7-2-3-7- Roughness 264
7-2-4- Membrane Performance 264
7-2-4-1- Liquid Entry Pressure of Water (LEP_w) 264
7-2-4-2- Permeability 264
7-2-4-3- Rejection 266
7-3- Results and Discussion 266
7-3-1- Effect of Ratio of PVDF Polymers of Different Molecular Weights 266
7-3-1-1- Viscosity Change 266
7-3-1-2- Thickness of the Top Layer 268
7-3-1-3- Surface Morphology 270
7-3-1-4- Porosity 273
7-3-1-5- Surface Contact Angle and Roughness 274
7-3-1-6- LEP_w 275
7-3-1-7- VMD Flux 277
7-3-2- Effect of Film-Penetration Time (τ) 277
7-3-2-1- Thickness of the Top Layer 277
7-3-2-2- Surface Morphology 281
7-3-2-3- Porosity 285
7-3-2-4- Surface Contact Angle and Roughness 285
7-3-2-5- LEP_w 286
7-3-2-6- VMD Flux 287
7-3-2-7- Salt Rejection 290
7-3-2-8- Polymer Blend H:L = 4:6 290
7-4- Conclusion 292
Acknowledgments 293
Chapter 8:
Conclusions and future works 298
8-1- ZTIMD and Its Feasibility 299
8-2- Mixed Matrix MD Nanocomposite Membranes 300
8-2-1- Hydrophilic Nanomaterials Incorporated MD Membranes 302
8-2-2- Effects of Backing Material, PVDF Blend Ratio, and Penetration Time 302
8-2-3- Superhydrophobic Nanomaterials Incorporated MD Membranes 304

8-3- Future works 305
8-3-1- ZTIMD at Pilot Scale 305
8-3-2- ZTIMD on a VMD Basis 305
8-3-3- Testing Durability, and Thermal and Mechanical Stability of the Developed Nanocomposite MD Membranes 306
8-3-4- Testing the Developed Nanocomposite MD Membranes in a DCMD Configuration 306
8-3-5- Effects of Nanomaterials Properties on the Membrane Performance 306

Appendix A:

Effects of superhydrophobic SiO_2 nanoparticles on the performance of PVDF flat sheet membranes for vacuum membrane distillation 307
A-2- Introduction 309
A-3- Experimental materials and method 311
A-3-1- Materials 311
A-3-2- Preparation of Dope Solution 311
A-3-3- Membrane Casting Method 312
A-3-4- Characterization of Dope Solution (Viscosity Measurement) 312
A-3-5- Membrane Characterization 313
A-3-5-1- Scanning Electron Microscopy (SEM) 313
A-3-5-2- Liquid Entry Pressure of Water (LEP_w) Measurements 313
A-3-5-3- Water Contact Angle Measurements 314
A-3-5-4- Membrane Surface Roughness 314
A-3-5-5- Energy Dispersive X-ray Spectroscopy (EDX) Analyses 314
A-3-5-6- Porosity and Pore Size Measurements 314
A-3-6- Vacuum Membrane Distillation (VMD) 315
A-3-7- ATR-FTIR Analyses 316
A-3-8- Nanoparticle Characterization 316
A-4- Results and Discussion 317
A-4-1- Dope Solution Viscosity 317
A-4-2- Membrane Characterization 317
A-4-2-1- Scanning Electron Microscopy (SEM) 317
A-4-2-2- LEP_w, Porosity, and Pore Size Measurements 320
A-4-3- Membrane Surface Properties 322
A-4-3-1- Water Contact Angle 322
A-4-3-2- Roughness Analysis 323
A-4-3-3- Particle Distribution (EDX Analyses) 325
A-4-3-4- ATR-FTIR Analyses 327

A-4-3-5- TEM Analysis 328
A-4-4- Membrane Performance 329
A-5- Conclusion 332

List of Figures

Fig. 1-1 Water scarcity map around the world [2] 2

Fig. 2-1 Direct Contact Membrane Distillation (DCMD) [4] 16

Fig. 2-2 Air Gap Membrane Distillation (AGMD) [4] 17

Fig. 2-3-(a), (b) Memstill configuration [4,24] 18

Fig. 2-4 Permeate Gap Membrane Distillation (PGMD) 19

Fig. 2-5 Sweep Gap Membrane Distillation (SGMD) [4] 20

Fig. 2-6 Vacuum Membrane Distillation (VMD) [4] 21

Fig. 2-7 Vacuum Gap Membrane Distillation (VGMD) 22

Fig. 2-8 Memsys Configuration [4,33] 23

Fig. 2-9 (a) Plate and frame module, (b) Supported flat sheet membrane [4] 25

Fig. 2-10 (a) Hollow fiber module, (b) Hollow fiber membrane [4] 26

Fig. 3-1 (a) General schematic of the proposed desalination plant on the cross-sectional temperature profile of Gulf of Oman *[72]* where enthalpy of seawater is extracted for DCMD configuration, (b) ZTIMD process flow diagram 60-61

Fig. 3-2 Applied algorithm to study the economic vability of the ZTIMD 63

Fig. 3-3 Water production cost vs. brine temperature where pre-treatment is as intense as that of RO or as simple as cartridge filtration at $T_{f,in}$=30 °C and $T_{p,in}$=15 °C, when (a) membrane price varies between 18.5 and 116 \$/m^2 at a constant membrane replacement rate and permeability of 15% and 0.00774 kg/m^{2}h.Pa, (b) membrane replacement rate varies between 5 and 20% at a constant membrane price and permeability of \$90/m^2 and 0.00774 kg/m^{2}h.Pa, (c) membrane permeability varies between 0.01161 and 0.00516 kg/m^{2}h.Pa at a constant membrane price and replacement rate of \$90/m^2 and 15%, IPT and SPT stand for Intense and Simplified Pre-Treatment, respectively 73-75

Fig. 3-4 (a) Overall, (b) total capital and (c) total O&M cost break-down when (1) intense and (2) simplified pre-treatment step is adopted to the ZTIMD process at a membrane price, replacement rate, and permeability of \$90/m^2, 15% and 0.00774 kg/m^{2}h.Pa, respectively, other costs in (a) includes cost of civil work, indirect capital, regular electrical energy, chemicals, spares, and labor 77-82

Fig. 3-5 Share of major contributors to the total water cost, i.e. intake and pre-treatment and purchased membrane costs, in total capital cost vs. brine temperature, at $T_{f,in}$=30 °C, $T_{p,in}$=15 °C, and a membrane price, replacement rate, and permeability of \$90/m^2, 15% and 0.00774 kg/m^{2}h.Pa, respectively 84

Fig. 3-6 Water production cost vs. permeate inlet temperature where pre-treatment is as intense as that of RO or as simple as cartridge filtration at $T_{f,in}$=30 °C, when (a) membrane price varies between 18.5 and 116 \$/m^2 at a constant membrane replacement rate and permeability of 15% and 0.00774 kg/m^{2}h.Pa, (b) membrane replacement rate varies between 5 and 20% at a constant membrane price and permeability of \$90/m^2 and 0.00774 kg/m^{2}h.Pa, (c) membrane permeability varies between 0.01161 and 0.00516 kg/m^{2}h.Pa at a constant membrane price and replacement rate of \$90/m^2 and 15% 86-88

Fig. 3-7 Share of purchased membrane and external heat exchanger costs, in total capital cost vs. permeate inlet temperature at $T_{f,in}$=30 °C, and a membrane price, replacement rate, and permeability of \$90/m^2, 15% and 0.00774 kg/m^{2}h.Pa, respectively 89

Fig. 3-8 Water production cost vs. process feed temperature where cartridge filtration is used for pre-treatment at $T_{f,out}$=27 °C and $T_{p,in}$=11 °C, when (a) membrane price varies in the range of 18.5-116 \$/m^2 at constant replacement rate of 15% and permeability of 0.00774 kg/m^2h.Pa, (b) membrane replacement rate varies in the range of 5-20% at a constant membrane price of \$90/m^2 and permeability of 0.00774 kg/m^2h.Pa, (c) membrane permeability varies between 0.01161-0.00516 kg/m^2h.Pa at a constant membrane price of \$90/m^2 and a replacement rate of 15% 92-93

Fig. 3-9 Effect of waste heat temperature on the water production cost for the best case scenario in this work, the ZTIMD coupled with cartridge filtration at a membrane price, replacement rate, and permeability of \$18.5/m^2, 5% and 0.01161 kg/m^2h.Pa, respectively, $T_{f,out}$=27 °C and $T_{p,in}$=11 °C 95

Fig. 3-10 A schematic of the underwater pipe for cooling the bottom seawater 105

Fig. 4-1 Effects of nanozeolites on both active and support layers of an FO membrane. © Elsevier. Reprinted from [148] with permission from Elsevier. Permission to reuse must be obtained from the rights holder. 149

Fig. 4-2 The proposed mechanisms for water transport trough a PP CNIM. © American Chemical Society. Reprinted from [154] with permission from American Chemical Society. Permission to reuse must be obtained from the rights holder. 157

Fig. 4-3 The proposed mechanisms for water transport trough a carboxylated carbon nanotubes incorporated PP membrane when PVDF served as glue to encapsulate the nanotubes within the membrane. © Elsevier. Reprinted from [166] with permission from Elsevier. Permission to reuse must be obtained from the rights holder. 158

Fig. 4-4 The free volume (shown in bright color) based upon molecular dynamics simulation results (a) Neat PVA membrane, (b) PVA/CNT membrane. © Elsevier. Reprinted from [156] with permission from Elsevier. Permission to reuse must be obtained from the rights holder. 159

Fig. 5-1 Experimental VMD setup for measuring the permeate flux 197

Fig. 5-2 Schematic of experimental setup for LEP_w tests 199

Fig. 5-3-a Top surface SEM images of the CuO/PVDF membranes at different concentrations of the nanoparticles where the black spots represent the surface pores 200

Fig. 5-3-b Cross-sectional SEM images of the CuO/PVDF membranes at different concentrations of the nanoparticles 202

Fig. 5-4 Ratio of the thickness of the finger-like layer to the total membrane thickness vs. nanoparticle concentration 204

Fig. 5-5 Viscosity of the dope suspension vs. nanoparticle concentration 205

Fig. 5-6 Surface pore size vs. nanoparticle concentration 206

Fig. 5-7 Micro-voids in sponge-like layer For M0.0 and M2.0 207

Fig. 5-8 Membrane porosity vs. concentration for the nanocomposite membranes of PVDF/CuO 207

Fig. 5-9 Membrane thickness vs. nanoparticle concentration 208

Fig. 5-10 EDX analysis of the different layers of M2.0 209

Fig. 5-11 Surface contact angle vs. concentration for the nanocomposite membranes of PVDF/CuO 210

Fig. 5-12 Pure water flux vs. nanoparticle concentration 211

Fig. 5-13 Effect of feed temperature on the pure water flux of the M0.0 and M2.0 212

Fig. 5-14 LEP_w vs. nanoparticle concentration 213

Fig. 5-15 Effects of the type of the hydrophilic nanomaterials on the membrane (a) porosity, (b) contact angle, and (c) pure water flux 214-215

Fig. 6-1 (a) Top surface (b) Cross-sectional SEM images of the SiO_2/PVDF membranes (M0.0, M2.0, and M7.0), the surface pores are specified by the black spots in top surface 230

Fig. 6-2 EDS mapping of C, F, and Si for M2.0 232

Fig. 6-3 Surface pore size and ratio of the thickness of the finger-like layer to the total membrane thickness vs. silica nanoparticle concentration 233

Fig. 6-4 Dope suspension viscosity vs. nanoparticle concentration at 25 ºC 234

Fig. 6-5 Pure water flux stability test for 4 different M2.0, feed temperature: 27.5 °C 235

Fig. 6-6 Pore wetting analysis, EDS mapping of Ag for M2.0 after 4.5 h filtration of silver nitrate 236

Fig. 6-7 Pure water flux stability test for 4 different M7.0-3396, feed temperature: 27.5 °C 238

Fig. 6-8 Top surface SEM images of the SiO_2/PVDF membranes with backing material (M0.0-3396, M2.0-3396, M5.0-3396, M7.0-3396 and M9.0-3396), the surface pores are specified by the black spots 239

Fig. 6-9 A comparison between the surface pore size of the membranes with and without the non-woven backing material 240

Fig. 6-10 Surface pore size and ratio of the thickness of the finger-like layer to the total membrane thickness vs. silica nanoparticles concentration – NWF supported membranes 241

Fig. 6-11 Membrane porosity vs. silica nanoparticles concentration– NWF supported membranes 242

Fig. 6-12 Surface contact angle vs. silica nanoparticle concentration – NWF supported membranes 242

Fig. 6-13 Surface contact angle vs. silica nanoparticles concentration –NWF supported and unsupported membranes 244

Fig. 6-14 LEP_w vs. silica nanoparticles concentration –NWF supported and unsupported membranes 245

Fig. 6-15 Pure water flux vs. silica nanoparticles concentration – NWF supported membranes 246

Fig. 6-16-a Elemental EDS analysis: (1) aqueous suspension of 0.001 wt.% hydrophilic silica nanoparticles and (2) permeate of VMD using M7.0-3396 after 4.5 h operation 248

Fig. 6-16-b SEM image (labeled as SEM) and EDS mapping images (the rest) for: (1) aqueous suspension of 0.1 wt.% hydrophilic silica nanoparticles, (2) aqueous suspension of 0.001 wt.% hydrophilic silica nanoparticles, and (3) VMD permeate from M7.0-3396 after 4.5 h operation 249

Fig. 7-1 Experimental VMD setup [16] 265

Fig. 7-2 Dope suspension viscosity vs. (a) polymer ratio in the presence (7.0 wt.% SiO_2) and absence of nanoparticles and (b) nanoparticle concentration at H:L = 2:8 at 25 ºC 267

Fig. 7-3 Top layer thickness vs. (a) H:L ratio and (b) casting dope viscosity in the presence of 7.0 wt.% SiO_2 nanoparticles with a penetration time of 3 min 268

Fig. 7-4 Cross-sectional (a) SEM and (b) EDS fluorine mapping for the membranes with a H:L ratio of 2:8 and 0:10 for a penetration time of 3 min 269

Fig. 7-5 Top surface SEM images of the supported SiO_2/PVDF membranes of different H:L ratios (nanoparticles concentration, 7.0 wt.%, penetration time,3 min) The surface pores are specified by the black spots in top surface 271

Fig. 7-6-a Surface pore size vs. H:L ratio (nanoparticle concentration,7.0 wt.%; penetration time, 3 min) 273

Fig. 7-6-b Overall (combined top layer and substrate) porosity vs. H:L ratio (nanoparticle concentration,7.0 wt.%; penetration time, 3 min) 274

Fig. 7-6-c Contact angle vs. H:L ratio (nanoparticle concentration,7.0 wt.%; penetration time, 3 min) 275

Fig. 7-6-d LEP_w and maximum pore size vs. H:L ratio (nanoparticle concentration,7.0 wt.%; penetration time, 3 min) 276

Fig. 7-6-e Pure water flux vs. H:L ratio (nanoparticles concentration, 7.0 wt.%; penetration time, 3 min; feed temperature, 27.5 °C; downstream pressure: 1.2 kPa) 277

Fig. 7-7 Top layer thickness vs. penetration time at a polymer ratio of H:L = 2:8 in the presence of 7.0 wt.% SiO_2 nanoparticles 278

Fig. 7-8 Cross-sectional (a) SEM and (b) EDS fluorine mapping for membranes with different penetration times, the nanoparticles concentration, 7.0 wt.%, the PVDF ratio, H:L = 2:8 280

Fig. 7-9 Top surface SEM images of the supported SiO_2/PVDF membranes at different penetration times, the nanoparticles concentration, 7.0 wt.%, the PVDF ratio, H:L = 2:8, the surface pores are specified by the black spots in the top surface 282

Fig. 7-10-a Surface pore size vs. penetration time (H:L = 2:8; SiO_2 nanoparticles, 7.0 wt.%) 284

Fig. 7-10-b Porosity vs. penetration time (H:L = 2:8; SiO_2 nanoparticles, 7.0 wt.%) 285

Fig. 7-10-c Contact angle vs. penetration time (H:L = 2:8; SiO_2 nanoparticles, 7.0 wt.%) 286

Fig. 7-10-d LEP_w and maximum pore size vs. penetration time (H:L = 2:8; SiO_2 nanoparticles, 7.0 wt.%) 287

Fig. 7-10-e Pure water flux vs. penetration time (H:L = 2:8; SiO_2 nanoparticles, 7.0 wt.%; feed temperature, 27.5 °C; downstream pressure: 1.2 kPa) 287

Fig. 7-11 Schematic of the effect of the penetration time on the membrane characteristics 289

Fig. 7-12 NaCl rejection for membranes of two different penetration times (H:L = 2:8; SiO_2 nanoparticles, 7.0 wt.%; feed temperature, 27.5 °C; downstream pressure: 1.2 kPa) 290

Fig. 8-1 A summary on the experimenal work of the thesis 301

Fig. A-1 Schematic diagram of the experimental LEP_w set-up 313

Fig. A-2 Schematic diagram of VMD set-up 316

Fig. A-3 Viscosity measurements of the polymer solution 317

Fig. A-4 SEM images of the PVDF flat sheet nanocomposite membranes: T for top surface, C for cross-section, B for 319

bottom surface

Fig. A-5 Effect of nanoparticles concentration on LEP_w 320

Fig. A-6 Effect of nanoparticles concentration on porosity 321

Fig. A-7 Effects of nanoparticles concentration on surface pore diameter 322

Fig. A-8 Effect of nanoparticles concentration on water contact angle 323

Fig. A-9 Three dimensional topographic images of neat PVDF and PVDF-SiO_2 nanocomposite membranes 324

Fig. A-10 Silicon (Si) and Fluorine (F) mapping of PVDF-SiO_2 nanocomposite membranes cross-sections 326

Fig. A-11 EDX images of flat sheet PVDF-SiO_2 nanocomposite membranes: MS-4 (first row) and MS-7 (third row) 327

Fig. A-12 FTIR spectra of the neat PVDF (MS-0), 2.0 wt.% SiO_2-PVDF (MS-2), 4.0 wt.% SiO_2-PVDF (MS-4) and 7.0 wt.% SiO_2-PVDF (MS-7) nanocomposite membranes 328

Fig. A-13 TEM images of superhydrophobic SiO_2 nanoparticles 329

Fig. A-14 Permeation flux of VMD as a function of nanoparticles concentration in dope solution 330

Fig. A-15 Analysis of membrane flux with artificial seawater, i.e., containing 35 g/L NaCl and artificial brackish water, i.e., 2 g/L aqueous NaCl solution 331

Fig. A-16 Comparative analysis of flux stability and rejection with time 331

List of Tables

Table 2-1 Comparison between MD and RO for desalination	14
Table 2-2 Comparison between different MD configurations	24
Table 2-3 Dominant mechanisms in mass transfer across the membrane in different MD configurations	35
Table 2-4 Heat transfer in different regions of an MD configuration (If there is no resistance in cooling surface)	38
Table 3-1 Assumptions for the economic feasibility analysis of the ZTIMD process	65
Table 3-2 A list of capital and operation and maintenance costs for the proposed ZTIMD desalination process	68-69
Table 3-3 Desalinated water cost in different processes	99
Table 3-4 Operating conditions of the ZTIMD with simplified pre-treatment	102
Table 3-5 Capital cost break-down calculations	104
Table 3-6 Operation and maintenance cost break-down calculations	104
Table 3-7 List of assumptions for calculation of the thickness of the insulation material	106
Table 4-1 Effects of nanomaterials on the performance of composite membranes in the ultrafiltration/microfiltration process (The most significant results)	127
Table 4-2 Effects of nanomaterials on the performance of composite membranes in the nanofiltration process (The most significant results)	136
Table 4-3 Effects of nanomaterials on the performance of composite membranes in the reverse osmosis process (The most significant results)	142
Table 4-4 Effects of nanomaterials on the performance of composite membranes in the forward osmosis process, active layer facing draw solution mode, AL-DS, (The most significant results)	147
Table 4-5 Effects of nanomaterials on the performance of composite membranes in the membrane distillation/pervaporation process (The most significant results)	154
Table 4-6 Changes in membrane physico-chemical properties and performance induced by nanoparticles (NP) incorporation	167-170
Table 5-1 The different features of reverse osmosis and membrane distillation in a desalination process	191
Table 5-2 Composition of the dope solution along with the nanoparticles concentration within the membrane matrix	194
Table 5-3 Surface roughness analysis of the CuO NPs incorporated membranes by ImageJ according to the ISO 4287/2000 standard (all the units in pixel)	210
Table 6-1 Surface roughness analysis of the hydrophilic SiO_2 nanocomposite membranes by ImageJ according to the ISO 4287/2000 standard (all the units in pixel)	243

Table 6-2 Nanocomposite PVDF membranes in membrane distillation 247

Table 7-1 Surface roughness analysis of the 7.0 wt.% hydrophilic SiO_2 incorporated nanocomposite membranes vs. H:L ratio by ImageJ and its plugin Roughness Calculation (all the units in pixel) 275

Table 7-2 Surface roughness analysis of the 7.0 wt.% hydrophilic SiO_2 incorporated nanocomposite membranes vs. penetration time by ImageJ and its plugin Roughness Calculation (all the units in pixel) 286

Table 7-3 Porosity, contact angle, LEP_w, VMD pure water flux of the 7.0 wt.% hydrophilic SiO_2 incorporated nanocomposite membranes for different penetration times where the blend ratio is 4:6 291

Table A-1 Composition of the dope solution for flat-sheet composite membrane preparation 312

Table A-2 Roughness parameters of the prepared PVDF nanocomposite flat sheet membranes 324

Abbreviation

AFM	*Atomic Force Microscopy*
AGMD	*Air Gap Membrane Distillation*
ALD	*Atomic Layer Deposition*
AOP	*Advanced Oxidation Process*
APTS	*3-Aminopropyltriethoxysilane*
ATR	*Attenuated Total Reflectance*
BET	***Brunauer Emmett Teller***
BP	*Bucky-Paper*
BPPO	*Brominated Poly(phenylene oxide)*
BSA	*Bovine serum albumin*
CA	*Cellulose acetate*
CNIM	*Carbon Nanotube Immobilized Membrane*
CNT	*Carbon Nanotube*
CTA	*Cellulose triacetate*
DCMD	*Direct Contact Membrane Distillation*
DLS	***Dynamic Light Scattering***
DMAc	*Dimethylacetamide*
DMF	*Dimethyformamide*
DMSO	*Dimethysulfoxide*
EDS	*Electron Dispersion Spectroscopy*
FO	*Forward Osmosis*
FTIR	*Fourier Transformed Infrared Spectroscopy*
GO	*Graphene Oxide*
GOR	*Gain Output Ratio*
H	*High Molecular Weight PVDF*
ICP	*Internal Concentration Polarization*
L	*Low Molecular Weight PVDF*
LEP_w	*Liquid Entry Pressure of Water*
MD	*Membrane Distillation*
MED	*Multi Effect Distillation*
MF	*Microfiltration*
MSF	*Multi Stage Flash*
MWCNT	*Multi-Walled Carbon Nanotube*
NF	*Nanofiltration*
NMP	*N-Methyl Pyrrolidone*
NP	*Nanoparticle*
NWF	*Non-Woven Fabric*
O&M	*Operation & Maintenance*
PA	*Polyamide*
PAI	*Poly(amide-imide)*
PAN	*Polyacrylonitrile*
PAS	*Polyarylsulfone*
PCTE	*Polycarbonate*
PDMS	*Polydimethylsiloxane*
PE	*Polyethylene*
PEI	*Polyethyleneimine*
PES	*Polyethersulfone*
PGMD	*Permeate Gap Membrane Distillation*
PI	*Polyimide*
PMMA	*Poly(methyl methacrylate)*
PP	*Polypropylene*
PSf	*Polysulfone*
PTFE	*Polytetrafluoroethylene*
PV	*Pervaporation*
PVA	*Poly(vinyl alcohol)*
PVC	*Polyvinyl chloride*
PVDF	*Polyvinylidene fluoride*
RO	*Reverse Osmosis*
RR	*Recovery Ratio*
SDS	*Sodium dodecyl sulfate*
SEM	*Scanning Electron Microscopy*
SGMD	*Sweep Gas Membrane Distillation*
SPES	*SulfonatedPolyethersulfone*
SWRO	*Seawater Reverse Osmosis*
TEM	*Transmission Electron Microscopy*
TIPS	*Thermally Induced Phase Separation*
TMOS	*Tetramethylorthosilicate*
TMP	*Transmembrane Pressure*
UF	*Ultrafiltration*
VC	*Mechanical Vapor Compression*
VGMD	*Vacuum Gap Membrane Distillation*
VIP	*Vapor Induced Precipitation*
VMD	*Vacuum Membrane Distillation*
VMEMD	*Vacuum Multi-Effect Membrane Distillation*
ZTIMD	*Zero Thermal Input Membrane Distillation*

Nomenclature

Symbol		Subscript	
a	Amortization factor	c	Coolant
A	Area	f	Feed
c	Concentration	g	Gas
C	Conductivity	in	inlet
C_m	Membrane coefficient	LMTD	Logarithmic mean of temperature difference
c_p	Specific heat capacity	m	Membrane interface
d	Diameter/Mean pore size	min	Minimum
D	Diffusion coefficient	out	outlet
dt	Temperature rise	p	Permeate
e	Electricity cost	pol	Polymer
f	Plant availability		
g	Gravity of Earth		
Gr	Grashof number		
h	Heat transfer coefficient/Heat exchanger cost per area		
i	Annual interest rate		
J	Flux		
k	Thermal conductivity		
K	Mass transfer coefficient		
k_B	Boltzmann constant		
Kn	Knudsen number		
l	Purchased piping cost per length/Gap thickness		
L	Length		
m	Mass flowrate/Weight		
M	Molecular weight		
m^*	Membrane cost per area		
n	Plant life time		
Nu	Nusselt number		
P	Pressure		
P^*	Vapor pressure		
P_s	Brake power		
Pr	Prandtl number		
q	Volume flowrate		
Q	Heat		
r	Pore radius/Replacement rate		
R	Universal gas constant/Rejection		
r_{max}	Maximum pore size		
RR	Recovery ratio		
t	Time		
T	Temperature		
U	Global heat transfer coefficient		
w	Weight		
W	Plant capacity		
γ	Surface tension		
δ	Membrane thickness		
ΔH_v	Heat of vaporization		
ε	Porosity		
η	Efficiency		
θ	Contact angle		
λ	Mean free path of the molecule		
μ	Viscosity		
Π	Thermal efficiency		
ρ	Density		
τ	Tortuosity/Penetration time		
Φ	Concentration polarization coefficient		
ψ	Temperature polarization coefficient		

List of Publications

Peer-Reviewed Articles

1. **Mohammadali Baghbanzadeh**, Dipak Rana, Christopher Q. Lan, Takeshi Matsuura, "*Zero thermal input membrane distillation, a zero-waste and sustainable solution for fresh water shortage*", Applied Energy, 187 (2017) 910-928.

2. **Mohammadali Baghbanzadeh**, Nadine Hirceaga, Dipak Rana, Christopher Q. Lan, Takeshi Matsuura, "*Effects of polymer ratio and film-penetration time on the properties and performance of nanocomposite PVDF membranes in membrane distillation*", Industrial & Engineering Chemistry Research, 55 (37) (2016) 9971-9982.

3. **Mohammadali Baghbanzadeh**, Dipak Rana, Christopher Q. Lan, Takeshi Matsuura, "*Effects of hydrophilic silica nanoparticles and backing material in improving the structure and performance of VMD PVDF membranes*", Separation and Purification Technology, 157 (2016) 60-71.

4. **Mohammadali Baghbanzadeh**, Dipak Rana, Takeshi Matsuura, Christopher Q. Lan, "*Effects of inorganic nano-additives on properties and performance of polymeric membranes in water treatment: a review*", Separation & Purification Reviews, 45 (2016) 141-167.

5. Johnson E. Efome, **Mohammadali Baghbanzadeh**, Dipak Rana, Takeshi Matsuura, Christopher Q. Lan, "Effects of superhydrophobic SiO2 nanoparticles on the performance of PVDF flat sheet membranes for Vacuum Membrane distillation", Desalination, 371 (2015) 47-57.

6. **Mohammadali Baghbanzadeh**, Dipak Rana, Christopher Q. Lan, Takeshi Matsuura, "*Effects of hydrophilic CuO nanoparticles on properties and performance of PVDF VMD membranes*", Desalination, 369 (2015) 75-84.

Book Chapters

7. **Mohammadali Baghbanzadeh**, Christopher Q. Lan, Dipak Rana, Takeshi Matsuura, (2016) "*Membrane distillation*, In: *Nanostructured Polymer Membranes, Volume 1: Processing and Characterization*", *P. M. Visakh, O. Nazarenko* (eds), Wiley-Scrivener Publishing, US, Ch. 11, pp. 419-455.

Conference Presentations

8. **Mohammadali Baghbanzadeh**, Dipak Rana, Christopher Q. Lan, Takeshi Matsuura, "*VMD desalination using nanocomposite membranes prepared by hydrophilic nano-additives*", 2016 AIChE Annual Meeting, San Francisco, USA, November 13-18, 2016.

9. **Mohammadali Baghbanzadeh**, Dipak Rana, Takeshi Matsuura, Christopher Q. Lan, "*Vacuum membrane distillation by hydrophilic nanoparticles incorporated membranes for desalination*", 65th Canadian Chemical Engineering Conference, Calgary, Canada, October 4-7, 2015.

10. **Mohammadali Baghbanzadeh**, Dipak Rana, Takeshi Matsuura, Christopher Q. Lan, "*Hydrophilic CuO nanoparticles, a great opportunity to enhance the VMD membrane performance*", Euromembrane 2015, Aachen, Germany, September 6-10, 2015.

11. **Mohammadali Baghbanzadeh**, Dipak Rana, Christopher Q. Lan, Takeshi Matsuura, "*The application of PVDF nanocomposite membranes in saline water desalination by vacuum membrane distillation*", 98th Canadian Chemistry Conference and Exhibition, Ottawa, Canada, June 13-17, 2015.

12. **Mohammadali Baghbanzadeh**, Dipak Rana, Christopher Q. Lan, Takeshi Matsuura, "*The use of hydrophilic CuO nanoparticles to enhance the MD membrane performance*", 64th Canadian Chemical Engineering Conference, Niagara Falls, Canada, October 19-22, 2014.

Statement of Contributions of Collaborators and Co-Authors

Chapter 2, Membrane distillation

Literature review was thoroughly done by **Mohammadali Baghbanzadeh**. He wrote the first draft and revised the book chapter during the review process according to the supervisors' and reviewers' comments.

Christopher Q. Lan provided supervision, guidance, and revision of the book chapter. Takeshi Matsuura and Dipak Rana helped with correction of the book chapter.

Chapter 3, Zero thermal input membrane distillation, a zero-waste and sustainable solution for fresh water shortage

Literature review, simulation of the process, technical calculations, and investigation of the economic feasibility of the process were thoroughly performed by **Mohammadali Baghbanzadeh**. He wrote the first draft of the manuscript and was responsible for its revision during the review process by the supervisors and journal reviewers. He was also responsible for drafting a point-to-point response to reviewers' comments before the manuscript was accepted by Applied Energy.

Christopher Q. Lan provided the idea of ZTIMD, and helped with concept development, structuring and revision of the manuscript. Takeshi Matsuura contributed to revision of the manuscript. Dipak Rana helped with correction and revision of the manuscript.

Chapter 4, Effects of inorganic nano-additives on properties and performance of polymeric membranes in water treatment: a review

Mohammadali Baghbanzadeh thoroughly did the literature review, wrote the first draft, revised the manuscript multiple times according to the supervisors' and reviewers' comments. He was also responsible for drafting a point-to-point response to reviewers' comments before the manuscript was accepted by Separation & Purification Reviews.

Christopher Q. Lan provided supervision, and helped with structuring and revision of the manuscript. Takeshi Matsuura contributed to revision of the manuscript. Dipak Rana helped with correction of the manuscript.

Chapter 5, Effects of hydrophilic CuO nanoparticles on properties and performance of PVDF VMD membranes

All of the lab works were carried out by **Mohammadali Baghbanzadeh**. **Mohammadali** measured viscosity of the dope solutions, fabricated the membranes and characterized them in terms of morphology, pore size, porosity, thickness, hydrophobicity, and roughness. He tested the membranes performance by measuring flux, selectivity, and LEP_w. Literature review and data analysis were thoroughly done by **Mohammadali Baghbanzadeh**, he wrote the first draft of the paper and revised the manuscript during the review process by considering the supervisors' and reviewers' comments. He also drafted the point-to-point response to reviewers' comments and finalized it according to supervisors' comments before the manuscript was accepted by Desalination.

Christopher Q. Lan and Takeshi Matsuura contributed to concept development, guidance in research, and manuscript revision. Dipak Rana provided the idea of using CuO nanoparticles and training of Mohammadali on laboratory techniques such as membrane fabrication and measurement of LEP_W, contact angle, and VMD flux. He also contributed to manuscript correction. In particular, Dipak Rana suggested the use of EDS mapping to identify the cross-sectional distribution of nanoparticles.

Chapter 6, Effects of hydrophilic silica nanoparticles and backing material in improving the structure and performance of VMD PVDF membranes

Mohammadali Baghbanzadeh provided the idea of using hydrophilic silica nanoparticles in PVDF membranes. He performed all of the lab works including measurement of viscosity of the dope solutions, membrane fabrication and characterization. He measured pore size, porosity and thickness, and analyzed membrane morphology, surface hydrophobicity and roughness. Membrane performance was evaluated by **Mohammadali Baghbanzadeh** through measuring flux, selectivity, and LEP_w. He tested more than 20 different backing materials and chose

Hollytex® 3396 as the appropriate substrate. Literature review and data analysis were thoroughly carried out by him. **Mohammadali** wrote the first draft of the manuscript and revised it during the review process based on comments from the supervisors and reviewers. He also drafted the point-to-point response to reviewers' comments and finalized it according to supervisors' comments before the manuscript was accepted by Separation and Purification Technology.

Christopher Q. Lan provided supervision, guidance in research, and manuscript revision. Takeshi Matsuura contributed to manuscript revision. Dipak Rana provided experimental guidance and helped with manuscript correction. In particular, Dipak Rana suggested the use of EDS to detect potential leaching of nanoparticles from membranes into permeate.

Chapter 7, Effects of polymer ratio and film-penetration time on the properties and performance of nanocomposite PVDF membranes in membrane distillation

Mohammadali Baghbanzadeh provided the idea of investigating the effects of polymer ratio and film-penetration time on the properties and performance of the PVDF membranes. He did most of the lab works except for those performed by Nadine Hirceaga, which are described briefly later in this section. **Mohammadali** measured viscosity of the dope solutions, fabricated most of the membranes, characterized all of them by measuring pore size, porosity and thickness, analyzing morphology, surface hydrophobicity, and roughness. He performed most of the membrane performance tests including flux, selectivity, and LEP_w measurements. Literature review and data analysis were thoroughly done by him. First draft of the manuscript was prepared by **Mohammadali** and he was responsible for the revision of the manuscript during the review process and based on the supervisors' and reviewers' comments. He also drafted the point-to-point response to reviewers' comments and finalized it according to supervisors' comments before the manuscript was accepted by Industrial & Engineering Chemistry Research.

Nadine Hirceaga joined the research group as a MEng student to assist **Mohammadali Baghbanzadeh** in some experiments reported in this paper. She was trained and supervised by **Mohammadali**. From the works she did during her stay in the research group (Spring/Summer 2015), some performance data such as flux, selectivity, and LEP_w results for a specific membrane (H:L = 2:8, τ = 3 min, SiO_2 concentration: 7.0 wt.%) were included in this manuscript

after been verified by **Mohammadali Baghbanzadeh** experimentally. Her efforts were appreciated by putting her name as a co-author.

Christopher Q. Lan and Takeshi Matsuura contributed to concept development, guidance in research, structuring, and revision of the manuscript. Dipak Rana helped with manuscript correction.

Appendix A, Effects of superhydrophobic SiO_2 nanoparticles on the performance of PVDF flat sheet membranes for vacuum membrane distillation

The idea of using superhydrophobic silica nanoparticles in PVDF membrane was provided by **Mohammadali Baghbanzadeh**. To assist **Mohammadali** for accomplishment of this paper, Johnson E. Efome was hired as a MASc student. **Mohammadali Baghbanzadeh** trained Johnson during the early stages of membrane characterization and performance tests. **Mohammadali** was involved in some of the characterization tests for the neat PVDF membrane, and regularly participated in discussion of concepts, trouble shooting, and revision of the manuscript.

Johnson E. Efome performed most of the experimental works including membrane development, characterization (morphology, pore size, porosity, thickness, hydrophobicity, and roughness), and MD performance tests (flux, selectivity, and liquid entry pressure of water (LEP_w)), except some characterizations for neat PVDF membrane. He thoroughly did the literature review, analyzed data, and wrote the first draft, revised the manuscript according to the supervisors', **Mohammadali Baghbanzadeh**'s and reviewers' comments. Johnson E. Efome was responsible for drafting a point-to-point response to reviewers' comments before the manuscript was accepted by Desalination.

Christopher Q. Lan and Takeshi Matsuura provided supervision, guidance, and revision of the manuscript. Dipak Rana helped with correction and submission of the manuscript.

It should be pointed out that some of the results involving the use of specialized instruments such as SEM and EDS were carried out by technicians/scientists in charge of these facilities in Carleton University.

Chapter 1:

Introduction

1-1- Introduction

Water scarcity, due to population and industrial growth, urbanization and intensified drought conditions, has become a serious threat in different areas of the world. It is predicted that over 1.8 billion people would be exposed to absolute water scarcity while two third of the world population would be living under water-stress conditions by 2025 [1]. Fig. 1-1 shows water scarcity map throughout the world.

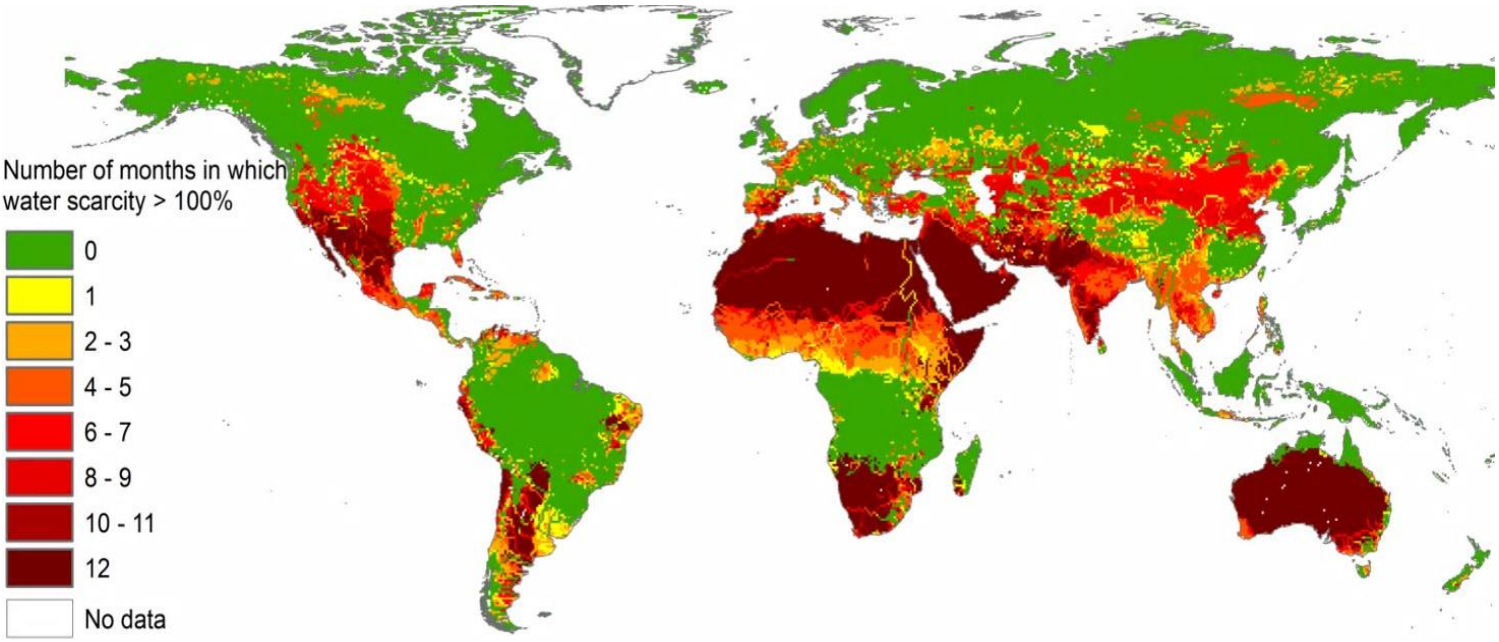

Fig. 1-1 Water scarcity map around the world [2]

While roughly 70% of the earth is covered by water, only 2.5% of the water is usable as freshwater [3]. Different approaches could be used to recover fresh water from the available sources including water catchment, wastewater reclamation and reuse, desalination, and water import. Among them, desalination has attracted much attention over the past few decades [4-11]. Different sources of raw waters can be used for desalination including seawater, brackish water, river water, and wastewater. Taking into consideration the large amounts of salted water stored in the oceans and seas, seawater desalination is potentially considered a sustainable solution for compensating the water shortage in countries with coastal areas.

A variety of different methods have been developed for desalination and membrane-based processes and thermal distillation technologies are number one and number two top contributors to the global market, respectively [8]. While membrane-based technologies such as Reverse

Osmosis (RO) are much more energy-efficient [12,13], thermal distillation processes are capable of maintaining their relative popularity in oil-rich regions such as the Middle East [1].
Currently, the water production from RO is economically more affordable than the other processes such as Membrane Distillation (MD). However, MD has demonstrated unique advantages that make it potentially competitive with the other desalination technologies, especially RO [8,13]. These advantages include 1) MD requires no transmembrane pressure while RO demands a large transmembrane pressure in the range of 44-82 bar depending on salt concentration [14]; 2) MD is able to work well at large water recovery ratio, while the operating pressure of RO would be extremely high if the water recovery ratio is too high (e.g., 60% or above); 3) MD is less subjected to fouling and scaling than RO; 4) while intense pre-treatment is necessary for RO, MD requires only simple pre-treatment such as cartridge filtration; 5) RO is electrically an energy intensive process where almost 40% of the overall costs are spent for electrical energy consumption [15] whereas MD requires very limited electricity consumption.

In spite of its favorable characteristics, MD has not yet been industrialized mainly due to two serious obstacles. First, huge thermal energy consumption required for water evaporation and second, low performance of MD membranes, especially at relatively low temperature, both of which control the overall costs of MD [16]. Therefore, any improvements in MD that would reduce its energy consumption and/or better the membrane performance would be of relevance in pushing MD towards being a commercially viable desalination technology.

1-2- Project Objectives

The objectives of this thesis are twofold:

- Verify the economic feasibility of a novel seawater desalination strategy, i.e., Zero Thermal Input Membrane Distillation (ZTIMD), for cost-effective, energy-saving, and waste-free seawater desalination at large scale. To achieve this goal, water production costs under different conditions were estimated using process simulation;
- Develop MD membranes with large fluxes at operation temperatures suitable for the proposed ZTIMD process.

To achieve the objectives, this work is divided into two segments: 1) ZTIMD simulation and feasibility study based on the data available in the literature and a few justified assumptions, 2)

experimental development of MD membranes incorporated with hydrophobic and hydrophilic nanoparticles.

For the ZTIMD simulation, fresh water production cost is chosen as the objective function and different case scenarios were made to study the effects of different parameters such as the complexity of the pre-treatment, operating conditions, and membrane characteristics on the economic feasibility of the proposed process.

1-2-1- Zero Thermal Input Membrane Distillation (ZTIMD)

ZTIMD proposes to extract the enthalpy of surface seawater for MD and use the cold bottom seawater as the heat sink (i.e., the coolant). Since the achievable temperature difference across the membrane will not be similar to that of the typical MDs, i.e. 40-60 °C, in the absence of external heating source, the proposed ZTIMD process would work at very low recovery ratios, less than 5%. Therefore, large amounts of raw seawater should be processed at industrial level, which might affect the costs associated with feed pumping, pre-treatment, etc. Furthermore, acquiring the coolant from the bottom sea would require a long underwater piping and additional electrical energy consumption to overcome the frictional pressure loss caused by pumping of seawater through the pipeline. Thus, the economic feasibility of the process needs to be investigated. For the simulation, two different case scenarios were made, where the pre-treatment can be estimated at different levels of complexity, i.e. that of the RO process which is intense and a more realistic pre-treatment for the ZTIMD process only by cartridge filtration. For each case, the major contributors to the production cost were determined, and their effect on the economic viability of the process was evaluated.

1-2-2- Nanocomposite MD Membranes

As discussed earlier, MD membranes play a major role in determining the overall cost in an MD desalination process. Many efforts have been devoted to improve the MD membranes performance via surface modification [17-19] and the use of polymeric additives [20,21]. However, the fabrication of nanocomposite membranes, which have already demonstrated great potential in the other applications, for MD has been out of the researchers' radar, and only a few works were reported in the literature applying carbon nanotubes [22] and modified hydrophobic $CaCO_3$ nanoparticles [23,24] to generate mixed matrix MD membranes. Considering the lack of

information on the use of nanomaterial incorporated membranes for MD, despite many promising results published for Ultrafiltration (UF) [25-27], Microfiltration (MF) [28-30], Nanofiltration (NF) [31-33], RO [34-36], and Forward Osmosis (FO) [37-39], it is the aim of this work to investigate the effects of nanomaterials on the properties, structure, and performance of the MD membranes.

Nanomaterials could be divided into two categories: 1) hydrophobic and 2) hydrophilic nanomaterials. The nano-additives of different hydrophobicity will definitely influence the membrane properties and structure, and consequently performance, in different fashion. Therefore, in this study, experimental works were designed in such a way to make it possible studying the effects of hydrophobicity of the nanomaterials on the membrane structure, characteristics, and performance, separately. To this end, different hydrophilic nanoparticles including CuO, $CaCO_3$, and SiO_2 as well as superhydrophobic SiO_2 nanoparticles were chosen as the nano-fillers to be embedded in a polyvinylidene fluoride (PVDF) matrix. Membrane morphology, membrane properties such as pore size, thickness, porosity, surface roughness, contact angle, and Liquid Entry Pressure of water (LEP_w), and membrane performance in terms of Vacuum Membrane Distillation (VMD) flux and selectivity were studied in the presence of the nano-fillers. It was tried to recognize the strength and weakness of the resulted membranes in each step and remove the flaws in the next step.

The membrane flux was evaluated at a low temperature of the feed stream, i.e. 27.5 °C. It was attempted to develop nanocomposite MD membranes whose fluxes, even when operated at such a low temperature, are equal to or more than those of the high temperature MD membranes, which are usually operated at temperatures as high as 60-80 °C.

1-3- Novelty of the Thesis

In this thesis, the concept of ZTIMD is proposed and developed for the first time with the purpose of the extraction of the solar energy stored in surface seawater to provide the MD process with the required thermal energy for evaporation that would make the process independent from external sources of thermal energy. In addition, economic feasibility of the process is also investigated through simulation and using literature data with a few verified and realistic assumptions.

Furthermore, this is the first time that hydrophilic nanoparticles are used to improve the structure, properties, and performance of the MD membranes.

1-4- Structure of the Thesis

A comprehensive literature review on the MD is provided in Chapter 2, while the evaluation of economic feasibility of the proposed ZTIMD process based on simulation results are given in Chapter 3.

For the experimental work, superhydrophobic SiO_2 nanoparticles as well as three different kinds of hydrophilic nanomaterials including CuO, $CaCO_3$, and amine modified SiO_2 were incorporated in PVDF membranes, and the resulted nanocomposite membranes were subjected to VMD performance tests. A comprehensive literature review on the effects of the nanomaterials on the properties and performance of the membrane-based processes for water treatment is given in Chapter 4, while the experimental results are presented in Chapters 5 to 7 plus Appendix A.

In chapter 5, two different hydrophilic nanoparticles, CuO and $CaCO_3$, and in Chapter 6, amine modified hydrophilic SiO_2 nanomaterials were embedded into PVDF membrane. The nanocomposite membranes at different loadings of the nano-additives were subjected to VMD test for determining the water flux and membrane selectivity. The membranes were further characterized by SEM to explore the effects of the nano-fillers concentration on their structure and properties for the purpose of interpretation of the results. It should be noted that the effect of non-woven fabric (NWF) backing material on the membrane properties and performance was also investigated in Chapter 6.

In Chapter 7, the best membrane obtained by the incorporation of the nanomaterials in Chapters 5, 6, and Appendix A was used as the base for further optimization by varying the ratio of the high and low molecular weight PVDF as the host polymer and also the penetration time, a critical parameter in preparation of supported membranes. To this end, different penetration times, defined as the period between the completion of membrane casting and the immersion in the coagulation bath, were tested, and the most appropriate penetration time that led to a better performance by considering the flux, selectivity, and LEP_w together was recommended.

Chapter 8 summarizes the results of this work, which proposed a disruptive ZTIMD desalination strategy that promises a cost-effective, energy-efficient, waste-free, and therefore truly more sustainable solution to the world freshwater demand, demonstrated its economic feasibility, and

developed novel MD membranes that may technically enable such a strategy. A few recommendations are also presented in terms of further studies that may help ready this technology for commercialization.

Finally, it should be mentioned that this thesis includes an Appendix A, which its results have been used for the final conclusions. In Appendix A, a study was performed to investigate the effects of the superhydrophobic SiO_2 nanomaterial on the structure, properties, and performance of the PVDF membranes. The concentration of the nano-fillers in the matrix of the polymeric membrane were changed to find the optimum loading, where the nanocomposite membranes demonstrated the best VMD performance in terms of flux. The morphology of nanocomposite membranes was investigated by SEM images, and characterized by measuring the surface pore size, porosity, thickness, surface roughness, contact angle, and LEP_w.

References

[1] V.G. Gude, Desalination and sustainability - An appraisal and current perspective, Water Res. 89 (2016) 87-106.

[2] the Guardian, Four billion people face severe water scarcity, new research finds, (February 2016).

[3] J.E. Efome, M. Baghbanzadeh, D. Rana, T. Matsuura, C.Q. Lan, Effects of superhydrophobic SiO2 nanoparticles on the performance of PVDF flat sheet membranes for vacuum membrane distillation, Desalination. 373 (2015) 47-57.

[4] A.E. Khalifa, Water and air gap membrane distillation for water desalination – An experimental comparative study, Separation and Purification Technology. 141 (2015) 276-284.

[5] S. Daer, J. Kharraz, A. Giwa, S.W. Hasan, Recent applications of nanomaterials in water desalination: A critical review and future opportunities, Desalination. 367 (2015) 37-48.

[6] M. Baghbanzadeh, D. Rana, C.Q. Lan, T. Matsuura, Effects of Inorganic Nano-Additives on Properties and Performance of Polymeric Membranes in Water Treatment, Separation & Purification Reviews. 45 (2016) 141-167.

[7] S. Miller, H. Shemer, R. Semiat, Energy and environmental issues in desalination, Desalination. 366 (2015) 2-8.

[8] M. Baghbanzadeh, D. Rana, T. Matsuura, C.Q. Lan, Effects of hydrophilic CuO nanoparticles on properties and performance of PVDF VMD membranes, Desalination. 369 (2015) 75-84.

[9] H.M. Hegab, L. Zou, Graphene oxide-assisted membranes: Fabrication and potential applications in desalination and water purification, J.Membr.Sci. 484 (2015) 95-106.

[10] H. Azizi Namaghi, A. Haghighi Asl, M. Pourafshari Chenar, Identification and optimization of key parameters in preparation of thin film composite membrane for water desalination using multi-step statistical method, Journal of Industrial and Engineering Chemistry. 31 (2015) 61-73.

[11] M. Baghbanzadeh, D. Rana, C.Q. Lan, T. Matsuura, Effects of hydrophilic silica nanoparticles and backing material in improving the structure and performance of VMD PVDF membranes, Separation and Purification Technology. 157 (2016) 60-71.

[12] N. Ghaffour, T.M. Missimer, G.L. Amy, Technical review and evaluation of the economics of water desalination: Current and future challenges for better water supply sustainability, Desalination. 309 (2013) 197-207.

[13] A.S. Hassan, H.E.S. Fath, Review and assessment of the newly developed MD for desalination processes, Desalin.Water Treat. 51 (2013) 574-585.

[14] S. Liyanaarachchi, L. Shu, S. Muthukumaran, V. Jegatheesan, K. Baskaran, Problems in seawater industrial desalination processes and potential sustainable solutions: a review, Reviews in Environmental Science and Bio-Technology. 13 (2014) 203-214.

[15] L. Ophek, L. Birnhack, O. Nir, E. Binshtein, O. Lahav, Reducing the specific energy consumption of 1st-pass SWRO by application of high-flux membranes fed with high-pH, decarbonated seawater, Water Res. 85 (2015) 185-192.

[16] S. Al-Obaidani, E. Curcio, F. Macedonio, G. Di Profio, H. Ai-Hinai, E. Drioli, Potential of membrane distillation in seawater desalination: Thermal efficiency, sensitivity study and cost estimation, J.Membr.Sci. 323 (2008) 85-98.

[17] M. Qtaishat, D. Rana, M. Khayet, T. Matsuura, Preparation and characterization of novel hydrophobic/hydrophilic polyetherimide composite membranes for desalination by direct contact membrane distillation, J.Membr.Sci. 327 (2009) 264-273.

[18] K.C. Chong, S.O. Lai, K.M. Lee, W.J. Lau, B.S. Ooi, Performance of Surface Modification of Polyvinylidene Fluoride Hollow Fiber Membrane in Membrane Distillation, 2nd International Conference on Sustainable Materials (Icosm 2013). 795 (2013) 137-140.

[19] D. Tong, X. Wang, M. Ali, C.Q. Lan, Y. Wang, E. Drioli, et al., Preparation of Hyflon AD60/PVDF composite hollow fiber membranes for vacuum membrane distillation, Separation and Purification Technology. 157 (2016) 1-8.

[20] S. Simone, A. Figoli, A. Criscuoli, M.C. Carnevale, A. Rosselli, E. Drioli, Preparation of hollow fibre membranes from PVDF/PVP blends and their application in VMD, J.Membr.Sci. 364 (2010) 219-232.

[21] E. Drioli, A. Ali, S. Simone, F. Macedonio, S.A. AL-Jlil, F.S. Al Shabonah, et al., Novel PVDF hollow fiber membranes for vacuum and direct contact membrane distillation applications, Separation and Purification Technology. 115 (2013) 27-38.

[22] K. Gethard, O. Sae-Khow, S. Mitra, Water Desalination Using Carbon-Nanotube-Enhanced Membrane Distillation, Acs Applied Materials & Interfaces. 3 (2011) 110-114.

[23] D. Hou, J. Wang, X. Sun, Z. Ji, Z. Luan, Preparation and properties of PVDF composite hollow fiber membranes for desalination through direct contact membrane distillation, J.Membr.Sci. 405 (2012) 185-200.

[24] D. Hou, G. Dai, H. Fan, J. Wang, C. Zhao, H. Huang, Effects of calcium carbonate nano-particles on the properties of PVDF/nonwoven fabric flat-sheet composite membranes for direct contact membrane distillation, Desalination. 347 (2014) 25-33.

[25] A.L. Ahmad, M.A. Majid, B.S. Ooi, Functionalized PSf/SiO2 nanocomposite membrane for oil-in-water emulsion separation, Desalination. 268 (2011) 266-269.

[26] A. Rahimpour, M. Jahanshahi, S. Khalili, A. Mollahosseini, A. Zirepour, B. Rajaeian, Novel functionalized carbon nanotubes for improving the surface properties and performance of polyethersulfone (PES) membrane, Desalination. 286 (2012) 99-107.

[27] Q. Wang, X. Wang, Z. Wang, J. Huang, Y. Wang, PVDF membranes with simultaneously enhanced permeability and selectivity by breaking the tradeoff effect via atomic layer deposition of TiO2, J.Membr.Sci. 442 (2013) 57-64.

[28] J. Li, Z. Xu, H. Yang, L. Yu, M. Liu, Effect of TiO2 nanoparticles on the surface morphology and performance of microporous PES membrane, Appl.Surf.Sci. 255 (2009) 4725-4732.

[29] G. Wu, S. Gan, L. Cui, Y. Xu, Preparation and characterization of PES/TiO2 composite membranes, Appl.Surf.Sci. 254 (2008) 7080-7086.

[30] N. Maximous, G. Nakhla, W. Wan, K. Wong, Preparation, characterization and performance of Al2O3/PES membrane for wastewater filtration, J.Membr.Sci. 341 (2009) 67-75.

[31] L.M. Jin, S.L. Yu, W.X. Shi, X.S. Yi, N. Sun, Y.L. Ge, et al., Synthesis of a novel composite nanofiltration membrane incorporated SiO2 nanoparticles for oily wastewater desalination, Polymer. 53 (2012) 5295-5303.

[32] J.n. Shen, C.c. Yu, H.m. Ruan, C.j. Gao, B. Van der Bruggen, Preparation and characterization of thin-film nanocomposite membranes embedded with poly(methyl

methacrylate) hydrophobic modified multiwalled carbon nanotubes by interfacial polymerization, J.Membr.Sci. 442 (2013) 18-26.

[33] R. Kumar, A.M. Isloor, A.F. Ismail, S.A. Rashid, A. Al Ahmed, Permeation, antifouling and desalination performance of TiO2 nanotube incorporated PSf/CS blend membranes, Desalination. 316 (2013) 76-84.

[34] J. Yin, E. Kim, J. Yang, B. Deng, Fabrication of a novel thin-film nanocomposite (TFN) membrane containing MCM-41 silica nanoparticles (NPs) for water purification, J.Membr.Sci. 423 (2012) 238-246.

[35] H.J. Kim, K. Choi, Y. Baek, D. Kim, J. Shim, J. Yoon, et al., High-Performance Reverse Osmosis CNT/Polyamide Nanocomposite Membrane by Controlled Interfacial Interactions, Acs Applied Materials & Interfaces. 6 (2014) 2826-2836.

[36] M. Fathizadeh, A. Aroujalian, A. Raisi, Effect of added NaX nano-zeolite into polyamide as a top thin layer of membrane on water flux and salt rejection in a reverse osmosis process, J.Membr.Sci. 375 (2011) 88-95.

[37] N. Niksefat, M. Jahanshahi, A. Rahimpour, The effect of SiO2 nanoparticles on morphology and performance of thin film composite membranes for forward osmosis application, Desalination. 343 (2014) 140-146.

[38] N. Ma, J. Wei, R. Liao, C.Y. Tang, Zeolite-polyamide thin film nanocomposite membranes: Towards enhanced performance for forward osmosis, J.Membr.Sci. 405 (2012) 149-157.

[39] D. Emadzadeh, W.J. Lau, T. Matsuura, A.F. Ismail, M. Rahbari-Sisakht, Synthesis and characterization of thin film nanocomposite forward osmosis membrane with hydrophilic nanocomposite support to reduce internal concentration polarization, J.Membr.Sci. 449 (2014) 74-85.

Chapter 2:

Membrane distillation

M. Baghbanzadeh, C. Q. Lan, D. Rana, T. Matsuura, (2016) Membrane distillation, In: Nanostructured Polymer Membranes, Volume 1: Processing and Characterization, Wiley-Scrivener Publishing, US, Ch. 11, pp. 419-455

Membrane distillation

Mohammadali Baghbanzadeh, Christopher Q. Lan*, Dipak Rana, Takeshi Matsuura
Department of Chemical and Biological Engineering, University of Ottawa, 161 Louis Pasteur Private, Ottawa, Ontario, K1N 6N5, Canada

Abstract

Membrane Distillation (MD) is a thermal-driven membrane-based separation process with great potential in applications such as desalination, wastewater treatment, and separation of volatile components from liquid mixtures. Since the formation of the MD concept in the 1960s, extensive studies have been devoted to both the understanding of the fundamental principles and improving the economic competitiveness of MD. This chapter strives to provide a comprehensive coverage of both the fundamentals and recent developments in association with the application, process design, and membrane fabrication in this field.

Keywords: Separation; Distillation membrane; Membrane characteristic; Transport phenomena;

2-1- Introduction

Membrane Distillation (MD), introduced in the late 1960s [1], is considered as a low cost and energy saving alternative to conventional separation processes such as distillation and Reverse Osmosis (RO). MD is a membrane-based thermal-driven separation process that uses vapor pressure difference across the membrane as the driving force for mass transfer. The major obstacle hindering the commercial application of MD include the unavailability of appropriate MD membranes with required characteristics at reasonable costs [2] and the huge process thermal energy demand that result in a process which is not economically appealing in comparison with the conventional separation processes such as RO [3]. Extensive efforts have been focused on the development of novel MD membrane based upon a better understanding of mass and heat transfer principles of MD [4] with significant advances in many different fronts. In an MD process, liquid molecules are evaporated at the liquid-vapor interface and only vapor

*Corresponding author. Tel.: 1 613 562 5800x2050.
E-mail address:Christopher.Lan@uottawa.ca (C.Q. Lan)

molecules are permitted to pass through the porous and hydrophobic medium. Finally, concentrated solution would be collected on the permeate side. The following are considered characteristic of the MD process [5]:

1. A porous membrane is needed.
2. The membrane should not be wetted by process liquid.
3. Capillary condensation should not take place inside the membrane pores.
4. Liquid is not permitted to pass through the membrane and only vapor should be transported across the membrane.
5. The membrane must be neutral to the vapor equilibrium of the different components in the process liquid.
6. At least one side of the membrane should be in direct contact with the process liquid.
7. For each component in the process liquid, the membrane operation driving force is a partial pressure gradient in the vapor phase across the membrane.

In a MD process, the feed does not need to be heated up to the boiling temperature of the volatile component. Therefore, the process will work at low operating temperatures compared to conventional processes. In addition, the operating pressure in an MD arrangement is much less than that of pressure-driven membrane processes such as RO, Microfiltration (MF), Ultrafiltration (UF), and Nanofiltration (NF), resulting in a separation process consuming less electric power, requiring materials of less mechanical strength, and being less sensitive to membrane fouling compared to the pressure-driven processes. Furthermore, MD permeate can theoretically approach a selectivity of 100%, which is similar to conventional thermal distillation processes and much more superior to pressure-driven membrane based processes. Table 2-1 compares the advantages and disadvantages of MD and RO for desalination.

Table 2-1 Comparison between MD and RO for desalination		
	Advantages	Disadvantages
RO	1)Established commercial processes; 2) Good membrane durability; 3) Near zero thermal energy consumption; 4) Compact systems with small footprint.	1) High operating pressure; 2) Need for mechanically strong systems; 3) Lower product quality compared to that of MD; 4) Limited water recovery; 5) Environmental liabilities due to rejection of large volumes of concentrated brines; 5) Membrane fouling a significant concern; 6) Rigid pre-treatment of feed required.
MD	1) No transmembrane pressure required; 2) Small power consumption; 3) Less tendency to fouling; 4) Use of low-grade energy; 5) Close to 100% salt rejection leading to high quality water products; 6) Working well with concentrated brines	1) High operating temperature in comparison with RO; 2) Consuming large quantities of thermal energy; 3) Membrane durability a hindrance; 4) Relatively small flux in comparison to RO; 5) Economically uncompetitive as stand-alone desalination process at present.

2-2- Applications of Membrane Distillation Technology

Membrane distillation has the potential of being used in water desalination, solution degassing, treatment of industrial effluents, purification of pharmaceuticals, processing of foods and removal of organic compounds, heavy metals from aqueous solutions [6-10] and radioactive wastes [11] and concentrating diluted non-volatile acids such as sulfuric acid and phosphoric acid [12].

MD could also be employed for recovery of volatile compounds from aqueous solutions. By applying a hydrophobic membrane, components more volatile than water would be transported through the membrane pores and consequently the other side would be enriched by those components. Such a process has the potential to be used for integrated systems. For instance, in a membrane bioreactor, by continuous removal of ethanol from broth during fermentation, MD could enhance the process yield [13].

Another example of MD application is HCl recovery from industrial effluents [14]. For instance, HCl might be used as the pickling liquor for removing surface oxides before electroplating and spent pickling liquors should be refined from the harmful heavy metals. While neutralization methods are traditionally used, MD process can be employed for acid recovery. In this process, water vapor and gaseous acid are transferred through the membrane pores to the permeate side. Vapor is condensed and gaseous acid is then dissolved [15].

The MD process could potentially be used for water treatment in place of RO provided to having high performance MD membranes which are comparable to the conventional RO membranes in terms of permeability and durability. Furthermore, a novel MD process which demands much less thermal energy input compared to the conventional MD processes needs to be developed. The main disadvantages of RO technology in water treatment are huge electrical energy consumption, limited water recovery and environmental liabilities in association with the rejection of large volumes of concentrated brines [16]. Furthermore, osmotic pressure increases significantly with the increase of the brine concentration and therefore, operation pressure and electrical energy consumption would increase dramatically with the increase of water recovery. In addition, fouling and scaling are important challenges in RO.

2-3- Different Kinds of Membrane Distillation Configuration

There are several configurations of MD systems, which are different based on the structure of the permeate side.

2-3-1- Direct Contact Membrane Distillation (DCMD)

Direct contact membrane distillation is the simplest MD configuration. The membrane is in direct contact with the liquid phase and has the ability of producing a high flux. Hot feed is in direct contact with the hot side of the membrane surface and vapor molecules pass through the membrane toward the permeate side and condensation takes place inside the module. The application of this configuration is in desalination and concentration of aqueous solutions [17,18]. Because of its simple structure and high flux, DCMD was exposed to a large amount of laboratory researches. The main disadvantage of this configuration is its low energy efficiency [4] and that is a great obstacle in its commercialization. As a result of a higher heat transfer

coefficient on the permeate side, DCMD has the highest heat conduction loss among the other configurations that will decrease its thermal efficiency [19,20]. Fig. 2-1 shows a schematic picture of DCMD concept.

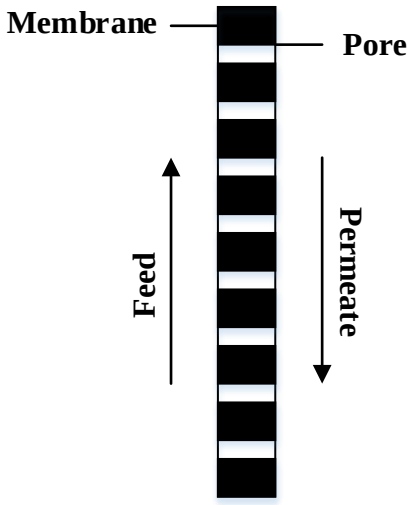

Fig. 2-1 Direct Contact Membrane Distillation (DCMD) [4]

2-3-2- Air Gap Membrane Distillation (AGMD)

In an air gap membrane distillation arrangement, there is a layer of air between the membrane and condensation surface. Hot side is similar to that of DCMD, but as well as the membrane, vapor molecules pass through the stagnant air to reach the cold surface inside the module. This configuration has a high energy efficiency with a relatively low flux. AGMD can be particularly used where the available energy is small [21]. Due to its greater mass transfer and thermal resistances, air gap controls the heat and mass transfer. The air gap is usually thicker than the membrane and its thermal conductivity is smaller, thus more heat energy in this configuration will be used to evaporate water in comparison with DCMD. Latent heat of vapor can be recovered by the condenser, if a low temperature feed as the cooling stream is used to condense vapor. Because of a low temperature difference across the membrane, this configuration has a low flux and larger surface area is required [18,21,22]. Fig. 2-2 shows a schematic of AGMD concept.

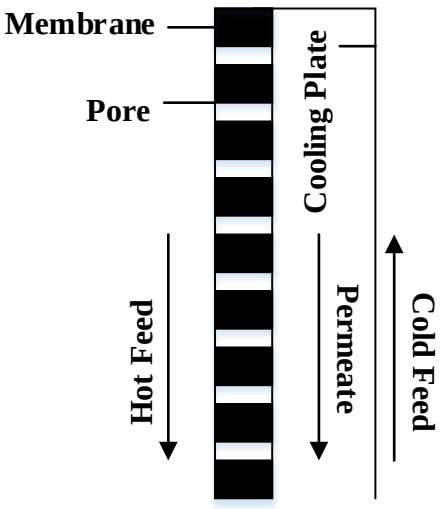

Fig. 2-2 Air Gap Membrane Distillation (AGMD) [4]

2-3-2-1- Memstill and Aquastill

Memstill (Fig. 2-3-a,b) is a novel configuration based on the energy-efficient AGMD idea. Desalination takes place in a counter current flow configuration. Cold feed solution flows through a condenser with non-permeable walls which results in an increment in its temperature. Then it is heated up using a source of energy and enters an evaporator that its walls consists of a microporous hydrophobic membranes. The condenser and membrane could be either tubular or flat sheet. It has been reported that depending on the cost of thermal energy provided, using Memstill for desalination would reduce the product cost to 0.26-0.50 $\$/m^3$ of water produced [20]. The low cost is due to the cheaper plant materials for the module compared to high pressure RO. Furthermore, there is the possibility of using low grade sources of heat such as waste heat to provide thermal energy for desalination. Memstill has the lowest thermal energy required among the other configurations (56-100 kWh/m^3) which would result in the highest Gain Output Ratio (GOR) that has been ever reported (11.2) [4]. Feed temperature should be within 80-90 °C and electrical energy required is almost 0.75 kWh/m^3 [23].

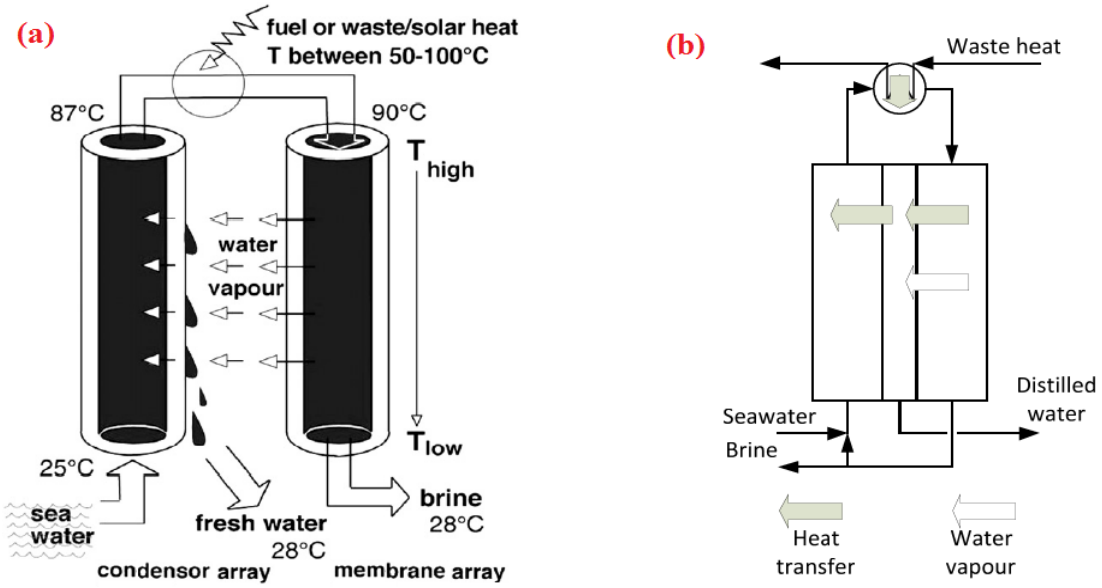

Fig. 2-3-(a), (b) Memstill configuration [4,24]

2-3-3- Permeate Gap Membrane Distillation (PGMD)

PGMD is a configuration between AGMD and DCMD. The air gap is inherently open to atmospheric air at ambient pressure. By closing the bottom distillate outlet and allowing the permeate to fill up the air gap, the permeate will be discharged from the top and such a configuration is called PGMD. In fact, stagnant air in AGMD is replaced by stagnant liquid in PGMD. An important advantage of this configuration compared to DCMD is the separation of permeate channel from the cooling stream. It results in the use of other fluids for cooling purpose. For instance, cold feed solution could be employed as the coolant and it would be preheated before entering the hot side. Actually, it provides the possibility of internal heat recovery. There is a thin foil between the permeate gap and coolant in this configuration that adds an extra thermal resistance to the system and reduces the effective temperature difference across the membrane. PGMD arrangement has higher permeate flux in contrast to AGMD [25] due to a faster condensation that takes place when vapor is directly mixed with colder liquid, and also a faster heat loss rate towards the polymeric film (foil) that is in contact with the coolant stream. Furthermore, at low feed temperatures, PGMD has lower specific thermal energy consumption compared to AGMD. A schematic of PGMD is given in Fig. 2-4.

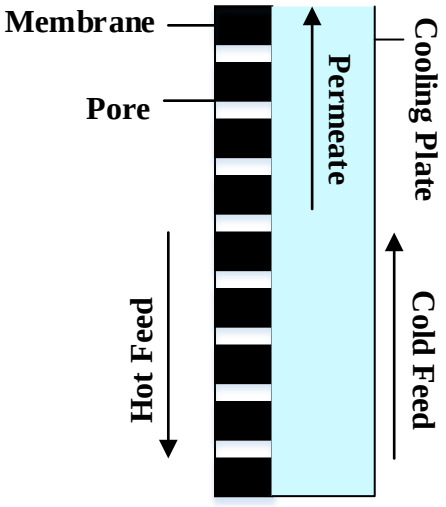

Fig. 2-4 Permeate Gap Membrane Distillation (PGMD)

2-3-4- Sweep Gas Membrane Distillation (SGMD)

In SGMD, there is an inert gas (stripping gas) instead of the stagnant air in AGMD to carry the vapor that leaves the membrane. Vapor is condensed in an external condenser. Unlike AGMD, the gas barrier for reducing heat loss is not stationary which results in an enhancement in the mass transfer coefficient. This configuration is used to remove volatiles from an aqueous solution [26,27]. Due to the greater driving force originating from the reduced vapor pressure on the permeate side, SGMD has higher mass transfer in comparison with AGMD and lower heat loss across the membrane than DCMD, but employing an external condenser and blower would increase its capital and operating costs. Fig. 2-5 presents a schematic of SGMD concept.

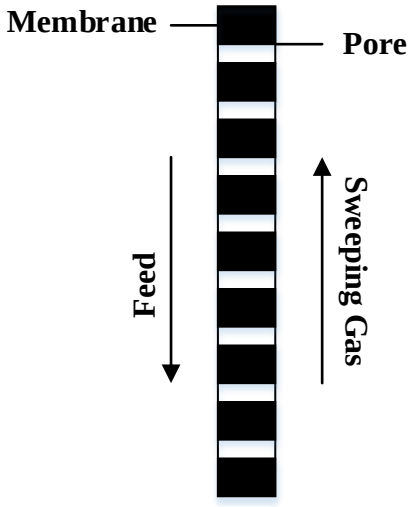

Fig. 2-5 Sweep Gap Membrane Distillation (SGMD) [4]

2-3-5- Vacuum Membrane Distillation (VMD)

In this configuration, the permeate side is vapor under reduced pressure, and it could be condensed in separate equipment such as an external condenser. In this arrangement, pressure is maintained below the equilibrium vapor pressure to improve mass transfer. VMD is beneficial for removing volatiles from an aqueous solution [28,29]. VMD is characterized by *first*: vaporization of the more volatile components at the liquid-vapor interface and *second*: diffusion of the vapor through the membrane pores according to a Knudsen mechanism. To maintain a vapor pressure difference across the membrane, the vapor permeate should be removed continuously from the vacuum chamber. By considering the fact that vapor pressure on the cold side can be reduced to near zero, VMD could provide the highest driving force at the same feed temperature compared to the other MD configurations. VMD is a suitable approach for reducing heat loss and reaching higher vapor flow rates. It should be mentioned that the possibility of liquid penetration into the membrane pores in this configuration is higher than the other arrangements and a membrane with a smaller mean pore size should be applied [6]. A schematic of VMD configuration is shown in Fig. 2-6.

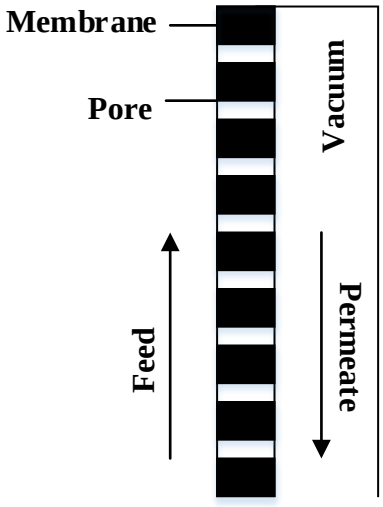

Fig. 2-6 Vacuum Membrane Distillation (VMD) [4]

2-3-5-1- Vacuum Gap Membrane Distillation (VGMD)

VGMD (Fig. 2-7) is a type of AGMD configuration in which a slight vacuum pressure is applied on the permeate side. In other words, VGMD is an arrangement between AGMD and VMD. It is different from VMD in a way that product water is condensed inside the module at the highest possible temperature. To create the vacuum pressure, an air ejector or a vacuum pump could be used [25]. By using a slight vacuum, electrical energy consumption would be significantly decreased compared to the conventional VMD process which works at a very high vacuum pressure, moreover, there would not be a need for a continuous evacuation in VGMD. Therefore, and to prevent vacuum loss due to the existence of non-condensable gases in feed solution, it is necessary to remove them first. To this end, degassing could be proposed as the preliminary step before the VGMD process. To degas the feed solution, hollow fiber membranes are typically employed under a vacuum pressure [30,31]. Higher the vacuum pressure means a greater level of degassing and consequently, a better VGMD performance. The performance of VGMD is greatly dependent on the vacuum pressure which is used on the permeate side. Higher vacuum would result in a better performance, however, it would result in more energy consumption and less effective internal heat recovery [25]. At a very small vacuum of 0.9 bar, VGMD demonstrated to have a performance between PGMD and AGMD in terms of permeate flux and specific thermal

energy consumption [25]. It is predicted that the VGMD function could be enhanced by increasing the vacuum pressure.

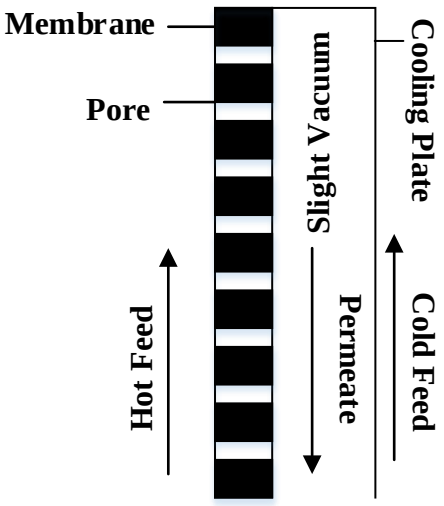

Fig. 2-7 Vacuum Gap Membrane Distillation (VGMD)

2-3-5-2- Memsys

Memsys (Fig. 2-8) is a novel configuration of VGMD that has employed an internal heat recycling concept to reduce the thermal energy consumption. It is known as Vacuum Multi-Effect Membrane Distillation (VMEMD) which combines the advantages of multi effect and vacuum concepts to make a multistage setup integrated into a compact plate and frame module. This configuration has been successfully commercialized [32]. A Memsys module consists of a steam raiser, multiple stages and a condenser. Each stage has several membrane and foil frames. Temperature difference between steam raiser and condenser provides a driving force for the entire process. Foils are made from metal coated Polypropylene (PP) and act as the condensation plates. Membranes are made from Polytetrafluoroethylene (PTFE) and serve as vapor channels. Feed solution flows in the space between foils and membrane frames. A vacuum pump is employed to generate vacuum pressure throughout the module, however, vacuum pressure varies from 0.1 to 0.3 bar in different stages [32]. Thermal energy consumption of Memsys process is within 175-350 kWh/m^3 that corresponds to a GOR of 3.6. Its electrical energy requirement is in

the range from 0.75 to 1.75 kWh/m^3, and feed solution temperature falls between 60 and100 °C, while the coolant temperature is less than 40 °C [4].

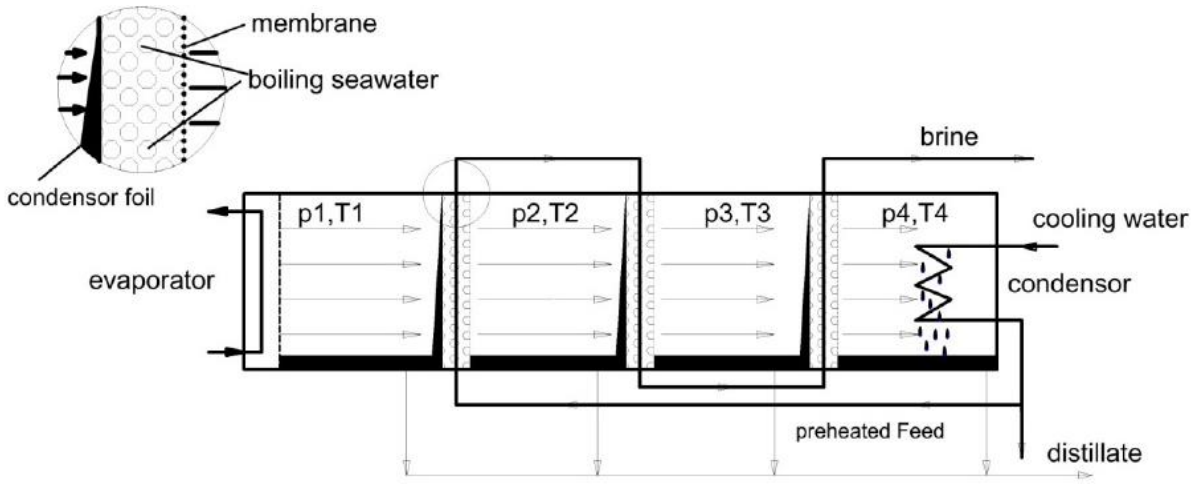

Fig. 2-8 Memsys Configuration [4,33]

2-3-5-3- Difference Between VMD and Pervaporation (PV)

Both VMD and PV are membrane-based separation processes in which hot solution is in direct contact with membrane on upstream side, while a vacuum pressure is employed on downstream side of the membrane. Membrane plays a significant role in differences between these two types of processes. In VMD configuration, porous and hydrophobic membranes are applied which their function is like a support for vapor-liquid interface and they do not influence the separation performance, but in pervaporation, dense and selective membranes are employed and the separation process is affected by the solubility and diffusivity of the components in the membrane. In VMD, vapor molecules cross the pores of the membrane, but in PV, diffusion is the dominant mechanism and vapor molecules are diffused through the membrane. In other words, VMD uses porous membranes, while non-porous membranes are applied in PV. Therefore, VMD usually achieves higher flux than that of PV [34].

Table 2-2 summarizes the differences between various configurations of MD.

Table 2-2 Comparison between different MD configurations

Configuration	Applicable Module	Advantages	Disadvantages
DCMD	1) Plate and Frame	1) Simple structure 2) High flux 3) A broad availability of research data	1) Low energy efficiency due to conductive heat loss 2) Coolant should be preferably the same as the permeate
AGMD	1) Plate and Frame	1) Simple structure; 2) Higher energy efficiency than DCMD 3) Capable of latent heat recovery	Smaller flux than DCMD due to smaller driving force at same feed/coolant temperature
PGMD	1) Plate and Frame 2) Spiral Wound	1) Simple structure; 2) Larger driving force and hence flux than AGMD at same feed/coolant temperature 3) Less conductive heat loss than DCMD 4) Capable of latent heat recovery	1) Smaller driving force and hence flux than DCMD at same feed/coolant temperature 2) Lower energy efficiency than AGMD due to conductive heat loss
SGMD	1) Plate and Frame 2) Hollow Fiber	1) Larger flux than AGMD due to turbulence on permeate side 2) Smaller conductive heat loss than DCMD	Need external condenser/air blower
VMD	1) Plate and Frame 2) Hollow Fiber 3) Spiral wound	1) Greatest driving force among the MD configurations, because the pressure on permeate side could be reduced to almost zero 2) High flux 3) Absence of conductive heat loss	1) Require membranes of large liquid entry pressure; 2) Need external condenser/vacuum pump 3) Challenge of maintaining vacuum at large scale 4) Increase water pH due to CO_2 removal
VGMD	1) Plate and Frame	1) Larger flux than AGMD due to larger driving force 2) Lower thermal energy consumption than AGMD 3) No need of external condenser 4) No need of continuous evacuation, less power consumption than VMD	1) Need degassing of feed 2) Maintenance of vacuum a challenge, especially at large scale 3) Complex system demanding careful sealing

2-4- Distillation Membranes

2-4-1- MD Modules

There are four major membrane modules which are plate and frame, hollow fiber, tubular and spiral wound [6].

2-4-1-1- Plate and Frame

In this module, membrane and spacers are placed between two plates. It is suitable for flat sheet membranes and can be applied for DCMD, AGMD, SGMD, and VMD configurations. Spacers are used to increase turbulence and reduce temperature polarization for enhancing the flow dynamics. Packing density in this module is within 100-400 m^2/m^3 [35]. Its effective area for the same volume is relatively smaller than the other modules, and a membrane support is required, but multiple layers of flat sheet membranes could be used to increase the effective area. On the other hand, the simplicity of its construction, cleaning and replacing damaged membranes make the module appropriate for laboratory applications to test the influence of membrane properties and process variables on the membrane performance. Indeed, this type of module is most commonly used in laboratory experiments. Figs. 2-9-a and b show a schematic of plate and frame module and flat sheet membrane.

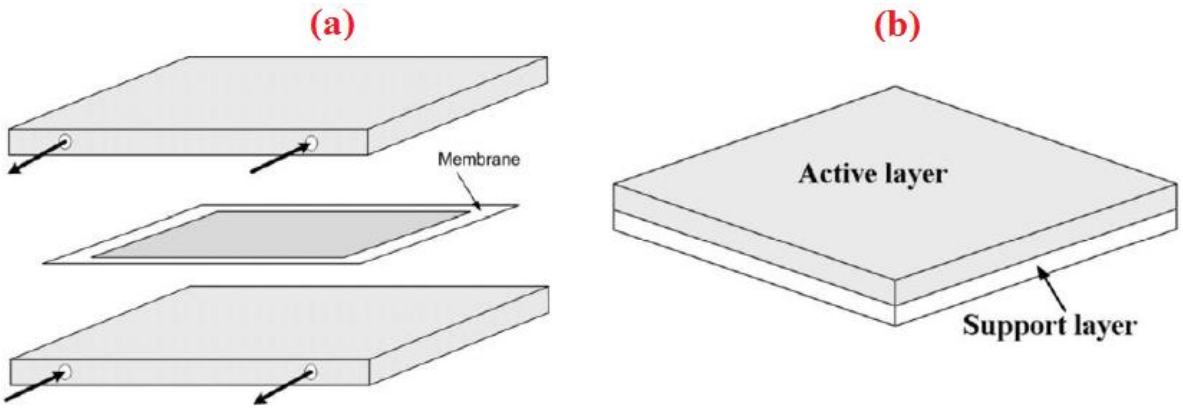

Fig. 2-9 (a) Plate and frame module, (b) Supported flat sheet membrane [4]

2-4-1-2- Hollow Fiber

In this module, thousands of hollow fibers are bundled and sealed into a housing. It is possible for the feed solution to flow inside or outside the fibers while the permeate product would be collected from the other side. According to the cooling fluid arrangement, presence of air gap, sweeping gas or negative pressure on the permeate side, DCMD, AGMD, SGMD or VMD configurations could be achieved. It has a very high packing density (about 3000 m^2/m^3) [36], and its energy consumption is very low which are two main advantages of this module, which further would result in the process being potentially applicable in industry. Although, its high tendency to fouling and difficulty to cleaning and replacing the broken hollow fibers are considered as the main disadvantages of this module. The broken hollow fibers could be detected by a liquid decay test [37-39]. Low efficient distribution of feed solution in the shell side may cause high degrees of temperature polarization. To reduce this effect in hollow fiber modules, cross flow patterns have been developed [40]. A schematic of hollow fiber module and hollow fiber membrane are given in Figs. 2-10-a and b.

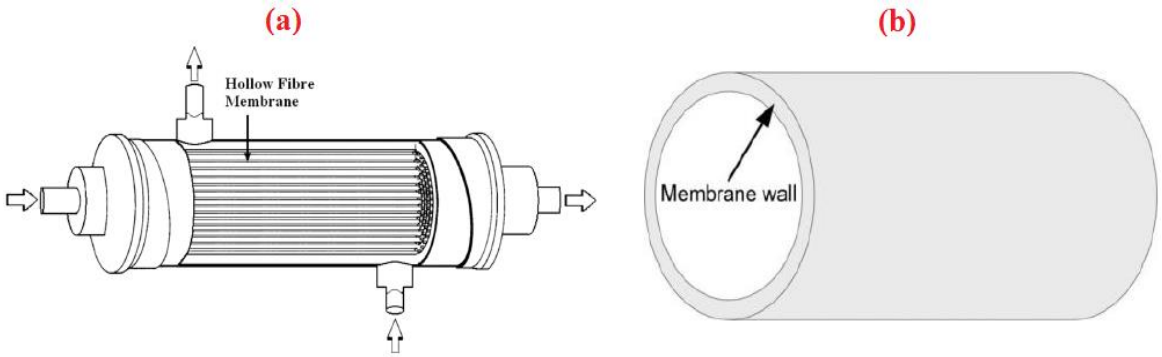

Fig. 2-10 (a) Hollow fiber module, (b) Hollow fiber membrane [4]

2-4-1-3- Tubular

In this module, there are two cylindrical chambers for hot and cold fluids and a tube shaped membrane is placed between the chambers. Its ease of cleaning, high effective area and low tendency to fouling make it a good option for commercial applications. However, having a high operating cost is considered to be a disadvantage of this module. Tubular modules could be used in DCMD, AGMD, and VMD configurations.

2-4-1-4- Spiral Wound

In this module, flat sheet membranes and spacers are enveloped and rolled around a perforated central collection tube. Feed flows in an axial direction through the membrane surface, and the permeate product moves radially to the center where it is accumulated by the collection tube. In this module a feed spacer mesh is used to keep the membranes separated, therefore, feed water will flow between the sheets, and then a separate permeate carrier is obtained on the opposite side of the membrane sheets to carry the permeate to the perforated tube for the collection of the product. Generating turbulence, lowering the boundary layers thickness close to the membrane surface, and helping reduce scaling and fouling potentials are the main concerns that need to be taken into account in a feed spacer design.

This module has average packing density, tendency to fouling, and energy consumption [6].

2-4-2- Applicable Membranes for MD

Flat sheet (Fig. 2-10-b) and hollow fiber (Fig. 2-11-b) are the two most common types of membrane in different applications. As shown in Fig 2-10-b, a supported flat sheet membrane is made up of two layers. A thin active layer and a porous support layer. Support layer provides sufficient mechanical strength and enables the active layer to be constructed as thin as possible to reduce the mass transfer resistance. It should be pointed out that unsupported flat sheet membranes are also common in MD. PP, PTFE, and polyvinylidene fluoride (PVDF) are materials which are used for flat sheet membranes fabrication, while PP, PVDF and PVDF-PTFE composite are mainly used for preparing hollow fiber membranes. Hollow fiber membranes have larger specific surface area than flat sheet ones, but they typically have low flux due to their poor flow dynamics and high degree of temperature polarization [41,42]. However, high-flux hollow fiber membranes (as high as that of flat sheet membranes) have been recently developed, such as hollow fiber membranes with a sponge-like structure and thin walls, dual-layer hydrophilic-hydrophobic fibers with a very thin effective hydrophobic PVDF layer (50 μm) [4].

2-4-2-1- Nanocomposite Membranes

Much attention has been paid to nanocomposite membranes in different membrane-based processes such as MF, UF, NF, RO, and FO [43-52]. However, using nanomaterials in

developing the MD membranes is considered to be a new concept and only a few studies have been reported in the literature in this direction. Carbon nanotubes [53], $CaCO_3$ [16,54,55], CuO [16], and SiO_2 [56,57] are the nanomaterials which were used for making the MD nanocomposite membranes. The use of hydrophobic nanomaterials was more often among those researches [54-56]. Interestingly and in spite of the nature of the MD membranes which highly demands hydrophobic surfaces, Baghbanzadeh et al. demonstrated that hydrophilic nanoparticles such as $CaCO_3$ [16], CuO [16], and SiO_2 [57] have a great potential in enhancing the membrane performance by increasing the permeability through enlarging the surface pore size, porosity, and reducing the thickness of the sponge-like layer which is considered to be the major contributor to the mass transfer resistance across the membrane. They showed that hydrophilic silica nanoparticles could increase the thickness of the finger-like layer significantly, and since such a membrane might be mechanically fragile in long term MD operation, nanocomposite membrane could be stabilized by a non-woven polyester backing material for a longer durability [57]. A quite large VMD pure water flux of 12.7 kg/m^2h was reported in their work when a feed temperature of 27.5 °C and an vacuum pressure of 1.2 kPa was used [57]. It is worth pointing out that the hydrophilic nanomaterials incorporated membranes demonstrated nearly perfect salt rejection in those studies [16,57].

2-4-3- Membrane Characteristics in MD

Hydrophobic microporous membranes are employed in MD processes. Generally, membranes in MD applications should have high thermal and chemical resistance at relatively high temperatures against basic and acidic solutions. In the following, the major characteristics of the membranes in an MD process are presented.

2-4-3-1- Liquid Entry Pressure (Wetting Pressure)

Liquid entry pressure (LEP) is the highest pressure that could be applied in MD without penetration of the liquid feed into the membrane pores. If the pressure exceeds this amount, liquid would enter the hydrophobic membrane. It depends upon maximum pore size and membrane hydrophobicity. Feed concentration would influence the LEP as well. For example, organic solutes usually reduce the LEP. Gostoli and Sarti [58] reported that by increasing the concentration of ethanol, LEP would linearly decrease. Generally, LEP is related to the nature of

organic matter, its concentration, and feed temperature [59]. Laplace equation (equation 2-1) can be used to determine LEP [60].

$$\Delta P = P_f - P_p = \frac{-2B\gamma_l \cos\theta}{r_{\max}} \quad (2\text{-}1)$$

P_f and P_p are the hydraulic pressure on the feed and permeate side, respectively, B is a geometric pore coefficient (equal to 1 for cylindrical pore), γ_l is liquid surface tension, θ and r_{max} are contact angle (between the solution and membrane surface) and maximum pore size, respectively. For an aqueous solution of NaCl, surface tension depends on the salt concentration (c_f) and can be calculated by equation 2-2 [61].

$$\gamma_l = \gamma_{l,water} + 1.467 c_f \quad (2\text{-}2)$$

$\gamma_{l,water}$ is pure water surface tension and equals to 72 mN/m at 25 °C. Considering equation 2-1, a membrane with a high contact angle (equivalent to high hydrophobicity), small pore size, low surface energy (equivalent to high hydrophobicity), and high surface tension is greatly desired in MD for reaching an appropriate LEP of the feed solution.

2-4-3-2- Membrane Thickness

Permeate flux is inversely related to the membrane thickness. It means a thicker membrane results in a lower permeate flux. It is due to an increase in mass transfer resistance when the membrane becomes thicker, however heat loss would decrease in this case. According to Lagana et al. [62], the optimum membrane thickness is in the range from 30 to 60 μm. Among the MD configurations, membrane thickness has the smallest impact in AGMP, because mass transfer is controlled by stagnant air gap thickness in the arrangement.

2-4-3-3- Porosity and Tortuosity

Porosity (ε) is defined as the ratio of the membrane pores volume to the total volume of the membrane. It varies between 30% and 85% in different membranes [63]. Higher porosity means higher thermal resistance (lower conductive heat loss) and permeability of the MD membranes due to a larger evaporation surface area, and results in an increment in the heat efficiency and flux. Although, mechanical strength decreases by increasing the porosity that brings about a

membrane with a high tendency to crack formation under mild pressures. The Smolder–Franken equation is used for calculating the porosity as follows [64]:

$$\varepsilon = 1 - \frac{\rho_m}{\rho_{pol}} \tag{2-3}$$

Where ρ_m and ρ_{pol} are the densities of membrane and polymer material, respectively.

Tortuosity is a parameter for determining the deviation of the pore structure from a cylindrical shape. Higher tortuosity means a more complicated transportation path and accordingly a smaller permeate flux. Macki-Meares suggested the following relationship between porosity and tortuosity [65].

$$\tau = \frac{(2-\varepsilon)^2}{\varepsilon} \tag{2-4}$$

2-4-3-4- Mean Pore Size and Pore Size Distribution

MD membranes usually have a pore size in the range from 0.1 to 1 μm [17,63]. Permeate flux increases with membrane pore size. Since pore size distribution in a membrane is not uniform, the mean pore size is usually used to characterize the membrane. The membrane pore size should be optimized in such a way that it provides an appropriate flux while not allowing the membrane to become wet. Scanning Electron Microscopy (SEM) and Atomic Force Microscopy (AFM) can be used to determine surface morphology of an MD membrane [16,56,57,66-68]. These analyses are able to estimate the porosity, pore size, and pore size distribution of a membrane. SEM is used to study the top and bottom surface as well as the cross section of the membrane while the sample needs to be gold/carbon sputtered before analysis. However, AFM can be used without sample preparation at ambient pressure and temperature. To measure the maximum and mean pore size besides the pore size distribution, bubble point with gas permeation method can be employed. The procedure has been explored elsewhere [34].

2-4-3-5- Thermal Conductivity

MD demands the membranes with low thermal conductivity because sensible heat transfer increases with thermal conductivity which would further result in a reduction in the permeate

flux as a result of the reduced interface temperature gradient [4]. Thermal conductivity of a membrane (k_m) consists of two contributors, i.e. polymer and gas thermal conductivities (k_{pol} and k_g, respectively). Since the thermal conductivities of air and water vapor are close to each other, it could be assumed that gas inside the pores only consists of a single component, and its thermal conductivity at a temperature close to 40 °C could be calculated by equation 2-5 [21].

$$k_g = 1.5 \times 10^{-3} \sqrt{T} \tag{2-5}$$

Finally, thermal conductivity of a MD membrane can be better estimated by a volume average of the polymer and gas resistances using equation 2-6 [69].

$$k_m = \left(\frac{\varepsilon}{k_g} + \frac{1-\varepsilon}{k_{pol}} \right)^{-1} \tag{2-6}$$

Where k_{pol} depends upon the temperature, degree of crystallinity, and the shape of the crystal. Thermal conductivities of most hydrophobic polymers are close to each other. Equation 2-7 has been suggested to calculate the thermal conductivity of PTFE [6].

$$k_{pol} = 4.86 \times 10^{-4} T + 0.253 \tag{2-7}$$

2-4-3-6- Membrane Fabrication

Among the materials used in membrane fabrication, PTFE has the highest hydrophobicity, good thermal and chemical stability, and oxidation resistance. But due to its relatively high thermal conductivity, it has fairly high heat loss due to conduction. However, PVDF and PP membranes also show appropriate hydrophobicity, thermal and chemical resistance and mechanical strength. New materials such as carbon nanotubes and fluorinated copolymers have been recently developed in membrane fabrication [4].

For membrane fabrication, different methods such as sintering, stretching, and phase inversion are mostly used.

Sintering is used to prepare PTFE membranes. Polymeric powder is pressed into a film or plate and sintered below the melting point. The membranes which are prepared by this method have a porosity within 10%-40% and their typical pore size is in the range from 0.2 to 20 μm [4].

PP and PTFE membranes could be manufactured by using a stretching process. In this method, polymeric layers are formed by extrusion from a polymeric powder at temperatures near the melting point that is combined with a rapid draw-down. The pore size of the membranes fabricated in this way is within 0.2-20 μm and their porosity is around 90% [4].

PVDF membranes could be made by applying phase the inversion method. In this process, a polymeric solution is prepared using an appropriate solvent and cast as a thin layer on non-woven polyester, PP backing material or PP scrim backing supports to make a supported membrane or on a glass plate to generate an unsupported membrane. Afterwards, the cast membrane is immersed in a non-solvent medium such as water, and the solution is converted to two phases (a solid polymer rich phase and a liquid rich phase). The pore size of such a membrane is within 0.2-20 μm while its porosity is approximately 80% [4].

2-5- Transport Phenomena in MD

In an MD process, heat and mass transfers take place in the same direction from the hot to cold side. Feed solution temperature drops by convection mechanism through the feed side boundary layer from T_f to $T_{f,m}$ at the membrane hot surface. Simultaneously, a part of liquid feed molecules are evaporated and transferred across the membrane to the cold permeate side. Along with the mass transfer through the membrane, heat is transported by conduction (sensible heat) and carried by the vapor molecules (latent heat) to the other side. In the cold side, depending on the MD configuration which is used, temperature decreases across the permeate boundary layer from $T_{p,m}$ at the membrane cold surface to a bulk temperature of T_p at the cold plate or stream. Therefore, the driving force for the transport phenomena is the vapor pressure difference between $T_{f,m}$ and $T_{p,m}$.

2-5-1- Mass Transfer in MD

Mass transfer in MD includes three steps. First of all, liquid feed solution vaporizes at the liquid-gas interface. Second, vapor molecules go through the membrane pores towards the cold

interface as a result of vapor pressure difference, and finally, according to the MD configurations, vapor molecules will be condensed in a liquid stream, stagnant or moving gas, or reduced pressure space. Thus, there are two main factors that control mass transfer. The first is the vapor pressure difference and the second is the membrane permeability. Mass transfer in MD is limited by mass transfer across the membrane if fluid dynamics on the hot and cold sides of the membrane shows a good condition with an appropriate turbulency.

A global transport equation for mass transfer through the membrane is given by equation 2-8 that correlates mass flux to vapor pressure difference across the membrane by introducing a membrane coefficient (C_m) that is related to the dominant mechanism for mass transfer in the membrane [6].

$$J = C_m(P_f - P_p) \tag{2-8}$$

Where P_f and P_p are the vapor pressure at the membrane feed and permeate interfaces, respectively, and could be calculated by the Antoine equation [70].

The following should be taken into consideration regarding the mass transfer in the membrane [4]:

1. Since the porosity of a membrane is always less than 100%, the effective area for mass transfer is less than the total area of the membrane.
2. Since the membrane pores do not go straight within the membrane matrix, i.e. a tortuosity of less than unity, vapor molecules travel a longer path than the membrane thickness.
3. Resistance to diffusion increases by the inner walls of the pores due to a decrease in momentum of the vapor molecules.

Regarding the presence or absence of air molecules inside the membrane pores, there are three basic mechanisms which would determine the mass transfer through the membranes: Knudsen diffusion (*K*), Poiseuille or viscous flow (*P*), and Molecular diffusion (*M*). However, a combination of them could also take place which is known as transition mechanism. When Knudsen is applicable, the molecule-pore wall collisions are dominant over molecule-molecule

collisions. Molecular diffusion would be the case when the vapor molecules collide with each other, while a Knudsen/Molecular mechanism happens when the vapor molecules collide with each other, and also diffuse through the air film. In Poiseuille flow (viscous flow), the gas molecules act as a continuous fluid driven by a pressure gradient [6]. To determine which mechanism plays the major role in mass transfer across the membrane, Knudsen number is defined by equation 2-9 as follows [4]:

$$Kn = \frac{\lambda}{d} \tag{2-9}$$

Where λ is the mean free path of the molecules (the average distance which is traveled by a molecule between consecutive collisions), while d is the mean pore size of the membrane. λ is obtained from the kinetic theory and using equation 2-10 [6].

$$\lambda = \frac{k_B T}{\sqrt{2}\pi P d_e^2} \tag{2-10}$$

Where k_B, T, and P are Boltzmann constant, absolute temperature, and average pressure within the membrane pores, respectively. In addition, d_e is the diameter of the molecule.

A large value of *Kn* means that the mean free path of vapor molecules is large in comparison with the membrane mean pore size, while a small amount of *Kn* proves that membrane has a large mean pore size. Table 2-3 shows different situations which may take place in mass transfer through a membrane in different MD configurations.

Table 2-3 Dominant mechanisms in mass transfer across the membrane in different MD configurations

MD Configuration	*Kn*	Mechanism	C_m
DCMD, PGMD, AGMD, and SGMD	Kn >1.0	Knudsen diffusion	$C_{Kn} = \frac{2\pi}{3}\frac{1}{RT}\left(\frac{8RT}{\pi M_W}\right)^{1/2}\frac{r^3}{\tau\delta}$
	0.01< *Kn* <1.0	Transition (Knudsen/Molecular)	$C_T = \frac{\pi}{RT}\frac{1}{\tau\delta}\left[\left(\frac{2}{3}\left(\frac{8RT}{\pi M_W}\right)^{\frac{1}{2}} r^3\right)^{-1} + \left(\frac{PD}{P_{air}} r^2\right)^{-1}\right]^{-1}$
	Kn <0.01	Molecular diffusion	$C_M = \frac{\pi}{RT}\frac{PD}{P_{air}}\frac{r^2}{\tau\delta}$
VMD	*Kn* >10.0	Knudsen diffusion	$C_{Kn} = \frac{2\pi}{3}\frac{1}{RT}\left(\frac{8RT}{\pi M_W}\right)^{1/2}\frac{r^3}{\tau\delta}$
	0.01< *Kn* <10.0	Transition (Knudsen/Poiseuille)	$C_T = \frac{\pi}{RT}\frac{1}{\tau\delta}\left[\left(\frac{2}{3}\left(\frac{8RT}{\pi M_W}\right)^{\frac{1}{2}} r^3\right)^{-1} + \left(\frac{r^4}{8\mu} P_{ave}\right)^{-1}\right]^{-1}$
	Kn <0.01	Poiseuille diffusion	$C_P = \frac{\pi r^4}{8\mu}\frac{P_{ave}}{RT}\frac{1}{\tau\delta}$

In AGMD configuration, mass transfer through the stagnant air is controlled by molecular diffusion and vapor molecules are transferred from the cold surface of membrane to the condensation film by molecular diffusion. The flux in an air gap layer is calculated by equation 2-11.

$$N_{Air\ \ Gap} = \frac{D}{RT}\frac{P}{l_{Air\ \ Gap} P_{lm}}\Delta P_{Air\ \ Gap} = C_{Air\ \ Gap}\Delta P_{Air\ \ Gap} \tag{2-11}$$

The total vapor flux in an AGMD can be estimated via equation 2-12 as follows:

$$N_{Vap-AGMP} = \left(\frac{1}{C_m} + \frac{1}{C_{Air\ \ Gap}} \right)^{-1} \Delta P_{Total} \qquad (2\text{-}12)$$

By considering equation 2-8 and Table 2-3, membrane coefficient is a function of temperature, pressure, membrane structure, and diffusing species, while the driving force (P_f-P_p) is a function of liquid solution temperature and composition at hot and cold membrane surfaces. Furthermore, it could be concluded that in a MD process, flux is enhanced by increasing the pore size and membrane porosity, and by reducing the membrane tortuosity and thickness. Although, when the thickness of membrane decreases, sensible heat loss increases. This suggests that an optimum thickness for the membrane should be found out.

2-5-2- Heat Transfer in MD

Heat transfer from bulk feed to the permeate side involves two steps. First of all, heat is transferred from the hot to cold side through the membrane as sensible heat and latent heat. Sensible heat is conducted across the membrane, while the latent heat is carried by the vapor molecules through the membrane pores. As a result of sensible and latent heat transfer, a temperature difference between the boundary layer and bulk liquid in the hot channel is generated that would result in the second step. In this phase, heat is transferred from the bulk feed to the hot side boundary layer by convection. It is worth mentioning that heat transfer in both steps are equal.

Heat transfer via convection in the feed boundary layer is given by equation 2-13.

$$Q_f = h_f (T_f - T_{f,m}) \qquad (2\text{-}13)$$

Where h_f represents heat transfer coefficient at the feed boundary layer.

Heat transfer across the membrane via conduction and vapor molecules movement is presented by equation 2-14.

$$Q_m = \frac{k_m}{\delta}(T_{f,m} - T_{p,m}) + J\Delta H_v \tag{2-14}$$

Where k_m, δ, J, and ΔH_v are membrane thermal conductivity, membrane thickness, permeate flux, and heat of vaporization, respectively.

$$Q_f = Q_m \qquad \rightarrow \qquad \frac{k_m}{\delta}(T_{f,m} - T_{p,m}) + J\Delta H_v = h_f(T_f - T_{f,m}) \tag{2-15}$$

It should be pointed out that the above equations are used for the heat transfer analysis at the hot side and across the membrane for all of the MD configurations except VMD in where heat conduction in the membrane is not applicable.

Surface temperatures of both sides of the membrane ($T_{f,m}$ and $T_{p,m}$) cannot be obtained experimentally, however, a mathematical iterative model according to equation 2-16 has been proposed by Termpiyakul et al. [71] for their estimation.

$$\begin{cases} T_{f,m} = T_f - \dfrac{J\Delta H_v + k_m(T_{f,m} - T_{p,m})/\delta_m}{h_f} \\ T_{p,m} = T_p - \dfrac{J\Delta H_v + k_m(T_{f,m} - T_{p,m})/\delta_m}{h_p} \end{cases} \tag{2-16}$$

Heat transfer on the permeate side of DCMD, SGMD, and VMD can be simulated by equation 2-17.

$$Q_p = h_p(T_{p,m} - T_p) \tag{2-17}$$

According to equation 2-18, heat transfer on the cold side of AGMD configuration includes two parts. The first is related to heat transfer across the stagnant air gap that occurs by conduction and vapor molecules transportation, and the second is for condensation in the permeate boundary layer. It is worth mentioning that for a PGMD configuration, since the vapor molecules become liquid as soon as they pass through the membrane, the second term related to latent heat in equation 2-18 will be ignored [72].

$$Q_{AG} = \frac{k_{AG}}{l_{AG}}(T_{p,m} - T_{film}) + J\Delta H_v = Q_p = h_p(T_{film} - T_p) \quad (2\text{-}18)$$

It should be noted that heat transfer coefficient (h_p) in the condensate film on a vertical plate is obtained via equation 2-19 [73].

$$h_p = \frac{2}{3}\sqrt{2}\left(\frac{k_{film}^3 \rho^2 g \Delta H_v}{\mu L(T_{film} - T_p)}\right)^{\frac{1}{4}} \quad (2\text{-}19)$$

If the air gap is thicker than 5 mm, free convection would take place between two vertical plates across the air gap region and heat coefficient could then be estimated by equation 2-20 [6].

$$Nu = c(\Pr Gr)^n \left(\frac{l}{L}\right)^{\frac{1}{9}} \quad , \quad \begin{cases} 10^5 < Gr < 10^7 \rightarrow \begin{cases} c = 0.07 \\ n = 1/3 \end{cases} \\ 10^4 < Gr < 10^5 \rightarrow \begin{cases} c = 0.2 \\ n = 1/4 \end{cases} \end{cases} \quad (2\text{-}20)$$

Table 2-4 summarizes the heat transfer in different MD arrangements.

Table 2-4 Heat transfer in different regions of an MD configuration (If there is no resistance in cooling surface)

MD Configuration	Q_f	Q_m	Q_{Gap}	Q_p	Natural Convection
DCMD	$h_f(T_f - T_{f,m})$	$\frac{k_m}{\delta}(T_{f,m} - T_{p,m}) + J\Delta H_v$	-	$h_{p,DCMD}(T_{p,m} - T_p)$	-
PGMD	$h_f(T_f - T_{f,m})$	$\frac{k_m}{\delta}(T_{f,m} - T_{p,m}) + J\Delta H_v$	$\frac{k_{PG}}{l_{PG}}(T_{p,m} - T_p)$	Q_{Gap}	If l>5 mm
AGMD	$h_f(T_f - T_{f,m})$	$\frac{k_m}{\delta}(T_{f,m} - T_{p,m}) + J\Delta H_v$	$\frac{k_{AG}}{l_{AG}}(T_{p,m} - T_{film}) + J\Delta H_v$	$h_p(T_{film} - T_p)$	If l>5 mm
SGMD	$h_f(T_f - T_{f,m})$	$\frac{k_m}{\delta}(T_{f,m} - T_{p,m}) + J\Delta H_v$	$h_A(T_{p,m} - T_{film}) + J\Delta H_v$	$h_p(T_{film} - T_p)$	-
VMD	$h_f(T_f - T_{f,m})$	$J\Delta H_v$	$J\Delta H_v$	$h_p(T_{film} - T_p)$	-

2-5-2-1- Thermal Efficiency and Heat Loss

In an MD process, thermal efficiency (Π) is defined as the ratio of latent heat of vaporization to the total (latent and sensible) heat [6]. Usually, thermal efficiency is enhanced by increasing the feed temperature, feed flow rate, and membrane thickness. On the other hand, it would decrease with an increase in feed concentration [74]. Equations 2-21 and 2-22 are used to calculate the thermal efficiency of a DCMD and AGMD process [18], respectively.

$$\Pi = \frac{J\Delta H_v}{\frac{k_m}{\delta}(T_{f,m} - T_{p,m}) + J\Delta H_v} \tag{2-21}$$

$$\Pi = 1 - \frac{\alpha T_a^{-2.1}}{\lambda}\left(\frac{(T_f - T_p)c_p}{\alpha T_a^{-2.1} + \beta} + \frac{k_a}{l}\right) \tag{2-22}$$

α and β are obtained experimentally for an air gap distance less than 5 mm, and T_a is the average MD temperature between 30 and 80 °C [75]. The c_p and k_a are specific heat and air gap thermal conductivity, respectively.

According to Martínez-Díez et al. [76], heat loss reduces by increasing the feed temperature and flow rate. Three sources of heat loss in an MD configuration are: 1) presence of air inside the membrane pores, 2) heat loss across the membrane via conduction, and 3) heat loss due to temperature polarization. To minimize heat loss in MD, degassing of feed solution, increasing the membrane thickness, setting up an air gap between the membrane and the condensation surface, and working in a turbulent regime have been suggested [6]. Using heat recovery in MD would result in better performance for the process, however it would need an external heat exchanger and a membrane with larger area that increases the capital costs.

2-5-3- Temperature and Concentration Polarization

In an MD process, the feed solution is evaporated at the membrane hot surface that would create a heat transfer boundary layer on the hot side. In addition, by condensing the vapor molecules in the other side, the permeate heat transfer boundary layer would also be established on the cold

side. The presence of boundary layers would bring about a temperature difference between the liquid-vapor interface and bulk fluids that is known as temperature polarization. It is estimated by equation 2-23 as follows:

$$\psi = \frac{T_{m,f} - T_{m,p}}{T_f - T_p} \tag{2-23}$$

For a VMD configuration, temperature polarization is characterized based upon equation 2-24 [17]:

$$\psi = \frac{T_f - T_{m,f}}{T_f - T_p} \tag{2-24}$$

Temperature polarization represents the effect of heat transfer boundary layers on total heat transfer resistance of the system [6]. It means by reducing the boundary layer resistances, the temperature difference between the liquid-vapor interface and bulk fluids becomes smaller and ψ approaches 1. In addition, if the heat transfer is controlled by the boundary layer resistances, system demonstrates a high degree of temperature polarization and ψ approaches zero. According to Alkhudhiri et al. [6], for DCMD arrangement, ψ is within 0.4-0.7. It is noteworthy mentioning that the temperature polarization is more important at high concentration, high temperature, and low feed velocity, when the boundary layer resistances become greater. Typically, by making the fluids more turbulent using a spacer, temperature polarization would be reduced.

Concentration polarization is defined according to equation 2-25 as the ratio of solute concentration on the membrane surface to that of the bulk feed, and is symbolized by Φ.

$$\Phi = \frac{c_m}{c_f} \tag{2-25}$$

Solute concentration on the membrane surface is obtained via equation 2-26 [6]:

$$c_m = c_f \exp\left(\frac{j}{\rho K}\right) \tag{2-26}$$

Where, ρ and K are the liquid density and mass transfer coefficient, respectively.

Since the accumulated solute on the membrane surface generates a diffusive flow back to the feed [6], concentration polarization and fouling should be taken into account in modeling purposes, and vapor flux cannot be only estimated by Knudsen, molecular, and Poiseuille flow mechanisms, due to the differences between the properties of boundary layer at the membrane surface and the bulk solution.

2-5-4- Fouling

Fouling is related to the creation of an additional layer on the membrane surface from the components which are present in the liquid solution. The additional layer could be due to biological fouling (by bacteria) or scaling as a result of high concentration solutions. Fouling and scaling would result in the blockage of the membrane pores, which would further reduce the effective area of the membrane, and finally decrease the permeate flux. Furthermore, the additional film acts as an extra resistance against heat transfer. Moreover, it may cause a pressure drop and severe temperature polarization effect.

Equation 2-27 is used to estimate the heat transfer in the additional layer that is generated as a result of fouling. Heat is transported through the layer via conduction.

$$Q_{fouling} = \frac{k_{fouling}}{\delta_{fouling}}(T_{f,fouling} - T_{f,m}) \qquad (2\text{-}27)$$

Fouling highly depends upon membrane and feed solution properties, module geometry, and operating conditions [77]. It can be inhibited by using pre-treatment methods or membrane cleaning. In addition, working at low temperature with high feed flow rate would bring about a decrease in tendency to fouling.

2-5-5- Operating Parameters

There are several parameters that influence vapor flux in an MD configuration, including:

2-5-5-1- Feed Temperature

Since vapor pressure increases exponentially with temperature according to the Antoine equation, considering equation 2-8, by increasing the feed temperature, permeate flux would exponentially increase. Srisurichan et al. [65] reported that using a feed solution of high temperature would increase the mass transfer coefficient in the membrane. Furthermore, it has been reported that by increasing the feed temperature, temperature polarization would decrease [69].

2-5-5-2- Permeate Temperature

Permeate flux decreases with an increase in permeate temperature, however, because vapor pressure variation with temperature is insignificant at low temperatures, the cold side temperature has smaller effects on permeate flux compared to the feed temperature [6].

2-5-5-3- Feed Concentration

By increasing the feed concentration, vapor pressure decreases, temperature polarization increases, and feed viscosity would exponentially increase which results in a reduction in driving force and eventually, a decrease in the permeate flux [6].

2-5-5-4- Feed Flow Rate

By increasing the feed flow rate or its velocity, turbulence increases that reduces hydrodynamic boundary layer thickness and subsequently, temperature polarization that would eventually result in an increment in convective heat transfer coefficient. Therefore, permeate flux would increase. The effects of feed flow rate on permeate flux are more significant at higher temperatures [6].

2-5-5-5- Air Gap Thickness

Permeate flux declines linearly by increasing the air gap distance in AGMD module [17]. Temperature gradient across the gap decreases by reducing the air gap thickness that results in the permeate flux enhancement.

2-5-5-6- Membrane Properties

Permeate flux increases with membrane porosity, while it is inversely proportional to the membrane tortuosity and thickness. In addition, membranes with larger pore size show a higher

flux, and the presence of backing material is favorable in mechanically stabilizing the membrane, although has a negative effect on vapor flux through the membrane.

2-6- Conclusion

Considering the contents above, membrane distillation (MD) is an emerging technology that has not yet been totally commercialized due to the expensive low performance MD membranes besides the huge thermal energy consumption throughout the process which would bring about a more expensive final product compared to the other membrane-based processes such as reverse osmosis. To overcome these problems, thermal energy consumption in MD needs to be optimized, while thermal energy input should be replaced by big sources of available cheap energy such as industrial waste heat. Moreover, novel MD membranes need to be developed which are appropriate in terms of permeability, selectivity, chemical and mechanical stability, and durability to further reduce the cost of the final product. To this end, nanocomposite membranes have been demonstrated to be suitable in improving the performance of the MD membranes. Nonetheless, Memsys has successfully developed a commercial MD module for salt water desalination [32]. The module uses novel concepts such as using a low grade heat for steam raiser stage (feed temperature lies between 50 and 80 °C), applying approximately high vacuum to the entire system (0.1-0.3 bar), and employing an internal heat recycling system to reduce the amount of thermal energy consumption.

References

[1] M. FINDLEY. Vaporization through Porous Membranes. Industrial & Engineering Chemistry Process Design and Development, 6 (1967) 226.

[2] A. Alklaibi, N. Lior. Membrane-distillation desalination: status and potential. Desalination, 171 (2005) 111.

[3] W.T. Hanbury, T. Hodgkiess. Membrane distillation - an assessment. Desalination, 56 (1985) 287.

[4] L.M. Camacho, L. Dumee, J. Zhang, J. Li, M. Duke, J. Gomez, et al. Advances in Membrane Distillation for Water Desalination and Purification Applications. Water, 5 (2013) 94.

[5] K. Smolders, A.C.M. Franken. Terminology for Membrane Distillation. Desalination, 72 (1989) 249.

[6] A. Alkhudhiri, N. Darwish, and N. Hilal. Membrane distillation: A comprehensive review. Desalination, 287 (2012) 2.

[7] J. Zuo, S. Bonyadi, and T. Chung. Exploring the potential of commercial polyethylene membranes for desalination by membrane distillation. J.Membr.Sci., 497 (2016) 239.

[8] S. Goh, J. Zhang, Y. Liu, and A.G. Fane. Membrane Distillation Bioreactor (MDBR) - A lower Green-House-Gas (GHG) option for industrial wastewater reclamation. Chemosphere, 140 (2015) 129.

[9] K.C. Wijekoon, F.I. Hai, J. Kang, W.E. Price, W. Guo, H.H. Ngo, et al. A novel membrane distillation-thermophilic bioreactor system: Biological stability and trace organic compound removal. Bioresour.Technol., 159 (2014) 334.

[10] K. Gethard, S. Mitra. Carbon nanotube enhanced membrane distillation for online preconcentration of trace pharmaceuticals in polar solvents. Analyst, 136 (2011) 2643.

[11] G. Zakrzewska-Trznadel, M. Harasimowicz, and A.G. Chmielewski. Concentration of radioactive components in liquid low-level radioactive waste by membrane distillation. J.Membr.Sci., 163 (1999) 257.

[12] U.K. Kesieme, H. Aral, M. Duke, N. Milne, and C.Y. Cheng. Recovery of sulphuric acid from waste and process solutions using solvent extraction. Hydrometallurgy, 138 (2013) 14.

[13] M. Gryta, A. Morawski, and M. Tomaszewska. Ethanol production in membrane distillation bioreactor. Catalysis Today, 56 (2000) 159.

[14] M. Tomaszewska, M. Gryta, and A. Morawski. Recovery of hydrochloric acid from metal pickling solutions by membrane distillation. Separation and Purification Technology, 22-3 (2001) 591.

[15] M. Tomaszewska. Membrane distillation - Examples of applications in technology and environmental protection. Polish Journal of Environmental Studies, 9 (2000) 27.

[16] M. Baghbanzadeh, D. Rana, T. Matsuura, and C.Q. Lan. Effects of hydrophilic CuO nanoparticles on properties and performance of PVDF VMD membranes. Desalination, 369 (2015) 75.

[17] K.W. Lawson, D.R. Lloyd. Membrane distillation. J.Membr.Sci., 124 (1997) 1.

[18] L. Martínez, F.J. Florido-Díaz. Theoretical and experimental studies on desalination using membrane distillation. Desalination, 139 (2001) 373.

[19] M.N. Chernyshov, G.W. Meindersma, and A.B. de Haan. Comparison of spacers for temperature polarization reduction in air gap membrane distillation. Desalination, 183 (2005) 363.

[20] G.W. Meindersma, C.M. Guijt, and A.B. de Haan. Desalination and water recycling by air gap membrane distillation. Desalination, 187 (2006) 291.

[21] A.-. Jönsson, R. Wimmerstedt, and A.-. Harrysson. Membrane distillation - a theoretical study of evaporation through microporous membranes. Desalination, 56 (1985) 237.

[22] A.M. Alklaibi, N. Lior. Membrane-distillation desalination: Status and potential. Desalination, 171 (2005) 111.

[23] K. Tarnacki, M. Meneses, T. Melin, J. van Medevoort, and A. Jansen. Environmental assessment of desalination processes: Reverse osmosis and Memstill®. Desalination, 296 (2012) 69.

[24] G.W. Meindersma, C.M. Guijt, and A.B. de Haan. Desalination and water recycling by air gap membrane distillation. Desalination, 187 (2006) 291.

[25] A. Cipollina, M.G. Di Sparti, A. Tamburini, and G. Micale. Development of a Membrane Distillation module for solar energy seawater desalination. Chem.Eng.Res.Design, 90 (2012) 2101.

[26] M.C. García-Payo, C.A. Rivier, I.W. Marison, and U. von Stockar. Separation of binary mixtures by thermostatic sweeping gas membrane distillation: II. Experimental results with aqueous formic acid solutions. J.Membr.Sci., 198 (2002) 197.

[27] M. Khayet, P. Godino, and J.I. Mengual. Nature of flow on sweeping gas membrane distillation. J.Membr.Sci., 170 (2000) 243.

[28] S. Bandini, C. Gostoli, and G.C. Sarti. Separation efficiency in vacuum membrane distillation. J.Membr.Sci., 73 (1992) 217.

[29] G.C. Sarti, C. Gostoli, and S. Bandini. Extraction of organic components from aqueous streams by vacuum membrane distillation. J.Membr.Sci., 80 (1993) 21.

[30] M. Rzechowicz, R.M. Pashley. A membrane method for degassing nonaqueous liquids. J.Colloid Interface Sci., 298 (2006) 321.

[31] M. Rzechowicz, R.M. Pashley. The effect of de-gassing on the efficiency of reverse osmosis filtration. J.Membr.Sci., 295 (2007) 102.

[32] K. Zhao, W. Heinzl, M. Wenzel, S. Büttner, F. Bollen, G. Lange, et al. Experimental study of the memsys vacuum-multi-effect-membrane-distillation (V-MEMD) module. Desalination,.

[33] W. Heinzl, S. Buettner, and G. Lange. Industrialized modules for MED Desalination with polymer surfaces. Desalination and Water Treatment, 42 (2012) 177.

[34] M. Khayet, T. Matsuura. Pervaporation and vacuum membrane distillation processes: Modeling and experiments. AIChE J., 50 (2004) 1697.

[35] S.-. Andersson, N. Kjellander, and B. Rodesjö. Design and field tests of a new membrane distillation desalination process. Desalination, 56 (1985) 345.

[36] K. Schneider, W. Hölz, R. Wollbeck, and S. Ripperger. Membranes and modules for transmembrane distillation. J.Membr.Sci., 39 (1988) 25.

[37] H. Guo, Y. Wyart, J. Perot, F. Nauleau, and P. Moulin. Low-pressure membrane integrity tests for drinking water treatment: A review. Water Res., 44 (2010) 41.

[38] W.T. Johnson. Predicting log removal performance of membrane systems using in-situ integrity testing. Filtration Sep., 35 (1998) 26.

[39] F. Banat, N. Jwaied, M. Rommel, J. Koschikowski, and M. Wieghaus. Desalination by a "compact SMADES" autonomous solarpowered membrane distillation unit. Desalination, 217 (2007) 29.

[40] L. Song, Z. Ma, X. Liao, P.B. Kosaraju, J.R. Irish, and K.K. Sirkar. Pilot plant studies of novel membranes and devices for direct contact membrane distillation-based desalination. J.Membr.Sci., 323 (2008) 257.

[41] S. Bonyadi, T.S. Chung. Flux enhancement in membrane distillation by fabrication of dual layer hydrophilic–hydrophobic hollow fiber membranes. J.Membr.Sci., 306 (2007) 134.

[42] S. Bonyadi, T. Chung. Highly porous and macrovoid-free PVDF hollow fiber membranes for membrane distillation by a solvent-dope solution co-extrusion approach. J.Membr.Sci., 331 (2009) 66.

[43] M. Baghbanzadeh, D. Rana, C.Q. Lan, and T. Matsuura. Effects of Inorganic Nano-Additives on Properties and Performance of Polymeric Membranes in Water Treatment. Separation & Purification Reviews, 45 (2016) 141.

[44] Y. Wang, J. Zhu, H. Huang, and H. Cho. Carbon nanotube composite membranes for microfiltration of pharmaceuticals and personal care products: Capabilities and potential mechanisms. J.Membr.Sci., 479 (2015) 165.

[45] A.M. Ferreira, E.B. Roque, F.V. da Fonseca, and C.P. Borges. High flux microfiltration membranes with silver nanoparticles for water disinfection. Desalination and Water Treatment, 56 (2015) 3590.

[46] R. Ding, H. Zhang, Y. Li, J. Wang, B. Shi, H. Mao, et al. Graphene oxide-embedded nanocomposite membrane for solvent resistant nanofiltration with enhanced rejection ability. Chemical Engineering Science, 138 (2015) 227.

[47] T. Arumugham, N.J. Kaleekkal, D. Rana, and M. Doraiswamy. Separation of oil/water emulsions using nano MgO anchored hybrid ultrafiltration membranes for environmental abatement. J Appl Polym Sci, 133 (2016).

[48] E. Bet-moushoul, Y. Mansourpanah, K. Farhadi, and M. Tabatabaei. TiO2 nanocomposite based polymeric membranes: A review on performance improvement for various applications in chemical engineering processes. Chem.Eng.J., 283 (2016) 29.

[49] D. Emadzadeh, W.J. Lau, M. Rahbari-Sisakht, H. Ilbeygi, D. Rana, T. Matsuura, et al. Synthesis, modification and optimization of titanate nanotubes-polyamide thin film nanocomposite (TFN) membrane for forward osmosis (FO) application. Chem.Eng.J., 281 (2015) 243.

[50] D. Qin, Z. Liu, D.D. Sun, X. Song, and H. Bai. A new nanocomposite forward osmosis membrane custom-designed for treating shale gas wastewater. Scientific Reports, 5 (2015).

[51] A.S. Al-Hobaib, K.M. AL-Sheetan, M.R. Shaik, N.M. Al-Andis, and M.S. Al-Suhybani. Characterization and Evaluation of Reverse Osmosis Membranes Modified with Ag2O Nanoparticles to Improve Performance. Nanoscale Research Letters, 10 (2015).

[52] A.M.A. El-Aassar. Improvement of reverse osmosis performance of polyamide thin-film composite membranes using TiO2 nanoparticles. Desalination and Water Treatment, 55 (2015) 2939.

[53] K. Gethard, O. Sae-Khow, and S. Mitra. Water Desalination Using Carbon-Nanotube-Enhanced Membrane Distillation. Acs Applied Materials & Interfaces, 3 (2011) 110.

[54] D. Hou, J. Wang, X. Sun, Z. Ji, and Z. Luan. Preparation and properties of PVDF composite hollow fiber membranes for desalination through direct contact membrane distillation. J.Membr.Sci., 405 (2012) 185.

[55] D. Hou, G. Dai, H. Fan, J. Wang, C. Zhao, and H. Huang. Effects of calcium carbonate nano-particles on the properties of PVDF/nonwoven fabric flat-sheet composite membranes for direct contact membrane distillation. Desalination, 347 (2014) 25.

[56] J.E. Efome, M. Baghbanzadeh, D. Rana, T. Matsuura, and C.Q. Lan. Effects of superhydrophobic SiO2 nanoparticles on the performance of PVDF flat sheet membranes for vacuum membrane distillation. Desalination, 373 (2015) 47.

[57] M. Baghbanzadeh, D. Rana, C.Q. Lan, and T. Matsuura. Effects of hydrophilic silica nanoparticles and backing material in improving the structure and performance of VMD PVDF membranes. Separation and Purification Technology, 157 (2016) 60.

[58] C. Gostoli, G.C. Sarti. Separation of liquid mixtures by membrane distillation. J.Membr.Sci., 41 (1989) 211.

[59] M.C. GarcÄ±´a-Payo, M.A. Izquierdo-Gil, and C. FernÃ¡ndez-Pineda. Wetting Study of Hydrophobic Membranes via Liquid Entry Pressure Measurements with Aqueous Alcohol Solutions. J.Colloid Interface Sci., 230 (2000) 420.

[60] A.C.M. Franken, J.A.M. Nolten, M.H.V. Mulder, D. Bargeman, and C.A. Smolders. Wetting criteria for the applicability of membrane distillation. J.Membr.Sci., 33 (1987) 315.

[61] J. Zhang, N. Dow, M. Duke, E. Ostarcevic, J. Li, and S. Gray. Identification of material and physical features of membrane distillation membranes for high performance desalination. J.Membr.Sci., 349 (2010) 295.

[62] F. Laganà, G. Barbieri, and E. Drioli. Direct contact membrane distillation: modelling and concentration experiments. J.Membr.Sci., 166 (2000) 1.

[63] M.S. El-Bourawi, Z. Ding, R. Ma, and M. Khayet. A framework for better understanding membrane distillation separation process. J.Membr.Sci., 285 (2006) 4.

[64] M. Khayet, T. Matsuura. Preparation and characterization of polyvinylidene fluoride membranes for membrane distillation. Ind Eng Chem Res, 40 (2001) 5710.

[65] S. Srisurichan, R. Jiraratananon, and A.G. Fane. Mass transfer mechanisms and transport resistances in direct contact membrane distillation process. J.Membr.Sci., 277 (2006) 186.

[66] Z. Chen, D. Rana, T. Matsuura, D. Meng, and C.Q. Lan. Study on structure and vacuum membrane distillation performance of PVDF membranes: II. Influence of molecular weight. Chem.Eng.J., 276 (2015) 174.

[67] J.C. Mierzwa, C.D. Vecitis, J. Carvalho, V. Arieta, and M. Verlage. Anion dopant effects on the structure and performance of polyethersulfone membranes. J.Membr.Sci., 421 (2012) 91.

[68] Y. Yang, D. Rana, T. Matsuura, S. Zheng, and C.Q. Lan. Criteria for the selection of a support material to fabricate coated membranes for a life support device. Rsc Advances, 4 (2014) 38711.

[69] J. Phattaranawik, R. Jiraratananon, and A.G. Fane. Heat transport and membrane distillation coefficients in direct contact membrane distillation. J.Membr.Sci., 212 (2003) 177.

[70] F.A. Banat, J. Simandl. Theoretical and Experimental-Study in Membrane Distillation. Desalination, 95 (1994) 39.

[71] P. Termpiyakul, R. Jiraratananon, and S. Srisurichan. Heat and mass transfer characteristics of a direct contact membrane distillation process for desalination. Desalination, 177 (2005) 133.

[72] A. Cipollina, M.G. Di Sparti, A. Tamburini, and G. Micale. Development of a Membrane Distillation module for solar energy seawater desalination. Chemical Engineering Research & Design, 90 (2012) 2101.

[73] S. Kimura, S. Nakao, and S. Shimatani. Transport phenomena in membrane distillation. J.Membr.Sci., 33 (1987) 285.

[74] S. Al-Obaidani, E. Curcio, F. Macedonio, G. Di Profio, H. Al-Hinai, and E. Drioli. Potential of membrane distillation in seawater desalination: Thermal efficiency, sensitivity study and cost estimation. J.Membr.Sci., 323 (2008) 85.

[75] G.L. Liu, C. Zhu, C.S. Cheung, and C.W. Leung. Theoretical and experimental studies on air gap membrane distillation. Heat and Mass Transfer, 34 (1998) 329.

[76] L. Martínez-Díez, F.J. Florido-Díaz, and M.I. Vázquez-González. Study of evaporation efficiency in membrane distillation. Desalination, 126 (1999) 193.

[77] S. Shirazi, C. Lin, and D. Chen. Inorganic fouling of pressure-driven membrane processes — A critical review. Desalination, 250 (2010) 236.

Chapter 3:

Zero thermal input membrane distillation, a zero-waste and sustainable solution for fresh water shortage

M. Baghbanzadeh, D. Rana, C. Q. Lan, T. Matsuura, Zero thermal input membrane distillation, a zero-waste and sustainable solution for fresh water shortage, Applied Energy, 187 (2017) 910-928.

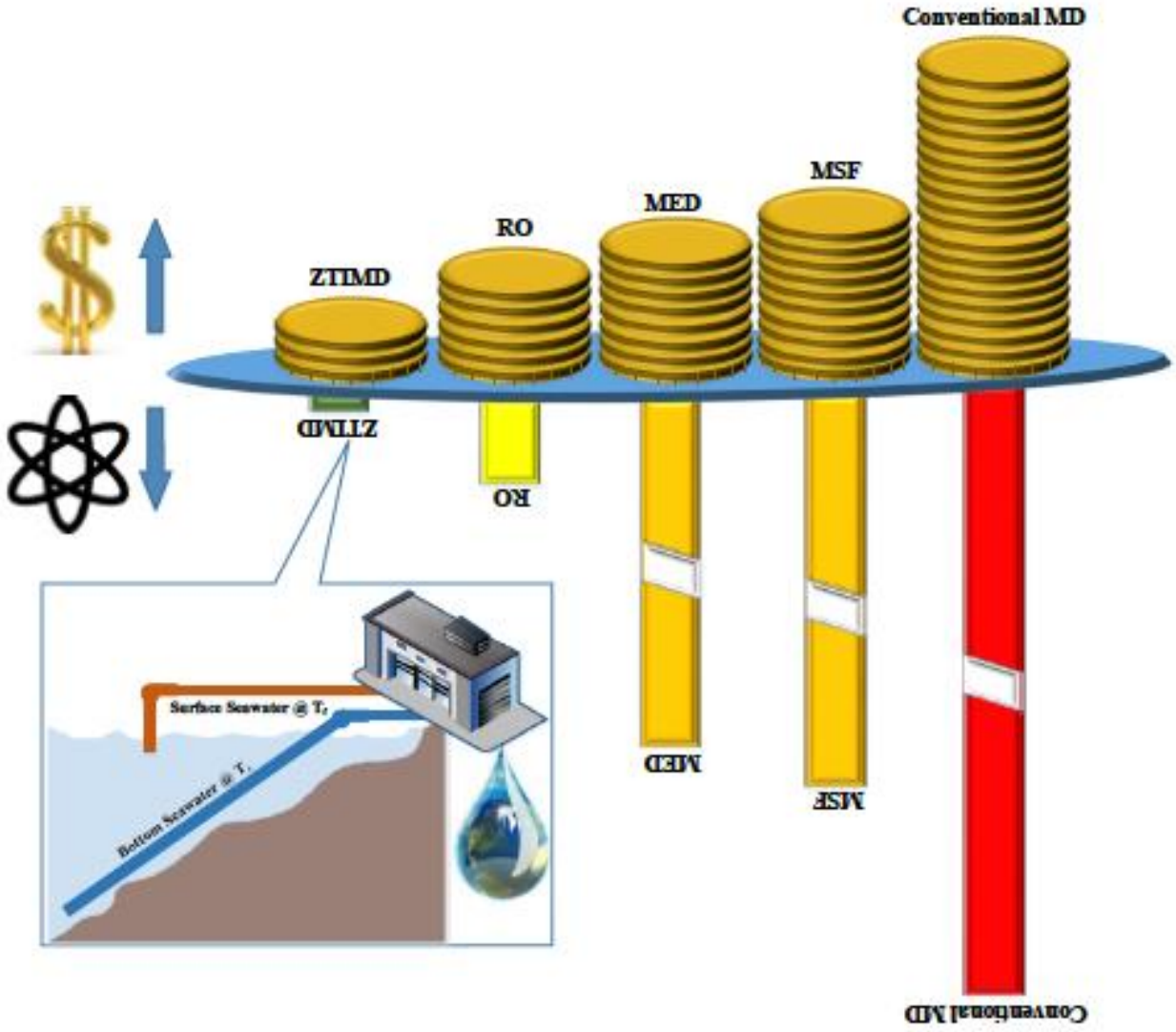
Conventional MD
MSF
MED
RO
ZTIMD
Surface Seawater @ T
Bottom Seawater @ T

Zero thermal input membrane distillation, a zero-waste and sustainable solution for freshwater shortage

Mohammadali Baghbanzadeh, Dipak Rana, Christopher Q. Lan*, Takeshi Matsuura

Department of Chemical and Biological Engineering, University of Ottawa, 161 Louis Pasteur Private, Ottawa, Ontario, Canada K1N 6N5

Abstract

The innovative concept of a zero-waste, energy efficient, and therefore sustainable desalination strategy, Zero Thermal Input Membrane Distillation (ZTIMD), is demonstrated to be economically more effective than existing seawater desalination technologies by simulation based on a single-pass Direct Contact Membrane Distillation process using surface seawater as the feed and bottom seawater as the coolant. Thermal energy required for water distillation in the process was satisfied by extracting the enthalpy of the surface seawater using the bottom seawater as the heat sink. Under one of the favorable conditions, the proposed ZTIMD process could produce pure water with a cost of \$0.28/m^3 at a specific energy consumption of 0.45 kWh/m^3, which is significantly lower than that of the major existing seawater desalination processes, including the currently dominating technology, Reverse Osmosis (\$0.45-2.00/m^3). Some major advantages promised by the ZTIMD include 1) With no requirement of external thermal energy input, ZTIMD is an inherently energy-saving process, 2) it is economically competitive to existing desalination technologies, and 3) it is waste-free.

*Corresponding author. Tel.: 1 613 562 5800x2050.
E-mail address:Christopher.Lan@uottawa.ca (C.Q. Lan)

Keywords: Membrane distillation; Zero thermal energy input; Waste-free; Desalination; Feasibility;

3-1- Introduction

Water scarcity due to population, agricultural, industrial growth and urbanization, which is further intensified by global warming and widespread droughts, has become a serious threat all over the world. Currently, one third of the global population is in short of clean water, and it is anticipated that over 1.8 billion people would experience absolute water shortage and two third of the population would be under water stress by 2025 worldwide *[1,2]*. Almost 70% of the earth surface is covered by water *[3]*, however, only 2.5% of that water is deemed to be usable as freshwater *[4]*. Recovering freshwater from undrinkable water bodies such as oceans and brackish waters by means of desalination has become increasingly important over the past few decades *[5-16]*. For instance, Singapore is planning to increase the share of desalination in their water supply market from 10% at present to 30% by 2061. China is expected to roughly quadruple their current desalination capacity by 2020. In California, the largest desalination plant in the western hemisphere will produce 50 million gallons of drinkable water every day from pacific seawater with an investment of $1 billion by 2016 *[1]*. According to a recent analysis by Frost & Sullivan, the global desalination capacity is predicted to double by 2020 *[17]*.

At present, desalination itself is not sustainable due to its consumption of extremely large quantities of energy, mainly fossil fuels *[16,18]*. As an example, Saudi Arabia with the largest desalination market in the world at a share of 17% *[1]*, consumes 1.5 million barrels of oil every day to generate a daily desalinated water of 3.3 million m^3 *[19]*. This oil-for-water strategy is making freshwater the new oil in reference to its unsustainability *[1]*. It is of interest to mention

that late Richard Smalley, a Nobel laureate of 1996 in chemistry, listed "energy" and "water" as the first and second among the top 10 problems facing the humanity for the next 50 years *[19]*. It has been argued that the use of renewable energy such as solar *[20-23]*, geothermal *[24,25]*, wind *[26,27]*, and tidal *[28,29]* for desalination would result in longer-term sustainable water supply. However, such a desalination process is not economically affordable at large scale up to now despite of the extensive efforts worldwide *[20,30,31]*.

The global desalination market is currently dominated by Reverse Osmosis (RO) *[3,9,32-38]* since it demands much less specific energy than thermal desalination processes *[39-42]*. Nevertheless, the 3-4 kWh/m^3 *[19,43-46]* specific energy consumption of RO still accounts for about 40% of the overall cost of the final product, which shows the process to be still quite energy intensive *[43]*. Furthermore, exergy analysis shows that remarkable irreversibility takes place in RO processes *[47-50]* and the aforementioned typical energy consumption in RO is approximately 600% more than the thermodynamic minimum energy required to reduce the salt concentration of seawater from 35,000 mg/L to that of drinkable water, i.e., 300 mg/L, at a water recovery of 40% *[51]*. In practice, commercial RO processes usually work at a water recovery in the range of 40-60%, which would generate even larger irreversibility. Other challenges in association with RO include its high operational pressure, sensitivity to the quality of raw feed, need for extensive feed pre-treatment, and the fouling and scaling problems *[9,34,52-54]*.

Membrane Distillation (MD) is considered as the most promising emerging technology which has the potential to compete with RO in the desalination market *[9,33]*. MD has important advantages that set it apart from other desalination technologies. These include 1) nearly complete salt rejection even at high salt concentration of feed where RO normally fails, 2)

possibility of using low grade heat, 3) ability of working at high water recoveries, 4) low tendency to fouling and scaling which would result in lower operation and maintenance costs and environmental impacts, and 5) chemical pre-treatment of the feed might be eliminated due to the mild operating conditions *[9,33,55-60]*. In addition, exergy analysis indicates that MD would be more appropriate if waste heat is available *[50]*.

Nevertheless, MD has not yet been industrialized as a stand-alone desalination process at large scale and related studies have mostly focused on integrating MD as part of a hybrid process such as RO/MD and nanofiltration (NF)/RO/MD, where MD is utilized to achieve high overall water recovery that is not realistic with RO or NF/RO *[61,62]*. One of the main constraints of conventional MD desalination is its requirement of large quantities of thermal energy input to pre-heat the feed *[62]*, which might be in the range of 600-9080 kWh/m^3 *[21]*.

Extensive efforts have been made to reduce the costs or increase the sustainability of energy for MD desalination, and different approaches have been proposed including 1) use of low grade heat such as waste heat from industrial facilities *[63,64]*, 2) use of renewable energy such as solar energy *[30,65]* and geothermal energy *[25]*, and 3) introducing new configurations designed to partially recover the thermal energy *[62,66,67]*.

Only a few techno-economic studies on MD desalination process are available in the literature, which provide valuable information on the key contributors to costs and the overall competence of the technology *[21,25,57,65,68,69]*. Al-Obaidani et al. *[57]* reported pure water costs of \$1.17/m^3 and \$1.25/m^3 for a Direct Contact Membrane Distillation (DCMD) process with and without heat recovery, respectively. For the DCMD plant without heat recovery, the authors showed that almost 61% of the operation and maintenance costs are spent to generate steam for

heating purpose. Therefore, one could considerably reduce the total water costs by reducing or eliminating the heat requirement. It was estimated that the pure water production cost via a DCMD process would drop to \$0.64/m^3 if the required thermal energy is obtained from a zero-cost source such as waste heat *[57]*, and MD would become quite competitive with the RO desalination process as a result. According to the data in the literature, pure water cost via Seawater RO (SWRO) varies between \$0.45/m^3 and \$2.00/m^3 in different areas of the world *[62,70]*. It has also been reported that the integration of MD and cheap industrial waste heat could result in a huge reduction in pure water production cost which might be as low as \$0.26/m^3 *[62,71]*. However, it is apparent that only in very limited circumstances industrial waste heat would be available at a rate that could fulfill the energy demand of a large scale MD desalination plant *[62]*.

To this end, seawater is a natural heat reservoir that promises to match any possible scale of desalination operations. However, to extract the enthalpy of seawater, a heat sink of a lower temperature is needed. Fortunately, the sea has the answer in itself, i.e., the low temperature bottom seawater. In a tropical region, the average surface and bottom seawater temperatures could be typically at around 30 °C and 10 °C (depending upon the depth), respectively *[72,73]*. The temperature difference between the seawater at the surface and bottom provides the basis for the proposed concept of Zero Thermal Input Membrane Distillation (ZTIMD).

This work establishes the feasibility of the novel concept of ZTIMD for cost-effective, energy-saving, and zero-waste stand-alone MD for large scale seawater desalination. It is demonstrated that, by using bottom seawater as the coolant, the huge thermal energy stored in surface seawater could be extracted for efficient MD, which eliminates the need for external thermal energy input, making it both energy efficient and cost-effective. Furthermore, this process would be able to

avoid discharging high concentration brines into the seawater, alleviating a common environmental liability of large scale seawater desalination plants, i.e. the increase of salinity of local seawater that threatens the aquatic ecosystem *[74,75]*. In addition, the moderate operational conditions of ZTIMD, including low transmembrane pressure and low water recovery, removing the need of chemical pre-treatment, which is required for RO, and therefore avoid discharge of waste chemicals into the environment. This is the first attempt to exploit the abundant thermal energy stored in surface seawater for sustainable MD desalination. The successful implementation of this strategy is expected to revolutionize the seawater desalination industry.

3-2- Methodologies

3-2-1- Zero Thermal Input Membrane Distillation (ZTIMD)

As shown in Fig. 3-1, a ZTIMD process could be a single stage DCMD process with an external heat exchanger to reject heat to the bottom seawater, and a storage tank to collect the product fresh water. Underwater piping is needed for the coolant to be pumped up from the bottom of the sea. As a practical example, a region in Gulf of Oman close to the Strait of Hormuz is considered as a case study in this paper. According to Fig. 3-1-a, seawater at a temperature of 10 °C is available at the depth of approximately 800 m from the surface. Water of even lower temperature would be accessible at deeper locations *[72,76]*.

Thermal energy consumption and membrane costs are two major contributors to the water production cost in a conventional MD desalination process. While the ZTIMD is a free thermal input process, working at extremely low recovery ratios, which is required to avoid external thermal energy inputs, would result in demand on large amounts of raw feed. As a consequence, pre-treatment may become a relatively expensive entity if an intense pre-treatment step similar to

that in RO is to be used. Fortunately, MD works at very small or, practically zero trans-membrane pressure and would less likely suffer from severe fouling, which justifies a much simpler pre-treatment *[60,68,77]*. In fact, it has been accepted that chemical pre-treatment could be disregarded for MD and the pre-treatment can be simplified to only cartridge filtration of the raw seawater *[68]*. Furthermore, it was reported that lower feed temperatures could potentially reduce the fouling tendency in a DCMD process *[62]*. Therefore, it would be even more so in ZTIMD since it works at very low temperatures (approximately 30 °C) in comparison with that in conventional MD (60-80 °C). In addition, the low working temperature may help minimize thermal aging of MD membranes and therefore elongate the durability of membrane for reduced production costs.

It should be pointed out that, since sensible heat of the feed is absorbed for water evaporation in a MD process, approximately 5.4 °C temperature decrease is associated with a water recovery of 1%. As a result, the temperature difference of 20 °C between the surface seawater and bottom seawater would allow only a water recovery of less than 4%. Going beyond this water recovery would require the heating of the concentrated brine by external thermal energy input for more passes to the incremental increase of water recovery. This is a small water recovery compared to the common practice in RO, which usually have a water recovery of 40-60% or even higher. In other words, a ZTIMD process is necessarily a single-pass MD process with a low water recovery. This small water recovery presents a unique advantage since it will make the concentration difference between the discharged concentrate and the natural seawater to be negligible, while the discharge of high concentration brines into the seawater on site has been an environmental liability to conventional desalination processes such as SWRO *[41,53,57,61,62,78,79]*. Furthermore, working at very low recovery ratios will considerably

decrease the possibility of scaling, which is a common problem in high recovery ratio SWRO processes due to the precipitation of alkaline earth metal salts in the concentrated brine on the membrane surface. This will further diminish the need for chemical treatment of feed and therefore further justify the simplification of pre-treatment for the proposed ZTIMD. Combination of the avoidance of chemical pre-treatment and the discharge of close-to-natural-seawater concentration would make the ZTIMD practically waste-free.

However, the limitations of the proposed ZTIMD process do create the following three major inherited challenges, 1) the low working temperature of 30 °C or less implies a small driving force for membrane distillation, which may significantly increase the cost of membranes; and 2) the small water recovery requires the pre-treatment of seawater of 15-20 times of a conventional desalination process or even more; and 3) bottom seawater needs to be pumped at a long distance to the plant site to serve as the coolant, which raises concerns over the added capital and O&M costs. In the following stimulations, we will demonstrate the feasibility of the ZTIMD strategy despite of these challenges. It should be mentioned that the temperature rise due to pumping power is estimated to be less than 0.01 °C using energy balance. Further assume heat transfer between seawater and the environment in pumping is negligible due to proper insulation (see the sample calculations at the end of this Chapter for thickness of insulation material), and the water temperature at the entrance of the DCMD unit equals to that at the pump inlet, at the surface or bottom of the sea.

(a)

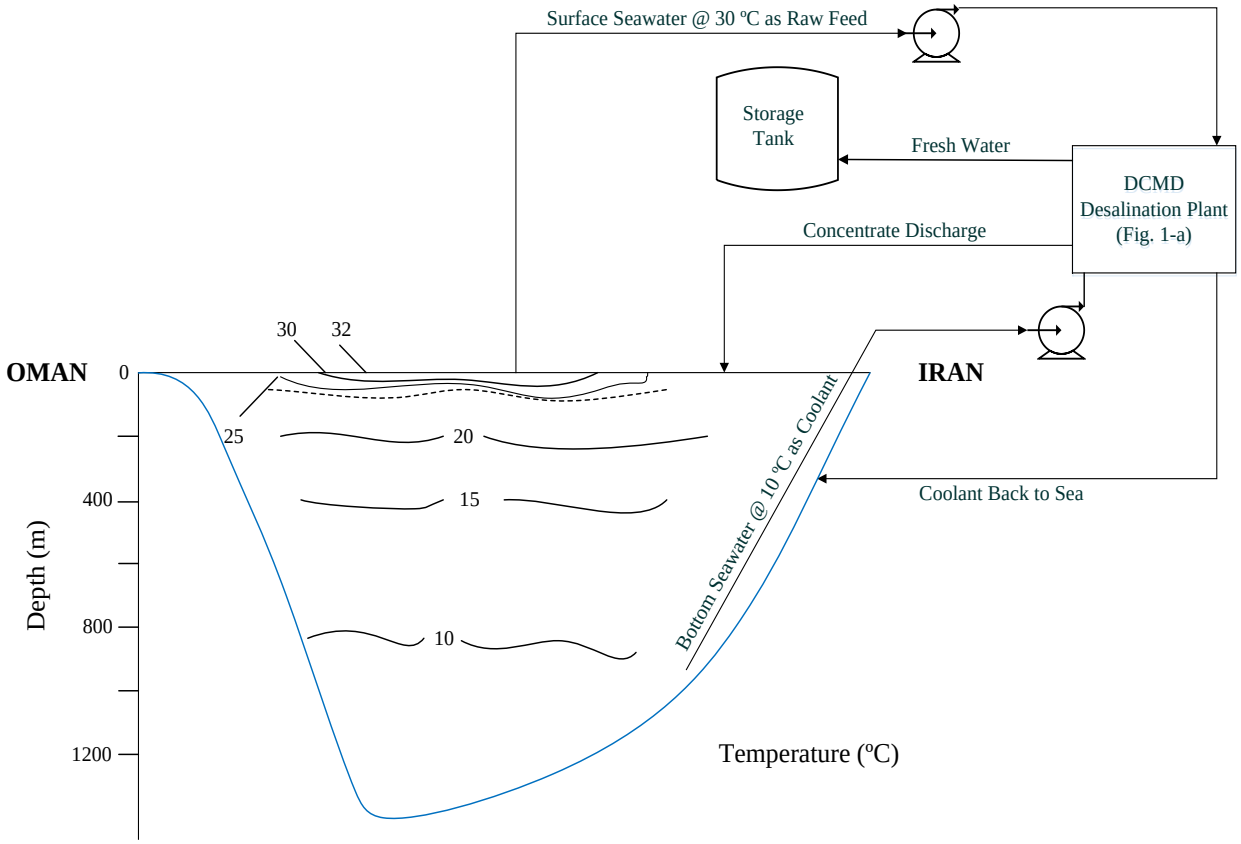
Surface Seawater @ 30 ºC as Raw Feed
Storage Tank
Fresh Water
DCMD Desalination Plant (Fig. 1-a)
Concentrate Discharge
OMAN
IRAN
30
32
0
25
20
15
10
400
800
1200
Depth (m)
Bottom Seawater @ 10 ºC as Coolant
Coolant Back to Sea
Temperature (ºC)

(b)

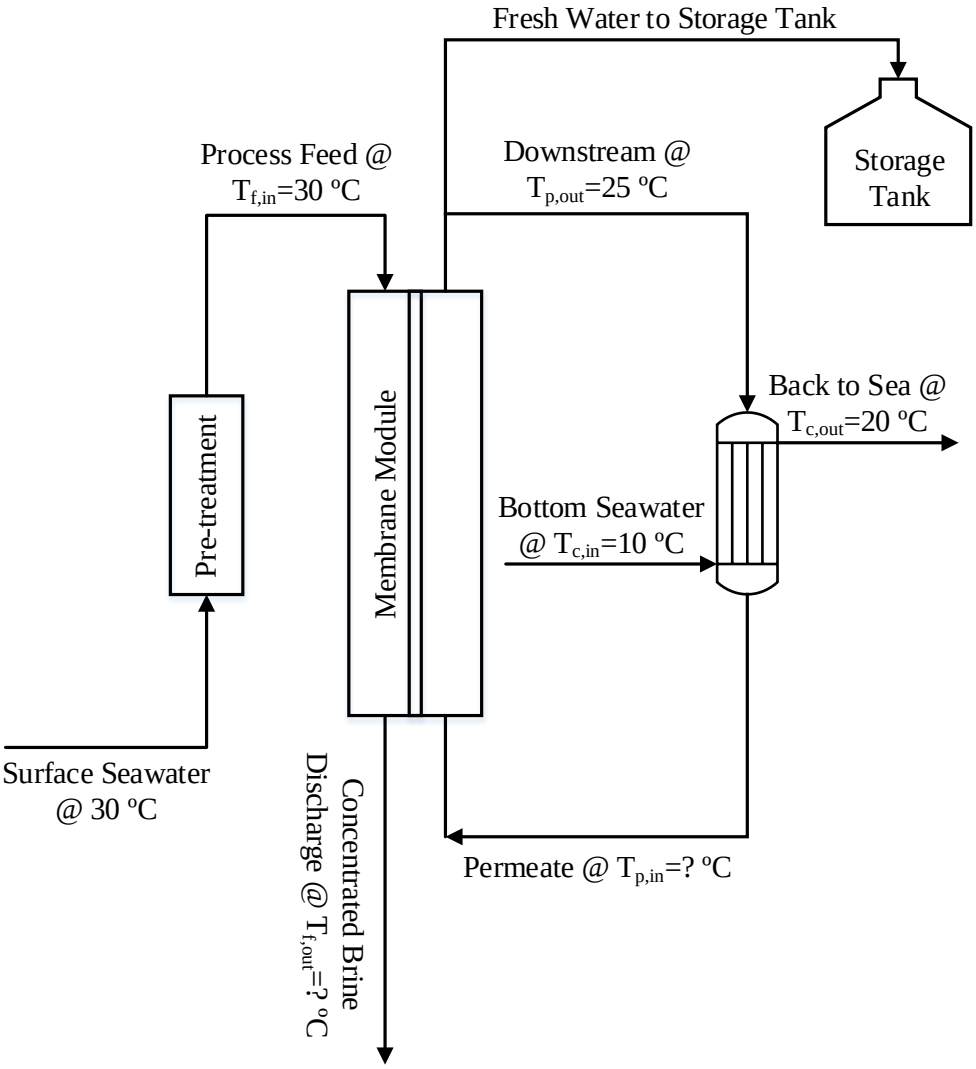

Fig. 3-1 (a) General schematic of the proposed desalination plant on the cross-sectional temperature profile of Gulf of Oman *[72]* where enthalpy of seawater is extracted for DCMD configuration, (b) ZTIMD process flow diagram

3-2-2- Process Simulation

To study the economic feasibility of the proposed ZTIMD, final product cost is taken as the objective function. A schematic diagram of a single-pass ZTIMD process is shown in Fig. 3-1-b with specifics of a few key parameters. The effects of some key process operating conditions, including temperature of concentrate discharge, $T_{f,out}$, and minimum approach temperature in the external heat exchanger, $\Delta T_{min} = [T_{p,in} - T_{c,in}]_{min}$, along with the membrane characteristics such as price, lifespan, and permeability on the objective function are investigated. The temperature of

the feed and coolant at the entrance of membrane module are assumed to be 30 °C and 10 °C, respectively.

The effect of thermal energy input on a single-pass DCMD process which is identical to the proposed ZTIMD process except the thermal energy input was also explored by increasing the process feed temperature, $T_{f,in}$, from 30 °C to 50 °C. Simulations are based on two case scenarios differ in pre-treatment assumptions, 1) with an intense pre-treatment similar to that of RO, and 2) with a simplified pre-treatment including only cartridge filtration. An algorithm of the simulation is presented in Fig. 3-2, and the related assumptions and equations are listed in Tables 3-1&2, respectively.

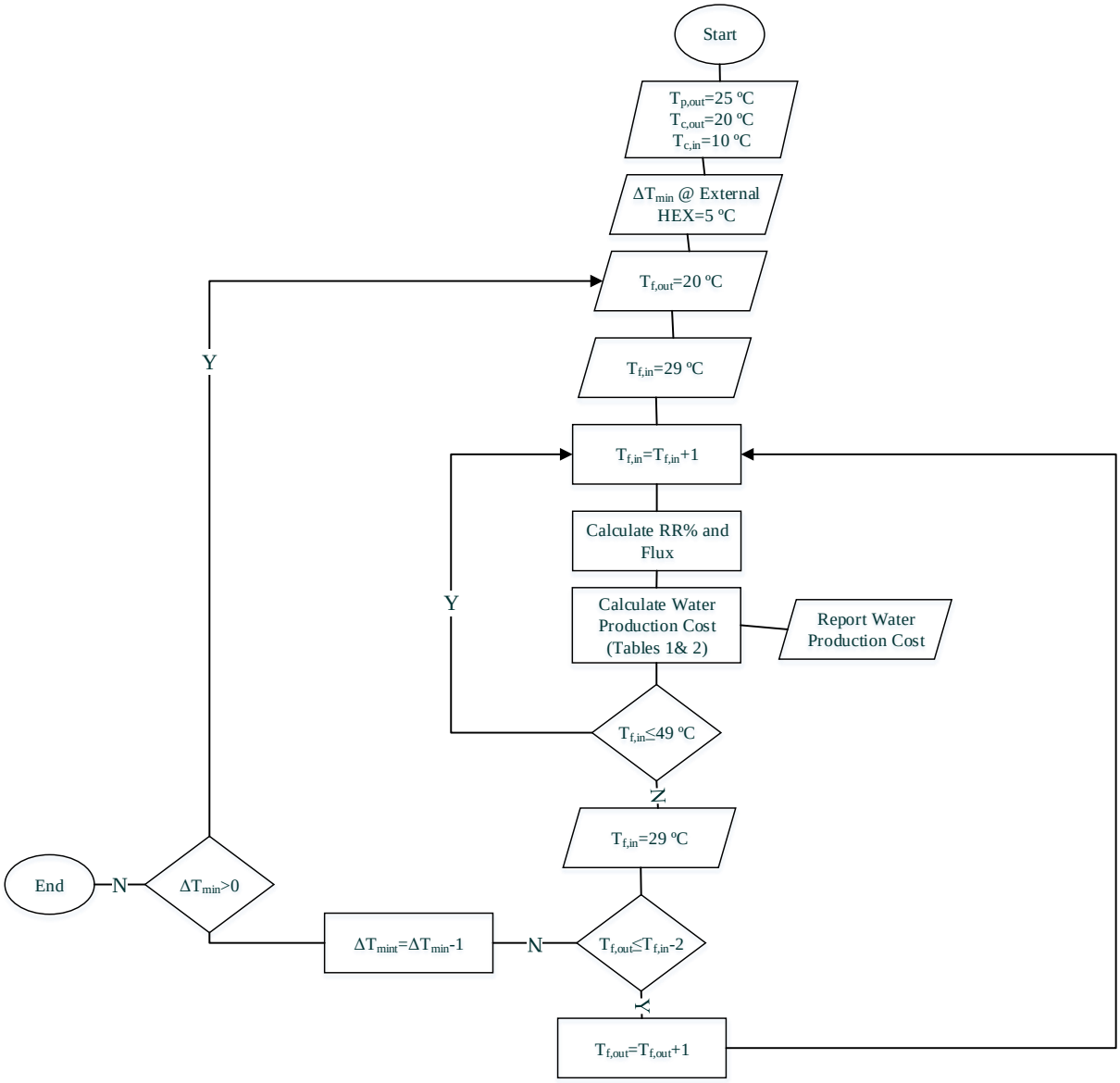

Fig. 3-2 Applied algorithm to study the economic vability of the ZTIMD

Considering the algorithm provided in Fig. 3-2, the bottom seawater enters the process at $T_{c,in}$=10 ºC, the surface seawater is fed to the system at $T_{f,in}$=30 ºC, or it can be elevated up to 50 ºC, by using an external heat source. It is assumed that permeate leaves the membrane module at $T_{p,out}$=25 ºC and coolant is discharged in the sea at $T_{c,out}$=20 ºC. In the first loop, effects of the process feed temperature, i.e. $T_{f,in}$, on the process efficiency and production cost will be explored. Temperature of concentrate discharge, i.e. $T_{f,out}$, is changed within a range of 20 to 28 ºC in the

second loop, while the minimum approach temperature in the external heat exchanger is varied from 5 to 1 ºC in the third loop by changing the permeate inlet temperature, i.e. $T_{p,in}$, from 15 to 11 ºC for the purpose of optimization. Production cost is used as the objective function for simulation and optimization, which were carried out by Microsoft Excel 2016 and VBA. The economic feasibility of ZTIMD is established by comparing the production costs of freshwater with those of the existing desalination technologies.

A list of assumptions made for the calculations in this work is given in Table 3-1.

Table 3-1 Assumptions for the economic feasibility analysis of the ZTIMD process

Plant availability (%)	90	**Storage cost (% of collector cost)** ***[30]***	20
Plant capacity (m^3/day)	24,000	**Steam HEX global heat transfer coefficient (W/m^2.C)** ***[57,80]***	2,500
Plant life (year)	20	**External HEX global heat transfer coefficient (W/m^2.C)** ***[80,81]***	700
Interest rate (%) ***[57,69,82]***	5	**Steam and external HEX efficiency**	0.8
Amortization factor [a]	0.08	**Steam HEX cost ($/$m^2$)** ***[57]***	2,000
DCMD feed pressure (kPa)	120	**External HEX cost ($/$m^2$)** ***[57]***	1,540
Raw feed temperature (ºC)	30	**Underwater piping installation costs ($)** ***[83]***	1,500,000
Permeate outlet temperature (ºC)	25	**Purchased underwater pipe cost for the coolant ($/ft)** ***[84]***	96.5
Coolant inlet (bottom seawater) temperature (ºC)	10	**Underwater pipe diameter (in)** [b]	40.5
Coolant outlet temperature (ºC)	20	**Underwater pipe length (m)**	1,100
Temperature polarization coefficient ***[85-91]***	0.7	**Cartridge filter cost ($/unit)** [c]	245
Membrane permeability (kg/m^2h.Pa) ***[85]***	0.00774	**Electricity cost ($/kWh)** ***[57]***	0.03
Membrane cost per unit area ($/$m^2$) ***[25,57,61,82]***	90	**Ordinary electrical energy consumption (kWh/m^3)** ***[57]***	0.045
Membrane replacement (%/year) ***[22,25,57,61,68,69,82,92,93]***	15	**Spares cost ($/$m^3$)** ***[57]***	0.033
Solar insolation in Muscat, yearly average (kW/m^2) ***[94]***	0.246	**Labor cost ($/$m^3$)** ***[57]***	0.03
Solar collector efficiency	0.8	**Chemical cost ($/$m^3$)** ***[57]***	0.018
Flat plate collector cost including solar racks ($/$m^2$) ***[92]***	208	**Steam cost ($/kg)** ***[57]***	0.007

[a] Amortization factor was calculated by $a = \frac{i(i+1)^n}{(i+1)^n-1}$ where i and n represent annual interest rate and plant life time, respectively *[61]*.

[b] Schedule 40-OD: 42-ASME

[c] Datum was obtained from personal communication with the manufacturer, GE Water, USA

Considering the information presented in Table 3-1 and regarding a daily water consumption of 150 L per person for a family of four in the Middle East *[1]*, the proposed plant would be large enough for a city with a population of almost 160,000 people. Membrane permeability was taken from the literature, 0.00774 kg/m^{2}h.Pa, *[85]* for the flux calculations and is considered an average value within the data available in the literature, while much higher permeabilities in the range of 0.01285–0.05178 kg/m^{2}h.Pa are estimated *[25,95]*. In addition, MD membrane price also changes significantly in the literature, and the prices were mostly those of membranes for the other membrane applications, most likely due to the lack of the data for MD membranes of industrial scale. For example, Al-Obaidani et al. used \$90/m^2 in their cost estimation analysis *[57]*, and a similar price was applied elsewhere *[25,61,82]*, however, a membrane price of \$116/m^2 *[96]*, \$36/m^2 *[22,97]*, and \$18.5/m^2 *[68]* was used in other cost evaluations. Regarding the membrane durability, it has been reported that MD membranes could withstand between 5 and 20 years, which is based on the lifespan of commercial RO membranes *[68]*, and also largely depends upon the raw feed quality. Therefore, membrane replacement cost varies from 5 to 20% of the purchased membrane cost *[22,25,57,61,68,69,82,92,93]*. In this work the center values of \$90/m^2, 15%, and 0.00774 kg/m^{2}h.Pa for membrane price, replacement rate, and permeability, respectively, are adopted, and a sensitivity analysis is carried out within the ranges of 18.5 to 116 \$/m^2, 5 to 20%, and 0.00516 to 0.01161 kg/m^{2}h.Pa, i.e. ±50% of that of the average value in the literature, 0.00774 kg/m^{2}h.Pa, while the upper limit of the permeability used in this study, i.e. 0.01161 kg/m^{2}h.Pa, is much less than the data available in the literature *[25,95]*.

Generally, the production cost is broken down into two categories. Capital cost and Operation and Maintenance (O&M) cost. Capital cost accounts for fixed, one-time expenses due to purchased equipment, installation, construction, land, depreciation, administrative etc., which

can be further divided into direct and indirect costs. Those expenses that are directly related to the production of a product such as equipment cost are considered as the direct capital cost, while the expenses that indirectly affect the production cost such as administrative fees are referred to as the indirect capital cost. Indirect capital cost could be roughly estimated as 10% of the direct capital cost *[57]*. It should be pointed out that land cost mostly depends on the project location, and was neglected by many other researchers *[21,22,68,69,92]*, and will not be taken into consideration in this study. Operation and maintenance cost represents the yearly expenses due to the operation and maintenance of the plant including cost of energy, spares, labor, etc. A list of capital and operation and maintenance costs which have been considered in this study is presented in Table 3-2.

Table 3-2 A list of capital and operation and maintenance costs for the proposed ZTIMD desalination process

Capital Costs	
Cost of civil work excluding the underwater piping ($)	$1945W^{0.8}$ *[57]*
Cost of purchased underwater piping ($)	(Required pipe length)×l
Cost of underwater piping installation ($) [a]	1,500,000 *[98]*
Cost of intake and pre-treatment ($)	$658(W/RR)^{0.8}$ *[57]* [b]
Cost of DCMD feed pumps ($)	$4.78 \times 10^{-6}\,(W/RR)\,P$ *[57]*
Cost of DCMD coolant pumps ($) [c]	*[84]*
Cost of membrane ($)	(Required membrane area)×m
Cost of heat exchangers ($)	(Required heat exchanger area)×h
Total direct capital costs ($)	Sum of all above costs
Indirect capital costs ($)	0.1×(Total direct capital costs) *[57]*
Total capital costs ($)	(Direct + Indirect capital costs)
Annual fixed charges ($/m^3)	$(a \times \text{Total capital costs})/(f \times W \times 365)$ *[57]*
Operation and Maintenance Costs	
Membrane replacement ($/year)	(Total cost of membrane)× r_m
Cost of electricity excluding the bottom seawater pumping ($/year)	(Annual electricity consumption)×e
Cost of electricity for pumping the coolant, i.e. bottom seawater ($/year)	(Annual electricity consumption)×e
Cost of chemicals ($/year)	(Specific chemical cost per m^3)×W
Cost of spares ($/year)	(Specific spears cost per m^3)×W
Cost of labor ($/year)	(Specific labor cost per m^3)×W

Total annual O&M costs ($/year)	Sum of all above costs
Annual O&M charges ($/m^3)	$(\text{Total annual O\&}M\ costs)/(f \times W \times 365)$ *[57]*
Total Water Cost	
Overall Water Cost ($/m^3)	(Annual fixed charges)+(Annual O&M charges)

Where W, l, RR, m, h, a, f, r_m, e represent for plant capacity, purchased piping cost per length, recovery ratio, membrane cost per area, heat exchanger cost per area, amortization factor, plant availability, membrane replacement rate, and electricity cost, respectively.

[a] Installation cost depends on the pipe length, which is further related to the depth that seawater is extracted, and is assumed to be 1100 m.

[b] This equation is used when pre-treatment cost is estimated as intense as that of the SWRO process.

[c] Purchased coolant pumps cost depends on the required power and is obtained by finding the frictional pressure loss in the pipe according to equation 3.

It should be noted that the ZTIMD is considered to be a process free from thermal energy input. However, in the case scenarios where surface seawater is heated by an external source of energy such as solar, fossil fuel, and waste heat, the required capital and O&M costs related to the external heat source, including the solar collectors along with the storage costs besides the expenses related to the steam generation need to be added to Table 3-2.

It is also worth mentioning that in our calculations, the recovery ratio (*RR*) was estimated according to energy balance (equation (3-1)), and the water vapor pressure (P^*) by equation (3-2), which was derived by combining Antoine equation and Raoult's law *[85,99]*. Water flux was calculated by multiplying the membrane permeability and logarithmic mean of vapor pressure difference around the membrane module in Fig 3-1-b.

$$\%RR = \frac{m_p}{m_f} \times 100 = \frac{C_p(T_{f,in} - T_{f,out})}{\Delta H_v} \times 100 \qquad (3\text{-}1)$$

Equation (1) was derived from the energy balance using the membrane module as the control volume if there is no conductive heat loss across the membrane *[62]*. Where m_p is the rate of freshwater production (same as membrane permeation rate), m_f the flow rate of feed, C_p the specific heat capacity of seawater, $T_{f,in}$ process feed temperature, $T_{f,out}$ temperature of concentrate discharge, and ΔH_v the latent heat of vaporization at the temperature of operation. The difference between the flow rate of feed and that of concentrated seawater is assumed to be negligible. The same equation is applicable on the downstream side of the MD module by using $T_{p,out}$ and $T_{p,in}$, respectively, instead of $T_{f,in}$ and $T_{f,out.}$

$$P^* = \left[\exp\left(16.3872 - \frac{3885.7}{T + 230.17}\right)\right](1 - x) \quad (3\text{-}2)$$

In equation (2), P^* (kPa) stands for the water vapor pressure at a temperature of T (ºC), and x represents the seawater salt concentration, 35 g/L in this study.

Furthermore, to find the additional electrical energy required for pumping the coolant from the bottom sea, and according to the Bernoulli's equation, energy equivalent to the pressure drop through the pipeline need to be supplied by the coolant pumps, while the frictional pressure loss (ΔP_f) per 100 ft of the pipe is obtained via Equation (3-3) *[100]*.

$$\Delta P_f = \frac{W^{1.8}\mu^{0.2}}{20{,}000 d^{4.8}\rho} \quad (3\text{-}3)$$

Where W and μ represent the coolant mass flow rate (lb/h) and its viscosity (cP), respectively, and d and ρ are internal pipe diameter (in) and fluid density (lb/ft^3), respectively.

3-2-3- Results and Discussion

To study the economic viability of the proposed ZTIMD, the unknown temperatures in Fig. 3-1-b, i.e. $T_{f,out}$ and $T_{p,in}$ were optimized. Optimization has been carried out by taking the water production cost as the objective function. Furthermore, major contributors to the overall cost need to be found out, and a sensitivity analysis on those crucial parameters was performed.

3-2-3-1- Effects of Concentrated Brine Discharge Temperature ($T_{f,out}$) on the Water Production Cost

Technically, water recovery decreases as $T_{f,out}$ (see eq. 1) increases, which will result in more investment on the feed section, including pumping, pre-treatment, etc. However, as the brine temperature ($T_{f,out}$) is elevated, driving force across the membrane will increase, which will bring about a higher water flux and accordingly lower membrane cost in the process. Therefore, an optimum brine temperature should exist at which the water production cost is minimized. Fig. 3-3 shows the water production cost versus $T_{f,out}$ in the range of 20 to 28 ºC for two case scenarios: 1) an intense pre-treatment (that of RO) is applied for the proposed ZTIMD and 2) pre-treatment is simplified to a more realistic condition including cartridge filtration only. The cost variations as a function of membrane price, durability, and permeability in each case scenario are also investigated, and the results of which are presented in Figs. 3-3-a, 3-3-b, and 3-3-c, respectively.

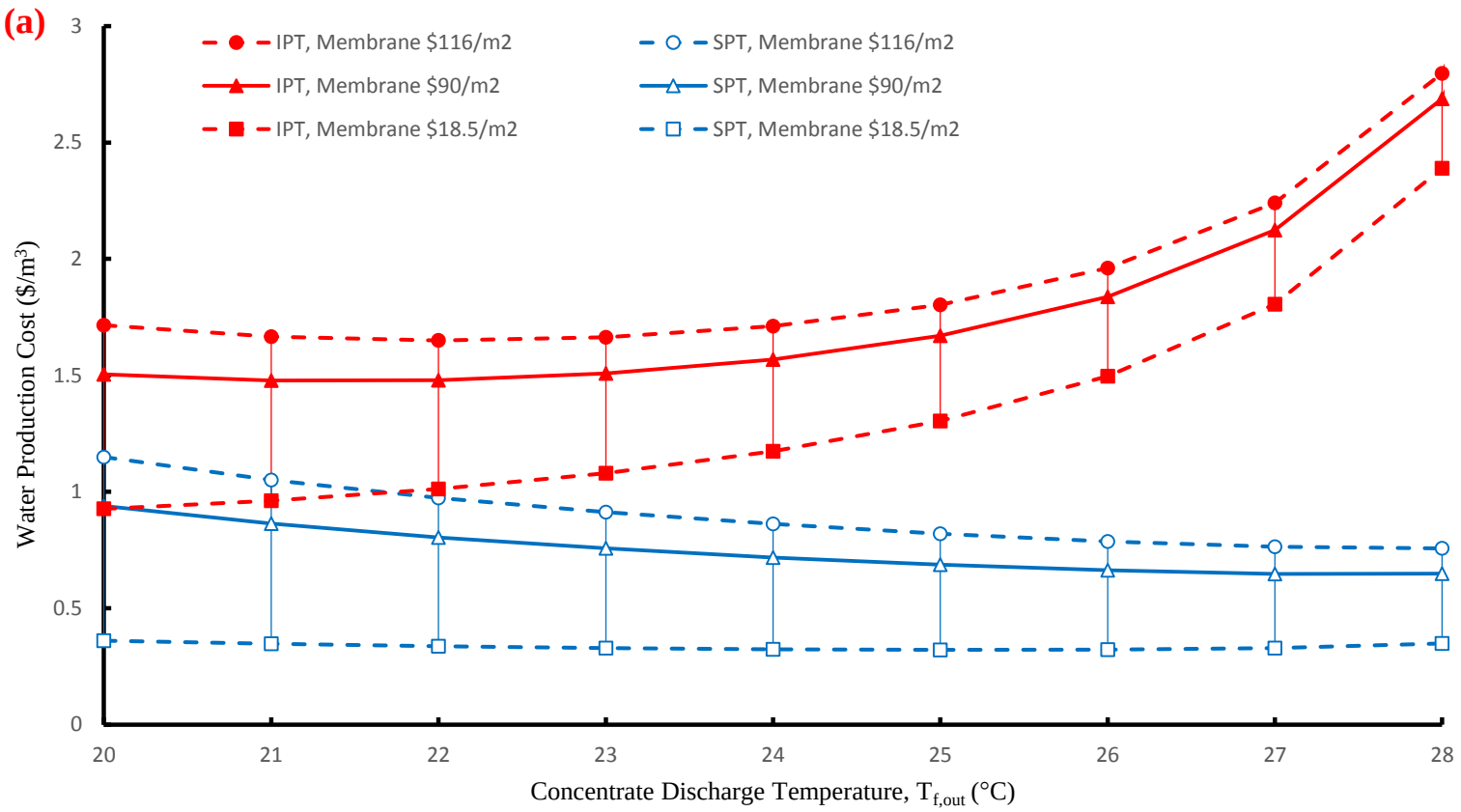
(a)
IPT, Membrane $116/m2
IPT, Membrane $90/m2
IPT, Membrane $18.5/m2
SPT, Membrane $116/m2
SPT, Membrane $90/m2
SPT, Membrane $18.5/m2
Water Production Cost ($/m3)
0
0.5
1
1.5
2
2.5
3
20
21
22
23
24
25
26
27
28
Concentrate Discharge Temperature, Tf,out (°C)

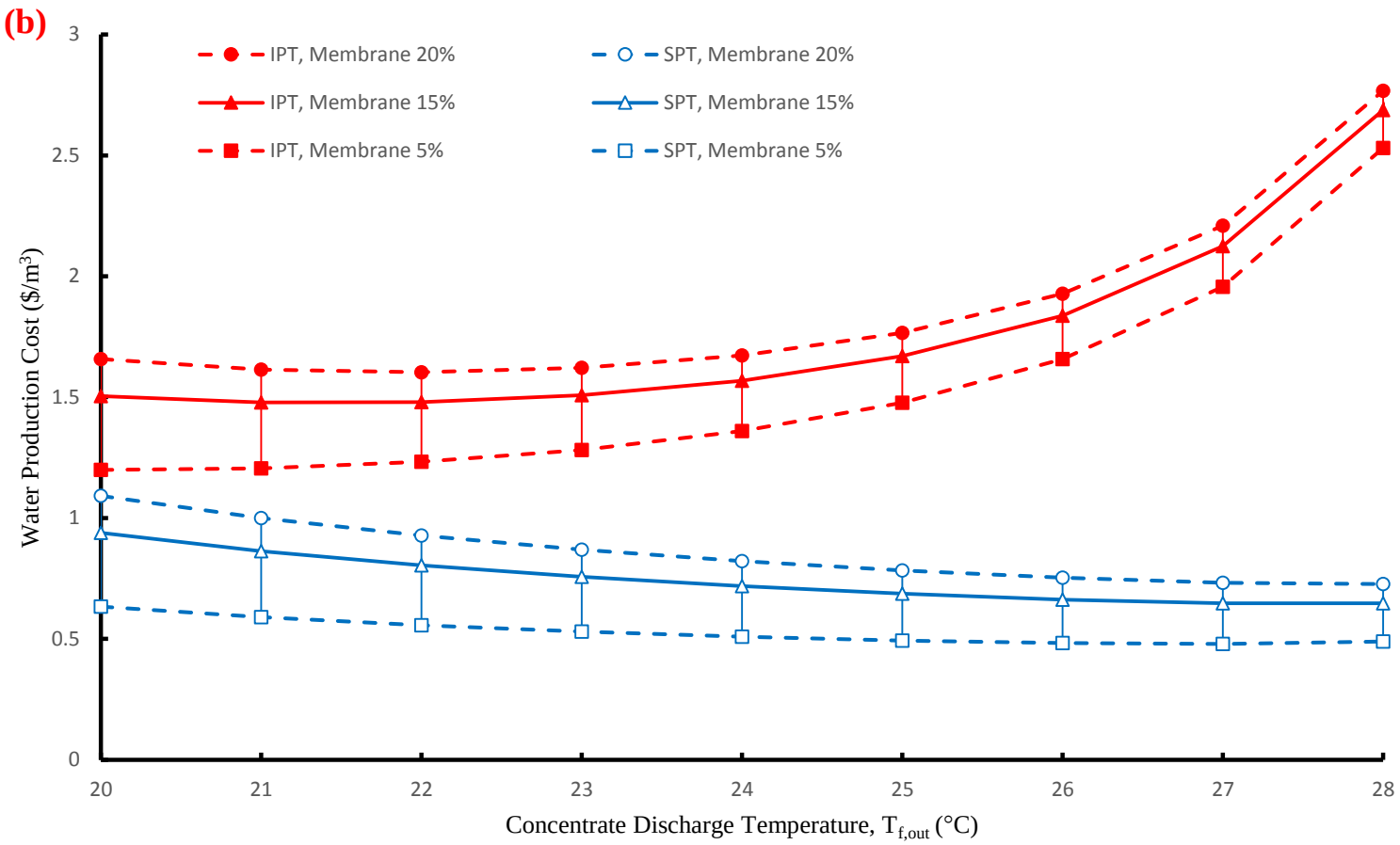
(b)
IPT, Membrane 20%
SPT, Membrane 20%
IPT, Membrane 15%
SPT, Membrane 15%
IPT, Membrane 5%
SPT, Membrane 5%
Water Production Cost ($/m3)
0
0.5
1
1.5
2
2.5
3
20
21
22
23
24
25
26
27
28
Concentrate Discharge Temperature, Tf,out (°C)

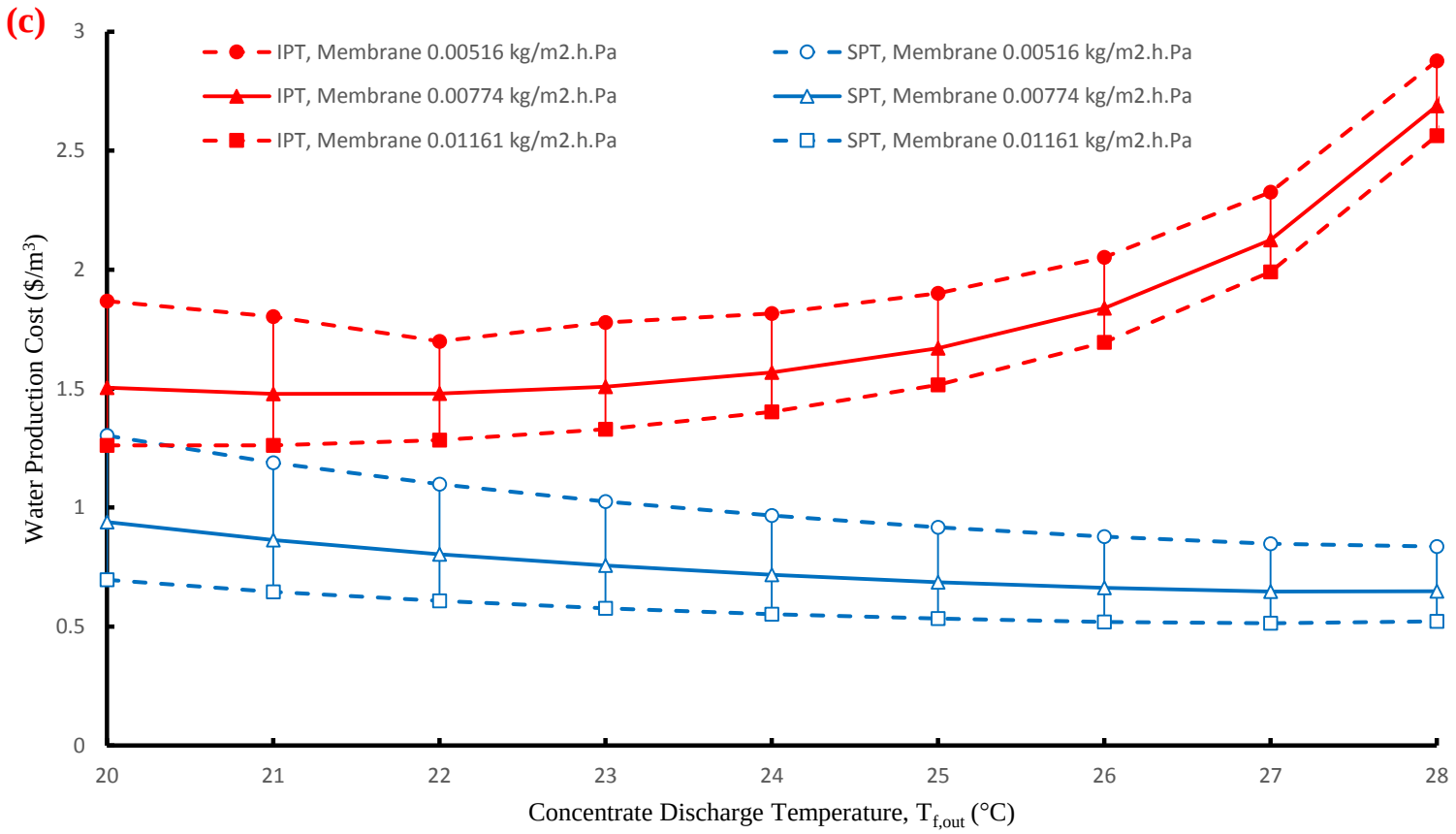

Fig. 3-3 Water production cost vs. brine temperature where pre-treatment is as intense as that of RO or as simple as cartridge filtration at $T_{f,in}$=30 °C and $T_{p,in}$=15 °C, when (a) membrane price varies between 18.5 and 116 \$/m^2 at a constant membrane replacement rate and permeability of 15% and 0.00774 kg/m^{2}h.Pa, (b) membrane replacement rate varies between 5 and 20% at a constant membrane price and permeability of \$90/m^2 and 0.00774 kg/m^{2}h.Pa, (c) membrane permeability varies between 0.01161 and 0.00516 kg/m^{2}h.Pa at a constant membrane price and replacement rate of \$90/m^2 and 15%, IPT and SPT stand for Intense and Simplified Pre-Treatment, respectively

As shown in Fig. 3-3, which were obtained using the center values of membrane price (\$90/m^2), replacement rate (15%), and permeability (0.00774 kg/m^{2}h.Pa), water production cost goes through a minimum for both case scenarios, i.e. \$1.48/m^3 at $T_{f,out}$=21 ºC for the intense pre-treatment and \$0.65/m^3 at $T_{f,out}$=27 ºC for the simplified pre-treatment. The results show that

when the surface seawater is fed to the system at 30 ºC with the assumptions in Table 3-1, a brine temperature of either 21 or 27 ºC depending on the complexity of the pre-treatment step would result in a minimum water production cost of 1.48 or 0.65 $/m^3. As expected, adopting the simplified pre-treatment brought about a much lower water production cost.

(a) Major Contributors to the Water Production Cost

To better understand the major contributors to the product cost at different levels of complexity of the pre-treatment step, overall (a), total capital (b), along with the operation and maintenance (c) cost broke-down for each case scenario at the optimum brine temperature and is presented in Fig. 3-4, when each membrane parameter is maintained at its center value.

(a-1)

Overall Cost Break-Down-Intense Pre-treatment
$T_{f,in}$ = 30 °C, $T_{f,out}$ = 21 °C

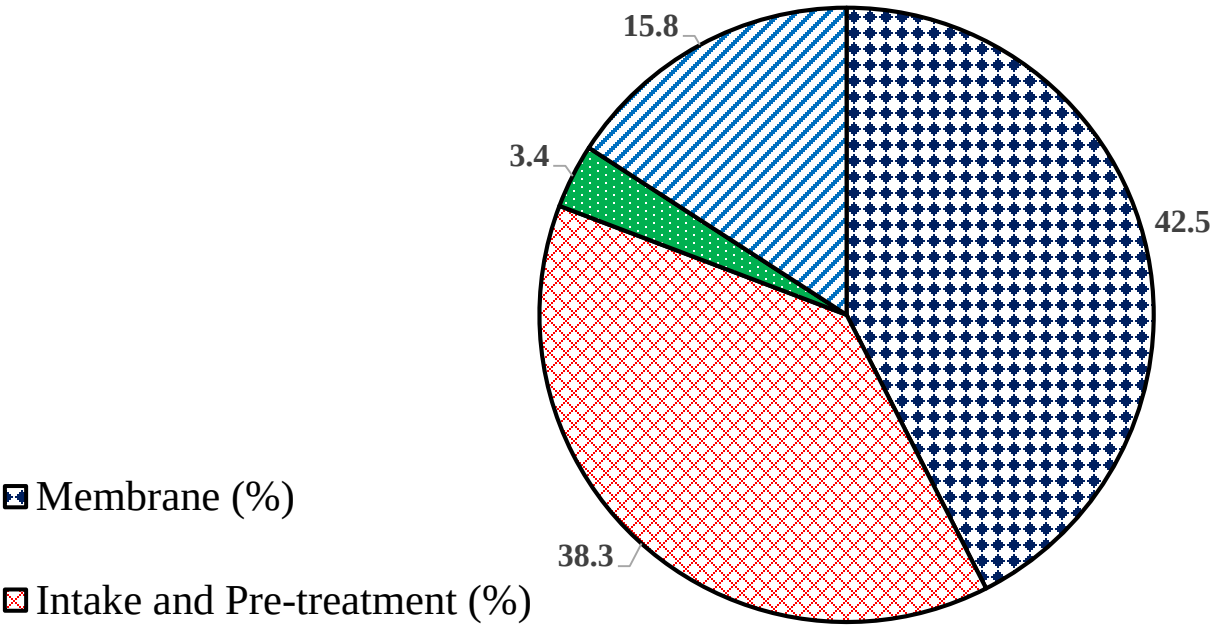

(a-2)

Overall Cost Break-Down-Simplified Pre-treatment
$T_{f,in}$ = 30 °C, $T_{f,out}$ = 27 °C

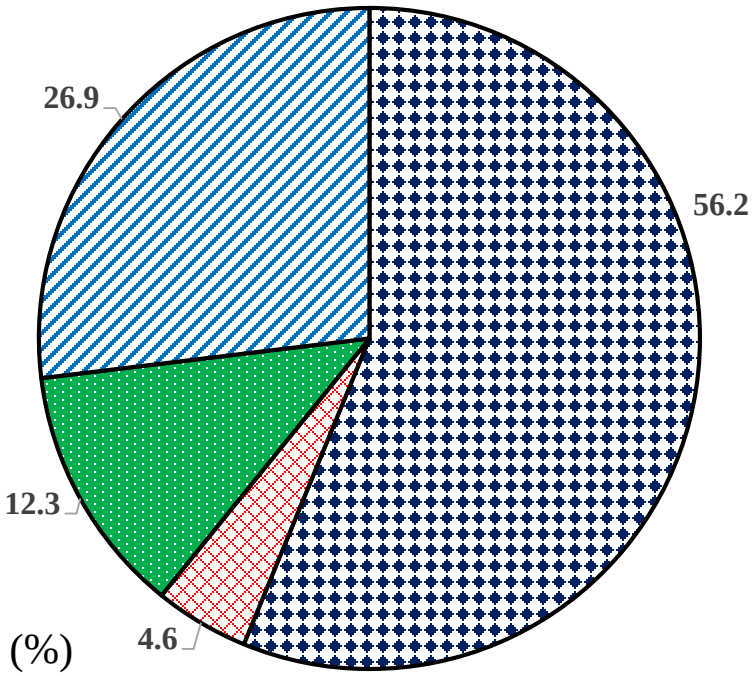

(b-1)

Total Capital Cost Break-Down-Intense Pre-treatment
$T_{f,in}$ = 30 °C, $T_{f,out}$ = 21 °C

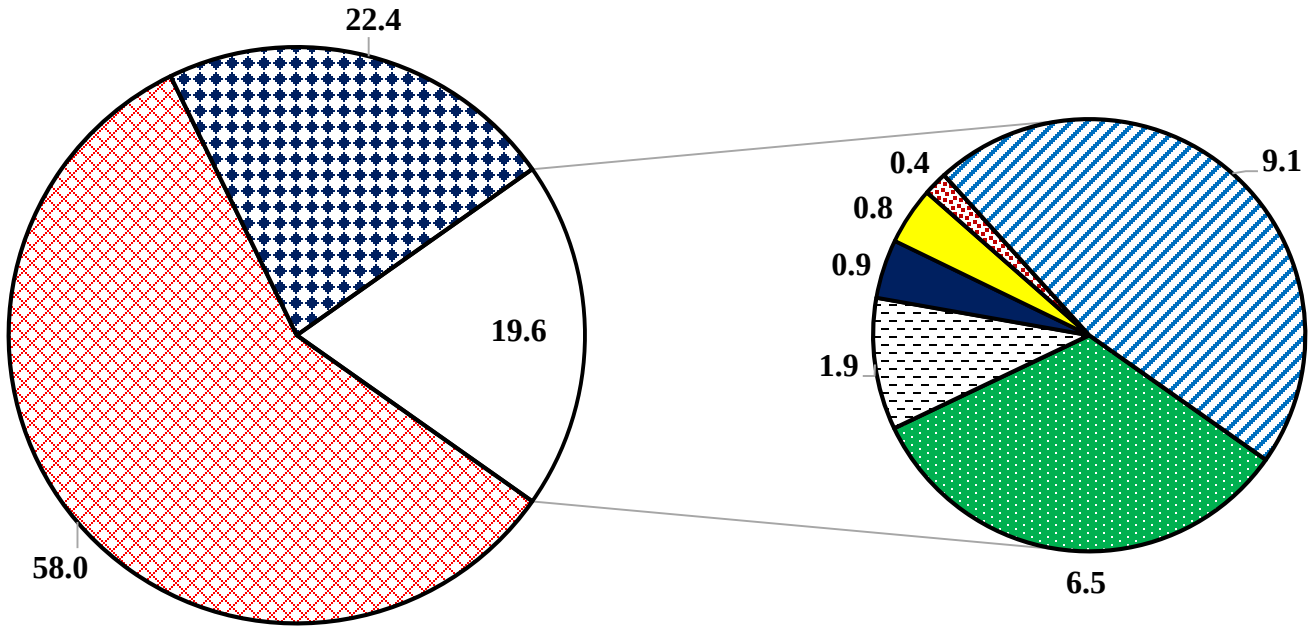

(b-2)

Total Capital Cost Break-Down-Simplified Pre-treatment
$T_{f,in}$ = 30 °C, $T_{f,out}$ = 27 °C

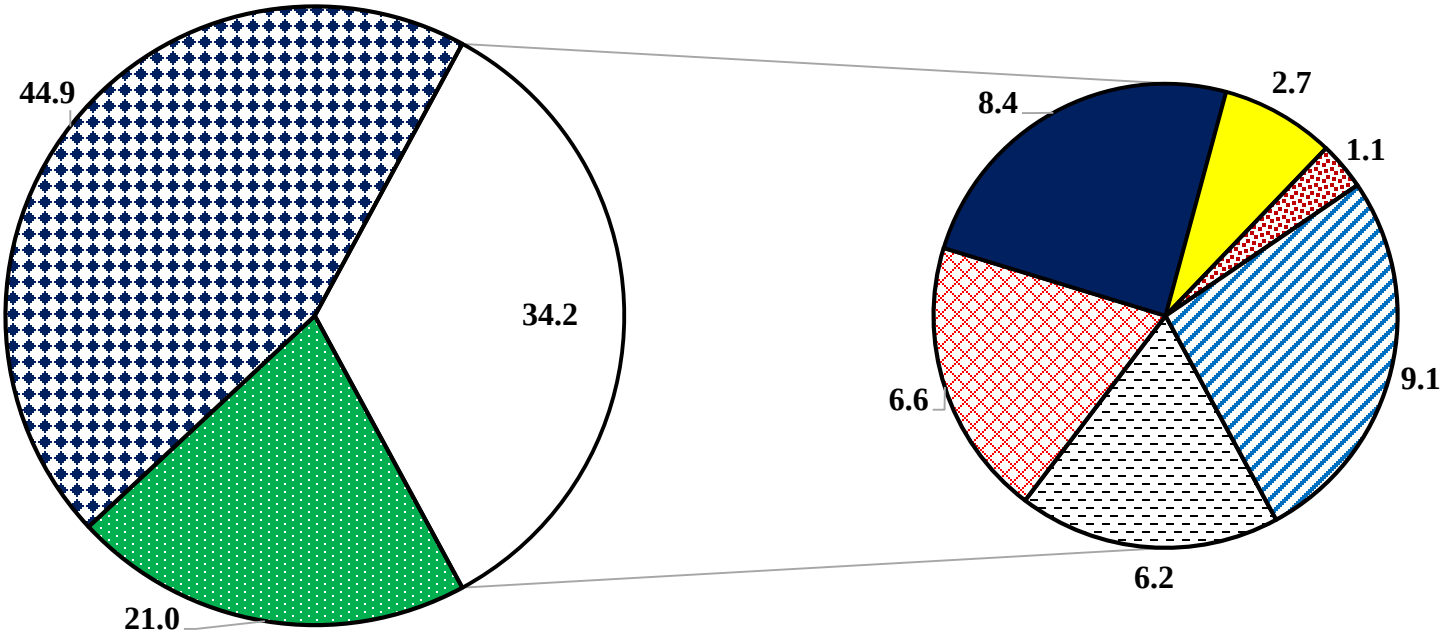

(c-1)

Total O&M Cost Break-Down-Intense Pre-treatment
$T_{f,in}$ = 30 °C, $T_{f,out}$ = 21 °C

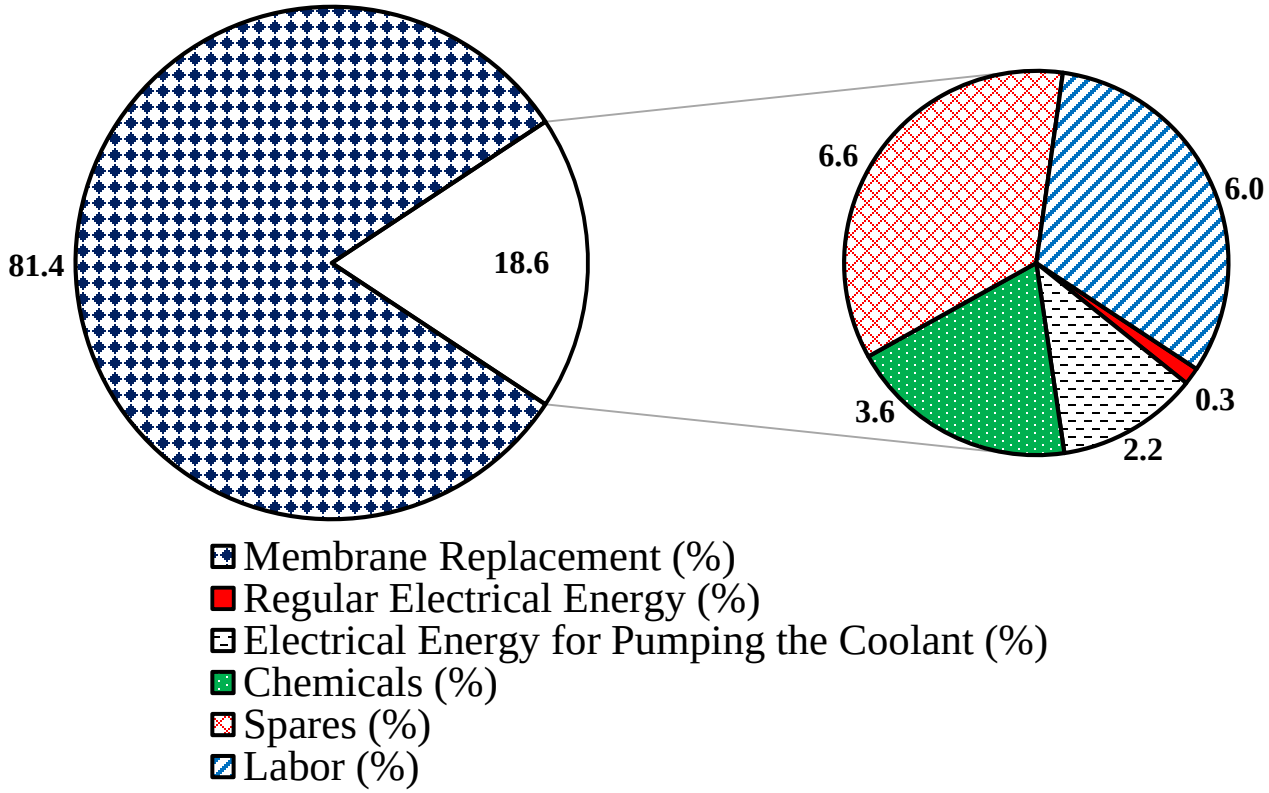

(c-2)

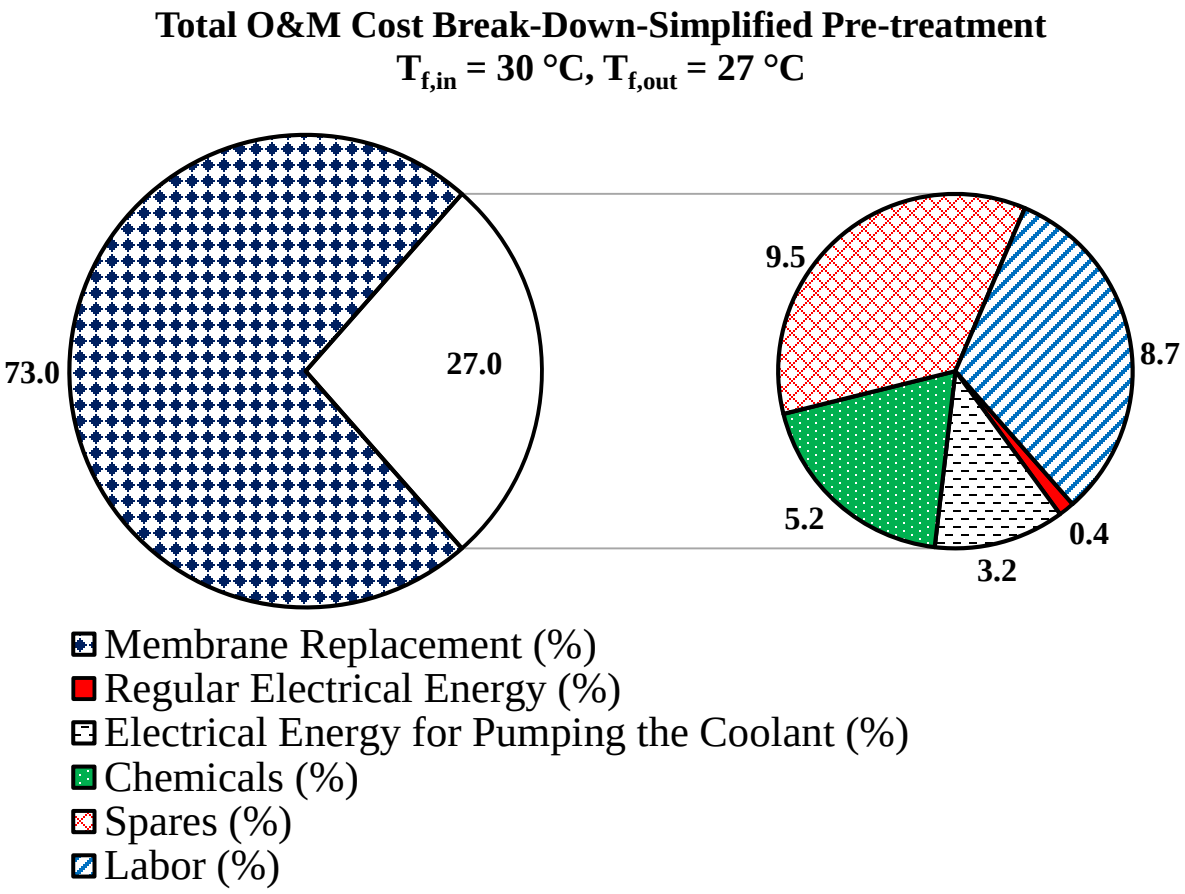

Fig. 3-4 (a) Overall, (b) total capital and (c) total O&M cost break-down when (1) intense and (2) simplified pre-treatment step is adopted to the ZTIMD process at a membrane price, replacement rate, and permeability of \$90/m^2, 15% and 0.00774 kg/m^2h.Pa, respectively, other costs in (a) includes cost of civil work, indirect capital, regular electrical energy, chemicals, spares, and labor

Considering Fig. 3-4-a, the additional costs for implementation of the ZTIMD compared to the regular DCMD desalination process, which include the costs associated with the feed (due to working at low recovery ratios) and coolant pumping, external heat exchanger, and underwater piping are not significant in comparison with the pre-treatment and membrane costs. They only take 3.4% and 12.3% of the overall costs for the ZTIMD coupled with intense and simplified

pre-treatment, respectively. As shown in Fig. 3-4-b-1 for the intense pre-treatment, pre-treatment (58%) and purchased membrane costs (22%) are the major contributors to the total capital cost of a ZTIMD process, while in Fig. 3-4-b-2 for the simplified pre-treatment, the pre-treatment cost goes down to 6.6% and the purchased membrane cost goes up to 44.9%, thus controlling the total capital cost. As for the O&M cost, membrane replacement cost is the major contributor for both intense (81.4%, Fig. 3-4-c-1) and simplified (73%, Fig. 3-4-c-2) pre-treatment. The energy costs associated with transportation of the bottom seawater to be used as the coolant at the external heat exchanger is surprisingly insignificant (less than 3% for both scenarios). This is because the seawater is pressurized at the bottom of the sea and the increase in water head by pumping is not necessary. The friction loss in the piping calculated by equation 3 is very small.

As discussed earlier in this section, the concentrated brine temperature would have opposite effect on the pre-treatment and membrane cost. This trend is clearly shown in Fig. 3-5 for both scenarios as the shares in the capital cost.

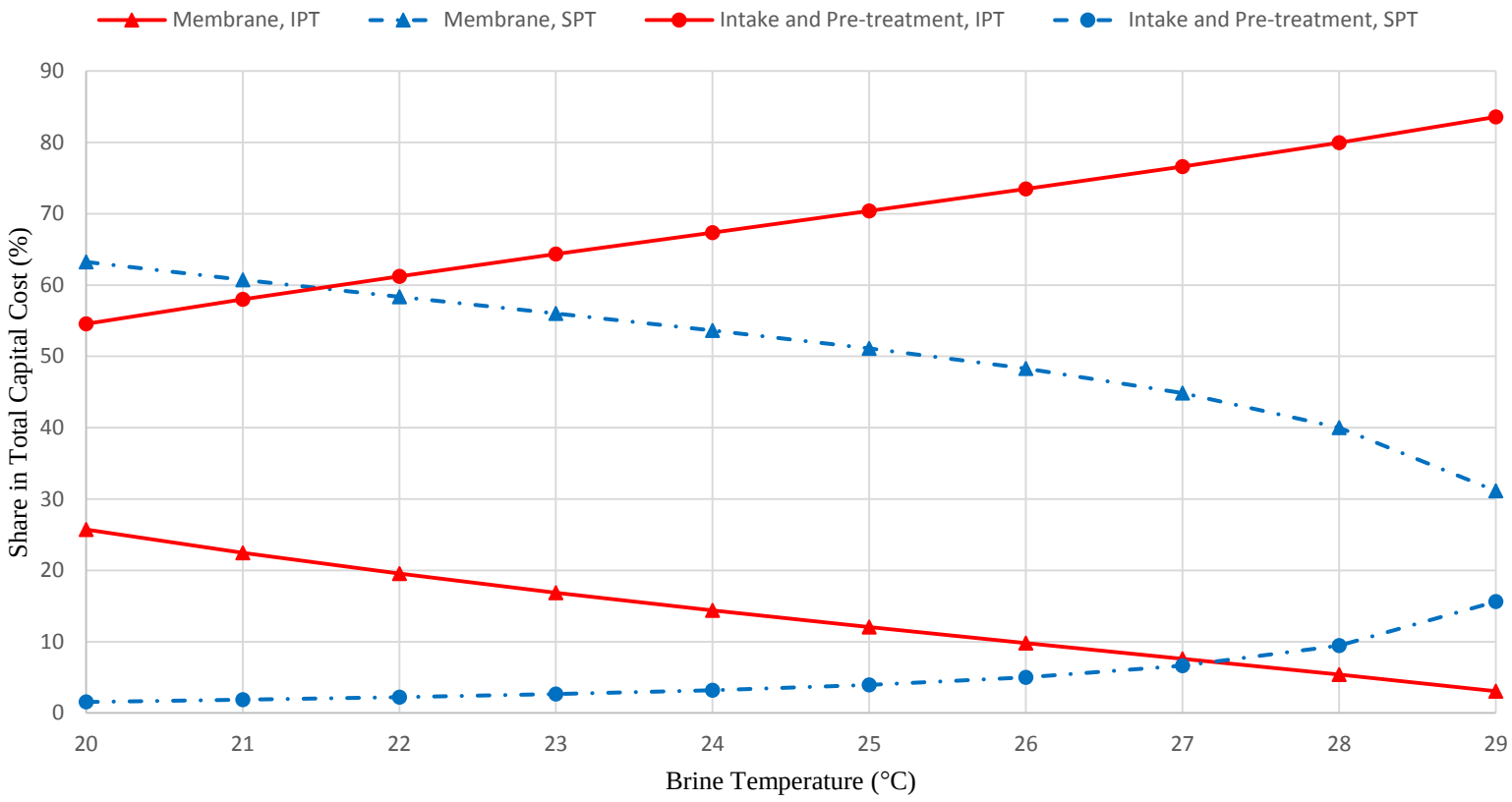

Fig. 3-5 Share of major contributors to the total water cost, i.e. intake and pre-treatment and purchased membrane costs, in total capital cost vs. brine temperature, at $T_{f,in}$=30 °C, $T_{p,in}$=15 °C, and a membrane price, replacement rate, and permeability of \$90/m^2, 15% and 0.00774 kg/m^{2}h.Pa, respectively

According to Fig. 3-5, the portion of intake and pre-treatment cost increases as the concentrated brine leaves the process at higher temperatures, mainly due to smaller recovery ratios and therefore larger amounts of feed to be processed at higher $T_{f,out}$ (recovery ratio decreases from 1.8% to 0.4% when $T_{f,out}$ increases from 20 to 28 ºC). On the other hand, increased concentrated brine temperature will result in lower purchased membrane and accordingly replacement costs due to the higher fluxes obtained through working at higher brine temperatures (water flux

increases from 3.7 to 7.2 kg/m^{2}h when $T_{f,out}$ increases from 20 to 28 ºC). These two opposite trends will lead to a minimum water production cost at a $T_{f,out}$ of 21 and 27 ºC for the ZTIMD coupled with intense and simplified pre-treatment, respectively.

(b) Effects of the Membrane Characteristics on the Water Production Cost

As shown in the previous section, membrane cost is the top contributor to the overall cost of a ZTIMD process when the pre-treatment step is approximated by cartridge filtration only. The range bars in Fig. 3-3 representing cost variation demonstrate that a cheaper, more durable and permeable membrane resulted in a cheaper product. When the pre-treatment step is approximated by that of the RO process, total water cost varies from 0.96 to 1.80 \$/m^2 at $T_{f,out}$=21 ºC depends upon the membrane price, lifespan, and permeability, while for the ZTIMD process coupled with the simplified pre-treatment step, product could be obtained in the range of 0.33-0.85 \$/m^2 at $T_{f,out}$=27 ºC depending on the membrane characteristics. Nonetheless, a best case scenario would be when a membrane with the price, replacement rate, and permeability of \$18.5/m^2, 5%, and 0.01161 kg/m^{2}h.Pa, respectively, used in a ZTIMD process with the simplified pre-treatment by cartridge filtration, where the product could be obtained at a cost as low as of \$0.28/m^3.

3-2-3-2- Effects of Minimum Approach Temperature in the External Heat Exchanger, (ΔT_{min}) on the Water Production Cost

Minimum approach temperature, ΔT_{min}, in the external heat exchanger in the ZTIMD process will be changed from 1 to 5 ºC by varying the permeate inlet temperature, i.e. $T_{p,in}$ in Fig 3-1-b, from 11 to 15 ºC. Considering the lowest ΔT_{min} of 1 ºC, $T_{p,in}$ is its lowest at 11 ºC, hence the largest heat exchanger is required to cool the downside stream. On the other hand, the downside

stream of the lowest $T_{p,in}$ enters the membrane module, resulting in the highest membrane flux and the lowest membrane purchase cost. In other words, lowering the ΔT_{min} has two opposing effects on the water production cost, by increasing the cost for heat exchanger, while decreasing the membrane purchase cost. Effects of $T_{p,in}$ (as well ΔT_{min}) on the water production cost is given in Fig. 3-6, where the solid lines represent the water production cost for the intense and simplified pre-treatment, when the membrane price, replacement rate, and permeability are at their central values. The effects of the variation of the membrane price, replacement rate, and permeability are shown by the range bars and broken lines in Figs. 3-6-a, 3-6-b, and 3-6-c, respectively.

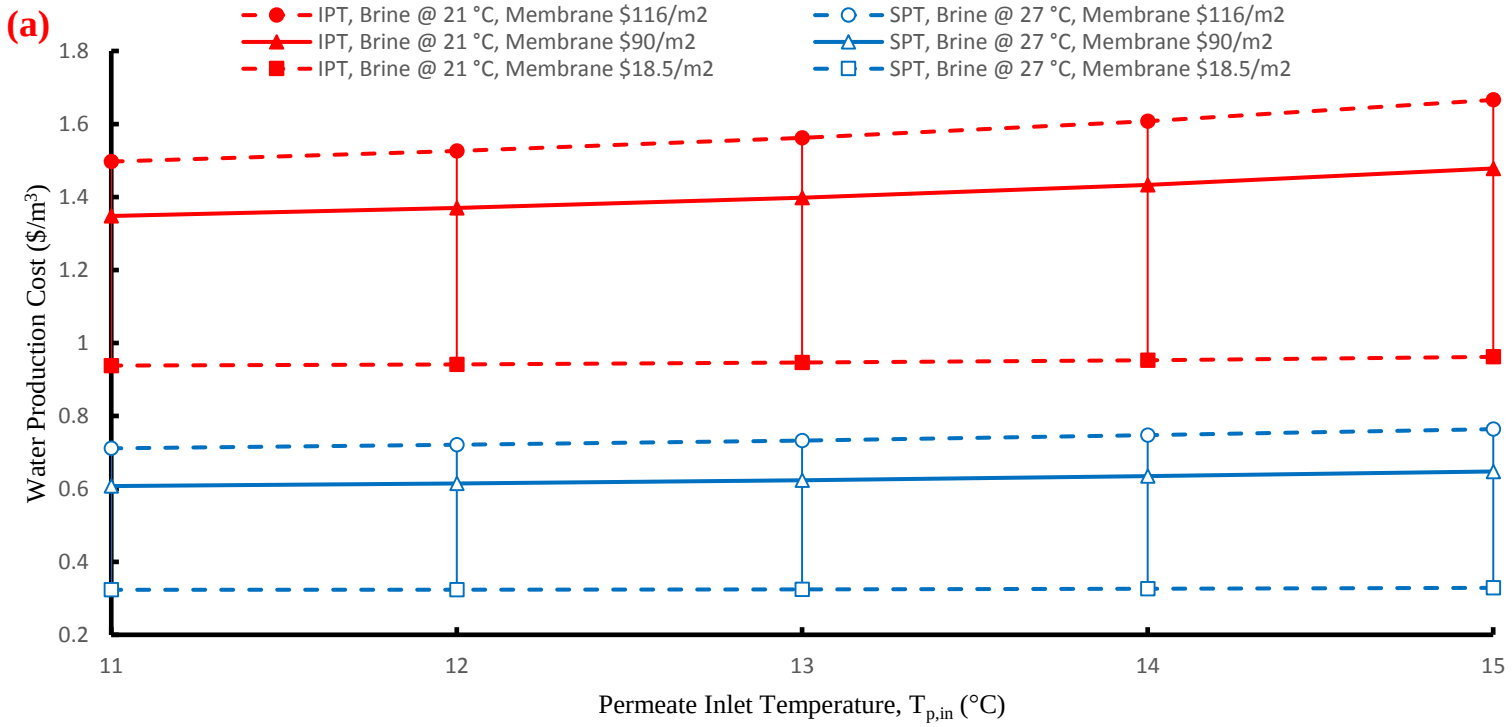

(b)

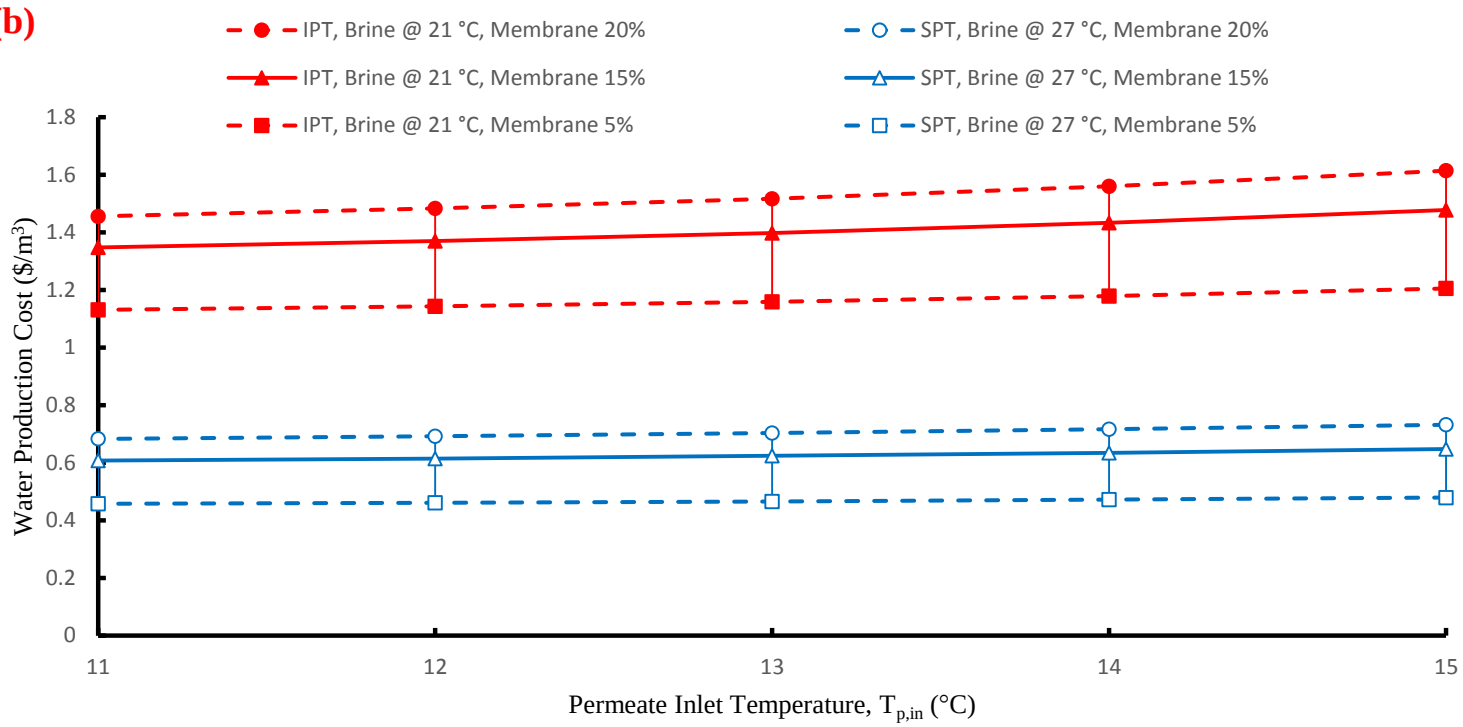
IPT, Brine @ 21 °C, Membrane 20%
SPT, Brine @ 27 °C, Membrane 20%
IPT, Brine @ 21 °C, Membrane 15%
SPT, Brine @ 27 °C, Membrane 15%
IPT, Brine @ 21 °C, Membrane 5%
SPT, Brine @ 27 °C, Membrane 5%
Water Production Cost ($/m³)
1.8
1.6
1.4
1.2
1
0.8
0.6
0.4
0.2
0
11
12
13
14
15
Permeate Inlet Temperature, T p,in (°C)

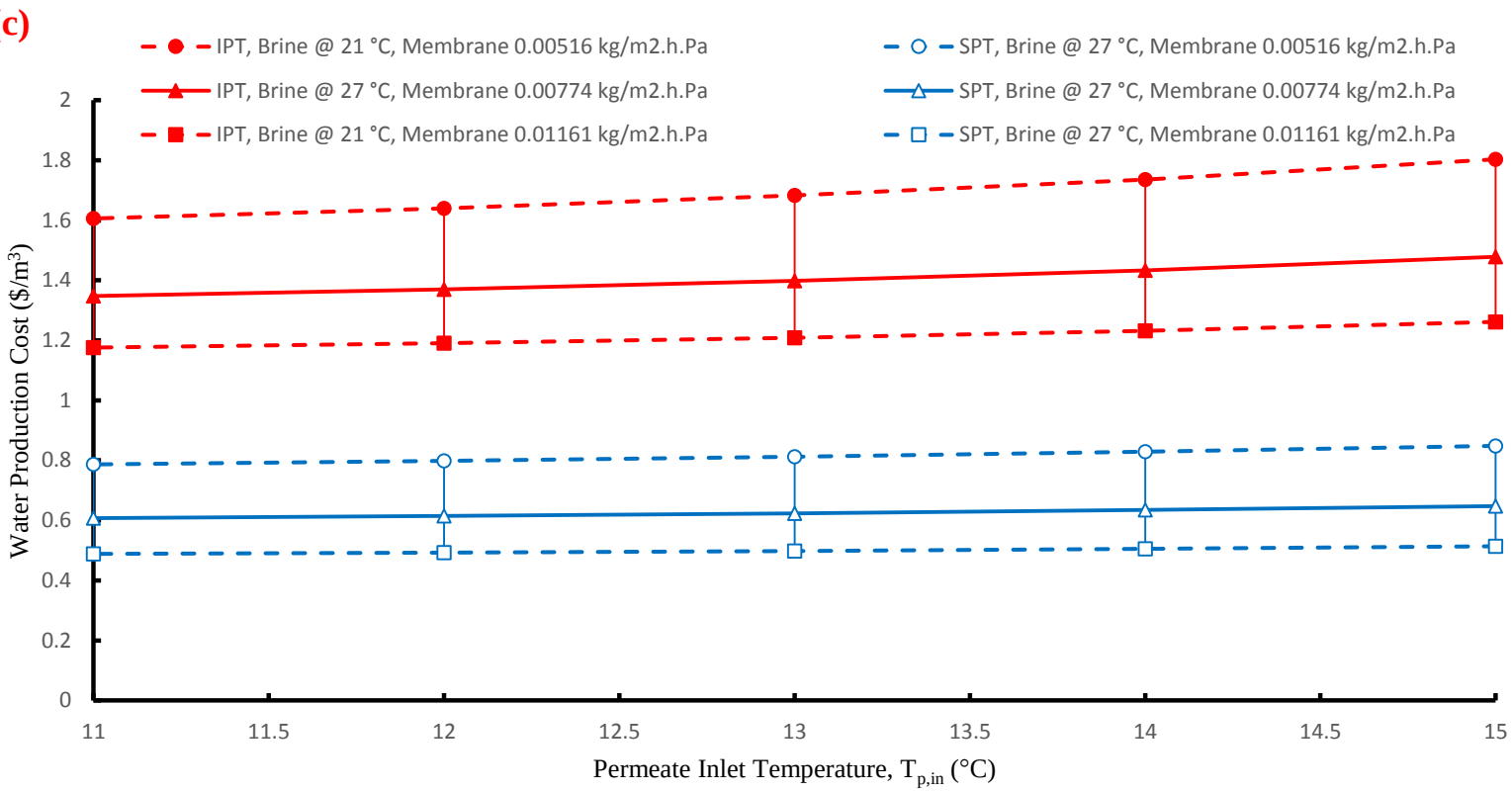

Fig. 3-6 Water production cost vs. permeate inlet temperature where pre-treatment is as intense as that of RO or as simple as cartridge filtration at $T_{f,in}$=30 °C, when (a) membrane price varies between 18.5 and 116 \$/m^2 at a constant membrane replacement rate and permeability of 15% and 0.00774 kg/m^{2}h.Pa, (b) membrane replacement rate varies between 5 and 20% at a constant membrane price and permeability of \$90/m^2 and 0.00774 kg/m^{2}h.Pa, (c) membrane permeability varies between 0.01161 and 0.00516 kg/m^{2}h.Pa at a constant membrane price and replacement rate of \$90/m^2 and 15%

As shown in Fig. 3-6, water production cost decreases by 8.8% from \$1.48/m^3 to \$1.35/m^3 when an intense pre-treatment is performed as $T_{p,in}$ decreases from 15 to 11 ºC, which is equivalent to a reduction in ΔT_{min} from 5 to 1 ºC, while for the simplified pre-treatment, water production cost is reduced by 6.2%, from \$0.65/m^3 to \$0.61/m^3, when $T_{p,in}$ decreases from 15 to 11 ºC. These results demonstrate that the effect of membrane cost reduction is dominant in determining the water production cost in comparison with the increase in the external heat exchanger cost. Fig. 3-

7 wherein the share of the membrane purchase cost and the external heat exchanger cost are shown to support this conclusion.

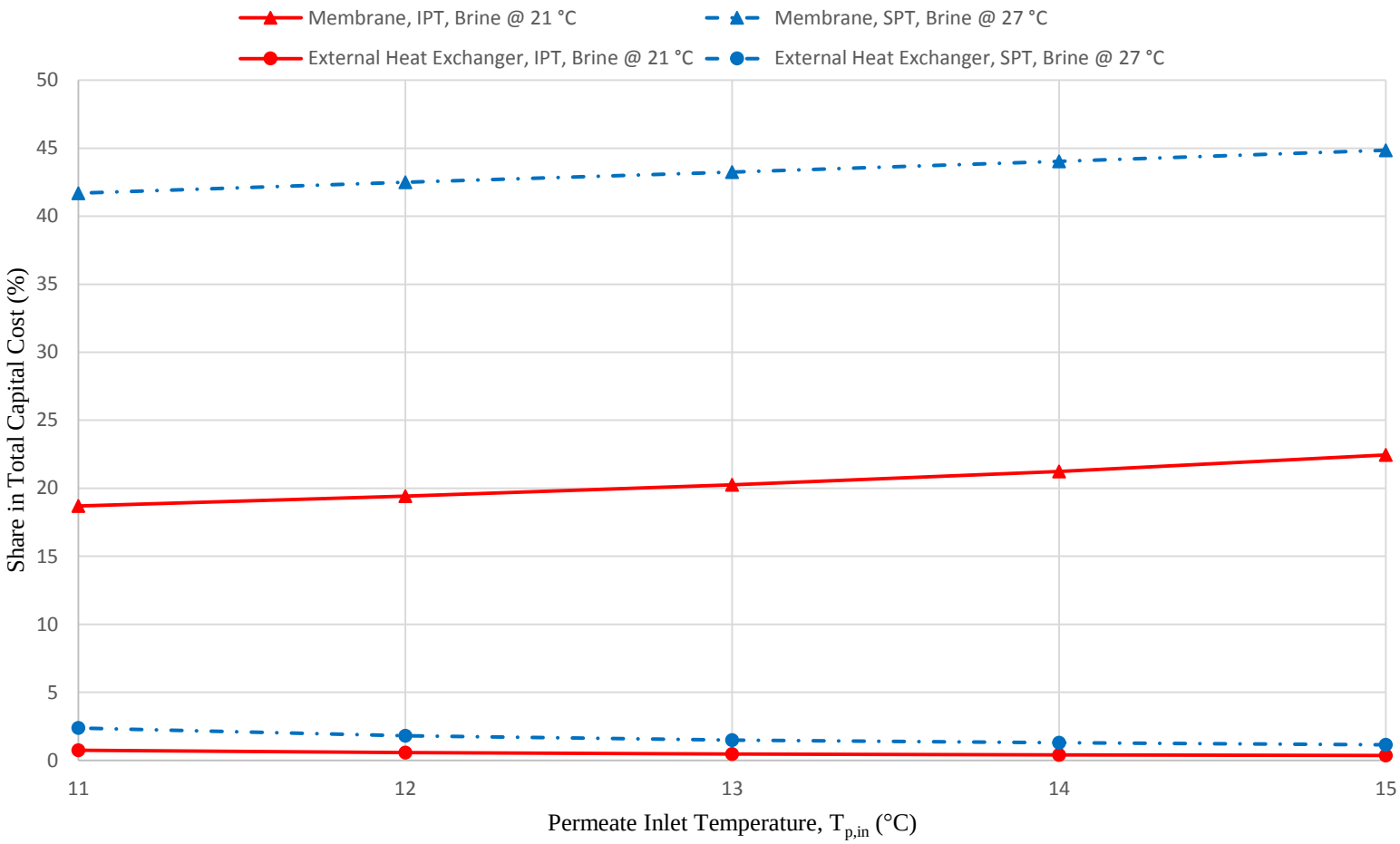

Fig. 3-7 Share of purchased membrane and external heat exchanger costs, in total capital cost vs. permeate inlet temperature at $T_{f,in}$=30 °C, and a membrane price, replacement rate, and permeability of \$90/m^2, 15% and 0.00774 kg/m^{2}h.Pa, respectively

According to Fig. 3-7, the share of the external heat exchanger cost increases only slightly as ΔT_{min} decreases, and it remained below 0.8% and 2.4% for the intense and simplified pre-treatment, respectively, demonstrating that the costs associated with the external heat exchanger

do not play a major role in controlling the product water cost. On the other hand, the share of the membrane purchase cost decreased from 22.4% to 18.7%, and 44.8% to 41.7%, for intense and simplified pre-treatment, respectively. It is worth mentioning that intake and pre-treatment cost is still a major contributor to the water production cost for the intense pre-treatment scenario by occupying approximately 58 to 61% of the total capital cost within the range of the ΔT_{min} variation. According to the results presented in Fig. 3-6, ΔT_{min} should be set at 1 ºC and permeate should enter the membrane module at 11 ºC to obtain the minimum total water cost.

3-2-3-3- Effects of Process Feed Temperature ($T_{f,in}$) on the Water Production Cost

As discussed earlier, huge thermal energy consumption is considered as a major obstacle in the commercialization of the MD process. Although, the proposed ZTIMD process is supposed to require no heat input, it would be worth investigating the effect of the process feed temperature, $T_{f,in}$, on the water production cost, especially when the recovery ratio is low. Looking into the flow sheet given in Fig. 3-1-b, the increase in $T_{f,in}$ will increase the water flux due to the enhanced driving force, which leads to the decrease in purchased membrane cost. At the same time, the recovery ratio will also increase and the feed seawater flowrate supplied to the membrane module will decrease. For instance, in one of the case studies where $T_{f,out}$ and $T_{p,in}$ are set equal to 27 and 11 ºC, respectively, with an increase in $T_{f,in}$ from 30 to 50 ºC, recovery ratio increases from almost 0.5% to 4.3% as a result of water flux increase from 7.6 to 24.7 kg/m^{2}h. Consequently, feed seawater flow rate decreases by almost 8 times. The heat required to elevate the temperature of the latter amount of feed seawater from 30 to 50 ºC is 28.9 kWh/m^3, which should be provided by an external heat source. Our calculations showed that the water

production cost would increase from \$0.61/m^3 to \$8.02/m^3, an enormous 1214.8% increase, when the solar energy is used as the heat source, while employing the fossil fuel would result in an increase from \$ 0.61/m^3 to \$ 6.56/m^3, i.e. 975.4% increase, when the simplified pre-treatment was adopted and $T_{f,out}$, $T_{p,in}$, membrane price, replacement rate, and permeability were set equal to 27 ºC, 11 ºC, \$90/m^2, 15%, and 0.00774 kg/m^2h.Pa, respectively. It should be pointed out that at $T_{f,in}$=50 ºC, more than 89% of the total capital cost is for the solar collectors and storage cost, when the solar energy is the heat source. On the other hand, more than 97% of the O&M cost was shared by the steam generation cost when fossil fuel was used to heat up the feed. It is worth mentioning that a cooling water temperature of 10 ºC due to the use of bottom seawater as the coolant and a low water recovery due to the adoption of a single-pass DCMD process are used in the simulation. The results with external thermal input using solar energy and fossil fuels therefore might be different from conventional DCMD processes using corresponding energy sources.

There are several reports in the literature on the viability of the MD desalination when the required external heat input is fulfilled by waste heat. In such a case, water production cost was evaluated to range from 0.26 to 0.65 \$/m^3 *[21,57,69,92,97,101]*. An investigation was made to study the effect of heating the seawater from 30 ºC to the process feed temperature, $T_{f,in}$ on the water production cost in the ZTIMD process, when the low grade waste heat at 100 ºC is used, and the results summarized in Fig. 3-8 for the simplified pre-treatment scenario and for the minimum approach temperature of 1 ºC ($T_{p,in}$ of 11 ºC). Again, the solid line represents the water

production cost corresponding to the center values of the membrane characteristic parameters, and the effect of each parameter is represented by the range bars and broken lines.

(a)

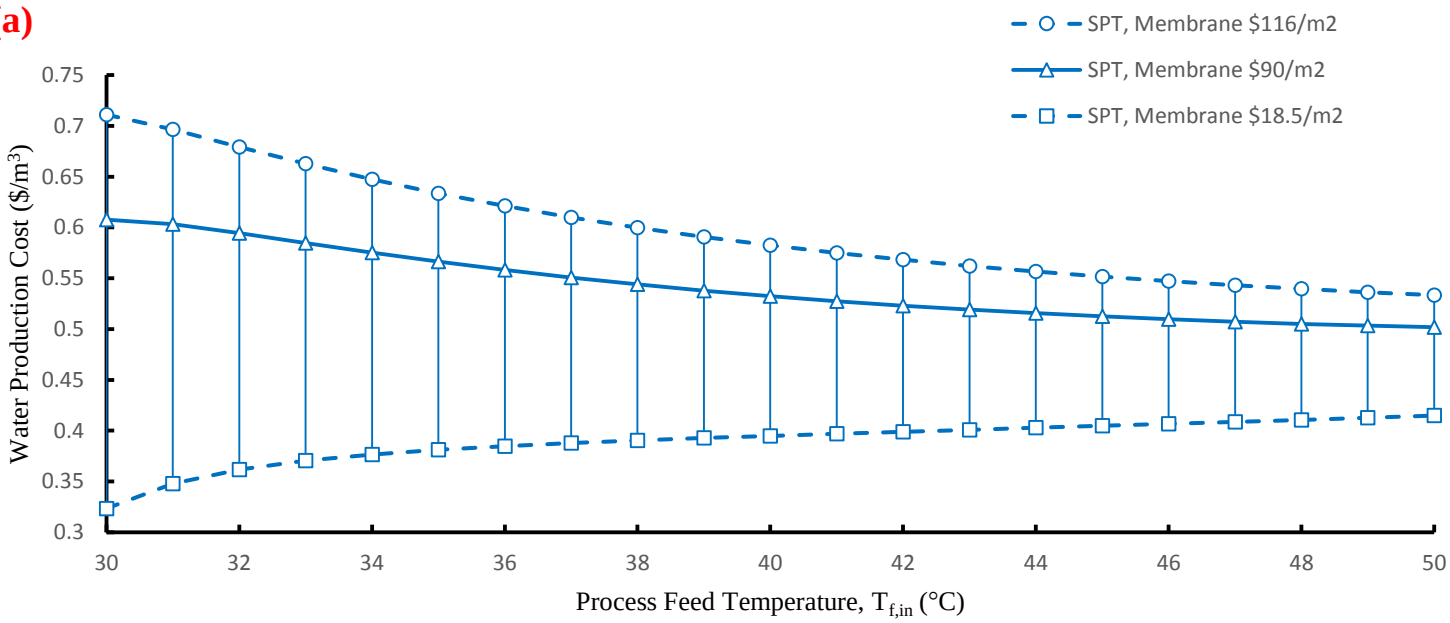

(b)

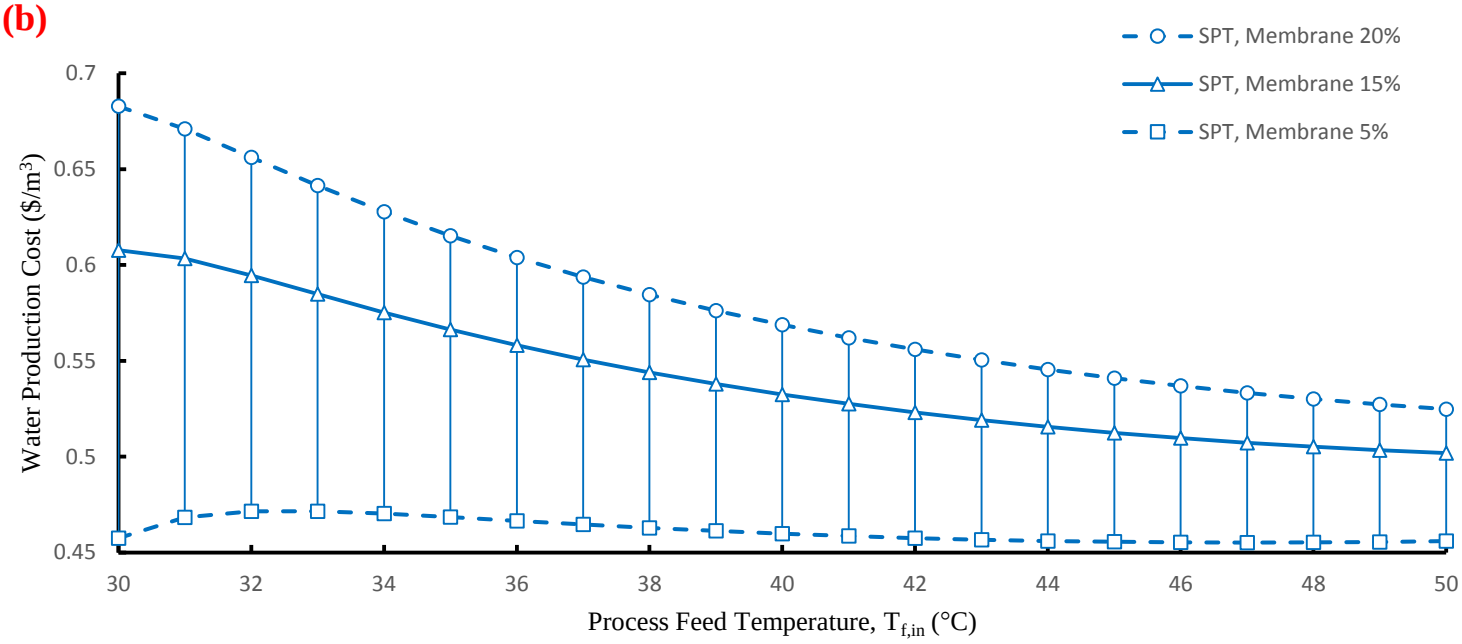
SPT, Membrane 20%
SPT, Membrane 15%
SPT, Membrane 5%
Water Production Cost ($/m3)
0.7
0.65
0.6
0.55
0.5
0.45
30
32
34
36
38
40
42
44
46
48
50
Process Feed Temperature, Tf,in (°C)

(c)

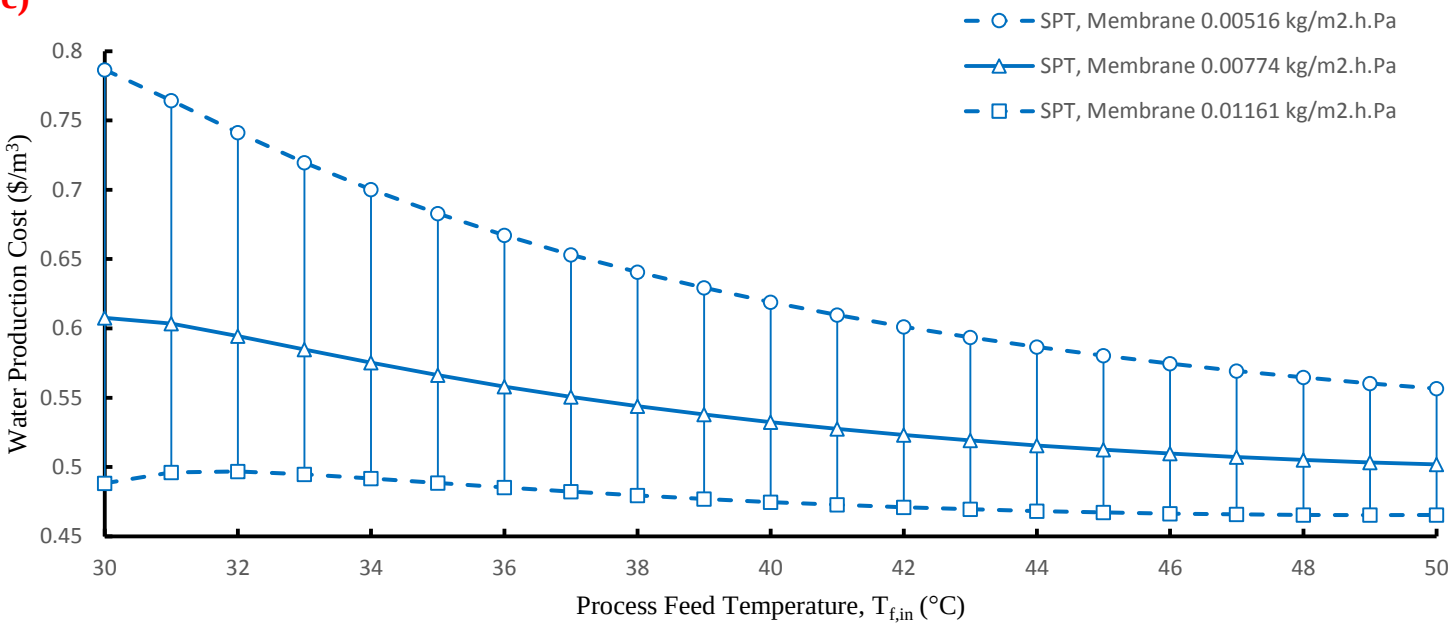
SPT, Membrane 0.00516 kg/m2.h.Pa
SPT, Membrane 0.00774 kg/m2.h.Pa
SPT, Membrane 0.01161 kg/m2.h.Pa
Water Production Cost ($/m3)
0.8
0.75
0.7
0.65
0.6
0.55
0.5
0.45
30
32
34
36
38
40
42
44
46
48
50
Process Feed Temperature, Tf,in (°C)

Fig. 3-8 Water production cost vs. process feed temperature where cartridge filtration is used for pre-treatment at $T_{f,out}$=27 °C and $T_{p,in}$=11 °C, when (a) membrane price varies in the range of 18.5-116 \$/m^2 at constant replacement rate of 15% and permeability of 0.00774 kg/m^{2}h.Pa, (b) membrane replacement rate varies in the range of 5-20% at a constant membrane price of \$90/m^2 and permeability of 0.00774 kg/m^{2}h.Pa, (c) membrane permeability varies between 0.01161-0.00516 kg/m^{2}h.Pa at a constant membrane price of \$90/m^2 and a replacement rate of 15%.

As shown in Fig. 3-8, when the center values are used, the water production cost decreases from \$0.61/m^3 to \$0.50/m^3 with the increase in $T_{f,in}$ from 30 to 50 ºC, indicating the merit of heating seawater using waste heat before it enters the MD module. However, in Fig. 3-8-a, the lower boundary of the water production cost increases with $T_{f,in}$, indicating the demerit of seawater heating when the membrane of the lowest price (18.5 \$/m^2) is available. On the other hand, a maximum is observed in the lower boundaries of Figs. 3-8-b (at a membrane replacement rate of 5%) and –c (at a membrane permeability of 0.01161 kg/m^{2}h.Pa) at $T_{f,in}$=33 ºC and 32 ºC, respectively. For instance, looking into the capital cost items for the process presented in Fig. 3-8-a, for a membrane cost of \$18.5/m^2, when $T_{f,in}$ increases from 30 to 50 ºC, share of membrane purchase cost decreases from 13.5% to 2.5%, while the portion of the steam heat exchanger cost increases from 0 to 54.9%, demonstrating that the heat exchanger becomes the dominating item in controlling the water production cost as $T_{f,in}$ increases. These results indicate that the utilization of even waste heat does not necessarily benefit the MD process due to the costs of heat exchanger.

Since the requirement of heat exchange surface is directly dependant on the temperature of waste heat, the effects of waste heat temperature in the range of 100-400 ºC was investigated with other conditions fixed at the scenario that enables the lowest water production cost of \$0.28/m^3 when no external thermal energy is used to heat the feed seawater. These conditions include simple

pre-treatment, membrane price \$18.5/m^2, replacement rate 5%, and permeability 0.01161 kg/m^2h.Pa. The results are displayed in Fig. 3-9.

It is worth mentioning that in the case of waste heat temperature of 100 ºC, and at $T_{f,in}$=50 ºC, more than 55% of the total capital cost is attributed to the cost of heat exchanger, while only 1.7% to the purchased membrane cost.

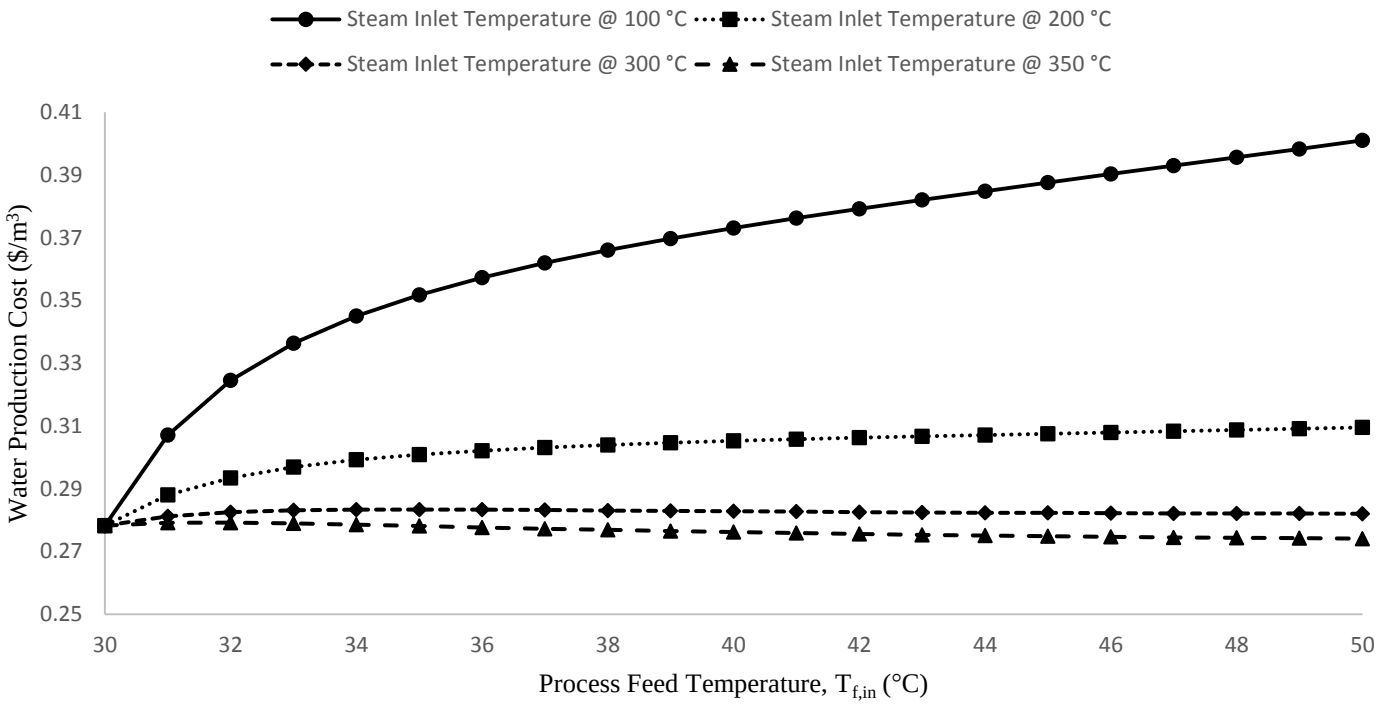

Fig. 3-9 Effect of waste heat temperature on the water production cost for the best case scenario in this work, the ZTIMD coupled with cartridge filtration at a membrane price, replacement rate, and permeability of \$18.5/m^2, 5% and 0.01161 kg/m^2h.Pa, respectively, $T_{f,out}$=27 °C and $T_{p,in}$=11 °C

As shown in Fig. 3-9, the water production cost decreases with the increase of the waste heat temperature. As well, when the waste heat temperature is less than 200 °C, increasing the process

feed temperature would increase the water production cost significantly, due to the fact that the heat exchanger cost is more dominant than the relatively low membrane cost. When the waste heat is available at temperatures of 300 and 350 °C, a maximum is observed in the water production cost at the process feed temperature of 35 and 32 °C, respectively. These results demonstrate that the cost of heat exchangers cannot be neglected in MD, especially when the temperature of the heat source is relatively low. They also point to a conclusion that is somewhat against the conventional wisdom, i.e., waste heat is not necessarily beneficial to MD unless its quality justifies its usage. It should be noted that it is rare to have waste heat available at a magnitude that is sufficient to sustain the operation of a stand-alone MD plant for desalination at large scale.

3-2-4- Feasibility of ZTIMD

Table 3-3 compares the water production cost of five different desalination technologies, i.e., Multi-Stage Flash (MSF), Multi-Effect Distillation (MED), RO, conventional MD, and ZTIMD. Thermal processes such as MSF and MED are dominant in regions with excessive access to oil, leading to concerns such as CO_2 emission and energy sustainability. For all the desalination technologies in Table 3-3, the scale benefits are obvious with the product cost remarkably lower at a larger scale. In addition to the scale, cost variations between similar processes mainly depend on location of desalination plant, quality of raw feed, and accessibility of the process to available energy sources.

Comparing the ZTIMD with other desalination technologies and according to section 3-2-1, while the primary merit of ZTIMD is that no external thermal energy is required for MD, there

are concerns in association with the increase of membrane costs at the low feed temperatures (and therefore small flux) and the introduction of additional costs including the pre-treatment of large volume of raw feed due to small water recovery and the pumping of bottom seawater as coolant. However, as shown in Table 3-3, the overall water production cost of \$0.61/m^3 when it is estimated on the basis of the center values for the membrane characteristic parameters, is quite competitive with the other processes.

The simulation results indicate that, at a typical scenario as presented in Fig. 3-1-b, i.e., when $T_{f,out}$ and $T_{p,in}$ are set at 27 and 11 °C, respectively, membrane is the top contributor to the water production cost, no matter if the simplified pre-treatment (56.9% of overall cost) or the intense pre-treatment (42.5% of overall cost) is to be used. As discussed in section 3-2-1, according to the operating conditions of the ZTIMD process, simplifying the pre-treatment to exclude chemical pre-treatment and therefore include cartridge filtration as the only major cost contributor is reasonable and commonly accepted for MD. In such a scenario, only about 3.3% of the overall cost is spent to process the raw surface seawater for the pre-treatment in ZTIMD. Furthermore, underwater piping and pumping of the bottom seawater together will add no more than 6.2% to the overall cost.

It should be noted that the center value we used for membrane price, i.e., \$90/m^2, is commonly used in feasibility studies of MD processes *[25,57,61,82]*, but is much higher than the lowest price of MD membranes in the literature, which is \$18.5/m^2 *[68]*. Furthermore, the fabrication of MD is simpler than RO and the price of commercial RO membrane could be as low as \$10-12/m^2 *[102,103]*. It is reasonable to expect the price of MD membranes to eventually fall down

to at least the level of commercial RO membranes once commercial MD desalination plants are in operation around the globe. Furthermore, the transmembrane pressure of ZTIMD is practically zero in comparison with that of RO, fouling and scaling of it is much less severe than that in RO, and the operation temperature of it, unlike that in conventional DCMD, is comparable to that of RO. As a result, it is reasonable to expect the membrane durability in ZTIMD processes to be made comparable to that of RO, if not significantly longer, as MD fabrication technologies perfects with time. Therefore, it is logical to use a membrane replacement rate of 5%, which is a realistic membrane replacement rate of commercial RO plants *[22,68,92]* as the lower limit in simulation. Finally, as aforementioned, the upper limit of the MD membrane permeability, which is 0.01161 $kg/m^2h.Pa$, is a conservative choice in comparison with literature data *[25,95]*.

When the membrane parameters are set to price $\$18.5/m^2$, replacement rate 5%, and permeability 0.01161 $kg/m^2h.Pa$, which seem by all means to be achievable according to the data available in the literature, water production cost will drop to as low as $\$0.28/m^3$, which would make the desalination as a much more affordable, much greener, and much more sustainable process. According to the results, any efforts in improving the MD membrane performance would eventually result in an even cheaper product by the process.

Table 3-3 Desalinated water cost in different processes		
Capacity (m^3/day)	**Water Production Cost ($/$m^3$)**	**Ref.**
Multi-Stage Flash (MSF)		
23,000-528,000	0.56-1.75	*[104]*
20,000	2.02	*[105]*
1	2.84	*[106]*
NA*	1.1-1.5	*[21,107]*
Multi-Effect Distillation (MED)		
91,000-320,000	0.52-1.01	*[104]*
12,000-55,000	0.95-1.5	*[104]*
20,000	0.89	*[108]*
72	2.0	*[109]*
NA*	0.46-0.85	*[21,107]*
Reverse Osmosis (RO)		
100,000-320,000	0.45-0.66	*[104]*
105,000	0.45-0.63	*[71]*
15,000-60,000	0.48-1.62	*[104]*
500	2.7	*[110]*
1	3.73	*[111]*
NA*	0.47-2.0	*[62]*
Conventional Membrane Distillation (MD)		
24,000	1.17-1.23	*[57]*
20,000	1.22	*[25]*
20,000	0.50 [a]	*[25]*
100	10-11.3 [b]	*[68]*
0.15-10	10.5-19.5	*[104]*
3.79	1.16	*[69]*
0.5	18.0-36.0	*[22]*
0.1	15.0-29.9	*[22]*
NA*	1.1-1.8	*[97]*
ZTIMD [c]		
24,000	0.61 [d]	This work
24,000	0.28 [e]	This work

* Not Applicable
[a] If geothermal energy used for heating purpose
[b] Cost in (€/m^3)
[c] With simplified pre-treatment
[d] Membrane price, replacement rate, and permeability at \$90/m^2, 15%, 0.00774 kg/m^2h.Pa
[e] Membrane price, replacement rate, and permeability at \$18.5/m^2, 5%, 0.01161 kg/m^2h.Pa

Data in Table 3-3 show that the ZTIMD process is economically more efficient than other desalination technologies. It is also interesting to compare the energy consumption of different desalination processes with that of the ZTIMD. Since the thermal energy required for evaporation is extracted from the surface seawater in the ZTIMD, the process would need no more than 0.45 kWh/m^3 electrical energy input. On the other hand, it has been reported that MSF

needs 26.4-83.0 kWh/m^3 energy input, while that of MED falls in the range of 39.7-105.7 kWh/m^3 *[21,42]*. As mentioned earlier, RO energy consumption is about 3-4 kWh/m^3 *[19,21,42,46]*. Specific energy consumption of conventional MD process varies in a large range between 600 to 9080 kWh/m^3 as reported in different studies *[21]*.

In this work, the simulation was carried out by using Gulf of Oman as the hypothetic site of operation. Nonetheless, this novel process could operate wherever the temperature difference between the surface and bottom seawater is sufficiently large.

It should be cautioned that the simulation was performed based on data obtained from laboratory and pilot scale studies reported in the literature. Validation of the results with pilot and demonstration scale plants is therefore warranted. Furthermore, the lack of time-tested commercial MD membranes due to the current lack of market demands, which is in turn dictated by the lack of economic viability of conventional MD processes, is another practical challenge. This problem, however, is expected to resolve itself when cost-effective and sustainable ZTIMD plants find their popularity in the market.

3-3- Conclusion

Conventional desalination processes, whether thermal or pressure-driven, are energy intensive and costly, which raises cost-effectiveness and sustainability as major concerns. While use of fossil fuels for desalination is unsustainable from the perspective of energy and environment, using renewable fuels for water makes the process economically unaffordable. We established the economic feasibility, energy saving, and environment-friendliness of a revolutionary

seawater desalination strategy, ZTIMD, which promises zero thermal energy consumption and zero-waste discharge, by extracting the solar thermal energy stored in surface seawater as the heat source for DCMD. The cold water at the bottom of the sea is used as the coolant and the temperature difference between the warm surface and the cold bottom seawaters provides the driving force. Economic evaluation was carried out using a typical temperature profile of seawater to the depth direction in Gulf of Oman. Two case scenarios were considered with respect to the pre-treatment of seawater: one in which the pre-treatment is as intense as that of the RO and the other is done by simplified pre-treatment using cartridge filters alone, which has been accepted as realistic for MD. It was concluded that for both case scenarios there is no or minimized merit of implementing any external heat sources, including free waste heat unless it is available at 350 °C or higher. When the centre values for the membrane characteristics are used, a water production cost of \$0.61/m^3 at a specific energy consumption of 0.45 kWh/m^3 could be achieved by ZTIMD, which is competitive comparing to that of the commercial SWRO processes. In a favorable scenario, water production cost of \$0.28/m^3 was found to be achievable.

It is worth emphasizing that the enthalpy of surface seawater would be able to match ZTIMD operations at any scale.

Furthermore, unlike SWRO processes that create environmental liabilities such as the discharge of large volumes of concentrate brine from the RO units to the operation site, which may cause significant stress to the local aquatic ecosystem *[74,75]*, the ZTIMD process promises not to alternate the local salt concentration of operation sea region and discharging no waste chemicals from pre-treatment as well. In other words, the zero-thermal energy input membrane distillation

process is also a zero-waste process. We expect the successful implementation of this strategy, which is sustainable from the perspectives of economics, energy, and environment, to revolutionize seawater desalination industry.

3-4- Sample Cost Calculation for the Best Case Scenario

The water production cost with the required details for the ZTIMD with a process flow diagram shown in Fig. 3-1-b when the membrane price, replacement rate, and permeability are assumed to be \$18.5/m^2, 5%, and 0.01161 kg/m^2h.Pa, respectively, is presented in this section. Specific values of key parameters used in the sample calculations are presented in Table 3-4. Temperatures at the membrane interface were obtained by assuming a temperature polarization factor of 0.7 *[85-91]*.

Table 3-4 Operating conditions of the ZTIMD with simplified pre-treatment

$T_{f,in}$ (°C)	$T_{f,out}$ (°C)	$T_{p,in}$ (°C)	$T_{p,out}$ (°C)	$T_{c,in}$ (°C)	$T_{c,out}$ (°C)
30	27	11	25	10	20
$T_{f,m,in}$ (°C)		$T_{f,m,out}$ (°C)	$T_{p,m,in}$ (°C)	$T_{p,m,out}$ (°C)	
29.25		24.6	13.4	25.75	
$P^*_{f,m,in}$ (kPa)		$P^*_{f,m,out}$ (kPa)	$P^*_{p,m,in}$ (kPa)	$P^*_{p,m,out}$ (kPa)	
3.95		3.00	1.54	3.33	
Membrane Flux (kg/m^2h)					
11.3					
Recovery Ratio (RR), Equation (2)					
0.00555					

Raw Feed Flowrate

$$Raw\ feed\ flowrate = \frac{W}{RR} = 4{,}321{,}223.7\ m^3/day$$

Coolant Flowrate

$$Coolant\ flowrate = \left(\frac{W \times \Delta H_v}{C_p \times \left(T_{p,out} - T_{p,in}\right)} - W\right) \times \frac{T_{p,out} - T_{p,in}}{T_{c,out} - T_{c,in}} = 1{,}262{,}767.1\, m^3/day$$

Electricity for Pumping

$$Frictional\ pressure\ loss\ within\ the\ underwater\ pipe = \Delta P_f = \frac{{m_c}^{1.8}\mu^{0.2}}{20{,}000 d^{4.8}\rho}$$

$$= 5.3\left(\frac{psi}{100ft}\right) \xrightarrow{Considering\ a\ pipe\ length\ of\ 1100\ m} \Delta P_f = 1{,}319.4\ kPa$$

$$Required\ pumping\ energy = 1319.4\ kJ/m^3 = 0.366\, kWh/m^3$$

Size of Heat Exchangers

$$Heat\ to\ be\ provided\ by\ the\ external\ heat\ exchanger =$$

$$\frac{Coolant\ flowrate \times C_p \times \left(T_{c,out} - T_{c,in}\right)}{\eta} = 760{,}561.4\ kW$$

$$Required\ external\ heat\ exchanger\ area = \frac{Heat\ to\ be\ provided\ by\ EHX}{U \times \Delta T_{LMTD}} = 437.2\, m^2$$

Surface Area of Membrane

$$Required\ membrane\ area = \frac{W \times \rho/24}{Flux} = 87{,}714.3\, m^2$$

Units of Cartridge Filters for Pre-treatment:

$$Required\ cartridge\ filters\ for\ pre-treatment = \frac{Raw\ feed\ flowrate}{Feed\ flowrate\ to\ cartridge}$$

$$\xrightarrow{Considering\ a\ cartridge\ flowrate\ of\ 540\ m^3/day} Number\ of\ cartridge\ filters = 8{,}003$$

3-4-1- Capital Cost

Table 3-5 Capital cost break-down calculations

Cost of civil work excluding the underwater piping ($)	$1945W^{0.8}$ [33]	6,201,000
Cost of purchased underwater piping ($)	(Required pipe length)×l	348,000
Cost of underwater piping installation ($)	[70]	1,500,000
Cost of intake and pre-treatment ($)	(Number of filters) ×(unit cost of filters)	1,961,000
Cost of DCMD feed pumps ($)	$4.78 \times 10^{-6}\ (W/RR)\ P$[33]	2,479,000
Cost of DCMD coolant pumps ($)	[57]	805,000
Cost of membrane ($)	(Required membrane area)×m*	1,623,000
Cost of heat exchangers ($)	(Required heat exchanger area)×h	673,000
Total direct capital costs ($)	Sum of all above costs	15,590,000
Indirect capital costs ($)	0.1×(Total direct capital costs) [33]	1,559,000
Total capital costs ($)	(Direct + Indirect capital costs)	17,149,000
Annual fixed charges ($/m^3)	$(a \times \text{Total capital costs})/(f \times W \times 365)$ [33]	0.18

3-4-2- Operation and Maintenance Cost

Table 3-6 Operation and maintenance cost break-down calculations

Membrane replacement ($/year)	(Total cost of membrane)× r_m	81,000
Cost of electricity excluding the bottom seawater pumping ($/year)	(Annual electricity consumption)×e	11,000
Cost of electricity for pumping the coolant, i.e. bottom seawater ($/year)	(Annual electricity consumption)×e	87,000
Cost of chemicals ($/year)	(Specific chemical cost per m^3)×W	142,000
Cost of spares ($/year)	(Specific spears cost per m^3)×W	260,000
Cost of labor ($/year)	(Specific labor cost per m^3)×W	237,000
Total annual O&M costs ($/year)	Sum of all above costs	818,000
Annual O&M charges ($/m^3)	(Total annual O&M $costs$)$/(f \times W \times 365)$ [33]	0.10

3-4-3- Overall Water Cost

$$Overall\ water\ cost = Annual\ fixed\ charges + Anuual\ O\&M\ charges = 0.28\ \$/m^3$$

3-4-4- Thickness of Required Insulation Material for Only 1 °C Increase in Coolant Temperature from Bottom of the Sea to the Surface

In this calculations, it is assumed that the environment seawater temperature is fixed at 30 °C from the bottom to surface of the sea (Worst Case Scenario).

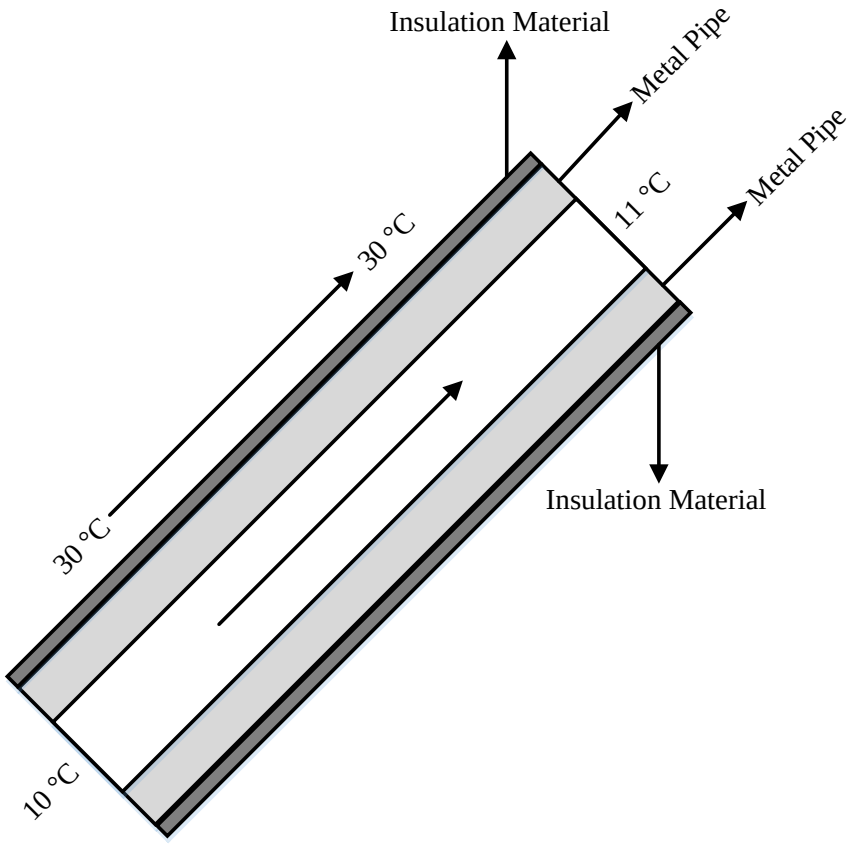

Fig. 3-10 A schematic of the underwater pipe for cooling the bottom seawater

Table 3-7 List of assumptions for calculation of the thickness of the insulation material	
ρ (kg/m^3)	999.7
$D_{i,Pipe}$ (m)	1.03
$r_{i,Pipe}$ (m)	0.51
$D_{o,Pipe}$ (m)	1.07
$r_{o,Pipe}$ (m)	0.53
k_{Steel} (W/mK)	50.2
Pipe Length (m)	1100
Viscosity (Ns/m^2)	0.001307
Coolant Flowrate (m^3/s)	14.73
Coolant Flowrate (kg/s)	14722.05
Surface Area (m^2)	0.83
Velocity (m/s)	17.72
Heat Capacity (J/kgK)	4181.3
k_{Water} (W/mK)	0.58

Energy Required for 1 °C Temperature Increase along the Pipe:

$$Q = mc_p\Delta T = 61557321.35\ W$$

Thermal Resistance of the Pipe:

$$R_{Steel\ Pipe} = \frac{\ln(\frac{r_o}{r_i})}{2\pi kl} = \frac{\ln(\frac{0.5334}{0.51435})}{2\pi \times 50.2 \times 1100} = 1.05 \times 10^{-7}$$

Convective Heat Transfer Coefficient inside the Pipe:

$$Re = \frac{\rho u D_i}{\mu} = \frac{999.7 \times 17.71867865 \times 1.0287}{0.001307} = 13941650.01$$

$$Pr = \frac{c_p \mu}{k_{Water}} = \frac{4181.3 \times 0.001307}{0.58} = 9.42$$

$$Nu = 0.027 \times Re^{4/5} \times Pr^{1/3} = 29616.57$$

$$h = \frac{Nu \times k_{Water}}{D_i} = 16698.37\ W/m^2K$$

Inner Surface Temperature of the Pipe:

$$\Delta T = \frac{Q}{h \times \pi \times D_i \times l} = 1.04\ ℃$$

$$T_{Inner\ Wall} = 10 + \Delta T = 11.04$$

Temperature Difference across the Metal Pipe:

$$\Delta T_{Steel\ Pipe} = Q \times R_{Steel\ Pipe} = 6.45\ ℃$$

$$T_{Outer\ Wall} = 11.04 + 6.45 = 17.49$$

Temperature Difference across the Insulation Material:

$$\Delta T_{Insulation\ Material} = 30 - 17.49 = 12.51\ ℃$$

Thermal Resistance of the Insulation Material ($\Delta T=29-(11+\Delta T_{\text{Steel Pipe}})$ °C):

$$R_{Insulation\ Material} = \frac{\Delta T_{Insulation\ Material}}{Q} = 2.03 \times 10^{-7}$$

Thickness of the Insulation Material (Fiberglass as Insulation Material, k=0.04 W/mK):

$$r_o = r_i exp(2\pi k_{Insulation\ Material} l \times R)$$

$$r_{o,Insulation\ Material} = 0.53 \times exp(2\pi \times 0.04 \times 1100 \times 2.03 \times 10^{-7})$$

$$r_{o,Insulation\ Material} = 0.53\ m$$

Thickness of the Insulation Material:

$$t = 2.99 \times 10^{-5}\ m$$

It should be pointed out that coolant would have a short residence time of about 62 s in the pipe from bottom of the sea to its surface that hypothetically could be the reason of an extremely small required insulation material thickness for an increase of only 1 °C in the coolant temperature. The above calculations show that the costs associated with the insulation material to maintain the coolant temperature at 10 °C within the pipe from bottom of the sea to the surface would be negligible.

References

[1] Gude VG. Desalination and sustainability - An appraisal and current perspective. Water Res 2016;89:87-106.

[2] Mehanna M, Saito T, Yan J, Hickner M, Cao X, Huang X et al. Using microbial desalination cells to reduce water salinity prior to reverse osmosis. Energy & Environmental Science 2010;3:1114-20.

[3] Shahzad MW, Thu K, Kim Y, Ng KC. An experimental investigation on MEDAD hybrid desalination cycle. Appl Energy 2015;148:273-81.

[4] Efome JE, Baghbanzadeh M, Rana D, Matsuura T, Lan CQ. Effects of superhydrophobic SiO2 nanoparticles on the performance of PVDF flat sheet membranes for vacuum membrane distillation. Desalination 2015;373:47-57.

[5] Khalifa AE. Water and air gap membrane distillation for water desalination – An experimental comparative study. Separation and Purification Technology 2015;141:276-84.

[6] Daer S, Kharraz J, Giwa A, Hasan SW. Recent applications of nanomaterials in water desalination: A critical review and future opportunities. Desalination 2015;367:37-48.

[7] Baghbanzadeh M, Rana D, Lan CQ, Matsuura T. Effects of Inorganic Nano-Additives on Properties and Performance of Polymeric Membranes in Water Treatment. Separation & Purification Reviews 2016;45:141-67.

[8] Miller S, Shemer H, Semiat R. Energy and environmental issues in desalination. Desalination 2015;366:2-8.

[9] Baghbanzadeh M, Rana D, Matsuura T, Lan CQ. Effects of hydrophilic CuO nanoparticles on properties and performance of PVDF VMD membranes. Desalination 2015;369:75-84.

[10] Hegab HM, Zou L. Graphene oxide-assisted membranes: Fabrication and potential applications in desalination and water purification. J Membr Sci 2015;484:95-106.

[11] Azizi Namaghi H, Haghighi Asl A, Pourafshari Chenar M. Identification and optimization of key parameters in preparation of thin film composite membrane for water desalination using multi-step statistical method. Journal of Industrial and Engineering Chemistry 2015;31:61-73.

[12] Baghbanzadeh M, Rana D, Lan CQ, Matsuura T. Effects of hydrophilic silica nanoparticles and backing material in improving the structure and performance of VMD PVDF membranes. Separation and Purification Technology 2016;157:60-71.

[13] Surwade SP, Smirnov SN, Vlassiouk IV, Unocic RR, Veith GM, Dai S et al. Water desalination using nanoporous single-layer graphene. Nature Nanotechnology 2015;10:459-64.

[14] Chen Y, Li Y, Chang H. Optimal design and control of solar driven air gap membrane distillation desalination systems. Appl Energy 2012;100:193-204.

[15] ElMekawy A, Hegab HM, Pant D. The near-future integration of microbial desalination cells with reverse osmosis technology. Energy & Environmental Science 2014;7:3921-33.

[16] Gude VG. Energy storage for desalination processes powered by renewable energy and waste heat sources. Appl Energy 2015;137:877-98.

[17] Desalination Plants to Double by 2020. October, 2015.

[18] Thu K, Kim Y, Amy G, Chun WG, Ng KC. A hybrid multi-effect distillation and adsorption cycle. Appl Energy 2013;104:810-21.

[19] Fthenakis V, Atia AA, Morin O, Bkayrat R, Sinha P. New prospects for PV powered water desalination plants: case studies in Saudi Arabia. Progress in Photovoltaics 2016;24:543-50.

[20] Napoli C, Rioux B. Evaluating the economic viability of solar-powered desalination: Saudi Arabia as a case study. Int J Water Resour Dev 2016;32:412-27.

[21] Khayet M. Solar desalination by membrane distillation: Dispersion in energy consumption analysis and water production costs (a review). Desalination 2013;308:89-101.

[22] Banat F, Jwaied N. Economic evaluation of desalination by small-scale autonomous solar-powered membrane distillation units. Desalination 2008;220:566-73.

[23] Salata F, Coppi M. A first approach study on the desalination of sea water using heat transformers powered by solar ponds. Appl Energy 2014;136:611-8.

[24] Gude VG. Geothermal source potential for water desalination - Current status and future perspective. Renew Sust Energ Rev 2016;57:1038-65.

[25] Sarbatly R, Chiam C. Evaluation of geothermal energy in desalination by vacuum membrane distillation. Appl Energy 2013;112:737-46.

[26] Gokcek M, Gokcek OB. Technical and economic evaluation of freshwater production from a wind-powered small-scale seawater reverse osmosis system (WP-SWRO). Desalination 2016;381:47-57.

[27] Guo L, Liu W, Li X, Liu Y, Jiao B, Wang W et al. Energy Management System for Stand-Alone Wind-Powered-Desalination Microgrid. IEEE Trans Smart Grid 2016;7:1079-87.

[28] Dansoh C. The viability of renewable energy and energy storage as the power source for municipal- scale reverse osmosis desalination. Desalin Water Treat 2015;55:3064-90.

[29] Zhao G, Su X, Cao Y, Su J, Liu Y. Experiments on the hydrodynamic performance of horizontal axis tidal current turbine and desalination of sea water. Int J Energy Res 2016;40:600-9.

[30] Fiorenza G, Sharma V, Braccio G. Techno-economic evaluation of a solar powered water desalination plant. Energy Conversion and Management 2003;44:2217-40.

[31] Zhou L, Tan Y, Wang J, Xu W, Yuan Y, Cai W et al. 3D self-assembly of aluminium nanoparticles for plasmon-enhanced solar desalination. Nature Photonics 2016;10:393.

[32] Inukai S, Cruz-Silva R, Ortiz-Medina J, Morelos-Gomez A, Takeuchi K, Hayashi T et al. High-performance multi-functional reverse osmosis membranes obtained by carbon nanotube.polyamide nanocomposite. Scientific Reports 2015;5:13562.

[33] Hassan AS, Fath HES. Review and assessment of the newly developed MD for desalination processes. Desalin Water Treat 2013;51:574-85.

[34] Shannon MA, Bohn PW, Elimelech M, Georgiadis JG, Marinas BJ, Mayes AM. Science and technology for water purification in the coming decades. Nature 2008;452:301-10.

[35] Heiranian M, Farimani AB, Aluru NR. Water desalination with a single-layer MoS2 nanopore. Nature Communications 2015;6:8616.

[36] Cohen-Tanugi D, McGovern RK, Dave SH, Lienhard JH, Grossman JC. Quantifying the potential of ultra-permeable membranes for water desalination. Energy & Environmental Science 2014;7:1134-41.

[37] Suss ME, Baumann TF, Bourcier WL, Spadaccini CM, Rose KA, Santiago JG et al. Capacitive desalination with flow-through electrodes. Energy & Environmental Science 2012;5:9511-9.

[38] Suárez F, Ruskowitz JA, Tyler SW, Childress AE. Renewable water: Direct contact membrane distillation coupled with solar ponds. Appl Energy 2015;158:532-9.

[39] Zhou J, Chang VW-, Fane AG. Environmental life cycle assessment of brackish water reverse osmosis desalination for different electricity production models. Energy & Environmental Science 2011;4:2267-78.

[40] Forrestal C, Xu P, Ren Z. Sustainable desalination using a microbial capacitive desalination cell. Energy & Environmental Science 2012;5:7161-7.

[41] Prante JL, Ruskowitz JA, Childress AE, Achilli A. RO-PRO desalination: An integrated low-energy approach to seawater desalination. Appl Energy 2014;120:104-14.

[42] Wakeel M, Chen B, Hayat T, Alsaedi A, Ahmad B. Energy consumption for water use cycles in different countries: A review. Appl Energy 2016;178:868-85.

[43] Ophek L, Birnhack L, Nir O, Binshtein E, Lahav O. Reducing the specific energy consumption of 1st-pass SWRO by application of high-flux membranes fed with high-pH, decarbonated seawater. Water Res 2015;85:185-92.

[44] Elimelech M, Phillip WA. The Future of Seawater Desalination: Energy, Technology, and the Environment. Science 2011;333:712-7.

[45] Tal A. Seeking sustainability: Israel's evolving water management strategy. Science 2006;313:1081-4.

[46] Ghaffour N, Lattemann S, Missimer T, Ng KC, Sinha S, Amy G. Renewable energy-driven innovative energy-efficient desalination technologies. Appl Energy 2014;136:1155-65.

[47] Spiegler KS, El-Sayed YM. The energetics of desalination processes. Desalination 2001;134:109-28.

[48] Criscuoli A, Drioli E. Energetic and exergetic analysis of an integrated membrane desalination system. Desalination 1999;124:243-9.

[49] Cerci Y. Exergy analysis of a reverse osmosis desalination plant in California. Desalination 2002;142:257-66.

[50] UNESCO Centre for Membrane Science and Technology. Emerging trends in desalination: a review, Comissioned by the National Water Commission and on Key Water Issues. October 2008;9.

[51] Busch M, Mickols WE. Reducing energy consumption in seawater desalination. Desalination 2004;165:299-312.

[52] Wang EN, Karnik R. WATER DESALINATION Graphene cleans up water. Nature Nanotechnology 2012;7:552-4.

[53] Liu Z, Bai H, Lee J, Sun DD. A low-energy forward osmosis process to produce drinking water. Energy & Environmental Science 2011;4:2582-5.

[54] Bajpayee A, Luo T, Muto A, Chen G. Very low temperature membrane-free desalination by directional solvent extraction. Energy & Environmental Science 2011;4:1672-5.

[55] Ali MT, Fath HES, Armstrong PR. A comprehensive techno-economical review of indirect solar desalination. Renewable and Sustainable Energy Reviews 2011;15:4187-99.

[56] Susanto H. Towards practical implementations of membrane distillation. Chem Eng Process 2011;50:139-50.

[57] Al-Obaidani S, Curcio E, Macedonio F, Di Profio G, Ai-Hinai H, Drioli E. Potential of membrane distillation in seawater desalination: Thermal efficiency, sensitivity study and cost estimation. J Membr Sci 2008;323:85-98.

[58] Chang H, Hsu J, Chang C, Ho C, Cheng T. Simulation study of transfer characteristics for spacer-filled membrane distillation desalination modules. Appl Energy, http://dx.doi.org/10.1016/j.apenergy.2015.12.030.

[59] Li G, Zhang L. Investigation of a solar energy driven and hollow fiber membrane-based humidification–dehumidification desalination system. Appl Energy 2016;177:393-408.

[60] Zaragoza G, Ruiz-Aguirre A, Guillén-Burrieza E. Efficiency in the use of solar thermal energy of small membrane desalination systems for decentralized water production. Appl Energy 2014;130:491-9.

[61] Macedonio F, Curcio E, Drioli E. Integrated membrane systems for seawater desalination: energetic and exergetic analysis, economic evaluation, experimental study. Desalination 2007;203:260-76.

[62] Camacho LM, Dumee L, Zhang J, Li J, Duke M, Gomez J et al. Advances in Membrane Distillation for Water Desalination and Purification Applications. Water 2013;5:94-196.

[63] Xu Y, Zhu B, Xu Y. Pilot test of vacuum membrane distillation for seawater desalination on a ship. Desalination 2006;189:165-9.

[64] Khraisheh M, Benyahia F, Adham S. Industrial case studies in the petrochemical and gas industry in Qatar for the utilization of industrial waste heat for the production of fresh water by membrane desalination. Desalination and Water Treatment 2013;51:1769-75.

[65] Banat F, Jwaied N. Economic evaluation of desalination by small-scale autonomous solar-powered membrane distillation units. Desalination 2008;220:566-73.

[66] Zhao K, Heinzl W, Wenzel M, Buettner S, Bollen F, Lange G et al. Experimental study of the memsys vacuum-multi-effect-membrane-distillation (V-MEMD) module. Desalination 2013;323:150-60.

[67] Meindersma G, Guijt C, de Haan A. Desalination and water recycling by air gap membrane distillation. Desalination 2006;187:291-301.

[68] Guillen-Burrieza E, Alarcon-Padilla D, Palenzuela P, Zaragoza G. Techno-economic assessment of a pilot-scale plant for solar desalination based on existing plate and frame MD technology. Desalination 2015;374:70-80.

[69] Lee J, Kim W. Numerical study on multi-stage vacuum membrane distillation with economic evaluation. Desalination 2014;339:54-67.

[70] Greenlee LF, Lawler DF, Freeman BD, Marrot B, Moulin P. Reverse osmosis desalination: Water sources, technology, and today's challenges. Water Res 2009;43:2317-48.

[71] Meindersma G, Guijt C, de Haan A. Desalination and water recycling by air gap membrane distillation. Desalination 2006;187:291-301.

[72] Michael Reynolds R. Physical oceanography of the Gulf, Strait of Hormuz, and the Gulf of Oman—Results from the Mt Mitchell expedition. Mar Pollut Bull 1993;27:35-59.

[73] Pous S, Carton X, Lazure P. Hydrology and circulation in the Strait of Hormuz and the Gulf of Oman - Results from the GOGP99 experiment: 1. Strait of Hormuz. Journal of Geophysical Research-Oceans 2004;109:C12037.

[74] Brika B, Omran AA, Addien OD. Chemical elements of brine discharge from operational Tajoura reverse osmosis desalination plant. Desalination and Water Treatment 2016;57:5345-9.

[75] Jamil S, Loganathan P, Kazner C, Vigneswaran S. Forward osmosis treatment for volume minimisation of reverse osmosis concentrate from a water reclamation plant and removal of organic micropollutants. Desalination 2015;372:32-8.

[76] Ezam M, Bidokhti AA, Javid AH. Numerical simulations of spreading of the Persian Gulf outflow into the Oman Sea. Ocean Science 2010;6:887-900.

[77] Koschikowski J, Wieghaus M, Rommel M. Solar thermal-driven desalination plants based on membrane distillation. Desalination 2003;156:295-304.

[78] Xevgenos D, Moustakas K, Malamis D, Loizidou M. An overview on desalination & sustainability: renewable energy-driven desalination and brine management. Desalin Water Treat 2016;57:2304-14.

[79] Wan CF, Chung T. Energy recovery by pressure retarded osmosis (PRO) in SWRO-PRO integrated processes. Appl Energy 2016;162:687-98.

[80] Backhurst JR, Marker JH. Coulson & Richardson's Chemical Engineering, Fluid Flow, Heat Transfer and Mass Transfer. Sixth ed. Oxford: Butterworth-Heinemann, Volume 1, 1999.

[81] Sinnott RK. Coulson & Richardson's Chemical Engineering, Chemical Engineering Design Third ed. Oxford: Butterworth-Heinemann, Volume 6, 2003.

[82] Macedonio F, Ali A, Poerio T, El-Sayed E, Drioli E, Abdel-Jawad M. Direct contact membrane distillation for treatment of oilfield produced water. Separation and Purification Technology 2014;126:69-81.

[83] Golomb D. Transport systems for ocean disposal of CO2 and their environmental effects. Energy Conversion and Management 1997;38:S279-86.

[84] Peters MS, Timmerhaus KD. Plant design and economics for chemical engineers. Fourth ed. : McGraw-Hill, 1991.

[85] Alkhudhiri A, Darwish N, Hilal N. Membrane distillation: A comprehensive review. Desalination 2012;287:2-18.

[86] Curcio E, Drioli E. Membrane distillation and related operations - A review. Separation and Purification Reviews 2005;34:35-86.

[87] Lawson KW, Lloyd DR. Membrane distillation. J Membr Sci 1997;124:1-25.

[88] MartinezDiez L, VazquezGonzalez M. Temperature polarization in mass transport through hydrophobic porous membranes. AIChE J 1996;42:1844-52.

[89] Martinez-Diez L, Vazquez-Gonzalez M. Effects of polarization on mass transport through hydrophobic porous membranes. Ind Eng Chem Res 1998;37:4128-35.

[90] Phattaranawik J, Jiraratananon R. Direct contact membrane distillation: effect of mass transfer on heat transfer. J Membr Sci 2001;188:137-43.

[91] Janajreh I, Suwwan D, Hashaikeh R. Assessment of direct contact membrane distillation under different configurations, velocities and membrane properties. Appl Energy, http://dx.doi.org/10.1016/j.apenergy.2016.05.020.

[92] Saffarini RB, Summers EK, Arafat HA, Lienhard JH. Economic evaluation of stand-alone solar powered membrane distillation systems. Desalination 2012;299:55-62.

[93] Drioli E, Curcio E, Di Profio G, Macedonio F, Criscuoli A. Integrating membrane contactors technology and pressure-driven membrane operations for seawater desalination - Energy, exergy and costs analysis. Chemical Engineering Research & Design 2006;84:209-20.

[94] Apricus Solar Co. L. Middle eastern solar insolation levels. 2012.

[95] Chiam C, Sarbatly R. Vacuum membrane distillation processes for aqueous solution treatment-A review. Chem Eng Process 2013;74:27-54.

[96] Drioli E, Lagana F, Criscuoli A, Barbieri G. Integrated membrane operations in desalination processes. Desalination 1999;122:141-5.

[97] Zuo G, Wang R, Field R, Fane AG. Energy efficiency evaluation and economic analyses of direct contact membrane distillation system using Aspen Plus. Desalination 2011;283:237-44.

[98] Golomb D. Transport systems for ocean disposal of CO2 and their environmental effects. Energy Conversion and Management 1997;38:S279-86.

[99] Smith JM, Van Ness HC, Abbott MM. Introduction to Chemical Engineering Thermodynamics, Seventh ed. New York: McGraw-Hill Comp, 2005.

[100] Branan C. Rules of thumb for chemical engineers. Third ed. United States of America: Gulf Professional, 2002.

[101] Hanemaaijer JH, van Medevoort J, Jansen AE, Dotremont C, van Sonsbeek E, Yuan T et al. Memstill membrane distillation - a future desalination technology. Desalination 2006;199:175-6.

[102] Zhu A, Rahardianto A, Christofides PD, Cohen Y. Reverse osmosis desalination with high permeability membranes - Cost optimization and research needs. Desalination and Water Treatment 2010;15:256-66.

[103] Yoon S. Membrane Bioreactor Processes: Principles and Applications. Florida, USA: CRC Press, 2016.

[104] Al-Karaghouli A, Kazmerski LL. Energy consumption and water production cost of conventional and renewable-energy-powered desalination processes. Renewable & Sustainable Energy Reviews 2013;24:343-56.

[105] Ayoub J, Alward R. Water requirements and remote arid areas: The need for small-scale desalination. Desalination 1996;107:131-47.

[106] SURI R, ALMARAFIE A, ALHOMOUD A, MAHESHWARI G. Cost-Effectiveness of Solar Water Production. Desalination 1989;71:165-75.

[107] Semiat R. Desalination: Present and future. Water Int 2000;25:54-65.

[108] GLUECKSTERN P. Potential Uses of Solar-Energy for Seawater Desalination. Desalination 1995;101:11-20.

[109] Milow B, Zarza E. Advanced MED solar desalination plants. Configurations, costs, future - Seven years of experience at the Plataforma Solar de Almeria (Spain). Desalination 1997;108:51-8.

[110] Fiorenza G, Sharma V, Braccio G. Techno-economic evaluation of a solar powered water desalination plant. Energy Conversion and Management 2003;44:2217-40.

[111] Ahmad G, Schmid J. Feasibility study of brackish water desalination in the Egyptian deserts and rural regions using PV systems. Energy Conversion and Management 2002;43:2641-9.

Chapter 4:

Effects of inorganic nano-additives on properties and performance of polymeric membranes in water treatment: a review

M. Baghbanzadeh, D. Rana, C. Q. Lan, T. Matsuura, Effects of inorganic nano-additives on properties and performance of polymeric membranes in water treatment, Separation & Purification Reviews, 45 (2016) 141-167

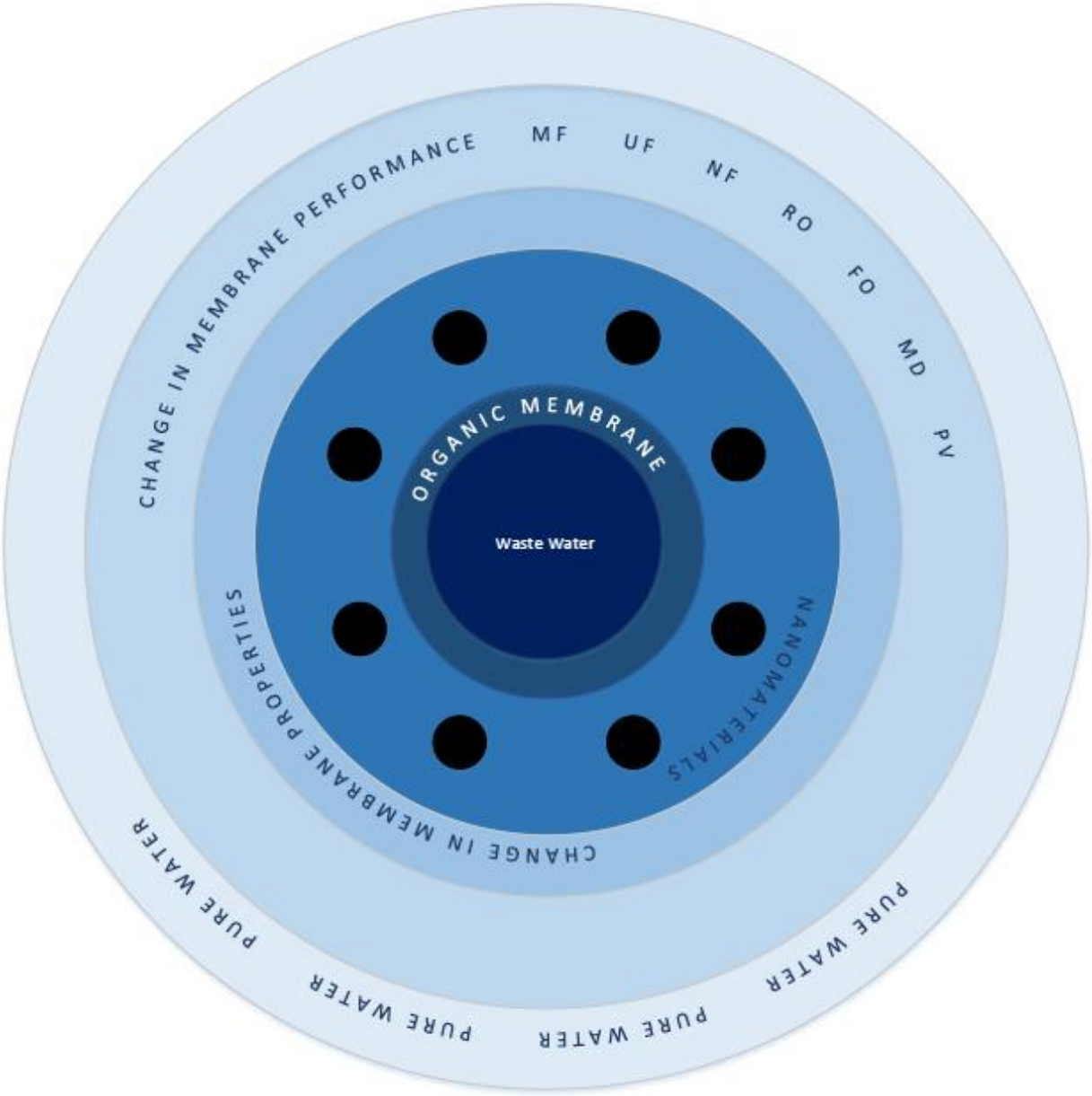
CHANGE IN MEMBRANE PERFORMANCE
MF
UF
NF
RO
FO
MD
PV
ORGANIC MEMBRANE
Waste Water
NANOMATERIALS
CHANGE IN MEMBRANE PROPERTIES
PURE WATER
PURE WATER
PURE WATER
PURE WATER
PURE WATER

Effects of inorganic nano-additives on properties and performance of polymeric membranes in water treatment: a review

Mohammadali Baghbanzadeh, Dipak Rana, Christopher Q. Lan*, Takeshi Matsuura
Department of Chemical and Biological Engineering, University of Ottawa, 161 Louis Pasteur Private, Ottawa, Ontario, Canada K1N 6N5

Abstract

Separation using selective polymeric membranes has been well-established as an energy-efficient and cost-effective technology in water treatment and many other applications involving aqueous solutions. However, limited chemical, thermal, and mechanical resistances besides their tendency to fouling, and inadequate pure water flux may often restrict their applications. To this end, inorganic materials as additives have been demonstrated to be able to enhance chemical, thermal, and fouling resistances, which demonstrate their great potential for developing novel membranes by using them as additives in polymer matrices. Considering the excellent characteristics of the nano-sized particles, this study reviews the effects of inorganic nano-additives on properties and performance of polymer/nanoparticle composite membranes. It has been demonstrated that using nanomaterials in a polymer matrix could enhance the mechanical strength and stiffness, wettability, selectivity, water permeability, and antifouling characteristics of the host polymer.

Keywords: Membrane-based water treatment processes; Inorganic nanomaterials; Organic membranes; Membrane properties; Membrane performance;

4-1- Introduction

The increase in water demand for domestic, agricultural and industrial uses resulted in much attention toward water and waste water treatment technologies during the last few decades. The

*Corresponding author. Tel.: Tel.: 1 613 562 5800x2050.
E-mail address:Christopher.Lan@uottawa.ca (C.Q. Lan), Rana@uottawa.ca (D. Rana)

water demand is predicted to increase by 50% over the next few decades [1]. Membrane filtration, advanced oxidation processes (AOPs), and UV irradiation are among the processes that have been used for this purpose [2] and membrane filtration is considered to be one of the most energy saving and cost efficient technologies [1, 3].

Depending upon the membrane pore size, mechanism of rejection, and driving force of mass transfer, membrane processes for the separation of liquids could be categorized as microfiltration (MF), ultrafiltration (UF), nanofiltration (NF), reverse osmosis (RO), forward osmosis (FO), membrane distillation (MD), and pervaporation (PV). In each process, membrane properties such as pore size, pore size distribution, cross-sectional structure, and surface chemistry would influence the performance of the membrane. In spite of their mechanical and chemical stability, narrower pore size distribution, higher porosity, and lower tendency to fouling in comparison with the polymeric membranes, ceramic membranes are very expensive, therefore, organic membranes are in priority for industrial applications [4]. However, the present polymeric membranes suffer from a trade-off between membrane permeability and selectivity, fouling problems and in some cases chemical resistance [5-10]. Therefore, the development of novel membranes with a combination of high permeability and selectivity beyond the trade-off line, with enhanced thermal, mechanical and chemical stability, and fouling resistance is still needed.

A method to prepare membranes of improved morphology and characteristics is to change the casting dope formulation by using different additives such as mineral fillers, polymers, surfactants, and non-solvents [9]. Similarly, the change in the composition of coagulation media is sometimes effective. The proper choice of additives may result in the formation of more desirable pore structures with better interconnectivity, an improvement in the surface properties such as wettability, and suppressing or encouraging the formation of macro-voids [11]. For instance, organic additives such as polymethyl methacrylate (PMMA) was reported to have improved the properties of the polyvinylidene fluoride (PVDF) membranes, leading to enhanced antifouling characteristics, but unfortunately have resulted in a reduction in membrane strength [12, 13]. Furthermore, hybrid membranes with a polymeric matrix embedded with inorganic fillers are regarded by some researchers as the next generation membranes [14] since hybrid

membranes combine the essential membrane forming capacity of organic polymers with some unique desirable features of selected inorganic additives [4]. For example, silica particles have been reported to provide enhanced mechanical stability to membranes [15], fast transport properties of aligned carbon nanotubes (CNTs) could be employed to enhance the flux of polymer membranes, shape selectivity and specific sorption of zeolites would help the polymers improve the membrane salt rejection, the catalytic properties of TiO_2 nanoparticles would influence the fouling resistance and water flux [16], and last example consists of how carboxyl, epoxy, and hydroxyl functional groups on edges and planes of graphene oxide (GO) would provide the membrane surface with a large negative zeta potential which prevents the accumulation of the bio-foulants on the membrane surface as a result of electrostatic repulsion between the surface and microorganism [17].

Nano-sized inorganic particles can be effectively used as additives in a membrane matrix due to their small size and high specific surface area [8]. Generally, a large surface area of the nano-sized materials increases the interfacial interactions between the particles and the polymer matrix, and consequently, will improve the thermal and mechanical stabilities of the formed composite membrane. In particular using nano-sized inorganic materials will enhance the level of mixing, especially, in polymer matrices with functional groups such as carbonyl and hydroxyl groups that allow hydrogen bonds to form with the inorganic network [18]. It has been revealed that using nanomaterials as additives in composite membranes could overcome material deficiencies, and improve permeate flux, surface wettability, and mechanical properties of the membrane [19]. It was also noted that the dispersion of these particles in membrane casting solutions to create a uniform surface is a big challenge and surface modification of the particles or using different surfactants such as sodium dodecyl sulfate (SDS) has been proposed as a possible solution for this problem [20].

Inorganic nanoparticles incorporated membranes have found a broad range of applications from gas separation [21, 22] to liquid separation including microfiltration [23, 24], ultrafiltration [25, 26], nanofiltration [20, 27], reverse osmosis [28, 29], forward osmosis [30, 31], membrane distillation [32, 33], and pervaporation [34, 35]. Many inorganic nanomaterials such as SiO_2,

zeolites, CNTs, TiO_2, Al_2O_3, Fe_3O_4, $CaCO_3$, GO, Ag, and ZrO_2 have been used to achieve this goal [19, 36-44]. However, the main purpose of using nanomaterials in polymeric membranes has been fouling mitigation and flux enhancement. The effects of inorganic fillers on the membrane properties and performance can be summarized as altering the skin layer thickness, its porosity, and pore size, controlling macro-void formation, changing the permeability of the membrane depending upon the concentration of nanomaterials and their dispersibility inside the casting solution, and altering the rejection characteristics of the membrane [6].

While extensive studies have demonstrated the great potentials of composite membranes enhanced by inorganic nano-additives as a new generation of membranes for water treatment applications, information on the commercial applications of these membranes are scarce at this stage. Nonetheless, some membrane manufacturers have made nano-composite membranes commercially available with encouraging results. For instance, QuantumFlux (Qfx) SW 75ES RO membranes, which are manufactured by NanoH_2O (El Segundo, California [45]), are commercially available nanocomposite membranes containing undisclosed inorganic nanoparticles. They have a similar salt rejection and a flux increased by 50-100% in comparison with the standard membranes containing no inorganic additive [46]. Furthermore, these membranes were compared with Filmtec SW30HRLE units of Lenntech (Delft, The Netherlands), which are standard commercial thin film membranes, at small and pilot scales. Results show similar salt rejection of the two types of membranes, but the water permeability of the Qfx units was 140-200% of that of the Filmtec units [47].

In this review, we strive to provide a comprehensive account of the most recent advances in the development of inorganic-organic composite membranes for water treatment with a focus on the effects of different inorganic nanomaterials on membrane properties and performance.

4-2- Nanomaterials as Additives for Enhanced Membrane Performance

As discussed earlier, the addition of nanomaterials into the host polymer is known as a promising approach to enhance the performance of a membrane-based process. Among the nanoparticles,

carbon nanotubes, silica, titania, and alumina have been known to be outstanding to enhance water treatment capacity.

4-2-1- Carbon Nanotube (CNTs)

Up to now, a lot of work has been allocated to the reinforcement of the polymers by using CNTs in a nanocomposite frame [48-53]. Of particular relevance, the narrow size distribution, uniformity of the tubes, atomic scale smoothness, chemically inert interior walls, and outstanding biofouling resistance have made CNTs an appropriate additive for enhancing the water flux, salt rejection, and biofouling properties of polymeric membranes [16].

Extremely high aspect ratio, molecularly smooth hydrophobic graphitic walls, and the nanoscale diameter are of the most important characteristics of CNTs, which result in efficient transportation of the water molecules through the nanotubes. The movement of water molecules through the nanotube is faster than that of other pore structures of comparable size [54].

Carbon nanotubes within a polymeric matrix would provide a pore network through their hollow nano-channels and interspaces, and via disarraying the polymer chain packing, which creates external nanoscale pathways within the membrane and helps the improvement of the matrix permeability [55, 56].

CNT-based membranes have less biofouling problems compared to the commercialized NF and RO membranes, which leads to lower operating costs [57]. Generally, carbon-based nanomaterials could deactivate bacteria and viruses [6]. In addition, vertically aligned CNT membranes have the capacity to be used for removing the microbial contaminants from drinking water [4]. CNTs could inhibit the microbial attachment and biofilm formation on the membrane surface. Furthermore, by functionalizing their surfaces and tips, CNTs could reduce hydrophilic and hydrophobic fouling of membranes.

4-2-2- Silica (SiO_2)

Silica is widely used as an inorganic additive in the fabrication of organic membranes due to its convenient operation, mild reactivity, mechanical strength, nontoxic nature, and the availability of its chemical properties [9, 40, 58-60]. It was reported that using silica nanoparticles in different concentrations resulted in an improvement of mechanical strength [61-66] and thermal stability [67-71] of the host polymers. As well, in some cases, silica nanoparticles influenced the polymerization reactions of the polymer matrix [72]. The most important reason for such a behavior is related to the interactions at the interface between the nano-fillers and the polymeric medium [73]. These strong interactions are due to the formation of immobilized amorphous layer of polymer molecules on the silica nanoparticles, which is ascribed to the smaller particle size and the better uniformity of their dispersion inside the solution [72].

4-2-3- Titanium Dioxide (TiO_2)

Their suitable chemical resistance, easily tunable morphology, surface properties, and catalytic functionality beside the antifouling properties of TiO_2 nanoparticles have made them applicable in membrane technology [3, 9, 74-77]. The photocatalytic properties of TiO_2 nanoparticles facilitate the decomposition of organic compounds. In a photocatalysis process, TiO_2 needs to be activated first by an appropriate amount of energy. This energy should be higher than the band gap of the semiconductor, which corresponds to ultraviolet wavelength in the case of TiO_2. Through absorbing the activation energy, the electron in the valence band is excited and jumps to the conduction band. Then a positively charged hole in the valence band will be left. The positively charged hole could react with the water molecules and oxidize them to hydroxyl free radicals ($^{\cdot}OH$). H^+ ions are also generated within the reaction. As a result of the reaction between the excited electron in the conduction band and the dissolved oxygen, oxygen radicals will be formed (O_2^-). The superoxide ions will further react with water molecules to produce hydroxide ions (OH^-) and peroxide radicals ($^{\cdot}OOH$). Peroxide radicals will be combined with hydrogen ions to form hydroxyl free radicals ($^{\cdot}OH$) and hydroxide ions (OH^-). The required number of electrons would participate in the reaction. The positively charged holes will also convert

hydroxide ions to hydroxyl free radicals. It means all the species will finally be converted to hydroxyl free radicals (˙OH) which are the main agent in attacking the pollutant molecule and microorganisms in waste water and converting them to carbon dioxide, water, and mineral acids [78-82]. Photocatalytic process mainly takes place close to the surface of the semiconductor, and a high specific surface area is always demanded. The nanoscale size of the TiO_2 nanoparticles provides the required surface area for the photocatalysis to improve the performance of the process.

Consequently, TiO_2 nanoparticles can be used for filtration purposes to increase the membrane resistance against fouling [83] by degrading the organic foulants which come into contact with the nanoparticles within the membrane matrix.

4-2-4- Aluminum Oxide (Al_2O_3)

Alumina nanoparticles are considered as the potential inorganic materials that can be used in organic membranes for the filtration purposes [84, 85], although, based on the available publications, they are not as popular as the above mentioned nanomaterials.

In addition to the nanomaterials which have already been discussed, there are a few works on the application of $CaCO_3$ [19, 86], Fe_3O_4 [39], Ag [41, 87], different types of zeolites [30, 88, 89], and Fe-Mn [90] nanoparticles in membrane-based processes for water treatment.

Ultrafiltration (UF), Microfiltration (MF), Nanofiltration (NF), Reverse Osmosis (RO), Forward Osmosis (FO), Membrane Distillation (MD), and Pervaporation (PV) are considered as the membrane-based separation processes for liquids. Since different membrane-based water treatment processes need membranes with distinct characteristics, the effects of incorporating nanoparticles on the membrane performance would depend on the process under the consideration. In other words, a nanoparticle that enhances the performance of a process may be harmful for the other process. Therefore, in this section, the effects of nanoparticles on different processes are investigated separately.

4-3- Nanomaterials Incorporated Polymeric Membranes in UF/MF

UF and MF processes separate particles and colloids from water based on size exclusion or particle capture and operate depending on pressure or concentration gradient across the membrane. Since UF and MF membranes are in direct contact with raw feed, the risk of fouling and biofouling of the membranes is higher than that of the step that follows. Fouling could be due to adsorption of organic molecules, microbial adhesion or deposition of particulates onto the membrane surface [91], leading to higher transmembrane pressure, reduced permeate flux, and chemical degradation of the membrane material, which further reduces its lifespan [92-94]. Mixed matrix membranes containing nanomaterials could be an approach to enhance the performance of UF/MF membranes. Polysulfone (PSf), polyacrylonitrile (PAN), polyethersulfone (PES), polyvinyl chloride (PVC), aliphatic and aromatic polyamides (PA), polyimides (PI), polyarylsulfone (PAS), and PVDF are among the most common polymers which have been used to prepare commercial MF and UF membranes [95]. A comprehensive review about the use of nanocomposite UF membranes and their effects on the process performance has been recently published by Goh et al.[8]. Table 4-1 highlights some of the most important works in which the nanomaterials were used in the ultrafiltration/microfiltration process.

Table 4-1 Effects of nanomaterials on the performance of composite membranes in the ultrafiltration/microfiltration process (The most significant results)

Nanomaterial	Host polymer	Nanomaterial concentration	Rejection increase	Water flux increase	Water flux (L/m^2h)	Remarks about the process	Ref.
SiO_2	PVDF	3.0 wt.% of TEOS	~ -6.8%	~ 266.0%	~ 301.0	*Rejection:* BSA (300 mg/L) *TMP:* 0.1 MPa	[40]
SiO_2	PSf	~ 4.8 wt.%	-	~ 1500.0%	~ 17.7	*Feed:* Oil in water emulsion *TMP:* 0.1 MPa (Flux was evaluated after 2 hr filtration)	[96]
CNT	PES	MWCNT/PES:0.5%	-	~ 727.3%	~ 91.0	*TMP:* 60 psi	[14]
CNT	PES	1.0 wt.%	~ 6.7%	~ 47.9%	~ 190.0	*Rejection and Fouling:* BSA (500 ppm)	[97]
CNT	BPPO	5.0 wt.%	~ -1.5%	~ 142.6%	~ 489.6	*Rejection:* Egg albumin (0.5 g/L)	[42]
TiO_2	PSf	2.0 wt.%	~ 5.3%	~ 67.3%	~ 491.0	*Rejection:* BSA (100 g/L) *TMP:* 1 bar	[98]
TiO_2	PVDF	No. of ALD cycles: 120	~ 74.7%	~ 164.9%	~ 191.2*	*Rejection:* BSA (1.0 g/L) *TMP:* 0.05 MPa	[3]
TiO_2	PVDF/SPES	4.0 wt.%	~ 66.9%	~ -42.7%	~ 618.6	*Fouling:* BSA (500 ppm)	[99]
TiO_2	PVDF	2.0 wt.%	-	~ -24.8%	~ 292.2	*Coagulation bath:* Water *Support:* Non-woven fabric	[100]
TiO_2	PES	2.0 wt.%	-	~ 26.0%	~ 442.9	*TMP:* 1.0 bar	[101]
Al_2O_3	PVDF	2.0 wt.%	~ 24.5%α	~ 37.6%α	~ 134.2	*Fouling:* BSA (0.1 g/L) *TMP:* 0.1 MPa	[84]
Al_2O_3	PVDF	3.0 wt.%	~ 1.6%	~ 286.3%	~ 129.2	*TMP:* 0.1 MPa	[37]
Al_2O_3	PCTE	No. of ALD cycles: 100	~ 44.5%	~ -61.0%	~ 4.8	*Rejection:* BSA (1.0 g/L) *TMP:* 2.0 bar	[102]
fCNT/GO	PVDF	1.0 wt.% (NPs/PVDF)	~ 14.3%	~ 239.7%	~ 203.0	*Rejection:* BSA (0.1 g/L)	[103]
TiO_2	PESβ	4.0 wt.%	-	~ 29.8%	~ 3720.0	-	[104]
TiO_2	PESβ	0.5 wt.%	-	~ 75.3%	~ 596.0	*Fouling:* BSA (2.0 g/L) *TMP:* 100.0 kPa	[24]
Al_2O_3	PESγ	Al_2O_3/PES:0.05	-	~ 46.3%	~ 1268.0*	Different TMPs, and concentration is stated as the ratio of Al_2O_3/PES	[85]

* $L/(m^2.h.bar)$
α Rejection and flux were evaluated in comparison with a composite membrane containing 1.0 wt.% of Al_2O_3 nanoparticles
β Microfiltration
γ Membrane Bioreactor (MBR)

4-3-1- Improvement of the Performance of UF/MF Membranes by Nano-additives

4-3-1-1- Permeability

Most researchers have confirmed the existence of an optimum concentration at which the permeability shows a maximum [13, 14, 24, 37, 40, 42, 84, 98, 101, 104-106]. It is attributed to the competition between the hydrophilicity and viscosity of the casting solution, which results in the maximum pore size at the threshold value. As well, at high particle concentrations sometimes pores are plugged causing a further reduction in the flux [13, 24, 37, 84, 97, 104].

In other works, water flux was related to pore plugging, surface hydrophilicity, and mean pore size [3, 97]. The flux depends on which factor is dominant at which concentration. For example, permeability is reduced by the addition of the nanomaterials at the low concentration, since the pore plugging dominates. As the particle concentration increases, surface hydrophilicity and mean pore size become dominant, and flux shows a maximum, while by further increasing the concentration, pore plugging plays the main role again, and permeability decreases [97].

It was reported that water flux increased continuously by the incorporation of nanomaterials without any reduction within a range of concentrations, [39, 85, 90, 96] which in one case, went up to 4.8 wt.% [96]. This behavior is attributed to the hydrophilicity enhancement and either increase in the surface roughness or membrane porosity. On the contrary, Li et al. [102] reported that by increasing the number of atomic layer deposition (ALD) cycles to deposit Al_2O_3 nanoparticles onto a polycarbonate (PCTE) membrane water flux decreased, which was attributed to the reduction of the mean pore size as the Al_2O_3 layer became thicker. In another work the flux continuously decreased when TiO_2 nanoparticles were added into a blended polymer matrix of PVDF and sulfonated polyethersulfone (SPES) [99]. TiO_2 nanoparticles could also enlarge the tiny nano-channels available between different GO nanosheets where they are placed between the layers of the graphene sheets to enhance the permeability of the nanocomposite membrane which is obtained [44]. Goh et al. [43] reported that the addition of GO nanosheets into a membrane of poly(amide-imide) (PAI) and polyethyleneimine (PEI) was

equivalent to shortening the cross-linking time by 60 min with almost 86% higher permeability and almost the same rejection. Zhang et al. [103] showed that a blend of functionalized MWCNTs and GO could increase the membrane permeability more than what the single particle did. The results were entirely well matched with the membrane porosity, pore size, surface roughness, and hydrophilicity.

It is worth mentioning that the contribution of nanoparticles into the surface roughness might result in an increase in flux due to an enlargement in the efficient filtration area [13, 37, 90]. As well, Cao et al. [38] investigated the effects of particle size on the membrane performance, and concluded that the membrane containing smaller nanoparticles showed the higher flux.

4-3-1-2- Rejection

In the UF and MF processes, solute rejection is determined mostly by the mean pore size. Thus, there is a trade-off between membrane permeability and selectivity [40, 96]. Typically, mean pore size reduction by nanomaterial incorporation enhances solute rejection [3, 99, 102]. Therefore, improving the flux and rejection simultaneously has been sought as the purpose of numerous works [3, 84, 98].

A threshold value for selectivity has also been observed. The rejection decrease at the concentrations above the optimum content has been related to the particle aggregation which brought about a membrane of poor morphology with larger surface pores in the vicinity of the particles aggregates [84, 98].

It is noteworthy that sometimes the addition of nanomaterials did not change its selectivity significantly [13, 37, 42].

According to Xu et al. [106] protein rejection was improved via the incorporation of GO and 3-aminopropyltriethoxysilane (APTS) functionalized GO in the PVDF membrane due to the absorptive action of the added carbon nanomaterials. It should be noted that the improvement was further for the membrane with the functionalized GO. Zhang et al. [103] showed that the

addition of oxygenized carbon nanomaterials brought about a denser surface with higher protein rejection in comparison with the neat PVDF.

4-3-1-3- Fouling

The fouling resistance can be improved by increasing the surface hydrophilicity via the addition of hydrophilic nanomaterials. Ag nanoparticles have exhibited anti-biofouling properties as well [41, 107, 108]. All the researchers have shown an enhancement in antifouling characteristics of the membranes as a result of nanomaterials incorporation [13, 14, 37, 38, 40, 85, 90, 96-100, 103, 105, 106, 109], mainly due to increase in hydrophilicity. Although particle agglomeration during the membrane fabrication can reduce the potential of antifouling effect due to the formation of defective pore structure which reduces fouling resistance [24, 84, 101]. Regarding the surface hydrophilicity and roughness which affect the fouling behavior of membranes, Xu et al. [106] concluded that surface hydrophilicity was dominant in their study since the neat PVDF with the smoothest surface showed the weakest antifouling performance.

4-3-1-4- Mechanical and Thermal Stability

Using nanomaterials in polymer matrices could enhance the thermal stability and mechanical strength of the composite membranes [13, 18, 37, 104]. The former effect is due to the interactions between nanoparticles and polymer chains, which increases the rigidity of the polymer substantially and also the energy required to break down the polymer chains, while the latter effect is because of cross-linking action of the nanomaterials which links the polymer chains together [104].

Again a threshold concentration was observed [24, 40, 98, 105, 110]. At lower concentrations, the nanoparticles act as the cross-linkers to endure the stress of the load, but at the higher concentrations, particle aggregation results in the formation of defects and stress convergence points under the loading forces, leading to deterioration of mechanical stability [17, 24]. Sometimes the nature of nano-additives is also effective in further strengthening the nanocomposite membrane. For instance, Wang et al. [105] reported that the unique mechanical properties, high aspect ratio, and high surface area of GO could increase the tensile strength of

the neat PVDF membrane. They also mentioned to lower elasticity which is obtained upon the addition of the GO nanosheets. In another study, Zhang et al. [103] demonstrated that the membrane with GO was mechanically stronger than the one with OMWCNT which was attributed to the higher specific surface area of graphene oxide rather than OMWCNT which is equivalent to a bigger contact area between the nanomaterials and polymer chains.

In a contrary study, Xu et al. [106] demonstrated that the addition of GO nanosheets into the PVDF matrix reduced the tensile strength. To overcome this problem, they showed that APTS functionalized GO nano-additives could increase the membrane tensile strength significantly. The mechanically stronger structure of the membrane with the functionalized GO was explained through the better dispersion of the nanosheets within the membrane matrix with lower degree of aggregation besides the promotional effect of APTS which penetrated into the membrane and entangled with PVDF matrix and resulted in stronger interactions between the available components within the membrane matrix.

4-3-2- Effects of the Nano-additives on the UF/MF Membranes Properties

4-3-2-1- Porosity and Mean Pore Size

The reports on porosity and mean pore size are often contradictory.

In some cases, it has led to a higher porosity and mean pore size [84, 85, 96, 101, 103], likely due to the hindrance effect of nanomaterials that reduces the interactions between solvent and polymer molecules. As a result, easier and faster diffusion of the solvent molecules from the polymer matrix to the coagulant (usually water) takes place, which further increases the porosity and mean pore size [111].

On the other hand, it has been reported that the addition of nanomaterials led to a reduction in both porosity and mean pore size [3, 38, 99, 100, 102]. It might be due to the deposition of nanomaterials in the membrane pores.

Another observation has been the existence of a threshold concentration of nanoparticles, below which porosity and mean pore size increase and above which they tend to decrease [14, 97, 98, 105, 106]. The decrease at high nanoparticle concentration might be due to the irregular standing of the nanomaterials in the membrane at the higher concentrations and the increase in the viscosity of the casting solution, which causes a delayed phase separation, creating a dense structure in the sub-layer. It is universally accepted that the viscosity of a suspension increases with the filler concentration [112]. At the low concentrations, nanomaterials act as the nucleating agents to increase the rate of nucleation of the polymer lean phase [105] and enhance the phase separation mostly due to an increment in the hydrophilicity of the casting solution, generating the larger mean pore size [14]. Xue et al. [106] considered the increase in amorphous nature of the PVDF membrane via the incorporation of GO nanosheets as a reason for the increase in the porosity of the nanocomposite membrane. They also mentioned that the APTS functionalized GO nanosheets could result in the larger mean pore size and higher porosity than the pure GO ones.

It is worth mentioning that Zhang et al. [103] revealed that oxidized carbon nanomaterials brought about a non-uniform pore size distribution after their incorporation in PVDF membrane.

There was also some evidence that the addition of Al_2O_3 nanoparticles did not affect the membrane pore sizes and its porosity [13, 24, 37].

4-3-2-2- Roughness

Membrane surface roughness mostly increased as a result of the addition of nanomaterials into the polymeric matrix [3, 13, 14, 37, 40, 42, 90, 103, 106], although there were also cases where the surface became smoother, and it is noteworthy mentioning that in all those works, TiO_2 nanoparticles were used as the additive [38, 99, 100].

As well, Rahimpour et al. [97] reported that there was a threshold concentration of multi-walled carbon nanotubes (MWCNTs). The roughness increases up to 1%, beyond which surface

roughness starts to decrease. This is attributed to change in demixing rate at different additive concentrations and the lower rate resulted in a smoother surface at the high concentrations.

4-3-2-3- Hydrophobicity/Hydrophilicity

In a UF or MF process, a hydrophilic membrane is highly demanded, therefore most of the works were aimed at preparing a more hydrophilic membrane [3, 13, 14, 18, 24, 37, 39, 42, 84, 85, 96, 97, 99-101, 103, 104, 106]. The enhanced hydrophilicity is mainly attributed to the hydrophilic nature of the nanomaterials or the change in membrane surface energy by the functionalization of nanoparticles surface before they are added to the polymer. Xu et al. [106] hypothesized that the reduction in the surface contact angle was due to the migration of the hydrophilic GO nano-fillers to the membrane surface which resulted in a lower interface energy within the phase inversion process which brought about a more hydrophilic surface.

It was also reported that there is a threshold concentration at which hydrophilicity shows a maximum [90, 98, 105]. The reason is that the surface roughness becomes dominant at higher additive concentration, which decreases the surface wettability [90].

In a contrary discussion, Zhang et al. [103] took the surface roughness into consideration and based upon the Wenzel model [113] concluded that a rougher surface would result in a more hydrophilic surface. In their study, they used functionalized MWCNTs, GO, and a blend of them as the nano-fillers and demonstrated that the membrane with the blended nanomaterials with the roughest surface possessed the highest hydrophilicity. They also discussed the synergistic interaction between functionalized MWCNT and GO that inhibited the agglomeration of each single nanomaterial in the blended membrane resulting in more efficient participation of the oxygen-containing functional groups in determining the surface hydrophilicity.

4-3-2-4- Morphology

Yu et al. [40] reported that by incorporating silica nanoparticles into the PVDF membrane, the cross-sectional morphology experienced a transition from finger-like macro-voids to a sponge-like structure. SiO_2 particles acted as the cross-linking agent between the polymeric chains and

restricted growth of finger-like cavities. At the higher contents of TEOS, i.e. precursor of SiO_2 nanoparticles, some massive aggregates in the polymeric matrix caused the membrane to lose its structure. In another study, surface images revealed that neat PES membrane consisted of cellular pores, but with the addition of small amounts of TiO_2 nanoparticles, within 1-2 wt.%, surface pores switched to a lacy structure. By further increasing the TiO_2 loading, the lacy structure returned into a cellular structure accompanied by the agglomerated nanoparticles, resulting in a poor skin layer arrangement [104]. Celik et al. [14] demonstrated that adding the carbon nanotubes into PES stopped the formation of macro-pores. In another work, it was observed that various quantities of finger-like macro-voids could be obtained as a result of the competition between the hydrophilicity of the casting suspension and its viscosity as the concentration of the filler materials increased [97, 98]. Oh et al. [100] revealed that formation of a thicker skin layer and a compact network inner layer with the blocked pores in the presence of the nanoparticles was attributed to an increment in the viscosity of the casting solution. Rahimpour et al. [99] showed that introducing TiO_2 nanoparticles into the blended matrix of PVDF/SPES resulted in the formation of a less porous sub-layer with more interconnectivity between the macro-voids. Moreover, SEM images taken by Liu et al. revealed that the thickness of the spongy layer in the membrane decreased with the presence of γ-Al_2O_3 nanoparticles [84]. According to Wang et al. [105] finger-like macro-voids became wider upon the addition of GO nanosheets into the PVDF matrix. The same behavior was reported by Xu et al. [106] and they also mentioned that the use of APTS functionalized GO could further widen the finger-like macro-voids of a PVDF membrane owing to the presence of hydrophilic functional groups on the GO surfaces. In another study, Zhang et al. [103] demonstrated that the addition of the oxidized carbon nanomaterials including functionalized carbon nanotube and graphene oxide resulted in a transition from finger-like structure for the neat PVDF to a sponge-like structure for the nanocomposite membranes due to the faster demixing rate as a result of the addition of the hydrophilic nanomaterials.

As a conclusion for this section, fouling mitigation by adding hydrophilic nanomaterials has been the major concern of the researchers. Different effects of nano-additives on UF/MF membrane

performance were, however, reported, depending on the researcher, due primarily to the poor control of membrane morphology and surface chemistry. Improvement in their control is therefore a key factor to develop high performance nanocomposite UF/MF membranes.

4-4- Nanomaterials Incorporated Polymeric Membranes in NF

NF membranes are designed for the selective separation of electrolytes from water based on their ionic radius and charge intensity. Unlike MF and UF membranes, which relies solely on size-rejection for separation, the separation of electrolytes by NF membranes is achieved by the combination of at least three mechanisms, i.e., size-exclusion, Donnan potential and dielectric exclusions [114]. As a result, NF membranes are capable of rejecting ions much smaller than its pore size. Surface properties of NF membranes such as pore size and surface charges are of great importance, which could be manipulated via the incorporation of nanomaterials in the host film to achieve a high performance membrane. Currently, Cellulose acetate (CA), PES, PSf, sulfonated PSf, and PA are the traditional organic materials which are used in industry [95]. Table 4-2 summarizes the most important results from the studies which used nanomaterials as the filler in a nanofiltration membrane.

Table 4-2 Effects of nanomaterials on the performance of composite membranes in the nanofiltration process (The most significant results)

Nanomaterial	Host polymer	Nanomaterial concentration	Rejection increase	Water flux increase	Water flux (L/m^2h)	Remarks about the process	Ref.
SiO_2	PA	1.5 wt.%	~ -7.4%	~ 47.1%	~ 10.0	*Feed:* Na_2SO_4 (1000 mg/L) *TMP:* 0.5 MPa	[20]
CNT	PA	PMMA/MWCNTs: 0.67 g/L	~ 22.0%	~ 62.2%	~ 68.4	*Rejection:* $MgCl_2$ (2000 mg/L)	[115]
TiO_2	PSf	1.0 wt.%	-	~ 192.0%	~ 378.8	*TMP:* 0.3 MPa	[116]
TiO_2	PES	TiO_2/MWCNT: 1.0 wt.%	~ 9.1%	~ 52.6%	~ 5.6	*Rejection:* Na_2SO_4(200 ppm) *Feed Pressure:* 5 bar	[117]
TiO_2	PA	5.0 wt.%	~ 8.6%[α]	~ 51.4%	~ 10.6	*Rejection:* $MgSO_4$(2000 ppm) *TMP:* 0.6 MPa	[118]
TiO_2	PA	1.0 wt.%	~ -15.7	~ 22.7%	~ 112.5	*Feed:* Na_2SO_4(1000 ppm) *TMP:* 300.0 psi	[119]
GO	PES	0.5 wt.%	~ 6.7%	~ 148.8%	~ 20.4	*Rejection:* Direct Red 16(30 mg/L) *TMP:* 0.4 MPa	[120]

[α] Rejection were evaluated in comparison with a composite membrane containing 1.0 wt.% of TiO_2 nanoparticles

4-4-1- Improvement of the Performance of NF Membranes by Nano-additives

4-4-1-1- Permeability

Via the incorporation of TiO_2, MWCNTs, and their hybrid as the nano-additives in a PES matrix, water flux increased compared to the neat PES membrane. It was attributed to disarray of polymer chains and their compactness, which resulted in the formation of free spaces at the interface between the polymer chains and the nano-fillers. The highest flux was achieved by the hybrid nanomaterials, followed by TiO_2 and MWCNTs. This is because hydrophilicity and membrane structure controlled the water flux. The TiO_2 incorporated membranes showed the highest hydrophilicity, but the particle aggregation caused pore blockage, and the flux became lower than the membrane with the hybrid nanomaterial. The addition of nanotubes to TiO_2 increased the compatibility of particles and the polymer matrix resulting in lower aggregation and higher water flux. It should be noted that the membrane mean pore size increased with the

concentration of hybrid nanomaterials, resulting in a higher flux for a membrane containing higher concentration of hybrid particles [117].

In another work, Mo et al. [119] confirmed that using TiO_2 nanoparticles increases the permeability of a neat PA membrane, which is attributed to enhanced surface hydrophilicity and larger pore size. Jin et al. [20] also reported that as the surface roughness increases, effective surface area will increase, which together with hydrophilicity enhancement raises the permeate flux. A higher flux was also obtained by Ganesh et al. [121] via the addition of GO nanosheets into the PSf matrix due to the enhanced hydrophilicity and morphology with bigger macro-voids and higher porosity.

Shen et al. [115] and Kumar et al. [116] observed a threshold concentration beyond which the flux starts to decrease, but it was still higher than that of the nascent membrane. At higher concentrations of nanomaterials, the membrane had a more compact structure with more blocked pores. In addition, due to the higher casting solution viscosity at those concentrations, the composite membranes possessed smaller pore size because of the delayed demixing between the solvent and non-solvent during the phase inversion process. It should be noted that mean pore size was dominant at the higher concentrations, and determined the flux, even though the hydrophilicity was enhanced with the concentration [116]. Zinadini et al. [120] also observed a maximum flux which was well matched with the surface contact angle (minimum), porosity (maximum), and pore size (maximum) behavior.

Lee et al. [118] observed a different trend. As their results revealed, water flux of their TiO_2/PA nanocomposite membranes slightly decreased up to the threshold TiO_2 concentration due to the formation of a tight PA layer. But above the threshold concentration, flux sharply increased due to the poor mechanical strength of the membranes, which was caused by the lower degree of in-situ polymerization. It might be improved by increasing the curing temperature during the interfacial polymerization process.

4-4-1-2- Rejection

By incorporating MWCNTs into PES membrane, Vatanpour et al. [117] showed that the rejection performance of a PES membrane increased due to the increase in the negative surface charge. The same observation was reported by Zinadini et al. [120] through the incorporation of GO nanoplates in PES membrane. Opposite results were obtained by Jin et al. [20], where the selectivity of a neat PA membrane decreased by the addition of silica nanoparticles. Reduction in salt rejection was also reported by Ng et al. [122] for TiO_2/PA nanocomposite membrane. It was attributed to loss in anionic character of PA membrane with –COOH groups in the presence of TiO_2 nanoparticles, which weakens the repulsion forces between $–COO^-$ and SO_4^{2-} ions in the feed solution.

An optimum concentration of nanomaterials for the maximum salt rejection has also been reported [115, 118]. The reason for a reduction in the rejection at higher than optimum concentrations was referred to the poor mechanical stability of the nanocomposite membrane [118] or the thickening of the active layer [115].

4-4-1-3- Fouling

Fouling in an NF process has detrimental effects such as higher operating pressure requirement, feed water loss, shorter membrane lifetime, limited recoveries, and higher operating costs [123]. There are numerous reports on fouling reduction by the incorporation of nanoparticles. Rahimpour et al. [124] showed that coating TiO_2 nanoparticles onto the membrane surface is more preferable than TiO_2 entrapment in PES membrane.

The smoother membrane with lower surface energy and more hydrophilicity has stronger antifouling abilities [101]. Upon the adsorption of water molecules by a hydrophilic surface, a water layer is formed that slows down the adsorption of the foulants onto the membrane surface [120]. Antifouling effect of nanomaterials has been reported [116, 117, 119, 120] due to improvement in surface hydrophilicity and smoothness, although Jin et al. [20] demonstrated that increment in surface roughness as a result of SiO_2 nanoparticles addition could surpass hydrophilicity improvement, and fouling was increased.

4-4-2- Effects of the Nano-additives on the NF Membranes Properties

4-4-2-1- Porosity and Mean Pore Size

Nanomaterials might generate a larger mean pore size when they are incorporated in the polymer matrix [20, 117, 119]. It is possible to observe a different behavior around a threshold concentration due to different demixing rates between the solvent and non-solvent during the phase inversion process as explained earlier [116]. Vatanpour et al. [117] mentioned that the presence of more hydrophilic nanoparticles in membrane could bring about a much larger mean pore size. As for porosity, it was reported hydrophilic TiO_2 and MWCNTs increased the porosity of virgin PES membrane [117]. It has been reported that GO nanosheets could extend the porosity of a nascent PSf membrane [121].

4-4-2-2- Roughness

Vatanpour et al. [117] reported that the addition of TiO_2 nanoparticles, carbon nanotubes and their hybrid made the membrane smoother than neat PES, although its smoothness depends upon the type of nanomaterial and its concentration in the polymeric matrix. Zinadini et al. [120] also showed that the PES membrane became smoother through the incorporation of GO nanoplates, although as the concentration of the nano-fillers increased, surface roughness increased. But Jin et al. [20] reported that a neat polyamide (PA) nanofiltration membrane became rougher as the silica nanoparticles concentration increased. To interpret the increase in PSf surface roughness via the addition of GO nanosheets, Ganesh et al. [121] stated that the hydrophilic nano-additives accelerated the solvent/non-solvent phase exchange rate which further resulted in the formation of spheres or nodules of polymers on the surface that is equivalent to a rougher surface.

4-4-2-3- Hydrophobicity/Hydrophilicity

It has been reported that using hydrophilic nanomaterials in nanofiltration membranes would result in a reduction in the surface contact angle [20, 116-119]. Zinadini et al. [120] stated that since the top surface of the membrane is exposed to water, i.e. non-solvent, in a phase inversion fabrication process, the hydrophilic GO nanoplates have this tendency to migrate onto the upper layers and make the PES surface more hydrophilic. Although at the high concentrations, particles

aggregation reduced the effective surfaces of the nanoplates and lowered the amount of hydrophilic functional groups that appeared on the top layer resulting in a less hydrophilic surface. The migration of GO nanosheets onto the upper layers within phase inversion process further proved by Ganesh et al. [121] for a PSf NF nanocomposite membrane.

4-4-2-4- Morphology

For a PES nanofiltration membrane, SEM images revealed that the neat membrane consisted of a thin dense top layer and a finger-like and porous sub-layer, while incorporating MWCNTs into the membrane resulted in a change in the finger-like structure to spherical macro-voids and higher porosity due to the presence of hydrophilic groups on the surface of nanotubes. However, introducing TiO_2 and a hybrid of MWCNT/TiO_2 into the neat PES membrane brought back the finger-like structure. In the case of hybrid materials, the width of the finger-like channels and subsequently, porosity reduced with an increment in the hybrid concentration, due to the viscosity increase during the phase inversion [117].

Zinadini et al. [120] demonstrated that wider finger-like macro-voids were obtained through the addition of GO nanoplates into the PES matrix. As well, lateral pores were formed within the membrane structure which further improved the membrane permeability. In another study, Ganesh et al. [121] stated that the use of GO nanosheets brought about the elongation of finger-like macro-voids.

In another work, size of the nodules in the polyamide layer increased by embedding the modified MWCNTs to the active layer, and at higher concentrations of the nanotubes, nodules disappeared and were replaced by a thick net structure [115].

According to this section, similar to the UF membranes, many efforts have been made to enhance the surface hydrophilicity of the NF membranes. The control of the surface charge is yet another factor to be considered especially for NF membranes.

4-5- Nanomaterials Incorporated Polymeric Membranes in RO

In an RO process, currently the greatest industrial desalination process by handling around 60% of the global desalination load [95, 125, 126], an external pressure is applied to reverse the natural flow of solvent which is from low to high solute concentration. In spite of typical filtration processes which size exclusion is considered as the predominant removal mechanism, RO involves a diffusive mechanism across the membrane. Fouling and biofouling are the main obstacles toward further industrial growth of RO technology and need to be prevented via feed pre-treatment, modification of membrane surface properties, optimization of process conditions and module geometry, and periodic cleaning [127]. Usually a smoother, more hydrophilic, and neutrally charged membrane shows a higher resistance against fouling [128-130]. As discussed earlier, the addition of nanomaterials such as silver [131, 132] to the organic host which is mostly PA and CA [95] seems also to be effective.

Table 4-3 summarizes the most important results from the works on using nanomaterials in RO membranes.

Table 4-3 Effects of nanomaterials on the performance of composite membranes in the reverse osmosis process (The most significant results)

Nanomaterial	Host polymer	Nanomaterial concentration	Rejection increase	Water flux increase	Water flux (L/m^2h)	Remarks about the process	Ref.
CNT	PA	0.1% (w/v)	~ -0.8%	~ 173.1%	~ 71.0	*Feed:* NaCl (2000 ppm)	[133]
NaX	PA	0.2% (w/v)	~ -35.3%	~ 174.6%	~ 32.4	*Feed:* NaCl (2000 ppm) *Operating Pressure:* 12 bar TMC: 0.15% (w/v) MPD: 3.0% (w/v)	[89]
AgA	PA	0.4% (w/v)	~ 2.0%	~ 60.0%	-	*Rejection:* NaCl (2000 ppm)	[134]
LTA	PA	0.2% (w/v)	~ -2.6%	~ 47.0%	-	*Rejection:* NaCl (2000 ppm) *Particle Size:* 97 nm	[88]
CNT	PA	15.0 (mg/g PA)	~ 216.7%	~ -12.5%	~ 28.0	*Rejection:* NaCl (4000 ppm) *PA concentration:* 10.0 wt.%	[135]
TiO_2	PA	-	~ 1.3%	~ -4.8%	~ 126.2	*Feed:* NaCl (2000 ppm)	[127]
TiO_2	PA	-	~ 0.1%	~ 9.1%	~ 23.9	*Feed:* NaCl (2000 ppm)	[136]
MCM-41	PA	0.1 wt.%	~ -0.2%	~ 61.9%	~ 46.3	*Rejection:* NaCl (2000 ppm)	[137]

4-5-1- Improvement of the Performance of RO Membranes by Nano-additives

4-5-1-1- Permeability

Normally, it is anticipated that the incorporation of impermeable nanoparticles will decrease the membrane permeability because those particles will reduce the space available for the permeation through polymer matrix. Therefore, any increase in membrane permeability is attributed to the formation of defective structure, which will lower the rejection [138].

Park et al. [139] showed that by increasing the silica nanoparticle concentration, flux first decreased slightly, while beyond the threshold value, there was a sharp increase in water flux. It was ascribed to the nanoparticle's interference in the interfacial polymerization, which lowers cross-linking degree in the active layer. Increase of curing temperature will probably make the active layer denser and more rigid.

There are some reports on nanoparticle's insignificant contribution to the membrane permeability [127, 135, 140].

All of the works other than the above mentioned reported enhanced permeability through the addition of nanomaterials into the PA active layer.

Zhang et al. [133] showed that membrane permeability increased significantly, as a result of carbon nanotubes incorporation, which was attributed to 1) fast liquid molecules transport characteristics of carbon nanotubes, 2) setting up a shorter path for transportation of the liquid molecules which pass through the nano-channels compared to when they travel across a dense structure with high tortuosity, 3) introducing the additional pores as a result of nanotubes interconnected network which is generated as a consequence of nanomaterials aggregation, and 4) enhanced surface hydrophilicity via the incorporation of carboxyl and hydroxyl groups in the membrane.

According to Fathizadeh et al. [89], nanozeolites brought about an increment in water flux of the neat PA membrane. A smoother surface together with the new flow paths which are created by the nano NaX help the liquid molecules pass through the polymer better. Lind et al. [134] also reported that the nanozeolites could enhance the membrane permeability, which was ascribed to hydrophilic nature of the nanocrystals, their contribution to altering the interfacial polymerization kinetics, and neat membrane structure. Lind et al. [88] also demonstrated that super hydrophilic nature of the nanozeolites and their internal pores create extra flow paths for the water molecules improving the water flux. They also reported that higher permeability is achieved via employing the nanozeolites with smaller sizes, since the smaller particles are more effective in increasing the membrane pore size.

Permeability enhancement via the addition of nanozeolites was further confirmed by Jeong et al. [28] due to the change in membrane morphology.

Kwak and Kim [136] showed that TiO_2 nanoparticles could increase the membrane water flux because of the water uptake characteristics of TiO_2 nanoparticles and surface hydrophilicity enhancement.

Yin et al. [137] used two different types of silica nanoparticles, porous MCM-41 silica and non-porous spherical silica. Membrane permeability increased by the incorporation of nanoparticles due to surface hydrophilicity enhancement and lower degree of cross-linking of the polymer matrix, which generated micro-porous defects around the nano-fillers and polymer interface. The permeability enhancement in porous MCM-41 silica case was further compared to the non-porous nanoparticles which proved that particle internal pores provide short flow paths for liquid molecules to pass through, and help the permeability improvement.

4-5-1-2- Rejection

Interestingly, most of the researchers reported that the rejection did not significantly change via the incorporation of nanomaterials [127, 134, 136, 137, 140]. Yin et al. [137] mentioned that this is due to the increased negative charge of the membrane in the presence of silica nanoparticles that overcomes the defective structure of membrane through the reduction in degree of polymer cross-linking.

An optimum concentration was reported by Park et al. [139] for silica nanoparticles to maximize the salt rejection.

Zhang et al. [133], on the other hand, reported that functionalized MWCNTs caused a significant reduction in NaCl rejection because of the formation of molecular scale voids, larger than the ionic size, between the nanotubes and polymer chains. Fathizadeh et al. [89] demonstrated that the addition of nanozeolite reduced salt rejection, since the imperfect interactions between nano NaX and monomers prevented the formation of strong bonds between nanozeolite and the polymer, resulting in the formation of defective pores. As well, particle agglomeration at the high concentrations brought about a defective structure. Lind et al. [88] also reported a reduction

in membrane rejection by the incorporation of nanozeolites. They showed that as the particles size increases, rejection performance is improved due to a reduction in pore size.

Nano-fillers might also generate a dense structure as a result of strong interactions between the nanomaterials and polymer matrix and produce a membrane of higher salt rejection [28, 135].

4-5-1-3- Fouling

In spite of the results of Vatanpour et al. [141] which show a great negative impact of a rough surface on the antifouling characteristics of a membrane due to the higher probability of foulant deposition onto the increased surface area, Rahman et al. [142] demonstrated that for the silver nanoparticles and antifouling polymer brushes incorporated RO membranes, hydrophilicity and surface energy are more important parameters in determining the level of bacterial attachment onto the surface. They stated that a more hydrophilic surface could absorb more water than the foulant. As well, lower surface energy weakens the van der Waals force between the foulant and membrane surface, which will result in more reversible fouling.

Ben-Sasson et al. [140] showed that Cu nanoparticles reduced the number of attached live bacteria onto the membrane surface remarkably (80-90%), which was attributed to the toxicity of the bound copper nanoparticles.

To improve anti-biofouling properties of an RO thin film composite membrane, Kim et al. [127] employed TiO_2 nanoparticles to use their photocatalytic bactericidal effects. They demonstrated that the photocatalytic nanoparticles could deactivate and kill the bacterial cells and prevent their adhesion onto the membrane surface.

Yin et al. [137] hypothesized that hydrophilicity improvement and increased negative charge as a result of silica nanoparticles incorporation could bring about an enhancement in antifouling characteristics of the membrane.

There are more works which confirm the improvement in antifouling characteristics via the addition of nanomaterials into the RO membrane [134, 136].

4-5-2- Effects of the Nano-additives on the RO Membranes Properties

4-5-2-1- Roughness

There are several contradictory reports. By incorporation of nanoparticles, the surface becomes smoother [28, 89], or rougher because of particle agglomeration at the membrane surface [133, 137]. It has also been reported that there was no significant change in the surface roughness because the nanomaterials were dispersed well through the polymer matrix [135, 140].

4-5-2-2- Hydrophobicity/Hydrophilicity

About the influence of particle size on the surface hydrophilicity, Lind et al. [88] demonstrated that smaller particles could enhance the hydrophilicity better. Yin et al. [137] showed that through the incorporation of porous MCM-41 silica nanoparticles, the surface contact angle decreased more than the non-porous silica nanospheres, since the hydrophilic internal pores were able to absorb water molecules by capillary effects. It should be noted that Shawky et al. [135] reported that the hydrophobic nature of MWCNTs resulted in an increment in surface contact angle as the nanotubes concentration increased, while, Ben-Sasson et al. [140] showed that the hydrophilicity of neat PA membrane did not change significantly as a result of Cu nanoparticles incorporation.

4-5-2-3- Morphology

A neat PA membrane has a leaf-like structure. Zhang et al. [133] reported a change to a nodular structure by the incorporation of functionalized MWCNTs. Fathizadeh et al. [89] exhibited that leaf-like morphology on the surface of the neat membrane was turned into hill and valley morphology by the addition of nano NaX into the polymer matrix, while Yin et al. [137] reported that porous MCM-41 nanoparticles did not affect the leaf-like structure of PA thin film layer.

As a conclusion for this section, the researchers have been successful in enhancing permeability of RO membrane without a significant compromise in selectivity by adding hydrophilic nanoparticles. As well, antifouling characteristics were improved, which is very important in RO application since the process deals with very high pressures, which further brings about more

probability for fouling issues. Higher the fouling potential means more expensive the process will be since the operating costs will be remarkably increased.

4-6- Nanomaterials Incorporated Polymeric Membranes in FO

More attention has been recently paid to the use of nanocomposite membranes in FO process for water treatment by different researchers. Table 4-4 outlines the related studies which will be discussed further through the following sections.

Table 4-4 Effects of nanomaterials on the performance of composite membranes in the forward osmosis process, active layer facing draw solution mode, AL-DS, (The most significant results)

Nanomaterial	Host polymer	Nanomaterial concentration	Rejection increase	Water flux increase	Water flux (L/m^2h)	Remarks about the process	Ref.
SiO_2	PA	0.05% (w/v)	~ 23.6%	~ 62.3%	~ 25.0	*DS:* NaCl (2.0 M) *FS:* NaCl (10.0 mM)	[143]
Silica gel[a]	PAN[b]	1.0 wt.%	~ -16.4[c]	~ 90.5%	~ 78.1	*DS:* $MgCl_2$ (0.5 M) *FS:* DI Water	[144]
CNT	PES[b]	2.0 wt.%	~ 20.7%	~ 46.3%	~ 12.0	*DS:* Glucose (2.0 M) *FS:* NaCl (10.0 mM)	[145]
CNT	PA	0.05% (w/v)	~ 27.6%[d]	~ 94.4%	~ 73.1	*DS:* NaCl (2.0 M) *FS:* NaCl (10.0 mM)	[146]
TiO_2	PSf[b]	0.5 wt.%	~ -3.1[d]	~ 93.1%	~ 30.9	*DS:* NaCl (0.5 M) *FS:* NaCl (10.0 mM)	[147]
NaY	PA	0.1% (w/v)	~ -18.8[e]	~ 42.5%	~ 30.2	*DS:* NaCl (1.0 M) *FS:* NaCl (10.0 mM)	[30]
NaY	PSf[b]	0.5 wt.%	~ -3.1[f]	~ 143.5%	~ 43.1	*DS:* NaCl (0.5 M) *FS:* DI Water	[148]

[a] Particle size ranged from 40 to 60 µm
[b] Particles were employed within the substrate matrix
[c] Rejection was evaluated by $MgCl_2$ (5.0 mM)
[d] Rejection was evaluated by NaCl (20.0 mM)
[e] Rejection was evaluated by NaCl (500.0 mg/L)
[f] Rejection was evaluated by NaCl (10.0 mM)

Unlike the RO, the osmotic pressure gradient is directly employed as the driving force in an FO process, and solvent migrates by diffusion from a feed of low concentration to a high concentration draw solution through a semi-permeable membrane to dilute the draw solution.

The membranes which are employed in FO application usually have an asymmetric structure with a thin selective layer supported by a porous sub-layer. Presently, cellulose triacetate (CTA) is mostly used to prepare FO commercial membranes [30, 144, 149].

In spite of its low operating costs and fouling tendency due to working at moderate operating conditions and achievable high recovery, internal concentration polarization (ICP) is considered as the main obstacle of FO process in water treatment area [146]. To minimize the ICP, a membrane with low structural parameter is highly demanded. In the structural parameter, support thickness, tortuosity, and porosity are combined to determine the support resistance against diffusion. In other words, in an FO process, a thinner support layer with smaller tortuosity and larger porosity is desirable.

Addition of nanomaterials either into the selective or substrate layer of an FO membrane could be considered as an approach to improve its performance, although Ma et al. [148] demonstrated that the addition of nanozeolites into the substrate layer [148] could have a superior effect than the active layer [30] in terms of water permeability. Emadzadeh et al. also reported that modifying the substrate structure, instead of the active layer, is effective to lower ICP [147, 150].

4-6-1- Improvement of the Performance of FO Membranes by Nano-additives

4-6-1-1- Permeability

It has been demonstrated that the addition of nanomaterials either into the selective or substrate layer could increase the membrane permeability and FO water flux [143, 145-150].

Emadzadeh et al. [147, 149] showed that the flux increased by incorporating TiO_2 nanoparticles into PSf membrane due to hydrophilicity enhancement, increase of porosity, and rougher surface, which leads to a larger filtration area [150].

Amini et al. [146] reported that in addition to increased hydrophilicity and surface roughness, flux improvement is also attributed to 1) the presence of nanotubes which provides the membranes with additional pores through their internal nano-channels and 2) the interfacial gaps between functionalized nanotubes and polymer chains, which bring about further passage for solvent transport. It is worth mentioning that the authors emphasized more on the latter reason because to extract solvent from the very small internal nano-channels a pressure needs to be applied.

Niksefat et al. [143] demonstrated that flux increase in a PA/PSf membrane through the incorporation of silica nanoparticles is attributed to 1) enhanced surface hydrophilicity, 2) increased surface roughness, 3) disruption of polymer chain packing as a result of the immobilization of the nanoparticles, and 4) change in cross-linking condition and interfacial polymerization process as the incorporation of the silica nanoparticles.

Ma et al. [148] mentioned that substrate permeability improvement through the contribution of NaY nanozeolites is due to the higher surface porosity of the substrate and more open structure of the PA selective layer. The authors suggested Fig. 4-1 as the possible mechanism for enhancing the FO water flux via the contribution of zeolite nanoparticles.

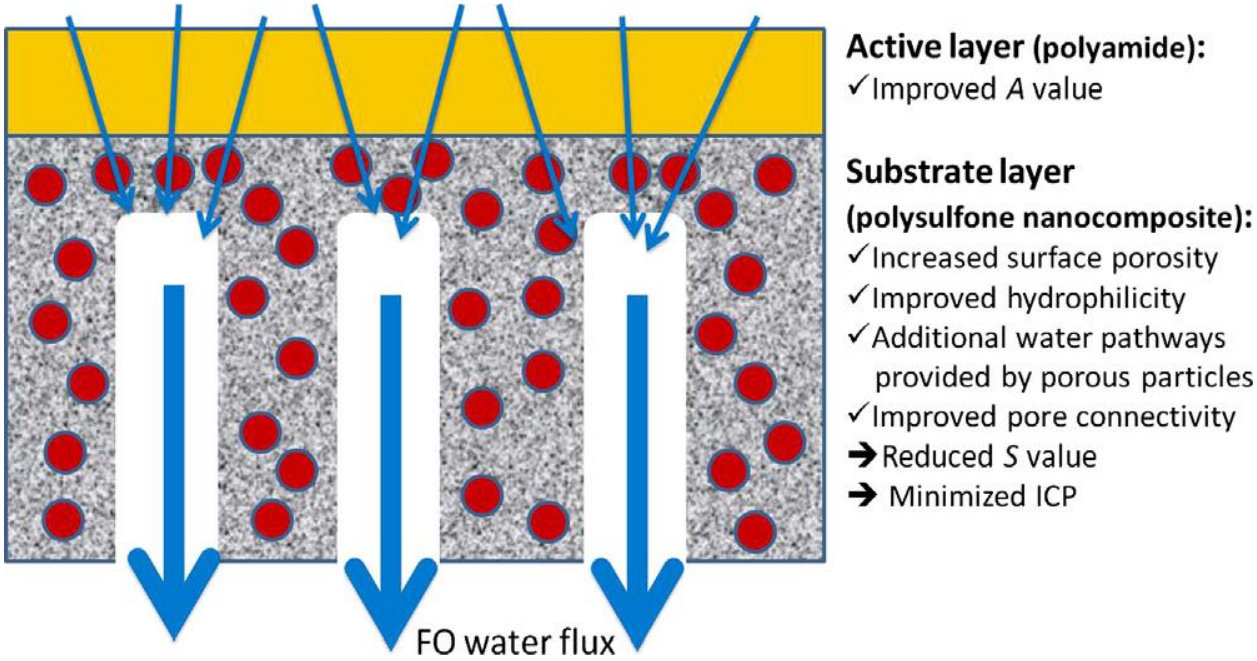

Fig. 4-1 Effects of nanozeolites on both active and support layers of an FO membrane. © Elsevier. Reprinted from [148] with permission from Elsevier. Permission to reuse must be obtained from the rights holder.

As it is clear in Fig. 4-1, increase in the flux is attributed to 1) enhancement of the permeability of the PA active layer and 2) minimized ICP as a result of reduced structural parameter through the incorporation of the nanozeolites. The increased surface porosity, enhanced hydrophilicity,

presence of additional water pathways provided by porous particles, and reduced tortuosity due to improved pore connectivity all contributed to a smaller structural parameter.

Wang et al. [145] also ascribed FO water flux improvement to the lower ICP value as a result of more open interior pore structure and smoother active layer, which is obtained via the incorporation of MWCNTs in the substrate of a PA/PES membrane.

A threshold concentration is also observed through different works. Lee et al. [144] revealed that substrate permeability and the FO membrane flux were enhanced via incorporation of silica gel micro-particles in a PAN substrate, which is mainly due to the addition of transport routes through the porous particles and the porosity increase in the substrate. Beyond the threshold concentration, flux began to decrease due to the agglomeration of the particles, which restricted the effective water transport through the substrate. Ma et al. [30] also reported that 0.1 wt/v% is the optimum concentration of NaY nanozeolites to maximize the permeability. The improved permeability is due to the 1) sub nanometer pores in the zeolite nanoparticles, 2) effect of nanoparticles on interfacial polymerization process, and 3) increased surface roughness as the incorporation of the nanozeolites.

4-6-1-2- Rejection

Salt rejection of an FO membrane changes differently by the incorporation of nanomaterials. It might be increased [145] or decreased [144, 147-149] with concentration based upon the nanoparticle. It has been reported that salt rejection is lowered by incorporating TiO_2 nanoparticles due to lower degree of cross-linking in the PA selective layer as a result of localized defects and agglomerated particles over the substrate surface, and its porous morphology. Emadzadeh et al. [150] revealed that at the higher concentration of the TiO_2 nanoparticles, the agglomerated particles would reduce the contact area of hydrophilic hydroxyl groups of the nanoparticles, leading to deterioration of the structural integrity of the membrane. Incorporation of silica gel micro-particles also caused the formation of a less tight selective layer with increasing particles concentration which reduced the membrane rejection [144]. It was also revealed that as the NaY nanozeolites concentration increased, localized defects appeared over

the membrane surface because of the looser integrity of the selective layer which resulted in a lower selectivity [148].

Furthermore, a threshold concentration has been reported in several works [30, 143, 146]. Decrease of salt rejection with an increase in filler concentration beyond the optimum value was ascribed to particles agglomeration which interferes with the interfacial polymerization, and a defective structure is obtained [143, 146]. It is worth quoting that Ma et al. [30] observed a minimum rejection at the concentration of 0.2wt/v%, and stated that the salt rejection increase at high concentrations of the NaY nanozeolites is attributed to a thicker active layer, which at the same time reduced the membrane permeability.

4-6-1-3- Fouling

To improve antifouling characteristics of a CTA FO membrane, Nguyen et al. [83] used Ag nanoparticles, while TiO_2 nanomaterials were employed to regenerate the silver nanoparticles by decomposing organic matters which covered them.

Fouling resistance of the neat FO membrane improved via the incorporation of the nanoparticles by restricting the growth of bacteria on the surface of the membrane. Silver nanoparticles alone reduced the bacterial growth by 4 times more than the neat membrane, while the incorporation of TiO_2 nanoparticles lowered bacterial concentration almost 11 times more than the neat CTA membrane, which is attributed to combined synergistic effects of both nanomaterials. Silver nanoparticles either release small amounts of Ag ions to induce cell death, or are attached to cell membrane, and influence its permeability and respiration [151], while TiO_2 nanoparticles hinder the Ag nanoparticles to be deactivated by the organic foulants.

It is worth mentioning that flux recovery of the membrane was enhanced by the incorporation of the nanoparticles, and the flux reduction as a result of biofouling was delayed. Furthermore, by altering the interfacial interactions between the membrane and biofilm, nanoparticles caused the fouling layer to be separated from the surface, much easier than before.

4-6-1-4- Mechanical and Thermal Stability

Pardeshi and Mungray [152] showed that functionalized montmorillonite nanoclay particles could improve the thermal stability of the neat poly vinyl alcohol (PVA) substrate. Wang et al. [145] also demonstrated that mechanical strength of the PA/PES forward osmosis membrane was enhanced by carbon nanotubes. Thus, the substrate does not need to be supported by a nonwoven fabric.

4-6-2- Effects of the Nano-additives on the FO Membranes Properties

4-6-2-1- Porosity and Mean Pore Size

Most of the researchers reported that membrane porosity increases as a result of incorporating nanomaterials [145, 147-149, 152]. Emadzadeh et al. [147, 149] mentioned that formation of longer finger-like voids in the TiO_2 nanoparticles incorporated substrate increased its porosity compared to the neat PSf membrane. Wang et al. [145] also reported that porosity increase is attributed to induced pores between the polymer chains and carbon nanotubes.

It is worth mentioning that Emadzadeh et al. [147, 149] and Wang et al. [145] revealed that average pore size was reduced by the addition of nanomaterials into the substrate.

4-6-2-2- Roughness

The incorporation of nanomaterials in either active or substrate layer mostly brought about a rougher surface [30, 83, 143, 146, 148, 149], although in some cases roughness increase was not significant, which could be due to the small amount of nanoparticles added to the polymer.

Emadzadeh et al. [149] mentioned that the presence of TiO_2 nanoparticles in the substrate could increase the surface roughness of thin film nanocomposite membrane of PA.

Increase in the surface roughness might be attributed to the nodular structure of the nanoparticles in the polymeric matrix [149] or to agglomeration of the nanoparticles especially at the higher concentrations [143].

4-6-2-3- Hydrophobicity/Hydrophilicity

Since a hydrophilic surface is highly demanded in an FO application, usually hydrophilic nano-additives are used to modify the surface of FO membranes [83, 143, 146-149]. However, Ma et al. [30] reported an increase in the surface contact angle via addition of NaY nanozeolites into the PA selective layer, which was attributed to an increment in the surface roughness through the contribution of nanoparticles.

4-6-2-4- Morphology

Emadzadeh et al. [147, 149] reported that the faster demixing rate during the phase inversion process by the addition of the hydrophilic TiO_2 nanoparticles created longer finger-like voids in the PSf substrate membrane. In a similar study, Emadzadeh et al. [150] illustrated that as the concentration of TiO_2 nanoparticles increases, viscosity of the dope solution increases, which slows down the phase separation kinetics, resulting in the formation of larger macro-voids within the membrane cross-section.

Lee et al. [144] demonstrated that upon addition of micro-scaled silica gel particles into the polymeric matrix, a larger number of straight finger-like macro-voids were formed.

Wang et al. [145] also mentioned that the addition of nano-fillers would change the rate of solvent/non-solvent exchange and thereby enhances the formation of more open interconnected pores.

The main focus of the researchers in employing the nanomaterials in FO membranes was on minimizing the ICP effect. To this end, the nano-fillers have been added into both selective and substrate layers. It seems adding nanoparticles into the substrate layer is more effective [30, 147, 148, 150]. To lower the structural parameter for increasing the permeability, porosity increase was mostly reported as a result of the nanomaterials incorporation in the polymeric FO membranes.

4-7- Nanomaterials Incorporated Polymeric Membranes in MD/PV

To acquire a better judgment about the results which have been obtained by using the nanomaterials as the additives in a membrane distillation/pervaporation process, Table 4-5 is provided.

Table 4-5 Effects of nanomaterials on the performance of composite membranes in the membrane distillation/pervaporation process (The most significant results)

Nanomaterial	Host polymer	Nanomaterial concentration	Rejection increase	Water flux increase	Water flux (kg/m^2h)	Remarks about the process	Ref.
CuO	PVDF	2.0 wt.%	NA*	~ 153.4%	~ 1.3	*Rejection:* NaCl (35 g/L) *Feed Temperature:* 27.5°C	[153]
CNT	PP	0.5 wt.%	~ 55.0%	~ 83.3%	~ 1980.0	*Feed:* NaCl/$MgSO_4$= 88:12 80°C & 0.5 ml/min	[154]
$CaCO_3$	PVDF	2.4 wt.%	-	~ 14.9%	~ 46.3	*Feed:* NaCl (3.5 wt.%) *Feed Temperature:* 80.5 °C	[19]
$CaCO_3$	PVDF	3.0 wt.%	-	~ 30.8%	~ 49.3	*Feed:* NaCl (35 g/L) *Feed Temperature:* 83.0°C	[86]
SiO_2	PDMS$^{\beta}$	15.0 wt.%	~ 25.0%$^{\alpha}$	~ -61.8%	~ 0.71	*Feed:* Dimethyl carbonate (DMC)/MeOH *Permeate side pressure:* 200.0 Pa	[155]
CNT	PVA$^{\beta}$	2.0 wt.%	~ 456.2%$^{\alpha}$	~ 224.6%	~ 0.07	*Feed:* Benzene/Cyclohexane *Permeate side pressure:* 1.0 kPa	[156]

* Rejection was perfect, i.e. more than 99.99% for both the neat and nanocomposite membranes
$^{\alpha}$ Rejection was evaluated by the separation factor
$^{\beta}$ Pervaporation

In MD and PV applications, partial vapor pressure difference across the membrane is considered as the driving force [7, 157]. In the MD, a process which is able to remove almost 100% of the non-volatile solute present in water [95], liquid molecules evaporate at the membrane interface and vapor molecules pass through the membrane pores to reach the permeate side, but in the PV process, liquid molecules are adsorbed by the membrane at its interface and evaporate while passing through the membrane, liquid and vapor molecules of the permeant are transported via diffusion within the non-porous membrane, and finally, vapor molecules are desorbed at membrane interface in the permeate side [158].

A hydrophobic membrane is highly demanded in an MD process to enhance the separation performance. On the other hand, either hydrophilic or hydrophobic membrane is used for PV, depending on whether aqueous or organic component of the feed is preferentially transported through the membrane. Hence, the membrane performance depends upon the feed properties. Polytetrafluoroethylene (PTFE) and PVDF are typically used in MD, and they are supposed to be hydrophobic with a reasonable porosity, but a challenge for their application in MD process is that they are expensive and difficult to process [159]. Therefore, finding a replacement for them in an MD configuration is desirable.

CNT Bucky-Paper (BP) membranes are among the very early footprint of nanomaterials in MD. BP is a non-woven paper like structure of randomly oriented CNTs. Their mean pore size was reported to be approximately 25 nm with a very high porosity (~90%) and specific surface area with a BET of ~200 m^2/g [159].

BP membranes were extensively studied by Dumée et al. [159-162] in a direct contact membrane distillation (DCMD) process.

It was also confirmed by Koo et al. [163] that using CNTs to produce BP structure on a commercial PVDF support could increase the flux and salt rejection compared to the commercial PVDF membrane. Furthermore, it was demonstrated that a plasma treated BP support could show a better performance compared to the commercial PSf membrane which is traditionally used as a support layer in thin film composite membranes in reverse osmosis (RO) processes [164].

The use of nanomaterials as the additives in an MD/PV membrane has not been as popular as it was in UF, MF and NF. In the following, nanomaterials mixed matrix membranes in MD/PV applications will be reviewed.

4-7-1- Improvement of the Performance of MD/PV Membranes by Nano-additives

4-7-1-1- Liquid Entry Pressure (LEP_w)

It has been exhibited that LEP_w of an MD membrane increases as a result of nanoparticles incorporation, which is attributed to altering the surface chemistry of the membrane [165] and a reduction in the maximum pore size [19]. On the other hand, Hou et al. [86] revealed that there was a threshold concentration at 3 wt.% beyond which LEP_w began to increase, which is consistent with the trend observed between the maximum pore size and concentration as discussed earlier in section 3-5-1. A similar behavior was also reported by Baghbanzadeh et al. [153] in a novel work where they used hydrophilic CuO nanoparticles to prepare PVDF/CuO nanocomposite membranes for a vacuum membrane distillation (VMD) desalination process. Change in LEP_w with the CuO nanoparticles concentration was governed by the surface pore size and LEP_w showed a minimum at 2.0 wt.% where the largest pore size was observed. It is worth mentioning that the minimum LEP_w (3.0 barg) was high enough to make the nanocomposite membrane applicable for the VMD application.

4-7-1-2- Permeability

Gethard et al. [154] showed that the sweep gas membrane distillation (SGMD) flux of PP carbon nanotube immobilized membrane (CNIM) was higher than a virgin PP membrane. This is because immobilized carbon nanotubes change the vapor-membrane interactions, and act as the sorbent sites for vapor transport. Due to their hydrophobic nature, carbon nanotubes reduce wetting and plugging of the pores by the liquid water molecules, resulting in an enhancement in the flux. As well, CNIM composite membrane exhibited higher mass transfer coefficient than the unmodified PP membrane, which was due to an increment in the diffusion coefficient.

To interpret the flux increase by the CNIM in SGMD process, Gethard et al. [32] proposed the following mechanisms as illustrated via Fig. 4-2.

1) Activated diffusion via adsorption on CNT surface, 2) Fast diffusion on CNTs surface, and 3) Hydrophobic effects of CNTs.

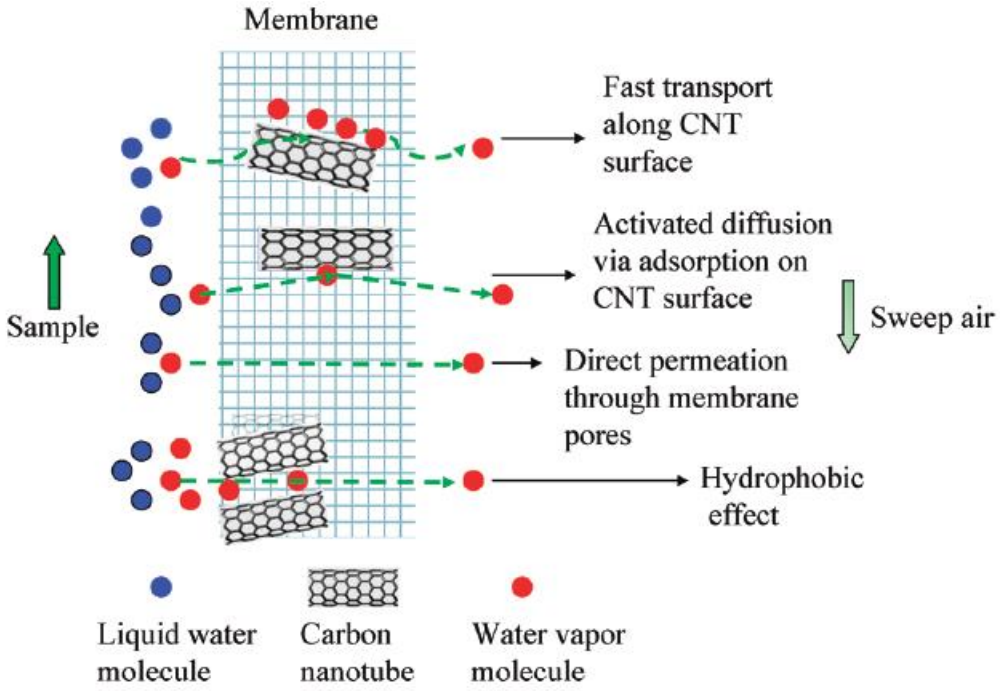

Fig. 4-2 The proposed mechanisms for water transport trough a PP CNIM. © American Chemical Society. Reprinted from [154] with permission from American Chemical Society. Permission to reuse must be obtained from the rights holder.

Vapor molecules may also be directly transported through the inner tubes of CNTs. In addition, due to their high aspect ratio, CNTs increase the functional surface area in a membrane. Furthermore, since CNTs are placed inside the pores, due to their high thermal conductivity, the temperature gradient through pore itself would be decreased, which results in a reduction in condensation inside the pores, and consequently increases the flux. The water condensation inside the pores reduces the surface hydrophobicity, and contributes to the attraction of more water molecules, which results in pore blockage and reduction in the flux.

In a similar study, Bhadra et al. [166] reported that carboxylated carbon nanotube incorporated PP membrane had a higher permeability and water flux in comparison with the carbon nanotube incorporated and unmodified PP membranes. Carboxylation improved interactions between the

nanotubes and polar water vapor molecules, resulting in enhanced desalination efficiency (Fig. 4-3). Membrane durability was also improved via the contribution of functionalized carbon nanotubes.

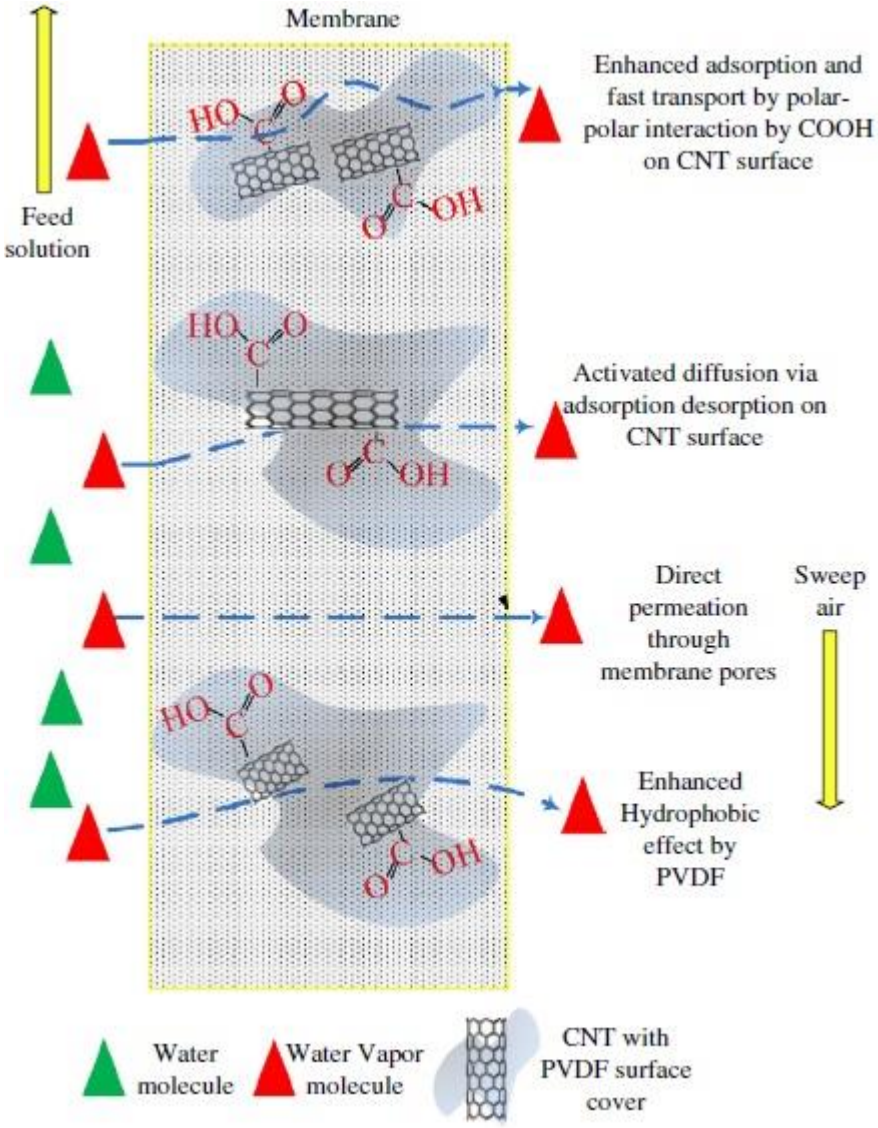

Fig. 4-3 The proposed mechanisms for water transport trough a carboxylated carbon nanotubes incorporated PP membrane when PVDF served as glue to encapsulate the nanotubes within the membrane. © Elsevier. Reprinted from [166] with permission from Elsevier. Permission to reuse must be obtained from the rights holder.

According to the molecular dynamics simulation results for a pervaporation membrane, the addition of the nanotubes would increase the membrane free volume (Fig. 4-4) and effectively

loosen the polymer chain packing, which is desirable for the permeants to pass through the membrane and improves the membrane performance. As well, nanotubes would provide additional nano-channels for a higher permeation rate [156].

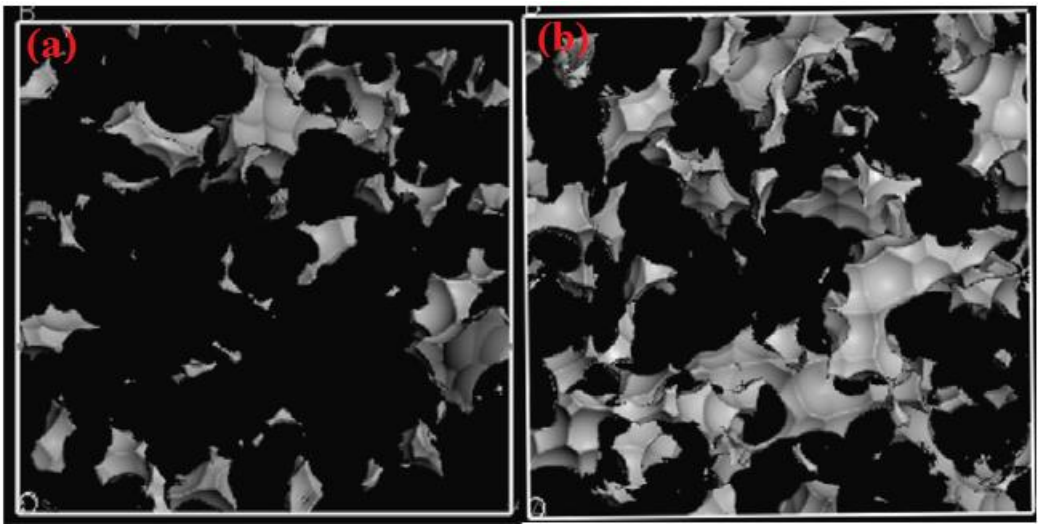

Fig. 4-4 The free volume (shown in bright color) based upon molecular dynamics simulation results (a) Neat PVA membrane, (b) PVA/CNT membrane. © Elsevier. Reprinted from [156] with permission from Elsevier. Permission to reuse must be obtained from the rights holder.

It was also reported that nanomaterials led to a reduction in MD/PV flux. Razmjou et al. [165] demonstrated that the super hydrophobic TiO_2 coated membrane had a lower average permeate flux in comparison with the neat PVDF membrane, which was explained by the hydrophobic nature of the treated membrane. As well, Wang et al. [155] showed that silica nanoparticles reduced the flux of a neat polydimethylsiloxane (PDMS) pervaporation membrane due to enhanced physical cross-linking and restricted plasticization by adding silica nanoparticles.

Hou et al. observed a threshold concentration of PVDF/$CaCO_3$ hollow fibers [19] and flat sheet membranes [86]. At lower concentrations, an increase in the porosity and the formation of a thinner skin layer enhanced the flux, but with a further increase in the concentration, mean pore size decreased and the skin layer became thicker, which resulted in a decrease in the permeate flux [19]. In terms of thermal efficiency, the membrane of optimum concentration also showed the best performance, while above the optimum concentration thermal efficiency was less than that of the neat PVDF membrane, which was attributed to the lower permeate flux and larger

thermal conductivity as a result of an excessive addition of $CaCO_3$ nanoparticles [19]. It is also worth mentioning that membrane durability was enhanced via the addition of the$CaCO_3$ nanoparticles, which was attributed to the narrower pore size distribution of the nanocomposite membrane [86]. Baghbanzadeh et al. [153] compared the effect of two different types of hydrophilic nanoparticles, i.e. CuO and $CaCO_3$, and based upon the results, CuO was superior to $CaCO_3$ in terms of improving the pure water flux of the neat PVDF membrane, where the former increased the flux by 153.4% and the latter enhanced the flux by 102.3% at 2.0 wt.% of the nano-fillers. Pure water flux met a maximum at 2.0 wt.% of the CuO nano-fillers. The flux behavior was thoroughly consistent with the cross-sectional morphology and surface pore size trend with the concentration. Although, the authors emphasized more on the surface pore size behavior.

4-7-1-3- Rejection

Gethard et al. [154] reported that immobilization of carbon nanotubes on the pores of a PP membrane results in an increment in its rejection performance. It is mainly because of the reasons which have been discussed in the previous section. As well, since CNTs act as both molecular transporters and sorbents, they can enhance the permeability of the target component over the others, thus increasing its selectivity. Hou et al. [19] also demonstrated that $CaCO_3$ nanoparticles enhance the rejection performance of a PVDF membrane.

According to Baghbanzadeh et al. [153], the increase in the water permeability was without any compromise in the salt rejection and both the neat and PVDF/CuO nanocomposite membrane showed a perfect rejection of NaCl (99.99%).

About the selectivity in a pervaporation process, it was shown that separation factor was improved by the nanomaterial addition, although those pervaporation processes were not employed for water treatment purpose [155, 167].

4-7-1-4- Fouling

Based upon the results of Razmjou et al. [165], permeate (water) of the super hydrophobic membrane of PVDF/TiO_2 had higher quality compared to that of the neat PVDF membrane

because of the partial pore wetting in the neat membrane. Moreover, the treated membrane possessed higher flux recovery after chemical cleaning of the membrane, which confirmed its better antifouling performance.

4-7-1-5- Mechanical and Thermal Stability

In comparison with a neat PVDF membrane, Kim et al. [15] demonstrated that mechanical properties including Young's modulus, tensile strength, and elongation at the break of a SiO_2 incorporated PVDF membrane were enhanced because the silica particles were confined between polymer chains as the cross-linkers, resulting in an increment in membrane rigidness. But thermal stability enhancement was not significant. It has been further confirmed by Hou et al. [19] that nanomaterials could act as the bridging point in the polymer matrix to enhance its mechanical and thermal strength. However, at high concentrations of the nanoparticles, the membrane becomes mechanically less stable due to the particles agglomeration. It is noteworthy that in another work, Hou et al. [86] showed that the effect of the $CaCO_3$ nanoparticles on thermal properties of the neat PVDF membrane was not significant.

Bhadra et al. [166] also demonstrated that carboxylated nanotubes in the PP CNIM could enhance thermal stability by increasing the degradation temperature.

As well, according to the results of Wang et al. [155], thermal and mechanical stability of the composite pervaporation membranes of PDMS improved as a result of the silica nanoparticles incorporation in the polymer matrix.

4-7-2- Effects of the Nano-additives on the MD/PV Membranes Properties

4-7-2-1- Porosity and Mean Pore Size

To incorporate silica nanoparticles in electro-spun nano-fibrous PVDF membranes, Kim et al. [15] used a sol-gel reaction of tetramethylorthosilicate (TMOS) followed by thermal treatment of the membrane. The authors showed that membrane porosity increased with the concentration of TMOS before thermal treatment was applied, while the mean pore size decreased. Porosity increase is attributed to the decrease in viscosity of the casting solution as confirmed earlier [168,

169]. The porosity decreased, however, after thermal treatment due to the increase of fiber diameter through membrane shrinkage [170, 171]. In another work, it was reported that the mean pore size and porosity of the flat sheet membrane with TiO_2 coating and fluorosilanization remained almost unchanged in comparison with the neat PVDF membrane [165]. As well, Hou et al. [19] demonstrated that mean pore size of a PVDF membrane decreases as a result of the addition of $CaCO_3$ nanoparticles, although membrane porosity showed a maximum at an optimum concentration beyond which it started to decrease because of the agglomeration of $CaCO_3$ particles in the casting dope, which decreased the dispersity of the nanoparticles and reduced the phase separation rate. It is noteworthy that pore size distribution became narrower with an increment in $CaCO_3$ concentration. In another work, Hou et al. [86] further confirmed that the addition of $CaCO_3$ nanoparticles narrowed the pore size distribution of a neat PVDF membrane. The results also demonstrated that porosity, mean pore size, and maximum pore size all showed a maximum at the concentration of 3.0 wt.% of the nano-fillers, which is attributed to the demixing rate change as the incorporation of the nanoparticles. Baghbanzadeh et al. [153] also expressed that upon the addition of hydrophilic CuO nanoparticles into the PVDF neat membrane, surface pore size met a maximum at the medium concentrations, while the porosity increase was not significant at those loadings.

4-7-2-2- Roughness

There were several works in which surface roughness of an MD membrane increased with the addition of nanomaterials into the host polymer [15, 19, 86, 165]. However, based upon the results in the work of Baghbanzadeh et al. [153], membrane surface became smoother upon the introduction of the CuO nano-additives to the PVDF membrane, however, as the filler concentration was elevated, surface roughness increased.

4-7-2-3- Hydrophobicity/Hydrophilicity

Hydrophobic nature of carbon nanotubes [154] or thermal treatment of the membranes after the addition of hydrophilic TiO_2 nanoparticles [15] resulted in more hydrophobic membranes. Hou et al. also reported that inorganic hydrophobic modified $CaCO_3$ nanoparticles could increase the hydrophobicity of a PVDF membrane [19, 86]. Baghbanzadeh et al. [153] showed that

hydrophilic CuO nanoparticles could increase the surface contact angle of the PVDF membrane at the medium concentrations of the hydrophilic nano-additives. The surface contact angle demonstrated a maximum in their study. At the concentrations less than that of the maximum, the contact angle paralleled the roughness behavior, it means rougher the surface higher the contact angle. But beyond that concentration and due to the presence of the hydrophilic nanomaterials over the membrane surface, contact angle decreased with the concentration.

In order to produce a super hydrophobic DCMD membrane, a microfiltration PVDF membrane was modified via roughening its surface by coating with TiO_2 nanoparticles through a low temperature hydrothermal process, and then reducing surface energy through surface fluorosilanization [165]. Introducing TiO_2 nanoparticles into the virgin membrane reduced the water contact angle, but after fluorosilanization, a super hydrophobic membrane with the water contact angle of more than 160˚ and self-cleaning properties was obtained. In a super hydrophobic membrane, a thin layer of air is formed between the surface and water droplets that can provide a membrane with a larger allowable pore size [172], lower heat loss via conduction, and subsequently higher water flux. As well, super hydrophobicity could result in an enhanced fouling behavior of the membrane as a result of reduction in the interactions between the feed and membrane surface [173, 174]. To develop a super hydrophobic surface, reducing the surface free energy via the functionalization with low surface energy materials, or creating a hierarchical nanostructure surface morphology through multilevel surface roughness could be applied [165].

4-7-2-4- Morphology

Hou et al. [19] demonstrated that using hydrophobic modified $CaCO_3$ nanoparticles optimized the sandwich-like morphology of the neat PVDF membrane, while mean pore size decreased as a result of the nanoparticle incorporation. The virgin hollow fiber PVDF membrane showed a three-layer structure, a sponge-like porous layer located between two layers of finger-like macro-voids. By adding the nanoparticles, the middle layer loosened, and its micro-pores became larger, which increased the membrane porosity. As well, finger-like macro-voids increased and became longer and narrower.

In a similar study, Hou et al. [86] reported that at low concentrations, hydrophobic modified $CaCO_3$ particles acted as the nucleating agents, increased the rate of phase inversion, and brought about a flat sheet membrane with higher porosity, larger mean pore size, and also larger micro-pores within the sponge-like layer. But at high concentrations, excess amounts of the nanoparticles agglomerated, acted as the anti-nucleating agents, which resulted in a membrane with dense structure and smaller mean pore size, that could reduce the membrane permeability.
In a different study and through using the hydrophilic CuO nanoparticles in a PVDF matrix, Baghbanzadeh at al. [153] showed that finger-like layer became thicker upon the addition of the hydrophilic nanomaterials. The ratio of the finger-like layer thickness to that of the entire membrane showed a maximum at the intermediate concentrations. This behavior was explained through faster diffusion of the non-solvent into the cast film at low concentrations due to the increase in the hydrophilicity of the dope in the presence of the hydrophilic CuO nanoparticles. The diffusion rate was declined as the fillers concentration increased as a result of the increase in the viscosity of the dope suspension. Another possible mechanism to interpret this behavior is about the nucleating capability of the hydrophilic nanoparticles which stimulated the growth of polymer lean phase at the low concentrations. However, the growth suppressed as the nanoparticles content increased in the casting dope due to the formation of the aggregated nanoparticles. It is noteworthy that the size of micro-voids in the sponge-like layer increased via the addition of the CuO nanoparticles which was ascribed to the affinity of the hydrophilic nano-fillers in the sponge-like layer to the non-solvent which increased the non-solvent influx in the bottom layer resulted in the larger micro-voids.

According to the discussion here and in comparison with the other membrane-based processes for water treatment, small amount of research has been dedicated to improve the MD and PV membranes performance through the use of inorganic nanomaterials which shows this direction is yet to be further investigated. Owing to the hydrophobic surface which is highly demanded for MD application, the selection of appropriate nanomaterials which could optimize both the membrane morphology and its surface chemistry seems to be a key factor. Based upon the results which have been reported for the other membrane-based technologies, hydrophilic nano-

additives have this capacity to enhance the membrane structure where they are used at appropriate concentrations. On the other hand, they most likely increase the surface hydrophilicity of the membrane, which has detrimental effects on the long term performance of an MD membrane. Therefore, much effort is called for to study the effects of nanomaterials type and characteristics on the membrane properties and performance in this field.

4-8- Discussion and Concluding Remarks

The brief summary of the review is as follows:

Experimental works demonstrated that adding SiO_2 nanoparticles into the polymer matrix resulted in enhanced mechanical strength besides an improvement in the membrane permeability. Carbon nanotubes have great potential in membrane applications for water treatment, and they are considered as a promising nano-additive in the modification of organic membranes, although there are several problems which may hinder their applications in membrane separation processes, e.g. surface defects, contamination by metal catalysts, and physical heterogeneities [175]. As well, it is necessary to modify their surface, whether tip or core, via functionalization to improve their abilities for providing a stable suspension as a casting dope. However, as a result of surface modification, nanotubes may lose their smooth neutral internal channels and interactions between water molecules and their functional groups will be developed, which slow down the water movement through the channel [176]. Among the obstacles facing the use of CNTs in membrane technologies for water treatment, synthesis and processing of nanotubes including costs of manufacturing, pre and post-treatments, functionalization, finding a route to scale up their production from lab-scale to industrial level, and finally their human health and environmental impacts, are of great importance, and they need to be further investigated.

TiO_2 nanoparticles are mostly used to enhance the hydrophilicity of the polymeric membranes, and subsequently produce a membrane with better antifouling properties. In this way, they can often increase the pure water flux. However, to reach the best performance of the TiO_2 nanoparticles in a polymer matrix, like the other nanomaterials, an optimum concentration should be sought and employed during the manufacturing process.

Owing to their high aspect ratio, low density, high strength and stiffness, GO nanosheets demonstrated to have the potential to improve the mechanical stability of the membrane. In addition, due to the presence of hydrophilic functional groups on their edges and planes they have this capability to enhance the fouling resistance of the membrane.

Finally, although the use of Al_2O_3, porous nanomaterials such as zeolites, $CaCO_3$, Ag, CuO, and etc. has not been exposed to large amount of research, the results are promising and attention is called to the ongoing works.

As it is clear from the discussions made above, using the nanomaterials in polymeric membranes resulted in various outcomes, and the results were very different from one study to the other. Nevertheless, all studies emphasize the importance of the procedures adopted for the fabrication of composite membranes, the kind of nanoparticles and their inherent nature, materials other than nanoparticles involved in membrane fabrication process, particle concentration, particle resource, methods which are employed to modify the particle surface, and subsequently their dispersion inside the casting solution.

As mentioned, they exhibited reverse effects in some situations, but in most cases, the advantages of nanoparticles incorporation in the polymeric membranes outweighed the disadvantages.

The main reason for the different behavior of nanomaterial incorporated membranes from those without nanoparticles is due to the enhanced interactions between the molecules in nano-scale, by which nanoparticle sites are used more effectively for fouling reduction and flux enhancement. However, it may also be possible that the membrane pores are plugged as a result of using overloaded nanoparticles, which reduces the water flux.

By considering the effects of SiO_2 nanoparticles on the mechanical strength of the membrane, fast water transport through the carbon nanotubes, antifouling and anti-biofouling properties of TiO_2, GO, and Ag nanomaterials, and superhydrophobic characteristics of functionalized $CaCO_3$ nanoparticles, hybrid nanomaterials can be suggested as an alternative way to expect a

synergistic effect of using different nanoparticles at the same time and in a homogeneous system. In addition, it was revealed that inorganic-organic membranes have been mostly used in pressure driven processes such as UF and NF, while much effort needs to be made to fabricate the membranes consistently for novel membrane technologies such as MD and FO. Furthermore, the effects of nanoparticle properties on the membrane characteristics should be further explored.

It should be noted that the investigated approach might be restricted by the limited nanomaterials concentration inside the polymer matrix, their agglomeration in the casting solution, and their poor stability over the membrane surface. Moreover, the quality of the permeate should be continuously monitored to ensure that the nanoparticles have not been released to the product, as well, ecotoxicity aspects of using nanoparticles in membrane technology is yet to be further investigated, and their release risk to the environment should be properly managed. Finally, those nanocomposite membranes could be taken into consideration for industrial applications which show outstanding characteristics in all aspects including high permeability, appropriate selectivity, good antifouling, anti-biofouling, and anti-scaling properties, low manufacturing cost, long term durability, environmental compatibility, and the ability to be employed easily in large scale which further would result in a lower final product cost.

In conclusion, Table 4-6 is provided based upon the discussions that have been made earlier to summarize the most important interpretations which are potentially applicable for different behaviors of the nanocomposite membranes compared to the neat ones as a result of nanomaterials incorporation.

Table 4-6 Changes in membrane physico-chemical properties and performance induced by nanoparticles (NP) incorporation

POROSITY AND PORE SIZE	
Increase	1) Hindrance effect of NPs that reduces the solvent/polymer interactions which allows the solvent to diffuse faster and easier from the polymer matrix to the coagulation bath 2) Hydrophilicity enhancement of the casting solution

Decrease	1) Viscosity increase of the casting solution 2) Deposition of nanomaterials in the membrane pores 3) Agglomeration of NPs at the high concentrations which reduces the phase separation rate
SURFACE ROUGHNESS	
Increase	1) Viscosity increase of the casting solution 2) Particles agglomeration on the membrane surface
Decrease	1) Hydrophilicity enhancement of the casting solution
HYDROPHOBICITY	
Increase	1) Addition of hydrophobic NPs 2) Increase of surface roughness as a result of NPs incorporation
Decrease	1) Addition of hydrophilic NPs or the contribution of their hydrophilic functional groups
EFFECTIVE PARAMETERS in MODIFYING MORPHOLOGY	
Change	1) NPs concentration 2) Hydrophilicity of the casting solution 3) Viscosity of the casting solution
WATER LIQUID ENTRY PRESSURE (LEP_w)	
Increase	1) Increase of surface hydrophobicity 2) Decrease of surface energy
Decrease	1) Increase of membrane maximum pore size

MECHANICAL and THERMAL STABILITY	
Increase	1) Cross-linking effect of NPs at the low concentrations which enhances the rigidity of the polymeric matrix
Decrease	1) Aggregation of NPs at the high concentrations which brings about a membrane with poor structure
FLUX	
Increase	1) Increase of membrane porosity and pore size 2) Increase of casting solution hydrophilicity 3) Enlargement of effective surface area due to the increase of surface roughness or NPs incorporation 4) Formation of free spaces at the interface between the polymer chains and the nano-fillers 5) Capillary effect of membrane pores as the surface hydrophilicity is improved 6) Decrease of temperature polarization as the surface hydrophobicity is enhanced (for MD) 7) Lowering the degree of polymerization in the presence of NPs since they interfere the interfacial polymerization 8) Decrease of pore wetting and its blockage when the surface hydrophobicity improves (for MD) 9) Lowering the vapor condensation through the membrane pores when thermal conductivity increases within the pores as a result of NPs contribution (for MD) 10) Contribution of new flow paths as the incorporation of NPs 11) Effects of NPs' internal pores which sometimes shorten the path that a vapor or liquid molecule would pass to reach the other side
Decrease	1) Increase of membrane thickness 2) Increase of membrane tortuosity 3) Increase of casting solution viscosity

	4) Blockage of membrane pores due to the particles agglomeration 5) Formation of a less porous sub-layer with more interconnectivity between the macro-voids as a result of NPs incorporation
REJECTION	
Increase	1) Decrease of membrane pore size 2) Increase of surface negative charge which enhances the repulsion forces between membrane surface and salt anions 3) A membrane with denser structure due to the strong interactions between nano-fillers and polymer matrix
Decrease	1) A membrane with defective structure as a result of particles aggregation at the high concentrations 2) Lowering the degree of cross-linking of active layer due to the incorporation of NPs 3) Existence of molecular scale voids between the NPs and polymer chains as a result of imperfect interactions
FOULING and BIOFOULING	
Increase	1) Membrane with defective structure as a result of particles agglomeration 2) Increase of surface roughness
Decrease	1) Enhancement of surface hydrophilicity 2) Nature of incorporated NPs like Ag, Cu, and TiO_2 3) Super hydrophobicity of the membrane surface since it sets up an air gap between the feed and surface 4) A membrane with lower surface energy which is equivalent to a weaker van der Waals force between the foulant and membrane surface

References

[1] Curcio, E., Profio, G.D., Fontananova, E., Drioli, E. (2015) Membrane Technologies For seawater Desalination And brackish Water Treatment. In: Basile A, Rastogi ACK (eds) *Advances in Membrane Technologies for Water Treatment.* Woodhead Publishing, Oxford, UK, Ch. 13, pp. 411-441

[2] Zhou, H., Smith, D. (2001) Advanced technologies in water and wastewater treatment. *Can. J. of Civil Eng.,* 28:49-66

[3] Wang, Q., Wang, X., Wang, Z., Huang, J., Wang, Y. (2013) PVDF membranes with simultaneously enhanced permeability and selectivity by breaking the tradeoff effect via atomic layer deposition of TiO2. *J. Membr. Sci.,* 442:57-64

[4] Koyuncu, I., Sengur, R., Turken, T., Guclu, S., Pasaoglu, M.E. (2015) Advances in Water Treatment By microfiltration, Ultrafiltration, and Nanofiltration. In: Basile A, Rastogi ACK (eds) *Advances in Membrane Technologies for Water Treatment.* Woodhead Publishing, Oxford, UK, Ch. 3, pp. 83-128

[5] Sears, K., Dumee, L., Schuetz, J., She, M., Huynh, C., Hawkins, S., Duke, M., Gray, S. (2010) Recent Developments in Carbon Nanotube Membranes for Water Purification and Gas Separation. *Materials,* 3:127-149

[6] Kim, J., Van der Bruggen, B. (2010) The use of nanoparticles in polymeric and ceramic membrane structures: Review of manufacturing procedures and performance improvement for water treatment. *Environ. Pollut.,* 158:2335-2349

[7] Camacho, L.M., Dumee, L., Zhang, J., Li, J., Duke, M., Gomez, J., Gray, S. (2013) Advances in Membrane Distillation for Water Desalination and Purification Applications. *Water,* 5:94-196

[8] Goh, P.S., Ng, B.C., Lau, W.J., Ismail, A.F. (2015) Inorganic Nanomaterials in Polymeric Ultrafiltration Membranes for Water Treatment. *Sep. Purif. Rev.,* 44:216-249

[9] Madaeni, S.S., Ghaemi, N., Rajabi, H. (2015) Advances in Polymeric Membranes for Water Treatment. In: Basile A, Rastogi ACK (eds) *Advances in Membrane Technologies for Water Treatment.* Woodhead Publishing, Oxford, UK, Ch.1, pp. 3-41

[10] Ji, Y. (2015) Membrane Technologies for Water Treatment and Reuse in the Gas and Petrochemical Industries. In: Basile A, Rastogi ACK (eds) *Advances in Membrane Technologies for Water Treatment.* Woodhead Publishing, Oxford, UK. Ch. 16, pp. 519-536

[11] Rahimpour, A., Madaeni, S.S. (2010) Improvement of performance and surface properties of nano-porous polyethersulfone (PES) membrane using hydrophilic monomers as additives in the casting solution. *J. Membr. Sci.,* 360:371-379

[12] Ochoa, N., Masuelli, M., Marchese, J. (2003) Effect of hydrophilicity on fouling of an emulsified oil wastewater with PVDF/PMMA membranes. *J. Membr. Sci.,* 226:203-211

[13] Yan, L., Li, Y.S., Xiang, C.B. (2005) Preparation of poly(vinylidene fluoride)(pvdf) ultrafiltration membrane modified by nano-sized alumina (Al2O3) and its antifouling research. *Polymer,* 46:7701-7706

[14] Celik, E., Park, H., Choi, H., Choi, H. (2011) Carbon nanotube blended polyethersulfone membranes for fouling control in water treatment. *Water Res.,* 45:274-282

[15] Kim, Y., Ahn, C.H., Choi, M.O. (2010) Effect of thermal treatment on the characteristics of electrospun PVDF−silica composite nanofibrous membrane. *Eur. Polym. J.,* 46:1957-1965

[16] Goh, P.S., Ismail, A.F., Ng, B.C. (2013) Carbon nanotubes for desalination: Performance evaluation and current hurdles. *Desalination,* 308:2-14

[17] Lee, J., Chae, H., Won, Y.J., Lee, K., Lee, C., Lee, H.H., Kim, I., Lee, J. (2013) Graphene oxide nanoplatelets composite membrane with hydrophilic and antifouling properties for wastewater treatment. *J. Membr. Sci.,* 448:223-230

[18] Luo, M., Tang, W., Zhao, J., Pu, C. (2006) Hydrophilic modification of poly(ether sulfone) used TiO2 nanoparticles by a sol–gel process. *J. Mater. Process Technol.,* 172:431-436

[19] Hou, D., Wang, J., Sun, X., Ji, Z., Luan, Z. (2012) Preparation and properties of PVDF composite hollow fiber membranes for desalination through direct contact membrane distillation. *J. Membr. Sci.,* 405:185-200

[20] Jin, L.M., Yu, S.L., Shi, W.X., Yi, X.S., Sun, N., Ge, Y.L., Ma, C. (2012) Synthesis of a novel composite nanofiltration membrane incorporated SiO2 nanoparticles for oily wastewater desalination. *Polymer,* 53:5295-5303

[21] Ahmad, J., Hagg, M.B. (2013) Polyvinyl acetate/titanium dioxide nanocomposite membranes for gas separation. *J. Membr. Sci.,* 445:200-210

[22] Khosravi, A., Sadeghi, M., Banadkohi, H.Z., Talakesh, M.M. (2014) Polyurethane-Silica Nanocomposite Membranes for Separation of Propane/Methane and Ethane/Methane. *Ind. Eng. Chem. Res.,* 53:2011-2021

[23] Lu, H., Zhang, L., Xing, W., Wang, H., Xu, N. (2005) Preparation of TiO2 hollow fibers using poly(vinylidene fluoride) hollow fiber microfiltration membrane as a template. *Mater. Chem. Phys.,* 94:322-327

[24] Wu, G., Gan, S., Cui, L., Xu, Y. (2008) Preparation and characterization of PES/TiO2 composite membranes. *Appl. Surf. Sci.,* 254:7080-7086

[25] de Lannoy, C., Soyer, E., Wiesner, M.R. (2013) Optimizing carbon nanotube-reinforced polysulfone ultrafiltration membranes through carboxylic acid functionalization. *J. Membr. Sci.,* 447:395-402

[26] Toroghi, M., Raisi, A., Aroujalian, A. (2014) Preparation and characterization of polyethersulfone/silver nanocomposite ultrafiltration membrane for antibacterial applications. *Polym. Adv. Technol.,* 25:711-722

[27] Peyravi, M., Jahanshahi, M., Rahimpour, A., Javadi, A., Hajavi, S. (2014) Novel thin film nanocomposite membranes incorporated with functionalized TiO2 nanoparticles for organic solvent nanofiltration. *Chem. Eng., J* 241:155-166

[28] Jeong, B., Hoek, E.M.V., Yan, Y., Subramani, A., Huang, X., Hurwitz, G., Ghosh, A.K., Jawor, A. (2007) Interfacial polymerization of thin film nanocomposites: A new concept for reverse osmosis membranes. *J. Membr. Sci.,* 294:1-7

[29] Kim, H.J., Choi, K., Baek, Y., Kim, D., Shim, J., Yoon, J., Lee, J. (2014) High-performance reverse osmosis CNT/polyamide nanocomposite membrane by controlled interfacial interactions. *Acs Appl. Mater. Interfaces,* 6:2826-2836

[30] Ma, N., Wei, J., Liao, R., Tang, C.Y. (2012) Zeolite-polyamide thin film nanocomposite membranes: Towards enhanced performance for forward osmosis. *J. Membr. Sci.,* 405:149-157

[31] Liu, X., Qi, S., Li, Y., Yang, L., Cao, B., Tang, C.Y. (2013) Synthesis and characterization of novel antibacterial silver nanocomposite nanofiltration and forward osmosis membranes based on layer-by-layer assembly. *Water Res.,* 47:3081-3092

[32] Gethard, K., Sae-Khow, O., Mitra, S. (2012) Carbon nanotube enhanced membrane distillation for simultaneous generation of pure water and concentrating pharmaceutical waste. *Sep. Purif. Technol.,* 90:239-245

[33] Abdallah, H., Moustafa, A.F., AlAnezi, A.A., El-Sayed, H.E.M. (2014) Performance of a newly developed titanium oxide nanotubes/polyethersulfone blend membrane for water desalination using vacuum membrane distillation. *Desalination,* 346:30-36

[34] Sairam, M., Patil, M.B., Veerapur, R.S., Patil, S.A., Aminabhavi, T.M. (2006) Novel dense poly(vinyl alcohol)–TiO2 mixed matrix membranes for pervaporation separation of water–isopropanol mixtures at 30 °C. *J. Membr. Sci.,* 281:95-102

[35] Shen, J., Chu, Y., Ruan, H., Wu, L., Gao, C., Van der Bruggen, B. (2014) Pervaporation of benzene/cyclohexane mixtures through mixed matrix membranes of chitosan and Ag+/carbon nanotubes. *J. Membr. Sci.,* 462:160-169

[36] Bottino, A., Capannelli, G., Comite, A. (2002) Preparation and characterization of novel porous PVDF-ZrO2 composite membranes. *Desalination,* 146:35-40

[37] Yan, L., Li, Y.S., Xiang, C.B., Xianda, S. (2006) Effect of nano-sized Al2O3-particle addition on PVDF ultrafiltration membrane performance. *J. Membr. Sci.,* 276:162-167

[38] Cao, X., Ma, J., Shi, X., Ren, Z. (2006) Effect of TiO2 nanoparticle size on the performance of PVDF membrane. *Appl. Surf. Sci.,* 253:2003-2010

[39] Huang, Z., Chen, K., Li, S., Yin, X., Zhang, Z., Xu, H. (2008) Effect of ferrosoferric oxide content on the performances of polysulfone-ferrosoferric oxide ultrafiltration membranes. *J. Membr. Sci.,* 315:164-171

[40] Yu, L., Xu, Z., Shen, H., Yang, H. (2009) Preparation and characterization of PVDF-SiO2 composite hollow fiber UF membrane by sol-gel method. *J. Membr. Sci.,* 337:257-265

[41] Yang, H., Lin, J.C., Huang, C. (2009) Application of nanosilver surface modification to RO membrane and spacer for mitigating biofouling in seawater desalination. *Water Res.,* 43:3777-3786

[42] Wu, H., Tang, B., Wu, P. (2010) Novel ultrafiltration membranes prepared from a multi-walled carbon nanotubes/polymer composite. *J. Membr. Sci.,* 362:374-383

[43] Goh, K., Setiawan, L., Wei, L., Si, R., Fane, A.G., Wang, R., Chen, Y. (2015) Graphene oxide as effective selective barriers on a hollow fiber membrane for water treatment process. *J. Membr. Sci.,* 474:244-253

[44] Xu, C., Xu, Y., Zhu, J. (2014) Photocatalytic antifouling graphene oxide-mediated hierarchical filtration membranes with potential applications on water purification. *Acs Appl. Mater. Interfaces,* 6:16117-16123

[45] Available from: www.nanoh2o.com May, 2015

[46] Kurth C.J., Koehler J.A.,Zhou M.,Holmberg B.A., Burk R.L. (2012) Reverse osmosis membranes, US Patent 8,177,978 B2

[47] Hofs, B., Schurer, R., Harmsen, D.J.H., Ceccarelli, C., Beerendonk, E.F., Cornelissen, E.R. (2013) Characterization and performance of a commercial thin film nanocomposite seawater reverse osmosis membrane and comparison with a thin film composite. *J. Membr. Sci.,* 446:68-78

[48] Ruan, S., Gao, P., Yang, X., Yu, T. (2003) Toughening high performance ultrahigh molecular weight polyethylene using multiwalled carbon nanotubes. *Polymer,* 44:5643-5654

[49] Coleman, J.N., Khan, U., Blau, W.J., Gun'ko, Y.K. (2006) Small but strong: A review of the mechanical properties of carbon nanotube-polymer composites. *Carbon,* 44:1624-1652

[50] Qu, X., Alvarez, P.J.J., Li, Q. (2013) Applications of nanotechnology in water and wastewater treatment. *Water Res.,* 47:3931-3946

[51] Dintcheva, N.T., Arrigo, R., Nasillo, G., Caponetti, E., La Mantia, F.P. (2013) Effect of the nanotube aspect ratio and surface functionalization on the morphology and properties of multiwalled carbon nanotube polyamide-based fibers. *J. Appl. Polym. Sci.,* 129:2479-2489

[52] Liu, Y., Kumar, S. (2014) Polymer/carbon nanotube nano composite fibers-a review. *ACS Appl. Mater. Interfaces,* 6:6069-6087

[53] Das, R., Ali, M.E., Abd Hamid, S.B., Ramakrishna, S., Chowdhury, Z.Z. (2014) Carbon nanotube membranes for water purification: A bright future in water desalination. *Desalination,* 336:97-109

[54] Kar, S., Bindal, R.C., Tewari, P.K. (2012) Carbon nanotube membranes for desalination and water purification: Challenges and opportunities. *Nano Today,* 7:385-389

[55] Mauter, M.S., Elimelech, M. (2008) Environmental applications of carbon-based nanomaterials. *Environ. Sci. Technol.,* 42:5843-5859

[56] Wang, X., Chen, X., Yoon, K., Fang, D., Hsiao, B., Chu, B. (2005) High flux filtration medium based on nanofibrous substrate with hydrophilic nanocomposite coating. *Environ. Sci. Technol.,* 39:7684-7691

[57] Ahn, C.H., Baek, Y., Lee, C., Kim, S.O., Kim, S., Lee, S., Kim, S., Bae, S.S., Park, J., Yoon, J. (2012) Carbon nanotube-based membranes: Fabrication and application to desalination. *J. Ind. Eng. Chem.,* 18:1551-1559

[58] Cho, J.W., Sul, K.I. (2001) Characterization and properties of hybrid composites prepared from poly(vinylidene fluoride-tetrafluoroethylene) and SiO2. *Polymer,* 42:727-736

[59] Ogoshi, T., Chujo, Y. (2005) Synthesis of poly(vinylidene fluoride) (PVdF)/silica hybrids having interpenetrating polymer network structure by using crystallization between PVdF chains. *J. Polym. Sci. Polym. Chem.,* 43:3543-3550

[60] Baghbanzadeh, M., Rashidi, A., Rashtchian, D., Lotfi, R., Amrollahi, A. (2012) Synthesis of spherical silica/multiwall carbon nanotubes hybrid nanostructures and investigation of thermal conductivity of related nanofluids. *Thermochim. Acta,* 549:87-94

[61] Vega-Baudrit, J., Navarro-Banon, V., Vazquez, P., Martin-Martinez, J.M. (2006) Addition of nanosilicas with different silanol content to thermoplastic polyurethane adhesives. *Int. J. Adhes. Adhes.,* 26:378-387

[62] Yao, X.F., Zhou, D., Yeh, H.Y. (2008) Macro/microscopic fracture characterizations of SiO2/epoxy nanocomposites. *Aerosp. Sci. Technol.,* 12:223-230

[63] Sprenger, S. (2013) Epoxy resin composites with surface-modified silicon dioxide nanoparticles: A review. *J. Appl. Polym. Sci.,* 130:1421-1428

[64] Wang, X., Wang, L., Su, Q., Zheng, J. (2013) Use of unmodified SiO2 as nanofiller to improve mechanical properties of polymer-based nanocomposites. *Composites Sci. Technol.,* 89:52-60

[65] Malay, O., Oguz, O., Kosak, C., Yilgor, E., Yilgor, I., Menceloglu, Y.Z. (2013) Polyurethaneurea-silica nanocomposites: Preparation and investigation of the structure-property behavior. *Polymer.,* 54:5310-5320

[66] Yang, J., Zhao, J. (2014) Preparation and mechanical properties of silica nanoparticles reinforced composite hydrogels. *Mater. Lett.,* 120:36-38

[67] Liu, Y.L., Hsu, C.Y., Wei, W.L., Jeng, R.J. (2003) Preparation and thermal properties of epoxy-silica nanocomposites from nanoscale colloidal silica. *Polymer,* 44:5159-5167

[68] Liu, W., Zhu, B., Zhang, J., Xu, Y. (2007) Preparation and dielectric properties of polyimide/silica nanocomposite films prepared from sol-gel and blending process. *Polym. Adv. Technol.,* 18:522-528

[69] Palza, H., Vergara, R., Zapata, P. (2011) Composites of polypropylene melt blended with synthesized silica nanoparticles. *Composites Sci. Technol.,* 71:535-540

[70] Song, H., Zheng, L. (2013) Nanocomposite films based on cellulose reinforced with nano-SiO2: microstructure, hydrophilicity, thermal stability, and mechanical properties. *Cellulose,* 20:1737-1746

[71] Bissadi, G., Kruczek, B. (2014) Thermal properties of silica/poly(2,6-dimethyl-1,4-phenylene oxide) films prepared by emulsion polymerization. *J. Therm. Anal. Calorim.,* 117:73-83

[72] Ab Rahman, I., Padavettan, V. (2012) Synthesis of silica nanoparticles by sol-gel: size-dependent properties, surface modification, and applications in silica-polymer nanocomposites-a review. *J. Nanomater.,* :132424

[73] Kickelbick, G. (2003) Concepts for the incorporation of inorganic building blocks into organic polymers on a nanoscale. *Prog. Polym. Sci.,* 28:83-114

[74] Madaeni, S.S., Ghaemi, N. (2007) Characterization of self-cleaning RO membranes coated with TiO2 particles under UV irradiation. *J. Membr. Sci.,* 303:221-233

[75] Teow, Y.H., Ahmad, A.L., Lim, J.K., Ooi, B.S. (2013) Studies on the surface properties of mixed-matrix membrane and its antifouling properties for humic acid removal. *J. Appl. Polym. Sci.,* 128:3184-3192

[76] Cruz, N.K.O., Semblante, G.U., Senoro, D.B., You, S., Lu, S. (2014) Dye degradation and antifouling properties of polyvinylidene fluoride/titanium oxide membrane prepared by sol-gel method. *J. Taiwan Inst. Chem. Eng.,* 45:192-201

[77] Ghasemzadeh, G., Momenpour, M., Omidi, F., Hosseini, M.R., Ahani, M., Barzegari, A. (2014) Applications of nanomaterials in water treatment and environmental remediation. *Front Env. Sci. Eng.,* 8:471-482

[78] Foster, H.A., Ditta, I.B., Varghese, S., Steele, A. (2011) Photocatalytic disinfection using titanium dioxide: spectrum and mechanism of antimicrobial activity. *Appl. Microbiol. Biotechnol.,* 90:1847-1868

[79] Lazar, M.A., Varghese, S., Nair, S.S. (2012) Photocatalytic Water Treatment by Titanium Dioxide: Recent Updates. *Catalysts,* 2:572-601

[80] Li, Q., Mahendra, S., Lyon, D.Y., Brunet, L., Liga, M.V., Li, D., Alvarez, P.J.J. (2008) Antimicrobial nanomaterials for water disinfection and microbial control: Potential applications and implications. *Water Res.,* 42:4591-4602

[81] Xu, C., Rangaiah, G.P., Zhao, X.S. (2014) Photocatalytic Degradation of Methylene Blue by Titanium Dioxide: Experimental and Modeling Study. *Ind. Eng. Chem. Res.,* 53:14641-14649

[82] Molinari, R., Argurio, P., Palmisano, L. (2015) Photocatalytic Membrane Reactors for Water Treatment. In: Basile A, Rastogi ACK (eds) *Advances in Membrane Technologies for Water Treatment.* Woodhead Publishing, Oxford, UK, Ch. 7, pp. 205-238

[83] Anh Nguyen, Zou, L., Priest, C. (2014) Evaluating the antifouling effects of silver nanoparticles regenerated by TiO2 on forward osmosis membrane. *J. Membr. Sci.,* 454:264-271

[84] Liu, F., Abed, M.R.M., Li, K. (2011) Preparation and characterization of poly(vinylidene fluoride) (PVDF) based ultrafiltration membranes using nano gamma-Al2O3. *J. Membr. Sci.,* 366:97-103

[85] Maximous, N., Nakhla, G., Wan, W., Wong, K. (2009) Preparation, characterization and performance of Al2O3/PES membrane for wastewater filtration. *J. Membr. Sci.,* 341:67-75

[86] Hou, D., Dai, G., Fan, H., Wang, J., Zhao, C., Huang, H. (2014) Effects of calcium carbonate nano-particles on the properties of PVDF/nonwoven fabric flat-sheet composite membranes for direct contact membrane distillation. *Desalination,* 347:25-33

[87] Sawada, I., Fachrul, R., Ito, T., Ohmukai, Y., Maruyama, T., Matsuyama, H. (2012) Development of a hydrophilic polymer membrane containing silver nanoparticles with both organic antifouling and antibacterial properties. *J. Membr. Sci.,* 387:1-6

[88] Lind, M.L., Ghosh, A.K., Jawor, A., Huang, X., Hou, W., Yang, Y., Hoek, E.M.V. (2009) Influence of zeolite crystal size on zeolite-polyamide thin film nanocomposite membranes. *Langmuir,* 25:10139-10145

[89] Fathizadeh, M., Aroujalian, A., Raisi, A. (2011) Effect of added NaX nano-zeolite into polyamide as a top thin layer of membrane on water flux and salt rejection in a reverse osmosis process. *J. Membr. Sci.,* 375:88-95

[90] Jamshidi Gohari, R., Lau, W.J., Matsuura, T., Ismail, A.F. (2013) Effect of surface pattern formation on membrane fouling and its control in phase inversion process. *J. Membr. Sci.,* 446:326-331

[91] Singh, R. (2015) Chapter Water and Membrane Treatment. In: Singh R (ed) *Membrane Technology and Engineering for Water Purification (Second Edition).* Butterworth-Heinemann, Oxford, UK, Ch. 2, pp. 81-178

[92] Lau, W.J., Goh, P.S., Ismail, A.F., Lai, S.O. (2014) Ultrafiltration as a pretreatment for seawater desalination: A review. *Membr. Water Treat.,* 5:15-29

[93] Butler, C.S., Boltz, J.P. (2014) Biofilm Processes and Control in Water and Wastewater Treatment. In: Ahuja S (ed) *Comprehensive Water Quality and Purification.* Elsevier, Waltham, MA, Ch. 3.6, pp. 90-107

[94] Sadr, S.M.K., Saroj, D.P. (2015) Membrane Technologies For municipal Wastewater Treatment. In: Basile A, Rastogi ACK (eds) *Advances in Membrane Technologies for Water Treatment.* Woodhead Publishing, Oxford, UK, Ch. 14, pp. 443-463

[95] Arribas, P., Khayet, M., García-Payo, M.C., Gil, L. (2015) Novel and Emerging Membranes for Water Treatment by Hydrostatic Pressure and Vapor Pressure Gradient Membrane Processes. In: Basile A, Rastogi ACK (eds) *Advances in Membrane Technologies for Water Treatment.* Woodhead Publishing, Oxford, UK, Ch. 8, pp. 239-285

[96] Ahmad, A.L., Majid, M.A., Ooi, B.S. (2011) Functionalized PSf/SiO2 nanocomposite membrane for oil-in-water emulsion separation. *Desalination,* 268:266-269

[97] Rahimpour, A., Jahanshahi, M., Khalili, S., Mollahosseini, A., Zirepour, A., Rajaeian, B. (2012) Novel functionalized carbon nanotubes for improving the surface properties and performance of polyethersulfone (PES) membrane. *Desalination,* 286:99-107

[98] Yang, Y., Zhang, H., Wang, P., Zheng, Q., Li, J. (2007) The influence of nano-sized TiO2 fillers on the morphologies and properties of PSFUF membrane. *J. Membr. Sci.,* 288:231-238

[99] Rahimpour, A., Jahanshahi, M., Rajaeian, B., Rahimnejad, M. (2011) TiO2 entrapped nano-composite PVDF/SPES membranes: Preparation, characterization, antifouling and antibacterial properties. *Desalination,* 278:343-353

[100] Oh, S.J., Kim, N., Lee, Y.T. (2009) Preparation and characterization of PVDF/TiO2 organic-inorganic composite membranes for fouling resistance improvement. *J. Membr. Sci.,* 345:13-20

[101] Razmjou, A., Mansouri, J., Chen, V. (2011) The effects of mechanical and chemical modification of TiO2 nanoparticles on the surface chemistry, structure and fouling performance of PES ultrafiltration membranes. *J. Membr. Sci.,* 378:73-84

[102] Li, F., Li, L., Liao, X., Wang, Y. (2011) Precise pore size tuning and surface modifications of polymeric membranes using the atomic layer deposition technique. *J. Membr. Sci.,* 385:1-9

[103] Zhang, J., Xu, Z., Mai, W., Min, C., Zhou, B., Shan, M., Li, Y., Yang, C., Wang, Z., Qian, X. (2013) Improved hydrophilicity, permeability, antifouling and mechanical performance of PVDF composite ultrafiltration membranes tailored by oxidized low-dimensional carbon nanomaterials. *J. Mater. Chem. A,* 1:3101-3111

[104] Li, J., Xu, Z., Yang, H., Yu, L., Liu, M. (2009) Effect of TiO2 nanoparticles on the surface morphology and performance of microporous PES membrane. *Appl. Surf. Sci.,* 255:4725-4732

[105] Wang, Z., Yu, H., Xia, J., Zhang, F., Li, F., Xia, Y., Li, Y. (2012) Novel GO-blended PVDF ultrafiltration membranes. *Desalination,* 299:50-54

[106] Xu, Z., Zhang, J., Shan, M., Li, Y., Li, B., Niu, J., Zhou, B., Qian, X. (2014) Organosilane-functionalized graphene oxide for enhanced antifouling and mechanical properties of polyvinylidene fluoride ultrafiltration membranes. *J. Membr. Sci.,* 458:1-13

[107] Zodrow, K., Brunet, L., Mahendra, S., Li, D., Zhang, A., Li, Q., Alvarez, P.J.J. (2009) Polysulfone ultrafiltration membranes impregnated with silver nanoparticles show improved biofouling resistance and virus removal. *Water Res.,* 43:715-723

[108] Lee, S.Y., Kim, H.J., Patel, R., Im, S.J., Kim, J.H., Min, B.R. (2007) Silver nanoparticles immobilized on thin film composite polyamide membrane: characterization, nanofiltration, antifouling properties. *Polym. Adv. Technol.,* 18:562-568

[109] Han, P., Yahui, H., Yang, W., Linlin, L. (2006) Preparation of polysulfone-Fe3O4 composite ultrafiltration membrane and its behavior in magnetic field. *J. Membr. Sci.,* 284:9-16

[110] Xiong, X., Li, Q., Zhang, X., Wang, L., Guo, Z., Yu, J. (2013) Poly(vinylidene fluoride)/silica nanocomposite membranes by electrospinning. *J. Appl. Polym. Sci.,* 129:1089-1095

[111] Kim, I., Lee, K., Tak, T. (2001) Preparation and characterization of integrally skinned uncharged polyetherimide asymmetric nanofiltration membrane. *J. Membr. Sci.,* 183:235-247

[112] Baghbanzadeh, M., Rashidi, A., Soleimanisalim, A.H., Rashtchian, D. (2014) Investigating the rheological properties of nanofluids of water/hybrid nanostructure of spherical silica/MWCNT. *Thermochim. Acta,* 578:53-58

[113] Wenzel, R. (1936) Resistance of solid surfaces to wetting by water. *Ind. Eng. Chem.,* 28:988-994

[114] Agboola, O., Maree, J., Mbaya, R. (2014) Characterization and performance of nanofiltration membranes. *Environ. Chem. Lett.,* 12:241-255

[115] Shen, J.n., Yu, C.c., Ruan, H.m., Gao, C.j., Van der Bruggen, B. (2013) Preparation and characterization of thin-film nanocomposite membranes embedded with poly(methyl methacrylate) hydrophobic modified multiwalled carbon nanotubes by interfacial polymerization. *J. Membr. Sci.,* 442:18-26

[116] Kumar, R., Isloor, A.M., Ismail, A.F., Rashid, S.A., Al Ahmed, A. (2013) Permeation, antifouling and desalination performance of TiO2 nanotube incorporated PSf/CS blend membranes. *Desalination,* 316:76-84

[117] Vatanpour, V., Madaeni, S.S., Moradian, R., Zinadini, S., Astinchap, B. (2012) Novel antibifouling nanofiltration polyethersulfone membrane fabricated from embedding TiO2 coated multiwalled carbon nanotubes. *Sep. Purif. Technol.,* 90:69-82

[118] Lee, H.S., Im, S.J., Kim, J.H., Kim, H.J., Kim, J.P., Min, B.R. (2008) Polyamide thin-film nanofiltration membranes containing TiO2 nanoparticles. *Desalination,* 219:48-56

[119] Mo, J., Son, S., Jegal, J., Kim, J., Lee, Y.H. (2007) Preparation and characterization of polyamide nanofiltration composite membranes with TiO2 layers chemically connected to the membrane surface. *J. Appl. Polym. Sci.,* 105:1267-1274

[120] Zinadini, S., Zinatizadeh, A.A., Rahimi, M., Vatanpour, V., Zangeneh, H. (2014) Preparation of a novel antifouling mixed matrix PES membrane by embedding graphene oxide nanoplates. *J. Membr. Sci.,* 453:292-301

[121] Ganesh, B.M., Isloor, A.M., Ismail, A.F. (2013) Enhanced hydrophilicity and salt rejection study of graphene oxide-polysulfone mixed matrix membrane. *Desalination,* 313:199-207

[122] Ng, L.Y., Mohammad, A.W., Leo, C.P., Hilal, N. (2013) Polymeric membranes incorporated with metal/metal oxide nanoparticles: A comprehensive review. *Desalination,* 308:15-33

[123] Aydiner, C. (2010) A novel approach based on distinction of actual and pseudo resistances in membrane fouling: "Pseudo resistance" concept and its implementation in nanofiltration of single solutions. *J. Membr. Sci.,* 361:96-112

[124] Rahimpour, A., Madaeni, S.S., Taheri, A.H., Mansourpanah, Y. (2008) Coupling TiO2 nanoparticles with UV irradiation for modification of polyethersulfone ultrafiltration membranes. *J. Membr. Sci.,* 313:158-169

[125] Ghaffour, N., Missimer, T.M., Amy, G.L. (2013) Technical review and evaluation of the economics of water desalination: Current and future challenges for better water supply sustainability. *Desalination,* 309:197-207

[126] Hassan, A.S., Fath, H.E.S. (2013) Review and assessment of the newly developed MD for desalination processes. *Desalin. Water. Treat.,* 51:574-585

[127] Kim, S., Kwak, S., Sohn, B., Park, T. (2003) Design of TiO2 nanoparticle self-assembled aromatic polyamide thin-film-composite (TFC) membrane as an approach to solve biofouling problem. *J. Membr. Sci.,* 211:157-165

[128] Ostuni, E., Chapman, R., Holmlin, R., Takayama, S., Whitesides, G. (2001) A survey of structure-property relationships of surfaces that resist the adsorption of protein. *Langmuir,* 17:5605-5620

[129] Vrijenhoek, E., Hong, S., Elimelech, M. (2001) Influence of membrane surface properties on initial rate of colloidal fouling of reverse osmosis and nanofiltration membranes. *J. Membr. Sci.,* 188:115-128

[130] Functional Nanostructured Materials and Membranes for Water Treatment. (2013) Wiley-VCH, Weinheim, Germany.

[131] Yang, H., Lin, J.C., Huang, C. (2009) Application of nanosilver surface modification to RO membrane and spacer for mitigating biofouling in seawater desalination. *Water Res.,* 43:3777-3786

[132] Yin, J., Yang, Y., Hu, Z., Deng, B. (2013) Attachment of silver nanoparticles (AgNPs) onto thin-film composite (TFC) membranes through covalent bonding to reduce membrane biofouling. *J. Membr. Sci.,* 441:73-82

[133] Zhang, L., Shi, G., Qiu, S., Cheng, L., Chen, H. (2011) Preparation of high-flux thin film nanocomposite reverse osmosis membranes by incorporating functionalized multi-walled carbon nanotubes. *Desalin, Water Treat.,* 34:19-24

[134] Lind, M.L., Jeong, B., Subramani, A., Huang, X., Hoek, E.M.V. (2009) Effect of mobile cation on zeolite-polyamide thin film nanocomposite membranes. *J. Mater. Res.,* 24:1624-1631

[135] Shawky, H.A., Chae, S., Lin, S., Wiesner, M.R. (2011) Synthesis and characterization of a carbon nanotube/polymer nanocomposite membrane for water treatment. *Desalination,* 272:46-50

[136] Kwak, S., Kim, S., Kim, S. (2001) Hybrid organic/inorganic reverse osmosis (RO) membrane for bactericidal anti-fouling. 1. Preparation and characterization of TiO2 nanoparticle self-assembled aromatic polyamide thin-film-composite (TFC) membrane. *Environ. Sci. Technol.,* 35:2388-2394

[137] Yin, J., Kim, E., Yang, J., Deng, B. (2012) Fabrication of a novel thin-film nanocomposite (TFN) membrane containing MCM-41 silica nanoparticles (NPs) for water purification. *J. Membr. Sci.,* 423:238-246

[138] Buonomenna, M.G. (2013) Nano-enhanced reverse osmosis membranes. *Desalination,* 314:73-88

[139] Park, K.T., Kim, S.G., Chun, B., Bang, J., Kim, S.H. (2010) Sulfonated poly(arylene ether sulfone) thin-film composite reverse osmosis membrane containing SiO2 nano-particles. *Desalin. Water Treat.,* 15:69-75

[140] Ben-Sasson, M., Zodrow, K.R., Qi Genggeng, Kang, Y., Giannelis, E.P., Elimelech, M. (2014) Surface Functionalization of Thin-Film Composite Membranes with Copper Nanoparticles for Antimicrobial Surface Properties. *Environ. Sci. Technol.*, 48:384-393

[141] Vatanpour, V., Madaeni, S.S., Moradian, R., Zinadini, S., Astinchap, B. (2011) Fabrication and characterization of novel antifouling nanofiltration membrane prepared from oxidized multiwalled carbon nanotube/polyethersulfone nanocomposite. *J. Membr. Sci.,* 375:284-294

[142] Rahaman, M.S., Therien-Aubin, H., Ben-Sasson, M., Ober, C.K., Nielsen, M., Elimelech, M. (2014) Control of biofouling on reverse osmosis polyamide membranes modified with biocidal nanoparticles and antifouling polymer brushes. *J. Mater. Chem. B*, 2:1724-1732

[143] Niksefat, N., Jahanshahi, M., Rahimpour, A. (2014) The effect of SiO2 nanoparticles on morphology and performance of thin film composite membranes for forward osmosis application. *Desalination,* 343:140-146

[144] Lee, J., Qi, S., Liu, X., Li, Y., Huo, F., Tang, C.Y. (2014) Synthesis and characterization of silica gel-polyacrylonitrile mixed matrix forward osmosis membranes based on layer-by-layer assembly. *Sep. Purif. Technol.,* 124:207-216

[145] Wang, Y., Ou, R., Ge, Q., Wang, H., Xu, T. (2013) Preparation of polyethersulfone/carbon nanotube substrate for high-performance forward osmosis membrane. *Desalination*, 330:70-78

[146] Amini, M., Jahanshahi, M., Rahimpour, A. (2013) Synthesis of novel thin film nanocomposite (TFN) forward osmosis membranes using functionalized multi-walled carbon nanotubes. *J. Membr. Sci.,* 435:233-241

[147] Emadzadeh, D., Lau, W.J., Matsuura, T., Rahbari-Sisakht, M., Ismail, A.F. (2014) A novel thin film composite forward osmosis membrane prepared from PSf-TiO2 nanocomposite substrate for water desalination. *Chem. Eng. J.,* 237:70-80

[148] Ma, N., Wei, J., Qi, S., Zhao, Y., Gao, Y., Tang, C.Y. (2013) Nanocomposite substrates for controlling internal concentration polarization in forward osmosis membranes. *J. Membr. Sci.,* 441:54-62

[149] Emadzadeh, D., Lau, W.J., Ismail, A.F. (2013) Synthesis of thin film nanocomposite forward osmosis membrane with enhancement in water flux without sacrificing salt rejection. *Desalination,* 330:90-99

[150] Emadzadeh, D., Lau, W.J., Matsuura, T., Ismail, A.F., Rahbari-Sisakht, M. (2014) Synthesis and characterization of thin film nanocomposite forward osmosis membrane with hydrophilic nanocomposite support to reduce internal concentration polarization. *J. Membr. Sci.,* 449:74-85

[151] Yu, B., Leung, K.M., Guo, Q., Lau, W.M., Yang, J. (2011) Synthesis of Ag-TiO2 composite nano thin film for antimicrobial application. *Nanotechnology,* 22:115603

[152] Pardeshi, P., Mungray, A.A. (2014) ,Synthesis, characterization and application of novel high flux FO membrane by layer-by-layer self-assembled polyelectrolyte. *J. Membr. Sci.,* 453:202-211

[153] Baghbanzadeh, M., Rana, D., Matsuura, T., Lan, C.Q. (2015) Effects of hydrophilic CuO nanoparticles on properties and performance of PVDF VMD membranes, *Desalination,* 369:75-84

[154] Gethard, K., Sae-Khow, O., Mitra, S. (2011) Water Desalination Using Carbon-Nanotube-Enhanced Membrane Distillation. *Acs Appl. Mater. Interfaces,* 3:110-114

[155] Wang, L., Han, X., Li, J., Zhan, X., Chen, J. (2011) Hydrophobic nano-silica/polydimethylsiloxane membrane for dimethylcarbonate-methanol separation via pervaporation. *Chem. Eng. J.,* 171:1035-1044

[156] Peng, F., Pan, F., Sun, H., Lu, L., Jiang, Z. (2007) Novel nanocomposite pervaporation membranes composed of poly(vinyl alcohol) and chitosan-wrapped carbon nanotube. *J. Membr. Sci.,* 300:13-19

[157] Liu, G., Wei, W., Jin, W. (2014) Pervaporation Membranes for Biobutanol Production. *Acs Sustainable Chem. Eng.,* 2:546-560

[158] Fauzi, N.F.I., Hasran, U.A., Kamarudin, S.K. (2013) Review on utilization of the pervaporation membrane for passive vapor feed direct methanol fuel cell. *2nd International Conference on Mechanical Engineering Research (Icmer 2013), Kuantan, Pahang, Malaysia, 1-3 July 2013,* 50:012056

[159] Dumee, L., Sears, K., Schuetz, J., Finn, N., Duke, M., Gray, S. (2010) Carbon nanotube based composite membranes for water desalination by membrane distillation. *Desalin, Water Treat.,* 17:72-79

[160] Dumee, L.F., Sears, K., Schuetz, J., Finn, N., Huynh, C., Hawkins, S., Duke, M., Gray, S. (2010) Characterization and evaluation of carbon nanotube Bucky-Paper membranes for direct contact membrane distillation. *J. Membr. Sci.,* 351:36-43

[161] Dumee, L., Germain, V., Sears, K., Schuetz, J., Finn, N., Duke, M., Cerneaux, S., Cornu, D., Gray, S. (2011) Enhanced durability and hydrophobicity of carbon nanotube bucky paper membranes in membrane distillation. *J. Membr. Sci.,* 376:241-246

[162] Dumee, L., Campbell, J.L., Sears, K., Schuetz, J., Finn, N., Duke, M., Gray, S. (2011) The impact of hydrophobic coating on the performance of carbon nanotube bucky-paper membranes in membrane distillation. *Desalination,* 283:64-67

[163] Koo, J., Han, J., Lee, S., Sohn, J., Choi, J. (2012) Development of Nano-carbon Bucky-Paper Membranes for Membrane Distillation. *Mater. Sci. Forum.,* 724:408-411

[164] Dumée, L., Lee, J., Sears, K., Tardy, B., Duke, M., Gray, S. (2013) Fabrication of thin film composite poly(amide)-carbon-nanotube supported membranes for enhanced performance in osmotically driven desalination systems. *J. Membr. Sci.,* 427:422-430

[165] Razmjou, A., Arifin, E., Dong, G., Mansouri, J., Chen, V. (2012) Superhydrophobic modification of TiO2 nanocomposite PVDF membranes for applications in membrane distillation. *J. Membr. Sci.,* 415:850-863

[166] Bhadra, M., Roy, S., Mitra, S. (2013) Enhanced desalination using carboxylated carbon nanotube immobilized membranes. *Sep. Purif. Technol.,* 120:373-377

[167] Peng, F., Pan, F., Sun, H., Lu, L., Jiang, Z. (2007) Novel nanocomposite pervaporation membranes composed of poly(vinyl alcohol) and chitosan-wrapped carbon nanotube. *J. Membr. Sci.,* 300:13-19

[168] Tan, S., Inai, R., Kotaki, M., Ramakrishna, S. (2005) Systematic parameter study for ultra-fine fiber fabrication via electrospinning process. *Polymer,* 46:6128-6134

[169] Huang, Z., Zhang, Y.-., Kotaki, M., Ramakrishna, S. (2003) A review on polymer nanofibers by electrospinning and their applications in nanocomposites. *Composites Sci. Technol.,* 63:2223-2253

[170] Choi, S., Lee, Y., Joo, C., Lee, S., Park, J., Han, K. (2004) Electrospun PVDF nanofiber web as polymer electrolyte or separator. *Electrochim. Acta,* 50:339-343

[171] Kim, Y., Ahn, C.H., Choi, M.O. (2010) Effect of thermal treatment on the characteristics of electrospun PVDF-silica composite nanofibrous membrane. *Eur. Polym. J.,* 46:1957-1965

[172] Ma, Z., Hong, Y., Ma, L., Su, M. (2009) Superhydrophobic Membranes with Ordered Arrays of Nanospiked Microchannels for Water Desalination. *Langmuir,* 25:5446-5450

[173] Zhang, H., Lamb, R., Lewis, J. (2005) Engineering nanoscale roughness on hydrophobic surface - preliminary assessment of fouling behaviour. *Sci. Technol. Adv. Mat.,* 6:236-239

[174] Privett, B.J., Youn, J., Hong, S.A., Lee, J., Han, J., Shin, J.H., Schoenfisch, M.H. (2011) Antibacterial Fluorinated Silica Colloid Superhydrophobic Surfaces. *Langmuir,* 27:9597-9601

[175] Mauter, M.S., Elimelech, M. (2008) Environmental applications of carbon-based nanomaterials. *Environ. Sci. Technol.,* 42:5843-5859

[176] Corry, B. (2011) ,Water and ion transport through functionalised carbon nanotubes: implications for desalination technology. *Energ. Environ. Sci.,* 4:751-759

Chapter 5:

Effects of hydrophilic CuO nanoparticles on properties and performance of PVDF VMD membranes

M. Baghbanzadeh, D. Rana, T. Matsuura, C. Q. Lan, Effects of hydrophilic CuO nanoparticles on properties and performance of PVDF VMD membranes, Desalination, 369 (2015) 75-84

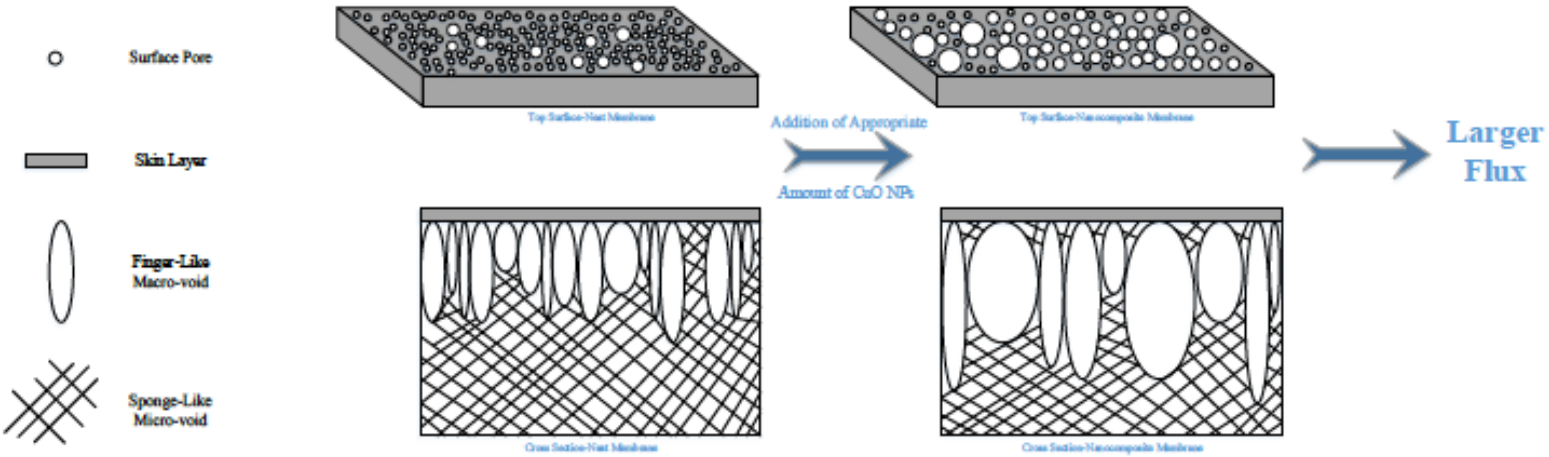
Surface Pore
Skin Layer
Finger-Like
Macro-void
Sponge-Like
Micro-void
Addition of Appropriate
Amount of CuO NPs
Larger
Flux

Effects of hydrophilic CuO nanoparticles on properties and performance of PVDF VMD membranes

Mohammadali Baghbanzadeh, Dipak Rana, Takeshi Matsuura, Christopher Q. Lan*

Department of Chemical and Biological Engineering, University of Ottawa, 161 Louis Pasteur Private, Ottawa, Ontario, Canada K1N 6N5

Abstract

In this study, composite membranes of hydrophilic CuO and $CaCO_3$ nanoparticles and polyvinylidene fluoride (PVDF) were developed by phase inversion method. The fabricated membranes were subjected to different characterizations including morphology study, pore size, porosity, and thickness measurement, wettability and surface roughness analysis. The membrane performance was examined in terms of pure water flux in vacuum membrane distillation (VMD), salt rejection, and liquid entry pressure of water (LEP_w). It was found that the membrane performance was optimized when 1.0 to 2.0 wt.% of CuO nanoparticles were embedded into the PVDF matrix via enhancing the membrane structure through enlarging surface pores and thickening the finger-like layer (in other words, thinning of the sponge-like layer). As a result, flux increased by 153.4% at the feed temperature of 27.5 °C and vacuum pressure of 1.2 kPa, when 2.0 wt.% of the CuO nanoparticles were embedded in PVDF. Membrane selectivity did not drop as a result of the CuO nanoparticles incorporation and was more than 99.99%. All the nanocomposite membranes showed reasonable contact angle and LEP_w, which proved appropriateness of the fabricated membranes for VMD application. Regarding the type of hydrophilic nanomaterials, CuO demonstrated better performance than $CaCO_3$ in terms of membrane permeability improvement.

Keywords: Hydrophilic CuO nanoparticles; Mixed matrix membrane; Membrane properties; Pure water flux; Vacuum membrane distillation;

*Corresponding author. Tel.: þ1 613 562 5800x2050.
E-mail address:Christopher.Lan@uottawa.ca (C.Q. Lan).

5-1- Introduction

The increase in water demand for domestic, agricultural and industrial uses and a remarkable reduction in desalination costs due to the technological improvements resulted in much attention toward saline water desalination technologies during the last few decades. Generally, desalination technologies could be divided into three different categories including: 1) Thermal processes such as Multi-stage Flash Distillation (MSF), Multiple Effect Distillation (MED), and Mechanical Vapor Compression (VC), 2) Membrane processes including Reverse Osmosis (RO), Forward Osmosis (FO), Ultrafiltration (UF), Microfiltration (MF), Nanofiltration (NF), and Membrane Distillation (MD), and 3) Hybrid processes combining different individual processes to enhance the total efficiency and to mitigate environmental liabilities.

It has been reported that around 63.7% of the produced pure water from desalination technologies is generated through membrane-based technologies while the remaining is achieved by thermal processes [1]. RO is now considered as the world's leading process for desalination [1,2], due to its relatively low specific energy consumption which would result in a lower pure water production cost.

MD is considered as an emerging technology which is claimed to become competitive with RO soon [2]. Table 5-1 presents a comparison between the RO and MD technologies in terms of process characteristics. It seems to be evident that MD has potential to compete in the desalination market provided that a high performance membrane is fabricated and the entire MD process is appropriately designed to minimize the thermal energy consumption.

Table 5-1 The different features of reverse osmosis and membrane distillation in a desalination process

Desalination Process	RO	MD
Fouling & Scaling Potential	High	Low
Feed Pre-treatment	Necessary	Could be ignored
Handling the High Concentration Feed	Sometimes fails	Able
Recovery Ratio	Limited (Increase in osmotic pressure with concentration)	Depends on feed temperature and complexity of the process
Brine Disposal	Depends on the recovery ratio	Depends on the recovery ratio
Electrical Energy Consumption	High	Negligible
Thermal Energy Consumption	Negligible	High
Operating Conditions	Harsh	Mild

Nanocomposite membranes demonstrated to have great potential in improving the membrane performance in terms of flux, rejection, antifouling characteristics, thermal, mechanical, and chemical stability in membrane water treatment including ultrafiltration [3-5], microfiltration [6-8], nanofiltration [9-11], reverse osmosis [12-14], and forward osmosis [15-17]. To this end, different nanomaterials such as SiO_2, carbon nanotubes (CNTs), TiO_2, Al_2O_3, $CaCO_3$, Ag, and nanozeolites have been used [5,16,18-23]. Nonetheless, very little information is available on the effects of different nanoparticles on the properties and performance of MD membranes even though some of the pioneering works have shown great potential of nanocomposite membranes for MD [23-25]. For instance, Gethard et al. [24] used carbon nanotubes in a polypropylene (PP) hollow fiber membrane and applied the prepared membranes in a Sweep Gas Membrane Distillation (SGMD) process and obtained almost 83.3% increase in the flux when a solution of

NaCl and $MgSO_4$ was used at 80 ºC as the feed. Hou et al. [23] [25] used hydrophobic modified $CaCO_3$ as the nano-additive to prepare a nanocomposite membrane of PVDF and $CaCO_3$ and employed those membranes in a Direct Contact Membrane Distillation (DCMD) configuration. According to their results and for a NaCl solution of 35 g/L, around 14.9% increase in the flux was observed when hollow fiber membranes were used at a feed temperature of 80.5 ºC [23], while almost 30.8% increase in the flux was obtained for the flat sheet membranes at 83 ºC [25].

To improve the performance of MD membranes via the incorporation of nanomaterials, appropriate selection of nanoparticles seems to be a key factor. Typically, nanoparticles can be divided into two different categories, hydrophobic and hydrophilic nanoparticles. It is usually assumed that the incorporation of hydrophobic particles into the membrane matrix results in a more hydrophobic membrane surface while the effect will be reversed by the incorporation of the hydrophilic ones. On the other hand, it has been demonstrated that hydrophilic nanoparticles are able to change the solvent/non-solvent exchange rate in the phase inversion process, which may result in a membrane of improved morphology. [10,11,26-28].

In this work, an attempt is made for the first time to develop mixed-matrix membranes by incorporating a hydrophilic nanoparticle, i.e., CuO nanoparticle, with polyvinylidene fluoride (PVDF). In a previous study, we have demonstrated that the PVDF membranes are appropriate for MD [29] even though PVDF's contact angle is less than 90^o and it is commonly accepted view that MD requires a contact angle of 90^o [30]. In this study, we further demonstrated that incorporating hydrophilic CuO nanoparticles with PVDF could result in membrane of sufficient liquid entry pressure of water (LEP_w) for Vacuum Membrane Distillation (VMD) with improved flux and satisfactory rejection.

Among the MD configurations which have been universally accepted, such as Direct Contact Membrane Distillation (DCMD), Air Gap Membrane Distillation (AGMD), Sweep Gas Membrane Distillation (SGMD), and Vacuum Membrane Distillation (VMD), the last one is selected in this study, since VMD is able to generate the highest achievable driving force for a given feed temperature. Moreover, VMD seems to be more economical from the view point of

energy consumption for a given driving force. As an illustrative example, according to Cabassud et al. [30], 1.3 kWh/m^3 of electrical energy is required to generate a vacuum pressure of 100 Pa at the permeate side. If water at an ambient temperature of 25 ºC, which has a saturation pressure of 3.166 kPa, is used as the feed for VMD at a vacuum pressure of 100 Pa, the driving force would be 3.066 kPa. However, according to Al-Obaidani et al. [31], for every 1 ºC temperature increase in feed temperature, around 1.82 kWh/m^3 thermal energy is required. Therefore, to obtain the same driving force in a DCMD configuration using the same water at ambient temperature of 25 ºC as both the coolant and the source of feed water, the feed needs to be heated up to 36.9 ºC (saturation pressure 6.232 kPa), which means around 21.7 kWh/m^3 thermal energy needs to be consumed. In other words, the thermal energy required to obtain the same driving force is almost 1600.0% that of the electrical energy required for each cubic meter of the permeate product in a VMD process in this particular case.

5-2- Experimental Methods

5-2-1- Materials

Polyvinylidene fluoride (PVDF) of different molecular weights, Kynar® 740, (Pellet, melt viscosity: 1850 ± 250 Pa.s; melting temperature: 160.1 ºC) and Kynar® HSV900 (Powder, melt viscosity: 4930 Pa.s; melting temperature: 165.1 ºC) were supplied as the host polymer by Arkema Inc. (Philadelphia, PA). To measure the melt viscosity, ASTM D3835 at 232 ºC was employed. Anhydrous N, N-dimethylacetamide (DMAc) as the solvent was purchased from Sigma–Aldrich with the purity of 99.9%. Hydrophilic spherical CuO and $CaCO_3$ nanoparticles were purchased from Skyspring Nanomaterials Inc. CuO nanoparticles had a purity of 99+% with the size of 40 nm, and $CaCO_3$ nanomaterials 97.5% and 15-40 nm. NaCl and n-butanol were supplied by Fisher Scientific and used as received.

5-2-2- Membrane Fabrication

To fabricate the membranes, phase inversion method was employed, and the casting solution and suspensions were prepared as follows:

5-2-2-1- Preparation of Casting Solution

To prepare the dope solution for the preparation of neat PVDF membrane, 1.25 wt.% water, 15 wt.% PVDF (HSV900:740 = 2:3 [29]), and 83.75 wt.% DMAc were mixed under vigorous stirring (180 rpm) for 72 h at 50 ºC. After the solution became homogeneous, it was left for 24 h at the room temperature to be degassed.

5-2-2-2- Preparation of Casting Suspension Containing Nanomaterials

To prepare the casting suspensions for the preparation of nanocomposite membranes, the required amounts of CuO (0.0 to 4.0 wt.% of the casting suspension based on Table 5-2) or $CaCO_3$ (1.0 and 2.0 wt.% of the casting suspension based on Table 5-2) nanoparticles were added into the dope solution and the resulted suspension was stirred by an overhead stirrer for 2 h until a uniform suspension was obtained.

Table 5-2 Composition of the dope solution along with the nanoparticles concentration within the membrane matrix

Membrane	**Dope solution concentration (wt.%)**			**Nanoparticles concentration in the dope suspension* (wt.%)**	
	PVDF	*DMAc*	*Water*	*CuO*	*$CaCO_3$*
M0.0	15	83.75	1.25	0.0	0.0
M0.5	15	83.75	1.25	0.5	-
M1.0	15	83.75	1.25	1.0	-
M2.0	15	83.75	1.25	2.0	-
M3.0	15	83.75	1.25	3.0	-
M4.0	15	83.75	1.25	4.0	-
Ṁ1.0	15	83.75	1.25	-	1.0
Ṁ2.0	15	83.75	1.25	-	2.0

* Dope suspension contains PVDF, DMAC, water, and the nanoparticles and the particles concentration is stated relative to the suspension

5-2-2-3- Membrane Preparation

The casting dope or the casting suspension was cast on a glass using a casting bar to make a thickness of 250 μm. After waiting for 15-30 s, the cast film together with the glass plate was immersed into a coagulation bath (distilled water at 25 ºC). The film was solidified and peeled off the glass plate spontaneously. The membrane was kept in the bath for 24 h while the liquid was replaced by distilled water until the solvent was completely removed from the system. Afterwards, the membrane was dried under room temperature.

5-2-3- Membrane Characterization

For better understanding of the effects of hydrophilic CuO and $CaCO_3$ nanoparticles on the membrane performance, membranes were characterized in terms of surface and cross-sectional structure, pore size, porosity, thickness, wettability (contact angle), and roughness.

5-2-3-1- Morphology

Both the top surface and the cross-section of the membrane were observed by Scanning Electron Microscope (SEM, Vega-II XMU VPSEM and Anatech Hummer VII). To observe the cross-section, the membrane was broken after its immersion in liquid nitrogen for a few seconds to obtain a clean cut cross-section. The membrane surfaces were gold or palladium sputtered before SEM observation.

5-2-3-2- Nanomaterials Distribution within the Membrane Layers

Electron dispersion spectroscopy (EDX) was applied to know the nanoparticle distribution to the depth direction of the membrane. EDX analysis was made by an instrument (EDX, Oxford Inca Energy 250X EDX).

5-2-3-3- Pore Size

The pore size of the top surface of the membranes was measured by SEM image analysis using the ImageJ software [32-36]. The surface pores were assumed to be perfectly circular. At least 60 pores were randomly selected from each membrane sample and average pore size was reported together with the standard deviation.

5-2-3-4- Porosity

Membrane porosity was determined according to the wet and dry method [32]. The membrane was first immersed for 12 h in n-butanol, with a much lower surface tension than water to ensure that the film was completely wetted before the membrane was weighed (w_1). Then, membrane was dried in an oven for 24 h at 50 ºC to make sure that the liquid has been thoroughly

evaporated before the membrane was weighed (w_2). The membrane porosity (ε) was obtained based upon equation 5-1.

$$\%\varepsilon = \frac{w_1\text{-}w_2}{A.\delta.\rho} \times 100 \quad (5\text{-}1)$$

Where A, δ, and ρ are membrane surface area (cm^2), thickness (cm), and n-butanol density (g/cm^3), respectively. To minimize the error, the average value of 3 separate measurements is reported as the membrane porosity.

5-2-3-5- Thickness

The membrane thickness was measured by a digital micrometer. Measurement was made at three different spots and the average is reported.

5-2-3-6- Wettability

The surface contact angle was measured by the VCA Optima Surface Analysis System (AST Products, Inc. Billerica, MA), a sessile drop and digitalized machine which has a camera, placing 2 µL of water droplet onto the membrane surface. The machine is able to capture static and dynamic pictures of the droplet, and calculates the surface contact angle via determining the tangent lines. Ten different locations were randomly chosen at the membrane surface, and the average value is recorded.

5-2-3-7- Roughness

The SEM surface image was subjected to ImageJ analysis to measure the surface roughness. The software has been already successfully used by the other researchers [29,32,35]. The program used in this work is called *SurfCharJ* [37] and the input to the software is a 32 bit SEM image. To convert a two dimensional picture into a three dimensional one, pixel values stand for distance z to the surface. The software assigns different pixel values to every single spot over the surface in the range of 0-255 in such a way that darker area with lower gray scale represents deeper void space and lighter area with higher gray scale corresponds to smooth polymer

medium. Based upon the difference between the pixel values of each spot, surface roughness will be analyzed.

5-2-4- Membrane Performance

Membrane performance is reported in terms of permeability in vacuum membrane distillation (VMD), rejection, and liquid entry pressure using the equipment shown schematically in Figs. 5-1 and 5-2.

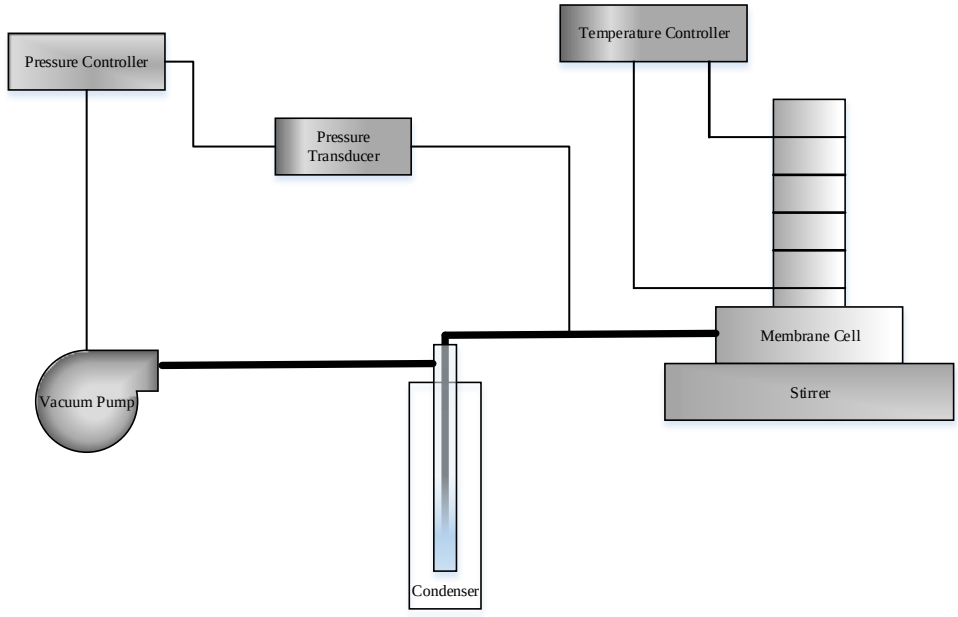

Fig. 5-1 Experimental VMD setup for measuring the permeate flux

According to Fig. 5-1, the experimental setup consists of a batch VMD cell with a feed chamber of 300 mL, equipped with a magnetic stirrer, a temperature controller to adjust the feed temperature to 27.5 ^{o}C, 40 ^{o}C, and 60 ^{o}C, a vacuum pump to control the pressure at 1.2 kPa abs on the permeate side, and a condenser cooled with liquid nitrogen to ensure that all permeate vapour is condensed in the cold trap.

5-2-4-1- Permeability

To measure the permeate flux, pure water was employed as the feed. The permeate flux was calculated by the following equation:

$$J = \frac{w}{A.t} \tag{5-2}$$

Where, *J* is flux in g/m^2.h, and *w*, *A*, and *t* are weight of the permeate collected (g), filtration area (m^2), and filtration time (h) respectively. Filtration area was 0.001134 m^2. For each membrane sample, flux was measured at least 3 times, and the average value is reported.

5-2-4-2- Rejection

To evaluate the membrane rejection characteristics, a solution of sodium chloride (35 g/L) was used as the feed in the VMD experimental setup and the salt concentration of the permeate was measured by a conductivity meter (OAKTON, CON 2700) to find the membrane selectivity via equation 5-3.

$$\%R = \frac{c_f - c_p}{c_f} \times 100 \tag{5-3}$$

Where R is rejection (%), and c_f and c_p are salt concentration at the feed and permeate sides, respectively.

5-2-4-3- Water Liquid Entry Pressure (LEP_w)

The LEP_w of the membrane was determined by the setup illustrated in Fig. 5-2. The membrane sample was mounted in the cell which was filled with water. The nitrogen gas pressure with the initial value of 1.0 barg was increased gradually at an interval of (2.0 psig) 0.14 barg and the pressure was kept constant at each pressure for 10 min. The pressure at which the first water droplet appears on the permeate side was recorded as LEP_w. Measurement was made three times for each membrane sample, and the average value is reported.

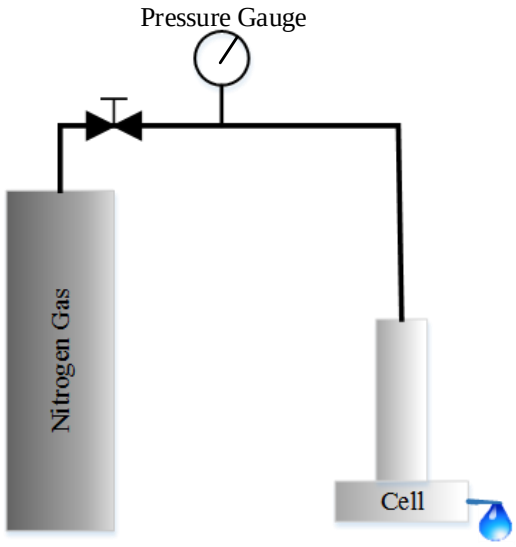

Fig. 5-2 Schematic of experimental setup for LEP_w tests

5-3- Results and Discussion

Figs. 5-3-a and 5-3-b show top and cross-sectional SEM images of PVDF/CuO nanocomposite membranes at different nanoparticle concentrations.

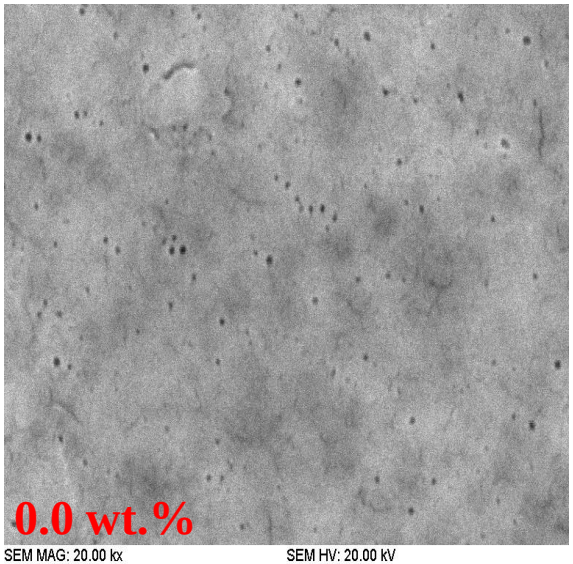
0.0 wt.%
SEM MAG: 20.00 kx
SEM HV: 20.00 kV
5 µm

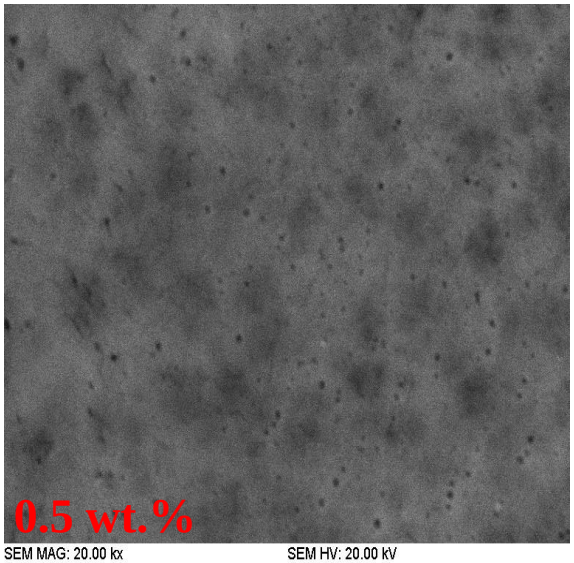
0.5 wt.%
SEM MAG: 20.00 kx
SEM HV: 20.00 kV
5 µm

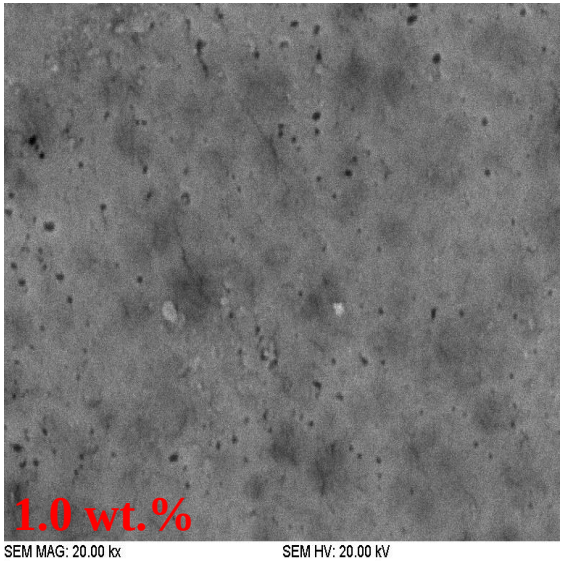
1.0 wt.%
SEM MAG: 20.00 kx
SEM HV: 20.00 kV
5 µm

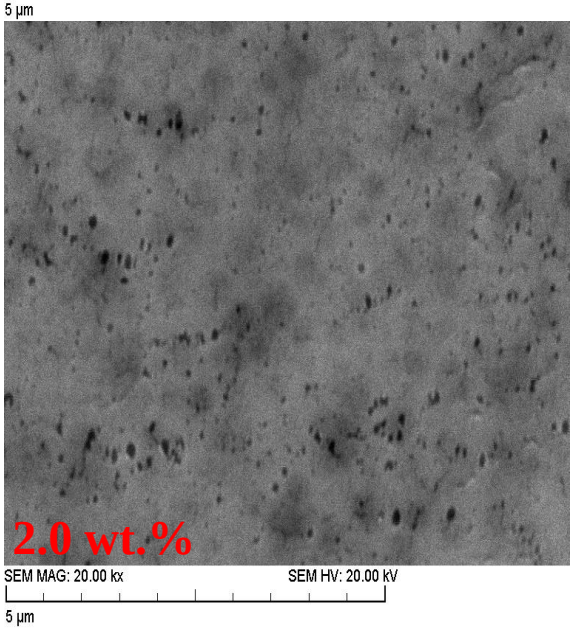
2.0 wt.%
SEM MAG: 20.00 kx
SEM HV: 20.00 kV
5 µm

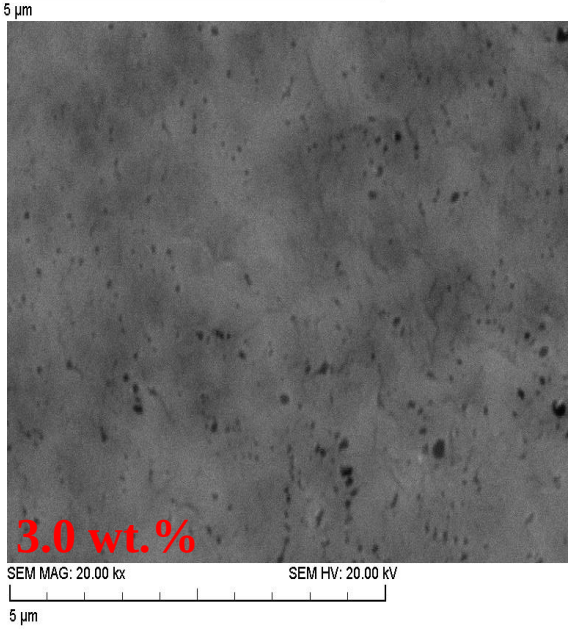
3.0 wt.%
SEM MAG: 20.00 kx
SEM HV: 20.00 kV
5 µm

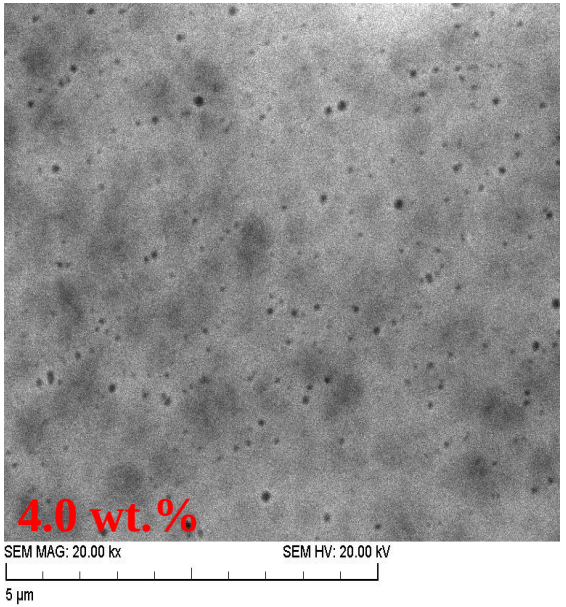
4.0 wt.%
SEM MAG: 20.00 kx
SEM HV: 20.00 kV
5 µm

Fig. 5-3-a Top surface SEM images of the CuO/PVDF membranes at different concentrations of the nanoparticles where the black spots represent the surface pores

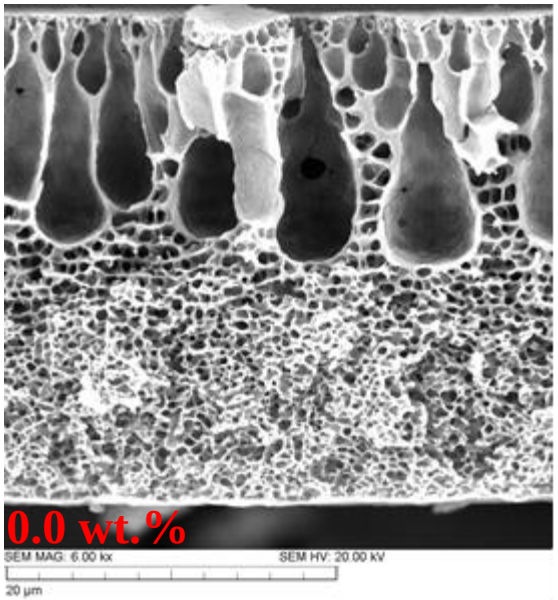
0.0 wt.%
SEM MAG: 6.00 kx
SEM HV: 20.00 kV
20 µm

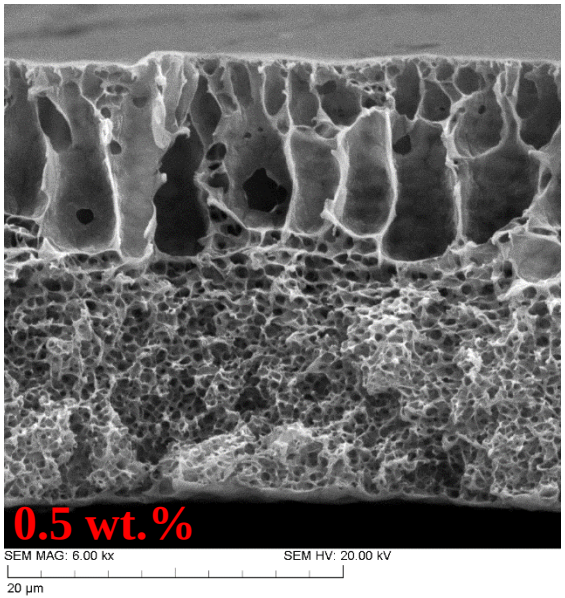
0.5 wt.%
SEM MAG: 6.00 kx
SEM HV: 20.00 kV
20 µm

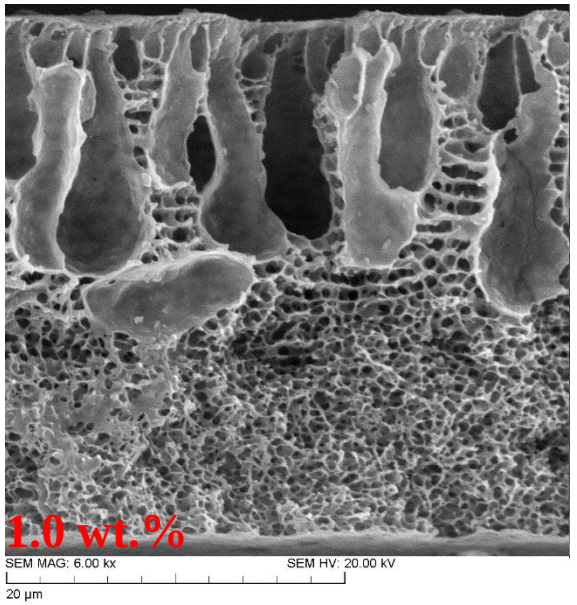
1.0 wt.%
SEM MAG: 6.00 kx
SEM HV: 20.00 kV
20 µm

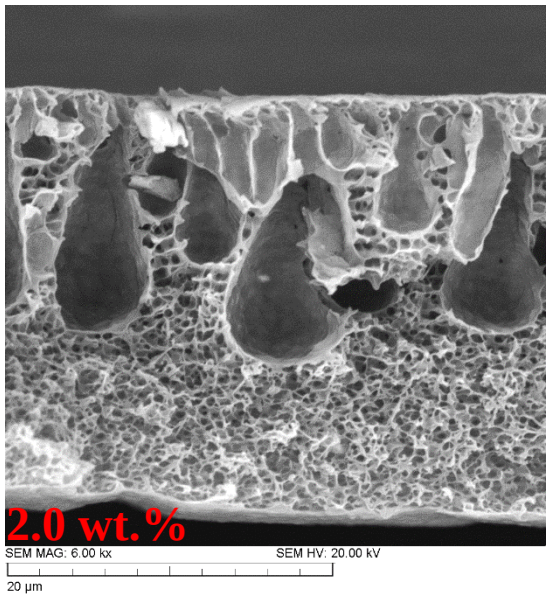
2.0 wt.%
SEM MAG: 6.00 kx
SEM HV: 20.00 kV
20 µm

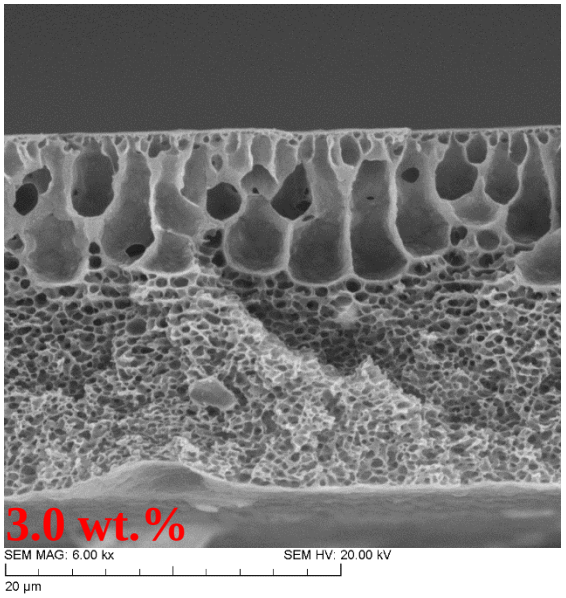
3.0 wt.%
SEM MAG: 6.00 kx
SEM HV: 20.00 kV
20 µm

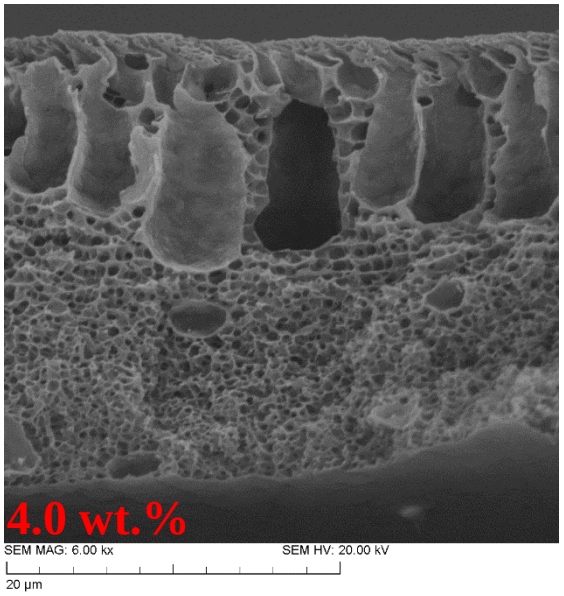
4.0 wt.%
SEM MAG: 6.00 kx
SEM HV: 20.00 kV
20 µm

Fig. 5-3-b Cross-sectional SEM images of the CuO/PVDF membranes at different concentrations of the nanoparticles

Figure 5-3-b shows typical asymmetric structures of the membrane with a thin top skin layer supported by a layer of finger-like macro-voids, which is followed by a thick layer of sponge-like structure. As for the effect of the nanoparticle concentration, it seems that the layer of finger-like voids goes deeper downward as the nanoparticle concentration increases from 0.0 to 2.0 wt.% and then moves upwards as the nanoparticle concentration further increases. This trend can be described more quantitatively as the ratio of the thickness of the finger-like layer to that of the entire membrane thickness is plotted versus the nanoparticle concentration as shown in Fig. 5-4. Clearly, there is a maximum of the ratio at the nanoparticle concentration of 1.0 wt.%.

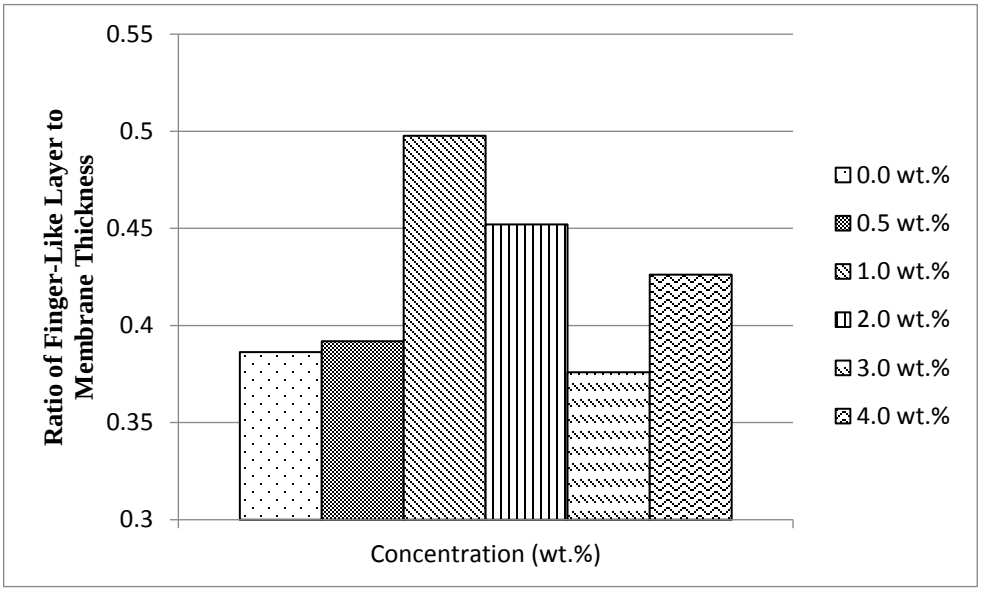

Fig. 5-4 Ratio of the thickness of the finger-like layer to the total membrane thickness vs. nanoparticle concentration

This trend is ascribed to the interplay of the factors governing the solvent/non-solvent exchange rate in the phase inversion process. When the amount of hydrophilic CuO nanoparticles in the casting is increased, the non-solvent water is drawn more deeply into the cast film, resulting in the increase of finger-like layer thickness. But when the nanoparticle concentration is further increased, the penetration of water into the cast film is suppressed due to increased viscosity of the cast nanoparticle/polymer suspension. Fig. 5-5 shows an almost linear increment in the

viscosity of the suspension as the nanoparticle concentration increases. The linear change of viscosity with the concentration is an evidence of appropriate stability of the suspensions [38].

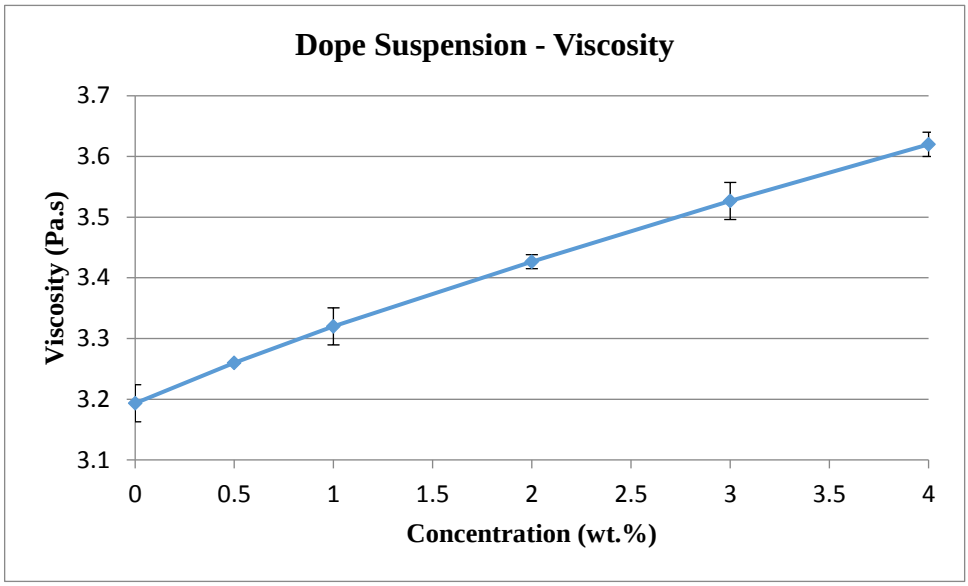

Fig. 5-5 Viscosity of the dope suspension vs. nanoparticle concentration

Another plausible interpretation is the presence of the nanoparticles in the polymer lean phase that is formed by phase separation. The size of the polymer lean phase grows faster as the hydrophilic nanoparticles are captured in it, resulting in larger pore sizes of the membrane. But the nanoparticles start to agglomerate at higher concentrations and a part of particles can no longer contribute to the growth of the polymer lean phase. As well, the particle agglomerates may block the macro-void spaces. Thus, the pore size starts to decrease.

The latter interpretation is corroborated by Fig. 5-6 where the surface pore size of the membrane is plotted versus nanoparticle concentration. The figure shows wide scattering of the measured pore sizes with long error bars. Yet, the average pore size seems to have a maximum of 110 nm at 2.0 wt.% of nanoparticles (M2.0).

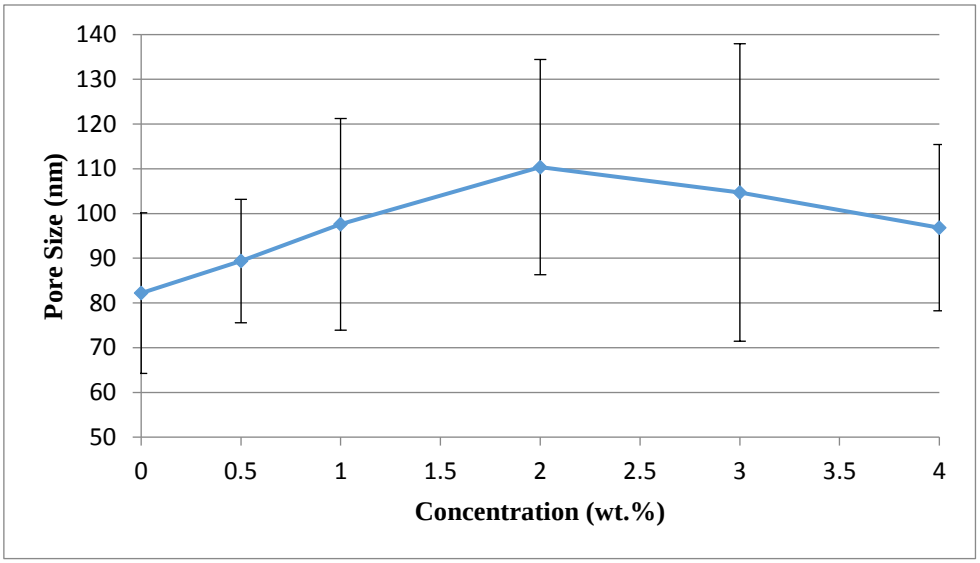

Fig. 5-6 Surface pore size vs. nanoparticle concentration

It is worth mentioning that the size of micro-voids in the sponge-like layer was also increased via the addition of the hydrophilic CuO nanoparticles. SEM images of sponge-like structure for the neat membrane and the one with 2.0 wt.% of CuO nanoparticles (M2.0) are given in Fig. 5-7. Micro-voids became larger by the addition of the nanoparticles and their average size was increased from 341 nm for the neat membrane to 426 nm for M2.0. It could be attributed to the hydrophilic nature of the nanoparticles when they have penetrated into the bottom layer. Since the particles tend to attract water, they would facilitate the non-solvent influx in the bottom layer during the fabrication process which would result in the larger micro-voids.

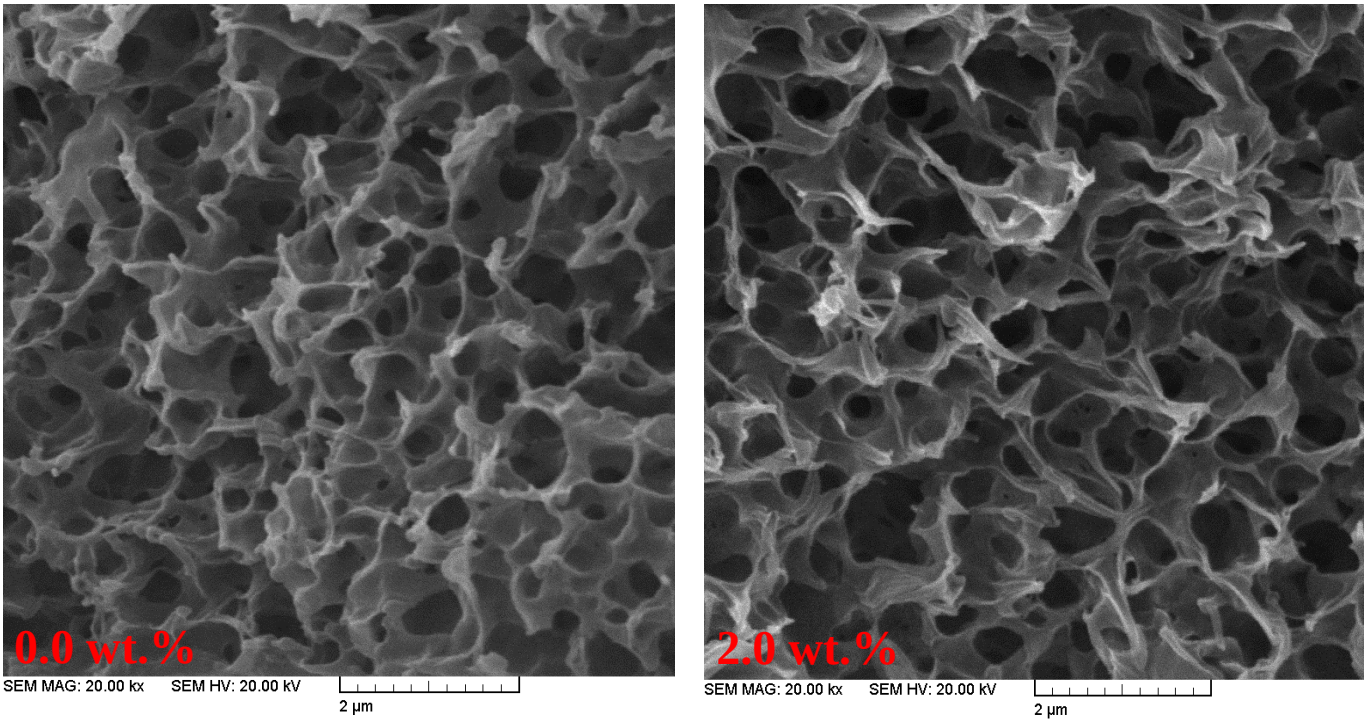

Fig. 5-7 Micro-voids in sponge-like layer For M0.0 and M2.0

Fig. 5-8 shows the membrane porosity versus concentration of nanoparticles.

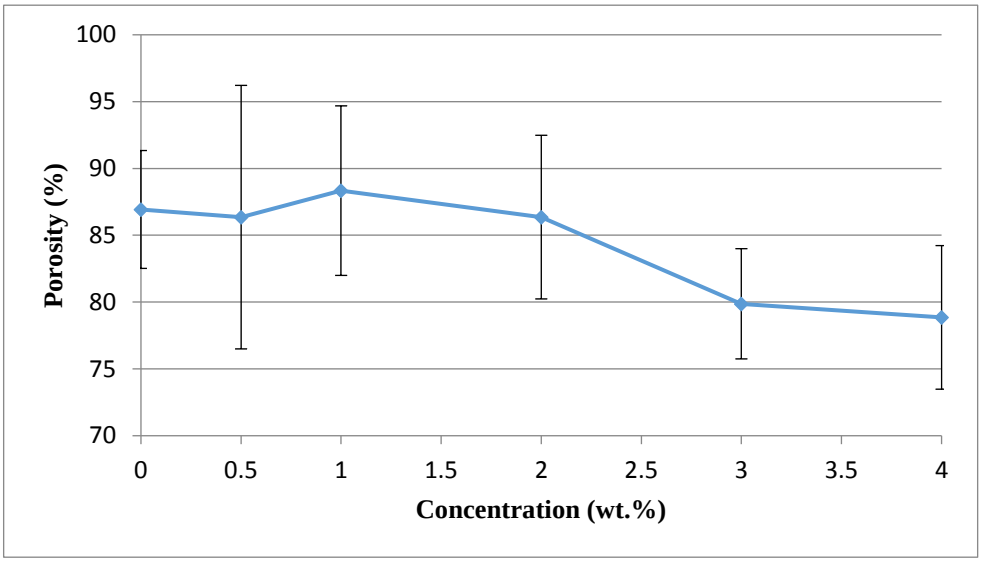

Fig. 5-8 Membrane porosity vs. concentration for the nanocomposite membranes of PVDF/CuO

Again a wide scattering in the measured porosity is observed with long error bars, which obscures the trend particularly in a concentration range below 1.0 wt.%. However, clear decreasing trend is observed in the range of concentration above 1.0 wt.%, which could be attributed to the agglomerated particles that occupy the membrane's void spaces.

The change in the membrane thickness with the nanoparticle concentration is given in Fig. 5-9.

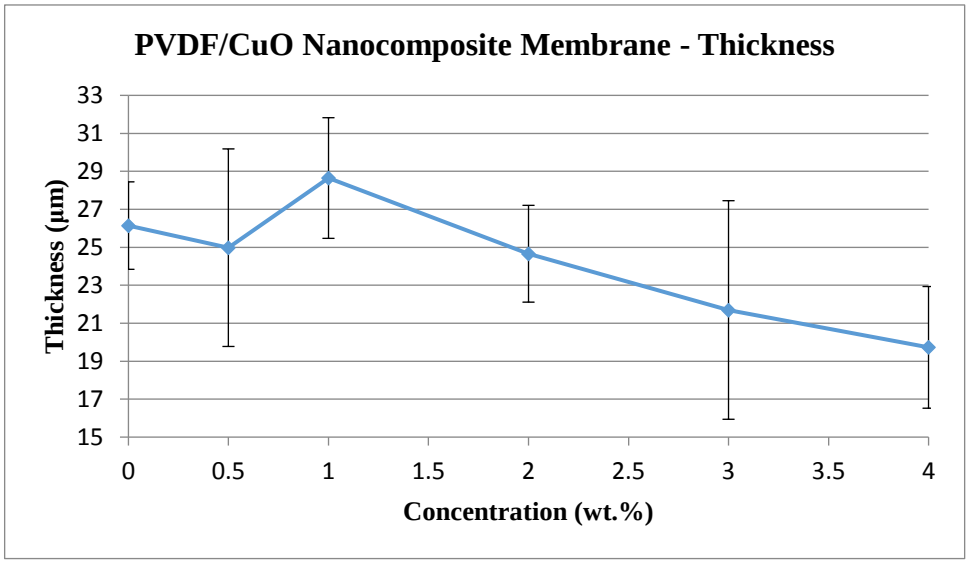

Fig. 5-9 Membrane thickness vs. nanoparticle concentration

The trend observed in Fig. 5-9 is similar to Fig. 5-8, i.e. the effect of nanoparticle concentration is insignificant in the concentration range lower than 1.0 wt.% due to the long error bars, followed by a clear decreasing trend of thickness beyond the concentration of 1.0 wt.%.

Fig. 5-10 gives EDX results that belong to the membrane with 2.0 wt.% of CuO nanoparticles (M2.0). From the figure, the particles are present on both surfaces, i.e. top and bottom, and also within the middle layers. In other words, hydrophilic CuO nanoparticles have been distributed throughout the membrane from top to bottom.

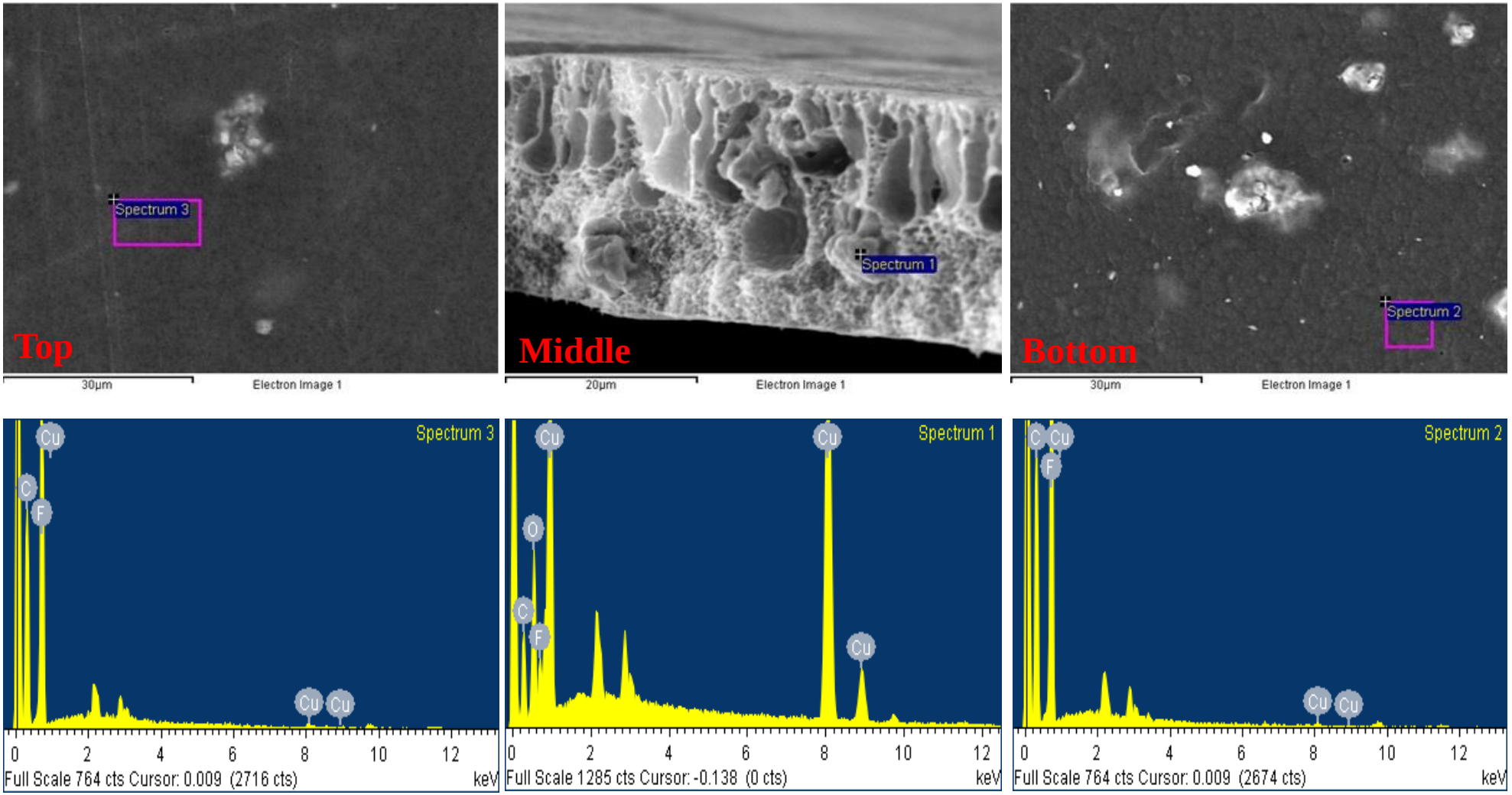

Fig. 5-10 EDX analysis of the different layers of M2.0

Table 5-3 gives the surface roughness of the fabricated membranes.

Table 5-3 Surface roughness analysis of the CuO NPs incorporated membranes by ImageJ according to the ISO 4287/2000 standard (all the units in pixel)

Concentration (wt.%)	Rq: Root mean square deviation	Ra: Arithmetical mean deviation	Rv: Lowest valley	Rp: Highest peak
0.0	11.7±0.2	9.3±0.1	-46.7±1.3	55.8±5.6
0.5	8.1±0.1	6.5±0.1	-31.7±0.7	36.4±0.8
1.0	9.7±0.2	7.7±0.1	-37.8±1.3	46.1±4.6
2.0	11.3±0.2	9.0±0.1	-43.3±0.9	52.5±3.1
3.0	15.9±0.5	12.6±0.4	-59.3±2.7	77.0±1.7
4.0	15.6±0.2	8.2±0.2	-38.6±1.0	48.9±2.4

From Table 5-3, upon introduction of the CuO nanoparticles into the membrane at 0.5 wt.%, the surface roughness decreased in comparison with that of the neat membrane. However, as the particle concentration was further increased, surface roughness increased and eventually leveled off.

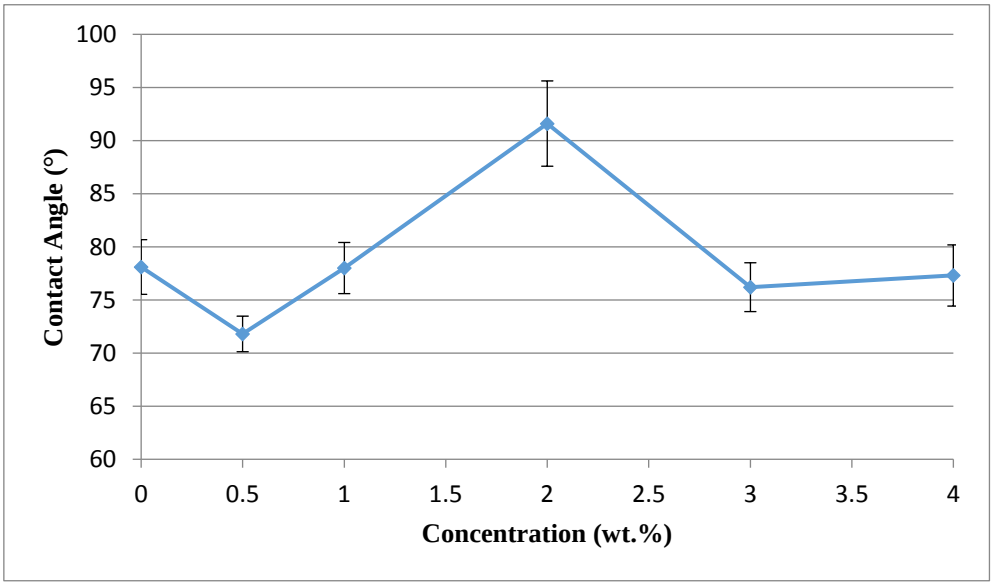

Fig. 5-11 Surface contact angle vs. concentration for the nanocomposite membranes of PVDF/CuO

Figure 5-11 shows the results of contact angle measurement. According to Fig. 5-11, contact angle decreases upon introduction of nanoparticles into the membrane but increases gradually until it reaches a maximum at 2.0 wt.% nanoparticle concentration and then decreases when the concentration is beyond 2.0 wt.%. These results can be interpreted by monitoring the surface

roughness data (Table 5-3). We hypothesize that, up to the concentration of 2.0 wt.% of the nanoparticles, most of the CuO particles migrated to the middle layers. Therefore, the surface was mostly covered by PVDF and the contact angle is governed not by surface chemistry but by surface roughness in a range of nanoparticle concentration from 0.0 to 2.0 wt.%. Indeed, the contact angle data paralleled the surface roughness data in the above range of nanoparticle concentration, i.e. lower the roughness parameter, the lower the contact angle and vice versa. However, nanoparticles appear to the membrane surface when the concentration is beyond 2.0 wt.% and start to increase the surface hydrophilicity due to their intrinsically hydrophilic nature, which reduces the contact angle. It should however be noted that the contact angles remained between 72º and 92º in the entire range of nanoparticle concentrations despite the addition of hydrophilic CuO nanoparticles and MD experiments were possible for all fabricated membranes.

Effects of the nanoparticle concentration on the membrane pure water flux is presented in Fig. 5-12, where flux shows a maximum at 2.0 wt.%.

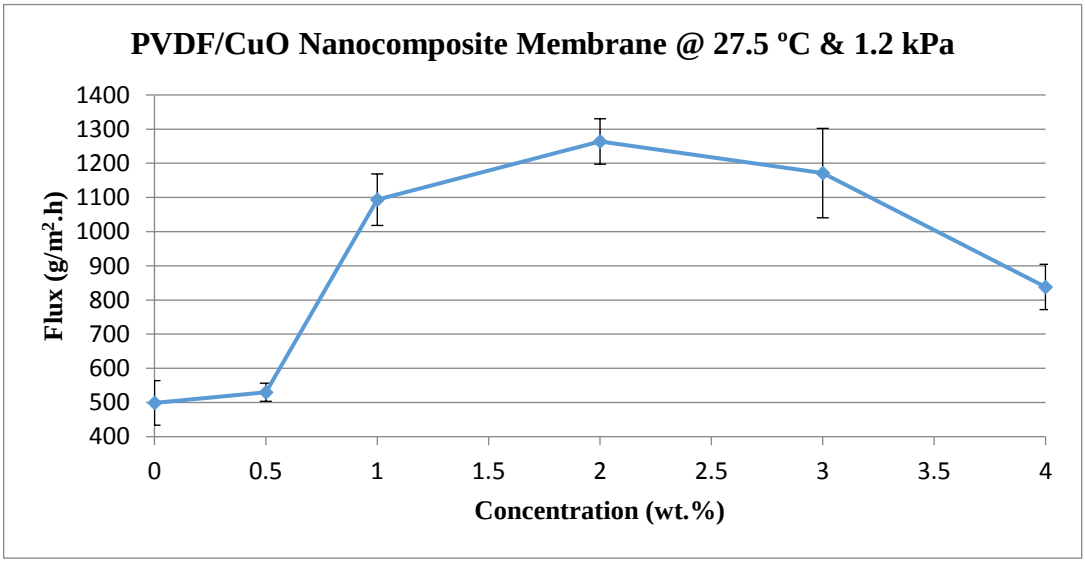

Fig. 5-12 Pure water flux vs. nanoparticle concentration

In Fig. 5-12, all the nanocomposite membranes demonstrated fluxes larger than the neat membrane and the maximum was 153.4% higher at the nanoparticle concentration of 2.0 wt.%. The trend observed in flux is consistent with the membranes characterization results, which are

shown in Figs. 5-4, 5-6 & 5-8. Based upon those results, the largest pore size (Fig. 5-6), the highest porosity (Fig. 5-8), the largest ratio of finger-like layer to the total membrane thickness (Fig. 5-4), all fall in the medium concentrations of either 1.0 or 2.0 wt.%, although M1.0 showed slightly higher porosity (Fig. 5-8) and the ratio of finger like layer thickness to the total membrane thickness (Fig. 5-4) than M2.0. M2.0 showed the higher flux due to the larger pore size (Fig. 5-6), which means that the role of the surface pore size is more important than the porosity and the finger-like structure both of which are considered as bulk property of the membrane.

Effects of the feed temperature on the pure water flux were then investigated for M0.0 and M2.0 and the results shown in Fig. 5-13.

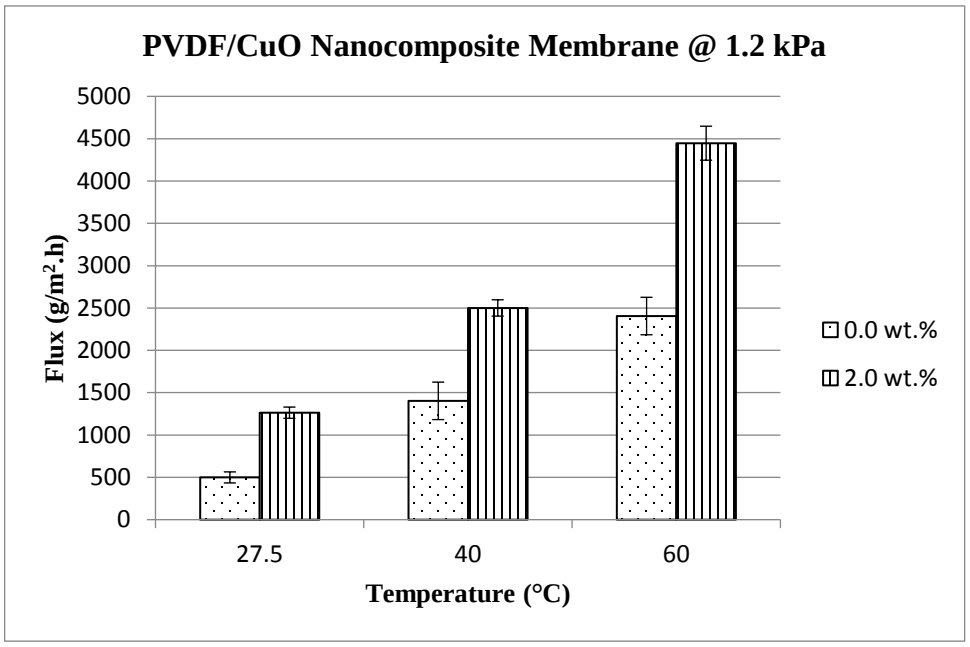

Fig. 5-13 Effect of feed temperature on the pure water flux of the M0.0 and M2.0

For both membranes flux increases with the feed temperature due to increased vapour pressure.

LEP_w is given as a function of nanoparticle concentration in Fig. 5-14. According to the Laplace equation there are two factors that govern LEP_w, i.e. pore size and the contact angle [38]. Looking into Fig. 5-6 (pore size) and Fig. 5-14 (LEP_w), Fig. 5-14 is the mirror image of Fig. 5-6,

indicating the Laplace equation is satisfied as far as the pore size is concerned. On the other hand, the Laplace equation becomes irrelevant since according to Fig. 5-11 contact angles are less than 90^{o} except for the data that corresponds to nanoparticle concentration of 2.0 wt.%. Thus, it is the pore size that governs the LEP_w.

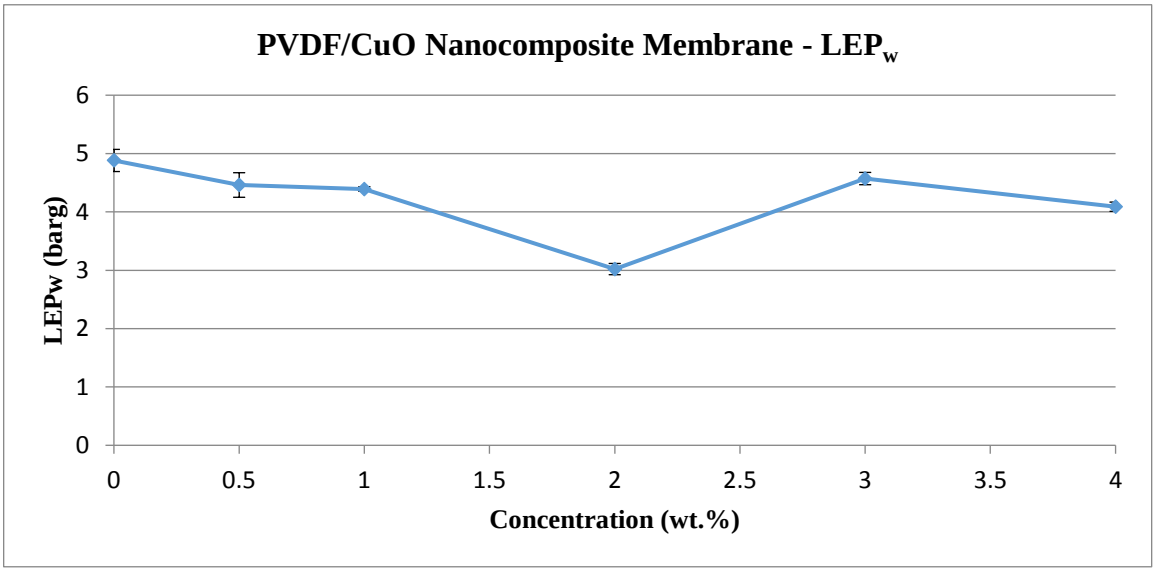

Fig. 5-14 LEP_w vs. nanoparticle concentration

It is noteworthy that the lowest LEP_w that belongs to M2.0 is 3.0 barg which is high enough for the membrane to be employed in VMD application.

It should be pointed out that the salt rejection test was performed with an aqueous solution of 35 g/L NaCl for both M0.0 and M2.0 and they showed a selectivity of more than 99.99%, which demonstrates the incorporation of the hydrophilic CuO nanoparticles brought about a higher flux without any reduction in the membrane selectivity.

To further investigate the effects of hydrophilic nanomaterials on the VMD membrane performance, 1.0 (Ṁ1.0) and 2.0 (Ṁ2.0) wt.% of $CaCO_3$ nanoparticles were added to the base PVDF polymer, and the resulted membranes were subjected to VMD test. Figs. 5-15-a to 5-15-c compare the effects of different hydrophilic nanoparticles on the membrane porosity, contact angle, and pure water flux at two different nanoparticle concentrations (1.0 and 2.0 wt.%). No

conclusion can be drawn about the porosity (Fig. 5-15-a) due to large scatter of the data. Contact angles are higher when CuO is added according to Fig. 5-15-b.

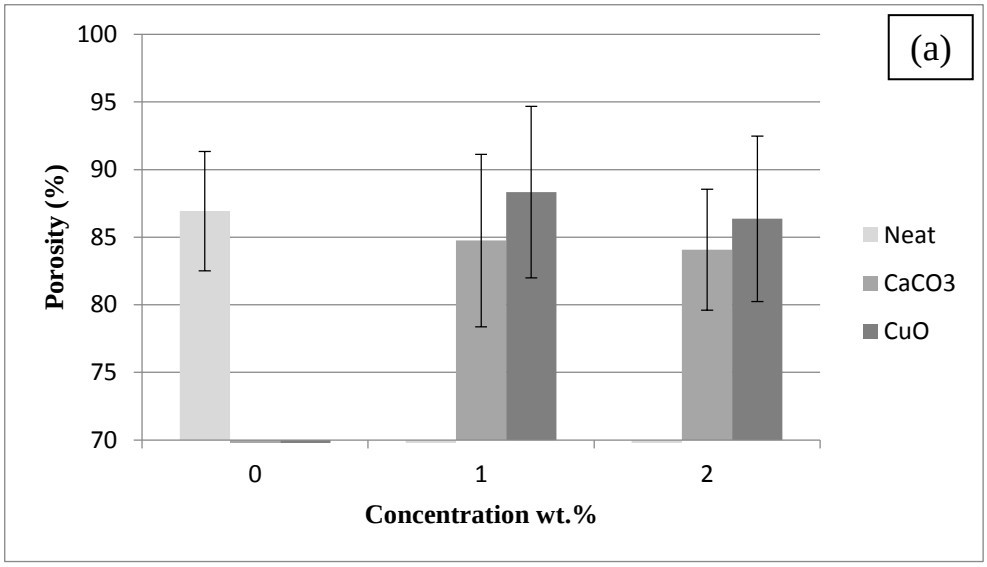

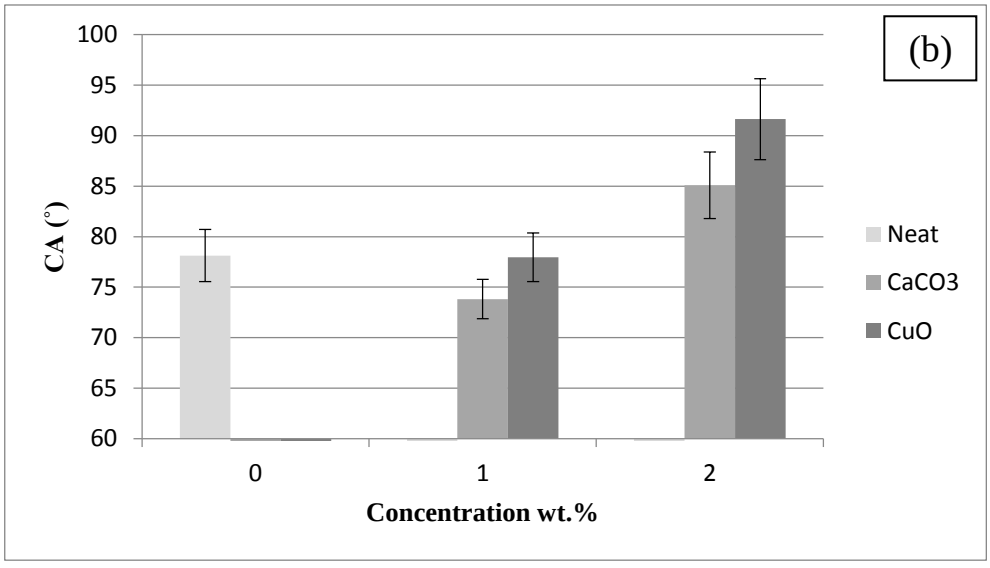

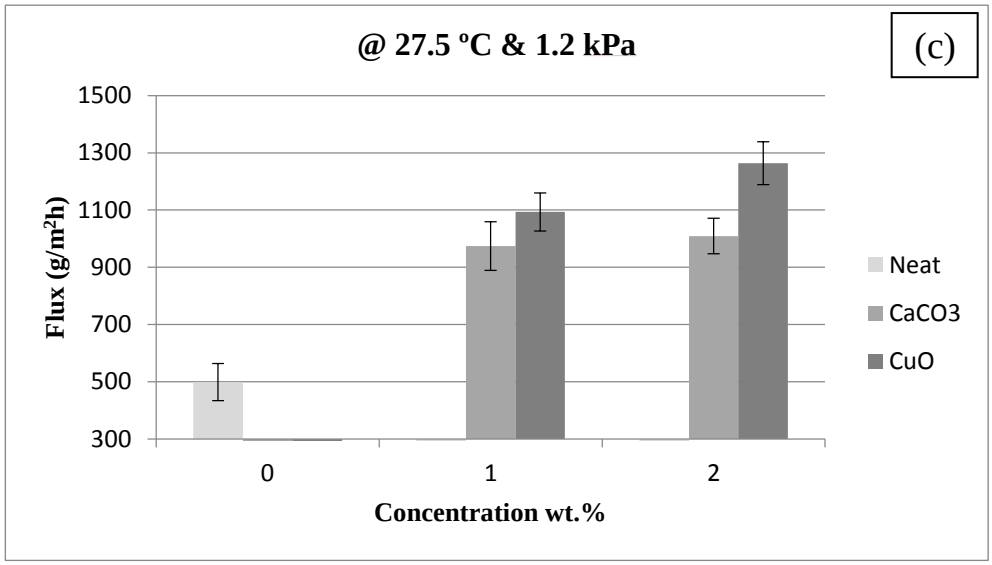

Fig. 5-15 Effects of the type of the hydrophilic nanomaterials on the membrane (a) porosity, (b) contact angle, and (c) pure water flux

Further, according to Fig. 5-15-c, the pure water flux was increased upon addition of both nanoparticles and the highest flux was observed at nanoparticle concentration of 2.0 wt.%. However, CuO nanoparticles demonstrated to be superior to $CaCO_3$ nanomaterials in terms of flux (increase of 153.4% vs. 102.3%, respectively, from the neat PVDF membrane when 2.0 wt.% is added) This may be due to either higher porosity (Fig. 5-15-a) or higher hydrophobicity (Fig. 5-15-b) of CuO than $CaCO_3$.

5-4- Conclusion

Effects of the hydrophilic nanoparticles on the properties and performance of the VMD membranes have been studied in this work. CuO nanoparticles were added into the PVDF matrix at different concentrations and the resulted membranes were characterized in terms of morphology, pore size, porosity, thickness, contact angle, and roughness. Their performance in VMD was also tested in terms of the flux and LEP_w. $CaCO_3$ nanomaterials, another type of hydrophilic particles, were also used for comparison. The following conclusions were drawn from the experimental results:

1) The addition of hydrophilic CuO nanoparticles was able to enhance the pore size and the thickness of finger-like layer. Slight increase in the membrane porosity was also observed at the medium concentrations of the nanoparticles.

2) The VMD performance was optimized at 2.0 wt.% of the CuO nanoparticles in the membrane where the flux increased 153.4% compared to the neat PVDF membrane at the feed temperature of 27.5 °C. In addition, no reduction in the membrane selectivity was observed.

3) The surface contact angle and LEP_w of that membrane were high enough, indicating that the membrane is applicable for MD.

4) The flux achieved at such a low feed temperature proved the usefulness of the membrane for area, not only desalination but also the other applications such as vacuum desiccant cooling and membrane evaporative cooling.

5) CuO nanoparticles revealed a better performance in terms of the pure water flux in comparison with the $CaCO_3$ nanomaterials.

6) Even though PVDF's contact angle is below 90^o and the CuO and $CaCO_3$ nanoparticles are hydrophilic, the composite membranes can be used for VMD.

In brief, hydrophilic nanoparticles have a great potential to improve the performance of the MD membranes, provided appropriate selection of the nanoparticles is made and their concentration in the membrane is well adjusted.

Acknowledgments

The authors would like to thank Arkema Inc. (Philadelphia, PA, USA) for generously offering the polymers (Kynar® 740 and Kynar® HSV900). Financial supports of NSERC Discovery and I2I grants are also gratefully acknowledged.

References

[1] N. Ghaffour, T.M. Missimer, G.L. Amy, Technical review and evaluation of the economics of water desalination: Current and future challenges for better water supply sustainability, Desalination. 309 (2013) 197-207.

[2] A.S. Hassan, H.E.S. Fath, Review and assessment of the newly developed MD for desalination processes, Desalin.Water Treat. 51 (2013) 574-585.

[3] A.L. Ahmad, M.A. Majid, B.S. Ooi, Functionalized PSf/SiO2 nanocomposite membrane for oil-in-water emulsion separation, Desalination. 268 (2011) 266-269.

[4] A. Rahimpour, M. Jahanshahi, S. Khalili, A. Mollahosseini, A. Zirepour, B. Rajaeian, Novel functionalized carbon nanotubes for improving the surface properties and performance of polyethersulfone (PES) membrane, Desalination. 286 (2012) 99-107.

[5] Q. Wang, X. Wang, Z. Wang, J. Huang, Y. Wang, PVDF membranes with simultaneously enhanced permeability and selectivity by breaking the tradeoff effect via atomic layer deposition of TiO2, J.Membr.Sci. 442 (2013) 57-64.

[6] J. Li, Z. Xu, H. Yang, L. Yu, M. Liu, Effect of TiO2 nanoparticles on the surface morphology and performance of microporous PES membrane, Appl.Surf.Sci. 255 (2009) 4725-4732.

[7] G. Wu, S. Gan, L. Cui, Y. Xu, Preparation and characterization of PES/TiO2 composite membranes, Appl.Surf.Sci. 254 (2008) 7080-7086.

[8] N. Maximous, G. Nakhla, W. Wan, K. Wong, Preparation, characterization and performance of Al2O3/PES membrane for wastewater filtration, J.Membr.Sci. 341 (2009) 67-75.

[9] L.M. Jin, S.L. Yu, W.X. Shi, X.S. Yi, N. Sun, Y.L. Ge, et al., Synthesis of a novel composite nanofiltration membrane incorporated SiO2 nanoparticles for oily wastewater desalination, Polymer. 53 (2012) 5295-5303.

[10] J.n. Shen, C.c. Yu, H.m. Ruan, C.j. Gao, B. Van der Bruggen, Preparation and characterization of thin-film nanocomposite membranes embedded with poly(methyl methacrylate) hydrophobic modified multiwalled carbon nanotubes by interfacial polymerization, J.Membr.Sci. 442 (2013) 18-26.

[11] R. Kumar, A.M. Isloor, A.F. Ismail, S.A. Rashid, A. Al Ahmed, Permeation, antifouling and desalination performance of TiO2 nanotube incorporated PSf/CS blend membranes, Desalination. 316 (2013) 76-84.

[12] J. Yin, E. Kim, J. Yang, B. Deng, Fabrication of a novel thin-film nanocomposite (TFN) membrane containing MCM-41 silica nanoparticles (NPs) for water purification, J.Membr.Sci. 423 (2012) 238-246.

[13] H.J. Kim, K. Choi, Y. Baek, D. Kim, J. Shim, J. Yoon, et al., High-Performance Reverse Osmosis CNT/Polyamide Nanocomposite Membrane by Controlled Interfacial Interactions, Acs Applied Materials & Interfaces. 6 (2014) 2826-2836.

[14] M. Fathizadeh, A. Aroujalian, A. Raisi, Effect of added NaX nano-zeolite into polyamide as a top thin layer of membrane on water flux and salt rejection in a reverse osmosis process, J.Membr.Sci. 375 (2011) 88-95.

[15] N. Niksefat, M. Jahanshahi, A. Rahimpour, The effect of SiO2 nanoparticles on morphology and performance of thin film composite membranes for forward osmosis application, Desalination. 343 (2014) 140-146.

[16] N. Ma, J. Wei, R. Liao, C.Y. Tang, Zeolite-polyamide thin film nanocomposite membranes: Towards enhanced performance for forward osmosis, J.Membr.Sci. 405 (2012) 149-157.

[17] D. Emadzadeh, W.J. Lau, T. Matsuura, A.F. Ismail, M. Rahbari-Sisakht, Synthesis and characterization of thin film nanocomposite forward osmosis membrane with hydrophilic nanocomposite support to reduce internal concentration polarization, J.Membr.Sci. 449 (2014) 74-85.

[18] L. Yu, Z. Xu, H. Shen, H. Yang, Preparation and characterization of PVDF-SiO2 composite hollow fiber UF membrane by sol-gel method, J.Membr.Sci. 337 (2009) 257-265.

[19] M. Bhadra, S. Roy, S. Mitra, Enhanced desalination using carboxylated carbon nanotube immobilized membranes, Separation and Purification Technology. 120 (2013) 373-377.

[20] F. Liu, M.R.M. Abed, K. Li, Preparation and characterization of poly(vinylidene fluoride) (PVDF) based ultrafiltration membranes using nano gamma-Al2O3, J.Membr.Sci. 366 (2011) 97-103.

[21] M. Ben-Sasson, X. Lu, E. Bar-Zeev, K.R. Zodrow, S. Nejati, G. Qi, et al., In situ formation of silver nanoparticles on thin-film composite reverse osmosis membranes for biofouling mitigation, Water Res. 62 (2014) 260-270.

[22] M.L. Lind, A.K. Ghosh, A. Jawor, X. Huang, W. Hou, Y. Yang, et al., Influence of Zeolite Crystal Size on Zeolite-Polyamide Thin Film Nanocomposite Membranes, Langmuir. 25 (2009) 10139-10145.

[23] D. Hou, J. Wang, X. Sun, Z. Ji, Z. Luan, Preparation and properties of PVDF composite hollow fiber membranes for desalination through direct contact membrane distillation, J.Membr.Sci. 405 (2012) 185-200.

[24] K. Gethard, O. Sae-Khow, S. Mitra, Water Desalination Using Carbon-Nanotube-Enhanced Membrane Distillation, Acs Applied Materials & Interfaces. 3 (2011) 110-114.

[25] D. Hou, G. Dai, H. Fan, J. Wang, C. Zhao, H. Huang, Effects of calcium carbonate nano-particles on the properties of PVDF/nonwoven fabric flat-sheet composite membranes for direct contact membrane distillation, Desalination. 347 (2014) 25-33.

[26] A. Razmjou, J. Mansouri, V. Chen, The effects of mechanical and chemical modification of TiO2 nanoparticles on the surface chemistry, structure and fouling performance of PES ultrafiltration membranes, J.Membr.Sci. 378 (2011) 73-84.

[27] E. Celik, H. Park, H. Choi, H. Choi, Carbon nanotube blended polyethersulfone membranes for fouling control in water treatment, Water Res. 45 (2011) 274-282.

[28] H. Wu, B. Tang, P. Wu, Novel ultrafiltration membranes prepared from a multi-walled carbon nanotubes/polymer composite, J.Membr.Sci. 362 (2010) 374-383.

[29] Z. Chen, D. Rana, T. Matsuura, Y. Yang, C.Q. Lan, Study on the structure and vacuum membrane distillation performance of PVDF composite membranes: I. Influence of blending, Separation and Purification Technology. 133 (2014) 303-312.

[30] L.M. Camacho, L. Dumee, J. Zhang, J. Li, M. Duke, J. Gomez, et al., Advances in Membrane Distillation for Water Desalination and Purification Applications, Water. 5 (2013) 94-196.

[31] S. Al-Obaidani, E. Curcio, F. Macedonio, G. Di Profio, H. Ai-Hinai, E. Drioli, Potential of membrane distillation in seawater desalination: Thermal efficiency, sensitivity study and cost estimation, J.Membr.Sci. 323 (2008) 85-98.

[32] J.C. Mierzwa, C.D. Vecitis, J. Carvalho, V. Arieta, M. Verlage, Anion dopant effects on the structure and performance of polyethersulfone membranes, J.Membr.Sci. 421 (2012) 91-102.

[33] Y. Yang, D. Rana, T. Matsuura, S. Zheng, C.Q. Lan, Criteria for the selection of a support material to fabricate coated membranes for a life support device, RSC Adv. 4 (2014) 38711-38717.

[34] S. Zhao, Z. Wang, J. Wang, S. Wang, Poly(ether sulfone)/Polyaniline Nanocomposite Membranes: Effect of Nanofiber Size on Membrane Morphology and Properties, Ind Eng Chem Res. 53 (2014) 11468-11477.

[35] O. Agboola, J. Maree, R. Mbaya, Characterization and performance of nanofiltration membranes, Environmental Chemistry Letters. 12 (2014) 241-255.

[36] D. Emadzadeh, W.J. Lau, T. Matsuura, M. Rahbari-Sisakht, A.F. Ismail, A novel thin film composite forward osmosis membrane prepared from PSf-TiO2 nanocomposite substrate for water desalination, Chem.Eng.J. 237 (2014) 70-80.

[37] ImageJ, January 2015.

[38] M. Baghbanzadeh, A. Rashidi, A.H. Soleimanisalim, D. Rashtchian, Investigating the rheological properties of nanofluids of water/hybrid nanostructure of spherical silica/MWCNT, Thermochimica Acta. 578 (2014) 53-58.

Chapter 6:

Effects of hydrophilic silica nanoparticles and backing material in improving the structure and performance of VMD PVDF membranes

M. Baghbanzadeh, D. Rana, C. Q. Lan, T. Matsuura, Effects of hydrophilic silica nanoparticles and backing material in improving the structure and performance of VMD PVDF membranes, Separation and Purification Technology, 157 (2016) 60-71

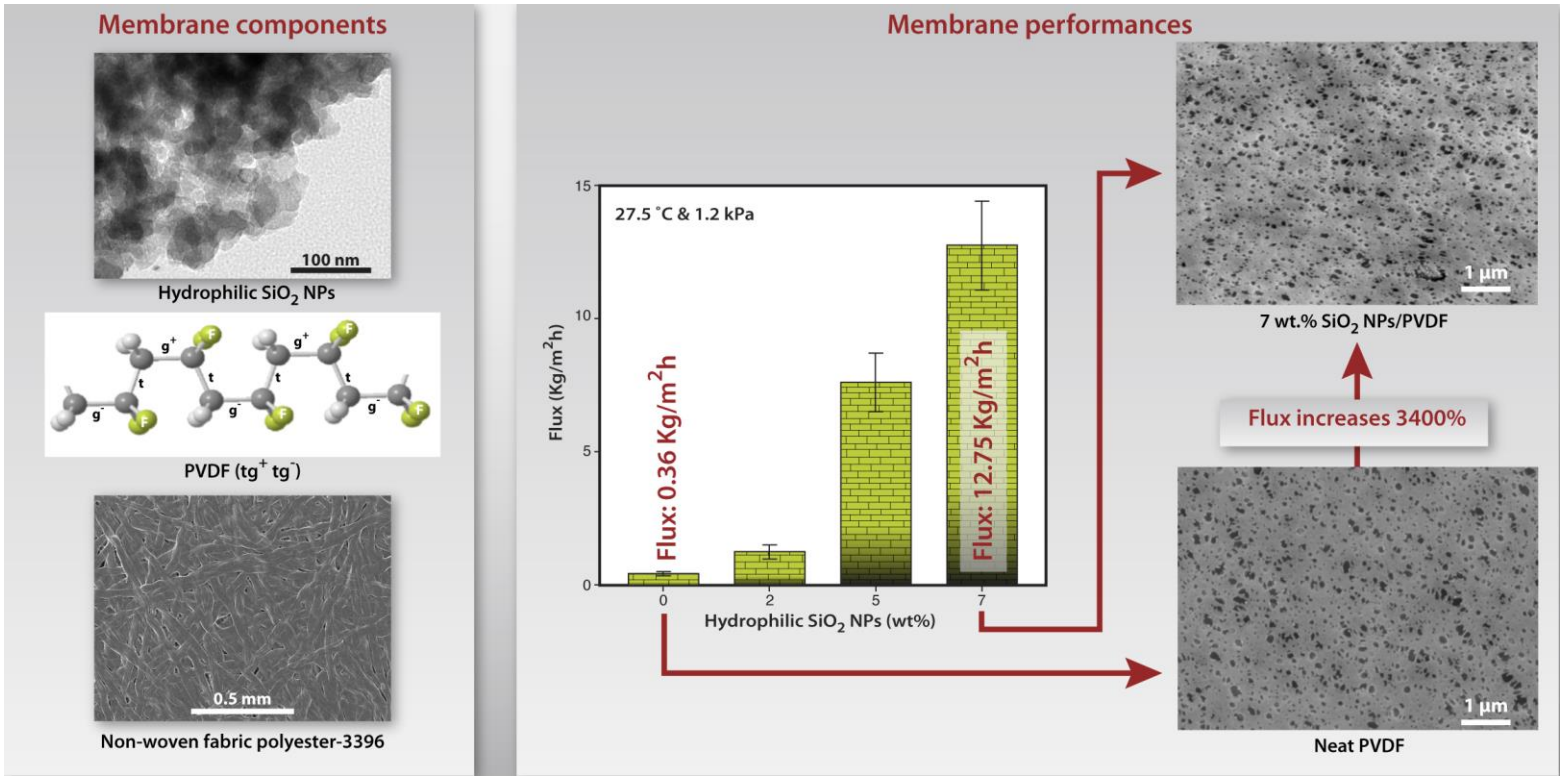
Membrane components
100 nm
Hydrophilic SiO_2 NPs
PVDF ($tg^+ tg^-$)
0.5 mm
Non-woven fabric polyester-3396
Membrane performances
27.5 °C & 1.2 kPa
Flux (Kg/m²h)
Flux: 0.36 Kg/m²h
Flux: 12.75 Kg/m²h
Hydrophilic SiO_2 NPs (wt%)
1 µm
7 wt.% SiO_2 NPs/PVDF
Flux increases 3400%
1 µm
Neat PVDF

Effects of hydrophilic silica nanoparticles and backing material in improving the structure and performance of VMD PVDF membranes

Mohammadali Baghbanzadeh, Dipak Rana, Christopher Q. Lan*, Takeshi Matsuura

Department of Chemical and Biological Engineering, University of Ottawa, 161 Louis Pasteur Private, Ottawa, Ontario, Canada K1N 6N5

Abstract

Effects of hydrophilic silica nanoparticles and Non-Woven Fabric (NWF) backing material on the properties and performance of the Polyvinylidene Fluoride(PVDF) membrane have been studied in this work. The nanocomposite membranes were prepared by the phase inversion method and characterized in terms of surface pore size, cross-sectional morphology, thickness, porosity, surface roughness and hydrophobicity. The fabricated membranes were subjected to Vacuum Membrane Distillation (VMD) experiments and their performance was evaluated through measuring the pure water flux and salt rejection. According to the results, effects of the hydrophilic nano-additives and NWF polyester enabled much higher VMD flux than the neat PVDF membrane when an appropriate amount of the nano-filler was added, possibly due to increase in the surface pore size and the reduction of the sponge-like layer thickness. The supported nanocomposite membranes possessed appropriate Liquid Entry Pressure (LEP_w) and mechanical strength, which make the membrane applicable in VMD process. When 7.0 wt.% of the silica nanoparticles was incorporated in a NWF supported membrane, the pure water flux became 12749.6 g/m^2h at feed temperature of 27.5 ºC and permeate side pressure of 1.2 kPa, representing a 2456% increase from the neat PVDF membrane. Almost complete NaCl rejection was also achieved when tested with 35 g/L NaCl aqueous solution.

Keywords: Hydrophilic SiO_2 nanoparticles; Non-woven fabric polyester; Finger-like layer; Sponge-like layer; Membrane structure; Flux; Vacuum membrane distillation (VMD);

*Corresponding author. Tel.: 1 613 562 5800x2050.
E-mail address:Christopher.Lan@uottawa.ca (C.Q. Lan)

6-1- Introduction

Saline water desalination has attracted extensive attentions during the last few decades. Water shortage due to the population and agricultural growth, and global warming in different areas of the world has forced people to find an alternative approach to alleviate the lack of fresh water. To this end, the desalination technology has demonstrated to be one of the most effective options [1-6]. Many processes could be used to remove the salty materials from the saline water, e.g., thermal processes such as Multiple Effect Distillation (MED) and Multi-stage Flash Distillation (MSF), Mechanical Vapor Compression (VC), and membrane-based processes. Currently desalination market is mainly dominated by the membrane-based processes [7-9], which include Reverse Osmosis (RO), Forward Osmosis (FO), Ultrafiltration (UF), Microfiltration (MF), Nanofiltration (NF), Membrane Distillation (MD) and the combination of two or more of them, due to the relatively low cost and energy consumption. While RO is presently placed on the top of these membrane processes [10-13], it has its own limitations such as strong tendency to fouling and scaling, limited product water recovery, huge electrical energy consumption required to work at extremely high operating pressures [14-17], which opens the way for the other membrane processes to enter into the competition in the desalination market. Particularly, MD has been demonstrated to be potentially applicable [18-22] provided a high performance durable membrane is available with high flux at relatively low operating temperatures to increase membrane life time and enable the utilization of low-quality thermal energy.

It is known that the membrane morphology and surface chemistry play a major role in determining the performance of the membranes, and they can be manipulated via different strategies in the manufacturing process, e.g., addition of nano-additives. The incorporation of nano-additives into neat membrane has been shown to be an appropriate approach in this direction as shown by the enhancement of the performance of the UF, MF, NF, RO, and FO membranes by numerous researchers [23]. However, the use of nanocomposite membranes in MD has been limited to only a few studies.

Gethard et al. [20] used carbon nanotube immobilized membrane (CNIM) in polypropylene (PP) in a sweep gas membrane distillation (SGMD) configuration and reported a higher flux than the neat PP membrane. In a similar work, Bhadra et al. [24] also observed an improvement in the PP membrane permeability through the addition of carboxylated carbon nanotubes. The

functionalized carbon nanotubes, especially the single walled ones, are very expensive to be used in commercial membrane production. In another attempt, Hou et al. [25,26] showed hydrophobic modified $CaCO_3$ nanoparticles to be effective in increasing the permeability of polyvinylidene fluoride (PVDF) membrane in direct contact membrane distillation (DCMD). In our recent works, it was shown that the addition of both superhydrophobic silica nanoparticles [27] and hydrophilic CuO nanoparticles [15] could significantly increase the flux of vacuum membrane distillation (VMD), but due to different mechanisms. Nevertheless, the fluxes obtained in these works, despite of the significant improvements in comparison to neat membranes, were still quite moderate and efforts dedicated to exploring more effective nano-additives are warranted.

The objective of this study is to investigate the effects of hydrophilic amino modified SiO_2 nanoparticles on the VMD performance of PVDF membranes. To the best of our knowledge, this work is the first attempt demonstrating that enclosure of hydrophilic silica nanoparticles could drastically increase the VMD flux of MD membranes without compromising hydrophobicity or salt rejection. This work was motivated by our earlier works, investigating the effects of hydrophilic CuO nanoparticles to lower the mass transfer resistance by increasing the fraction of the finger-like layer structure within the membrane layer and the compatibility of the silica nanoparticles with the dope solution, besides their mechanical strength and non-toxic nature [28]. The effects of backing materials on both the flux and stability of the membranes were also studied.

6-2- Experimental Methods

6-2-1- Materials

Two kinds of PVDF, Kynar® 740, (Pellet, melt viscosity: 1850 ± 250 Pa.s; melting temperature: 160.1 ºC) and Kynar® HSV900 (Powder, melt viscosity: 4930 Pa.s; melting temperature: 165.1 ºC) generously supplied by Arkema Inc. (Philadelphia, PA) were blended. DMAc and silver nitrate with the purity of 99.9% and 99+%, respectively, were supplied by Sigma–Aldrich. Hydrophilic amino modified SiO_2 nanoparticles with the size of 10-20 nm and 99.8% purity were purchased from Skyspring Nanomaterials Inc. NWF polyester, Hollytex® 3396 was supplied by Kavon Filter Products Co. (Farmingdale, NJ) and used as the backing material. Sodium chloride and n-butanol were provided by Fisher Scientific and used as received.

6-2-2- Membrane Fabrication

To make the membranes, phase inversion method was used. First, 1.25 wt.% water and 15 wt.% PVDF (HSV900:740 = 2:3 [29,30]) were dissolved in 83.75 wt.% DMAc under stirring at 180 rpm and 50 °C for 72 h to prepare the base polymeric solution. The homogenous solution was then degassed for 24 h before the required amount of the hydrophilic silica nanoparticles was added into the solution, and the resulting mixture was further stirred at the room temperature for 2 h. Then, the prepared suspension was cast by a casting bar either on a glass plate to make unsupported membranes or on a backing material to make supported membranes. The cast film together with the glass plate or the backing material was immersed in the water bath of 25 °C after standing on the glass plate or the backing material for approximately 15-30 s. The membranes were kept in the water bath for 24 h while the water was replaced by the fresh water several times to ensure the solvent was removed from the system. The membranes were then dried at room temperature.

In this study, five different unsupported membranes were fabricated by adding 0.0, 2.0, 5.0, 7.0 and 9.0 wt.% of the hydrophilic silica nanoparticles to the base polymeric solution. The membranes are coded as M0.0, M2.0, M5.0, M7.0, and M9.0. Similarly, five supported membranes were prepared and named as M0.0-3396, M2.0-3396, M5.0-3396, M7.0-3396, and M9.0-3396.

6-2-2-1- Viscosity of the Dope Suspension

The viscosity of the dope suspensions containing different amounts of the nano-particles was measured by a rotational rheometer (Brookfield, Synchro-Lectric viscometer model: LVF) at 25 ºC. An appropriate spindle with a suitable motor speed was applied to measure the suspension viscosity three times and the average value was calculated.

6-2-3- Membrane Characterization

All the membranes were characterized through Scanning Electron Microscope (SEM) analysis, surface pore size, porosity, and thickness measurement and analysis of the surface characteristics via evaluating their roughness and wettability by measuring the surface contact angle to better understand the changes in the structural properties of the membranes.

6-2-3-1- Morphology

Top surface and cross-sectional structure of the membranes were observed by SEM analysis (SEM, Vega-II XMU VPSEM and Anatech Hummer VII). For the cross-section study, a piece of membrane was first immersed in the liquid nitrogen for around 15-20 s, and then broken (for unsupported membrane) or cut by a very sharp scissor (for supported membrane) to obtain a clean cut of the membrane. Furthermore, all the samples were gold sputtered before SEM assessment to make them conductive.

6-2-3-2- Nanomaterials Distribution within the Membrane Layers

To ensure that the hydrophilic silica nanoparticles have been uniformly distributed within the membrane, electron dispersion spectroscopy (EDS) mapping of Si was carried out (EDX, Oxford Inca Energy 250X EDX). Samples were gold sputtered before doing the analysis.

6-2-3-3- Pore Size

Surface pore size was measured by using the top-view SEM images where approximately 150 pores were randomly chosen and assumed to be perfect circles. For this purpose, ImageJ software was employed [15,31-35] and the average value is reported.

6-2-3-4- Porosity

To measure the porosity, the wet and dry method was used [31]. The membrane sample was kept in n-butanol for 12 h to make sure all the pores have been filled with the liquid before it was weighed (w_1). Then, the wet membrane was oven dried at 50 °C for 24 h to obtain the weight of the dry sample (w_2). The membrane porosity was calculated by using the equation 6-1, where A (cm^2) and δ (cm) are effective surface area and thickness, respectively, and ρ (g/cm^3) represents the density of n-butanol.

$$\%\varepsilon = \frac{w_1 - w_2}{A.\delta.\rho} \times 100 \qquad (6\text{-}1)$$

The test was repeated at least three times and the average value was calculated.

6-2-3-5- Thickness

The thickness of the membrane was measured at different spots either by a digital micrometer or analyzing the cross-sectional SEM images via ImageJ and the average value was recorded.

6-2-3-6- Wettability

Surface hydrophobicity of the membranes was evaluated by measuring the surface contact angle by a VCA Optima Surface Analysis System (AST Products, Inc. Billerica, MA). A 2 μL droplet was placed on the membrane surface and the contact angle was measured. Ten different spots on the membrane surface were randomly selected and the average value is reported.

6-2-3-7- Roughness

ImageJ and its plugin *SurfCharJ* [36] have been demonstrated to be suitable tools for estimating the surface roughness of a membrane [15,29,31,34]. The surface roughness was evaluated by *SurfCharJ* program in this work using the top-view SEM images with appropriate magnification through a procedure which has been explained in our previous study [15].

6-2-4- Membrane Performance

The permeability and salt rejection performance of the membranes with and without the backing material were investigated by a VMD system. The experimental setup consisted of a static cell which was wrapped with a heating tape to control the feed temperature. A stirrer was used to increase the turbulence of the liquid in the cell, and to minimize the temperature and concentration polarization. On the permeate side, a vacuum pump was installed to generate a vacuum pressure of 1.2 kPa and the permeate vapour was collected in the condenser cooled by liquid nitrogen. A detailed schematic of the setup along with the operational procedure are given elsewhere [15,27].

6-2-4-1- Permeability

Membrane permeability was evaluated in terms of VMD flux given by equation 6-2.

$$J = \frac{w}{A.t} \tag{6-2}$$

Where *J*, *w*, *A*, and *t* are flux (g/m^2h), mass of the collected permeate (g), effective surface area of the membrane (0.001134 m^2), and filtration time (h) respectively. This test was performed for each membrane at least six times and the average value is reported.

6-2-4-2- Rejection

To measure the selectivity of the membranes, VMD test was carried out for the artificial seawater as the feed with the concentration of 35 g NaCl per litter. The conductivities of the feed (C_f) and permeate (C_p) were measured by a conductivity meter (OAKTON, CON 2700) and the salt rejection (*R*) was calculated via the equation 6-3.

$$\%R = \frac{C_f - C_p}{C_f} \times 100 \tag{6-3}$$

6-2-4-3- Water Liquid Entry Pressure (LEP_w)

LEP_w is the highest pressure applicable without letting liquid water permeate through the membrane pores. LEP_w was tested using a static cell loaded with liquid water in the feed

chamber. Pressure was applied on the liquid from a nitrogen cylinder and increased stepwise by an increment of 0.14 barg (2 psig) every 10 min until the first water droplet was observed at the cell outlet. This pressure was recorded as the LEP_w. The measurement was repeated at least three times and the average value is reported. A detailed schematic of the experimental setup is presented elsewhere [15].

6-2-4-4- Nanoparticles Leaching

The possibility of the nanoparticles leakage into the permeate was investigated by elemental EDS analysis and EDS mapping of Si in the VMD permeate (EDX, Oxford Inca Energy 250X EDX). Two aqueous suspensions of hydrophilic silica nanoparticles with the concentration of 0.1 and 0.001 wt.%, respectively, were prepared as standard solutions to ensure the nanoparticles are detectable at least up to a concentration of 0.001 wt.%. To this end, 6 mL of the suspension was placed on sample holder and put on a hot plate at 80 °C under fume hood for 2 h until the entire solvent evaporation. The as prepared sample was then carbon sputtered and analyzed for elemental EDS and EDS mapping.

6-3- Results and Discussion

6-3-1- Effects of Hydrophilic SiO_2 Nanoparticles on the Properties and VMD Performance of Nanocomposite Membrane

Figs. 6-1-a and 6-1-b show the top and cross-sectional SEM images of the unsupported membranes at different nanoparticle concentrations (M0.0, M2.0, and M7.0).

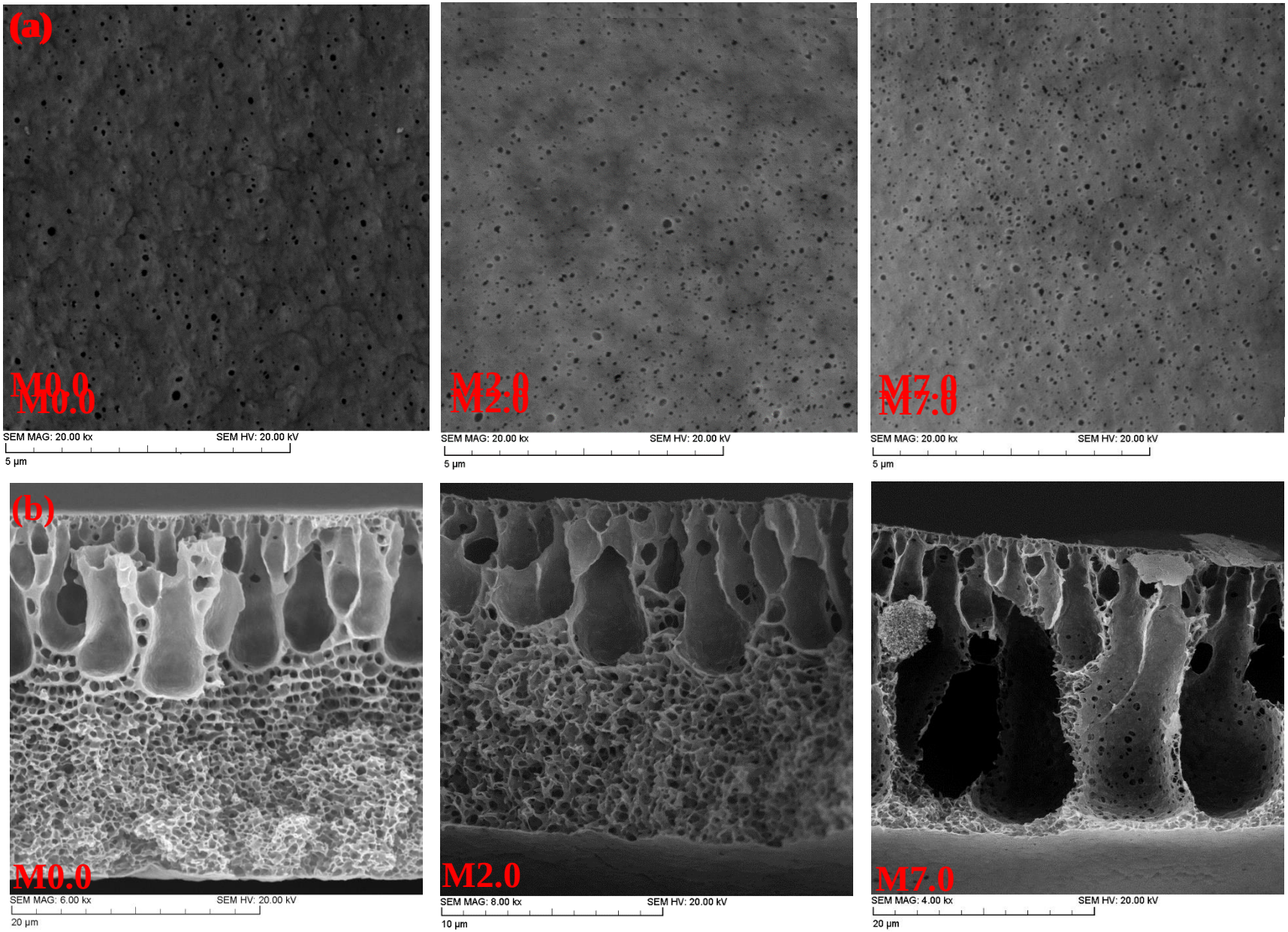
(a)
M0.0
SEM MAG: 20.00 kx
SEM HV: 20.00 kV
5 µm
M2.0
SEM MAG: 20.00 kx
SEM HV: 20.00 kV
5 µm
M7.0
SEM MAG: 20.00 kx
SEM HV: 20.00 kV
5 µm
(b)
M0.0
SEM MAG: 6.00 kx
SEM HV: 20.00 kV
20 µm
M2.0
SEM MAG: 8.00 kx
SEM HV: 20.00 kV
10 µm
M7.0
SEM MAG: 4.00 kx
SEM HV: 20.00 kV
20 µm

Fig. 6-1 (a) Top surface (b) Cross-sectional SEM images of the SiO_2/PVDF membranes (M0.0, M2.0, and M7.0), the surface pores are specified by the black spots in top surface

EDS mapping of different elements for M2.0 is given in Fig. 6-2 to show the uniformity of the dispersion of the hydrophilic silica nanoparticles across the cross-section with C and F mapping images corresponding to PVDF and Si mapping image presenting SiO_2 distribution. Fig. 6-2 shows that SiO_2 nanoparticles dispersed uniformly across the cross-section of the membrane. It should be pointed out that the dense colored layer that could be seen on the top of each image corresponds to the membrane surface instead of being part of the cross-section of the membrane. In other words, this Si mapping image also confirms the existence of SiO_2 nanoparticles on the surface of the membrane.

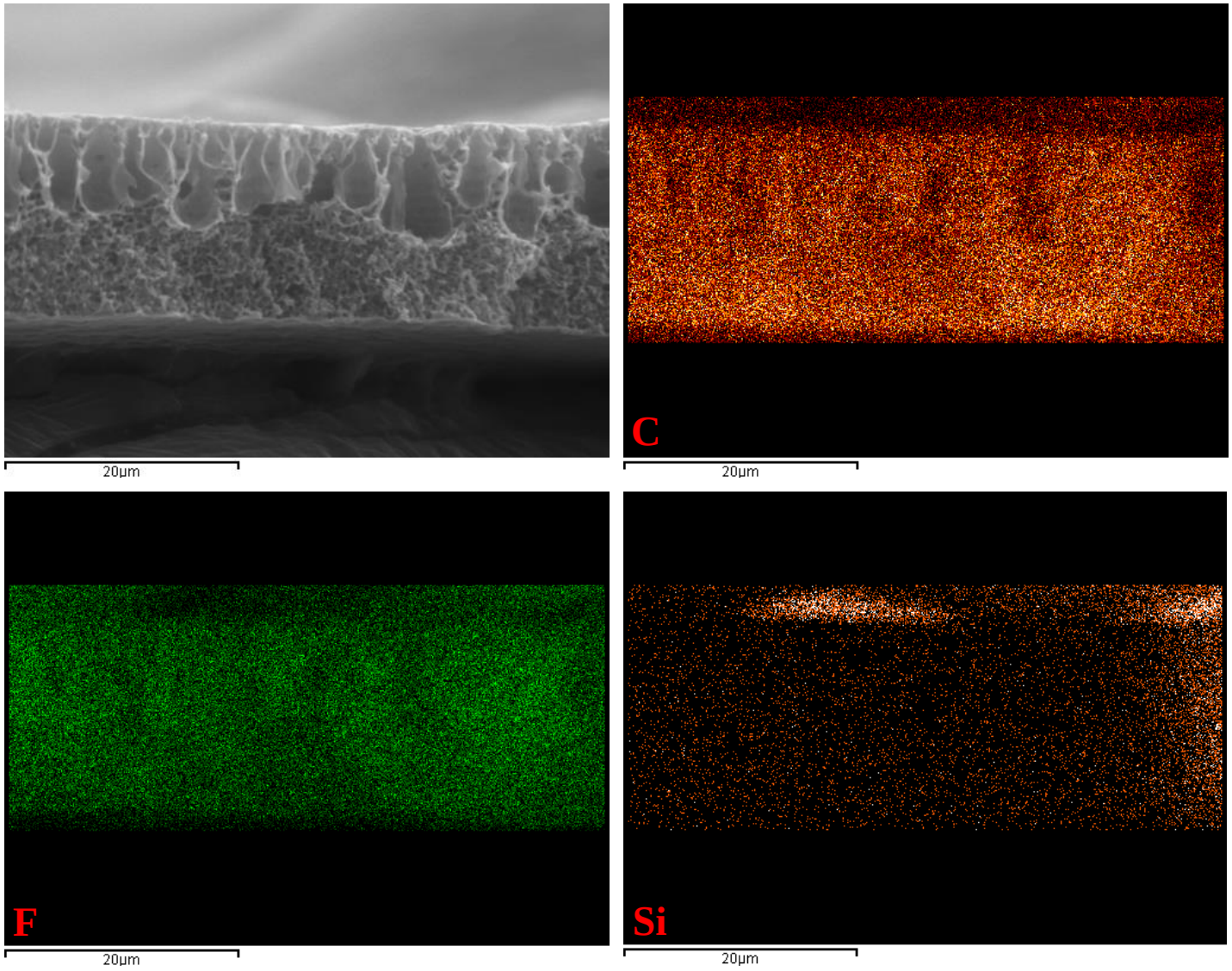

Fig. 6-2 EDS mapping of C, F, and Si for M2.0

From Fig. 6-1-a, the number of the surface pores increased with an increase in nanoparticle concentration. The pore size has also increased (Fig. 6-3), e.g., 47.3% increase from the neat PVDF (M0.0) membrane was observed with membrane M7.0. As shown in Fig. 6-1-b, all the membranes had an asymmetric structure with a very thin skin layer at the top, a finger-like layer in the middle, and a sponge-like layer at the bottom. The finger-like layer became thicker with the increase in the nanoparticle concentration, resulted in a decrease of sponge-like layer thickness as the overall membrane thickness remained largely constant. Fig. 6-3 shows the change in the ratio of the thickness of the finger-like layer to that of the entire membrane with the nanoparticle concentration. According to Figs. 6-1-b and 6-3, sponge-like layer has almost disappeared at 7.0 wt.% silica nanoparticle concentration (M7.0).

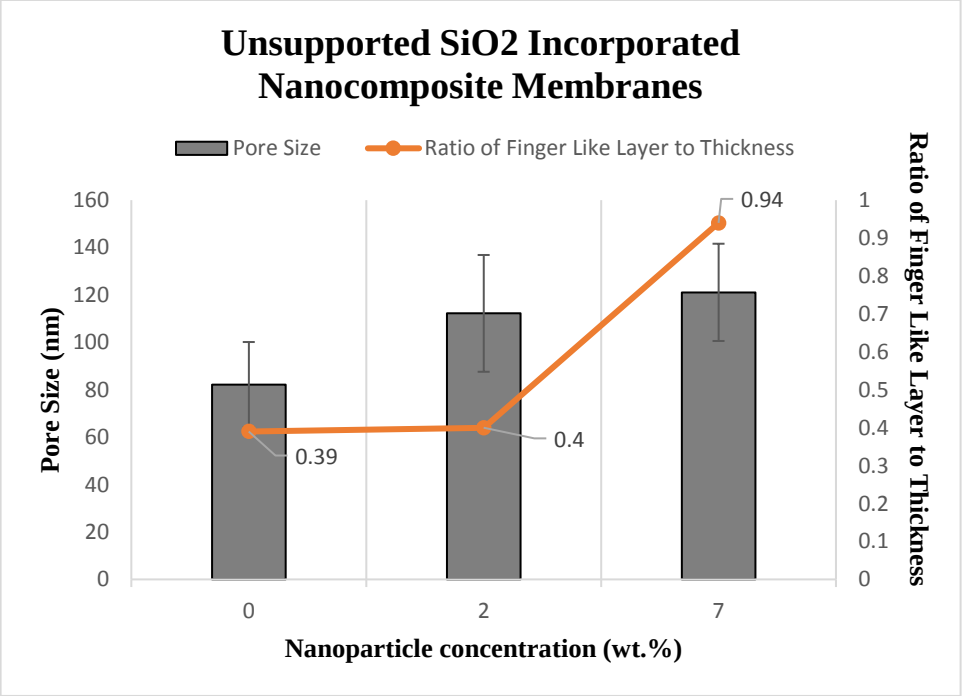

Fig. 6-3 Surface pore size and ratio of the thickness of the finger-like layer to the total membrane thickness vs. silica nanoparticle concentration

The increase of surface pore size and finger-like layer thickness is ascribed to the intrusion of a larger amount of non-solvent (water) into the cast film as the concentration of hydrophilic nanoparticles in the casting dope is increased. The viscosity increase with an increment in the

nanoparticle concentration (Fig. 6-4) seems to be not high enough to compromise the effect of the hydrophilicity enhancement. The viscosity shows a linear change with the concentration of the nano-fillers that further demonstrates the suitable stability of the casting suspensions [37].

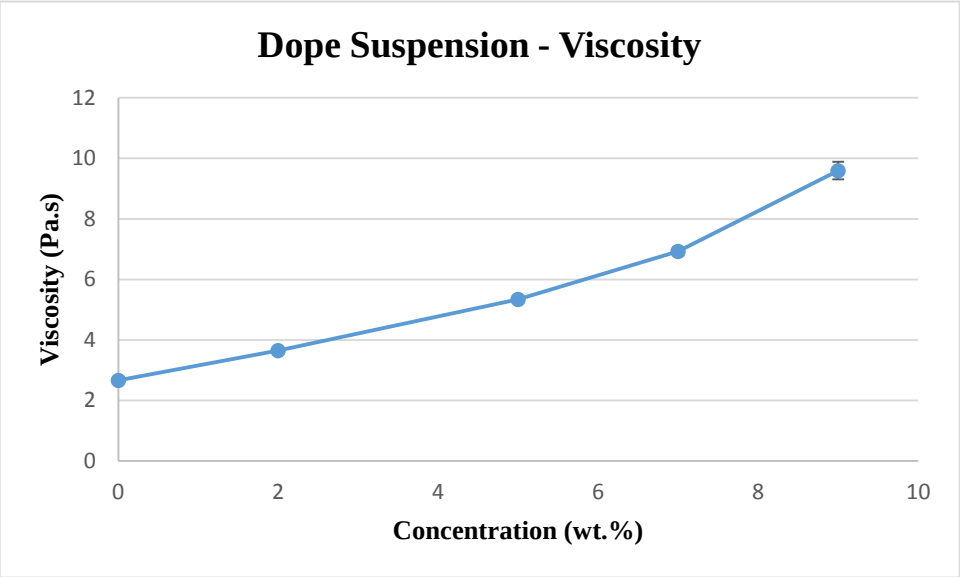

Fig. 6-4 Dope suspension viscosity vs. nanoparticle concentration at 25 ºC

Furthermore, nanoparticles acted as additional nucleating agents and as the concentration of the hydrophilic nano-additives increased, more nucleating agents had the chance to penetrate into the polymer lean phase, helped its growth to take place faster, which resulted in the larger surface pore size.

To investigate the stability of the SiO_2 incorporated nanocomposite membranes with time, four different samples of the unsupported membrane with 2.0 wt.% of silica nano-additives were tested with three consecutive VMD cycles, each cycle was under vacuum for 1.5 h. The results are shown in Fig. 6-5.

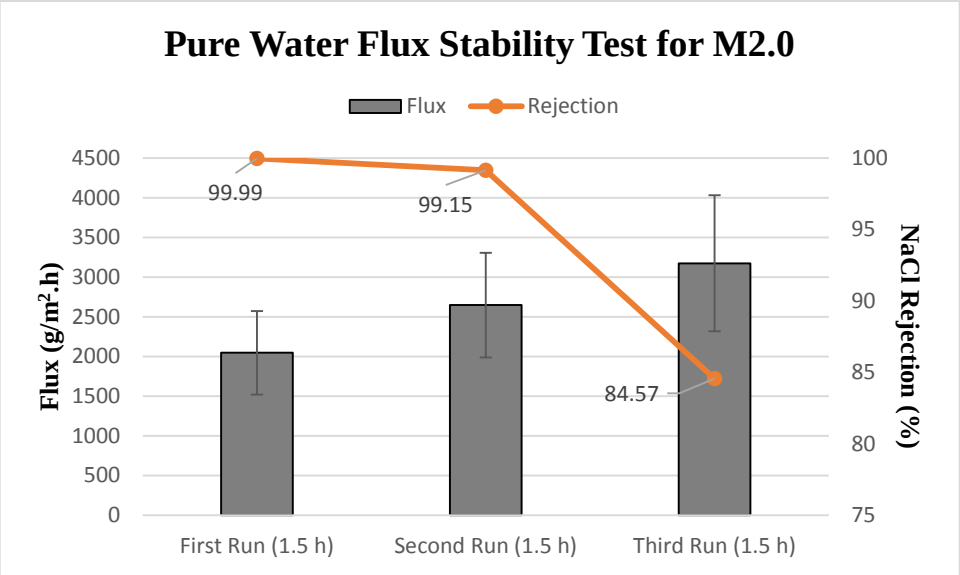

Fig. 6-5 Pure water flux stability test for 4 different M2.0, feed temperature: 27.5 °C

From Fig. 6-5, the flux of M2.0 membrane in the first cycle was above 2000 g/m^{2}h, showing the flux enhancement by the addition of nanoparticles as our previous studies have shown that the pure water flux of the neat PVDF membrane, i.e. M0.0, was 498.8±65.2 under the same conditions [15]. These results indicate that the nanocomposite membranes could sustain a much higher flux and similar salt rejection in comparison to the neat membranes. However, as also shown in Fig. 6-5, the flux increased progressively in the three cycles with a significant decrease of NaCl rejection in the third cycle. From these results, we can conclude that the nanocomposite membranes were deteriorating during the consecutive VMD tests and leakage likely occurred in the third cycle. To elucidate the mechanism of the membrane deterioration, M2.0 membrane was subjected to VMD for 4.5 hr with a solution of 1.0 wt.% silver nitrate, and the membrane was then rinsed with distilled water for three times before being subjected to EDS mapping for silver distribution across the membrane (Fig. 6-6).

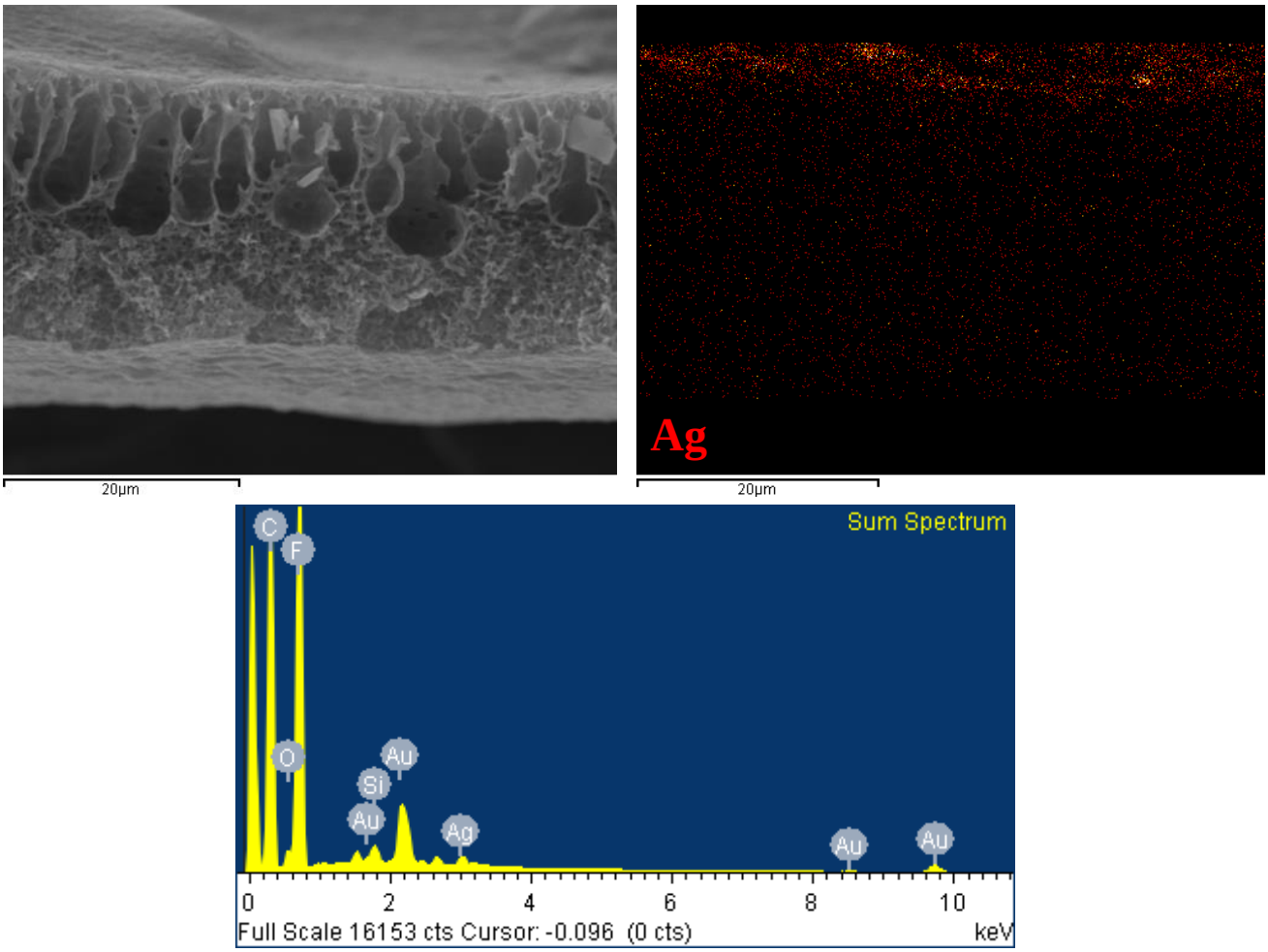

Fig. 6-6 Pore wetting analysis, EDS mapping of Ag for M2.0 after 4.5 h filtration of silver nitrate

Based upon Fig. 6-6 and in the same scale of noise, it could be concluded that there was no silver present in the membrane matrix and only small amounts of $AgNO_3$ were deposited on the membrane surface (dense colored layer on top of the membrane cross-section). In other words, pore wetting was not the cause of the aforementioned membrane leakage. Furthermore, when M7.0 was subjected to consecutive VMD cycles, significant leakage was observed in the second cycle (total 3 h) and the tests with 9.0 wt.% nanoparticle indicated severe leakage in the first cycle of VMD test. These results seem to suggest with little doubt that mechanical failure, which might be associated with the reduction of the sponge-like layer, was the cause of the incremental deterioration of the nanocomposite membrane with the progressive increase of nano-particles from 2.0 to 9.0 wt.%.

6-3-2- Effects of backing material on the Properties and VMD Performance of Nanocomposite Membrane

Our studies with unsupported nanocomposite membranes revealed that addition of hydrophilic SiO_2 nanoparticles would allow the reduction of the thickness of the sponge-like layer, which is a major contributor to mass transfer resistance of MD membranes. However, doing so would also bring about a significant disadvantage, i.e., the weakening of mechanical strength of membrane. The nanocomposite membranes, however, could resist pore wetting and therefore have a potential to be applied for MD if the mechanical weakness is overcome.

We hypothesized that coating nanocomposite membrane on an appropriate macro-porous backing material would significantly improve the mechanical strength of the nanocomposite membrane without compromising its flux. To test this hypothesis, we cast dope solution containing different concentrations of hydrophilic SiO_2 nanoparticles on a backing material selected from a previous study [32], i.e., (Hollytex® 3396) and a series of VMD and membrane characterization were carried out.

The improved durability of the supported nanocomposite membrane in comparison with the unsupported nanocomposite membrane was obvious. As shown in Fig. 6-7, the fluxes and salt rejection of M7.0-3396 were virtually unchanged during the three consecutive VMD cycles. Salt rejection was stable at a high level of 99.5% or above during the entire course of VMD test (Fig. 6-7), indicating that membrane integrity was not compromised.

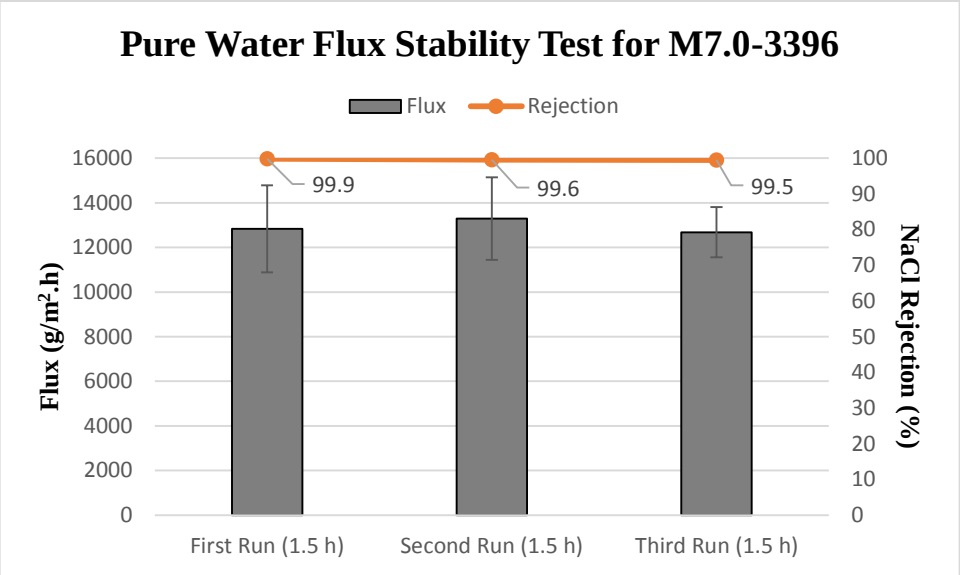

Fig. 6-7 Pure water flux stability test for 4 different M7.0-3396, feed temperature: 27.5 °C

The enhanced stability of supported membranes could be tentatively explained by the anchoring effects of the support materials, which was observed in our previous studies as well [32].

Top-view SEM images of the supported membranes for different nanoparticle concentration are given in Fig. 6-8.

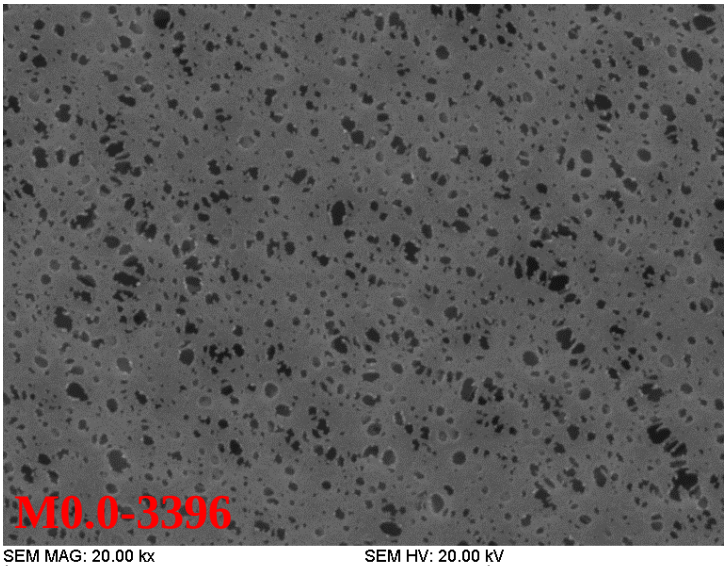
M0.0-3396
SEM MAG: 20.00 kx
SEM HV: 20.00 kV
5 µm

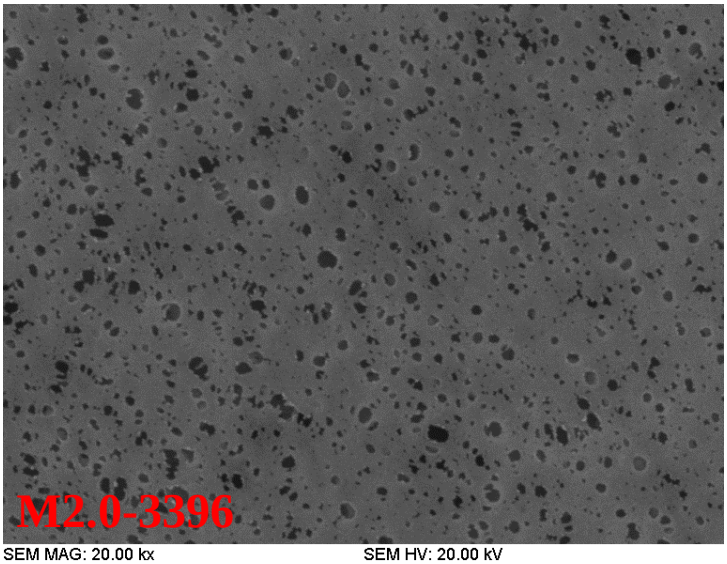
M2.0-3396
SEM MAG: 20.00 kx
SEM HV: 20.00 kV
5 µm

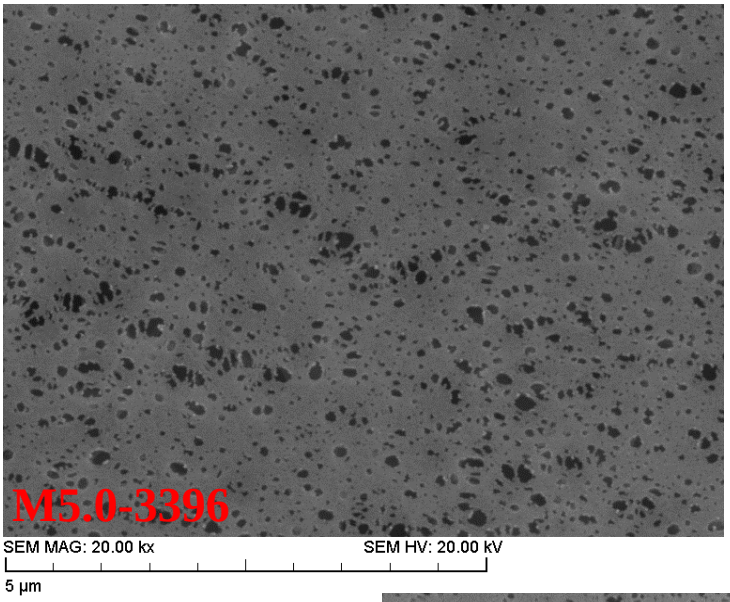
M5.0-3396
SEM MAG: 20.00 kx
SEM HV: 20.00 kV
5 µm

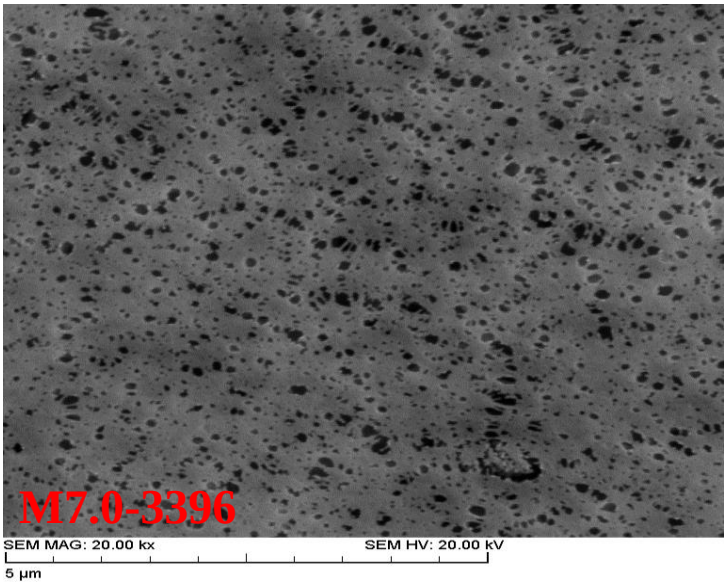
M7.0-3396
SEM MAG: 20.00 kx
SEM HV: 20.00 kV
5 µm

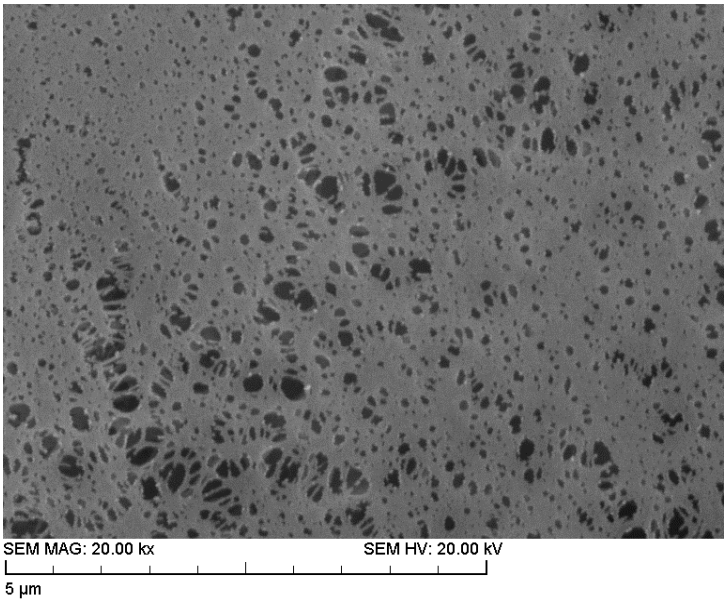
SEM MAG: 20.00 kx
SEM HV: 20.00 kV
5 µm

Fig. 6-8 Top surface SEM images of the SiO_2/PVDF membranes with backing material (M0.0-3396, M2.0-3396, M5.0-3396, M7.0-3396 and M9.0-3396), the surface pores are specified by the black spots

From the top SEM images given in Figs 6-1-a and 6-9, the pore sizes of the unsupported and supported membranes were calculated and shown in Fig. 6-9, which shows that the pore sizes of the supported membranes are larger than the unsupported membranes. This is because the cast membrane shrinks less during the phase inversion and drying processes due to the anchoring effect of the non-woven backing material.

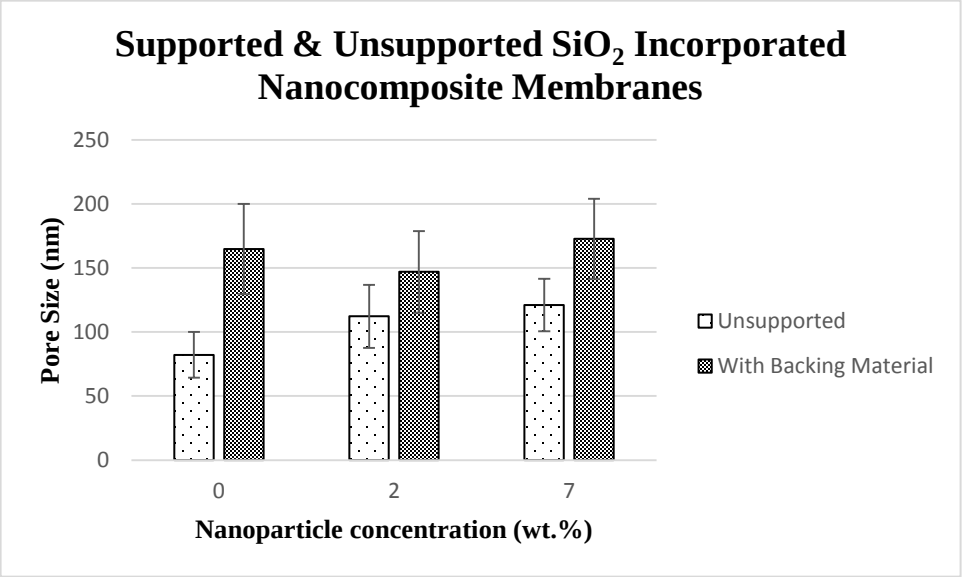

Fig. 6-9 A comparison between the surface pore size of the membranes with and without the non-woven backing material

The change in the surface pore size of the supported membranes with the concentration of the hydrophilic SiO_2 nanoparticles is shown in Fig. 6-10.

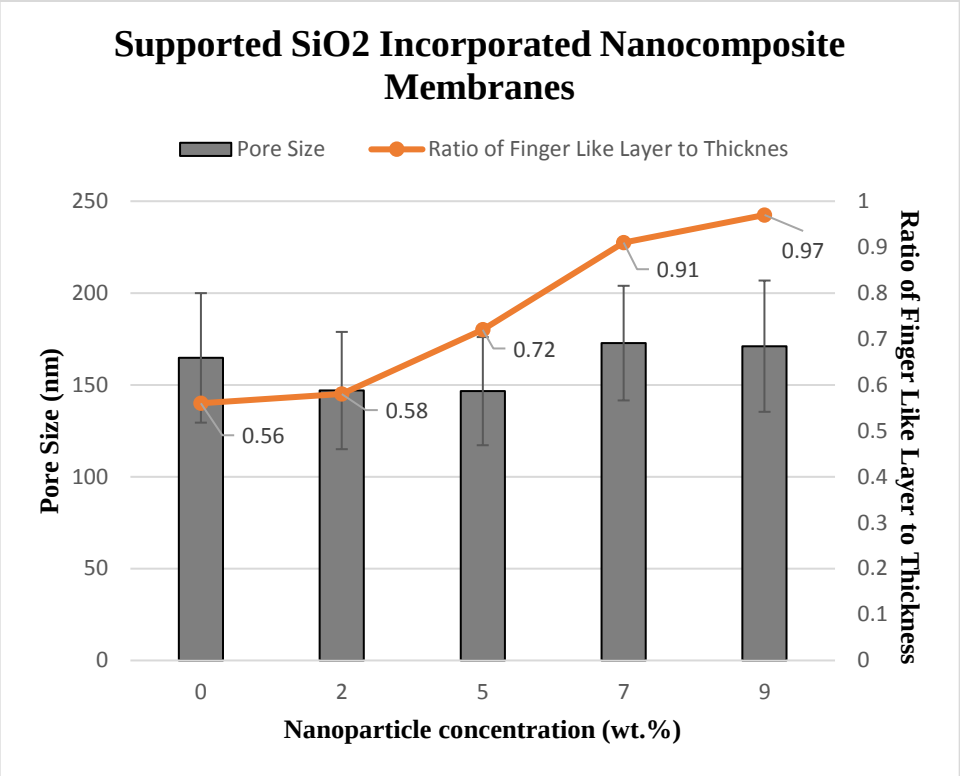

Fig. 6-10 Surface pore size and ratio of the thickness of the finger-like layer to the total membrane thickness vs. silica nanoparticles concentration – NWF supported membranes

According to Fig. 6-10, the surface pore size of the supported membranes did not change significantly with the nano-filler concentration. The effect of the nanoparticle concentration on the ratio of the thickness of the finger-like layer to that of the entire membrane (excluding the backing material) is also given in Fig. 6-10. Similar to the unsupported membrane (see Fig. 6-3), the ratio increased with the nanoparticle concentration.

Thus, it can be concluded that the phase inversion took place in a similar fashion regardless of the presence of the backing material. In other words, by considering the results from Figs. 6-3 and 6-10, both the unsupported and supported membranes showed the same cross-sectional behavior via the addition of the hydrophilic nano-additives that further demonstrated that the hydrophilic silica nanoparticles controlled the asymmetric structure of the membrane during the manufacturing process, while the major effect of the backing material was on the enlargement of the surface pore size along with stabilizing the membrane structure.

The porosity change with increasing nanoparticle concentration is illustrated in Fig. 6-11. It is worth noting that the porosity of the neat PVDF membrane (M0.0) and 3396 backing material (without coating) was reported to be 86.9% [15] and 11.6% [32], respectively.

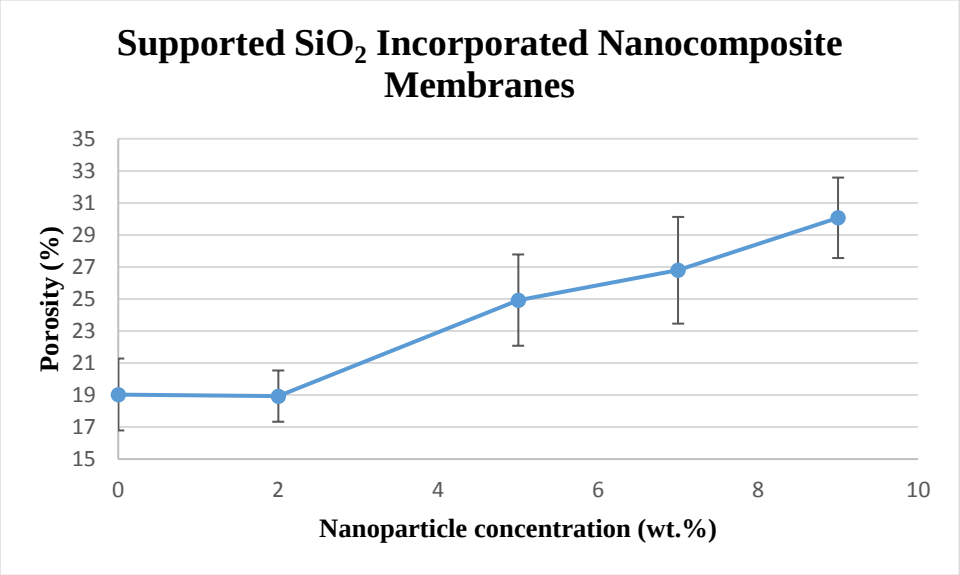

Fig. 6-11 Membrane porosity vs. silica nanoparticles concentration– NWF supported membranes

The porosity increases with the increase in the nanoparticles concentration together with the increase in finger-like macro-void fraction (Fig. 6-10).

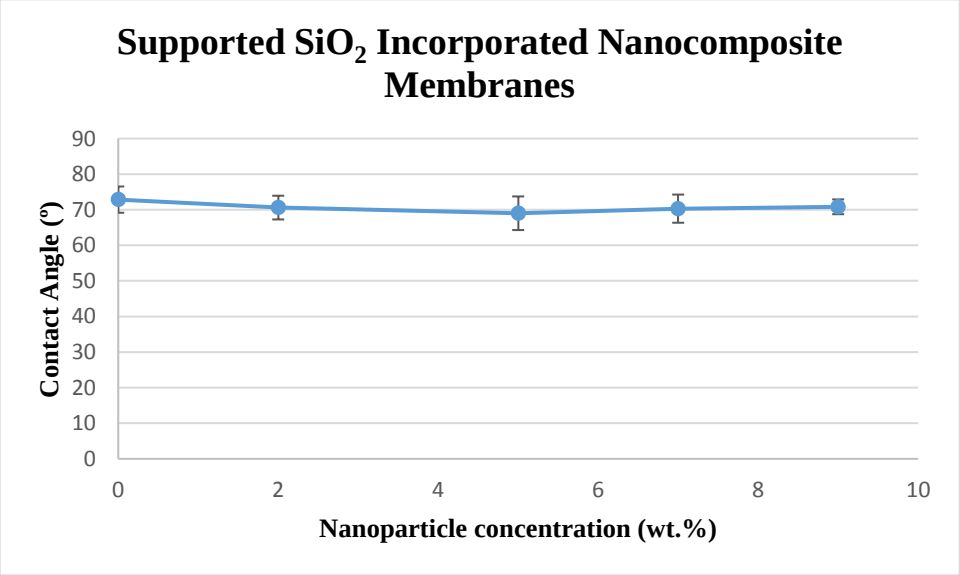

Fig. 6-12 Surface contact angle vs. silica nanoparticle concentration – NWF supported membranes

The effect of nanoparticle concentration on the contact angle of the supported membrane is shown in Fig. 6-12. From the figure, the nanoparticle concentration did not affect the contact angle significantly ($P > 0.05$) and the values are similar to the contact angles of the neat PVDF membranes reported in the literature. For instance, membranes of contact angle of 67.5º [38], 72.1º [26], 82.9º [39], and 83.6º [40,41] have been reported in the literature for a neat PVDF membrane. It should be pointed out that, although the contact angles are below 90º, our results and literature data have demonstrated beyond doubt that these membranes could have a large enough LEP_w to allow the membranes for MD applications [15,26,27,29,30].

Comparison of some other membrane characteristics was made between unsupported and supported membranes. Table 6-1 shows the surface roughness, another surface characteristic that is obtained from the top surface image analysis.

Table 6-1 Surface roughness analysis of the hydrophilic SiO_2 nanocomposite membranes by ImageJ according to the ISO 4287/2000 standard (all the units in pixel)

Membrane	Rq: Root mean square deviation	Ra: Arithmetical mean deviation	Rv: Lowest valley	Rp: Highest peak
Unsupported				
M0.0	3.3±0.3	2.6±0.2	-17.9±4.3	19.2±4.5
M2.0	3.9±0.2	3.1±0.2	-18.5±4.2	18.4±1.7
M7.0	4.2±0.7	3.3±0.5	-18.2±4.2	19.5±2.4
With Backing Material				
M0.0-3396	4.6±0.1	3.5±0.1	-19.9±1.0	25.8±1.2
M2.0-3396	4.2±0.2	3.3±0.2	-19.0±1.5	25.0±1.2
M5.0-3396	4.8±0.4	3.7±0.3	-22.2±2.3	28.3±1.7
M7.0-3396	5.0±0.5	3.8±0.4	-23.6±1.7	26.7±2.2
M9.0-3396	5.3±0.6	4.1±0.4	-22.8±2.9	28.6±1.8

According to Table 6-1, for the unsupported membrane, roughness kept increasing with an increase in nanoparticle loading while for the supported (with backing material) membrane roughness decreased from 0.0 to 2.0 wt.% of nanoparticle loading and increased thereafter. It could be attributed to the aggregation of the nanoparticles on the surface when their concentration is high. The same behavior was also reported in our previous work where the hydrophilic CuO nanoparticles were used in a PVDF matrix [15]. The effect of the backing material on the contact angle is shown in Fig. 6-13.

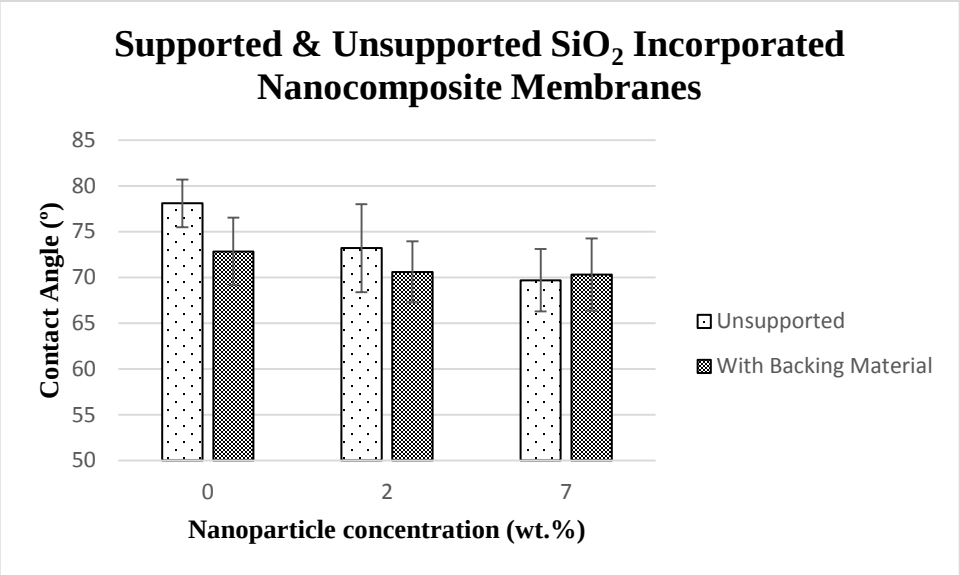

Fig. 6-13 Surface contact angle vs. silica nanoparticles concentration –NWF supported and unsupported membranes

From Fig. 6-13, the surface contact angle of the coated membranes was slightly less than the uncoated membrane, probably due to their larger surface pore sizes, however, the difference becomes insignificant at the high nanoparticle concentration. This trend could probably be explained by the interplay of pore size and surface roughness. As the nanoparticle concentration increases, roughness of the supported membrane grows faster than the unsupported membrane and all the supported membranes are rougher than the unsupported ones. Thus, the decrease of contact angle with increasing pore size and the increase of contact angle with increasing surface roughness compete with each other, and eventually the latter effect becomes dominant.

As it was mentioned earlier, MD demands the membranes with adequate LEP_w, higher than 1 barg. Therefore, LEP_w for all the membranes, both supported and unsupported was tested and is reported versus the nano-fillers concentration in Fig. 6-14.

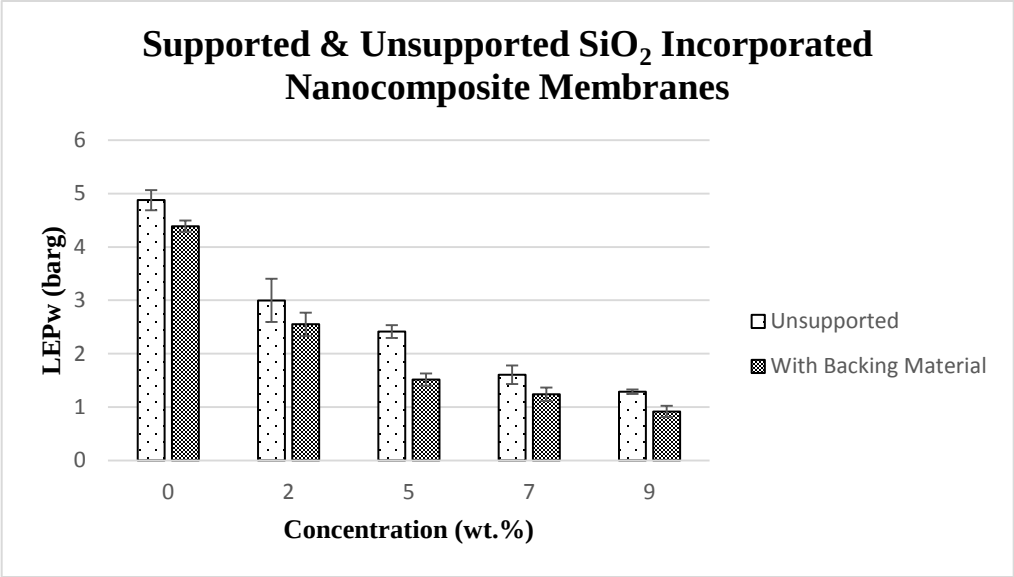

Fig. 6-14 LEP_w vs. silica nanoparticles concentration –NWF supported and unsupported membranes

Fig. 6-14 shows that the LEP_w decreased with the concentration of the silica nanoparticles, which is thoroughly consistent with the surface pore size. As it was discussed earlier, the higher the concentration of the nano-fillers, the larger the size of the surface pore size would be, and according to Laplace equation LEP_w decreases as the pore size becomes larger [42]. This theory is also valid when the supported membrane are compared with the unsupported ones, where the backing material brought about the membranes with larger pores and accordingly lower LEP_w.

Fig. 6-15 shows the effect of nanoparticle concentration on the pure water VMD flux where the VMD test was performed at 27.5 ºC and 1.2 kPa. It should be noted that the pure water VMD test failed for M9.0-3396 and the results were scattered with a large error bar, which is tentatively attributed to the large portion of the finger-like macro-voids and the diminish of sponge-like layer within the membrane structure.

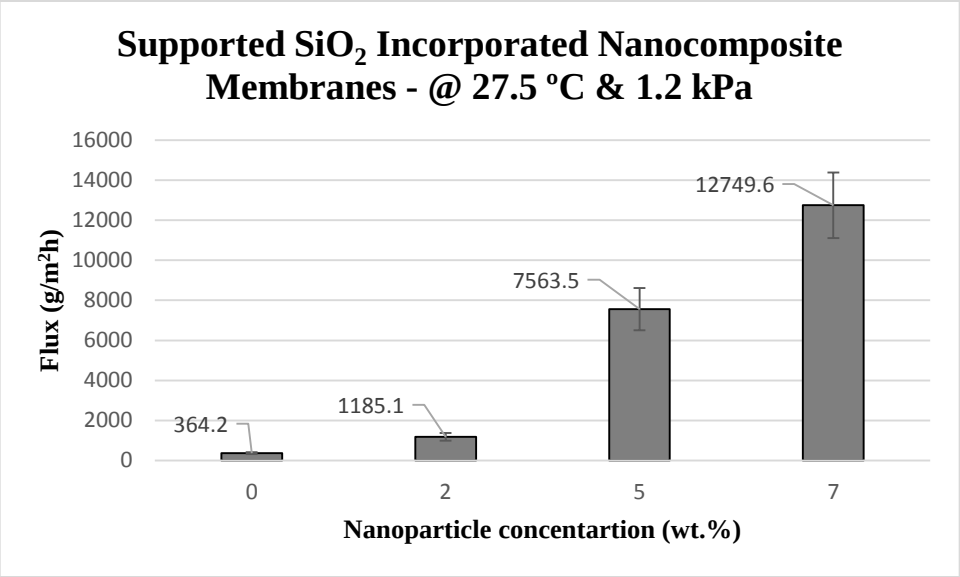

Fig. 6-15 Pure water flux vs. silica nanoparticles concentration – NWF supported membranes

Fig. 6-15 shows that the flux of M7.0-3396, which was 12749.6 g/m^{2}h, was 3400% of that of M0.0-3396, indicating a dramatic increase of flux when appropriate amount of amino modified SiO_2 was included as nano-additives. The pure water flux of M7.0-3396 is indeed remarkable considering the feed temperature of 27.5 ºC.

As listed in Table 6-2, adding different nano-additives resulted in drastically different increase of fluxes with nanocomposite membranes compared to their corresponding neat membranes, ranging from 28.1% in a previous study [25] to 2456% in this work. The flux of the best membrane of this study, which was a supported nanocomposite membrane with hydrophilic SiO_2 nanoparticles as additive, had a flux 9.8, 12.7, and 4.4 times of that when CuO [15], $CaCO_3$ [15], and superhydrophobic SiO_2 [27] nanoparticles were used, respectively. It is also more than 3 times of the fluxes reported by another group, i.e., 4.0 [26] and 4.1 [25] kg/m^{2}h, which were obtained with $CaCO_3$ nanocomposite membranes at higher feed temperatures of 33 and 30 ºC, respectively, using DCMD configuration. It is noteworthy pointing out that the highest flux of this study is 95.4% larger than the pure water flux of the commercial PVDF GVHP membrane which was used in a VMD process where a feed temperature of 25 ºC and vacuum pressure of 1.6 kPa was employed [43].

Furthermore, it is worth mentioning that the unsupported neat PVDF membrane (M0.0) possessed larger flux than the neat PVDF membrane with backing material (M0.0-3396). This is ascribed to the lower porosity and higher thickness of M0.0-3396 in comparison with M0.0.

Table 6-2 Nanocomposite PVDF membranes in membrane distillation

Nanomaterial	**Nanomaterial concentration**	**Neat membrane water flux (kg/m^2h)**	**Nanocomposite membrane water flux (kg/m^2h)**	**Water flux increase[α]**	**Rejection increase[α]**	**Remarks about the process**	**Ref.**
SiO_2 (Superhydrophobic)	7.0 wt.%	~ 0.7	~ 2.9	~ 292.4%	-[β]	*Rejection:* NaCl (35 g/L) *Feed Temperature:* 27.0°C *MD Configuration:* VMD	[27]
CuO (Hydrophilic)	2.0 wt.%	~ 0.5	~ 1.3	~ 153.4%	-[β]	*Rejection:* NaCl (35 g/L) *Feed Temperature:* 27.5°C *MD Configuration:* VMD	[15]
$CaCO_3$ (Hydrophilic)	2.0 wt.%	~ 0.5	~ 1.0	~ 102.3.4%	-	*Feed Temperature:* 27.5°C *MD Configuration:* VMD	[15]
$CaCO_3$ (Hydrophobic modified)	2.4 wt.%	~ 3.2	~ 4.1	~ 28.1%	-	*Feed:* NaCl (3.5 wt.%) *Feed Temperature:* 30.0 °C *MD Configuration:* DCMD	[25]
$CaCO_3$ (Hydrophobic modified)	3.0 wt.%	~ 3.0	~ 4.0	~ 33.3%	-	*Feed:* NaCl (35 g/L) *Feed Temperature:* 33.0 °C *MD Configuration:* DCMD	[26]
Neat PVDF GVHP[ɤ]	NA	~ 6.5	NA	NA	NA	*Membrane:* Commercial PVDF GVHP *Feed Temperature:* 25.0 °C *MD Configuration:* VMD	[43]
SiO_2 (Hydrophilic)	7.0 wt.%	~ 0.5	~ 12.7	~ 2456.0%	-[β]	*Rejection:* NaCl (35 g/L) *Feed Temperature:* 27.5 °C *MD Configuration:* VMD	Current Study

[α] Increase is evaluated compared to the neat membrane
[β] Rejection was perfect, i.e. more than 99.99% for both the neat and nanocomposite membranes
[ɤ] Flux for a neat commercial PVDF GVHP membrane in a VMD process with almost the same operating conditions as this work is presented for comparison purpose

Elemental EDS analysis for the VMD permeate from M7.0-3396 after the third cycle (4.5 h of operation) is presented in Fig. 6-16-a, while EDS mapping for the present elements is given in Fig. 6-16-b.

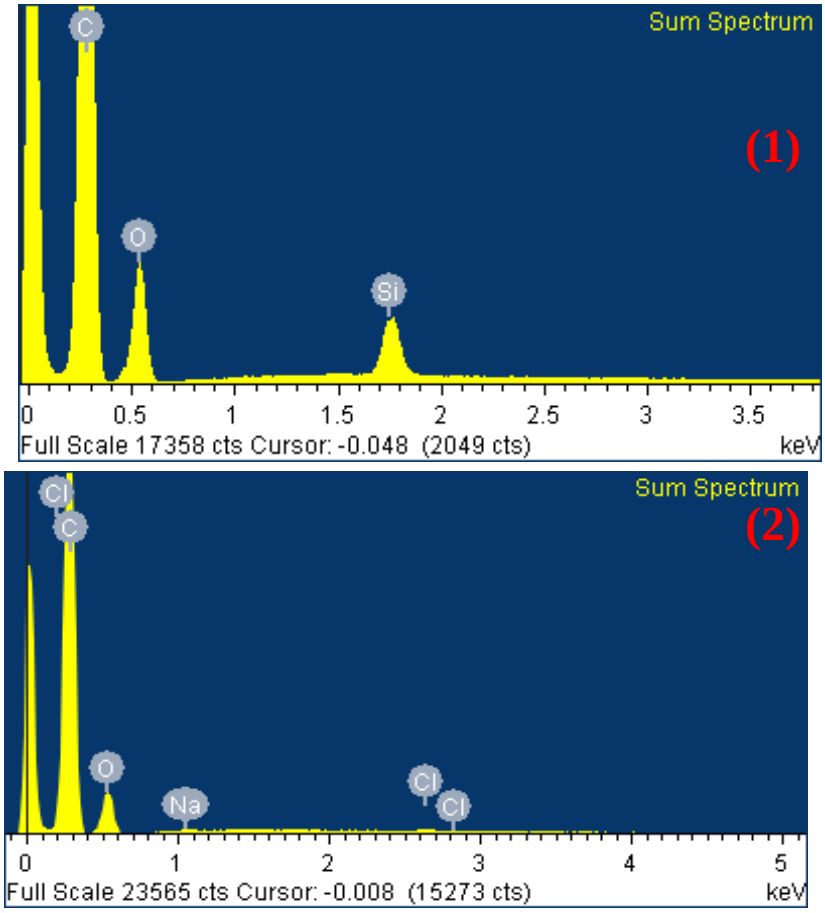

Fig. 6-16-a Elemental EDS analysis: (1) aqueous suspension of 0.001 wt.% hydrophilic silica nanoparticles and (2) permeate of VMD using M7.0-3396 after 4.5 h operation

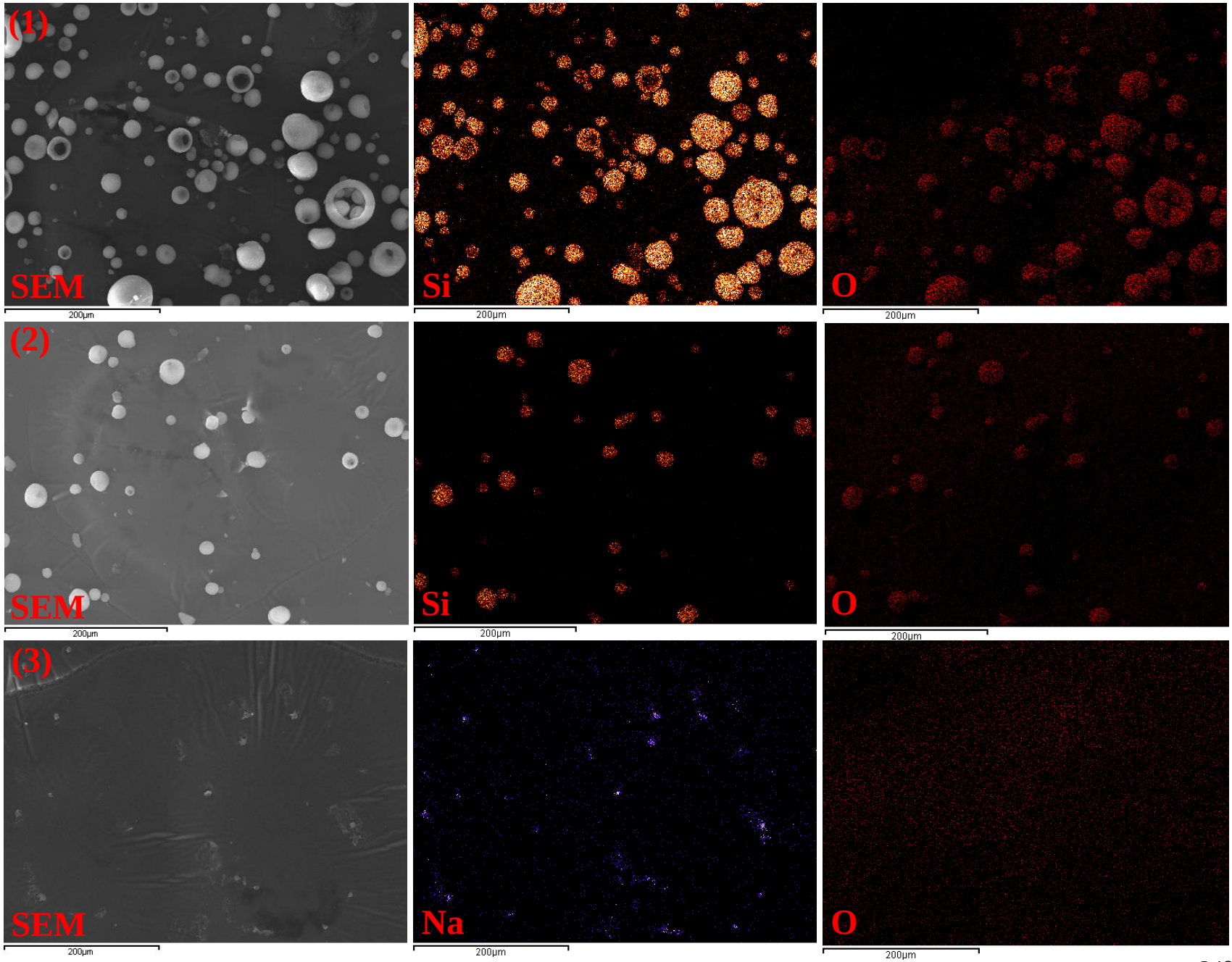
(1)
SEM
200μm
Si
200μm
O
200μm
(2)
SEM
200μm
Si
200μm
O
200μm
(3)
SEM
200μm
Na
200μm
O
200μm

Fig. 6-16-b SEM image (labeled as SEM) and EDS mapping images (the rest) for: (1) aqueous suspension of 0.1 wt.% hydrophilic silica nanoparticles, (2) aqueous suspension of 0.001 wt.% hydrophilic silica nanoparticles, and (3) VMD permeate from M7.0-3396 after 4.5 h operation

Considering Fig. 6-16-a, for the aqueous suspension with 0.001 wt.% hydrophilic SiO_2 nanoparticles in water, only Si, O, and C (sample was carbon sputtered) were detected via EDS analysis. The results for the aqueous suspension with lower amount of the nanoparticles demonstrate that the SiO_2 nanoparticles are detectable at least up to a concentration of 0.001 wt.%. No silica was detected for the VMD permeate after 3 consecutive VMD cycles for 4.5 h which shows the stability of the hydrophilic nano-additives within the membrane matrix of M7.0-3396. The presence of trace sodium and chlorine in the permeate as shown in both Figs. 6-16-a and 6-16-b is probably due to the existence of salt impurities in the water.

6-4- Conclusion

Nanocomposite membranes of PVDF and hydrophilic SiO_2 nanomaterials with and without backing material were fabricated via phase inversion process in this study. The membranes were subjected to structural properties characterization and VMD performance tests. It was revealed that addition of hydrophilic silica nanoparticles in PVDF membrane could lower the thickness of the sponge-like layer, which is one of the major contributors to mass transfer resistance in MD, and enlarge the pore size and porosity of PVDF membrane as well. This phenomenon is attributed to the facilitated demixing in the phase inversion process caused by the addition of hydrophilic silica nanoparticles. Such pore and cross-sectional structures of the membrane were confirmed to have a favourable effect on the VMD flux. Furthermore, NWF polyester backing material was found to be able to significantly enhance the mechanical strength of the membrane and make them capable of enduring repeated VMD tests. It was also found that the pore size in the supported nanocomposite membrane was larger than that of unsupported nanocomposite membranes. The effects of the hydrophilic SiO_2 nanoparticles and NFW polyester resulted in a supported nanocomposite membrane that is durable under the tested conditions

and capable of achieving a pure water flux of 12749.6 g/m^{2}h at a feed water temperature of 27.5 ºC when 7.0 wt.% of the nano-filers were included, which corresponds to 2456% increase compared to that of the neat PVDF membrane. It was also demonstrated that the nanoparticles were well stabilized in the membrane matrix and the release of the nanoparticles into the permeate was not a matter of concern in this study.

Acknowledgments

The generous gift of the polymers (Kynar® 740 and Kynar® HSV900) by Arkema Inc. (Philadelphia, PA, USA) is greatly acknowledged by the authors. Financial supports of NSERC Discovery and I2I grants are also highly appreciated.

References

[1] A.E. Khalifa, Water and air gap membrane distillation for water desalination – An experimental comparative study, Separation and Purification Technology. 141 (2015) 276-284.

[2] S. Daer, J. Kharraz, A. Giwa, S.W. Hasan, Recent applications of nanomaterials in water desalination: A critical review and future opportunities, Desalination. 367 (2015) 37-48.

[3] S. Miller, H. Shemer, R. Semiat, Energy and environmental issues in desalination, Desalination. 366 (2015) 2-8.

[4] H.M. Hegab, L. Zou, Graphene oxide-assisted membranes: Fabrication and potential applications in desalination and water purification, J.Membr.Sci. 484 (2015) 95-106.

[5] S. Roy, M. Bhadra, S. Mitra, Enhanced desalination via functionalized carbon nanotube immobilized membrane in direct contact membrane distillation, Separation and Purification Technology. 136 (2014) 58-65.

[6] J. Kuipers, S. Porada, Wireless desalination using inductively powered porous carbon electrodes, Separation and Purification Technology. 120 (2013) 6-11.

[7] E Curcio, GD Profio, E Fontananova, E Drioli, 13 - Membrane technologies for seawater desalination and brackish water treatment, in: Basile A, Rastogi ACK (Eds.), Advances in Membrane Technologies for Water Treatment, Woodhead Publishing, Oxford, 2015, pp. 411-441.

[8] N. Ghaffour, T.M. Missimer, G.L. Amy, Technical review and evaluation of the economics of water desalination: Current and future challenges for better water supply sustainability, Desalination. 309 (2013) 197-207.

[9] H.J. Kim, K. Choi, Y. Baek, D. Kim, J. Shim, J. Yoon, et al., High-Performance Reverse Osmosis CNT/Polyamide Nanocomposite Membrane by Controlled Interfacial Interactions, Acs Applied Materials & Interfaces. 6 (2014) 2819-2829.

[10] F.J. Garcia Latorre, S.O. Perez Baez, A. Gomez Gotor, Energy performance of a reverse osmosis desalination plant operating with variable pressure and flow, Desalination. 366 (2015) 146-153.

[11] J. Duan, E. Litwiller, I. Pinnau, Preparation and water desalination properties of POSS-polyamide nanocomposite reverse osmosis membranes, J.Membr.Sci. 473 (2015) 157-164.

[12] F. Guo, A. Servi, A. Liu, K.K. Gleason, G.C. Rutledge, Desalination by Membrane Distillation using Electrospun Polyamide Fiber Membranes with Surface Fluorination by Chemical Vapor Deposition, Acs Applied Materials & Interfaces. 7 (2015) 8225-8232.

[13] H. Dong, L. Zhao, L. Zhang, H. Chen, C. Gao, W.S. Winston Ho, High-flux reverse osmosis membranes incorporated with NaY zeolite nanoparticles for brackish water desalination, J.Membr.Sci. 476 (2015) 373-383.

[14] T.H. Chong, S. Loo, A.G. Fane, W.B. Krantz, Energy-efficient reverse osmosis desalination: Effect of retentate recycle and pump and energy recovery device efficiencies, Desalination. 366 (2015) 15-31.

[15] M. Baghbanzadeh, D. Rana, T. Matsuura, C.Q. Lan, Effects of hydrophilic CuO nanoparticles on properties and performance of PVDF VMD membranes, Desalination. 369 (2015) 75-84.

[16] R.K. McGovern, J.H. Lienhard V, On the potential of forward osmosis to energetically outperform reverse osmosis desalination, J.Membr.Sci. 469 (2014) 245-250.

[17] L. Karimi, L. Abkar, M. Aghajani, A. Ghassemi, Technical feasibility comparison of off-grid PV-EDR and PV-RO desalination systems via their energy consumption, Separation and Purification Technology. 151 (2015) 82-94.

[18] G. Guan, X. Yang, R. Wang, A.G. Fane, Evaluation of heat utilization in membrane distillation desalination system integrated with heat recovery, Desalination. 366 (2015) 80-93.

[19] Y. Liao, C. Loh, R. Wang, A.G. Fane, Electrospun Superhydrophobic Membranes with Unique Structures for Membrane Distillation, Acs Applied Materials & Interfaces. 6 (2014) 16035-16048.

[20] K. Gethard, O. Sae-Khow, S. Mitra, Water Desalination Using Carbon-Nanotube-Enhanced Membrane Distillation, Acs Applied Materials & Interfaces. 3 (2011) 110-114.

[21] J. Lee, Y. Kim, W. Kim, L. Francis, G. Amy, N. Ghaffour, Performance modeling of direct contact membrane distillation (DCMD) seawater desalination process using a commercial composite membrane, J.Membr.Sci. 478 (2015) 85-95.

[22] W.G. Shim, K. He, S. Gray, I.S. Moon, Solar energy assisted direct contact membrane distillation (DCMD) process for seawater desalination, Separation and Purification Technology. 143 (2015) 94-104.

[23] M. Baghbanzadeh, D. Rana, C.Q. Lan, T. Matsuura, Effects of inorganic nano-additives on properties and performance of polymeric membranes in water treatment, Separation & Purification Reviews. (2015).

[24] M. Bhadra, S. Roy, S. Mitra, Enhanced desalination using carboxylated carbon nanotube immobilized membranes, Separation and Purification Technology. 120 (2013) 373-377.

[25] D. Hou, J. Wang, X. Sun, Z. Ji, Z. Luan, Preparation and properties of PVDF composite hollow fiber membranes for desalination through direct contact membrane distillation, J.Membr.Sci. 405 (2012) 185-200.

[26] D. Hou, G. Dai, H. Fan, J. Wang, C. Zhao, H. Huang, Effects of calcium carbonate nano-particles on the properties of PVDF/nonwoven fabric flat-sheet composite membranes for direct contact membrane distillation, Desalination. 347 (2014) 25-33.

[27] J.E. Efome, M. Baghbanzadeh, D. Rana, T. Matsuura, C.Q. Lan, Effects of superhydrophobic SiO2 nanoparticles on the performance of PVDF flat sheet membranes for vacuum membrane distillation, Desalination. 373 (2015) 47-57.

[28] M. Baghbanzadeh, A. Rashidi, D. Rashtchian, R. Lotfi, A. Amrollahi, Synthesis of spherical silica/multiwall carbon nanotubes hybrid nanostructures and investigation of thermal conductivity of related nanofluids, Thermochimica Acta. 549 (2012) 87-94.

[29] Z. Chen, D. Rana, T. Matsuura, Y. Yang, C.Q. Lan, Study on the structure and vacuum membrane distillation performance of PVDF composite membranes: I. Influence of blending, Separation and Purification Technology. 133 (2014) 303-312.

[30] Z. Chen, D. Rana, T. Matsuura, D. Meng, C.Q. Lan, Study on structure and vacuum membrane distillation performance of PVDF membranes: II. Influence of molecular weight, Chem.Eng.J. 276 (2015) 174-184.

[31] J.C. Mierzwa, C.D. Vecitis, J. Carvalho, V. Arieta, M. Verlage, Anion dopant effects on the structure and performance of polyethersulfone membranes, J.Membr.Sci. 421 (2012) 91-102.

[32] Y. Yang, D. Rana, T. Matsuura, S. Zheng, C.Q. Lan, Criteria for the selection of a support material to fabricate coated membranes for a life support device, Rsc Advances. 4 (2014) 38711-38717.

[33] S. Zhao, Z. Wang, J. Wang, S. Wang, Poly(ether sulfone)/Polyaniline Nanocomposite Membranes: Effect of Nanofiber Size on Membrane Morphology and Properties, Ind Eng Chem Res. 53 (2014) 11468-11477.

[34] O. Agboola, J. Maree, R. Mbaya, Characterization and performance of nanofiltration membranes, Environmental Chemistry Letters. 12 (2014) 241-255.

[35] D. Emadzadeh, W.J. Lau, T. Matsuura, M. Rahbari-Sisakht, A.F. Ismail, A novel thin film composite forward osmosis membrane prepared from PSf-TiO2 nanocomposite substrate for water desalination, Chem.Eng.J. 237 (2014) 70-80.

[36] ImageJ, SurfCharJ, 2015.

[37] M. Baghbanzadeh, A. Rashidi, A.H. Soleimanisalim, D. Rashtchian, Investigating the rheological properties of nanofluids of water/hybrid nanostructure of spherical silica/MWCNT, Thermochimica Acta. 578 (2014) 53-58.

[38] Q. Wang, X. Wang, Z. Wang, J. Huang, Y. Wang, PVDF membranes with simultaneously enhanced permeability and selectivity by breaking the tradeoff effect via atomic layer deposition of TiO2, J.Membr.Sci. 442 (2013) 57-64.

[39] L. Yu, Z. Xu, H. Shen, H. Yang, Preparation and characterization of PVDF-SiO2 composite hollow fiber UF membrane by sol-gel method, J.Membr.Sci. 337 (2009) 257-265.

[40] L. Yan, Y.S. Li, C.B. Xiang, Preparation of poly(vinylidene fluoride)(pvdf) ultrafiltration membrane modified by nano-sized alumina (Al2O3) and its antifouling research, Polymer. 46 (2005) 7701-7706.

[41] L. Yan, Y.S. Li, C.B. Xiang, S. Xianda, Effect of nano-sized Al2O3-particle addition on PVDF ultrafiltration membrane performance, J.Membr.Sci. 276 (2006) 162-167.

[42] A.C.M. Franken, J.A.M. Nolten, M.H.V. Mulder, D. Bargeman, C.A. Smolders, Wetting criteria for the applicability of membrane distillation, J.Membr.Sci. 33 (1987) 315-328.

[43] M. Khayet, K. Khulbe, T. Matsuura, Characterization of membranes for membrane distillation by atomic force microscopy and estimation of their water vapor transfer coefficients in vacuum membrane distillation process, J.Membr.Sci. 238 (2004) 199-211.

Chapter 7:

Effects of polymer ratio and film-penetration time on the properties and performance of nanocomposite PVDF membranes in membrane distillation

M. Baghbanzadeh, N. Hirceaga, D. Rana, T. Matsuura, C. Q. Lan, Effects of polymer ratio and film-penetration time on the properties and performance of nanocomposite PVDF membranes in membrane distillation, Industrial & Engineering Chemistry Research, 55 (37) (2016) 9971-9982

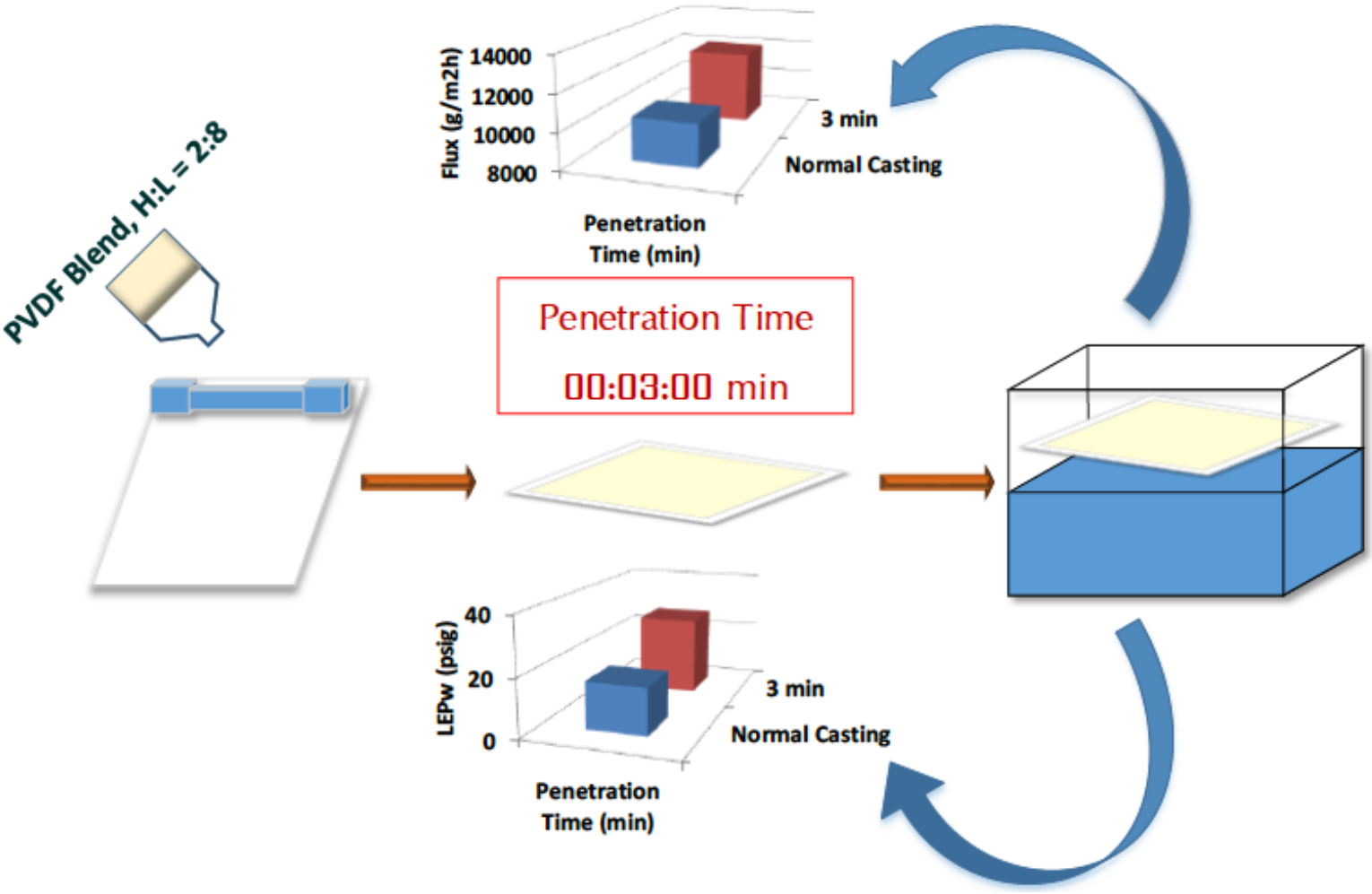
PVDF Blend, H:L = 2:8
Flux (g/m2h)
14000
12000
10000
8000
Penetration Time (min)
3 min
Normal Casting
Penetration Time
00:03:00 min
LEPw (psig)
40
20
0
Penetration Time (min)
3 min
Normal Casting

Effects of polymer ratio and film-penetration time on the properties and performance of nanocomposite PVDF membranes in membrane distillation

Mohammadali Baghbanzadeh, Nadine Hirceaga, Dipak Rana, Takeshi Matsuura, Christopher Q. Lan*

Department of Chemical and Biological Engineering, University of Ottawa, 161 Louis Pasteur Private, Ottawa, Ontario, Canada K1N 6N5

Abstract

Nanocomposite membranes were prepared for Vacuum Membrane Distillation (VMD) by casting the dope suspension on top of a non-woven polyester backing material. The dope consisted of 7.0 wt.% hydrophilic SiO_2 nanoparticles and the Polyvinylidene Fluoride (PVDF) blend of high molecular weight (H) and low molecular weight (L). The effects of the blend ratio (H:L) and the penetration time (τ), defined as the period between the completion of membrane casting and the immersion in the coagulation bath, on the membrane properties and performance were studied. It was found that the VMD flux is governed by the pore size and thickness of the top layer (defined as the layer formed above the backing material), both of which are affected by the H:L ratio and the penetration time. Results indicate that the VMD flux increased as the portion of L in the casting dope increased at constant τ, while a maximum flux was observed at τ = 2 min when the penetration time was changed at constant H:L ratio. It was also observed that the Liquid Entry Pressure of water (LEP_w) of membranes changed with the PVDF blend ratio and penetration time due to alteration of the maximum pore size. Considering all the data collected, the combination of H:L = 2:8 and penetration time of 3 min was identified as the best condition for the preparation of nanocomposite membranes, achieving one of the highest VMD fluxes, 12.1 kg/m^{2}h at 27.5 °C and 1.2 kPa, an improved LEP_w of 27.0 psig and a near complete NaCl rejection.

*Corresponding author. Tel.: 1 613 562 5800x2050.
E-mail address:Christopher.Lan@uottawa.ca (C.Q. Lan)

Keywords: Penetration time; Dope suspension viscosity; PVDF blend ratio; Hydrophilic SiO_2 nanoparticles; Membrane structure; Vacuum Membrane Distillation (VMD);

7-1- Introduction

Desalination has been shown to be a promising technology in compensating for the lack of fresh water throughout the world [1-11]. Membrane Distillation (MD) is deemed to have the potential of being developed into an appropriate alternative for Reverse Osmosis (RO) in the desalination market [12-22]. While currently the cost of pure water production of MD is still much higher than that of RO, this goal seems to be achievable by establishing an MD process that can be operated with small energy consumption, and by developing high performance MD membranes of large flux and good durability [23-26].

Tremendous efforts have been made in the past decade to develop membranes for MD applications [27]. More recently, researchers have begun to explore the possibility of improving MD membrane performance by surface modification [28-30], use of polymeric additives [27, 31], and incorporating nanoparticles in the membrane matrix [16, 20, 32-37]. Of particular relevance, recent studies of our group have found the use of hydrophilic nanomaterials such as CuO [16] and SiO_2 [33] to be effective in lowering the thickness of the sponge-like layer and enlarging the surface membrane pore size, thus increasing the flux. We found that the incorporation of 7.0 wt.% hydrophilic silica nanoparticles in a polymer solution together with the use of a Non-Woven Fabric (NWF) backing material could increase the pure water flux of the neat Vacuum Membrane Distillation (VMD) PVDF membrane by 2456%, achieving a flux of almost 12.7 kg/m^2h at a feed temperature of 27.5 °C [33]. Nevertheless, although the incorporation of hydrophilic silica nanoparticles was found not to compromise the membrane surface hydrophobicity, the membranes thus made only had a Liquid Entry Pressure of water (LEP_w) of 18 psig [33], highlighting an important aspect of the membrane that needs further improvement.

On another related recent development, it was demonstrated that blending PVDF of two different molecular weights could significantly affect the membrane properties and VMD performance, hypothetically due to the varied viscosities of the dope solution thus prepared [38, 39]. These two PVDF polymers of different molecular weights were miscible and the casting solutions made of them were stable at all compositions. This previous research suggests that the polymer blend of an appropriate ratio could enhance VMD performance by improving the membrane structure [38].

These studies, however, were carried out in the absence of nanoparticles with a relatively small VMD fluxes in comparison with the membranes incorporated with appropriate amounts of silica nanoparticles. It would therefore be of interest to investigate the effects of the polymer ratio on membrane properties and performance in the presence of silica nanoparticles.

In the fabrication of membranes using the Diffusion Induced Phase Separation (DIPS) approach, which is also widely used in preparation of MF and UF membranes, the dope solution is first cast on a supporting surface, and then, after being put in a controlled environment for a certain period of time for a thin film to form, is immersed in a non-solvent which is typically water at a certain temperature to induce the phase inversion and formation of membrane. Extensive studies with UF membranes [40-43] have shown that the evaporation time, which is the term used by the researchers to describe the period between the time when the film of dope solution is cast on the supporting surface and the time when the film is submerged in a non-solvent medium (e.g., water) to induce phase inversion, has significant impacts on the properties of corresponding membranes. It was demonstrated that longer evaporation time in the fabrication of UF membranes would generally result in a denser membrane with smaller surface pore size, lower water flux, and slightly higher rejection characteristics [40-42, 44-46]. Nevertheless, although the potentially significant effects of evaporation time have been noted previously [47], very few works have been done to explore these effects in the development of MD membranes. One example of related research involves the use of surface modifying macromolecules (SMM) to increase the hydrophobicity of Poly(ether sulfone) (PES) membranes. It was found that the surface contact angle increased with the evaporation time when SMM were employed, hypothetically by allowing enough time for SMM to migrate onto the membrane surface [43].

It should be pointed out that the term evaporation time could be misleading to a certain extent since it suggests that partial solvent evaporation is the primary cause for the observed effects of this particular treatment, i.e., film maturation, on membrane properties. However, while no evaporation data were presented in the aforementioned reports, significant solvent evaporation seems to be unlikely during the "evaporation time". As a matter of fact, during the period of this particular treatment in the fabrication of MF or UF membranes, the temperature was typically controlled in the range from 95 °C [40-42] to 110 °C [43], which is quite low compared to the normal boiling temperature of the solvent, *N*-Methyl Pyrrolidone (NMP) (i.e., 202 °C). In the case of PVDF MD membrane fabrication, film maturation is carried out at the ambient temperature for a

period of several minutes and the solvent used for dope solution preparation, i.e., N,N-Dimethylacetamide (DMAc), has a normal boiling point of 165.1 °C. As a logical consequence, little solvent evaporation was observed in this period. On the other hand, several minutes seem to be sufficient for part of the solvent to penetrate into the backing material. We therefore choose to use the term film-penetration time instead of evaporation time, although the latter has been used quite extensively in previous studies concerning MF and UF membranes. It is anticipated that different rates of penetration of the casting dope, depending on its viscosity, into the backing material in an MD membrane would result in different membrane structures and morphologies, and consequently different membrane performance.

In the current study, we systematically investigated the effects of two parameters, i.e., the ratio of PVDF polymers of different molecular weights and the film-penetration time, on the structure and performance of nanocomposite MD membranes, which is the first time such a research has been reported. It should be noted that nanoparticle concentration was maintained constant at 7.0 wt.% in the casting dope in this work according to the results of our previous study [33].

7-2- Materials and Methods

7-2-1- Materials

Kynar® 740, (Pellet, MW: 410 kDa, melt viscosity: 1850 ± 250 Pa.s; melting temperature: 160.1 ºC) and Kynar® HSV900 (Powder, MW: contains 24.92% 92,840 kDa and 75.08% 1367 kDa, melt viscosity: 4930 Pa.s; melting temperature: 165.1 ºC) as two different kinds of PVDF, were kindly provided by Arkema Inc. (Philadelphia, PA). In this study, the polymers are coded as L and H respectively. DMAc with a purity of 99.9% was purchased from Sigma–Aldrich. Hydrophilic amino modified SiO_2 nanoparticles with a purity of 99.8% and size of 10-20 nm were supplied by Skyspring Nanomaterials Inc. NWF polyester, Hollytex® 3396 was provided by Kavon Filter Products Co. (Farmingdale, NJ) and used as the substrate. Sodium chloride and n-butanol were supplied by Fisher Scientific and used as received.

7-2-2- Membrane Fabrication

The membranes were made by the phase inversion method. To this end, a polymeric solution of 15 wt.% PVDF, 83.75% wt.% DMAc and balance water was stirred for 72 h at 50 ºC with a

speed of 180 rpm. As mentioned earlier, the blend of Kynar® 740 and Kynar® HSV900 at different ratios was used as the host polymer. Then, a specific quantity of hydrophilic silica nanoparticles was added to the solution and the resulted mixture was subjected to vigorous agitation for 2 h to prepare the casting dope. Then the dope was cast on a backing material by using a casting bar to a thickness of 250 µm. After a penetration time of 15-30 s (called normal method), 2, 3, 4, 6, and 9 min, the cast film together with the backing material was immersed in the coagulation bath containing distilled water at 25 °C. The so fabricated membranes were left in the bath for 24 h while the water was replaced with fresh distilled water several times to make sure that the solvent has been thoroughly removed from the membrane matrix. Finally, membranes were dried at ambient temperature to be used for characterizations and VMD tests.

7-2-3- Membrane Characterization

To study the effects of the PVDF blend ratio and penetration time on the membrane structure, the supported membranes were subjected to structural examination including top-view and cross-sectional Scanning Electron Microscope (SEM) analysis, elemental mapping by Electron Dispersion Spectroscopy (EDS), surface pore size, porosity, thickness, surface hydrophobicity, and roughness measurements. All the membranes were also tested for VMD performance evaluation.

7-2-3-1- Morphology

The surface and cross-section of the membranes were studied by SEM (SEM, Vega-II XMU VPSEM and Anatech Hummer VII). PVDF distribution within the membrane matrix was studied by the fluorine mapping via EDS analysis (EDX, Oxford Inca Energy 250X EDX). To prepare the samples for cross-sectional analysis, a small piece of membrane was cut by very sharp scissors after immersion in liquid nitrogen for 15-20 s. The samples were then either gold (for SEM) or carbon (for EDS) sputtered to make them conductive and ready for analysis.

7-2-3-2- Pore Size

More than 200 pores were randomly chosen from the top surface SEM images and the pore size was measured via ImageJ software assuming the pores are circular and the average value was

recorded. This method was successfully employed elsewhere [16, 48-52]. Maximum pore size was reported as the average of the top 10% biggest pores among the measurements.

7-2-3-3- Porosity

Membrane porosity was measured by the wet and dry method [16]. The membrane samples were immersed in n-butanol for 12 h to ensure that the membrane pores were completely filled with the liquid. Afterward, the wet membranes were oven dried at 50 °C for 24 h. The porosity was calculated based on the weight difference between the wet and dry membrane according to equation 7-1 where w_1 andw_2 are the weight (g) of the wet and dry membrane, respectively, and A (cm^2), δ (cm), and ρ (g/cm^3) represent the membrane effective surface area and thickness, and the density of n-butanol, respectively.

$$\%\varepsilon = \frac{w_1\text{-}w_2}{A.\delta.\rho} \times 100 \qquad (7\text{-}1)$$

It should be mentioned that residual solvent on the membrane surfaces was removed before weighing the wet samples. Three samples were used for each membrane and the average value was reported.

7-2-3-4- Thickness

The entire membrane thickness was measured by using a digital micrometer. The measurement was made at more than four different spots of each membrane sheet and the average value was calculated. The top layer (defined as the layer formed above the backing material) thickness was measured using the SEM cross-sectional images. For this purpose, at least 6 different cross-sectional images of the same membrane were taken into consideration.

7-2-3-5- Viscosity of Dope Suspension

Viscosity of the casting dope was measured by a rotational rheometer (Brookfield, Synchro-Lectric viscometer model: LVF) at 25 ºC. The viscosity measurement was repeated at least three times by using an appropriate spindle and motor speed, and the average value was recorded.

7-2-3-6- Wettability

Membrane surface hydrophobicity was assessed by measuring the surface contact angle. A VCA Optima Surface Analysis System (AST Products, Inc. Billerica, MA) was used for this purpose. Different sites on the membrane surface were arbitrarily chosen and the contact angle was measured by placing a 2 μL droplet on the selected spot. The contact angle is reported as the average of at least ten different measurements.

7-2-3-7- Roughness

ImageJ and its plugin *Roughness Calculation* [53] were applied to the top-view SEM images for evaluating the surface roughness of the membranes. This measuring tool was already demonstrated to be an appropriate approach for estimating film roughness [16, 38, 39, 48, 51]. The details of the method are given elsewhere [16].

7-2-4- Membrane Performance

The performance of the developed membranes in this study was evaluated in terms of LEP_w, membrane permeability, and salt rejection. The details of the methods are as follows.

7-2-4-1- Liquid Entry Pressure of Water (LEP_w)

The experimental setup for measuring the LEP_w is presented elsewhere [16]. It consists of a static cell which was filled with distilled water. The cell was connected to a nitrogen cylinder which was equipped with a pressure regulator to control the pressure. Pressure was read by an inline pressure gauge. To obtain the LEP_w for each membrane, pressure was increased stepwise at an interval of 2 psig. The pressure was kept constant for 10 min at each step to observe if the liquid exited from the cell outlet. The pressure at which the liquid appeared at the cell outlet was recorded as the LEP_w. The test was repeated with at least three different membrane coupons, and the average value was reported.

7-2-4-2- Permeability

Membrane permeability was measured by a laboratory made VMD test unit (Fig. 7-1). The experimental procedure is given in our previous works [16, 34]. Briefly, a cylindrical vessel of ca

300 mL was used as the VMD permeation cell. After mounting the membrane on a sintered metal plate placed at the bottom of the cell, liquid (water) was filled in the feed chamber and the permeate side of the cell was connected to a vacuum pump. The feed temperature was controlled by a heating tape wrapped around the cell. Vacuum was controlled on the permeate side by a pressure transducer to generate the required driving force for the process. As a result of vapor pressure difference between two sides of the membrane, the vapor was transported through the membrane and collected in a cold trap which was cooled by liquid nitrogen.

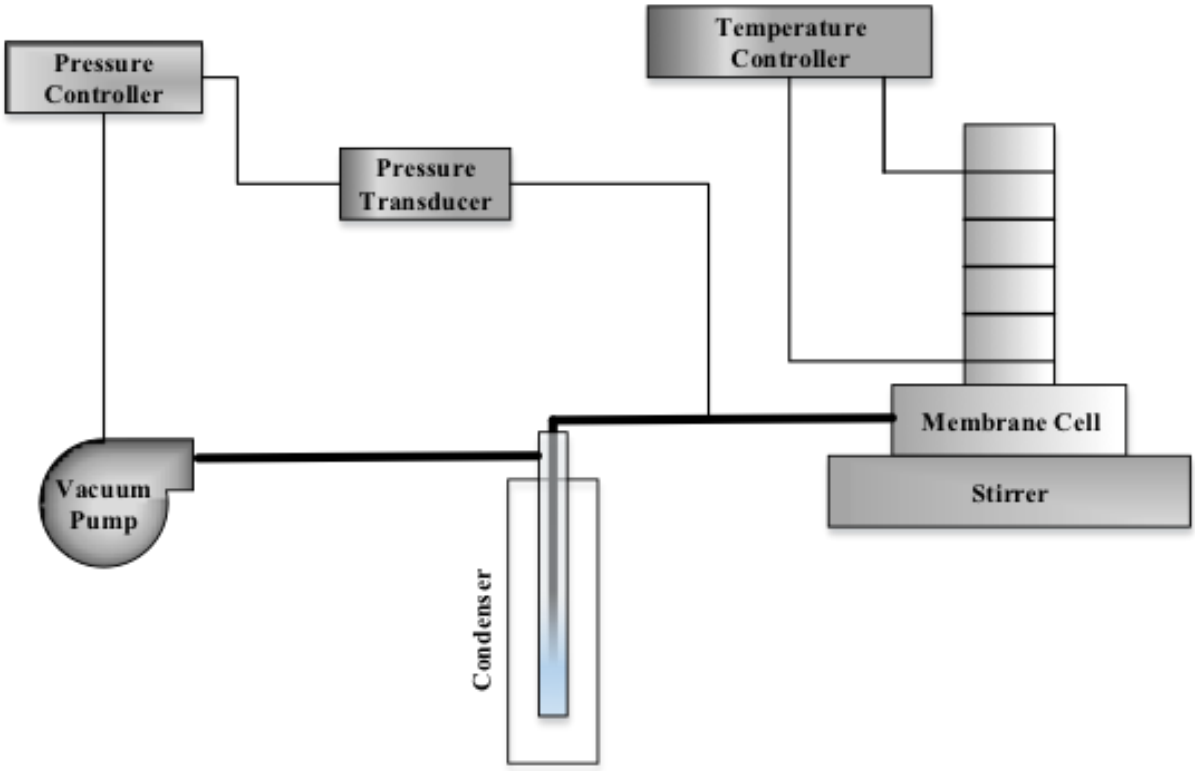

Fig. 7-1 Experimental VMD setup [16]

VMD flux was calculated by equation 7-2 where *J*, *w*, *A*, and *t* are flux (g/m^{2}h), mass of the collected permeate (g), effective surface area of the membrane (0.001134 m^2), and filtration time (h) respectively.

$$J = \frac{w}{A.t} \qquad (7\text{-}2)$$

The VMD test was repeated at least six times for each membrane and the average value was reported.

7-2-4-3- Rejection

The salt rejection ability was assessed using a feed aqueous solution of 35 g/L NaCl. The rejection, *R* was calculated by equation 7-3, where C_f and C_p are the feed and permeate conductivity (µS) respectively.

$$\%R = \frac{C_f - C_p}{C_f} \times 100 \quad (7\text{-}3)$$

Solution conductivity was measured by a conductivity meter (OAKTON, CON 2700).

7-3- Results and Discussion

7-3-1- Effect of Ratio of PVDF Polymers of Different Molecular Weights

7-3-1-1- Viscosity Change

The viscosity of the dope suspension at varied concentration of the hydrophilic SiO_2 nanoparticles and ratio of PVDF polymers of high (H) and low (L) molecular weights (i.e., the H:L ratio) are presented in Fig. 7-2. Fig. 7-2-a shows the effect of the polymer blend ratio (H:L) on the viscosity when the nanoparticle loading was fixed to 7.0 wt.%, while Fig. 7-2-b shows the effect of the nanoparticle concentration when the polymer ratio is constant at H:L = 2:8.

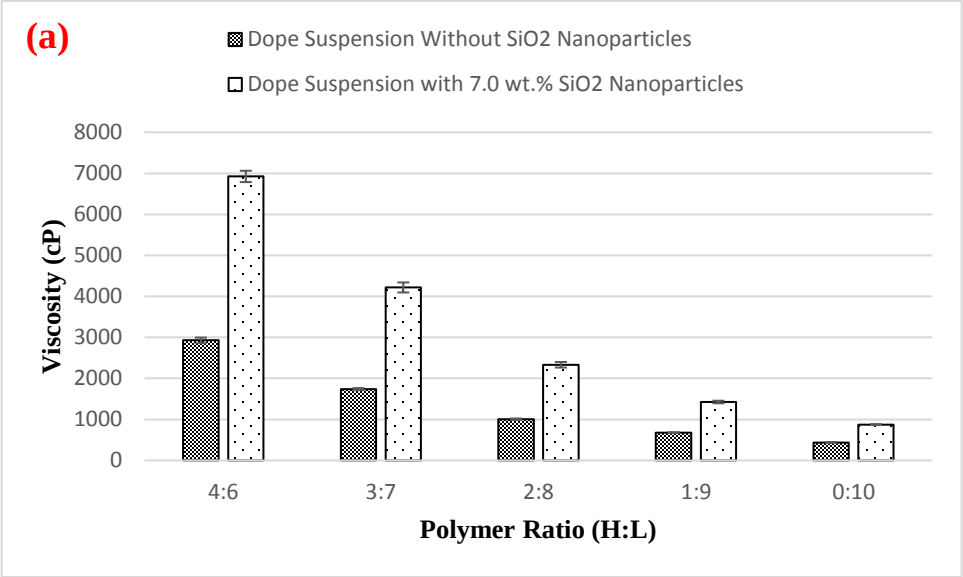

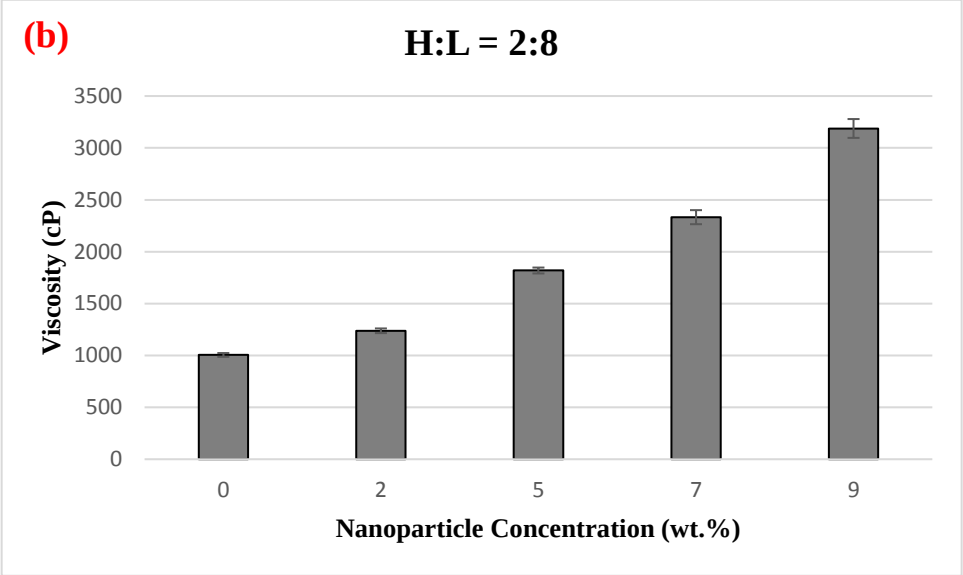

Fig. 7-2 Dope suspension viscosity vs. (a) polymer ratio in the presence (7.0 wt.% SiO_2) and absence of nanoparticles and (b) nanoparticle concentration at H:L = 2:8 at 25 ºC

As shown in Fig. 7-2, the suspension viscosity decreased with a decrease in (H:L) ratio and increased with nanoparticle concentration. The linear increase in the viscosity of the suspension with concentration of the silica nanoparticles in Fig. 7-2-b shows the stability of the suspensions [54].

7-3-1-2- Thickness of the Top Layer

Fig. 7-3 presents the effect of the (H:L) ratio and casting dope viscosity on the top layer (PVDF/SiO_2 layer above the backing material) thickness. From now on, the silica content and penetration time are maintained constant at 7.0 wt.% and 3 min, respectively, when the H:L ratio is changed.

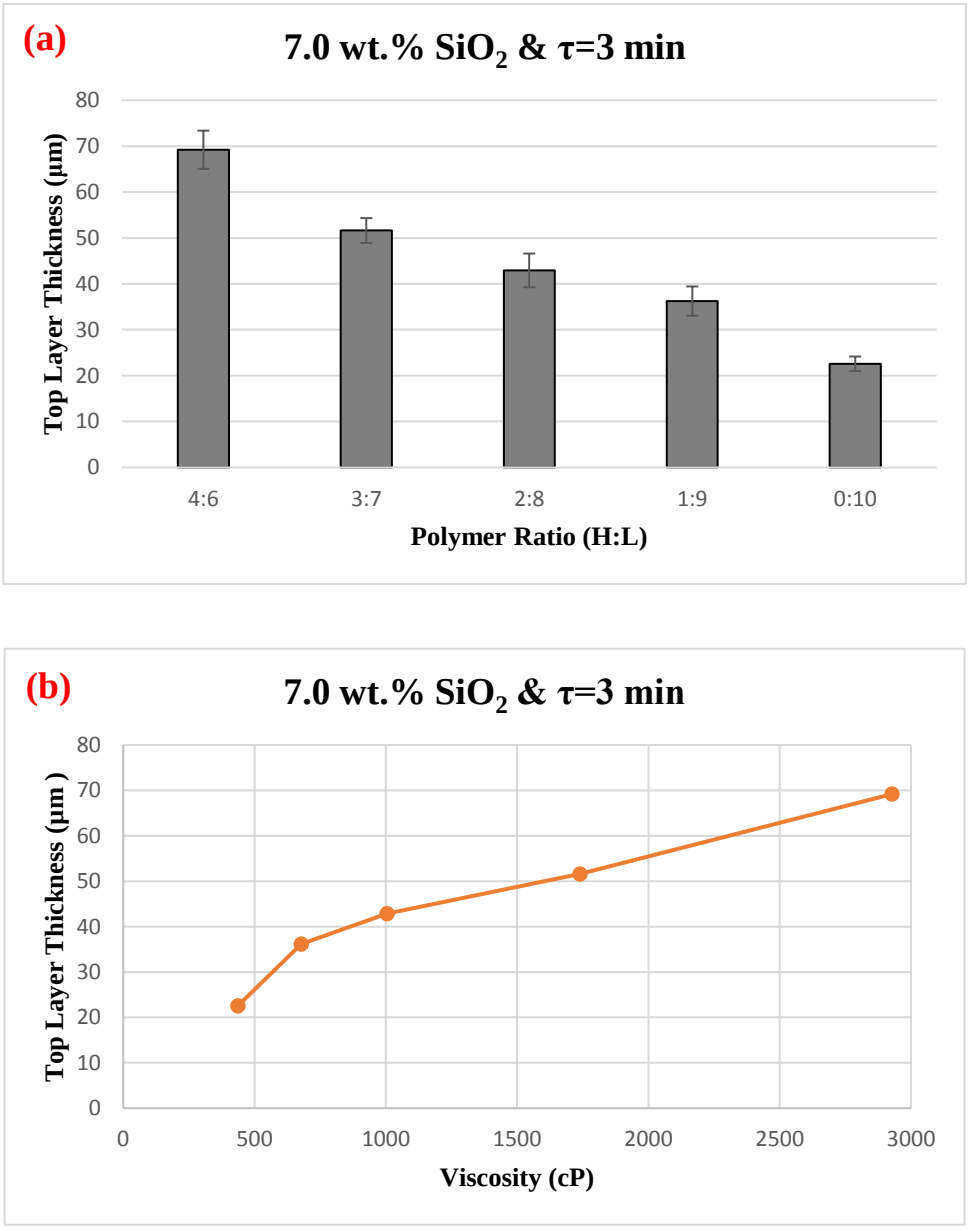

Fig. 7-3 Top layer thickness vs. (a) H:L ratio and (b) casting dope viscosity in the presence of 7.0 wt.% SiO_2 nanoparticles

with a penetration time of 3 min

From Fig. 7-3-a, the top layer thickness decreased with a reduction in H:L ratio. In Fig. 7-3-b, an almost linear increase in the top layer thickness versus viscosity of the casting dope suspension is observed. It is hypothesized that more casting dope penetrated into the backing material pores as the viscosity decreased due to a reduction in the portion of high molecular weight PVDF in the dope, reducing the amount of casting dope left on the top of the backing material. Fig. 7-4 shows EDS fluorine mapping across the membrane cross-section for two membranes with different H:L ratios, i.e. 2:8 and 0:10, and at the same penetration time, i.e. τ = 3 min.

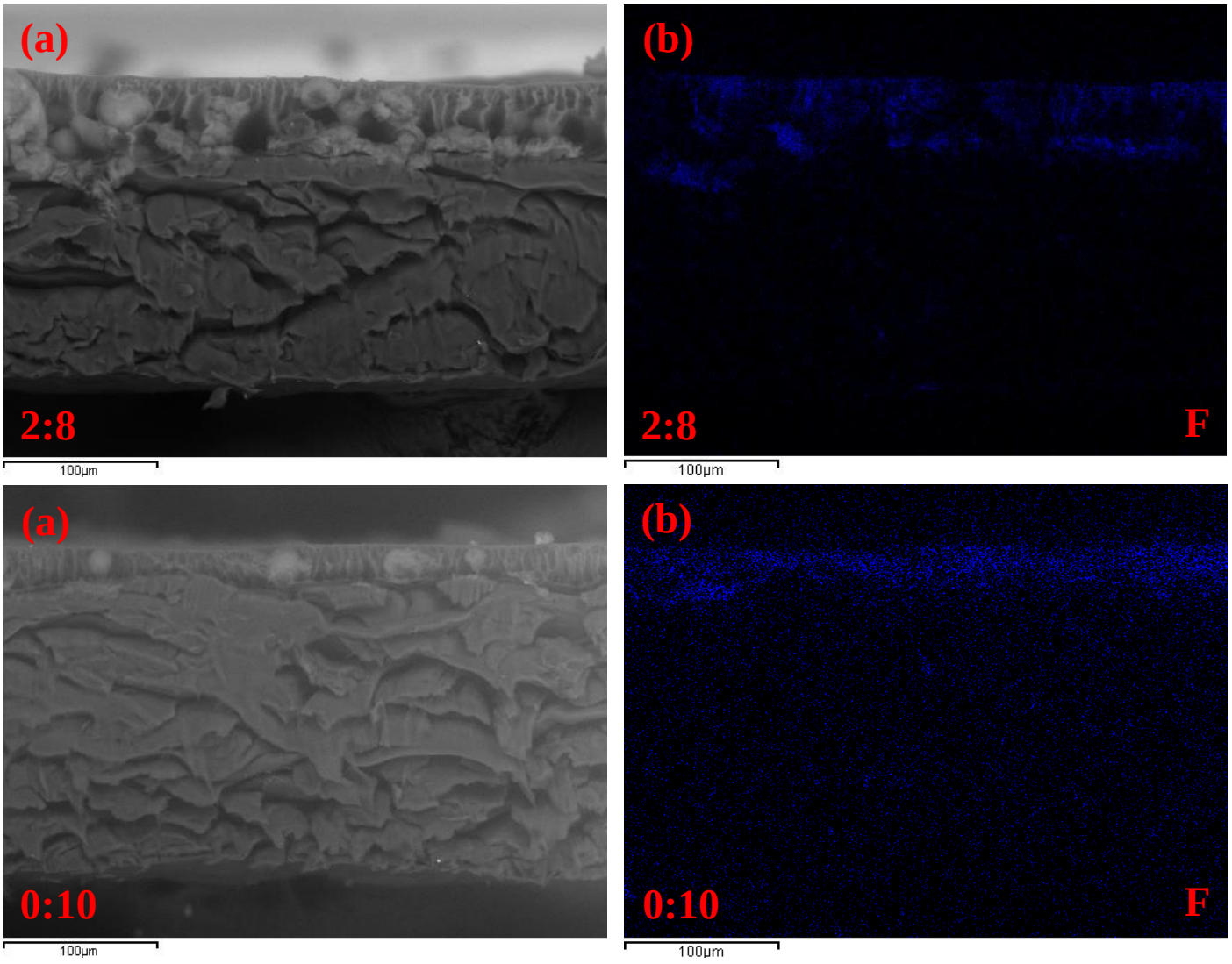

Fig. 7-4 Cross-sectional (a) SEM and (b) EDS fluorine mapping for the membranes with a H:L ratio of 2:8 and 0:10 for a penetration time of 3 min

In Fig. 7-4-b the bright spots represent fluorine atoms of PVDF. It is clear from the figure that the top PVDF layer becomes thinner while more PVDF penetrates into the backing material as the dope suspension viscosity decreases with an H:L ratio from 2:8 to 0:10.

7-3-1-3- Surface Morphology

The SEM images for different H:L ratios are given in Fig. 7-5. According to the figure, the surface morphology looks similar among the first three H:L ratios, i.e., 4:6, 3:7 and 2:8, which is distinctively different from those at 1:9 and 0:10. The pore size also became significantly larger at small H:L ratios (i.e., 1:9 and 0:10).This is confirmed by the results shown in Fig. 7-6-a. On the basis of the ANOVA analysis, the change in pore size is not significant when the H:L ratio changes in the range from 4:6 to 2:8 or from 1:9 to 0:10 ($P > 0.05$). However, the pore size changes significantly from the H:L ratio of 2:8 to 1:9 ($P < 0.05$). It should be noted that the error bars, which represent the standard deviation, do appear to overlap with each other even when 2:8 and 1:9 are compared. However, the statistical analysis results show that the difference between these two samples is significant due to the large sample sizes (*n* is in the range of 221-673).

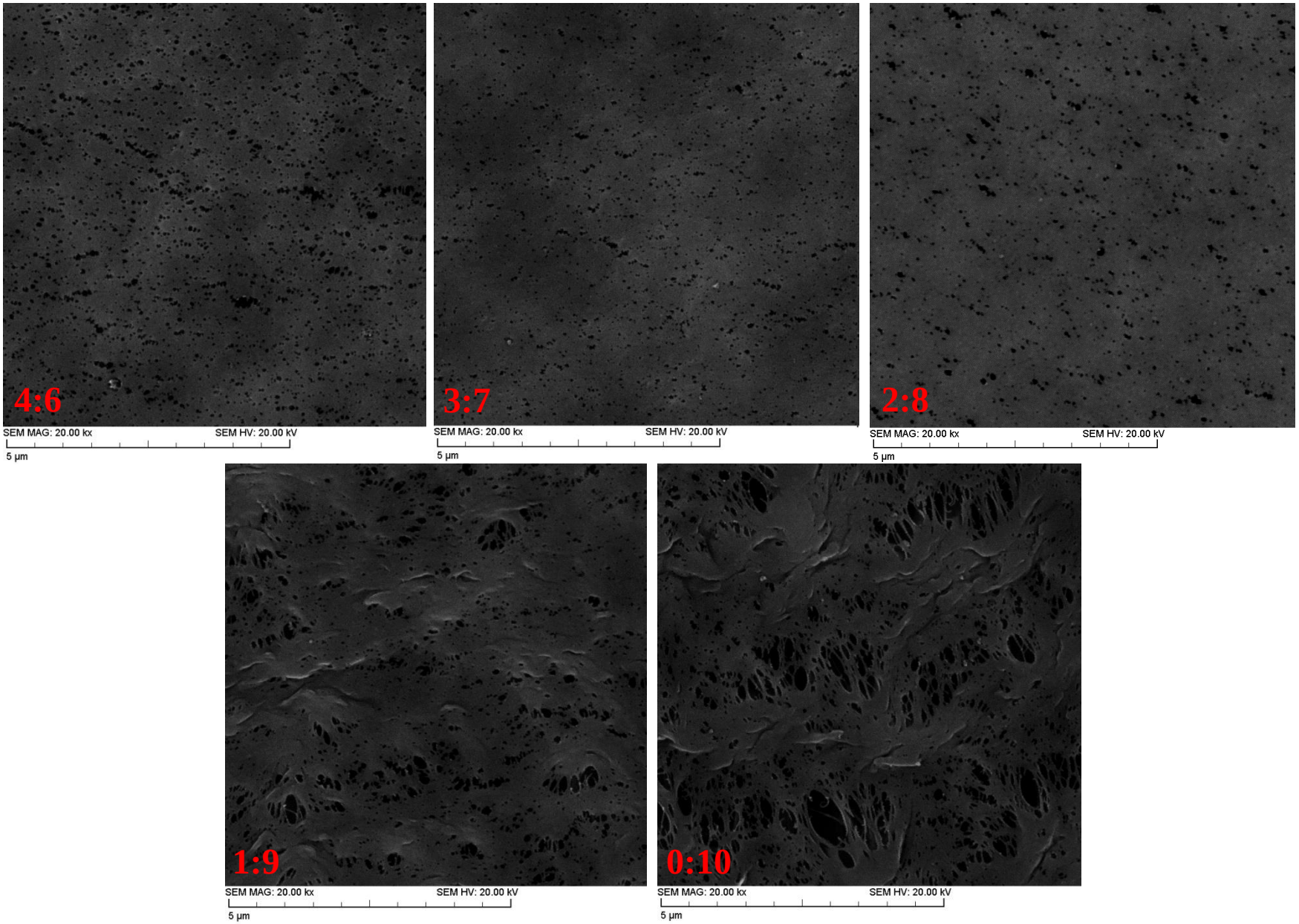
4:6
SEM MAG: 20.00 kx
SEM HV: 20.00 kV
5 µm
3:7
SEM MAG: 20.00 kx
SEM HV: 20.00 kV
5 µm
2:8
SEM MAG: 20.00 kx
SEM HV: 20.00 kV
5 µm
1:9
SEM MAG: 20.00 kx
SEM HV: 20.00 kV
5 µm
0:10
SEM MAG: 20.00 kx
SEM HV: 20.00 kV
5 µm

Fig. 7-5 Top surface SEM images of the supported SiO_2/PVDF membranes of different H:L ratios (nanoparticles concentration, 7.0 wt.%, penetration time,3 min) The surface pores are specified by the black spots in top surface

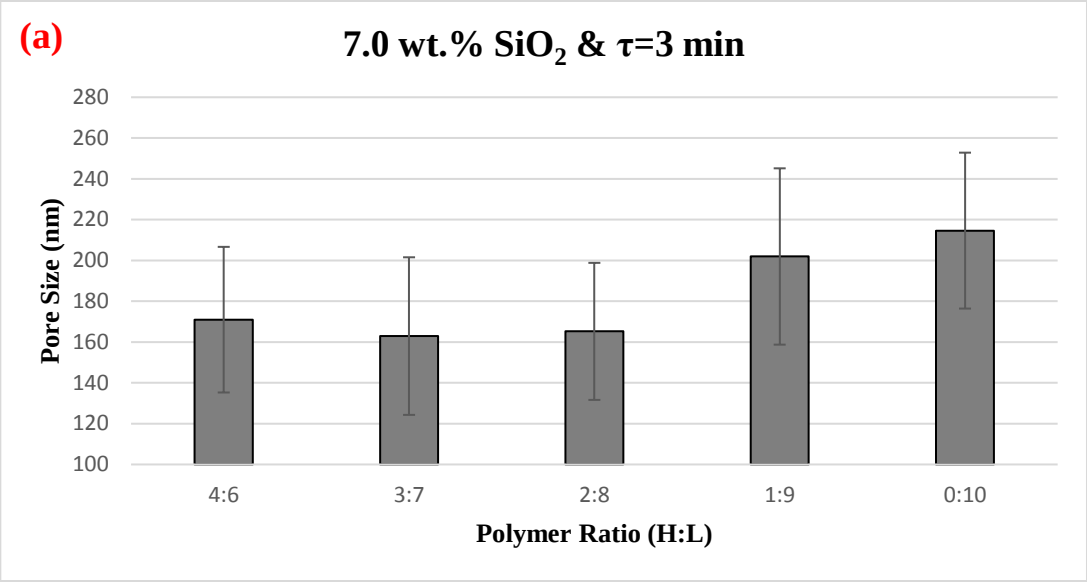

Fig. 7-6-a Surface pore size vs. H:L ratio (nanoparticle concentration,7.0 wt.%; penetration time, 3 min)

7-3-1-4- Porosity

From Fig. 7-6-b, porosity increased slightly with the decrease of H:L ratio down to 2:8 ($P > 0.05$). This is because of the increase in the solvent/non-solvent exchange rate with the decrease in viscosity. As a result, more non-solvent (water) was drawn into the membrane. The porosity however decreased slightly with the further reduction in H:L ratio ($P > 0.05$). This is because the casting solution that has penetrated deeper into the pores of the backing material was coagulated and packed densely in the pore.

It is noteworthy that, due to challenges in peeling off the top layer from the substrate, the porosity reported here is the overall porosity. Furthermore, the thickness of the substrate (152 µm) was several times of that of the top layer, which was in the range of 22.6 – 69.2 µm. As a result, the substrate porosity, which is reported to be as low as 11.5% [49, 55], had a significant contribution to the overall porosity. In other words, both the values and the variations of the porosity of the top layer at different polymer ratios should be much larger than what are reported in Fig. 7-6-b.

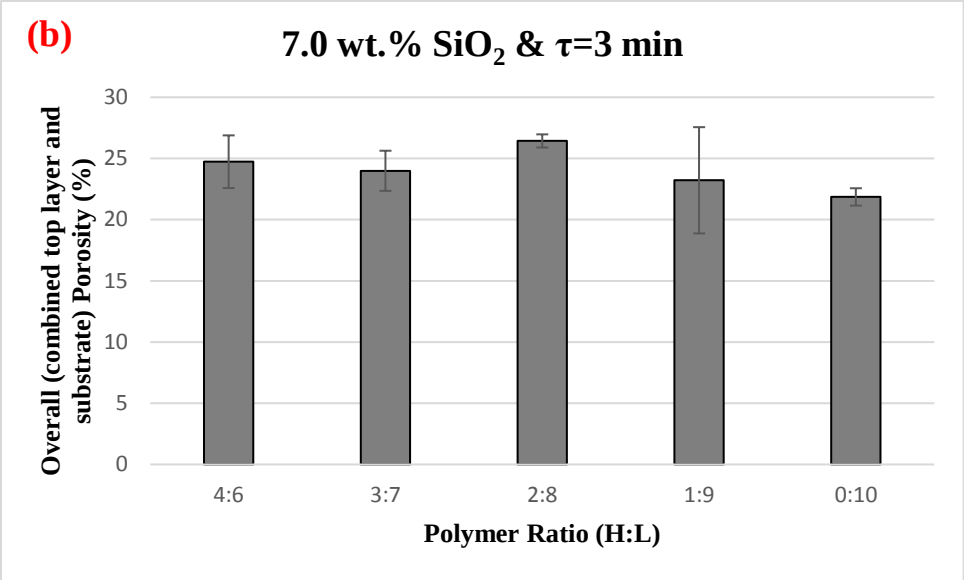

Fig. 7-6-b Overall (combined top layer and substrate) porosity vs. H:L ratio (nanoparticle concentration,7.0 wt.%; penetration time, 3 min)

7-3-1-5- Surface Contact Angle and Roughness

In Fig. 7-6-c, Contact angle decreased with the H:L ratio, which was especially notable when the H:L ratio was below 2:8. This could be explained tentatively by the large pore size observed at the membrane surface, into which water entered flattening the water droplet on the membrane surface. It should be noted that it has been demonstrated repeatedly in this and previous studies that PVDF membranes with a contact angle of much less than 90° still have a LEP_w that would allow the application of such membranes for VMD [16, 33, 34, 38, 39, 49], indicating that a contact angle of 90° is not necessarily the criterion to determine the applicability of a membrane for VMD experiments. What really matters is the LEP_w of a membrane, which is dependent not only on the contact angle but also on the pore size according to the Laplace equation [56].

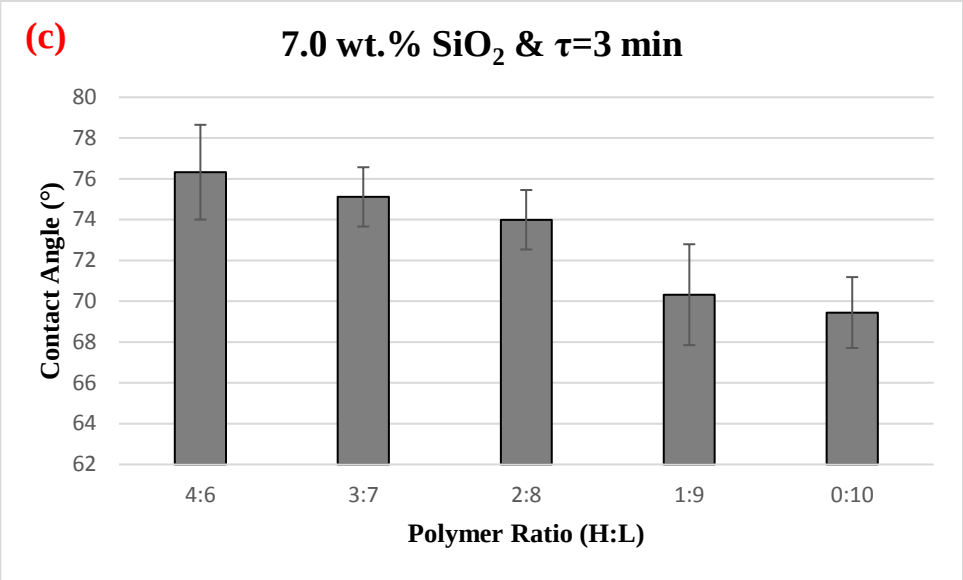

Fig. 7-6-c Contact angle vs. H:L ratio (nanoparticle concentration,7.0 wt.%; penetration time, 3 min)

Surface roughness analysis is provided in Table 7-1 to further interpret the change in surface contact angle as the dope suspension viscosity changes.

Table 7-1 Surface roughness analysis of the 7.0 wt.% hydrophilic SiO_2 incorporated nanocomposite membranes vs. H:L ratio by ImageJ and its plugin Roughness Calculation (all the units in pixel)

Polymer Ratio (H:L) Penetration time (3 min)	**Rq: Root mean square deviation**	**Ra: Arithmetical mean deviation**
4:6	60.8±0.7	59.7±0.8
3:7	59.0±0.2	57.6±0.3
2:8	56.0±0.2	54.5±0.1
1:9	53.5±0.3	51.9±0.1
0:10	50.6±0.7	48.5±0.4

According to Table 7-1, the surface roughness parameters decreased with the decrease in H:L ratio. The change in the surface hydrophilicity with the H:L ratio could be further attributed to the surface roughness as a smoother surface resulted in a slightly less hydrophobic surface.

7-3-1-6- LEP_w

LEP_w in Fig. 7-6-d shows a maximum at H:L = 2:8.

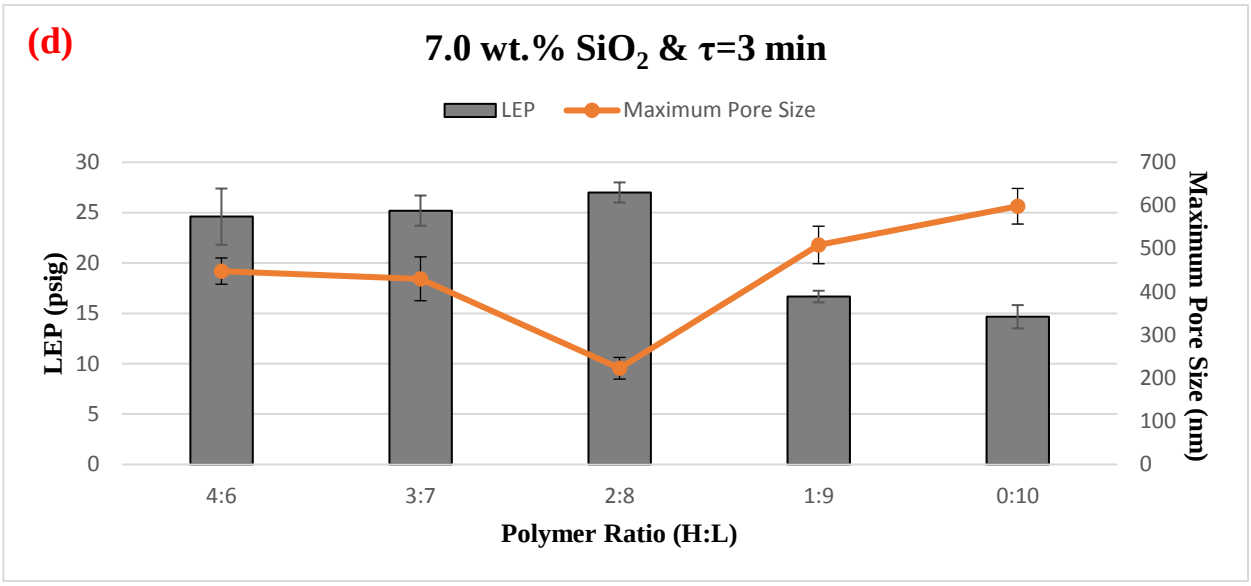

Fig. 7-6-d LEP_w and maximum pore size vs. H:L ratio (nanoparticle concentration,7.0 wt.%; penetration time, 3 min)

It is worth mentioning that, as shown in Fig. 7-6-d, the maximum pore size was 222.9 nm at H:L ratio 2:8, which is approximately half of that at 4:6 and 3:7 and one third of that at 0:10. The LEP_w was determined by the interaction of two different membrane properties, the maximum pore size and hydrophobicity as represented by the contact angle [56]. Fig. 7-6-c reports a decrease in contact angle, which predicts a decrease in LEP_w, with an increase in H:L ratio. However, Fig. 7-6-d shows a minimum of the maximum pore size at H:L ratio 2:8, which corresponds to the largest LEP_w of 27.0 psig at a maximum pore size of 222.9 nm, which was 51.8% of that at 3:7 (430.1 nm) and 43.8% of that at 1:9. These results seem to suggest that the effect of the remarkably small maximum pore size at the H:L ratio of 2:8 was more dominant than the decreasing contact angle. The significantly small LEP_w value at 1:9 and 0:10, on the other hand, appears to be the concerted effect of small contact angle and large maximum pore size under these conditions. It should be pointed out that statistical analysis demonstrated that the difference in LEP_w from 4:6 to 3:7 and 1:9 to 0:10 is not significant ($P > 0.05$), however, the P-value is less than 0.05 from 3:7 to 2:8 and 2:8 to 1:9 showing the significance of the difference between the maximum LEP_w and LEP_w for blend ratios of 3:7 and 1:9. In addition, ANOVA analysis proved that the maximum pore size at the H:L ratio of 2:8 is significantly lower than the other data points.

7-3-1-7- VMD Flux

In Fig. 7-6-e, VMD pure water flux keeps increasing with a reduction in the H:L ratio. This is ascribed to a decrease in the thickness of the membrane top layer (Fig. 7-3) and an increase in pore size (Fig. 7-6-a) with a decrease in the H:L ratio. It is noteworthy that a flux of around 21.3 kg/m^{2}h was achieved at H:L = 0:10, which represents the pure low molecular weight PVDF. However, this membrane could not last more than one VMD cycle (1.5 h), which is attributed to its weak mechanical strength.

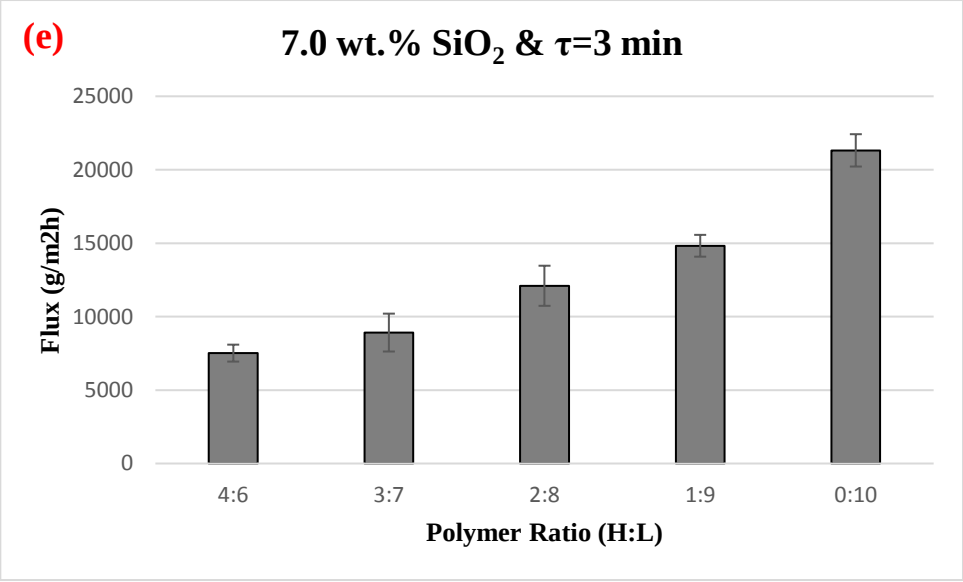

Fig. 7-6-e Pure water flux vs. H:L ratio (nanoparticles concentration, 7.0 wt.%; penetration time, 3 min; feed temperature, 27.5 °C; downstream pressure: 1.2 kPa)

7-3-2- Effect of Film-Penetration Time (τ)

The effects of the penetration time (τ) on the membrane properties and performance were studied. The nanoparticle concentration and H:L ratio are maintained constant at 7.0 wt.% and 2:8, respectively, while penetration time was changed from 0.25-0.50 minutes up to 9 minutes.

7-3-2-1- Thickness of the Top Layer

Fig. 7-7 shows the effect of penetration time on the thickness of the top layer.

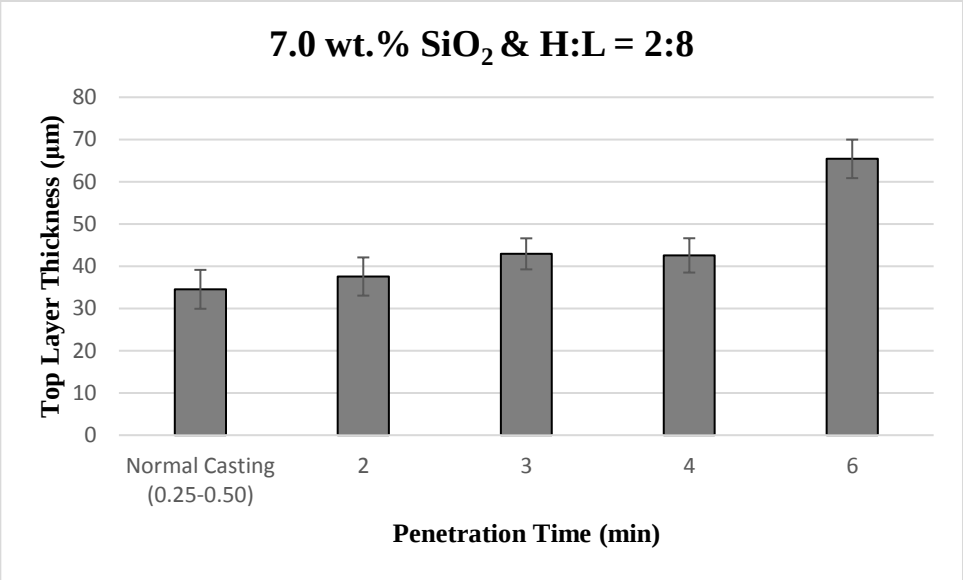

Fig. 7-7 Top layer thickness vs. penetration time at a polymer ratio of H:L = 2:8 in the presence of 7.0 wt.% SiO_2 nanoparticles

From Fig. 7-7, the top layer thickness increases with penetration time when the penetration time is equal to or less than 6 min ($P < 0.05$ when τ changes from 2 to 3 and 4 to 6). This result is quite interesting and unexpected since more casting dope is supposed to flow into the substrate pores and less casting dope is left behind for the top layer formation as the penetration time increases.

The results shown in Fig. 7-7 can be tentatively interpreted in the following way. PVDF macromolecules are entangled in the casting dope, forming a polymer gel around the nanoparticles. The formation of such polymer/nanoparticles gel is evidenced by an increase in viscosity upon addition of the nanoparticle into the polymer solution (Fig. 7-2). During the film-penetration period, both polymer/nanoparticle gel and solvent enter into the substrate pores but it is the solvent that enters preferentially, leaving behind the concentrated polymer/nanoparticle gel as the nascent top layer. The penetration, however, still causes the loss of a small amount of polymer with the solvent into the matrix of the backing material, resulting in the thinning of the top layer. On the other hand, when the top layer is brought into contact with non-solvent (water) in the coagulation bath, solvent/non-solvent exchange takes place and the top layer swells as the non-solvent migrates into the top layer, which is evidenced later by the porosity increase with increasing penetration time (Fig. 7-10-b), because non-solvent influx is greater than the solvent

outflux due to the hydrophilic nature of the nanoparticle. With an increase in penetration time, more polymer penetrates into the backing material with the solvent, causing more severe thinning. However, the concentration of polymer/nanoparticle gel increases as well and so does the top layer swelling more. Thus, the top layer thickness increases with the penetration time as far as the swelling surpasses the thinning. In other words, the top layer thickness is determined by two competing processes, i.e., thinning and swelling. The data shown in Fig. 7-7 seem to indicate that swelling was more dominant in the early stages of the penetration up to $\tau = 6$ min, however, for a longer penetration time, thinning became the controlling process since there was not sufficient polymer left on the top layer to swell. As evidence, when the penetration time was as long as 9 min, the nascent top layer became too thin to cover the entire surface of the backing material. The above hypothesis is further justified by Fig. 7-8, which shows the EDS fluorine mapping across the membrane cross-section for membranes of different penetration times.

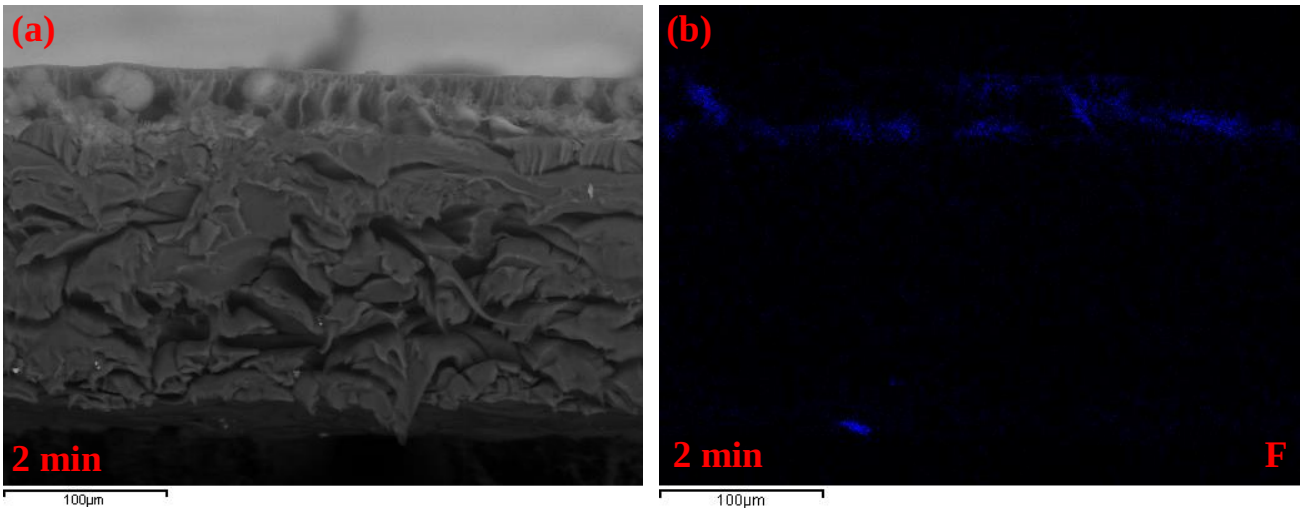
(a)
2 min
100µm
(b)
2 min
F
100µm

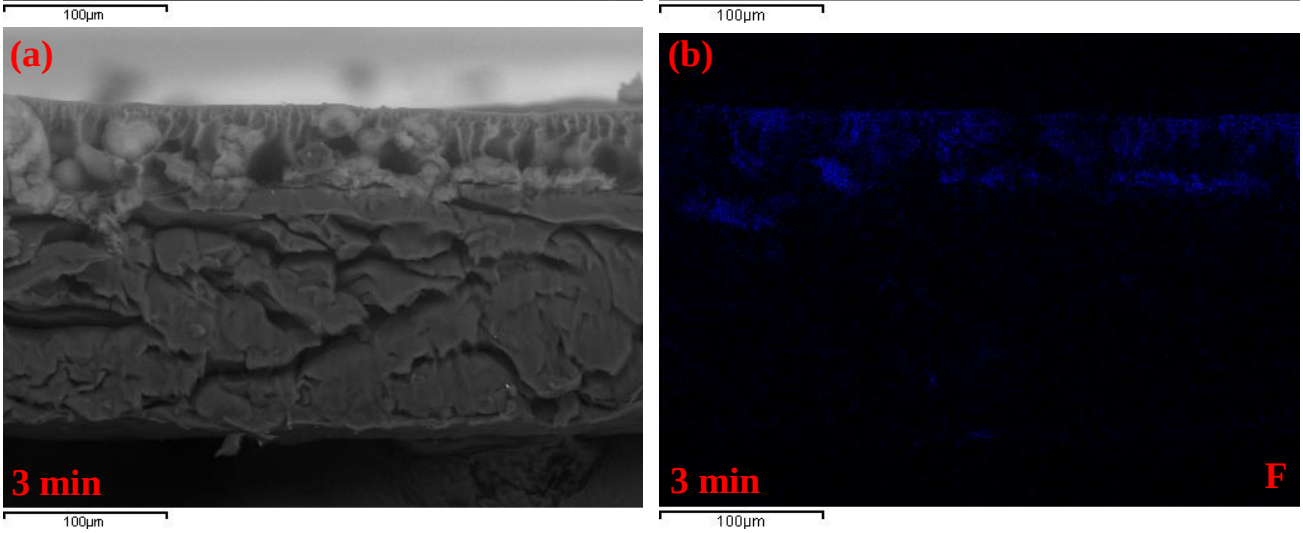
(a)
3 min
100µm
(b)
3 min
F
100µm

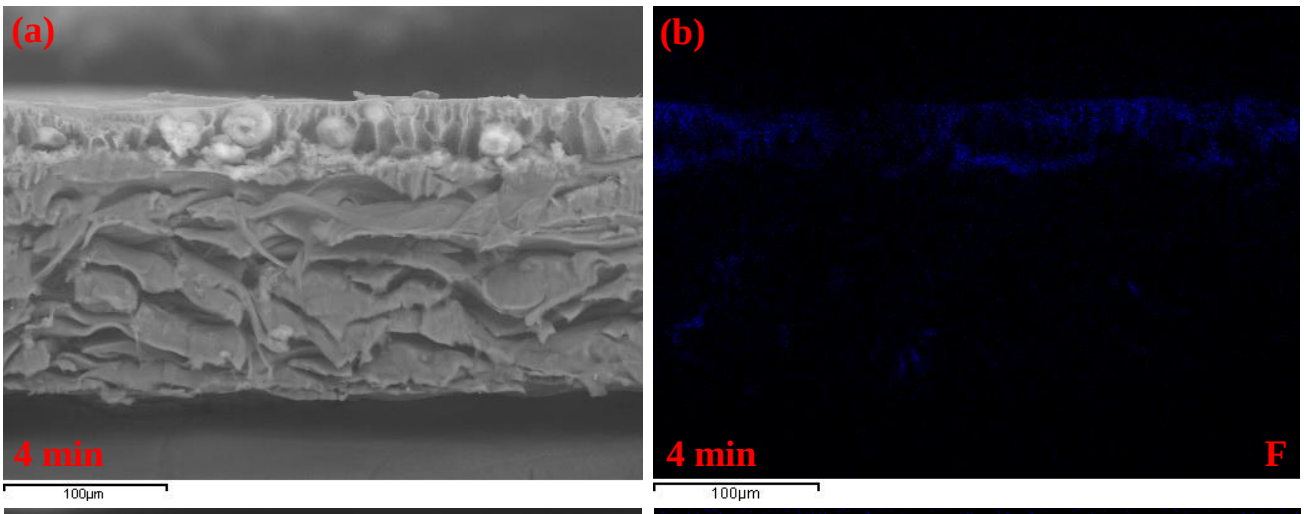
(a)
4 min
100µm
(b)
4 min
F
100µm

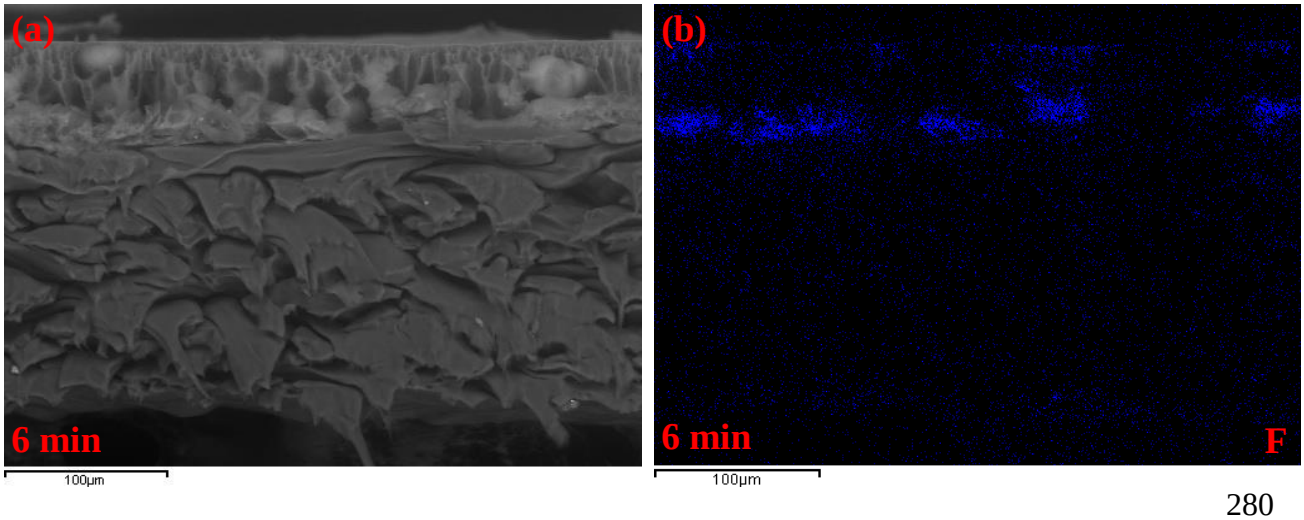
(a)
6 min
100µm
(b)
6 min
F
100µm

Fig. 7-8 Cross-sectional (a) SEM and (b) EDS fluorine mapping for membranes with different penetration times, the nanoparticles concentration, 7.0 wt.%, the PVDF ratio, H:L = 2:8

From Fig. 7-8-b, the thickness of the bright surface layer increases as the penetration time increases, corresponding to the thickening of the top PVDF layer shown in Fig. 7-8-a. The bright spots are hardly observed in the backing material until the penetration time becomes as long as 6 min. Even for 6 min, the color intensity in the backing material is much less than Fig. 7-4-b for the PVDF ratio of 0:10. By comparing Figs. 7-4 and 7-8, therefore, it could be concluded that the penetration of PVDF into the backing material was suppressed to a much lower level in the experiments where the effect of the penetration time was investigated.

7-3-2-2- Surface Morphology

Figure 7-9 shows the SEM images of the membrane surface.

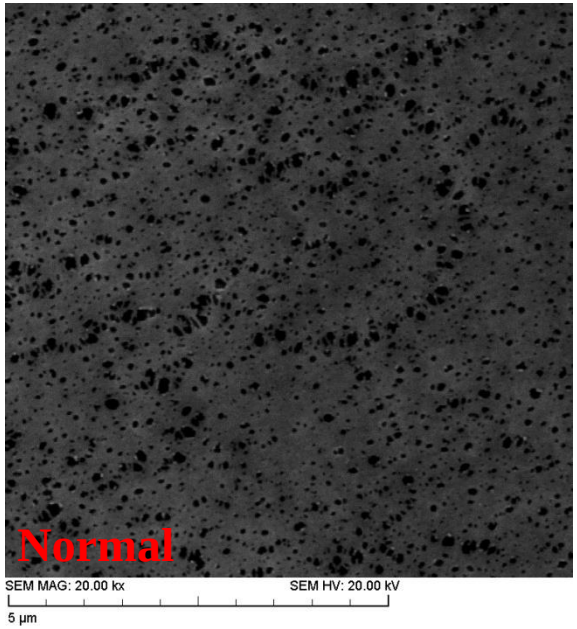
Normal
SEM MAG: 20.00 kx
SEM HV: 20.00 kV
5 µm

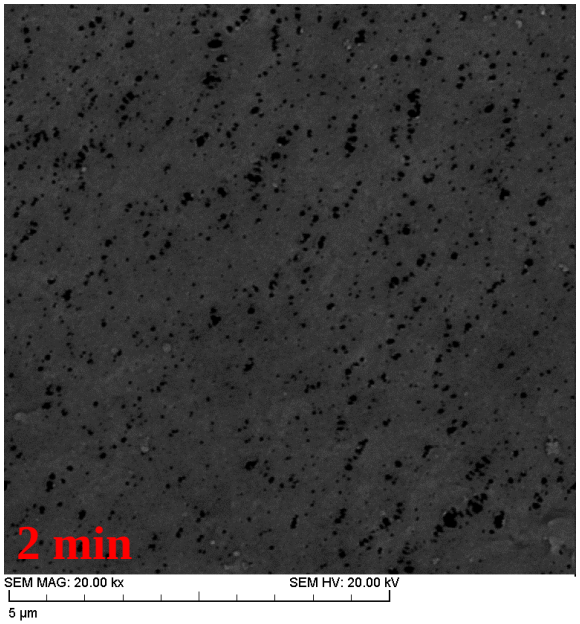
2 min
SEM MAG: 20.00 kx
SEM HV: 20.00 kV
5 µm

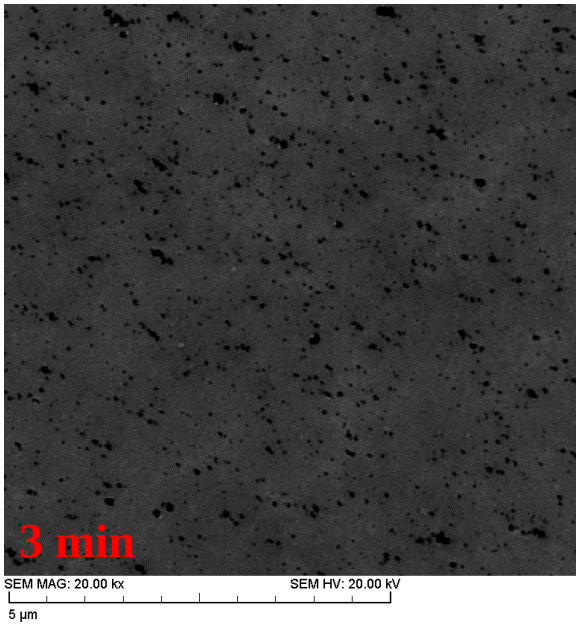
3 min
SEM MAG: 20.00 kx
SEM HV: 20.00 kV
5 µm

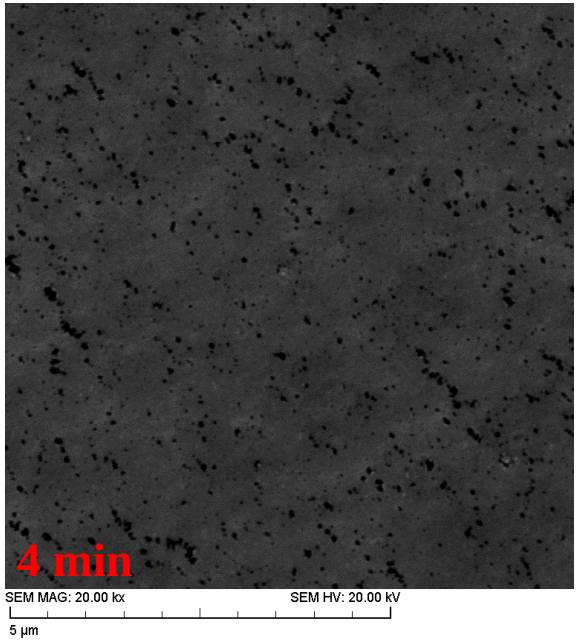
4 min
SEM MAG: 20.00 kx
SEM HV: 20.00 kV
5 µm

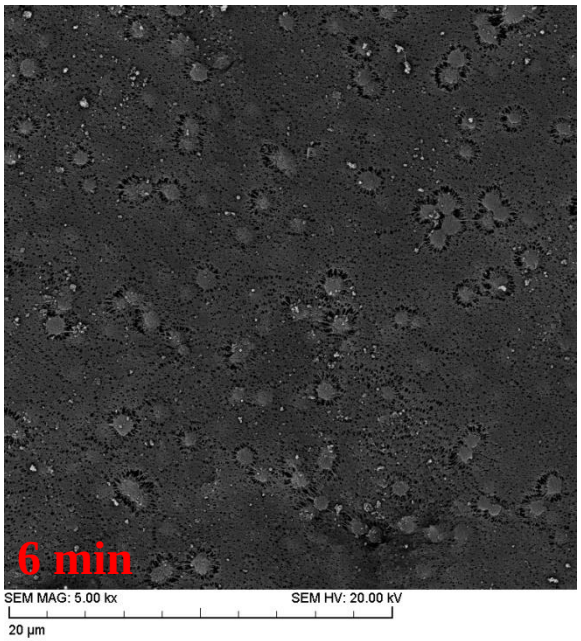
6 min
SEM MAG: 5.00 kx
SEM HV: 20.00 kV
20 µm

Fig. 7-9 Top surface SEM images of the supported SiO_2/PVDF membranes at different penetration times, the nanoparticles concentration, 7.0 wt.%, the PVDF ratio, H:L = 2:8, the surface pores are specified by the black spots in the top surface

There is no significant change in the surface image while the penetration time is less than or equal to 4 min. There is a change at the penetration time of 6 min where many circular centers are seen from which pores are developed radially. The primary component of these centers is likely nanoparticles that have agglomerated as their concentration increases with the increase in the penetration time.

It is worth mentioning that for the penetration times of 9 min or longer ($\tau \geq 9$ min), the number of the circular centers increased and the surface was only partially covered by the coated layer, leaving many pores visible at the backing material surface. The membrane shrank quickly when it was taken off the coagulation bath. It was therefore concluded that most of the polymer penetrated into the open pores of the backing material together with the solvent when the penetration time was equal or more than 9 min.

The change in pore size with penetration time is given in Fig. 7-10-a. There is a maximum of the pore size at $\tau = 2$ min. Similar to what we discussed about the significance of the data presented in Fig. 7-6-a, there is a certain degree of overlapping of the error bars between the pore sizes at a penetration time of 2 min and those at 0.25-0.50 and 3 min. However, the pore size at 2 min penetration time is still significantly larger than those at both 0.25-0.50 and 3.0-min ($P < 0.05$) since the sample sizes are very large (n=720, 491, and 221 for 0.25-0.50, 2.0, and 3.0 min penetration time, respectively).

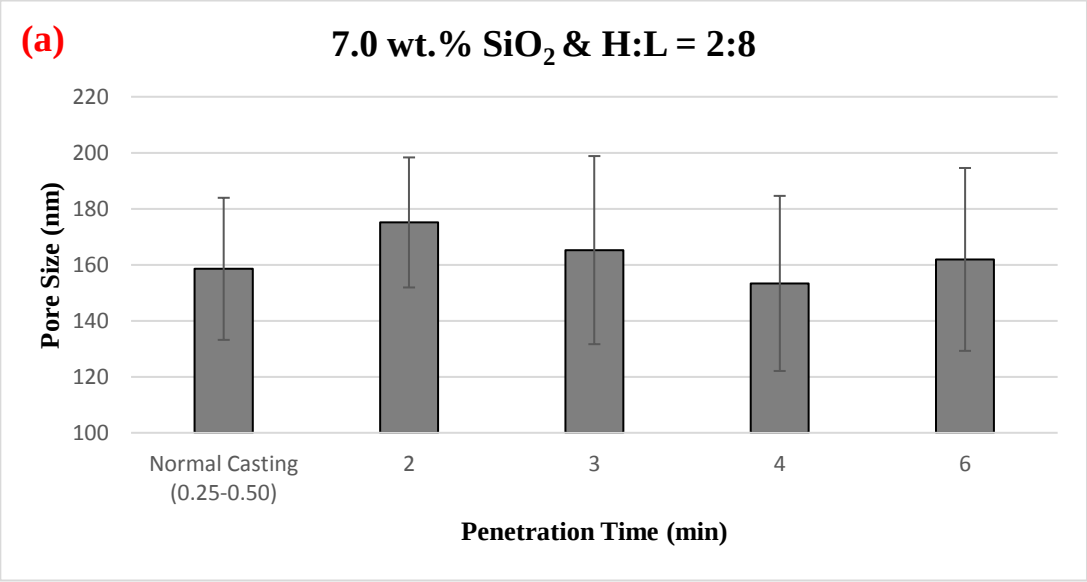

Fig. 7-10-a Surface pore size vs. penetration time (H:L = 2:8; SiO_2 nanoparticles, 7.0 wt.%)

7-3-2-3- Porosity

Figure 7-10-b shows the effect of penetration time on the porosity.

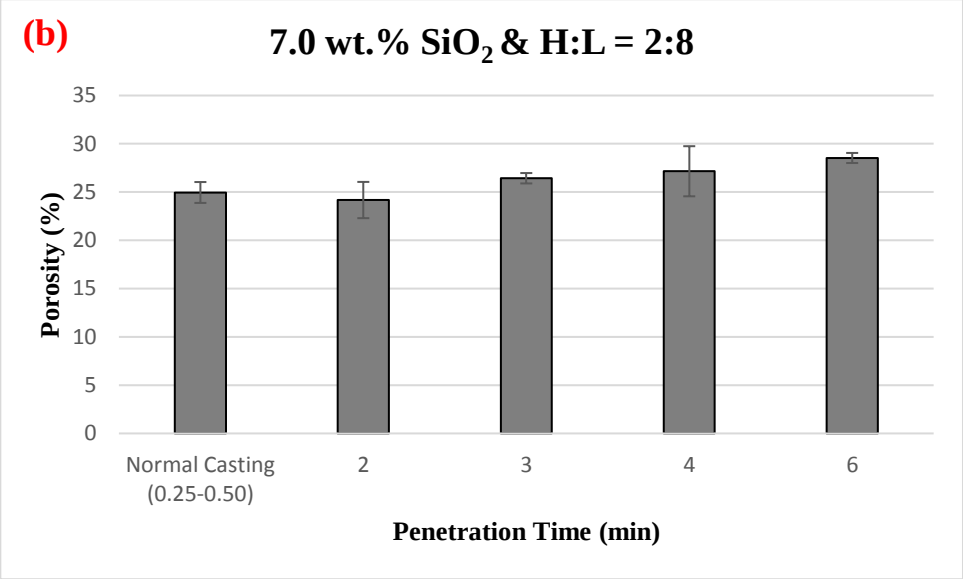

Fig. 7-10-b Porosity vs. penetration time (H:L = 2:8; SiO_2 nanoparticles, 7.0 wt.%)

Porosity increased gradually with the penetration time ($P < 0.05$). This is because of an increase in swelling of the top layer as discussed earlier. Similar to what was discussed in Section 8-3-1-4, the constant and small porosity of the backing material had a significant impact on the overall porosity and the actual porosity of the top layer and its variation at different penetration times should be much larger than what are reported in Fig. 7-10-b.

7-3-2-4- Surface Contact Angle and Roughness

According to Fig. 7-10-c, the contact angle increased with penetration time. This might be explained by the increase in surface roughness (shown in Table 7-2) due to the Wenzel or Cassie effect. In any case, the effects of penetration time on contact angle and roughness parameters are not very strong.

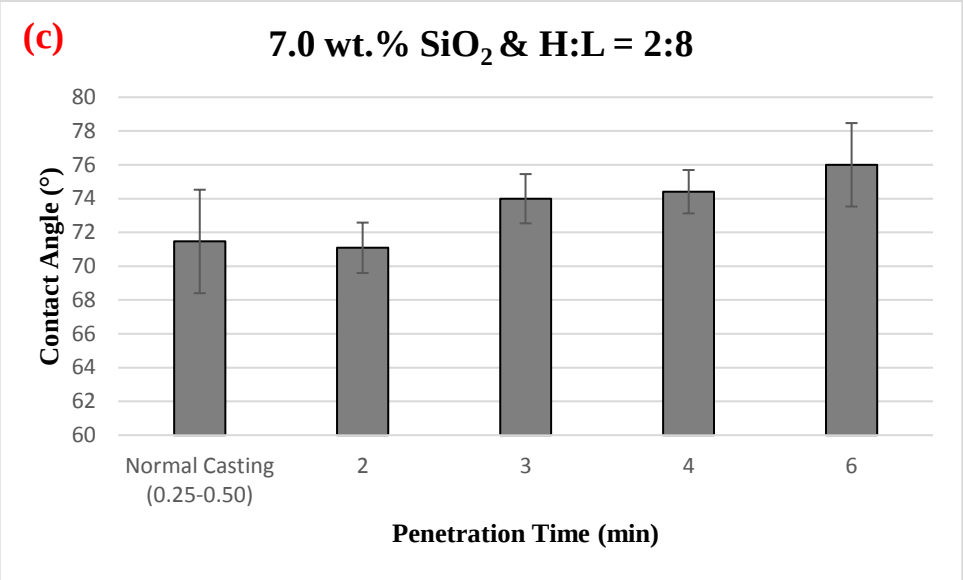

Fig. 7-10-c Contact angle vs. penetration time (H:L = 2:8; SiO_2 nanoparticles, 7.0 wt.%)

Table 7-2 Surface roughness analysis of the 7.0 wt.% hydrophilic SiO_2 incorporated nanocomposite membranes vs. penetration time by ImageJ and its plugin Roughness Calculation (all the units in pixel)

Penetration Time (min) Polymer Ratio (H:L = 2:8)	**Rq: Root mean square deviation**	**Ra: Arithmetical mean deviation**
Normal Casting (0.25-0.50)	54.6±0.2	52.5±0.3
2	55.4±0.2	52.7±0.1
3	56.0±0.1	55.6±0.2
4	56.4±0.1	55.5±0.2
6	57.4±0.4	56.2±0.2

7-3-2-5- LEP_w

In Fig. 7-10-d, a maximum in LEP_w was observed at τ = 3 min. A 66.7% increase in LEP_w was observed in comparison with the normal casting method at τ = 3 min. Looking at maximum pore size behavior in the same figure, the maximum pore size shows a minimum at exactly τ = 3 min. In addition, by considering Fig. 7-10-c, the surface becomes more hydrophobic with a longer penetration time, which is in favour of the LEP_w. However, a reduction in LEP_w beyond a penetration time of 3 min demonstrates that according to the Laplace equation [56], effect of maximum pore size is dominant at the longer penetration times, and the LEP_w is controlled by the maximum pore size, rather than the average pore size or the contact angle.

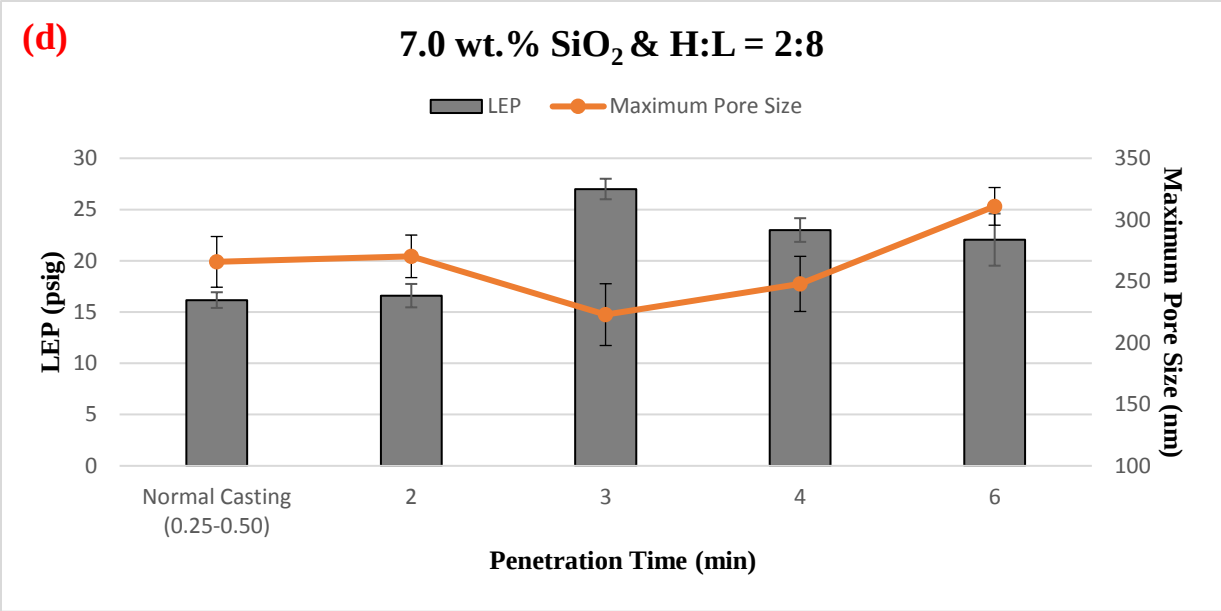

Fig. 7-10-d LEP_w and maximum pore size vs. penetration time (H:L = 2:8; SiO_2 nanoparticles, 7.0 wt.%)

7-3-2-6- VMD Flux

Figure 7-10-e shows that a maximum of VMD flux appeared at τ = 2 min. The maximum flux was 13.8 kg/m^2h, which is 33.4% larger than the flux from normal casting method.

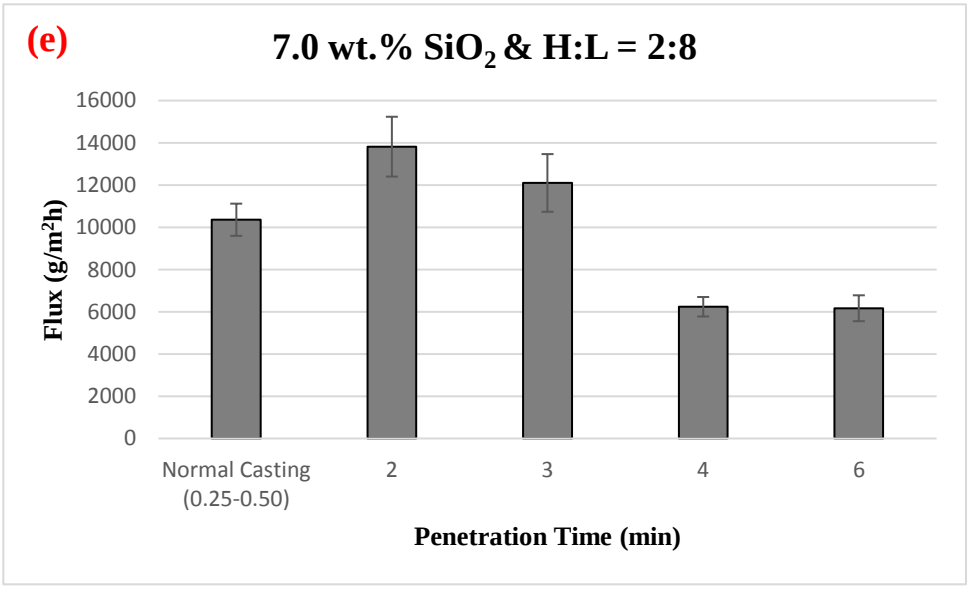

Fig. 7-10-e Pure water flux vs. penetration time (H:L = 2:8; SiO_2 nanoparticles, 7.0 wt.%; feed temperature, 27.5 °C; downstream pressure: 1.2 kPa)

This can be ascribed to the maximum average pore size that appeared at $\tau = 2$ min (Fig. 7-10-a). The steep decline in the flux at $\tau = 4$ and 6 min can be explained by the increase of top layer thickness as presented in Fig. 7-7 and decrease of substrate porosity as a result of the penetration of casting solution into the substrate macro-channels at the long penetration times as given in Fig. 7-8. As shown schematically in Fig. 7-11, there are three variables controlling the VMD flux, 1) surface pore size, 2) effective thickness of the top layer, and 3) the porosity of the top layer. According to Fig. 7-10-a, pore size met a maximum at a penetration time of 2 min, while Fig. 7-7 shows that the thickness of top layer increased with the penetration time, with a sharper rate at the longer penetration times. It should be pointed out that Fig. 7 also showed that there was detectable penetration of the cast layer into the backing layer, especially, at the longer penetration times, i.e. 6 min. Since the vapor molecules have to diffuse through the macro-channels inside the backing material, the polymer leaked into these channels would function as an extension of the top layer. In other words, effective thickness of the top layer would be larger than what were determined by SEM imaging, which is reported in Fig. 7-7. Therefore, it can be concluded that the maximum flux obtained at 2 min penetration was the result of the maximum pore size, second least top layer thickness. The impact of the gradually increasing porosity of the top layer seems not to be dominant in this case. Furthermore, the sharp decrease of flux at 4 min penetration time or longer could be explained by the concerted effects of small pore size and large top layer thickness. Once again, the impact of the slightly larger top layer porosity at these conditions seems to be overwritten by that of the pore size and top layer thickness.

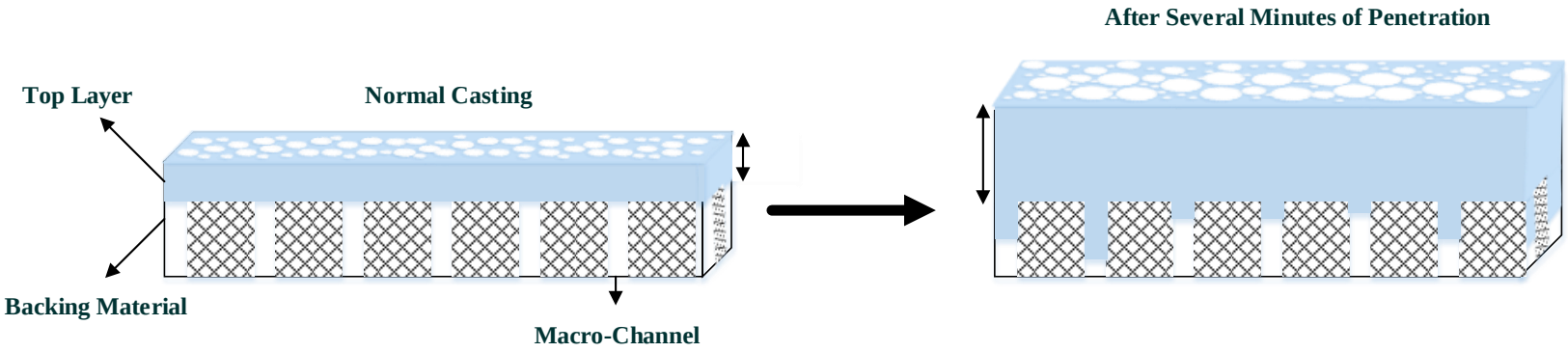

Fig. 7-11 Schematic of the effect of the penetration time on the membrane characteristics

7-3-2-7- Salt Rejection

In Fig. 7-10-e, two of the high fluxes are 13.8 and 12.1 kg/m^{2}h at τ = 2 and 3 min, respectively. The salt rejection of these membranes was examined by 3 cycles of the VMD experiments, with the downstream side kept under vacuum for 1.5 h at each cycle. The results are presented in Fig. 7-12. As shown in Fig. 7-12, NaCl rejection decreased considerably for the membrane of τ = 2 min, while nearly 100% NaCl rejection was maintained for the membrane of τ = 3 min. This is because the LEP_w was much higher at τ = 3 min than τ = 2 min (Fig. 7-10-d). The membrane with longer penetration time possessed almost 62.7% higher LEP_w and could be stable for a longer time. Obviously, therefore, 3 min is the best choice for the penetration time in this study.

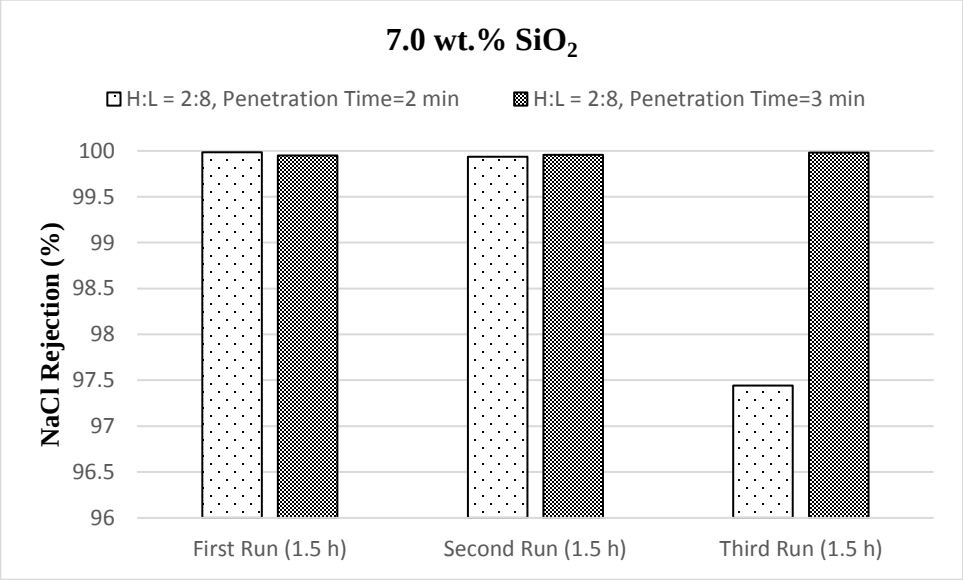

Fig. 7-12 NaCl rejection for membranes of two different penetration times (H:L = 2:8; SiO_2 nanoparticles, 7.0 wt.%; feed temperature, 27.5 °C; downstream pressure: 1.2 kPa)

7-3-2-8- Polymer Blend H:L = 4:6

Some experiments were further conducted with the membranes fabricated from a different polymer blend of H:L = 4:6 and the results are given in Table 7-3. It should be noted that trends observed in porosity, contact angle and LEP_w are almost the same as the blend ratio of H:L = 2:8. The flux however decreased continuously as the penetration time increased. This is because much denser polymer/nanoparticle gel was left behind at the top surface of the backing material during dope penetration.

Table 7-3 Porosity, contact angle, LEP_w, VMD pure water flux of the 7.0 wt.% hydrophilic SiO_2 incorporated nanocomposite membranes for different penetration times where the blend ratio is 4:6

Penetration Time (min)	Porosity (%)	Contact Angle (°)	LEP_w (psig)	Flux (kg/m^{2}h)
Normal Casting (0.25-0.50)	26.8±3.3	70.3±4.0	18.0±1.8	12.7±0.2
2	25.5±2.9	76.2±2.2	18.7±1.2	11.7±1.0
3	24.7±2.1	76.3±1.7	24.6±2.8	7.5±0.6
6	26.3±0.7	84.9±5.1	20.8±1.9	3.5±0.3

Regarding all above mentioned, the dope suspension viscosity and penetration time seem to have significant influence on the membrane characteristics and accordingly its performance. Therefore, and to reach the best performance of the fabricated membranes, the manufacturing procedure needs to be optimized based on the materials which are used.

Considering all the data presented in this work, the combination of H:L = 2:8 and penetration time of 3 min appears to be the best conditions for the preparation of nanocomposite membranes with an LEP_w of 27.0 psig, a 99.9 % NaCl rejection and a VMD flux of 12.1 kg/m^{2}h at a feed temperature of 27.5 °C and vacuum pressure of 1.2 kPa, which is approximately 86.2% higher than that of the VMD flux of a commercial PVDF GVHP membrane obtained at 25.0 °C and a slightly higher vacuum pressure of 1.6 kPa [57].

Generally speaking, the use of nanocomposite membranes in MD could be considered as a new concept and only a few studies have been carried out to investigate the effects of nanomaterials on the membrane characteristics and performance [16, 20, 33, 34, 36, 37]. Among those, even fewer works have been devoted to VMD application and three of them were published by our research group with different nanoparticles as additives. When CuO and $CaCO_3$ nanomaterials were used as nano-additives, VMD fluxes of 1.3 and 1.0 kg/m^{2}h were achieved, respectively [16]. The addition of superhydrophobic SiO_2 nanoparticles led to a flux of 2.9 kg/m^{2}h [34], and nanocomposite membranes with hydrophilic SiO_2 nanoparticles exhibited a flux of 12.7 kg/m^{2}h [33]. All these VMD tests were conducted at the same operating conditions, i.e. at a feed temperature of 27.0-27.5 °C and a vacuum pressure of 1.2-6.5 kPa. It should be noted that the nanocomposite membrane with a blend ratio and penetration time of H:L = 2:8 and 3 min, respectively, demonstrated approximately 50.0% higher LEP_w than the blend ratio of H:L = 4:6 (the best membrane that was reported in another publication and made by the normal method [33]).

7-4- Conclusion

Hydrophilic SiO_2 nanoparticles incorporated supported membranes were developed in this work with concentration of the nano-additives remained constant at 7.0 wt.%. Effects of the PVDF blend ratio (viscosity) and penetration time on the membrane structure, characteristics, and performance were investigated. According to the results, the thickness of the top layer on the substrate increased with the penetration time, while a thinner top layer was obtained as the portion of the high molecular weight PVDF (H) decreased in the dope suspension. It was demonstrated that the membrane surface became rougher and more hydrophobic as the penetration time increased, however, a smoother and slightly less hydrophobic surface was acquired by reducing the PVDF blend ratio (H:L) in the casting suspension. Surface pore size became larger as the concentration of low molecular weight PVDF (L) was elevated in the casting dope while the pore size had a maximum at penetration time of 2 min. A maximum LEP_w was observed when an intermediate penetration time of 3 min was applied during the membrane fabrication process at constant H:L polymer ratio or at a H:L polymer ratio of 2:8 when penetration time was kept constant. The change in LEP_w was attributed to the change in maximum pore size and surface contact angle. It was shown that the LEP_w would influence the membrane salt rejection, and a membrane with higher LEP_w could last longer in terms of selectivity. Based upon the VMD pure water results, membrane permeability was controlled by the surface pore size at the short penetration times, while the top layer thickness was indicated to be the dominant factor in determining the membrane permeability at the long penetration times. At the end, optimization of the membrane structure and performance by elongating the penetration time would depend on the casting dope suspension viscosity, and the membrane with a PVDF ratio of H:L = 2:8 and penetration time of 3 min with a LEP_w and pure water flux of 27.0 psig and 12.1 kg/m^2h at a feed temperature of 27.5 °C, respectively, is reported to be the best membrane in this study.

Acknowledgments

Authors would like to thank the kind gift of the polymers (Kynar® 740 and Kynar® HSV900) by Arkema Inc. (Philadelphia, PA, USA). Financial supports of NSERC Discovery and I2I grants are also highly appreciated.

References

(1) Khalifa, A. E. Water and air gap membrane distillation for water desalination – An experimental comparative study*Separation and Purification Technology* **2015**, 276-284.

(2) Daer, S.; Kharraz, J.; Giwa, A.; Hasan, S. W. Recent applications of nanomaterials in water desalination: A critical review and future opportunities*Desalination* **2015**, 37-48.

(3) Gabriel, K. J.; El-Halwagi, M. M.; Linke, P. Optimization across the Water-Energy Nexus for Integrating Heat, Power, and Water for Industrial Processes, Coupled with Hybrid Thermal-Membrane Desalination*Ind Eng Chem Res* **2016**, *12*, 3442-3466.

(4) Miller, S.; Shemer, H.; Semiat, R. Energy and environmental issues in desalination*Desalination* **2015**, 2-8.

(5) Hegab, H. M.; Zou, L. Graphene oxide-assisted membranes: Fabrication and potential applications in desalination and water purification*J. Membr. Sci.* **2015**, 95-106.

(6) Roy, S.; Bhadra, M.; Mitra, S. Enhanced desalination via functionalized carbon nanotube immobilized membrane in direct contact membrane distillation*Separation and Purification Technology* **2014**, 58-65.

(7) Xu, R.; Lin, P.; Zhang, Q.; Zhong, J.; Tsuru, T. Development of Ethenylene-Bridged Organosilica Membranes for Desalination Applications*Ind Eng Chem Res* **2016**, *7*, 2183-2190.

(8) Zhao, D.; Chen, S.; Wang, P.; Zhao, Q.; Lu, X. A Dendrimer-Based Forward Osmosis Draw Solute for Seawater Desalination*Ind Eng Chem Res* **2014**, *42*, 16170-16175.

(9) Perez-Moreno, V.; Bonilla-Suarez, C. B.; Fortanell-Trejo, M.; Pedraza-Aboytes, G. Seawater Desalination Using Modified Ceramic Membranes*Ind Eng Chem Res* **2012**, *17*, 5900-5904.

(10) Esfahani, I. J.; Kim, J. T.; Yoo, C. K. A Cost Approach for Optimization of a Combined Power and Thermal Desalination System through Exergy and Environmental Analysis*Ind Eng Chem Res* **2013**, *32*, 11099-11110.

(11) Odu, S. O.; van der Ham, A. G. J.; Metz, S.; Kersten, S. R. A. Design of a Process for Supercritical Water Desalination with Zero Liquid Discharge*Ind Eng Chem Res* **2015**, *20*, 5527-5535.

(12) Guan, G.; Yang, X.; Wang, R.; Fane, A. G. Evaluation of heat utilization in membrane distillation desalination system integrated with heat recovery*Desalination* **2015**, 80-93.

(13) Liao, Y.; Loh, C.; Wang, R.; Fane, A. G. Electrospun Superhydrophobic Membranes with Unique Structures for Membrane Distillation*Acs Applied Materials & Interfaces* **2014**, *18*, 16035-16048.

(14) Lee, J.; Kim, Y.; Kim, W.; Francis, L.; Amy, G.; Ghaffour, N. Performance modeling of direct contact membrane distillation (DCMD) seawater desalination process using a commercial composite membrane*J. Membr. Sci.* **2015**, 85-95.

(15) Shim, W. G.; He, K.; Gray, S.; Moon, I. S. Solar energy assisted direct contact membrane distillation (DCMD) process for seawater desalination*Separation and Purification Technology* **2015**, 94-104.

(16) Baghbanzadeh, M.; Rana, D.; Matsuura, T.; Lan, C. Q. Effects of hydrophilic CuO nanoparticles on properties and performance of PVDF VMD membranes*Desalination* **2015**, *0*, 75-84.

(17) Alkhudhiri, A.; Darwish, N.; Hilal, N. Membrane distillation: A comprehensive review*Desalination* **2012**, *0*, 2-18.

(18) Efome, J. E.; Rana, D.; Matsuura, T.; Lan, C. Q. Enhanced performance of PVDF nanocomposite membrane by nanofiber coating: A membrane for sustainable desalination through MD*Water Res.* **2016**, 39-49.

(19) Shin, Y.; Sohn, J. Mechanisms for scale formation in simultaneous membrane distillation crystallization: Effect of flow rate*Journal of Industrial and Engineering Chemistry* **2016**, 318-324.

(20) Gethard, K.; Sae-Khow, O.; Mitra, S. Water Desalination Using Carbon-Nanotube-Enhanced Membrane Distillation*Acs Applied Materials & Interfaces* **2011**, *2*, 110-114.

(21) Song, L.; Li, B.; Sirkar, K. K.; Gilron, J. L. Direct contact membrane distillation-based desalination: Novel membranes, devices, larger-scale studies, and a model*Ind Eng Chem Res* **2007**, *8*, 2307-2323.

(22) Wang, K. Y.; Foo, S. W.; Chung, T. Mixed Matrix PVDF Hollow Fiber Membranes with Nanoscale Pores for Desalination through Direct Contact Membrane Distillation*Ind Eng Chem Res* **2009**, *9*, 4474-4483.

(23) Xu, Y.; Zhu, B.; Xu, Y. Pilot test of vacuum membrane distillation for seawater desalination on a ship*Desalination* **2006**, *1-3*, 165-169.

(24) Khraisheh, M.; Benyahia, F.; Adham, S. Industrial case studies in the petrochemical and gas industry in Qatar for the utilization of industrial waste heat for the production of fresh water by membrane desalination*Desalination and Water Treatment* **2013**, *7-9*, 1769-1775.

(25) Jansen, A. E.; Assink, J. W.; Hanemaaijer, J. H.; van Medevoort, J.; van Sonsbeek, E. Development and pilot testing of full-scale membrane distillation modules for deployment of waste heat*Desalination* **2013**, 55-65.

(26) Sarbatly, R.; Chiam, C. Evaluation of geothermal energy in desalination by vacuum membrane distillation*Appl. Energy* **2013**, 737-746.

(27) Drioli, E.; Ali, A.; Simone, S.; Macedonio, F.; AL-Jlil, S. A.; Al Shabonah, F. S.; Al-Romaih, H. S.; Al-Harbi, O.; Figoli, A.; Criscuoli, A. Novel PVDF hollow fiber membranes for vacuum and direct contact membrane distillation applications*Separation and Purification Technology* **2013**, 27-38.

(28) Qtaishat, M.; Rana, D.; Khayet, M.; Matsuura, T. Preparation and characterization of novel hydrophobic/hydrophilic polyetherimide composite membranes for desalination by direct contact membrane distillation*J. Membr. Sci.* **2009**, *1-2*, 264-273.

(29) Chong, K. C.; Lai, S. O.; Lee, K. M.; Lau, W. J.; Ooi, B. S. Performance of Surface Modification of Polyvinylidene Fluoride Hollow Fiber Membrane in Membrane Distillation*2nd International Conference on Sustainable Materials (Icosm 2013)* **2013**, 137-140.

(30) Tong, D.; Wang, X.; Ali, M.; Lan, C. Q.; Wang, Y.; Drioli, E.; Wang, Z.; Cui, Z. Preparation of Hyflon AD60/PVDF composite hollow fiber membranes for vacuum membrane distillation*Separation and Purification Technology* **2016**, 1-8.

(31) Simone, S.; Figoli, A.; Criscuoli, A.; Carnevale, M. C.; Rosselli, A.; Drioli, E. Preparation of hollow fibre membranes from PVDF/PVP blends and their application in VMD*J. Membr. Sci.* **2010**, *1–2*, 219-232.

(32) Baghbanzadeh, M.; Rana, D.; Lan, C. Q.; Matsuura, T. Effects of Inorganic Nano-Additives on Properties and Performance of Polymeric Membranes in Water Treatment*Separation & Purification Reviews* **2016**, *2*, 141-167.

(33) Baghbanzadeh, M.; Rana, D.; Lan, C. Q.; Matsuura, T. Effects of hydrophilic silica nanoparticles and backing material in improving the structure and performance of VMD PVDF membranes*Separation and Purification Technology* **2016**, 60-71.

(34) Efome, J. E.; Baghbanzadeh, M.; Rana, D.; Matsuura, T.; Lan, C. Q. Effects of superhydrophobic SiO2 nanoparticles on the performance of PVDF flat sheet membranes for vacuum membrane distillation*Desalination* **2015**, *0*, 47-57.

(35) Bhadra, M.; Roy, S.; Mitra, S. Enhanced desalination using carboxylated carbon nanotube immobilized membranes*Separation and Purification Technology* **2013**, 373-377.

(36) Hou, D.; Wang, J.; Sun, X.; Ji, Z.; Luan, Z. Preparation and properties of PVDF composite hollow fiber membranes for desalination through direct contact membrane distillation*J. Membr. Sci.* **2012**, 185-200.

(37) Hou, D.; Dai, G.; Fan, H.; Wang, J.; Zhao, C.; Huang, H. Effects of calcium carbonate nano-particles on the properties of PVDF/nonwoven fabric flat-sheet composite membranes for direct contact membrane distillation*Desalination* **2014**, *0*, 25-33.

(38) Chen, Z.; Rana, D.; Matsuura, T.; Yang, Y.; Lan, C. Q. Study on the structure and vacuum membrane distillation performance of PVDF composite membranes: I. Influence of blending*Separation and Purification Technology* **2014**, 303-312.

(39) Chen, Z.; Rana, D.; Matsuura, T.; Meng, D.; Lan, C. Q. Study on structure and vacuum membrane distillation performance of PVDF membranes: II. Influence of molecular weight*Chem. Eng. J.* **2015**, *0*, 174-184.

(40) Mosqueda-Jimenez, D.; Narbaitz, R.; Matsuura, T.; Chowdhury, G.; Pleizier, G.; Santerre, J. Influence of processing conditions on the properties of ultrafiltration membranes*J. Membr. Sci.* **2004**, *1-2*, 209-224.

(41) Mosqueda-Jimenez, D.; Narbaitz, R.; Matsuura, T. Manufacturing conditions of surface-modified membranes: effects on ultrafiltration performance*Separation and Purification Technology* **2004**, *1*, 51-67.

(42) Mosqueda-Jimenez, D.; Narbaitz, R.; Matsuura, T. Effects of preparation conditions on the surface modification and performance of polyethersulfone ultrafiltration membranes*J Appl Polym Sci* **2006**, *6*, 2978-2988.

(43) Suk, D.; Chowdhury, G.; Matsuura, T.; Narbaitz, R.; Santerre, P.; Pleizier, G.; Deslandes, Y. Study on the kinetics of surface migration of surface modifying macromolecules in membrane preparation*Macromolecules* **2002**, *8*, 3017-3021.

(44) Pei, G.; Cheng, G.; Du, Q. Preparation of chelating resin filled composite membranes and selective adsorption of Cu(II)*J. Membr. Sci.* **2002**, *1*, 85-93.

(45) Bindal, R. C.; Hanra, M. S.; Misra, B. M. Novel solvent exchange cum immersion precipitation technique for the preparation of asymmetric polymeric membrane*J. Membr. Sci.* **1996**, *1*, 23-29.

(46) Jian, X.; Dai, Y.; He, G.; Chen, G. Preparation of UF and NF poly (phthalazine ether sulfone ketone) membranes for high temperature application*J. Membr. Sci.* **1999**, *1–2*, 185-191.

(47) Khayet, M.; Matsuura, T. *Membrane Distillation;* Elsevier: Amsterdam, 2011; .

(48) Mierzwa, J. C.; Vecitis, C. D.; Carvalho, J.; Arieta, V.; Verlage, M. Anion dopant effects on the structure and performance of polyethersulfone membranes*J. Membr. Sci.* **2012**, 91-102.

(49) Yang, Y.; Rana, D.; Matsuura, T.; Zheng, S.; Lan, C. Q. Criteria for the selection of a support material to fabricate coated membranes for a life support device*Rsc Advances* **2014**, *73*, 38711-38717.

(50) Zhao, S.; Wang, Z.; Wang, J.; Wang, S. Poly(ether sulfone)/Polyaniline Nanocomposite Membranes: Effect of Nanofiber Size on Membrane Morphology and Properties*Ind Eng Chem Res* **2014**, *28*, 11468-11477.

(51) Agboola, O.; Maree, J.; Mbaya, R. Characterization and performance of nanofiltration membranes*Environmental Chemistry Letters* **2014**, *2*, 241-255.

(52) Emadzadeh, D.; Lau, W. J.; Matsuura, T.; Rahbari-Sisakht, M.; Ismail, A. F. A novel thin film composite forward osmosis membrane prepared from PSf-TiO2 nanocomposite substrate for water desalination*Chem. Eng. J.* **2014**, 70-80.

(53) Roughness Calculation. (November 2015).

(54) Baghbanzadeh, M.; Rashidi, A.; Soleimanisalim, A. H.; Rashtchian, D. Investigating the rheological properties of nanofluids of water/hybrid nanostructure of spherical silica/MWCNT*Thermochimica Acta* **2014**, *0*, 53-58.

(55) Yang, Y.; Rana, D.; Matsuura, T.; Lan, C. Q. The heat and mass transfer of vacuum membrane distillation: Effect of active layer morphology with and without support material*Separation and Purification Technology* **2016**, 56-62.

(56) Franken, A. C. M.; Nolten, J. A. M.; Mulder, M. H. V.; Bargeman, D.; Smolders, C. A. Wetting criteria for the applicability of membrane distillation*J. Membr. Sci.* **1987**, *3*, 315-328.

(57) Khayet, M.; Khulbe, K.; Matsuura, T. Characterization of membranes for membrane distillation by atomic force microscopy and estimation of their water vapor transfer coefficients in vacuum membrane distillation process*J. Membr. Sci.* **2004**, *1-2*, 199-211.

Chapter 8:

Conclusions and future works

MD is considered as a separation process that can address the current challenges of desalination processes most effectively. However, despite MD's potential as one of the technologies that are competitive to the already established desalination processes such as RO, commercial MD plants have not yet been constructed as a stand-alone process. The reason is found in the high production cost of water caused primarily by the following two hindering barriers: 1) thermal energy required for vaporization of water and 2) insufficient performance of currently available MD membranes.

In this work, it is attempted to find the ways which would enable us to overcome those obstacles and pave the way for further improvement of MD. More specifically, to alleviate the external thermal energy supply, a novel and waste-free Zero Thermal Input MD (ZTIMD) desalination process, in which the thermal energy stored in surface seawater alone is utilized for the evaporation of water, is proposed. As well, the performance improvement of MD membrane is attempted by developing novel MD membranes via incorporation of nanomaterials. The following conclusions have been derived from this work.

8-1- ZTIMD and Its Feasibility

In ZTIMD, enthalpy of surface seawater is extracted by using bottom seawater as the coolant, which provides the process with the required temperature difference. To make the best use of the temperature difference between sea surface and bottom, and to avoid requirement of external thermal energy, ZTIMD is necessarily a single-pass process, which limits its water recovery ratio (amount of product water divided by the feed water) to 5% or less. However, the low recovery ratio can be considered as an inherent advantage of the process. Because the salinity of the concentrate discharge is only marginally higher than the natural seawater, the disposal of the concentrated brine imposes little environmental problems, unlike RO and other conventional desalination processes.

Economic analysis of the ZTIMD process was carried out for two cases where the pre-treatment of feed seawater is made at two different levels of complexity. In one case an intense pre-treatment such as that of SWRO process was assumed, and in the other the pre-treatment was

hypothetically carried out by cartridge filtration only, which is considered by many researchers as realistic. In each case scenario, effects of the key process operating conditions and the membrane characteristics such as price, lifetime, and permeability, on the water production cost was evaluated. It was found that fresh water could be produced, in the best scenario of the ZTIMD process, at a cost of $\$0.28/m^3$, which is approximately half of the cost of the current RO process. Some major advantages of ZTIMD include 1) the process requires no external thermal energy input and is therefore inherently energy-saving; 2) it is economically competitive to existing technologies; and 3) it is waste-free. However, releasing the cold seawater from the coolant line into the sea at a temperature of 20 °C, i.e. 10 °C less than that of the surface seawater, seems to be a challenge considering environmental regulations, nonetheless, it could be resolved by discharging it at the bottom layers of the sea.

8-2- Mixed Matrix MD Nanocomposite Membranes

On another front, novel membranes were developed, aimed at the improvement in VMD flux while maintaining the selectivity of membrane. For this purpose, manipulation of the membrane structure was targeted by incorporating nanomaterials in the membrane matrix as fillers. It was demonstrated that the hydrophobicity of the nanomaterials could affect the membrane structure and consequently its performance in various fashions. Moreover, there is a threshold filler content beyond which the membrane becomes either less permeable and/or mechanically more fragile. Fig. 8-1, visually summarizes the experimental works that were done throughout this PhD project.

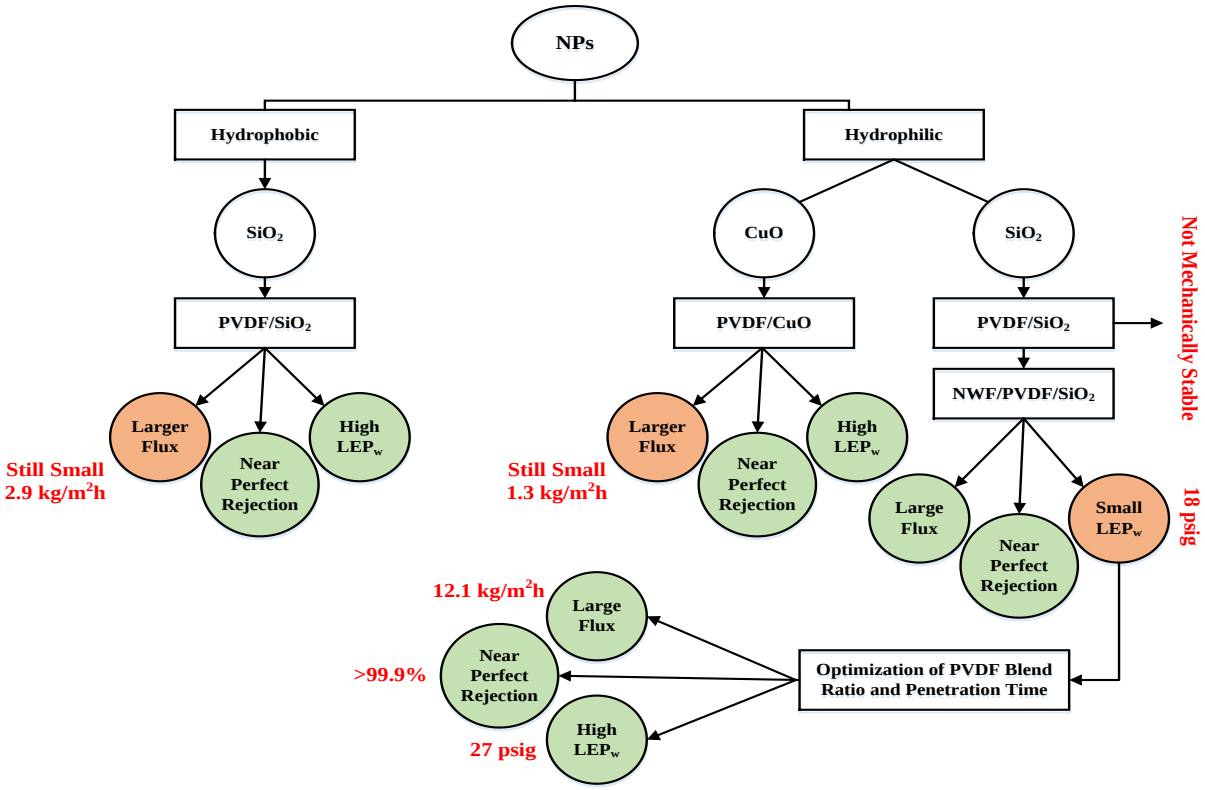

Fig. 8-1A summary on the experimenal work of the thesis

Generally speaking, nano-additives are divided into two different categories, hydrophobic and hydrophilic nanoparticles. At the early stage, superhydrophobic SiO_2 nanomaterials were incorporated in PVDF membrane (results shown in Appendix A). The resulted nanocomposite membrane possessed high LEP_w, near perfect rejection, and larger VMD flux in comparison with the neat PVDF membrane (almost 290% higher), however, its flux was not adequate to make the membrane an appropriate candidate for the proposed ZTIMD. Therefore, focus shifted to hydrophilic nanoparticles and primarily CuO nanomaterials. Again, the developed nanocomposite membranes demonstrated high LEP_w, almost perfect rejection, and higher VMD flux compared to the neat PVDF membrane (almost 150% increase), but the flux was not satisfying when the membrane was considered to be used in ZTIMD process. Therefore, another type of hydrophilic nanoparticles, i.e. SiO_2, was employed. According to the results, nanocomposite membranes of PVDF/SiO_2 demonstrated a desirable cross-sectional structure with reduced sponge-like layer thickness, however, they were not mechanically stable to withstand long VMD operation. Consequently, much attention was paid to improving of the mechanical stability of the membranes by adding another layer of the NWF backing material.

Results showed that the nanocomposite membranes of NWF/PVDF/SiO_2 possessed large enough VMD flux (almost 2450% increase in comparison with the neat PVDF membrane), near perfect rejection, and adequate LEP_w to be used for membrane distillation. Although, there was still more room to improve their relatively small LEP_w for the purpose of achieving a longer durability. To this end, a few key parameters in membrane fabrication process were targeted and according to the results, LEP_w increased by 50% through optimizing the PVDF blend ratio and penetration time. At the end, a membrane with quite large flux (12.1 kg/m^2h) at low temperature, i.e. 27.5 °C, almost complete rejection, and reasonable LEP_w (27 psig) was obtained when NWF/PVDF/SiO_2 nanoparticles were prepared at a filler concentration of 7.0 wt.%, PVDF blend ratio of H:L = 2:8, and penetration time of 3 min.

8-2-1- Hydrophilic Nanomaterials Incorporated MD Membranes

It was demonstrated that the portion of sponge-like layer that was the major source of the mass transfer resistance of the asymmetric membrane decreased as a result of the incorporation of the hydrophilic CuO and SiO_2 nanoparticles in PVDF membrane. For instance, in the case of CuO nanoparticles, the ratio of finger-like layer to the overall membrane thickness increased (therefore the ratio of sponge-like layer decreased) by 28.2% when the filler concentration increased from 0.0 to 1.0 wt.%, while the increase was 141.0% when SiO_2 concentration was increased from 0.0 to 7.0 wt.%. The PVDF/hydrophilic nanomaterials incorporated membranes possessed larger surface pores in comparison with the neat PVDF membrane. As a consequence, SiO_2 particle incorporated membranes exhibited higher fluxes. It is worth mentioning that the surface hydrophobicity of the PVDF membrane was not compromised by the addition of the hydrophilic nanomaterials and the LEP_w of the nanocomposite membranes were high enough to be used in VMD, although their LEP_ws were smaller than the neat PVDF membrane.

8-2-2- Effects of Backing Material, PVDF Blend Ratio, and Penetration Time

One of the drawbacks of the membrane with the reduced sponge-like layer is the decrease in the mechanical strength. As a result, membrane durability decreased significantly and feed liquid leaked into the permeate due to mechanical failure of the membrane structure, which further resulted in a reduced membrane selectivity. To increase the membrane durability, nanocomposite membranes were cast on a non-woven fabric (NWF) backing material. More than 20 different

backing materials were tested for this purpose (data not shown), and Hollytex® 3396 was chosen due to demonstration of the best performance by possessing the reasonable penetration of casting dope into the substrate. The results showed that the supported membranes could withstand the VMD process during the tested period (three consecutive VMD cycles), which was limited to the equipment and time constraints. Furthermore, the PVDF membrane supported by the backing material had a larger pore size compared to the membrane without backing material. However, the additional mass transfer resistance of the backing material brought about a smaller flux of the membrane.

It should be pointed out that at the optimum concentration of the hydrophilic nanoparticles, VMD flux of the nascent PVDF membrane at 27.5 °C and 1.2 kPa increased by 153.4% and 2456%, respectively, when 2.0 wt.% CuO and 7.0 wt.% SiO_2 were added (the membrane with SiO_2 nanoparticles was supported).

Thus the highest VMD flux (12.7 kg/m^{2}h at 27.5 °C and 1.2 kPa) was achieved by the NWF/PVDF/hydrophilic SiO_2membrane with 7.0 wt.% of filler content. However, the LEP_w of the membrane was slightly compromised. It should be noted that the PVDF used for the fabrication of the membrane was a blend of two different molecular weights, High (H) and Low (L), with a blend ratio of H:L = 4:6. The LEP_w of this membrane was 18 psig, only slightly above the required value of 14.5 psig for VMD. To increase the LEP_w, the effects of the blend ratio and the penetration time of the casting dope were investigated. It was found that the maximum LEP_w of 27.0 psig (50 % increase from 18 psig) was achieved at the H:L = 2:8 and the penetration time = 3.0 min, with VMD flux of 12.1 kg/m^{2}h at 27.5 °C and 1.2 kPa, (only less than 5% smaller than 12.7 kg/m^{2}h).

In summary, customizing the membrane manufacturing protocol is necessary to optimize the performance of the membrane fabricated from a given material. In addition, for the fabrication of membranes supported by a backing material, the coating parameters such as filler concentration, dope suspension viscosity, and penetration time should be taken into serious consideration to optimize the membrane performance.

8-2-3- Superhydrophobic Nanomaterials Incorporated MD Membranes

On the other hand, it was found that incorporating the superhydrophobic SiO_2 nanoparticles in the PVDF membrane could increase the VMD flux at 27 °C and 6.5 kPa by 292.4% when the nanoparticle was added at the optimum concentration of 7.0 wt.%. This was attributed to the pore size increase as a result of the addition of nanoparticles. It is interesting to note that the addition of superhydrophobic nanoparticles resulted in a denser but improved cross-sectional structure with hypothetically more interconnectivity between the pores. Furthermore, the nano-filler incorporation slightly lowered LEP_w from the nascent PVDF membrane, despite the increase in surface contact angle.

In the following, the major findings of the works done in the thesis are summarized:

1. Simulation according to the literature data and a few justifiable assumptions revealed that ZTIMD is economically competitive with the conventional desalination technologies. The process is inherently energy efficient and independent from external thermal energy input. It works at low temperatures, there is no transmembrane pressure in ZTIMD and therefore pre-treatment would be much simpler in comparison with the conventional desalination technologies such as RO. On the other hand, since the process works at very low recovery ratios, membrane's tendency to scaling would be negligible and accordingly chemical pre-treatment could be excluded from the process. Given all these benefits, ZTIMD would become waste free and environmentally friendly. Hence, the process is much more sustainable compared to the conventional desalination technologies such as RO.
2. Different nanoparticles (whether different in nature or hydrophobicity) have different effects on the membrane properties, however, they would drastically improve the VMD flux of the neat PVDF membrane with compromising the LEP_w.
3. Both hydrophilic and hydrophobic nanoparticles are able to increase the surface pore size of the neat PVDF membrane.
4. Incorporation of the hydrophilic nanoparticles in PVDF membrane results in a reduction in the thickness of the sponge-like layer, the major resistance against mass transfer across the membrane, and accordingly increases the membrane flux, however, it would compromise the membrane mechanical strength and LEP_w. It should be pointed out that the surface hydrophobicity of the PVDF membrane was not significantly compromised as a result of the inclusion of the hydrophilic nanoparticles.
5. Using a proper backing material improves the mechanical stability of the membrane.

6. Penetration time of the cast polymer into the backing material has significant impact on the membrane structure and accordingly on both flux and LEP_w.

7. The incorporation of hydrophobic nanoparticles visibly changed the structure of the sponge-like layer. The interconnectivity of the micro-pores hypothetically improved, which led to an increase in the membrane flux. Moreover, inclusion of the hydrophobic nanoparticles increased the surface contact angle, however, it did not lead to a significant change of LEP_w.

8-3- Future works

This novel work has opened a new way towards sustainable seawater desalination with studies on both membrane development and process design.

8-3-1- ZTIMD at Pilot Scale

Our research group has presented for the first time the innovative concept of using thermal energy stored in seawater for energy efficient, environmentally friendly, and economically feasible drinking water production at industrial level. The idea is revolutionary in nature, and it needs further work and efforts to become mature. The results presented in this study were obtained by using the literature data through simulation showing the great potential of the ZTIMD process for a sustainable and waste-free desalination process. However, implementing the project at a pilot scale with the simulated operating conditions would definitely help in better understanding the challenges lying ahead of the technology in its commercialization, and should be considered as the priority in the next step.

8-3-2- ZTIMD on a VMD Basis

Furthermore, in this study, the ZTIMD process was simulated by using a DCMD configuration. Considering the temperature difference between the sea surface and bottom, it was discussed earlier that the driving force would not be as high as that of the conventional MD processes. Therefore, membrane cost would be a major contributor to the overall costs of the simulated ZTIMD process. On the other hand, VMD can theoretically generate the highest driving force at the same feed temperature among the MD configurations. Thus, larger flux would be theoretically achievable by adopting VMD to ZTIMD process compared to DCMD configuration. However, generating the vacuum and working under such a low pressure

continuously and especially at large scale would be certainly challenging. Hence, it would be worth studying the viability of ZTIMD on the basis of VMD.

8-3-3- Testing Durability, and Thermal and Mechanical Stability of the Developed Nanocomposite MD Membranes

This thesis and the associated publications have revealed for the first time that hydrophilic nanomaterials could be used as the nano-additives for the development of the mixed matrix MD membranes. The results obtained are very promising, however, we are still in the beginning of a long way, and making the idea work at the industrial level would certainly need more time, much effort, and better facilities. This study aimed at improvement of the permeability of the MD membranes, while maintaining a high level of salt rejection, and the target was successfully achieved. The nanocomposite membranes fabricated in this work demonstrated larger fluxes than the currently available MD membranes at low feed temperatures. However, as already mentioned, the membrane durability is an important parameter in commercializing the MD process for seawater desalination. Therefore, testing the membrane durability in terms of pore wetting, thermal, and mechanical stability should be put in the priority for the future work. In addition, even though fouling in MD especially at low operating temperatures is not as severe as in RO, it would still be interesting to study the resistance of the membranes against fouling and biofouling to justify such an expectation.

8-3-4- Testing the Developed Nanocomposite MD Membranes in a DCMD Configuration

Furthermore, nanocomposite membranes prepared in this work were only tested for VMD. It would be interesting to evaluate the membranes in a DCMD configuration since the simulation of the ZTIMD was carried out with the DCMD process.

8-3-5- Effects of Nanomaterials Properties on the Membrane Performance

Last but not least, effects of nanomaterials characteristics such as size, morphology, thermal conductivity, etc. on the properties and performance of the MD membranes need to be further investigated.

Appendix A:

Effects of superhydrophobic SiO_2 nanoparticles on the performance of PVDF flat sheet membranes for vacuum membrane distillation

J. E. Efome, M. Baghbanzadeh, D. Rana, T. Matsuura, C. Q. Lan, Effects of superhydrophobic SiO_2 nanoparticles on the performance of PVDF flat sheet membranes for vacuum membrane distillation, Desalination, 371 (2015) 47-57

Effects of superhydrophobic SiO_2 nanoparticles on the performance of PVDF flat sheet membranes for vacuum membrane distillation

Johnson E. Efome, Mohammadali Baghbanzadeh, Dipak Rana*, Takeshi Matsuura, Christopher Q. Lan*

Department of Chemical and Biological Engineering, University of Ottawa, 161 Louis Pasteur Private, Ottawa, Ontario, Canada K1N 6N5

Abstract

Polyvinylidene Fluoride (PVDF)/SiO_2 flat sheet composite membranes were prepared for Vacuum Membrane Distillation (VMD) by the phase inversion immersion precipitation process. The effect of blending superhydrophobic SiO_2 nanoparticles into the PVDF dope solution was studied. The concentration of the nanoparticles in the dope solution was varied at different wt.% (1.0, 2.0, 4.0, 6.0, 7.0, 8.0, and 10.0 wt.%). The prepared membranes were characterized by scanning electron microscopy, water contact angle, porosity, liquid entry pressure of water, Fourier transformed infrared spectroscopy, and VMD at feed temperatures of 27.0 °C. The nanoparticles enhanced the membrane performance through an increase in surface pore size, leading to increased vapour flux with a maximum at 7.0 wt.%. The salt rejection was greater than 99.98% when a 35 g/L NaCl solution was used as feed. At this concentration, the largest macro-voids were achieved. Beyond 7.0 wt.%, the sponge-like layer became predominant and the flux was reduced. With a vapour flux increase of up to 4 times (from 0.7 to 2.9 kg/m^2 h) when compared to the neat membrane, this nanocomposite membrane could be of great potential in the desalination process through VMD.

Keywords: Polyvinylidene fluoride; Superhydrophobic SiO_2 nanoparticles; Sponge-like layer thickness; Vacuum membrane distillation;

*Corresponding author. Tel.: Tel.: 1 613 562 5800x2050.
E-mail address:Christopher.Lan@uottawa.ca (C.Q. Lan), Rana@uottawa.ca (D. Rana)

A-2- Introduction

The demand for drinkable water is showing an increasing trend due to the rise in global population. The total amount of water on earth is believed to be constant that goes through a re-cycling process. Though 70% of the earth is covered by water, only 2.5% is fresh water, the rest being saline and ocean based [1]. With the increasing effects of global temperature rise (climate changes), surface water is suffering from constant evaporation creating more shortage of portable water and making the saline water more saline. The situation does not seem not to be improving along with difficult challenges associated with controlling global warming and pollution [1]. Since there has not been a cost effective means to circumvent the crisis, global health, economic growth and even social welfare are at risk.

It is therefore imperative that other means of fresh water is required to meet the rising population demand such as desalination of sea water to portable water. Several conventional processes like Ultrafiltration (UF), Microfiltration (MF) Reverse Osmosis (RO) and multistage vacuum evaporation have been employed for water treatment but an emerging separation technique is needed [2]. Membrane Distillation (MD) is proving to be more efficient than other processes because of: (i) Lower operating pressure than RO, (ii) Close to 100% salt rejection, (iii) Lower energy consumption than multistage evaporation, and (iv) Lower operating temperature. MD has been used for different applications such as in the food industry, environmental protection and pharmaceuticals. In MD the driving force is the difference in vapour pressure across the micro-porous membrane created by the temperature gradient across the membrane [2].

Following extensive research on MD [3-31], different configurations have been analysed: Vacuum Membrane Distillation (VMD), Air Gap Membrane Distillation (AGMD), Direct Contact Membrane Distillation (DCMD) and Sweep Gas Membrane Distillation (SGMD) [6,9]. Irrespective of which configuration is being applied, a membrane which meets specific characteristics is always employed to carry out the separation process. In all MD configurations, one of the membrane characteristics is hydrophobicity which determines the wettability of the membrane surface. Hydrophobic membranes do not get wet easily, hence allowing only water vapour and not liquid to pass through the pores at pressures lower than the liquid entry pressure (LEP_w). At pressures greater than the LEP_w, the micro-pores become wet and part of the feed

solution seeps onto the permeate side, thus allowing for no separation [3,4,8]. Researchers have used several polymers in preparing hydrophobic membranes because these polymers have presented low surface energies, high chemical resistance, thermal stability, and good mechanical strengths. These polymers include; Polyvinylidene Fluoride (PVDF), Polypropylene (PP), Polyethylene (PE) and Polytetrafluoroethylene (PTFE) amongst which PVDF is the most widely used [27,28]. Several techniques of membrane preparation have also been investigated in preparing membrane distillation membranes. These include; Thermally Induced Phase Separation (TIPS), immersion precipitations, Vapour Induced Precipitation (VIP), and air casting of polymer solution, all of which involve some kind of solvent for polymer dissolution. The most widely used solvents for PVDF membrane preparation are Dimethysulfoxide (DMSO), Dimethyformamide (DMF), and Dimethylacetamide (DMAc) which are capable of completely dissolving the polymer at moderate temperatures [6,9,27,28].

In the last decade of research in MD, scientists have placed special focus on the hydrophobicity of the developed membranes because an efficient MD process must result in reliable flux measurements and consistent conductivity readings of the resulting permeate. As such researchers have developed several means of achieving hydrophobic (water contact angle greater than 90°) and even superhydrophobic (contact angle greater than 130°) membrane surfaces [9]. Kuo et al. [16] obtained novel composite membranes by using alcohol as the coagulation agent through the phase invasion precipitation method. The membranes were reported to have contact angles greater than 130°. Razmjou et al. [24] fabricated hydrophobic membranes by coating the PVDF surface with TiO_2 which resulted in membranes with contact angles greater than 130°.

Recent research works have also included techniques to enhance the porosity, flux, and mechanical strength of the membranes. A blend of high and low molecular weight PVDF was used by Chen et al. [5,6] to prepare flat sheet membranes of high porosity and improved LEP_w. Fontananova et al. [12] prepared membranes from PVDF copolymer (PVDF-co-hexafluoropropylene) and PVDF homopolymer. The copolymer membranes posed greater resistance to mass transport than the homopolymer due to a bi-layer formed at the top and bottom surfaces of the membrane. High porosity membranes were made by Khayet and Matsuura [14] using water as a pore forming agent. Wang and Chung [29] produced a mixed

matrix hollow fiber membrane with high flux and porosity by adding hydrophobic clay particles into the dope. Other researchers have used a blend of polymers for the dope solution preparation. Yang et al. [32] fabricated membranes on support materials which were shown to enhance the flux by up to 15 fold when compared to the unsupported membrane.

The present research was carried out to fabricate hydrophobic PVDF/nanoparticles flat sheet composite membranes using superhydrophobic SiO_2 nanoparticles as additives. The hydrophobic porous membranes where prepared by the phase inversion precipitation method using deionised water as the non-solvent additive and DMAc as the solvent. The membrane properties were investigated at different concentrations of the nanoparticles. They were characterized by Scanning Electron Microscopy (SEM), VMD, porosity, Liquid Entry Pressure of water (LEP_w), and water contact angle. The rejection of the membranes was also tested for desalination by using synthetic salt water.

A-3- Experimental materials and method

A-3-1- Materials

Polyvinylidene Fluoride (PVDF) polymer of two different molecular weights: Kynar® 740 and Kynar® HSV 900 was supplied as resins powder from Arkema Inc., Philadelphia, PA. PVDF exists in the α, β, and γ phases. However, Kynar is mostly in the α phase [6] and the structure of PVDF is presented in the graphical abstract. Dimethylacetamide (DMAc, > 99%) used as solvent was supplied by Sigma Aldrich Inc., St. Louis, MO. The pore forming agent and coagulation agent employed were deionised water (conductivity < 10 μS) produced by Millipore Q BIOCEL unit, Millipore, Billerica, MA. Superhydrophobic silica nanoparticles (purity: ≥ 99.8, particle size: 10-20 nm, surface area: 100-140 m^2/g), surface modified with single layer organic chains were supplied by SkySpring Nanomaterials Inc. (Houston, TX). Butan-1-ol (> 99.8%) was from Sigma Aldrich Inc., St. Louis, MO.

A-3-2- Preparation of Dope Solution

The dope solution was prepared by mixing PVDF (15 wt.%), DMAc (83.75 wt.%) and water (1.25 wt.%) together at a stirrer rotation of 180 rpm and 50°C for 72 h to ensure complete polymer dissolution and solution homogeneity. The solution was then allowed to de-gas for 24 h

at room temperature. The required amount of nanoparticles was then added to the required quantity of dope solution and the suspension was stirred at 100 rpm for 2 h to yield the dope solution with expected final wt.% (1.0, 2.0, 4.0, 6.0, 7.0, 8.0, and 10.0) of nanoparticles. Hereafter ‘‘nanoparticles concentration’’ means the nanoparticle concentration in the dope. The compositions for the respective concentrations are listed in Table A-1.

Table A-1 Composition of the dope solution for flat-sheet composite membrane preparation

Membrane Code	Dope Solution Concentration			Nanoparticles Concentration in the Dope Suspension
	PVDF (wt.%)	DMAc (wt.%)	Water (wt.%)	
MS-0	15	83.75	1.25	0.0
MS-1	15	83.75	1.25	1.0
MS-2	15	83.75	1.25	2.0
MS-4	15	83.75	1.25	4.0
MS-6	15	83.75	1.25	6.0
MS-7	15	83.75	1.25	7.0
MS-8	15	83.75	1.25	8.0
MS-10	15	83.75	1.25	10.0

* Dope solution was prepared before addition of nanoparticles, so the nanoparticles wt.% is relative to dope solution.

A-3-3- Membrane Casting Method

The dope solution containing the nanoparticle at the desired wt.% was then cast on a glass plate using a casting bar (0.25 mm thickness) at a speed of approximately 7 cm s^{-1}. The plate was then exposed to air for 10 s, followed by immersion into deionised water at ambient temperature. Upon completion of phase inversion, the solidified polymer sheet was peeled off the plate, transferred into fresh deionised water at ambient temperature and kept there for 24 h. Thereafter, the sheet was allowed to dry at room temperature for 24 h. The dried membranes were then subjected to characterization.

A-3-4- Characterization of Dope Solution (Viscosity Measurement)

Viscosity measurement was carried out with the aid of a rotational rheometer (Brookfield, Synchro-Lectric viscometer model: LVF). The solution to be analysed was poured into the testing valves and a suitable spindle connected and immersed into the solution. A suitable motor speed was selected and the spindle was allowed to rotate for 5-7 minutes until the monitor on the dial attained a constant value. The viscosity was calculated according to the rotation speed, spindle factor, and rotation factor. Three measurements per solution were performed and the average was reported.

A-3-5- Membrane Characterization

A-3-5-1- Scanning Electron Microscopy (SEM)

The top surface and cross-sectional images were taken using a SEM system (Tescan, Vega-II XMU with Oxford Inca Energy 250X EDS). After being immersed in liquid nitrogen to embrittle, the membrane sample was broken and fixed on a metal holder using a conductivity tape. The sample was then sputtered with a conductivity metal (Gold, > 99.8%) coating under vacuum. The coating instrument employed was Anatech Hummer VII. SEM images were then taken at randomly selected locations and at suitable magnifications.

A-3-5-2- Liquid Entry Pressure of Water (LEP_w) Measurements

The LEP_w of the membranes was measured using the setup shown in Fig. A-1, and the following approach [10]. A static liquid reservoir was installed with a membrane sample of surface area 0.00131 m^2 and filled with 200 ml of deionised water at ambient temperature. Compressed nitrogen from a cylinder was used to apply pressure on the liquid and a regulator was used to control the increment at 2.0 psig per 10 min until water dripped off continuously from the cell outlet. A pressure gauge connected on the line displayed the operating pressure. For each membrane, three samples were analysed and the average was reported. The pressure at which water was seen dripping off the cell was noted as the LEP_w.

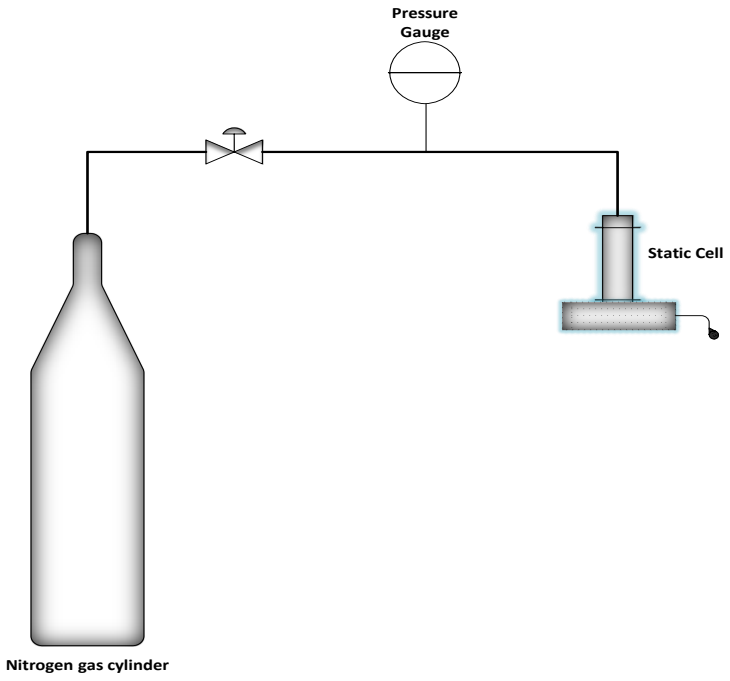

Fig. A-1 Schematic diagram of the experimental LEP_w set-up

A-3-5-3- Water Contact Angle Measurements

The surface of each membrane was analysed for its hydrophobicity by measuring the water contact angle using a VCA Optima surface Analysis system (AST Products Inc., Billerica, MA). A 1 μL water droplet was dropped on the membrane surface using a micro syringe (Hamilton Company, Reno, NV) followed by a 10 s wait period, then the angle was measured. Measurements were taken from 8 randomly selected spots and the average was reported.

A-3-5-4- Membrane Surface Roughness

The top surface of flat sheet membranes was analysed for roughness. A well suited software ImageJ was employed for the analysis. The SEM images were converted to a 32 bits image and an inbuilt plugin of ImageJ (*SurfCharJ*) could read the 7.5 μm x 7.5 μm size images to determine the roughness by computing the root mean square roughness (R_q) and the average roughness (R_a).

A-3-5-5- Energy Dispersive X-ray Spectroscopy (EDX) Analyses

To investigate how the nanoparticles are dispersed within the flat-sheet membranes, EDX analysis of the membrane cross-section was conducted using an Oxford Inca Energy 250X EDX apparatus.

A-3-5-6- Porosity and Pore Size Measurements

Three pieces were cut from randomly selected spots of a membrane sheet (area, 0.001884 m^2) and subjected to porosity measurements [21] using butan-1-ol. The pieces of membrane were kept immersed in a petri-dish that contained butanol for 24 h. They were then blotted, weighed and oven dried at 50°C for 2 h, followed by weighing again after drying. The porosity was calculated using the equation below and the average value was reported.

$$\%\varepsilon = \frac{m1\text{-}m2}{\rho.A.\delta} x100\% \qquad \text{(A-1)}$$

Where ε is the porosity (%), m_1 (g) is the weight of the wet membrane, m_2 (g) is the weight of the dry membrane, ρ (g/L) is the liquid density (butan-1-ol), A (m^2) is the effective surface area of the membrane, and δ (m) is the membrane thickness measured using a micrometer.

Pore size measurement of the flat sheet membranes was carried out by applying the ImageJ software on the top SEM image. Approximately 100 pores were randomly selected from the image and the average value was reported.

A-3-6- Vacuum Membrane Distillation (VMD)

VMD experiments were carried out to evaluate the performance of the composite membranes. The setup used for VMD is shown in Fig. A-2 following a previous research work [5, 6]. The module consisted of a feed chamber with a permeation base where the membrane (0.00113 m^2) was placed. A vacuum pump was used to apply vacuum (94.8 kPa) on the permeate side so that the permeated water vapour could be collected. The feed chamber was maintained at 27.0 °C with the use of a heating coil connected to a temperature control bath and kept under agitation to minimise temperature polarization effects. The procedure involved a 1 h pre-treatment by which air and moisture were sucked out of the lines. By doing so, the system was allowed to reach a steady state. All cold traps were cooled with liquid nitrogen. After the permeate vapour was collected in cold trap 3 during the 1 h pre-treatment, the vacuum line was switched to cold trap 2 where the permeate vapour was collected to measure the flux. Cold trap 1 was installed to prevent the oil contamination of the vacuum pump. The experiment was conducted for a predetermined time and the flux calculated using equation A-2.

$$\text{Flux} = \frac{\text{w}}{\text{t.A}} \qquad \text{(A-2)}$$

Where w (g) is the weight of condensate, t (h) is the time of flux collection, A (m^2) is the effective membrane surface area.

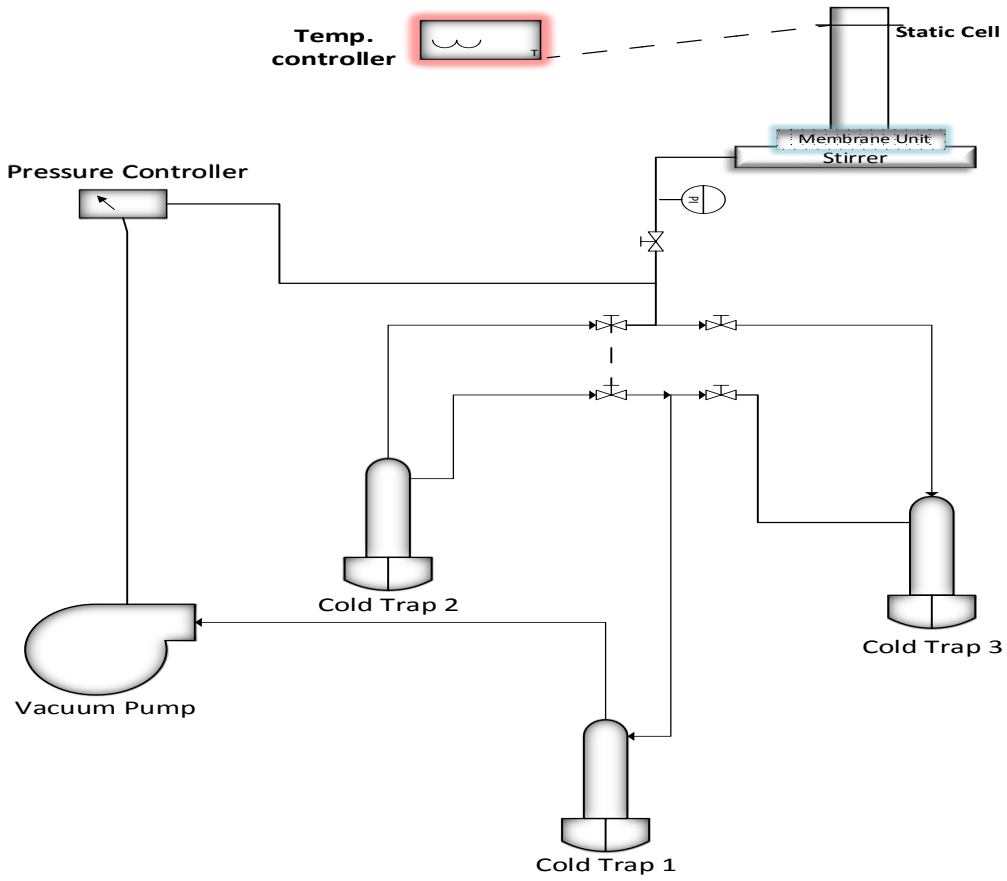

Fig. A-2 Schematic diagram of VMD set-up

A-3-7- ATR-FTIR Analyses

The prepared membranes were subjected to Attenuated Total Reflectance (ATR) - Fourier Transformed Infrared Spectroscopy (FTIR) spectroscopy by the Agilent tech-Cary630 (Agilent, Canada) spectrometer equipped with a diamond sampling accessory. The surface of the dried membranes were analysed by pressing and fixing the sample on the prism, and the IR spectra were recorded at 4 cm^{-1} resolution in the range of 650-3000 cm^{-1} with 64 scans.

A-3-8- Nanoparticle Characterization

The nanoparticles characterization was done to check for particle shape and surface properties (presence of pores). Transmission Electron Microscopy (TEM) (FEI Tecnai G2 F20 equipped with Oxford Aztec TEM with 80 mm SDD detector) was applied to observe the nano-structure of the silica nanoparticles. Samples were prepared by dispersing super hydrophobic silica power

into methanol. A drop of methanol was used for the dispersion of the nanoparticles on carbon-coated copper grids operating at 300 kV.

A-4- Results and Discussion

A-4-1- Dope Solution Viscosity

Fig. A-3 shows the results of viscosity measurements done at room temperature. It clearly illustrates a drastic increase in viscosity as nanoparticle concentration increases. Thus solvent/non-solvent exchange rate is significantly lowered at high nanoparticle concentration. It is worth noting that the viscosity of the dope solution increased from 3.2 Pa.s of SM-0 (without blending nanoparticles) to 15.0 Pa.s of SM-10 (nanoparticles concentration 10.0 wt.%).

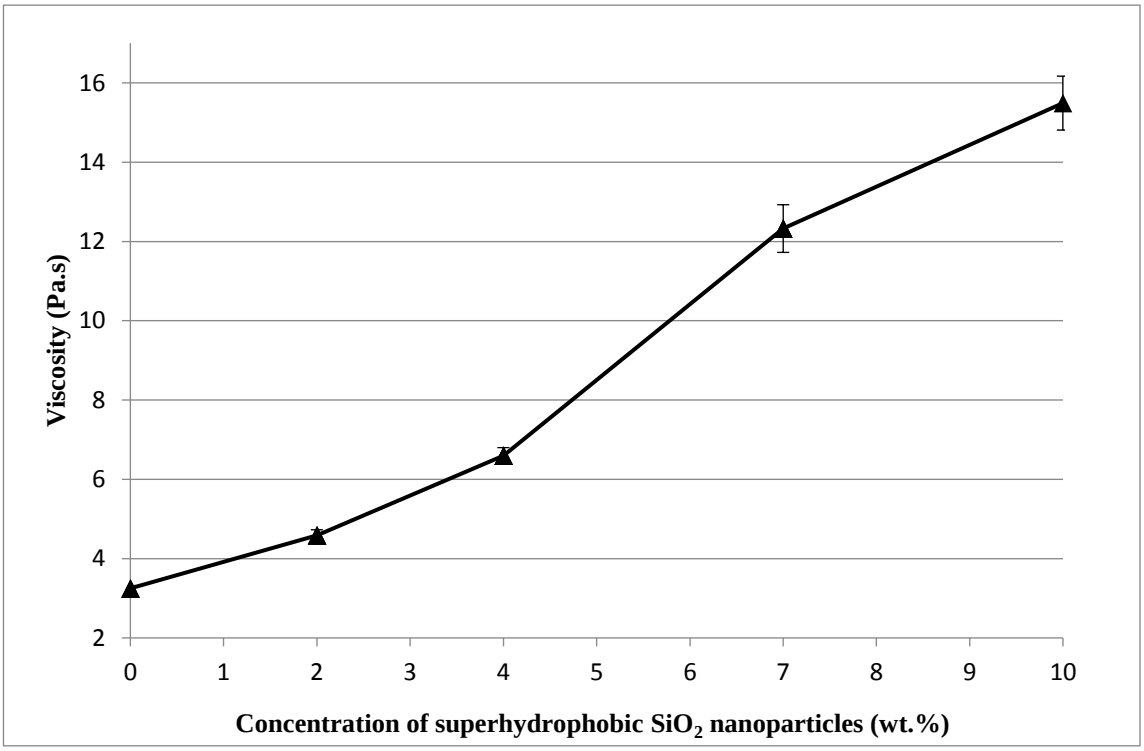

Fig. A-3 Viscosity measurements of the polymer solution

A-4-2- Membrane Characterization

A-4-2-1- Scanning Electron Microscopy (SEM)

To investigate the morphological changes associated with the addition of SiO_2 nanoparticles, SEM images of the top (T), cross-section (C) and bottom (B) of the membranes were taken as shown in Fig. A-4. From the cross-sectional images, it is seen that the membranes have an

asymmetric structure with a thin top skin layer, a finger-like macro-voids region, and a lower sponge-like layer. The effect of blending SiO_2 nanoparticles in the dope solution can be visually appreciated as a drastic change in the morphology is seen in the nanocomposite membranes (SM-4, SM-7, SM-10) when compared to the neat PVDF membrane (SM-0).

The top surface of the nanocomposite membranes presents a typical micro-porous surface showing a larger pore diameter but fewer in number than the neat PVDF membrane. Pores are formed by the phase inversion process. Demixing (presence of two phases; the polymer rich phase responsible for the solid continuous region and the phase with lesser polymer carrying the pore forming agents) plays a key role in pore formation. The higher the rate of demixing the lesser the appearance of the two phases, implying lesser pores will be formed [4-7].

Since water is the non-solvent coagulation media and the SiO_2 nanoparticles are superhydrophobic in nature and disperse well in the dope solution, water molecules are compelled to come together during solvent/non-solvent exchange to form larger droplets forming pores of larger sizes. Hence, the pore size increases upon addition of SiO_2 nanoparticles. Further increase in the nanoparticles concentration is supposed to increase the pore size progressively but the SEM images shows that the average pore sizes are approximately the same irrespective of concentration increase. This is ascribed to the weakened effect of hydrophobic nanoparticles as a result of their agglomeration.

As the SiO_2 nanoparticles concentration increases from MS-0-C to MS-10-C, a drastic change in the cross-sectional morphology is noticed. The membranes show a denser structure with smaller finger-like macro-voids. The finger-like layer disappears gradually, making it difficult to differentiate the finger-like layer from the sponge-like layer. This observation indicates that nanoparticles have a significant effect in the morphology of the membranes. During the solvent/non-solvent exchange process, the increased viscosity caused by increase in nanoparticles concentration (see Fig. A-3), poses greater resistance to the diffusion, resulting in the formation of fewer macro-voids but longer in depth [5-7,11]. This shows that at concentration > 10.0 wt.%, the membrane loses its asymmetric morphology, adapting to a more symmetric morphology made up primarily of the sponge-like layer and very dense. It is noted that the flux of the hydrophilic CuO nanoparticles incorporated PVDF composite membranes

which increases with increasing concentration of nanoparticles due to the enlarging surface pores and thickening the finger-like layer [33].

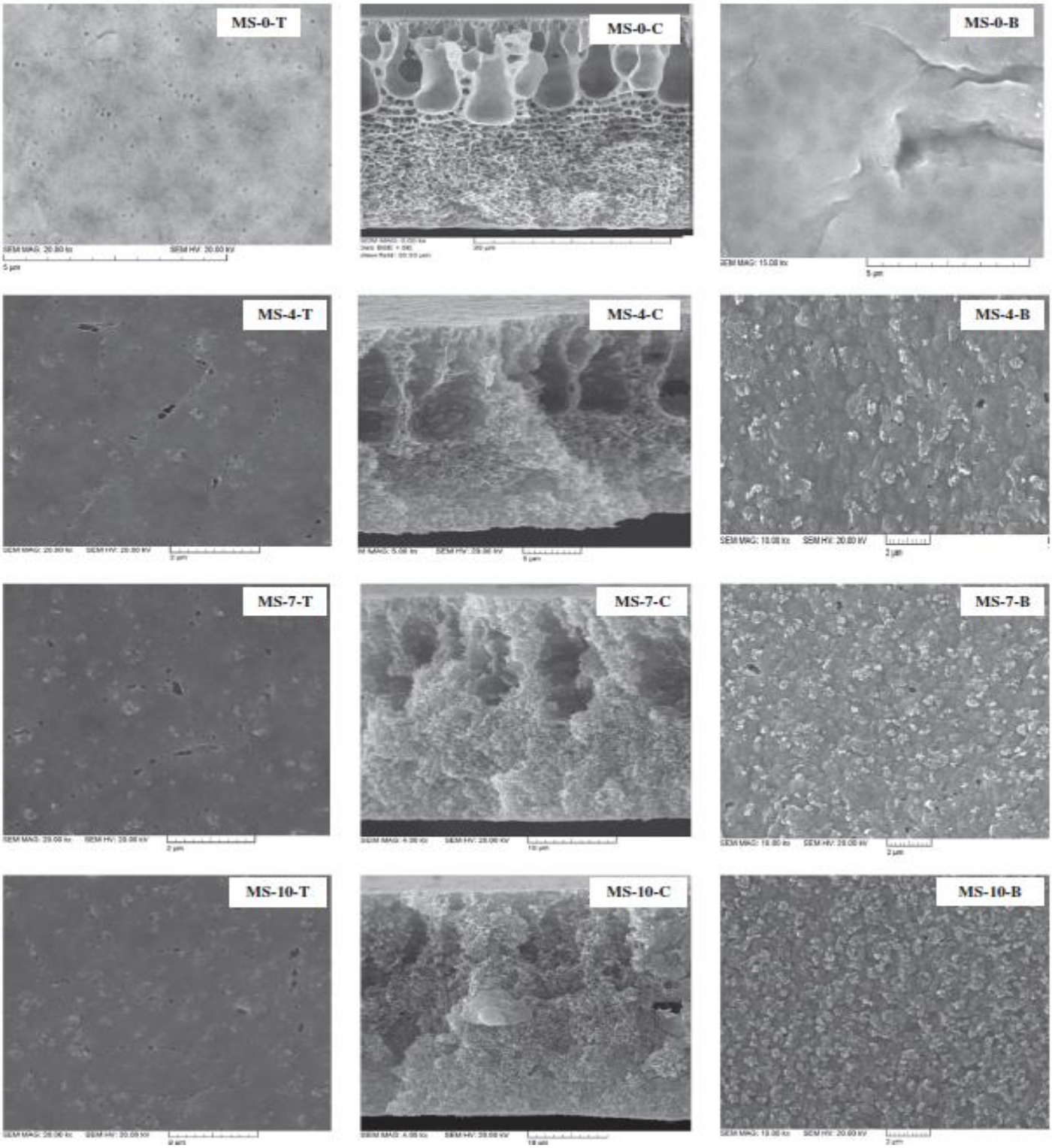

Fig. A-4 SEM images of the PVDF flat sheet nanocomposite membranes: T for top surface, C for cross-section, B for bottom surface

A-4-2-2- LEP_w, Porosity, and Pore Size Measurements

VMD membranes are supposed to be able to support pressures of at least 3.0 bars [27,31] to prevent water from fully penetrating the pores and disrupting the separation process. The experimental data for LEP_w is presented in Fig. A-5. The results show that all PVDF-SiO_2 blended membranes have values above 45.0 psi (3.1 bar) with the maximum shown at nanoparticles concentration of 10.0 wt.%, it can thus be concluded that these membranes are suitable for VMD processes.

The decrease in LEP_w from the neat PVDF to the nanocomposite membrane is tentatively attributed to the increase in the surface pore size but amongst the nanocomposite membranes, the LEP_w value maintains an increase due to the decrease in membrane porosity with an increase in nanoparticles concentration.

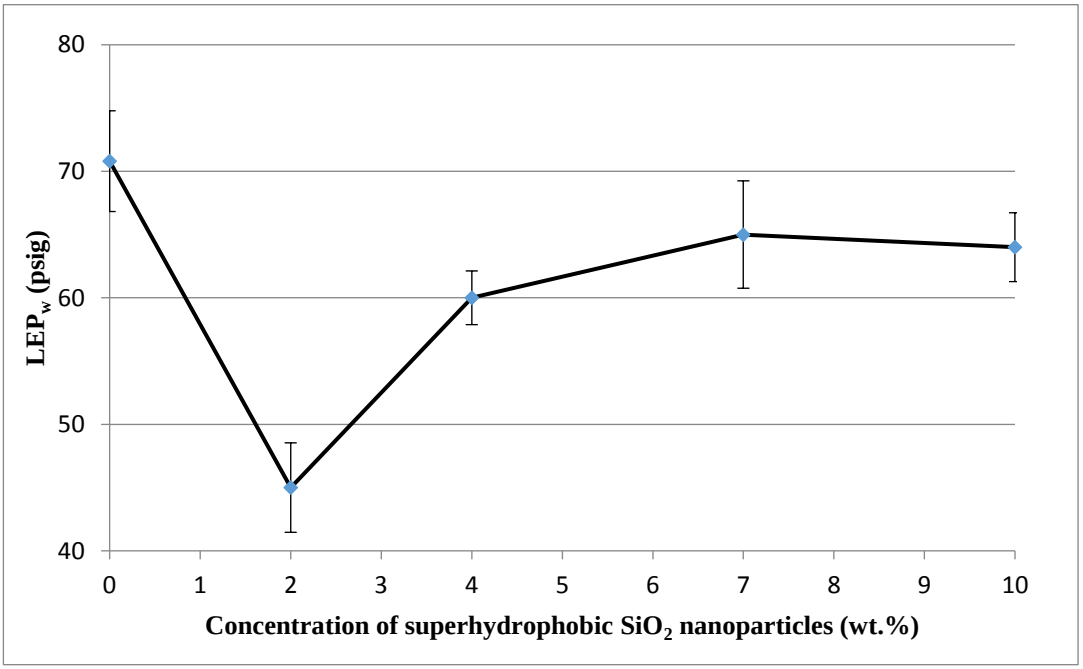

Fig. A-5 Effect of nanoparticles concentration on LEP_w

This further supports the fact that the surface pore sizes did not experience a great change amongst the blended membranes because if it did, the LEP_w would have seen a drop also caused by increased pore size.

The effect of the nanoparticle concentration on porosity is shown on Fig. A-6. The neat membrane presented the highest porosity value > 85% and the minimum value below 50% were shown at the nanoparticle concentration of 10.0 wt.%.

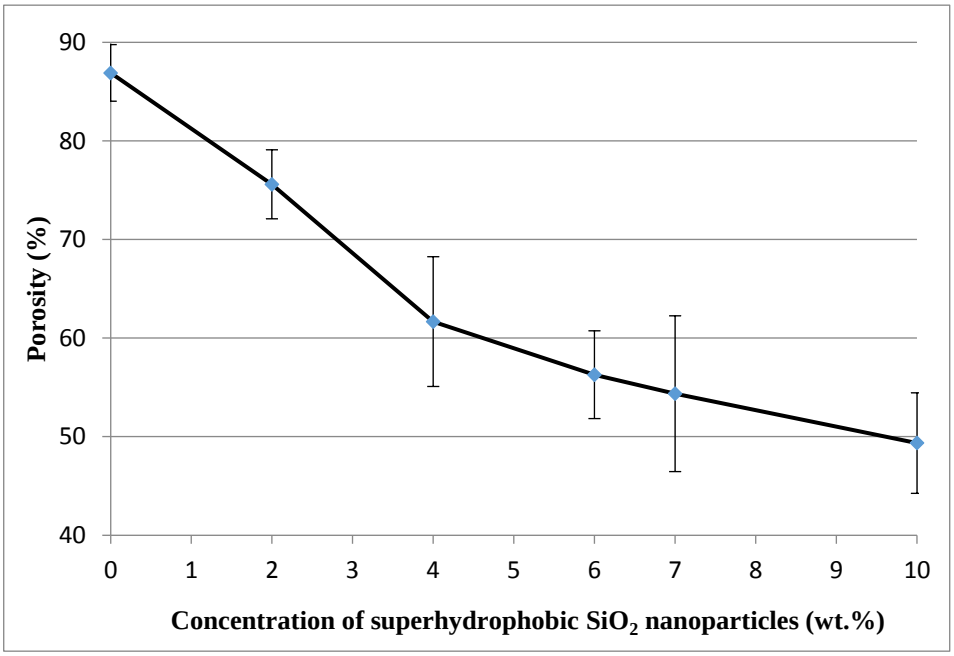

Fig. A-6 Effect of nanoparticles concentration on porosity

This decrease in porosity ties with the increase in viscosity [7,11] which caused the membrane to lose most of the finger-like layer and produced a denser sponge-like layer. The SEM images of MS-4-C, MS-7-C and MS-10-C also confirm this phenomenon. The increase in the membrane dense nature reduces the micro-voids hence the porosity drops.

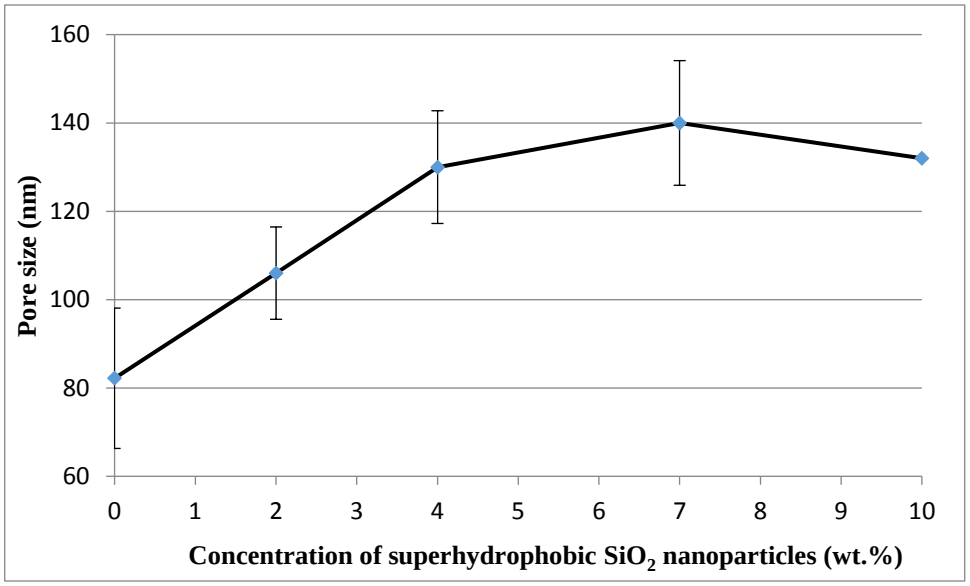

Fig. A-7 Effects of nanoparticles concentration on surface pore diameter

Fig. A-7 shows the pore size at the surface on the prepared membranes. As expected from the SEM top surface images (MS-0-T, MS-4-T, MS-7-T, MS-10-T), the pore size increases from nanoparticles concentration of 0.0 to 4.0 wt.% before levelling off.

A-4-3- Membrane Surface Properties

A-4-3-1- Water Contact Angle

The results of the water contact angle measurements are presented in Fig. A-8. Since the nanoparticles used were superhydrophobic in nature, it was expected to increase the hydrophobicity of the nanocomposite membranes to near superhydrophobic levels. Though a superhydrophobic surface was not obtained, the hydrophobicity was enhanced. All nanocomposite membranes showed values greater than the neat PVDF membrane, with the maximum contact angle attained (94°) at the nanoparticle concentration of 10.0 wt.%.

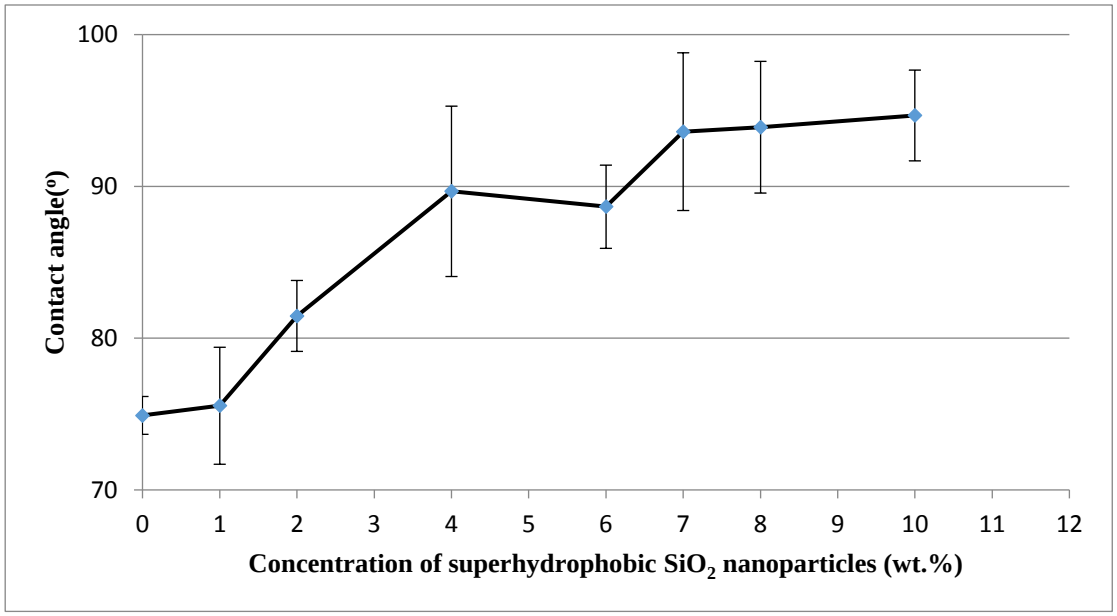

Fig. A-8 Effect of nanoparticles concentration on water contact angle

It should be noted that, the contact angle of the dense composite membrane prepared by complete solvent evaporation showed significantly higher values than the corresponding porous membrane. For example, dense membrane that corresponds to MS-10 demonstrated features of a superhydrophobic surface with a contact angle > 135°. This disparity in contact angle measurements could be explained by the fact that the dense membrane surface roughness is greater than the porous membrane [15-17] as a result of nanoparticles being exposed close to the surface.

A-4-3-2- Roughness Analysis

Roughness parameters were obtained from the SEM top surface images using the *SurfCharJ* plugin of ImageJ software and the results shown in Table A-2. The average roughness (R_a) defines the arithmetic average of the absolute values of the measured peak heights from a one dimensional plane, the root mean square (R_q) refers to the standard deviation and R_p denotes the maximum profile peak height. ImageJ surface analysis of the surface is shown in Fig. A-9.

Table A-2 Roughness parameters of the prepared PVDF nanocomposite flat sheet membranes			
Membrane Code	**R_a**	**R_q**	**R_p**
MS-0	15.53	19.65	242
MS-4	27.88	50.58	255
MS-7	28.03	52.19	255
MS-10	27.28	49.35	255

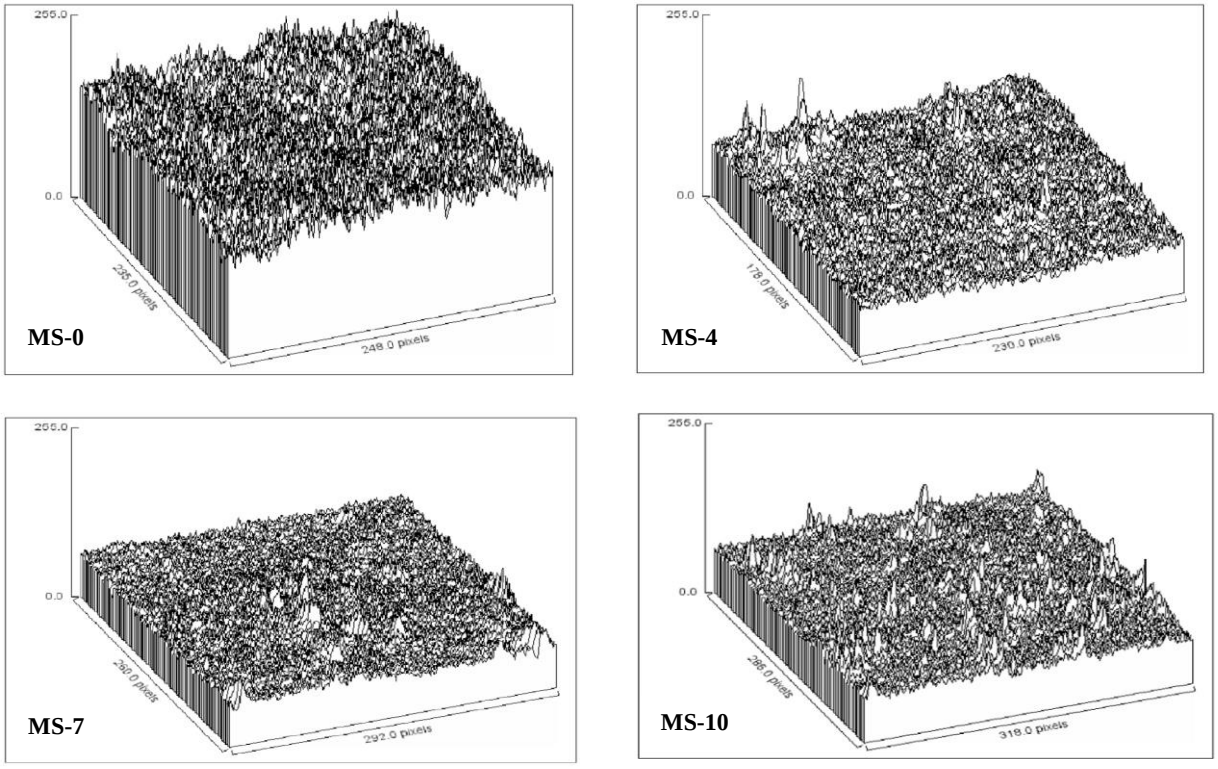

Fig. A-9 Three dimensional topographic images of neat PVDF and PVDF-SiO_2 nanocomposite membranes

It can be seen from the results that, the MS-0 membrane (neat PVDF membrane) had the smoothest surface with a R_a of 15.53 nm when compared to MS-4, MS-7, and MS-10 nanocomposite membranes. Amongst the nanocomposite membranes, there is not significant variation in the roughness parameters. This ties with the minimal variation in the water contact angle values seen amongst the nanocomposite membranes (Fig. A-8). It is thus evident that the presence of the nanoparticles increased the surface roughness [11,15], which led to an increase in the contact angle.

A-4-3-3- Particle Distribution (EDX Analyses)

Silicon mapping was performed across the cross-section of the nanocomposite membrane MS-2 and MS-7 to check for nanoparticle distribution and agglomeration as seen in Fig. A-10. Fluorine mapping is also shown in Fig. A-10 since PVDF was the base polymer and fluorine should be seen all across the cross-section. From the figure, it is seen that the nanoparticles are distributed with little or no agglomeration across the cross-section since clusters of colours are not observed. The greater intensity of the coloration seen in MS-7 denotes an increase in concentration from 2.0 to 7.0 wt.% nanoparticles.

According to Fig. A-11, three regions of the cross-section of MS-4 and MS-7 nanocomposite membranes were subjected to EDX. A section close to the top thin layer, the middle section and a section close to the bottom were sampled. It could be seen that, the nanoparticles dispersed uniformly throughout the cross-section as shown by nearly equal Si peaks at the different locations. Detailed analysis of the wt.% of silicon at these locations has shown that its concentration reduces very slightly from the top to bottom. This could be due to the difference in densities between the nanoparticles and the polymer solution.

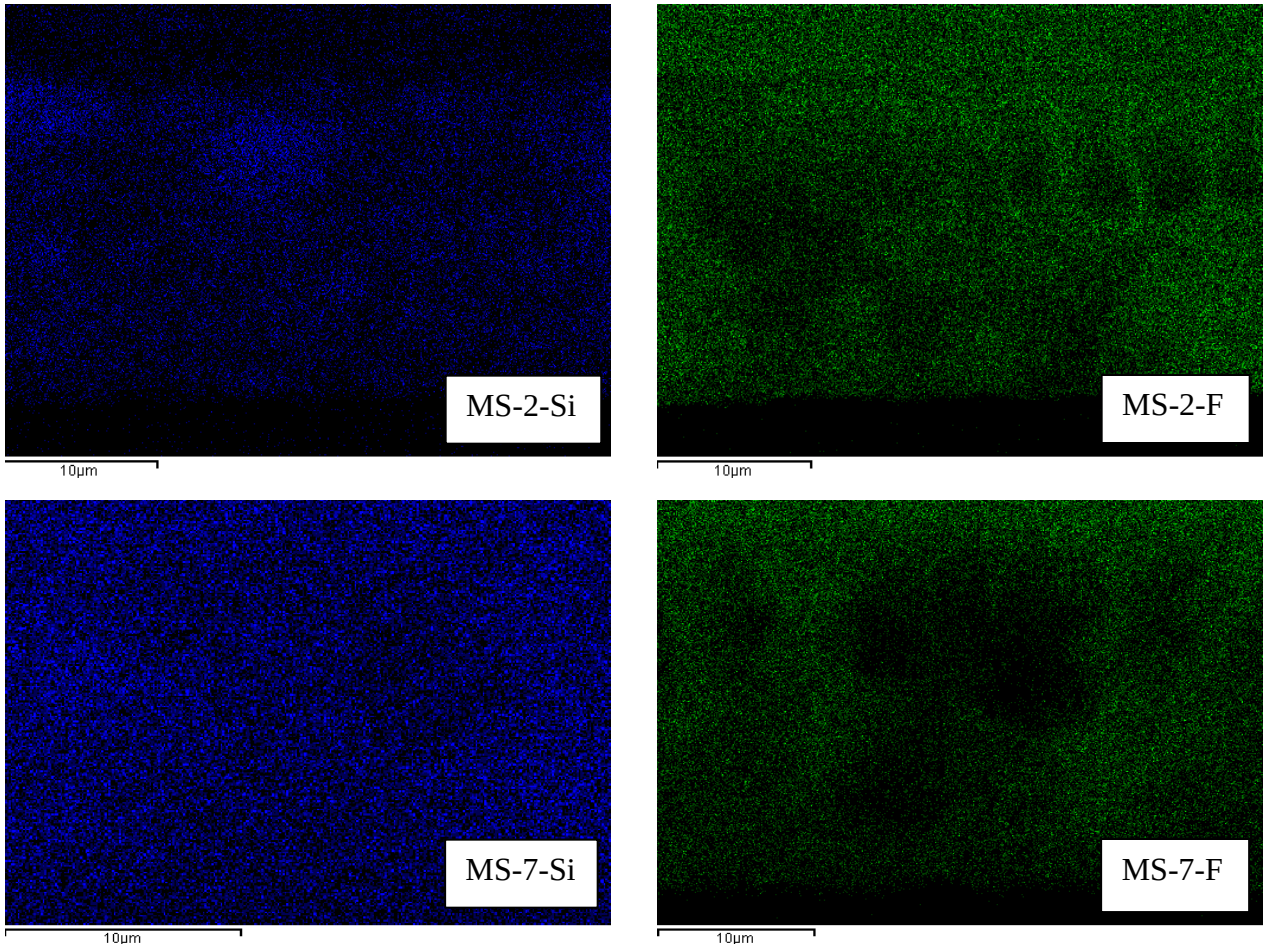

Fig. A-10 Silicon (Si) and Fluorine (F) mapping of PVDF-SiO_2 nanocomposite membranes cross-sections

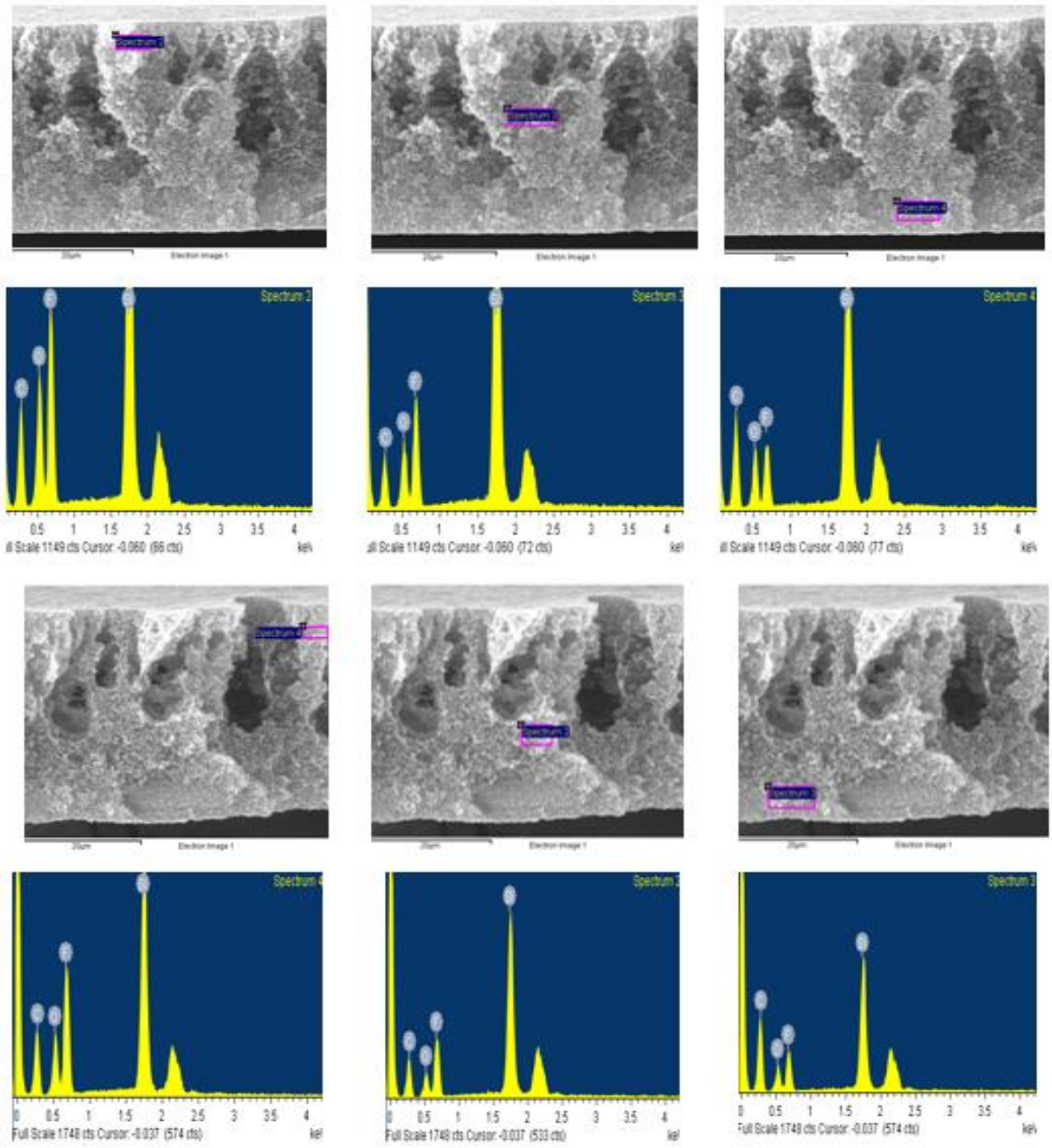

Fig. A-11 EDX images of flat sheet PVDF-SiO_2 nanocomposite membranes: MS-4 (first row) and MS-7 (third row)

A-4-3-4- ATR-FTIR Analyses

The ATR-FTIR spectra of the prepared membranes with varying nanoparticles concentrations are presented in Fig. A-12. PVDF being a semi-crystalline polymer has five possible polymorphs alternating between α-β transition states. All the membrane samples showed main absorption

peaks at 840, 880, 1070, 1180 and 1400 cm^{-1} wave number, indicating that the PVDF polymer is made up of the α and β crystals [12,24]. Since both crystals are present, it demonstrates that the phase inversion precipitation process did not create any chemical changes in the crystalline structure of the polymer.

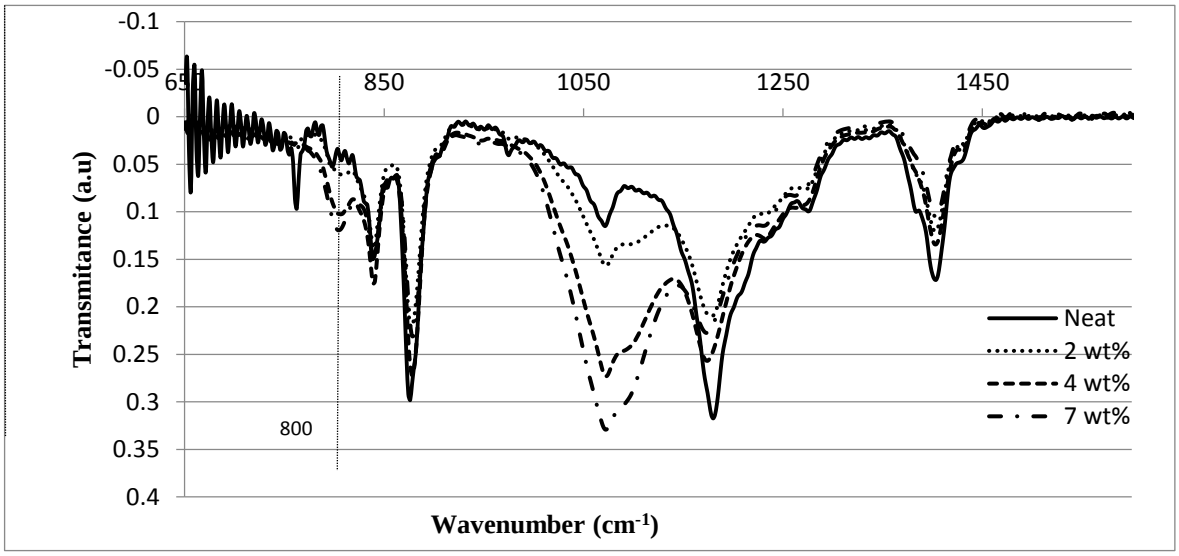

Fig. A-12 FTIR spectra of the neat PVDF (MS-0), 2.0 wt.% SiO_2-PVDF (MS-2), 4.0 wt.% SiO_2-PVDF (MS-4) and 7.0 wt.% SiO_2-PVDF (MS-7) nanocomposite membranes

The appearance of an absorbance peak at 800 cm^{-1}, a characteristic SiO_2 peak, and the increase of its transmittance with an increase in the nanoparticles concentration, suggests the inclusion of nanoparticles in the membrane.

A-4-3-5- TEM Analysis

Fig. A-13 shows the nanoparticles TEM images of particle shape and diameter. From the results, it could be seen that, the nanoparticles are near spherical and have diameters ranging from 10-20 nm which are compatible with the specifics provided by the manufacturer.

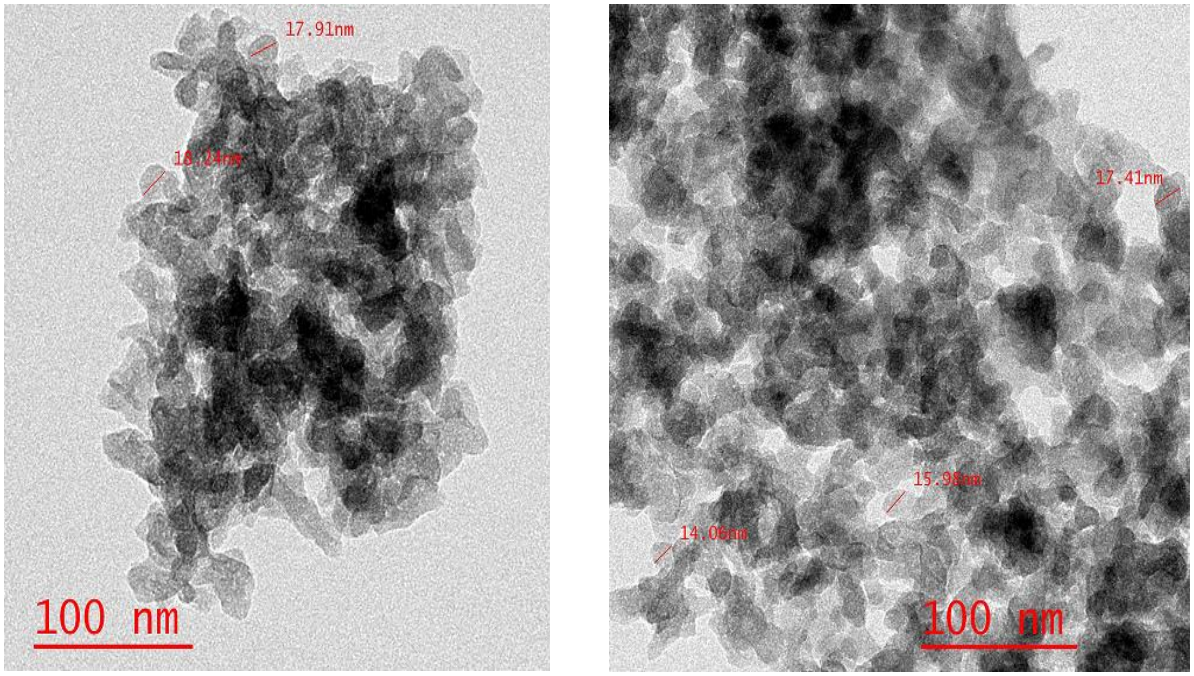

Fig. A-13 TEM images of superhydrophobic SiO_2 nanoparticles

A-4-4- Membrane Performance

The effect of changing nanoparticles concentration on the pure water flux of the composite membranes is shown in Fig. A-14. From the results, it is evident that the flux increases upon addition of nanoparticles from MS-0 to MS-4 and as the nanoparticles concentration further increases, shows a maximum at the nanoparticle concentration of 7.0 wt.% (MS-7). This trend parallels to the pore size change in Fig. A-7, which also shows a maximum at 7.0 wt.% due to the agglomeration of nanoparticles at higher concentrations. The decrease in porosity with an increase in nanoparticles concentration (see Fig. A-6) also contributes to the flux decrease at concentrations higher than 7.0 wt.%. It is also likely that some of the pores formed at the high nanoparticle concentration were dead-end pores through which no flow occurred [25].

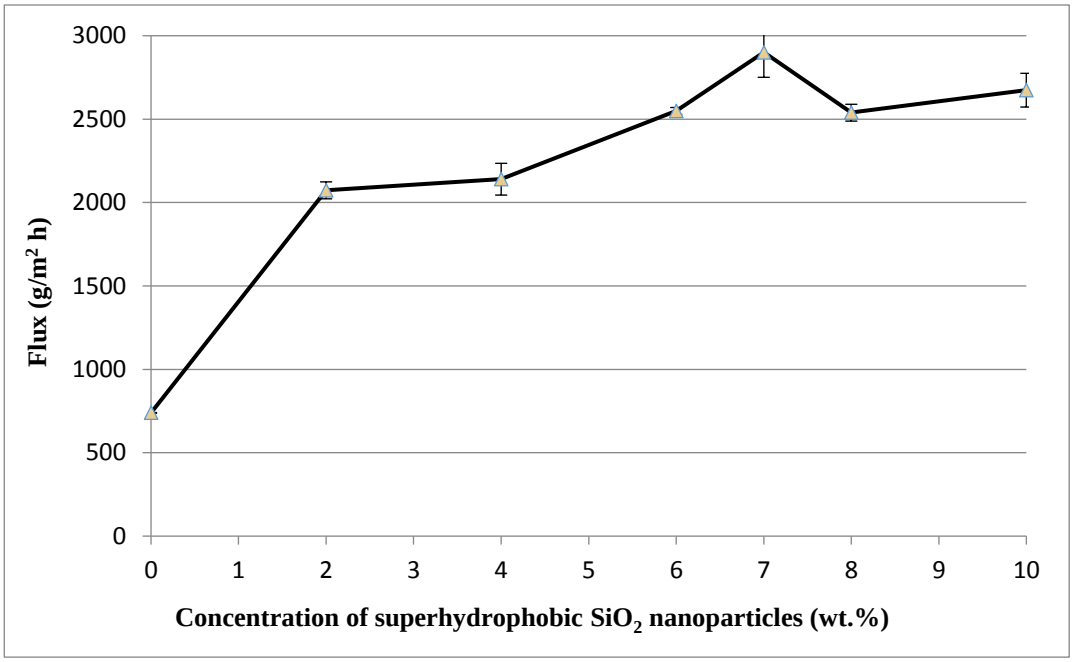

Fig. A-14 Permeation flux of VMD as a function of nanoparticles concentration in dope solution

The nanocomposite membranes where further tested for salt rejection with a 35 g/L NaCl solution to mimic sea water and 2 g/L NaCl brackish water as the feed at 27.0 °C. The conductivity of the salt water feed (510 mS) yielded a permeate solution (< 70 μS) denoting a salt rejection > 99.98% at the maximum flux of 2.9 kg m^{-2} h^{-1} while the brackish water (3.94 mS) yielded a permeate of < 50 μS giving a 99.99% rejection (Fig. A-15) for the MS-7 nanocomposite membrane which contained 7.0 wt.% superhydrophobic nanoparticles. This flux corresponds to 4 times higher than the VMD flux of the neat membrane, implying incorporating nanoparticles of up 7.0 wt.% in the dope solution is optimal under the investigated conditions.

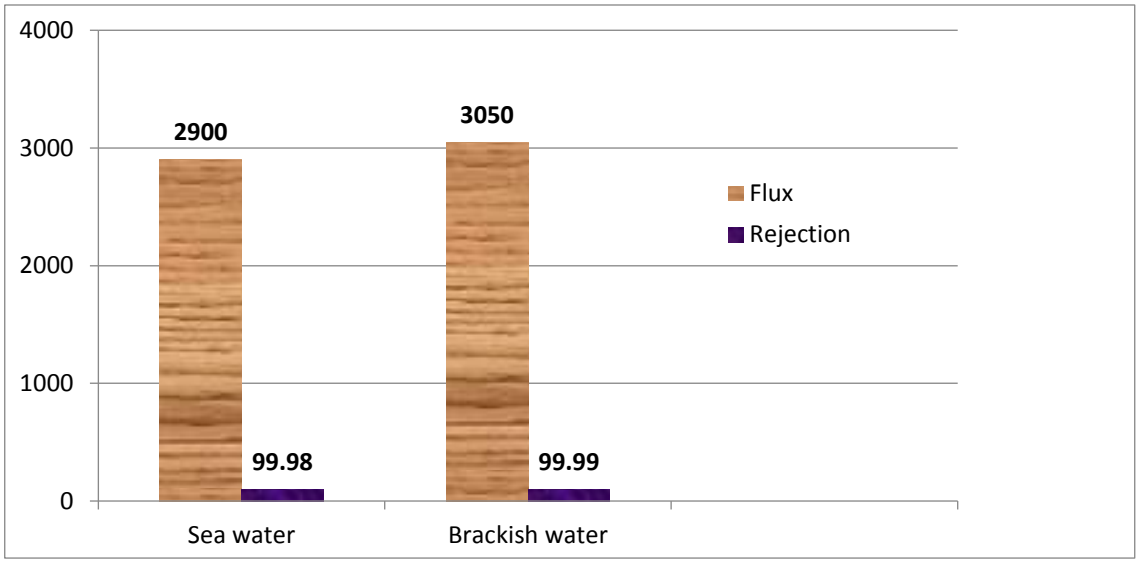

Fig. A-15 Analysis of membrane flux with artificial seawater, i.e., containing 35 g/L NaCl and artificial brackish water, i.e., 2 g/L aqueous NaCl solution

Usually, greater flux is associated with higher porosity [12], which was not the case in this study. Despite having the highest porosity, the neat PVDF membrane showed the lowest flux, implying vapour flux does not depend solely on the porosity but also on the resistance to the vapour movement across the membrane (dense crystalline nature) [7]. The MS-7 nanocomposite flux was analysed with respect to time to study the flux and rejection stabilities. Fig. A-16 shows an initial drop in flux of about 0.5% and then the flux levels off to 2991 g/m^2 h. The same trend of very small decrease of performance in the first four hours also applies to the rejection. It can thus be deduced that, for the time duration specified, the flux and rejection of the fabricated membrane were stable.

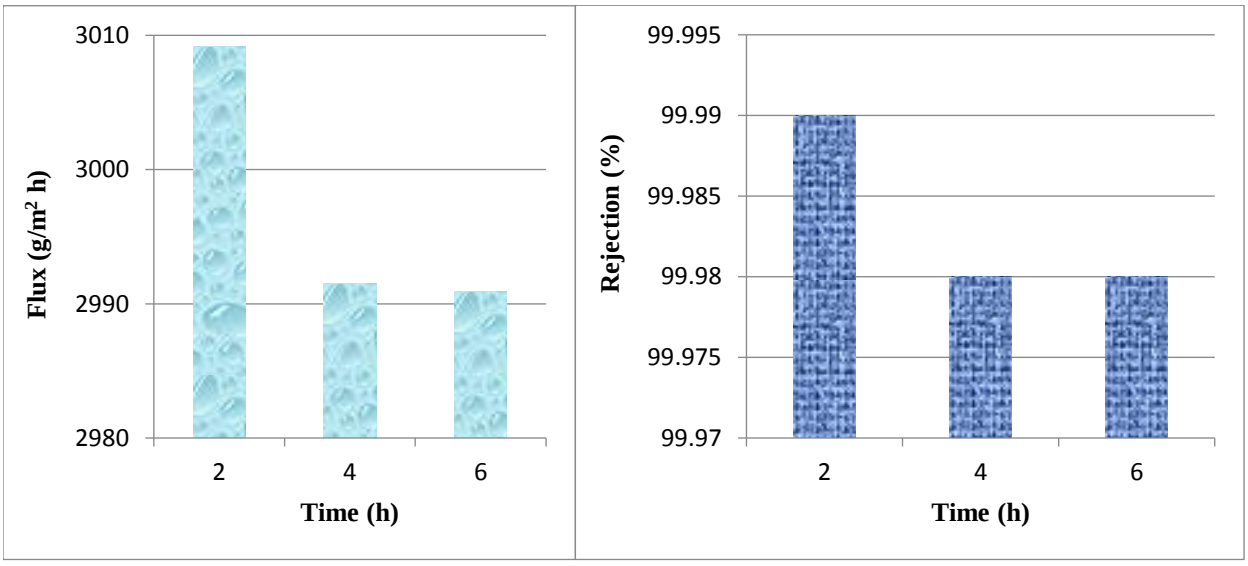

Fig. A-16 Comparative analysis of flux stability and rejection with time

When compared to the neat PVDF, all the nanocomposite membranes showed a greater flux, implying the increased pore size.

A-5- Conclusion

In Summary, flat sheet nanocomposite PVDF-SiO_2 membranes were prepared by the phase inversion technique, characterized by various methods and their performance in VMD was investigated. The experimental results showed that the addition of superhydrophobic SiO_2 nanoparticles have varying effects. The nanocomposite membrane morphology showed an asymmetric structure with a finger-like macro-void layer and a sponge-like layer, the ratio of which had an impact on the VMD performance of the membrane. The maximum flux was observed at the nanoparticle concentration of 7.0 wt.% with an average flux of around 3.0 kg/m^2 h, which was 4 times higher than the neat PVDF membrane. A salt rejection of more than 99.98% indicates that the fabricated membrane is satisfactory for membrane distillation. The results denote that 7.0 wt.% is the concentration most suitable for the studied VMD conditions. It was observed that the porosity decreased while the flux increased with increase in nanoparticles concentration. It is thus evident that the VMD flux does not depend solely on the porosity of the membrane but also on the crystalline nature of the membrane. On the other hand, all nanocomposite membranes showed an increased pore size compared to the neat PVDF membranes thus pore size also accounted for the increased flux. It is hence likely that the flux is determined by the interplay of surface pores size and bulk porosity. Also, all nanocomposite membranes had LEP_w values > 3 bar making them suitable for VMD applications. The study concludes that PVDF blended with superhydrophobic SiO_2 nanoparticles is suitable for VMD processes for desalination of seawater.

Acknowledgments

Special thanks to Arkema Inc. (Philadelphia, PA) for their generously offer of the polymers (Kynar® 740 and Kynar® HSV 900). Financial supports of the NSERC Discovery (Grant # RGPIN 288226-2010) and the I2IPJ (Grant # 463142-2014) grants are also gratefully acknowledged.

References

[1] (a) Anonymous, The United Nations Document Index, The United Nations Publications, New York, NY, 2005, 22.03.2005, Retrieved May 12, 2015; (b) Anonymous, International Decade for Action "Water for Life" 2005-2015, The UN-Water Decade Programme on Advocacy and Communication (UNW-DPAC), doi: ///www.un.or/waterforlifedecade/, Retrieved May 12, 2015; (c) Anonymous, Managing Water Under Uncertainty and Risk, The United Nations World Water Development Repot (WWDR4), 4th Edition, UNESCO, Paris, France, 2012, ISBN: 978-92-3-104235-5; (d) Anonymous, Water in a Sustainable World, The United Nations World Water Development Repot 2015, UNESCO, Paris, France, 2015, ISBN: 978-92-3-100071-3

[2] Abu-Zeid, M. A. E., Zhang, Y., Dong, H., Zhang, L., Chen, H., & Hou, L. (2015). A comprehensive review of vacuum membrane distillation technique. *Desalination, 356*, 1–14.

[3] Bian, X., Shi, L., Yang, X., & Lu, X. (2011). Effect of nano-TiO_2 particles on the performance of PVDF, PVDF-g-(maleic anhydride), and PVDF-g-poly(acryl amide) membranes. *Industrial & Engineering Chemistry Research, 50*(21), 12113–12123.

[4] Bonyadi, S., & Chung, T. S. (2007). Flux enhancement in membrane distillation by fabrication of dual layer hydrophilic-hydrophobic hollow fiber membranes. *Journal of Membrane Science, 306*(1-2), 134–146.

[5] Chen, Z., Rana, D., Matsuura, T., Yang, Y., & Lan, C. Q. (2014). Study on the structure and vacuum membrane distillation performance of PVDF composite membranes: I. Influence of blending. *Separation and Purification Technology, 133*, 303–312.

[6] Chen, Z., Rana, D., Matsuura, T., Meng, D., & Lan, C. Q. (2015). Study on the structure and vacuum membrane distillation performance of PVDF membranes: I. Influence of molecular weight. *Chemical Engineering Journal, 276*, 174–184.

[7] Chiam, C., & Sarbatly, R. (2013). Vacuum membrane distillation processes for aqueous solution treatment - A review. *Chemical Engineering and Processing: Process Intensification, 74*, 27–54.

[8] Cui, A., Liu, Z., Xiao, C., & Zhang, Y. (2010). Effect of micro-sized SiO_2-particle on the performance of PVDF blend membranes via TIPS. *Journal of Membrane Science, 360*(1-2), 259–264.

[9] Dong, Z., Ma, X., Xu, Z., You, W., & Li, F. (2014). Superhydrophobic PVDF–PTFE electrospun nanofibrous membranes for desalination by vacuum membrane distillation. *Desalination, 347*, 175–183.

[10] Drioli, E., Ali, A., & Macedonio, F. (2015). Membrane distillation: Recent developments and perspectives. *Desalination, 356*, 56–84.

[11] Fan, H., & Peng, Y. (2012). Application of PVDF membranes in desalination and comparison of the VMD and DCMD processes. *Chemical Engineering Science, 79*, 94–102.

[12] Fontananova, E., Jansen, J. C., Cristiano, A., Curcio, E., & Drioli, E. (2006). Effect of additives in the casting solution on the formation of PVDF membranes. *Desalination, 192*(1-3), 190–197.

[13] Hou, D., Dai, G., Fan, H., Wang, J., Zhao, C., & Huang, H. (2014). Effects of calcium carbonate nano-particles on the properties of PVDF/nonwoven fabric flat-sheet composite membranes for direct contact membrane distillation. *Desalination, 347*, 25–33.

[14] Khayet, M., & Matsuura, T. (2011). *Membrane Distillation*: *Principles and Applications*, Ch. 12, pp. 323–359, Elsevier, Amsterdam, The Netherlands.

[15] Koo, J., Han, J., Sohn, J., Lee, S., & Hwang, T. (2013). Experimental comparison of direct contact membrane distillation (DCMD) with vacuum membrane distillation (VMD). *Desalination and Water Treatment, 51*(31-33), 6299–6309.

[16] Kuo, C., Lin, H., Tsai, H., Wang, D., & Lai, J. (2008). Fabrication of a high hydrophobic PVDF membrane via nonsolvent induced phase separation. *Desalination, 233*(1-3), 40–47.

[17] Li, G., Shen, L., Luo, Y., & Zhang, S. (2014). The effect of silver-PAMAM dendrimer nanocomposites on the performance of PVDF membranes. *Desalination, 338*, 115–120.

[18] Li, X., Zhang, M., He, J., Wu, D., Meng, J., & Ni, P. (2014). Effects of fluorinated SiO2 nanoparticles on the thermal and electrochemical properties of PP nonwoven/PVdF-HFP composite separator for li-ion batteries. *Journal of Membrane Science, 455*, 368–374.

[19] Naidu, G., Jeong, S., Choi, Y., Jang, E., Hwang, T., & Vigneswaran, S. (2014). Application of vacuum membrane distillation for small scale drinking water production. *Desalination, 354*, 53–61.

[20] Ortiz de Zárate, J. M., Peňa, L., & Mengual, J. I. (1995). Characterization of membrane distillation membranes prepared by phase inversion. *Desalination, 100*(1-3), 139–148.

[21] Peng, P., Fane, A. G., & Li, X. (2005). Desalination by membrane distillation adopting a hydrophilic membrane. *Desalination, 173*(1), 45–54.

[22] Pourjafar, S., Jahanshahi, M., & Rahimpour, A. (2013). Optimization of TiO2 modified poly(vinyl alcohol) thin film composite nanofiltration membranes using taguchi method. *Desalination, 315*, 107–114.

[23] Qtaishat, M., Khayet, M., & Matsuura, T. (2009). Novel porous composite hydrophobic/hydrophilic polysulfone membranes for desalination by direct contact membrane distillation. *Journal of Membrane Science, 341*(1-2), 139–148.

[24] Razmjou, A., Arifin, E., Dong, G., Mansouri, J., & Chen, V. (2012). Superhydrophobic modification of TiO_2 nanocomposite PVDF membranes for applications in membrane distillation. *Journal of Membrane Science, 415-416*, 850–863.

[25] Salimi, A., & Yousefi, A. A. (2003). Analysis method: FTIR studies of β-phase crystal formation in stretched PVDF films. *Polymer Testing, 22*(6), 699–704.

[26] Devi, S., Ray, P., Singh, K., & Singh, P. S. (2014). Preparation and characterization of highly micro-porous PVDF membranes for desalination of saline water through vacuum membrane distillation. *Desalination, 346*, 9–18.

[27] Teoh, M. M., & Chung, T. (2009). Membrane distillation with hydrophobic macrovoid-free PVDF–PTFE hollow fiber membranes. *Separation and Purification Technology*, *66*(2), 229–236.

[28] Tijing, L. D., Choi, J., Lee, S., Kim, S., & Shon, H. K. (2014). Recent progress of membrane distillation using electrospun nanofibrous membrane. *Journal of Membrane Science, 453*, 435–462.

[29] Wang, P., & Chung, T. (2015). Recent advances in membrane distillation processes: Membrane development, configuration design and application exploring. *Journal of Membrane Science, 474*, 39–56.

[30] Wang, X., Zhang, L., Sun, D., An, Q., & Chen, H. (2009). Formation mechanism and crystallization of poly(vinylidene fluoride) membrane via immersion precipitation method. *Desalination, 236*(1-3), 170–178.

[31] Winter, D., Koschikowski, J., & Wieghaus, M. (2011). Desalination using membrane distillation: Experimental studies on full scale spiral wound modules. *Journal of Membrane Science*, *375*(1-2), 104–112.

[32] Yang, Y., Rana, D., Matsuura, T., Zheng, S., & Lan, C. Q. (2014). Criteria for the selection of a support material to fabricate coated membranes for a life support device. *RSC Advances*, *4*(73), 38711–38717.

[33] Baghbanzadeh, M., Rana, D., Matsuura, T., & Lan, C. Q. (2015). Effects of hydrophilic CuO nanoparticles on properties and performance of PVDF VMD membranes. *Desalination*, *369*, 75–84.